Novel β-Substituted (Alkoxy and Methylthio) Porphyrinoids: Synthesis, Characterization and Optical Properties

A Thesis Submitted for the Degree of

DOCTOR OF PHILOSOPHY

by
Anup Rana

School of Chemistry
University of Hyderabad
Hyderabad-500 046
INDIA

April 2015

Dedicated
to
মা-বাবা

CONTENTS

DECLARATION

I hereby declare that the matter embodied in the thesis entitled **"*Novel β-substituted (alkoxy and methylthio) porphyrinoids: synthesis, characterization and optical properties*"** is the result of investigations carried out by me in School of Chemistry, University of Hyderabad, Hyderabad, India under the supervision of **Dr. Pradeepta K. Panda** and it has not been submitted elsewhere for the award of any degree or diploma or membership, etc. This work is also free from plagiarism. I hereby agree that my thesis can be deposited in Shodhganga/INFLIBNET.

In keeping with the general practice of reporting scientific investigations, due acknowledgements have been made wherever the work described is based on the findings of other investigators. Any omission or error that might have crept in is sincerely regretted.

April 2015 **Anup Rana**

UNIVERSITY OF HYDERABAD

Central University (P.O.), Hyderabad-500046, India

Dr. Pradeepta K Panda
Associate Professor
School of Chemistry

Tel: 91-40-23134818 (Office)
Fax: 91-40-23012460
E-mail: pradeepta.panda@uohyd.ac.in
pradeepta.panda@gmail.com
pkpsc@uohyd.ernet.in

CERTIFICATE

This is to certify that the work described in this thesis entitled "***Novel ß-substituted (alkoxy and methylthio) porphyrinoids: synthesis, characterization and optical properties***" has been carried out by Mr. Anup Rana bearing Regd. No. 08CHPH46 under my supervision for partial fulfillment for the award of Doctor of Philosophy in Chemistry and the same has not been submitted elsewhere for any degree, which is a plagiarism free thesis.

Dean
School of Chemistry
University of Hyderabad
Hyderabad-500 046
India

Dr. Pradeepta K Panda
(Thesis supervisor)

PREFACE

The thesis entitled "Novel β-substituted (alkoxy and methylthio) porphyrinoids: synthesis, characterization and optical properties" consists of nine chapters. It deals with the syntheses and characterizations of novel β-(alkoxy and methylthio) porphyrinoids developed in our group. These include porphyrins and its isomer, porphycenes, and expanded porphyrins viz. stretched porphycenes and sapphyrins. C**hapter 1** basically deals with a historical overview of porphyrins including generalized introduction to isomeric and *π*-extended expanded porphyrinoids. Further, a detailed overview is provided about β-alkoxyporphyrinoids in context of their synthesis and application. **Chapter 2** gives a brief account of the methods and materials used in our investigation. In **chapter 3** we have discussed about fluorescence quenching method for solution and vapor phase sensing of environmentally hazardous high energy materials by using porphyrins and their Zn(II) complexes. **Chapter 4** deals with the synthesis of type-I tetrachlorotetramethoxyporphyrin along with its characterization, photophysical and NLO properties. In **chapter 5** we describe the synthesis of β-octamethoxyporphycene, two positional isomers of tetrachloroteramethoxyporphycenes along with their M(II) complexes. We have evaluated these molecules to understand the substitution effect at the porphycene periphery to find their suitablity for possible application as photosensitizers in PDT. C**hapter 6** gives an account on the synthesis of octamethylthioporphycene along with their M(II) complexes. The photophysical, electrochemical, NLO and transient absorption properties of these molecules were characterized in detail. In **chapter 7** we have discussed about the synthesis of three new octamethoxy substituted stretched porphycenes. These molecules were investigated in details to understand their photophysical, solid state structure, electrochemical, NLO and transient absorption properties to evaluate effect of substituents. In **chapter 8** we synthesized decamethoxysapphyrin and its 27-N-benzyl congener. These molecules were charecterised by solid state structure, ^{1}H NMR, photophysical and electrochemical properties. The anion binding and protonation of sapphyrins were evaluated by absorption spectroscopy. Further, structural diversity of 27-N-benzyl congener was probed in detail. Finally, **chapter 9** summarizes the overall achievement and future prospective.

April 2015 **Anup Rana**

Acknowledgement

It is impossible to achieve any goal individually, requires well-organized team work. This dissertation work is no exception. A large number people involved in the whole process that helped and inspired me directly or indirectly to carry out my PhD work smoothly during my stay in HCU. Therefore, it is time to acknowledge them for their kind help and inspiration. It is practically difficult for me to remember and name each and every person at this time. I would like to express my apology in advance to those that falls in this category. It's a reflection of my inadequate memory, not your contribution.

First and foremost, I would like to thank my supervisor Dr. Pradeepta K. Panda for his generous support and encouragement over the years and for giving me the opportunity to explore this exciting field of chemistry. He is the best guide I have ever seen, who has shaped my career to what I am today.

I would like to thank the former and present Dean, School of Chemistry, for their constant inspiration and for allowing me to use the available facilities. I am extremely thankful individually to all the faculty members of the School for their kind help and cooperation at various stages of my stay in the campus. I thank all the non-teaching staff of the School of Chemistry for their assistance on various occasions.

Council of Scientific and Industrial Research (CSIR), India is gratefully acknowledged for providing me fellowship. Also, I gratefully acknowledge to DRDO, India for providing financial assistance.

I am also grateful to our collaborators who helped make the present work much better. Dr. S. Venugopal Rao, ACRHEM, University of Hyderabad and his research group, particularly Debasis Swain is gratefully acknowledged for carrying out NLO studies included in the thesis. I would also like to thank Prof. Dongho Kim and his research group, particularly Sangsu Lee, Yonsei University, South Korea, for carrying out NLO and excited state photodynamic studies. Further, I thank to Prof. Jacek Waluk, Institute of Physical Chemistry, Polish Academy of Sciences, Poland; for being part of our collaborations. My sincere thanks also extend to Prof. A. Samanta and his research group, School of Chemistry, UOH; for their help during PhD work.

A special thank goes to all my lab mates. I have been fortunate enough to enjoy each of your company like a family member. A big thank to all of you: Naren, Sanjeev, Tridib, Ritwik, Brijesh, Nandakishore, Sathish, Obaiah, Vikranth, Prameela, Sandip, Kurumurthy, Nagamaiah, Swayam, Dharini, Mounika, Gitarani and Dhwaneet. I would also wish to thank Souradip, Preethi, Chandrasekhar and Prasad who extended their assistance to me during project stay.

My pleasant association with some friends and seniors inside and outside UOH such as Ranjit Da, Dinu da, Maity da, Paromita di, Santanu da, Palash da, Utpal da, Suparna di, Susrut da, Nayan, Raja, Satya, Navendu, Suman, Kaushik, Kallol, Sugata, Rudra, Sanatan, Sudipta, Tanmoy, Susanta da, is unforgettable.

I would like to thank my school of chemistry seniors and friends Abhijit da, Prashant da, Bhaswati di, Teja bhai, Sashi, Santhosh, Ganesh, Shrinivas, Ravindra, Naveen, Manoj, Ramana, Vanaja, Saktivel, Tamilsaran, Arindam, Arun, Sandeep, Mehboob, Arjun, Anish, Ganesh, Vignesh, Dharavath, Sridevi, Ram babu, Yashin, Krishnachary, Srinivas, Karunakar, Sekhar, Gupta, Hari, Rajgopal, Sathish, R. Kishore, Kishore, Ramesh, Anand, Sudalai, Seshadri, Venu, Suryanayaran, Rajesh, Ramesh, Anji, Srinivas, D. K., Krishnachaitanya, Bharat, Supratim, Pramiti, Paulami, Sutanuka, Arpita, Sabari, Subhra, Geetha, Olivia, Sneha, Debparna, Shalini di, Shubhabrata, Dipta, Gangadhar, Manojveer, Naidu, Sudhir, Narayana, Malkappa, Chandrasekhar, Ragavaiah, Lingaiah, Ramu, Babu and all others whose names are not mentioned due to limited space.

Finally, I would like to express my love and gratitude to my parents, sister, brother and family for their unconditional love, support and blessings. They made me what I am today and I owe everything to them. Dedicating this thesis to them is a minor recognition for their relentless support and love.

April 2015 **Anup Rana**

University of Hyderabad

Hyderabad-500 046

India

List of abbreviations

1D	One dimensional
2D	Two dimensional
3D	Three dimensional
Anhyd.	Anhydrous
AMP	Adenosine mono phosphate
AcOH	Acetic acid
Bcl-2	B-cell lymphoma 2
BCOD	Bicyclo[2.2.2]octadiene
br	Broad
$BF_3.(OEt)_2$	Borontrifluoride diethyletherate
Boc	t-butoxycarbonyl
Calcd.	Calculated
CV	Cyclic voltammetry
CT	Charge transfer
Conc.	Concentaration
d	Doublet
DPV	Differential pulse voltammetry
DCM	Dichloromethane
DCE	1,2-Dichloroethane
DDQ	2,3-Dichloro-5,6-dicyano-1,4-benzoquinone
DNT	2,4-dinitrotoluene
DMNB	2,3-dimethyl-2,3-dinitrobutane
DMSO	Dimethylsulfoxide
DMF	N,N-Dimethylformamide
Equiv.	Equivalent
ESI	Electrospray ionization
fs	femto second
FT	Fourier transform

FWHM	Full width at half maximum
GM	Göppert-Mayer
HRMS	High resolution-mass spectrometry
HOMO	Highest occupied molecular orbital
HMX	Octahydro-1,3,5,7-tetranitro-1,3,5,7-tetrazocine
h	Hour (s)
Hz	Hertz
H_2TPP	*meso*-tetraphenylporphyrin
HPLC	High performance liquid chromatography
HMTD	Hexamethylene triperoxide diamine
IC	Internal conversion
ICT	Internal charge transfer
IR	Infrared
IMS	Ion-mobility spectrometry
KHz	Kilo hertz
LUMO	Lowest unoccupied molecular orbital
LDMS	Laser desorption mass spectrometry
LCMS	Liquid chromatography mass spectrometry
m	Multiplet
m	Meta
m/z	Mass/charge
min	Minute (s)
MHz	Mega hertz
M	Molar
MO	Molecular orbital
naph	Naphthalene
NATO	North Atlantic Treaty Organization
NMR	Nuclear magnetic resonance
NICS	Nucleus independent chemical shifts
NB	Nitrobenzene
NM	Nitromethane

nm	nanometer
NOESY	Nuclear Overhauser effect spectroscopy
NLO	Nonlinear optical
NIR	Near infra-red
$Ni(acac)_2$	Nickel(II)acetylacetonate
o	Ortho
ORTEP	Oak Ridge Thermal Ellipsoid Program
OPA	Optical parametric amplifier
ORMOSIL	Organically modified silica
p	Para
PA	Picric acid
PDT	Photo dynamic therapy
$Pd(OAc)_2$	Palladium(II)acetate
$Pd(PPh_3)_2Cl_2$	Bis(triphenylphosphine)palladium(II)chloride
Pd/C	Palladium(0) on activated charcoal
ps	Pico second
^{i}Pr	*iso*-Propyl
^{n}Pr	*n*-Propyl
Py	Pyridine
PETN	Pentaerythritol tetranitrate
q	Quatret
quin	Quintet (pentet)
RDX	1,3,5-Trinitro-1,3,5-triazacyclohexane
s	Singlet or second
sex	Sextet
sep	Septet
sec	Second
SCE	Saturated Calomel Electrode
SV	Stern-Volmer
SOMO	Singly occupied molecular orbital
TATP	Triacetone triperoxide

TBAF	Tetrabutylammonium fluoride
TBACl	Tetrabutylammonium chloride
TBABr	Tetrabuylammonium bromide
$TBAPF_6$	Tetrabutylammonium hexafluorophosphate
TPA	Two photon absorption
TEMPO	2,2,6,6-Tetramethylpiperidinyloxy
TNT	2,4,6-trinitrotoluene
TNB	2,4,6-trinitrobenzene
Tetryl	2,4,6-Trinitrophenylmethylnitramine
TFA	Trifluoroacetic acid
THF	Tetrahydrofuran
TLC	Thin layer chromatography
TMS	Tetramethylsilane
TCSPC	Time correlated single-photon counting
t	Triplet
p-TsOH	para-Toluene sulfonic acid
TEA	Triethylamine
UV-Vis	Ultraviolet-Visible
VP	Vapor pressure
WLC	White light continuum
XRD	X-Ray diffraction

CHAPTER 1

Introduction

1.1 History of porphyrin

The name "porphyrin" emanates from the Greek word *porphyros* (πορφύρα) meaning purple. The history of porphyrin consists of two aspects, one is biological-geological at least 2.3 billion year old during evolution of life and another is chemical-medical which began at early 1840 by treatment of powdered and dried blood with conc. H_2SO_4 and washed the precipitate to free iron, but their procedure was inaccurate.[1] In this way they have synthesized (Berzelius, 1840, Scherer, 1841; Mulder, 1844) iron free hematin which showed red coloration in water solution. Thus, they have proved red coloration of blood was not due to iron.[2] Later, in 1867, Thudichum purified iron free hematin, called cruentine, which has bright red fluorescence and crystallized it, however his pioneering work remains neglected.[2] Hoppe-Seyler (1879) studied chlorophyll derived porphyrin, phylloporphyrin, which is structurally similar to hematin and has red fluorescence.[3] Thus he indirectly introduced the name "porphyrin" with prefix "haemato" and "phyllo".[1] In 1883, Soret discovered sharp absorption band of hemoglobin around near UV-region, subsequently referred as Soret band.[1] The clinical porphyrin studies were introduced by Schultz (1874) with the discovery of congenital porphyria, a genetic disorder caused by deposition of porphyrin in bone, and teeth, and further, its excretion through urine makes the latter wine red in color.[1] In 1880, McMunn has discovered a dark pigment called "urohaematin" in urine of a patient, who had been administered with sodium salicylate and later discovered cytochromes (myohematin) in 1884. Stockvis (1889) first discovered sulphonal induced acute porphyria and studied urinary pigment as it is closely related to, but different from hematin.[1] Probably, patients with acute porphyria might have inspired the epic story of "vampire and werewolf" in Hollywood because of their swollen face, hands and madness in behavior caused by phototoxicity. The madness of King George III was also probably caused by acute case of porphyria. Later, Günther clinically divided the type of porphyria, helping to resolve some of the misunderstanding in 1911. In 1912, Küster first proposed the correct structure of porphyrin, but it was not accepted at that time.[3] Mayer-Betz (1913) discovered the phototoxicity of hematoporphyrin by injecting himself, with hematoporphyrin causing porphyria like symptoms, which prevailed for few months.[3] Further, work related to chlorophyll by Willstätter, fetch him Nobel Prize in 1915.[3] Milroy first reported the general synthesis of porphyrin.[4] A new era of porphyrin research was initiated through the study of a famous patient Mathias Petry, whose urine was highly concentrated with uroporphyrin.[2] Later, work on Mathias Petry by Fischer led him to de novo synthesis of chlorohemin, which proved the

structure of porphyrin, first proposed by Küster earlier, honored him with Nobel Prize in 1930 and with it began the new era of synthetic porphyrin chemistry.[5]

1.2 Porphyrin-the pigment of life

It is believed that without porphyrin life in earth is not viable. If we go back to 2.3 billion year ago in the Archean eon era the life on earth was dominated by bacteria and archaea in atmosphere devoid of oxygen. The evolution of photosynthetic cyanobacteria (Figure 1.1) changed the earth and its atmosphere forever.[6] The process involves the conversion of water

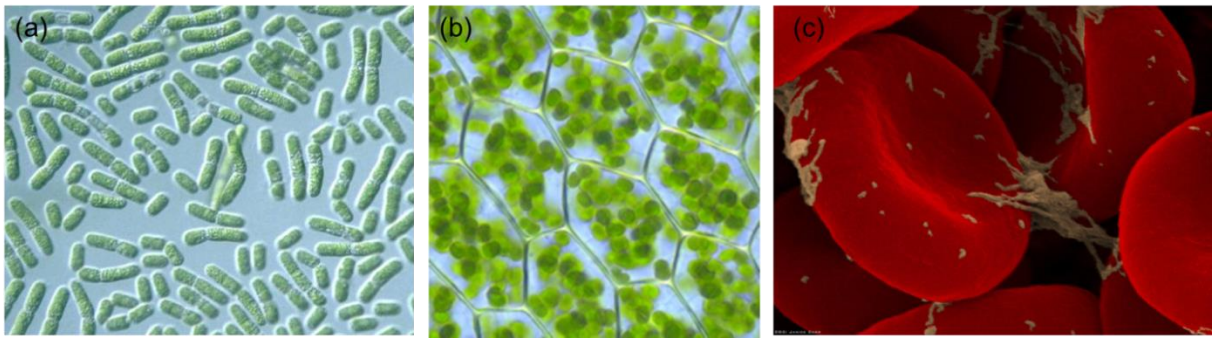

Figure 1.1 (a) Cyanobacteria (b) chloroplast in leaf and (c) red blood cells.

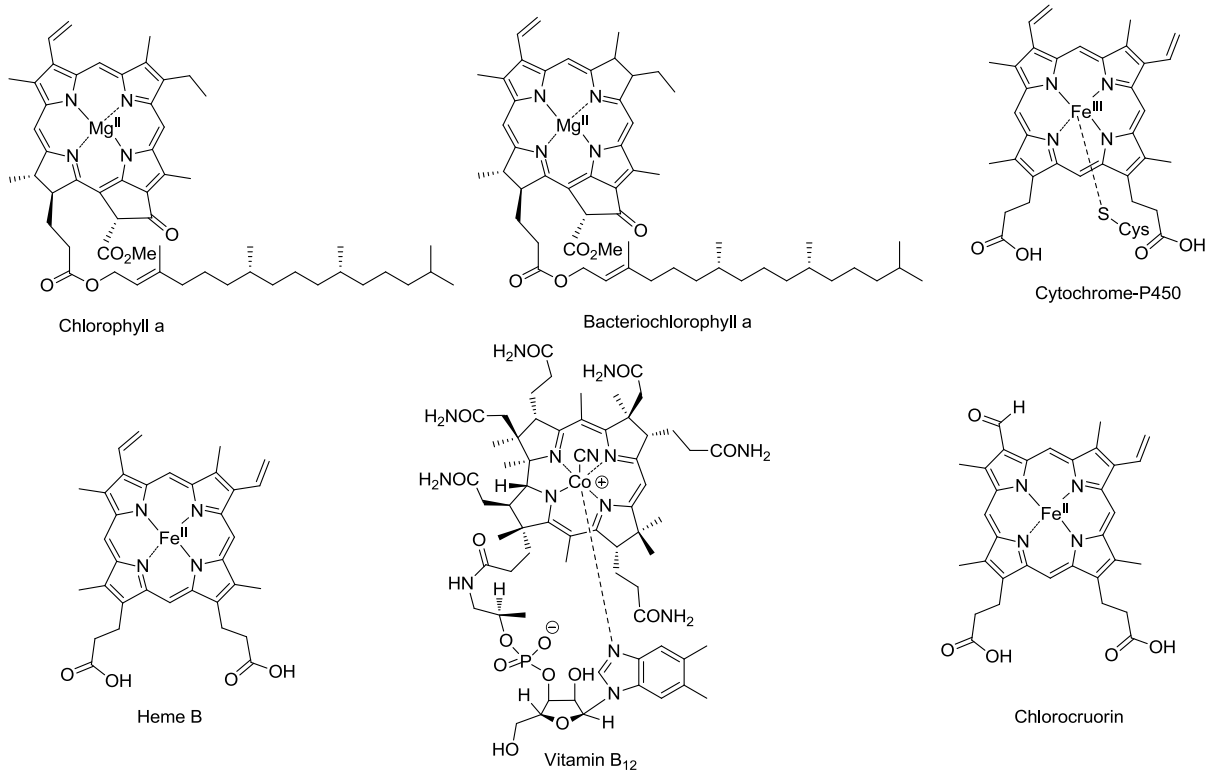

Figure 1.2 Some of the naturally occurring porphyrinoids of biological importance.

to molecular oxygen led to change reduced atmosphere to oxidisable environment and this event is known as “the great oxygenation event”. After that the event of life changed in earth

with evolution of eukaryotic organisms of diverse flora and fauna. Since then, porphyrin containing proteins play major roles from energy harvesting from light to reduce it to energy. For example, chlorophyll (Figure 1.2) in plant converts light energy to chemical energy with production of life saving oxygen. It is this oxygen, an outcome of photosynthesis, which is transported by heme containing protein like hemoglobin (Figure 1.2) and stored in cell by another heme protein, namely myoglobin and oxidised by yet another heme protein, cytochrome (Figure 1.2) to produce energy essential for life. Further, many biologically important catalytic oxidative processes involve heme containing proteins viz. catalase, peroxidase and transferrin. Also, Vitamin B_{12} (Figure 1.2) plays an important role in normal functioning of brain, nervous system and formation of blood. This ubiquity of action, reinforced by their visually appealing colors, has led Battersby to call the porphyrin and other tetrapyrrolic macrocycles as the "pigment of life".[7]

1.3 Scope of the Field

Porphyrins are a class of biologically important compounds consisting of 18π-aromatic macrocyclic systems, which resembles to [18]annulene. Further, these macrocyles exhibit rich photophysical properties and coordination chemistry, and the latter attribute is highlighted by their ability to form coordination complex with almost all metal ions, along with several non-metals and metalloids in the periodic table.[8] More importantly, porphyrin research no more limited to the fascination of synthetic organic chemists but have evolved further with wide interest of researchers cutting across several disciplines viz. biology, medicine, physics, engineering and theoretical studies. They have wide application in the field of material chemistry, opto-electronics, dye sensitized solar cells, catalysis, gas sensors, photo-inactivation of virus and bacteria, as photosensitizers for photodynamic therapy (PDT) of cancer, etc.[8] Though research on porphyrins initiated much earlier in 19th century but corresponding isomeric and expanded analogues started after 1960. Similar to porphyrin, isomeric porphyrins also exhibit interesting photophysical properties and coordination chemistry and hence, possess potential application in the above mentioned fields.[8] Expanded porphyrins display ability to bind with lager metal ions of lanthanide and actinide series. Also, expanded porphyrins possess red shifted absorption, and hence may find application towards deep penetrating PDT application. Interestingly, in their protonated forms, these macrocycles display strong affinity towards anions, an attribute not noticed in general for porphyrin.[9] Further, the expanded porphyrin with more than six pyrrole moieties in the

macrocycle, open up the field to study their aromaticity with practical examples, e.g. Hückel vs Möbius aromaticity.[9]

1.4 Nomenclature

Generally, in five member heterocyclic ring (e.g. pyrrole **1.1**, furan and thiophene) 2,5-positions are called α-position and 3,4-positions are called β-position. Similar nomenclature is used when these heterocycles are incorporated into macrocycles, though this convention is less traditional.[10] In macrocycles, "*meso*" or *meso* like term are used in general for bridging atom that separates two heterocyclic components. Due to complexity in applying IUPAC

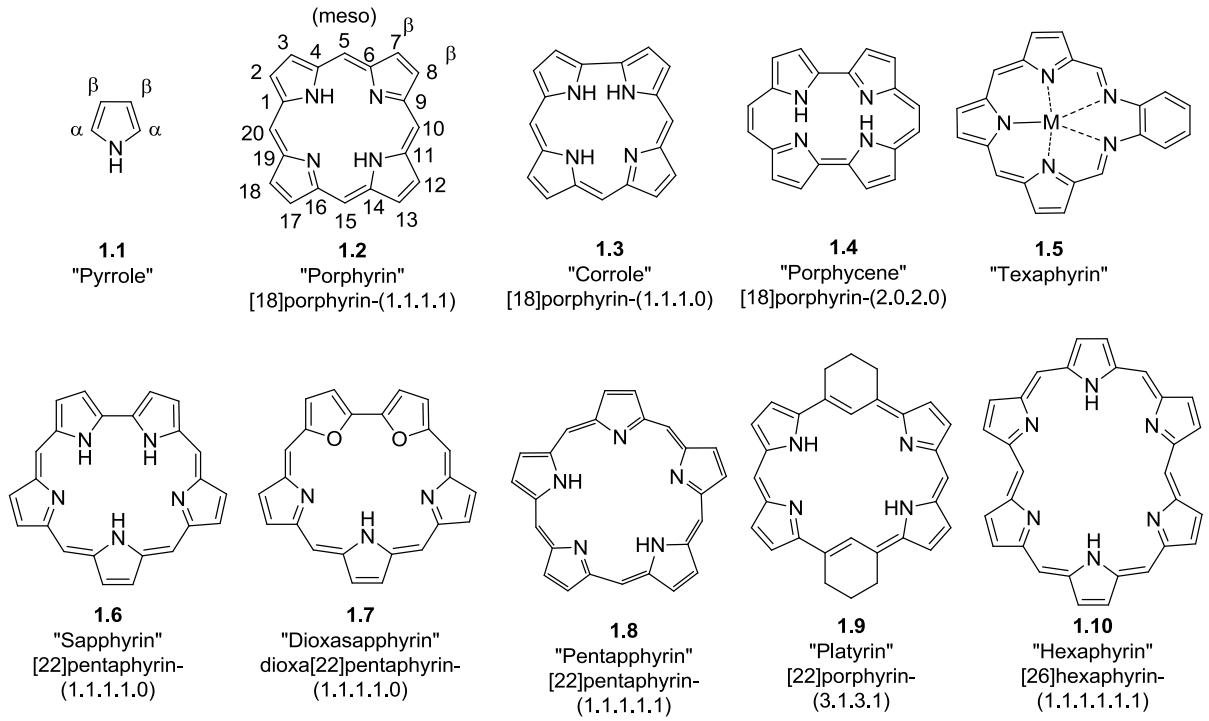

Figure 1.3 Nomenclature of some macrocycles by Franck's systematic approach.

nomenclature, many macrocycles are popularized by trivial names given by their original creators. These trivial names are generally based on either structural feature or color of the macrocycle, and ended with suffix "phyrin" or "rin" derived from porphyrin. This trend first initiated by R. B. Woodward with trivial name "sapphyrin" **1.6** for a pentapyrrolic macrocycle due to deep blue sapphire color in solid state,[11] followed by J. L. Sessler with trivial name "rubyrin" a hexapyrrolic macrocycle resembling its color to ruby.[12] Similarly, the trivial name texaphyrin **1.5** originated from Texas like shape of the macrocycle,[13] whereas, hexaphyrin **1.10** and heptaphyrin originated from number of pyrrole units present.[14] Further, LeGoff referred his vinylogous porphyrin with trivial name platyrin **1.9** originated

from Greek word "platys" means "wide".[15] But in modern context Franck's systematic approach is widely accepted for nomenclature of macrocycles.[16] According to this nomenclature porphyrin **1.2** would be termed as [18]porphyrin-(1.1.1.1) indicating a 18π-electronic system where each pyrrole unit connected through single sp^2-hybridised centers. Similarly, the porphyrin isomer porphycene **1.4** would be termed as [18]porphyrin-(2.0.2.0) and corrole **1.3** as [18]porphyrin-(1.1.1.0). Further, expanded porphyrin, sapphyrin **1.6** is named [22]pentaphyrin-(1.1.1.1.0) and similarly, rubyrin is [26]hexaphyrin-(1.1.0.1.1.0). If macrocycle contains heterocycles other than pyrrole, i.e. dioxasapphyrin **1.7** would be dioxa-[22]pentaphyrin-(1.1.1.1.0).

1.5 Contracted and isomeric porphyrins

First example of contracted porphyrin, corrole **1.3** was introduced by Johnson and coworkers during the synthesis of Vitamin B_{12}.[17] Similar to porphyrin; corrole is an 18π-aromatic macrocycle, however acts as a trianionic ligand and has its ability to stabilized metal ions in higher oxidation state. But in contrast to porphyrin, corrole is more acidic and can form stable anions with aqueous alkali.[8,10,18] However, the chemistry of corrole remained less developed

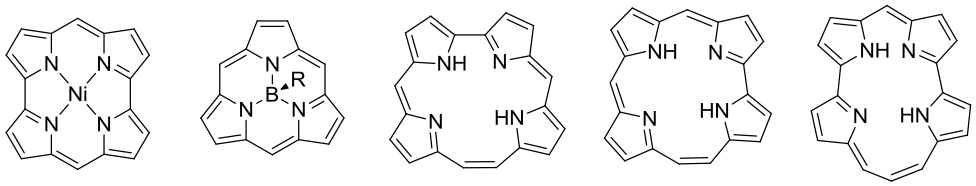

Figure 1.4 Contracted and isomeric porphyrins.

due to difficulties associated with its synthesis. Recently, Zeev Gross and coworkers (1999) reported the one pot facile synthesis of meso-triarylcorrole, triggering interest in its application in various fields like catalysis, sensor, dye sensitized solar cell, water splitting cell and biomedical application like PDT.[19] Also, very recently Shinokubo and coworkers introduced Ni(II) complex of 16 π-electronic anti-aromatic contracted porphyrin, Ni(II)-norcorrole **1.11**, which acts as electroactive species with stable performance in rechargeable battery.[20] One of the noteworthy new introductions in true contracted porphyrin family, subporphyrin **1.12**, first introduced by Osuka and coworkers, is a 14π-aromatic tripyrrolic macrocycle, which may find wide application in various fields similar to porphyrin.[21] However, these subporphyrins consist of central boron atom, which is used as template

during synthesis, and synthesis of boron-free freebase subporphyrin still remains a challenge to porphyrin chemists.

Though first example of contracted porphyrin was reported much earlier, but first example of isomeric porphyrin, i.e. porphycene **1.4** reported by annulene chemist, Vogel and coworkers in 1986 by reshuffling meso methine carbons.[22] Subsequently, almost after eight years, Vogel and Sessler independently reported three new porphyrin isomers; corrphycene (**1.13**),[23] hemiporphycene **1.14**[24] and isoporphycene **1.15**,[25] however these macrocycles didn't receive wider attention because of associated synthetic difficulties. Porphycene being the most stable porphyrin isomer, hence attracted considerable attention.[26] Further details regarding porphycenes are discussed in chapter 5 of this thesis.

1.6 Expanded porphyrins

Expanded porphyrins can be generate by two ways, first by increasing the number of bridging atoms by keeping four pyrrole units constant and second by introducing extra heterocycles and/or simultaneous addition of bridging atom(s) and heterocyclic rings onto the porphyrin moiety.[9a] Sessler defined expanded porphyrin as any macrocycle that contains pyrrole, furan, thiophene, or other heterocyclic subunits linked together either directly or through one or more spacer atoms in such a manner that the internal ring pathway contains at least 17 atoms.[9b] Compare to isomeric and contracted porphyrins, expanded porphyrin field is more diverse and hence, very difficult to highlight their all aspects in this overview. After all, expanded porphyrin field was initiated by serendipitous synthesis of sapphyrin **1.6** by R. B. Woodward during synthesis of vitamin B_{12}, which he highlighted in aromaticity symposium in Sheffield in 1966.[27] However, Johnson first reported the synthesis of sapphyrin as its dioxa analogue[28] and Woodward's all aza sapphyrin was later reported by Dolphin in 1983.[11] Though initially it was anticipated that its larger core can help bind with larger metal ions in higher oxidation state, but its failure to do so led to dwindling interest towards this macrocycle. However, it gained much interest when Sessler and coworkers discovered its anion binding ability, both in solution and solid states, in its diprotonated state.[29] Additional details about sapphyrins are discussed in chapter 8 of this thesis.

First synthesis of 22 π-electronic vinylogous porphyrin called platyrin **1.9** was reported by Berger and LeGoff in 1978, but its metallated derivatives proved to be very insoluble and rather unstable.[15] Later, Franck and coworkers reported the synthesis of vinylogous porphyrins by acid catalysed condensation approaches. Notably, N,N′,N″,N‴- tetramethyl

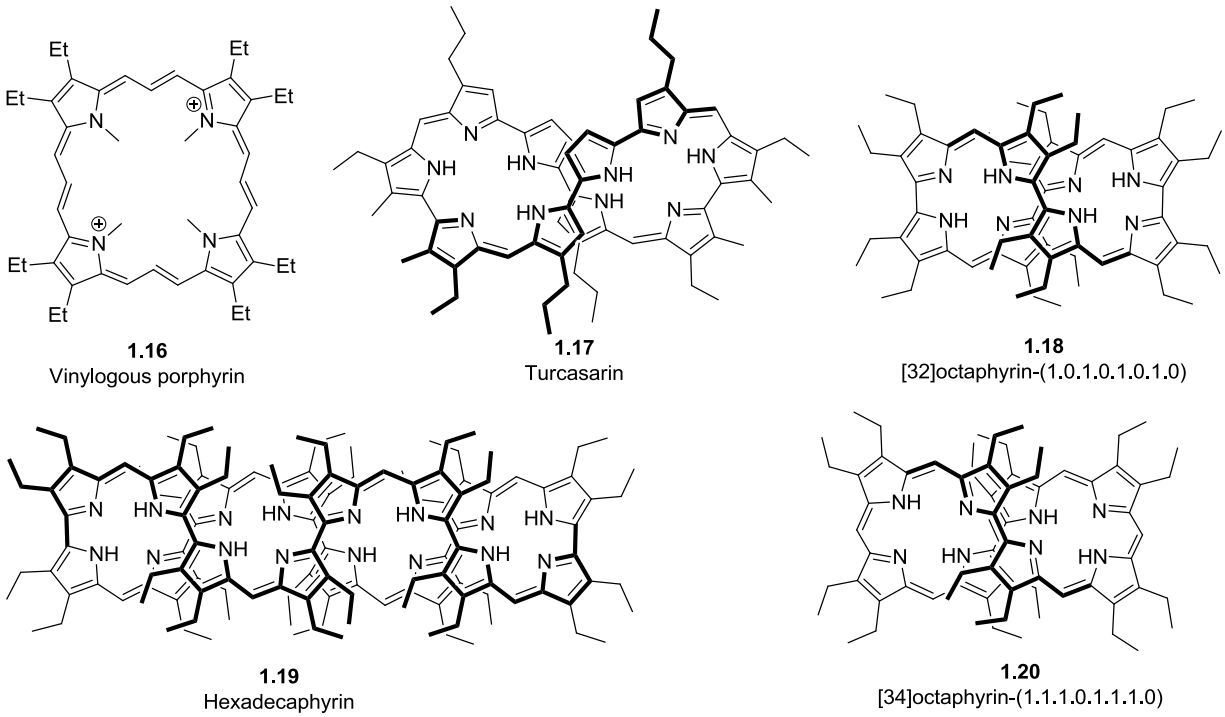

Figure 1.5 Few important examples of expanded porphyrins.

[26]porphyrin-(3.3.3.3) **1.16** and its tetraoxa analogue show record molar extinction coefficient (λ_{max} = 528 nm, ε = 1-1.6 × 10^6 $M^{-1}cm^{-1}$).[30] Soon after the synthesis of porphycene, Vogel and coworker reported expanded porphycene analogues by inclusion of additional acetylene bridges between α,α′-fused pyrrole positions of porphycene, called expanded porphycene or stretched porphycene.[31] Later they also reported the furan derived expanded analogues. Details about stretched porphycene and its corresponding analogues are discussed in chapter 7 of this thesis.

Eventually, Sessler and coworker introduced Schiff base derived expanded porphyrin analogue called texaphyrins **1.5**, which displayed an ability to complex with lanthanides.[13] Notably, water soluble Gd(III)-complex of texaphyrins known as motexaphin gadolinium (MGd) is a promising anticancer agent that allows clear MRI contrast. Also, they have widely studied other Schiff base derived expanded porphyrins for applications like anion sensor and liquid crystallinity.[32]

Another serendipitous addition by Sessler and coworker during synthesis of pentapyrrolic macrocycle, changed importance of expanded porphyrin, with discovery of turcasarin **1.17**, first expanded porphyrin to display figure-eight configuration both in solution and solid state.[33] Turcasarin is a decapyrrolic 40π-nonaromatic macrocycle existing in two inter-

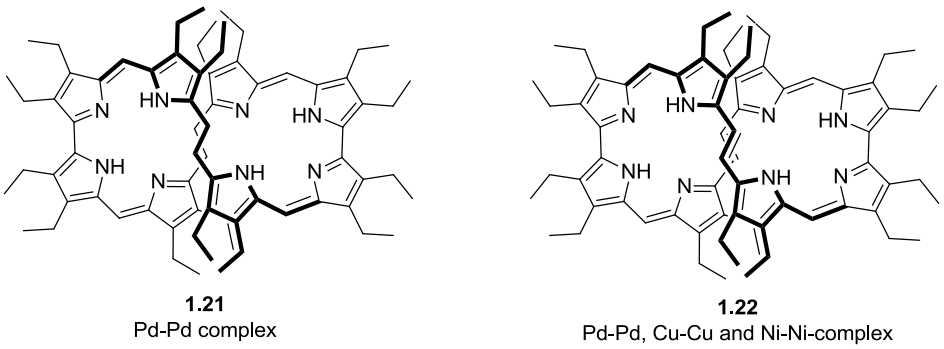

Figure 1.6 Figure-eight motif of octaphyrins.

convertible limiting helical conformations. Subsequently, Vogel and coworkers reported first octapyrrolic expanded porphyrin, [32]octaphyrin-(1.0.1.0.1.0.1.0) **1.18**, also adopted a chiral figure-eight configuration.[34] These reports attracted the attention of researcher towards synthesis of figure-eight motifs, which probably adopted by the macrocycles owing to conformational flexibility and effective nonbonding interaction. Interestingly, figure-eight motif in expanded porphyrin introduced the concept of supramolecular chirality and probably arises from their conformational flexibility. Further, Vogel and coworkers (1999) succeed in separation of β-alkyl substituted octaphyrins and its bis Pd(II) complexes (**1.21**-**22**) to their corresponding enantiomers.[35] Setsune and coworker made a notable contribution by synthesizing expanded porphyrin containing 24 pyrrole units and able to characterise [64]hexadecaphyrin-(1.0.1.0.1.0.1.0.1.0.1.0.1.0.1.0) **1.19** by X-ray diffraction, which still remains the largest structurally characterized expanded porphyrin.[36a-b] Recently, Setsune and coworker used cyclooctapyrroles, towards direct determination of absolute configuration of chiral carboxylic acids[36c] and very recently, employed them as chiro-optical sensing of oligonucleotides, which provides strong CD response with high thymine containing nucleotides.[36d]

Recently, expanded porphyrin provided effective platform to recognized Möbius aromatic system.[9d] Möbius aromaticity is a concept that predicts aromatic character in 4nπ cyclic conjugation with a singly twisted Möbius topology.[37] This concept was first introduced by Heilbronnerin in 1964 and by Zimmermann in 1966, and is fascinating for both synthetic chemists and theoretical researchers.[38] However, it is not easy to merge two conflicting structural elements i.e. the fully conjugated macrocyclic network and twisted π-system topology in a single molecule. Despite these difficulties, Herges and coworkers reported a [16]annulene that has twisted Möbius topology and moderate aromatic character.[38d] In general, aromaticity of macrocycle is very sensitive to ^{1}H NMR chemical shift and calculated

nucleus independent chemical shifts (NICS) (Figure 1.7).[39] The ^{1}H NMR chemical shifts of peripheral β-protons are diagnostic to aromaticity. Hückel aromatic and antiaromatic species exhibits diatropic and paratropic ring current respectively and similar type of ring current also observed for Möbius aromatic and antiaromatic systems. Further there is a detectable difference in photophysical properties of aromatic and antiaromatic compounds studied in details by Kim and coworkers (Figure 1.7).[9d] Generally, common aromatic expanded porphyrin consists of a sharp soret like absorption band as well as distinct low energy Q-type bands, a weak but detectable fluorescence, relatively long excited state lifetime and large two-photon absorption (TPA) cross section. In contrast, a broad and ill-defined absorption spectrum without Q-type band, no fluorescence, very short excited state lifetime and small TPA cross section value are the characteristics of antiaromatic compounds.

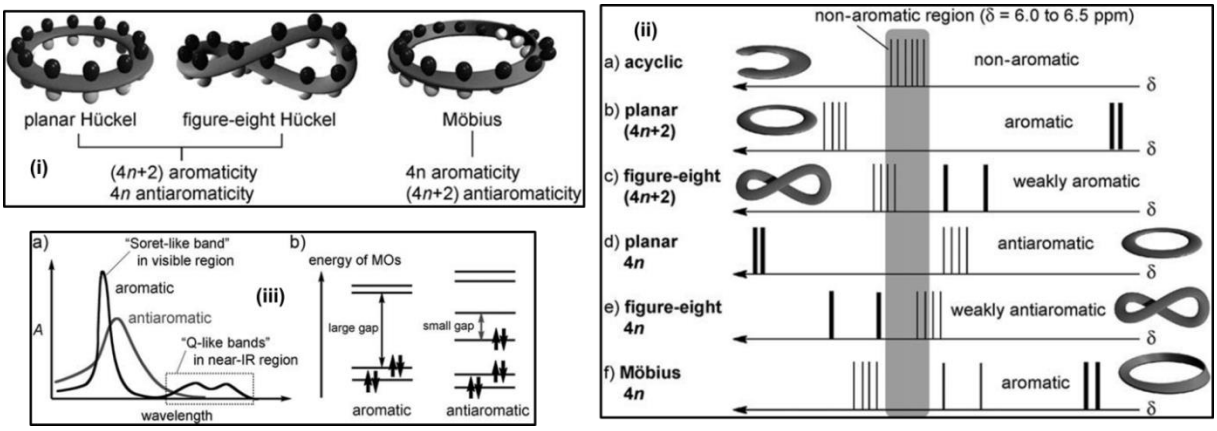

Figure 1.7 (i) Schematic representation of topology of π-conjugated systems; (ii) Typical ^{1}H NMR spectra of a) acyclic π-conjugated oligopyrrole and b-f) expanded porphyrins (each topology and number of π electron are shown). A normal line indicates the signals of the outer pyrrolic β protons and bold line indicates those of inner protons. (iii) Typical UV-Vis-NIR absorption spectra and molecular orbital diagrams of aromatic/antiaromatic expanded porphyrins.

Subsequent to Herges work, Latos-Grażyński and coworker reported first dynamic Hückel-Möbius expanded porphyrin system, di-*p*-benzi[28]hexaphyrin that undergoes solvent and temperature dependent conformational change between Hückel and Möbius topology.[40] Subsequently, Osuka and coworkers reported first stable Möbius aromatic system, bispalladium complex of [36]octaphyrin(1.1.1.1.1.1.1.1) **1.23** and also his group found that many of their previously reported metal complexes of hexaphyrin consist of Möbius topology.[41] Again, Latos-Grażyński and coworkers reported a rare Möbius antiaromatic compound, i.e. a cationic 18π-Pd(II)vacataporphyrin, exhibiting a weak paratropic ring

current.[42] Further, first structurally characterized Möbius antiaromatic compound was reported by Osuka and coworkers for a bisphosphorus[30]hexaphyrin **1.24**.[43]

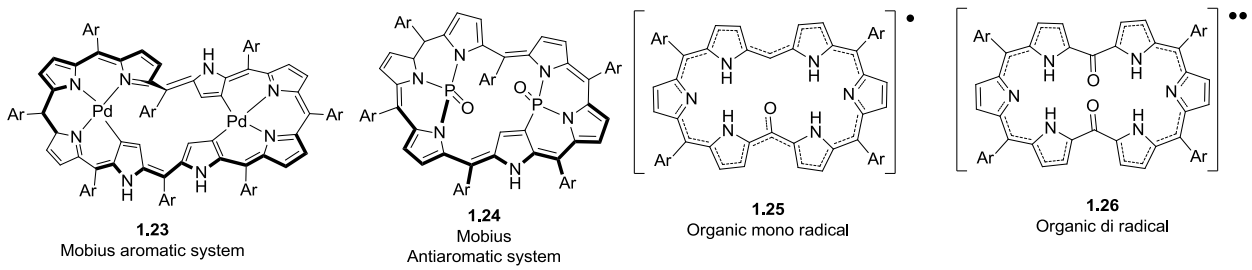

Figure 1.8 Recent examples of some important expanded porphyrins.

An important recent addition by Osuka and coworkers, is the isolation of stable organic radicals derived from expanded porphyrin. The oxygenated product of 5,20-*meso*-free hexaphyrin assigned as first stable (ambient condition) monoradical expanded porphyrinoid **1.25**[44] and subsequently, they have also isolated stable biradicals **1.26**[45] from meso-dioxygenated hexaphyrin, which exhibits characteristic unassignable broad NMR spectrum, ESR activity, magnetic susceptibility in solid state and a broad low energy band in absorption spectrum.

One of most remarkable addition to expanded porphyrin family was the synthesis of cyclo[8]pyrrole or [30]octaphyrin-(0.0.0.0.0.0.0.0) **1.27**, where all pyrrole α-positions are directly linked and have strong absorption in NIR region (~1100 nm), making it a promising material for optical storage and signalling device.[46] Also, it can extract sulphate ion from aqueous media[47] and in presence of electron deficient compound can form discotic liquid crystals.[48] Further, recent development on the synthesis of π-extended cyclo[8]pyrrole resulted further red shifted low energy band in UV-Vis-NIR spectra.[49] Remarkably, acenapthene fused pyrrole derived cyclo[8]pyrrole reported by Okujima and coworkers exhibits intense NIR band at 1482 nm.[50]

Another significant contribution is from Chandrasekhar and coworkers via the development of five member heterocycle derived (except N) expanded porphyrins, exhibiting unusual structural and photophysical properties.[51] In contrast to octaphyrin-(1.0.1.0.1.0.1.0), which exists in figure-eight conformation and nonaromatic, core modified [34]octaphyrin **1.28** reported by Chandrasekhar and coworkers, exhibits planar core and aromatic character.[51c] Also, they have reported core modified 42π-aromatic conjugated dodecaphyrin, which exhibits record TPA cross section (108000 GM).[52] Introduction of first stable smaragdyrin

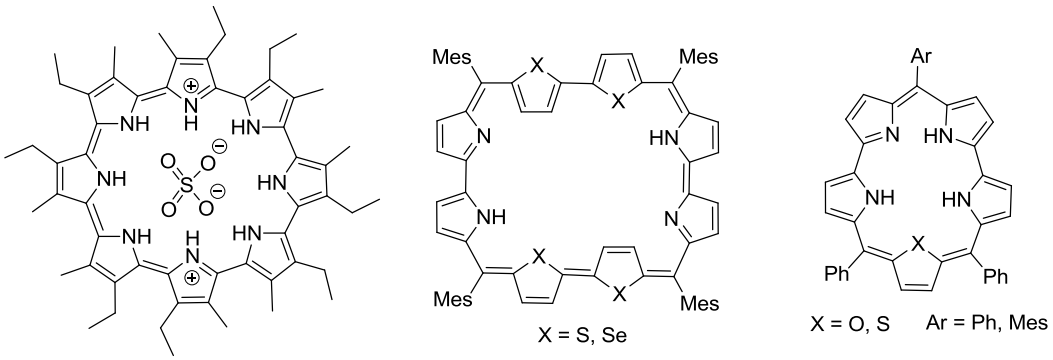

1.27
Cyclo[8]pyrrole

1.28
Hetero atom substituted octaphyrin

1.29
Stable smaragdyrins

Figure 1.9 Cyclo[8]pyrrole and some core modified expanded porphyrins.

1.29, a conjugated 22π-aromatic pentapyrrolic macrocycle was another important contribution form Chandrasekhar and coworkers.[53] Further, Ravikanth and coworker recently introduced boron complex of smaragdyrins, which act as fluorescent anion sensors.[54] They have also developed a series of porphyrin-smaragdyrin dyads and BODIPY-porphyrin-smaragdyrin triads, which act as efficient energy transfer device and hence can act as multi-chromophoric system for material application.[54e]

1.7 π-extended porphyrinoids

The π-extended porphyrinoids have low HOMO-LUMO energy gap, owing to their extended π-conjugation, and hence led to bathochromically shifted absorption spectra.[55] Recently, it received wider attention due to its potential application in various fields such as near infrared (NIR) dye stuffs, optical materials, nonlinear optics, organic semiconductors, photosensitizers for photodynamic therapy (PDT), and dye-sensitized solar cells.[56] The π-extension can be achieved either by oxidative coupling of periphery of macrocycle or by using annulated pyrrolic precursors. Though, the synthesis of π-extended porphyrins initiated much earlier, but π-extended isomeric and expanded porphyrins are still in their infancy stage. As it is impossible to cover details about π-extended porphyrinoids, we will discuss about few important landmarks in this field. For example, Anderson and coworker, reported a novel tetraaanthrcenyl fused porphyrin **1.30** by oxidative coupling of meso-tetraanthrylporphyrin, which displays exceptionally low HOMO-LUMO band gap, with lowest energy band at 1417 nm in absorption spectrum.[57] The anthracene fused porphyrin **1.31** was reported by Ono and coworkers possesses strong absorption in NIR region.[58] Further, Osuka and coworkers extended this strategy to expanded porphyrins via synthesis of bisanthracene-fused hexaphyrins **1.32**[59] and bisporphyrin-fused hexaphyrins **1.33**,[60] which exhibit Q-type band

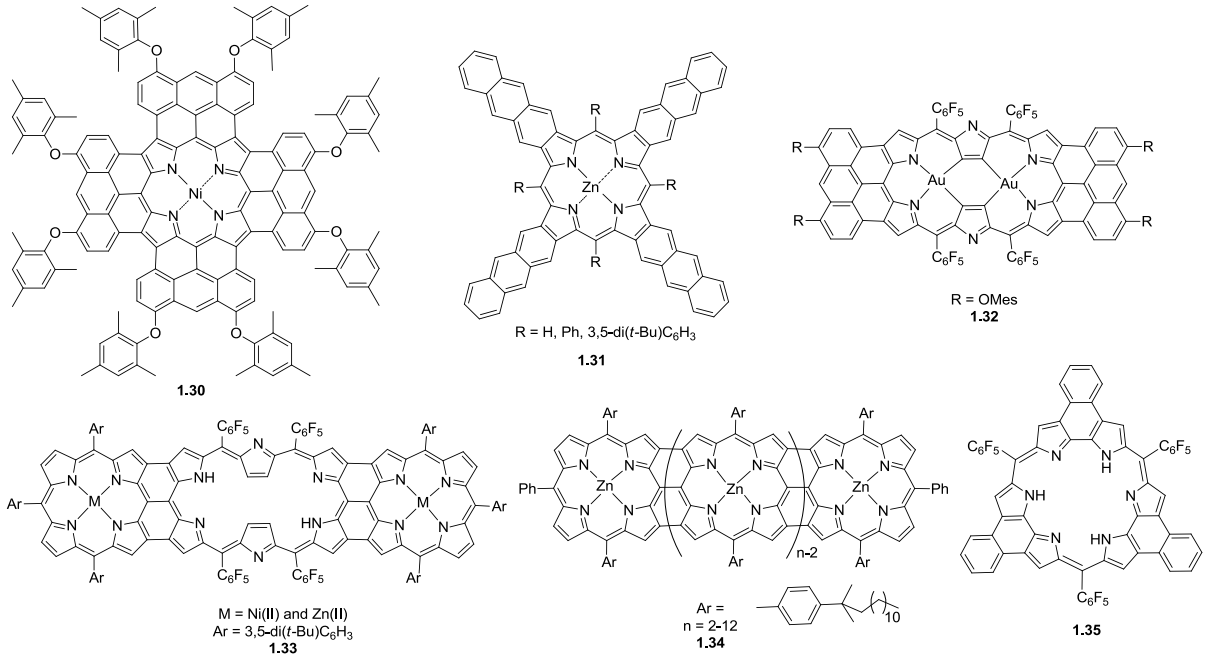

Figure 1.10 Some remarkable examples of π-extended porphyrinoids.

maxima at 1467 and 1912 nm respectively, further lowering the HOMO-LUMO band gap. Most remarkably, Osuka and coworker reported covalently triply fused Zn(II)-porphyrin oligomers (n = 2-12) **1.34** whose absorption reached to IR region and exhibits strong TPA cross section.[61] Similarly, Sessler and coworkers introduced naphthobipyrrole derived first planar antiaromatic rosarin **1.35**, which undergoes reversible proton coupled reduction to 26-π aromatic system via 25-π dicationic radical species.[62]

1.8 β-substituted porphyrinoids

All naturally occurring porphyrinoids consist of β-substituted analogues.[8] Therefore, initial research was primarily engrossed on β-substituted porphyrins. The close resemblance of β-substituted porphyrinoids with naturally occurring porphyrinoids make them comparatively better promising material towards application like light harvesting antenna, photosensitizers for photodynamic treatment of cancer.[8] Also, compared to *meso*-substituted porphyrinoids, properties of β-substituted analogues are much sensitive to the type of substituents present at their periphery. Therefore, β-substituents while retaining the basic properties of macrocycles, however help in effectively tuning the photophysical properties and also can enhance their solubility in organic solvents; thereby making them most studied, compared to their basic macrocyclic units. For example, due to poor solubility of basic porphine and porphycene, their β-alkyl analogues are studied in much detail. Again, β-substituted porphyrinoids are excellent test bed to check reactivity of *meso* positions and some substituents can act as

excellent leaving group, allowing further transformation at their periphery. In spite of these advantages, still synthesis of β-substituted porphyrinoids is highly challenging, either due to difficulty associated with the synthesis of substituted pyrroles, or varied reactivity of these substituted pyrroles. As our primary focus is on β-substituted porphyrinoids, therefore we have discussed in details about substituent effect on various porphyrinoids (porphyrin and its isomeric and expanded analogues) in corresponding chapters.

1.8.1 β-alkoxysubstituted porphyrinoids

The methoxy group in β-position of pyrrole moiety acts as electron donor, making porphyrinoids electron rich in nature. Also, methoxy group can enhance the hydrophilicity and help further derivatize upon deprotection, thereby enhancing its importance in biomedical application. In this context, it is worth mentioning about a family of naturally occurring

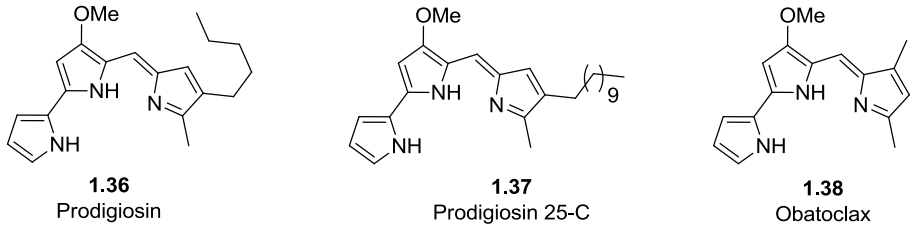

1.36 Prodigiosin **1.37** Prodigiosin 25-C **1.38** Obatoclax

Figure 1.11 Some novel naturally occurring and artificial Prodigiosins.

tripyrrolic moieties, which contain a common 4-methoxy, 2,2′-bipyrrole ring system, known as prodigiosin. Prodigiosin **1.36**, an active red pigment, exhibits antimalarial, antibacterial and most importantly anticancer activity. It was first isolated from micro-organisms namely, *Serratia* and *Streptomyces* as secondary metabolite product.[63] Notably, prodigiosin 25-C **1.37** has been studied extensively for its promising immunosuppressive and anticancer activity.[64] Also, Obatoclax **1.38**, an abiotic prodigiosin, which acts as Bcl-2 (B-cell lymphoma 2), is undergoing Phase II clinical trial for treatment of lung cancer.[65]

The field of β-methoxysubstituted porphyrinoids was initiated by Merz and coworkers with the synthesis of 3,4-dimethoxypyrrole, which finds wide application as conducting polypyrroles, owing to its ability to electro-polymerize at low oxidation potential.[66] Though it got popularized in polymer chemistry, but finds little application in porphyrinoid chemistry, despite wide potentiality in various applications owing to its instability at ambient condition and highly reactive nature. In 1993, Merz and coworkers synthesized β-octametoxyporphyrin **1.39a**, possessing strongest diamagnetic ring current, where inner imino protons resonate at

highly shielded region (-4.41 ppm).[67] Subsequently, they generalised the synthesis of 3,4-dialkoxypyrrole and hence able to synthesize several β-octaalkoxy and β-octaalkoxy-*meso*-tetra-arylporphyrins (**1.39a-d** and **1.40a-g**).[68] Most prominently, widely accepted Cheng and LeGoff condensation and Lindsey method were found to be insufficient and resulted with

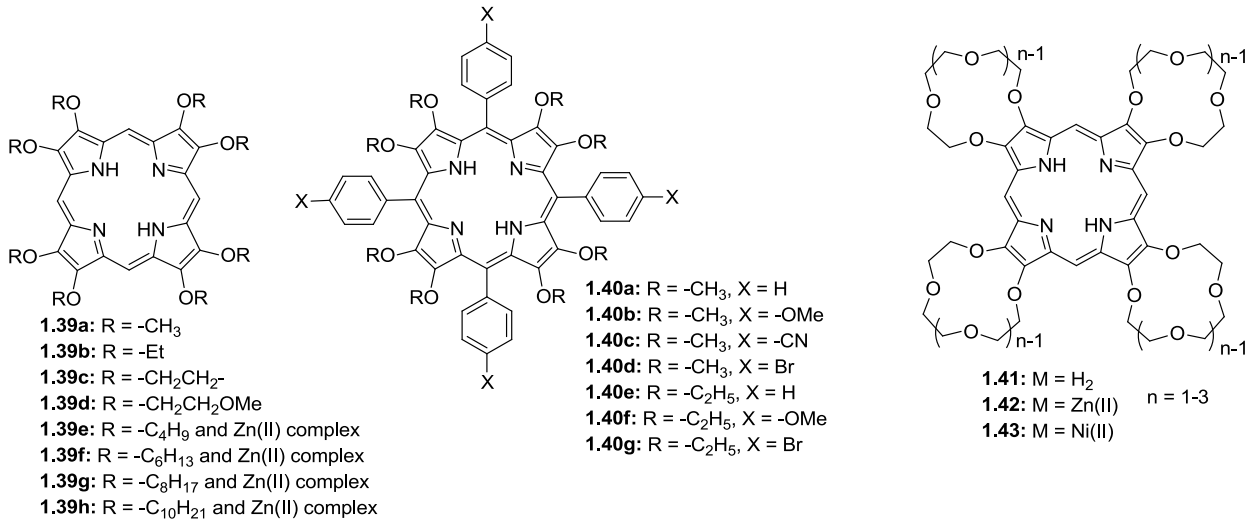

Figure 1.12 *Meso* and β-substituted octaalkoxyporphyrins and their M(II) complexes.

poor yield of porphyrins. The best result was obtained by following the protocol developed by Treibs and Häberle (AcOH/Pyridine and air). In 1996, Ono and coworkers reported the synthesis of several β-crown ether substituted porphyrins (**1.41-43**) and they have also reported β-alkoxyporphyrins (**1.39e-h**) with larger alkyl chain to explore their possible liquid crystalline properties.[69] Sessler and coworkers found that calix[4]pyrrole **1.44** synthesized from highly electron rich 3,4-methoxypyrrole binds selectively with fluoride ion and could prove useful as HPLC column media, due to its lower affinity and fast complexation and decomplexation rate.[70] Further, Merz and coworker developed facile multi-gram synthesis of 3,4-dialkoxypyrrole in four steps from commercially available 2,5-dimethoxy-2,5-dihydrofuran.[71] Chen and coworkers reported an electron rich metal-metal bonded octamethoxyporphyrin dimer $Rh_2(omp)_2$ (where omp; β-octamethoxyporphyrin), from the reaction of (omp)RhH with TEMPO and photolysis of (omp)RhR (R = Me, ^{i}Pr).[72] In 2001, Sessler and coworkers reported the synthesis of tetramethoxybipyrrole derived sapphyrin **1.47** by employing [3+1+1] condensation approach, which could be useful to synthesize sapphyrins, without synthesis of intermediate bipyrrole.[73] Again, Sessler and coworker reported Schiff base derived hydrazinophyrins (**1.45a-d**) and uranium alaskaphyrins (**1.46a-d**) from 3,4-dialkoxypyrrole, found to be liquid crystalline in nature forming columnar

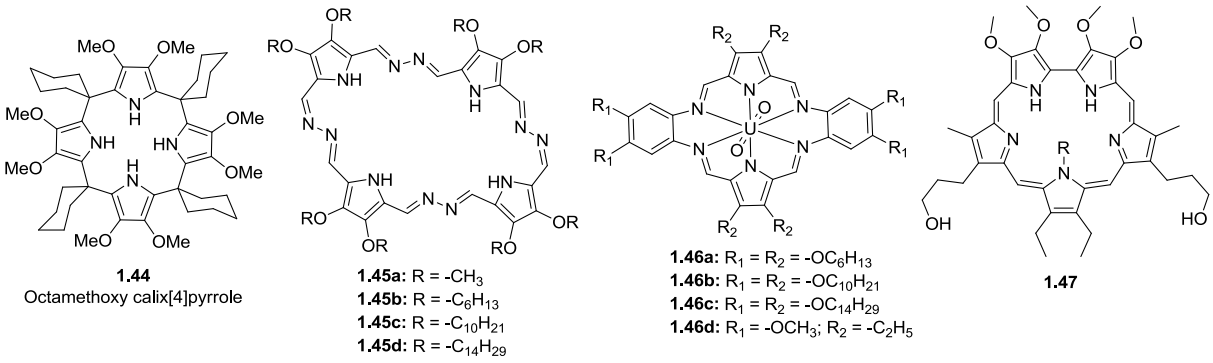

Figure 1.13 Some alkoxy substituted calixpyrrole, hydrazinophyrins, alaskaphyrins uranyl complex and sapphyrin.

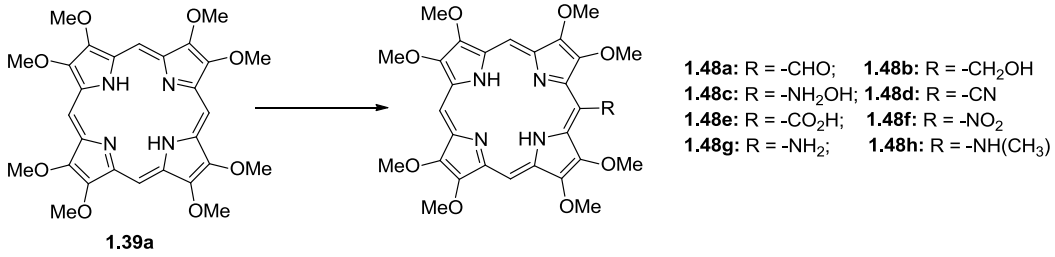

Figure 1.14 Synthesis of nona-substituted octamethoxyporphyrins.

mesophases.[74] In 2005, Krishnan and coworker able to functionalize β-octamethoxyporphyrin for the first time at its *meso*-position to form several nonasubstituted porphyrins (**1.48a-h**) effectively.[75] Therefore, we can conclude from the above developments that alkoxypyrrole derived macrocycles are mostly confined to porphyrin only, and majority of their aspects remains unexplored.

1.9 References

1. With, T. K. *Int. J. Biochem.* **1980**, *11*, 189.
2. Dolphin, D. *The Porphyrins, Structure and Synthesis Part A* **1978**, *1*, 29.
3. Warren, M. J.; Smith, A. G. *Tetrapyrroles: Birth, Life and Death* **2009**, 5.
4. Milroy, J. A. *Biochem. J.* **1918**, *12*, 318.
5. Fischer, H.; Zeile, K. *Justus Liebigs Ann. Chem*. **1929**, *468*, 98.
6. Olson, J. M. *Photosynth. Res*. **2006**, *88*, 109.
7. Battersby, A. R.; Fookes, C. J. R.; Matcham, G. W. J.; McDonald, E. *Nature* **1980**, *285*, 17.
8. (a) *The Porphyrin Handbook* (Eds.: K. M. Kadish; K. M. Smith; R. Guilard) Academic Press, San Diego, **2000**, *1-9*. (b) *Handbook of Porphyrin Science* (Eds.: K. M. Kadish; K. M. Smith; R. Guilard) World Scientific Publishing, Singapore, **2010**.

9. (a) The Porphyrin Handbook, **2000**, *2*, 55. (b) Sessler, J. L.; Seidel, D. *Angew. Chem. Int. Ed.* **2003**, *42*, 5134. (c) Saito, S.; Osuka, A. *Angew. Chem. Int. Ed.* **2011**, *50*, 4342. (d) Yoon, Z. S.; Osuka, A.; Kim, D. *Nat. Chem*. **2009**, *1*, 113.
10. Sessler, J. L.; Weghorn, S. J. *Expanded, Contracted & Isomeric Porphyrins* **1997**, 4.
11. Bauer, V. J.; Clive, D. L. J.; Dolphin, D.; Paine III, J. B. P.; Harris, F. L.; King, M. M.; Loder, J.; Wang, S-W. C.; Woodward, R. B. *J. Am. Chem. Soc.* **1983,** *105*, 6429.
12. Sessler, J. L.; Morishima, T.; Lynch, V. *Angew. Chem. Int. Ed. Engl.* **1991**, *30*, 977.
13. (a) Sessler, J. L.; Hemmi, G.; Mody, T.; Murai, T.; Burrell, A.; Young, S. W. *Acc. Chem. Res*. **1994**, *27*, 43. (b) Sessler, J. L.; Král, V.; Hoehner, M.; Chin, K. O. A.; Dávila, R. M. *Pure Appl. Chem*. **1996**, *68*, 1291.
14. Charriére, R.; Jenny, T. A.; Rexhausen, H.; Gossauer, A. *Heterocycles*, **1993**, *36*, 1561.
15. Berger, R. A.; LeGoff, E. *Tetrahedron Lett.* **1978**, *19*, 4225.
16. Gosmann, M.; Frack, B. *Angew. Chem. Int. Ed. Engl*. **1986**, *25*, 1100.
17. Johnson, A. W.; Kay, I. T. *Proc. Chem. Soc. London* **1964**, 89.
18. Jasat, A.; Dolphin, D. *Chem. Rev.* **1997**, *97*, 2267.
19. (a) Aviv, I.; Gross, Z. *Chem. Commun*. **2007,** 1987. (b) Aviv-Harel, I.; Gross, Z. *Chem. Eur. J.* **2009**, *15*, 8382. (c) Flamigni, L.; Gryko, D. T. *Chem. Soc. Rev*. **2009**, *38*, 1635. (d) Paolesse, R.; Jaquinod, L.; Nurco, D. J.; Mini, S.; Sagone, F.; Boschi, T.; Smith, K. M. *Chem. Commun*. **1999**,1307.
20. (a) Ito, T.; Hayashi, Y.; Shimizu, S.; Shin, J-Y.; Kobayashi, N.; Shinokubo, H. *Angew. Chem. Int. Ed*. **2012**, *51*, 8542. (b) Shin, J.-Y.; Yamada, T.; Yoshikawa, H.; Awaga, K.; Shinokubo, H. *Angew. Chem. Int. Ed*. **2014**, *53*, 3096.
21. (a) Inokuma, Y.; Kwon, J. H.; Ahn, T. K.; Yoo, M.-C.; Kim, D.; Osuka, A. *Angew. Chem. Int. Ed*. **2006**, *45*, 961. (b) Inokuma, Y.; Osuka, A. *Dalton Trans*. **2008**, 2517.
22. Vogel, E.; Kocher, M.; Schmickler, H.; Lex, J. *Angew. Chem. Int. Ed. Engl.* **1986**, *25*, 257.
23. (a) Sessler, J. L.; Brucker, E. A.; Weghorn, S. J.; Kister, M.; Schäfer, M.; Lex, J.; Vogel, E. *Angew. Chem. Int. Ed. Engl.* **1994**, *33*, 2308. (b) Aukauloo, M. A.; Guilard, R. *New. J. Chem*. **1994**, *18*, 1205.
24. (a) Callot, H. J.; Rohrer, A.; Tschamber, T. *New. J. Chem*. **1995**, *19*, 155. (b) Vogel, E.; Bröring, M.; Weghorn, S. J.; Scholz, P.; Deponte, R.; Lex, J.; Schmickler, H.; Schaffner, K.; Braslavsky, S. E.; Müller, M.; Pörting, S.; Sessler, J. L.; Fowler, C. J. *Angew. Chem. Int. Ed*. **1997**, *36*, 1651.

25. (a) Vogel, E. *J. Heterocyclic Chem*. **1996**, *33*, 1461. (b) Vogel, E.; Scholz, P.; Demuth, R.; Erben, C.; Bröring, M.; Schmickler, H.; Lex, J.; Hohlneicher, G.; Bremm, D.; Wu, Y.-D. *Angew. Chem. Int. Ed*. **1999**, *38*, 2919.
26. (a) Sánchez-García, D.; Sessler, J. L. *Chem. Soc. Rev.* **2008**, *37*, 215. (b) Stockert, J. C.; Cañete, M.; Juarranz, A.; Villanueva, A.; Horobin, R. W.; Borrell, J. I.; Teixidó, J.; Nonell, S. *Curr. Med. Chem.* **2007**, *14*, 997.
27. Woodward, R. B. *Aromaticity Conference, Sheffield, U.K.*, **1966**.
28. Broadhurst, M. J.; Grigg, R.; Johnson, A. W. *J. Chem. Soc. D, Chem. Commun.* **1969**, 1480.
29. (a) Sessler J. L.; Cry, M.; Lynch, V.; McGhee, E.; Ibers, J. A. *J. Am. Chem. Soc.* **1990**, *112*, 2810. (b) Shionoya, M.; Furuta, H.; Lynch, V.; Harriman, A.; Sessler, J. L. *J. Am. Chem. Soc.* **1992**, *114*, 5714.
30. (a) Gosmann, M.; Franck, B. *Angew. Chem. Int. Ed. Engl*. **1986**, *25*, 1100. (b) Knübel, G.; Franck, B. *Angew. Chem. Int. Ed. Engl.* **1988**, *27*, 1170. (c) Wessel, T.; Franck, B.; Möller, M.; Rodewald, U.; Läge, M. *Angew. Chem. Int. Ed. Engl.* **1993**, *32*, 1148. (d) Franck, B.; Nonn, A.; Fuchs, K.; Gosmann, M. *Liebigs Ann. Chem*. **1994**, 503.
31. (a) Jux, N.; Koch, P.; Schmickler, H.; Lex, J.; Vogel, E. *Angew. Chem. Int. Ed. Engl.* **1990**, *29*, 1385. (b) Vogel, E.; Jux, N.; Rodriguez-Val, E.; Lex, J.; Schmickler, H. *Angew. Chem. Int. Ed. Engl.* **1990**, *29*, 1387. (c) Mártire, D. O.; Jux, N.; Aramendía, P. F.; Negri, R. M.; Lex, J.; Braslavsky, S. E.; Schaffner, K.; Vogel, E. *J. Am. Chem. Soc.* **1992**, *114*, 9969.
32. (a) Sessler, J. L.; Murai, T.; Lynch, V.; Cyr, M. *J. Am. Chem. Soc.* **1988**, *110*, 5586. (b) Young, S. W.; Fan, Q.; Harriman, A.; Sessler, J. L.; Dow, W. C.; Mody, T. D.; Hemmi, G. W.; Hao, Y.; Miller, R. A. *Proc. Natl. Acad. Sci. USA* **1996**, *93*, 6610. (c) Sessler, J. L.; Miller, R. A. *Biochem. Pharmacol*. **2000**, *59*, 733. (d) Hannah, S.; Lynch, V.; Guldi, D. M.; Gerasimchuk, N.; MacDonald, C. L. B.; Magda, D.; Sessler, J. L. *J. Am. Chem. Soc*. **2002**, *124*, 8416. (e) Wei, W.-H.; Wang, Z.; Mizuno, T.; Cortez, C.; Fu, L.; Sirisawad, M.; Naumovski, L.; Magda, D.; Sessler, J. L. *Dalton Trans.* **2006**, 1934. (f) Evans, J. P.; Xu, F.; Sirisawad, M.; Miller, R.; Naumovski, L.; Ortiz de Montellano, P. R. *Mol. Pharmacol.* **2007**, *71*, 193. (g) Zahedi Avval, F.; Berndt, C.; Pramanik, A.; Holmgren, A. *Biochem. Biophys. Res. Commun*. **2009**, *379*, 775.
33. Sessler, J. L.; Weghorn, S. J.; Lynch, V.; Johnson, M. R. *Angew. Chem. Int. Ed. Engl.* **1994**, *33*, 1509.

34. (a) Vogel, E.; Bröring, M.; Fink, J.; Rosen, D.; Schmickler, H.; Lex, J.; Chan, K.W. K.; Wu, Y.-D.; Plattner, D. A.; Nendel, M.; Houk, K. N. *Angew. Chem. Int. Ed. Engl*. **1995**, *34*, 2511. (b) Bröring, M.; Jendrny, J.; Zander, L.; Schmickler, H.; Lex, J.; Wu, Y.-D.; Nendel, M.; Chen, J.; Plattner, D. A.; Houk, K. N.; Vogel, E. *Angew. Chem. Int. Ed. Engl.* **1995**, *34*, 2515.
35. Werner, A.; Michels, M.; Zander, L.; Lex, J.; Vogel, E. *Angew. Chem. Int. Ed*. **1999**, *38*, 3650.
36. (a) Setsune, J.-i.; Katakami, Y.; Iizuna, N. *J. Am. Chem. Soc.* **1999**, *121*, 8957. (b) Setsune, J.-i.; Maeda, S. *J. Am. Chem. Soc*. **2000**, *122*, 12405. (c) Lintuluoto, J. M.; Nakayama, K.; Setsune, J.-i. *Chem. Commun.* **2006**, 3492. (d) Ie, M.; Setsune, J.-i.; Eda, K.; Tsuda, A. *Org. Chem. Front*. **2015**, *2*, 29.
37. (a) Rzepa, H. S. *Chem. Rev.* **2005**, *105*, 3697. (b) Herges, R. *Chem. Rev.* **2006**, *106*, 4820.
38. (a) Heilbronner, E. *Tetrahedron Lett.* **1964**, *5*, 1923. (b) Zimmerman, H. E. *J. Am. Chem. Soc.* **1966**, *88*, 1564. (c) Mauksch, M.; Gogonea, V.; Jiao, H.; Schleyer, P. von R. *Angew. Chem. Int. Ed.* **1998**, *37*, 2395. (d) Ajami, D.; Oeckler, O.; Simon, A.; Herges, R. *Nature* **2003**, *426*, 819. (e) Schleyer, P. von R.; Jiao, H. *Pure Appl. Chem*. **1996**, *68*, 209.
39. (a) Mo, Y.; Schleyer, P. von R. *Chem. –Eur. J.* **2006**, *12*, 2009. (b) Wannere, C. S.; Sattelmeyer, K. W.; Schaefer III, H. F.; Schleyer, P. von R. *Angew. Chem. Int. Ed*. **2004**, *43*, 4200. (c) Wannere, C. S.; Schleyer, P. von R. *Org. Lett.* **2003**, *5*, 865. (d) Wannere, C. S.; Schleyer, P. von R. *Org. Lett*. **2003**, *5*, 605. (e) Wannere, C. S.; Moran, D.; Allinger, N. L.; Hess Jr., B. A.; Schaad, L. J.; Schleyer, P. von R. *Org. Lett*. **2003**, *5*, 2983. (f) Schleyer, P. von R.; Maerker, C.; Dransfeld, A.; Jiao, H.; van Eikema Hommes, N. J. R. *J. Am. Chem. Soc.* **1996**, *118*, 6317. (g) Schleyer, P. von R.; Manoharan, M.; Wang, Z.-X.; Kiran, B.; Jiao, H.; Puchta, R.; van Eikema Hommes, N. J. R. *Org. Lett.* **2001**, *3*, 2465. (h) Steiner, E.; Fowler, P. W. *Org. Biomol. Chem*. **2004**, *2*, 34. (i) Aihara, J.; Makino, M. *Bull. Chem. Soc. Jpn*. **2009**, *82*, 675. (j) Aihara, J.; Horibe, H. *Org. Biomol. Chem*. **2009**, *7*, 1939.
40. Stępień, M.; Latos-Grażyński, L.; Sprutta, N.; Chwalisz, P.; Szterenberg, L. *Angew. Chem. Int. Ed*. **2007**, *46*, 7869.
41. (a) Tanaka, Y.; Saito, S.; Mori, S.; Aratani, N.; Shinokubo, H.; Shibata, N.; Higuchi, Y.; Yoon, Z. S.; Kim, K. S.; Noh, S. B.; Park, J. K.; Kim, D.; Osuka, A. *Angew. Chem. Int. Ed.* **2008**, *47*, 681. (b) Park, J. K.; Yoon, Z. S.; Yoon, M.-C.; Kim, K. S.;

Mori, S.; Shin, J.-Y.; Osuka, A.; Kim, D. *J. Am. Chem. Soc.* **2008**, *130*, 1824. (c) Sankar, J.; Mori, S.; Saito, S.; Rath, H.; Suzuki, M.; Inokuma, Y.; Shinokubo, H.; Kim, K. S.; Yoon, Z. S.; Shin, J.-Y.; Lim, J. M.; Matsuzaki, Y.; Matsushita, O.; Muranaka, A.; Kobayashi, N.; Kim, D.; Osuka, A. *J. Am. Chem. Soc.* **2008**, *130*, 13568. (d) Kim, K. S.; Yoon, Z. S.; Ricks, A. B.; Shin, J.-Y.; Mori, S.; Sankar, J.; Saito, S.; Jung, Y. M.; Wasielewski, M. R.; Osuka, A.; Kim, D. *J. Phys. Chem. A* **2009**, *113*, 4498. (e) Saito, S.; Shin, J.-Y.; Lim, J. M.; Kim, K. S.; Kim, D.; Osuka, A. *Angew. Chem. Int. Ed.* **2008**, *47*, 9657. (f) Tokuji, S.; Shin, J.-Y.; Kim, K. S.; Lim, J. M.; Youfu, K.; Saito, S.; Kim, D.; Osuka, A. *J. Am. Chem. Soc.* **2009**, *131*, 7240. (g) Inoue, M.; Kim, K. S.; Suzuki, M.; Lim, J. M.; Shin, J.-Y.; Kim, D.; Osuka, A. *Angew. Chem. Int. Ed.* **2009**, *48*, 6687. (h) Koide, T.; Youfu, K.; Saito, S.; Osuka, A. *Chem. Commun*. **2009**, 6047. (i) Lim, J. M.; Shin, J.-Y.; Tanaka, Y.; Saito, S.; Osuka, A.; Kim, D. *J. Am. Chem. Soc*. **2010**, *132*, 3105.

42. Pacholska-Dudziak, E.; Skonieczny, J.; Pawlicki, M.; Szterenberg, L.; Ciunik, Z.; Latos-Grażyński, L. *J. Am. Chem. Soc.* **2008**, *130*, 6182.
43. Higashino, T.; Lim, J. M.; Miura, T.; Saito, S.; Shin, J.-Y.; Kim, D.; Osuka, A. *Angew. Chem. Int. Ed.* **2010**, *49*, 4950.
44. Koide, T.; Kashiwazaki, G.; Suzuki, M.; Furukawa, K.; Yoon, M.-C.; Cho, S.; Kim, D.; Osuka, A. *Angew. Chem. Int. Ed*. **2008**, *47*, 9661.
45. Koide, T.; Furukawa, K.; Shinokubo, H.; Shin, J.-Y.; Kim, K. S.; Kim, D.; Osuka, A. *J. Am. Chem. Soc*. **2010**, *132*, 7246.
46. Siedel, D.; Lynch, V.; Sessler, J. L. *Angew. Chem. Int. Ed*. **2002**, *41*, 1422.
47. Eller, L. R.; Stępień, M.; Fowler, C. J.; Lee, J. T.; Sessler, J. L.; Moyer, B. A. *J. Am. Chem. Soc*. **2007**, *129*, 11020.
48. Stępień, M.; Donnío, B.; Sessler, J. L. *Angew. Chem. Int. Ed*. **2007**, *46*, 1431.
49. (a) Okujima, T.; Jin, G.; Matsumoto, N.; Mack, J.; Mori, S.; Ohara, K.; Kuzuhara, D.; Ando, C.; Ono, N.; Yamada, H.; Uno, H.; Kobayashi, N. *Angew. Chem. Int. Ed*. **2011**, *50*, 5699. (b) Sarma, T.; Panda, P. K. *Chem. –Eur. J*. **2011**, *17*, 13987. (c) Roznyatovskiy, V. V.; Lim, J. M.; Lynch, V. M.; Lee, B. S.; Kim, D.; Sessler, J. L. *Org. Lett*. **2011**, *13*, 5620.
50. Okujima, T.; Ando, C.; Mack, J.; Mori, S.; Hisaki, I.; Nakae, T.; Yamada, H.; Ohara, K.; Kobayashi, N.; Uno, H. *Chem. –Eur. J*. **2013**, *19*, 13970.
51. (a) Chandrashekar, T. K.; Venkatraman, S. *Acc. Chem. Res.* **2003**, *36*, 676. (b) Misra, R.; Chandrashekar, T. K. *Acc. Chem. Res.* **2008**, *41*, 265. (c) Anand, V. G.; Pushpan,

S. K.; Venkatraman, S.; Dey, A.; Chandrashekar, T. K.; Joshi, B. S.; Roy, R.; Teng, W.; Senge, K. R. *J. Am. Chem. Soc.* **2001**, *123*, 8620. (d) Anand, V. G.; Venkatraman, S.; Rath, H.; Chandrashekar, T. K.; Teng, W.; Senge, K. R. *Chem. –Eur. J*. **2003**, *9*, 2282. (e) Rath, H.; Sankar, J.; PrabhuRaja, V.; Chandrashekar, T. K.; Nag, A.; Goswami, D. *J. Am. Chem. Soc.* **2005**, *127*, 11608. (f) Kumar, R.; Misra, R.; Chandrashekar, T. K.; Nag, A.; Goswami, D.; Suresh, E.; Suresh, C. H. *Eur. J. Org. Chem*. **2007**, 4552.

52. Rath, H.; Prabhuraja, V.; Chandrashekar, T. K.; Nag, A.; Goswami, D.; Joshi, B. S. *Org. Lett.* **2006**, *8*, 2325.
53. (a) Narayanan, S. J.; Sridevi, B.; Chandrashekar, T. K. *Org. Lett*. **1999**, *1*, 587. (b) Pareek, Y.; Ravikanth, M.; Chandrashekar, T. K. *Acc. Chem. Res*. **2012**, *45*, 1801.
54. (a) Pareek, Y.; Ravikanth, M.; Chandrashekar, T. K. *Acc. Chem. Res.* **2012**, *45*, 1801. (b) Rao, M. R.; Ravikanth, M. *J. Org. Chem.* **2011**, *76*, 3582. (c) Rao, M. R.; Ravikanth, M. *Eur. J. Org. Chem*. **2011**, 1335. (d) Pareek, Y.; Ravikanth, M. *Eur. J. Org. Chem*. **2011**, 5390. (e) Khan, T. K.; Ravikanth, M. *Eur. J. Org. Chem*. **2011**, 7011.
55. Mori, H.; Tanaka, T.; Osuka, A. *J. Mater. Chem. C* **2013**, *1*, 2500.
56. (a) Lash, T. D. *The Porphyrin Handbook*; Academic Press: New York, **2000**; Vol. *2*. (b) Zhi, L.; Müllen, K. *J. Mater. Chem.* **2008**, *18*, 1472. (c) Roznyatovskiy, V. V.; Lee, C.-H.; Sessler, J. L. *Chem. Soc. Rev*. **2013**, *42*, 1921.
57. Davis, N. K. S.; Thompson, A. L.; Anderson, H. L. *J. Am. Chem. Soc*. **2011**, *133*, 30.
58. Yamada, H.; Kuzuhara, D.; Takahashi, T.; Shimizu, Y.; Uota, K.; Okujima, T.; Uno, H.; Ono, N. *Org. Lett*. **2008**, *14*, 2947.
59. Naoda, K.; Mori, H.; Aratani, N.; Lee, B. S.; Kim, D.; Osuka, A. *Angew. Chem. Int. Ed*. **2012**, *51*, 9856.
60. Mori, H.; Tanaka, T.; Lee, S.; Lim, J. M.; Kim, D.; Osuka, A. *J. Am. Chem. Soc*. **2015**, *137*, 2097.
61. Tsuda, A.; Osuka, A. *Science* **2001**, *293*, 79.
62. Ishida, M.; Kim, S.-J.; Preihs, C.; Ohkubo, K.; Lim, J. M.; Lee, B. S.; Park, J. S.; Lynch, V. M.; Roznyatovskiy, V. V.; Sarma, T.; Panda, P. K.; Lee, C. H.; Fukuzumi, S.; Kim, D.; Sessler, J. L. *Nat. Chem*. **2013**, *5*, 15.
63. Fürstner, A. *Angew. Chem. Int. Ed*. **2003**, *42*, 3582.

64. (a) Yamamoto, D.; KIyozuka, Y.; Uemura, Y.; Yamamoto, C.; Takemoto, H.; Hirata, H.; Tanaka, K.; Hioki, K.; Tsubura, A. *J. Cancer. Res. Clin. Oncol*. **2000**, *126*, 191. (b) Montaner, B.; Perez-Toma, R. *Life Sciences* **2001**, *68*, 2025.
65. (a) Konopleva, M.; Watt, J.; Contractor, R.; Tsao, T.; Harris, D.; Estrov, Z.; Bornmann, W.; Kantarjian, H.; Viallet, J.; Samudio, I.; Andreeff, M. *Cancer Res*. **2008**, *68*, 3413. (b) Rahmani, M.; Aust, M. M.; Attkisson, E.; Williams, D. C. Jr.; Ferreira-Gonzalez, A.; Grant, S. *Blood* **2012**, *119*, 6089.
66. (a) Merz, A.; Schwarz, R.; Schropp, R. *Adv. Mater.* **1992**, *4*, 409. (b) Merz, A.; Graf, S. *J. Electroanal. Chem.* **1996**, *412*, 11. (c) Gassner, F.; Graf, S.; Merz, A. *Synth. Met*. **1997**, *87*, 75. (d) Merz, A.; Kronberger, J.; Dinsch, L.; Neudeck, A.; Petr, A.; Prakanyi, L. *Angew. Chem. Int. Ed.* **1999**, *38*, 1442. (e) Darmanin, T.; Guittard, F. *J. Mater. Chem.* **2009**, *19*, 7130. (f) Darmanin, T.; Guittard, F. *J. Am. Chem. Soc.* **2009**, *131*, 7928. (g) Arroyave, F. A.; Reynolds, J. R. *Macromolecules* **2012**, *45*, 5842. (h) Krondak, M.; Broncová, G.; Anikin, S.; Merz, A.; Mirsky, V. M. *J. Solid State Electrochem.* **2006**, *10*, 185.
67. Merz, A.; Schropp, R.; Lex, J. *Angew. Chem. Int. Ed. Engl.* **1993**, *32*, 291.
68. Merz, A.; Schropp, R.; Dötterl, E. *Synthesis* **1995**, 795.
69. (a) Murashima, T.; Uchihara, Y.; Wakamori, N.; Uno, H.; Ogawa, T.; Ono, N. *Tetrahedron Lett*. **1996**, *37*, 3133. (b) Murashima, T.; Wakamori, N.; Uchihara, Y.; Ogawa, T.; Uno, H.; Ono, N. *Mol. Cryst. Liq. Cryst*. **1996**, *278*, 165.
70. Gale, P. A.; Sessler, J. L.; Allen, W. E.; Tvermoes, N. A.; Lynch, V. *Chem Commun*. **1997**, 665.
71. Merz, A.; Meyer, T. *Synthesis* **1999**, 94.
72. Feng, M.; Chan, K. S. *J. Organomet. Chem*. **1999**, *584*, 235.
73. Shevchuk, S. V.; Davis, J. M.; Sessler, J. L. *Tetrahedron Lett*. **2001**, *42*, 2447.
74. (a) Sessler, J. L.; Callaway, W.; Dudek, S. P.; Date, R. W.; Lynch, V.; Bruce, D. W. *Chem Commun*. **2003**, 2422. (b) Sessler, J. L.; Callaway, W. B.; Dudek, S. P.; Date, R. W.; Bruce, D. W. *Inorg. Chem.* **2004**, *43*, 6650.
75. Panda, P. K.; Krishnan, V. *J. Chem. Sci*. **2005**, *117*, 73.

CHAPTER 2

Materials and Methods

This chapter provides detail insight about the materials used, instrumentation and methods employed for various studies. Also, the procedures used for the purification of solvents and chemicals are described. Further, we have discussed about the synthetic procedure of literary known compounds employed during the course of our investigations.

2.1 General experimental

2.1.1 Solvents

2.1.1.1 Solvent for reactions[1]

Pyrrole was distilled before use. Dichloromethane (DCM), 1,2-dichloroethane (DCE), and dimethylformamide (DMF) were dried by distillation over calcium hydride. Tetrahydrofuran (THF) and diethyl ether were dried by passing through columns of activated alumina, followed by distillation over sodium metal, in presence of benzophenone as indicator. Ethanol and methanol were dried by using activated magnesium turnings with iodine. Chloroform, benzyl alcohol and acetone were dried by distilling over anhydrous potassium carbonate. Toluene and benzene were refluxed with sodium and benzophenone until blue color appears and distilled before use. $POCl_3$ was distilled before use.

2.1.1.2 NMR solvents

Chloroform-d_1, D_2O, MeOH-d_4 and DMSO-d_6 were purchased from Sigma Aldrich/Acros Organics/Cambridge isotope Inc.

2.1.1.3 Solvents for optical measurement

DMSO, $CHCl_3$, CH_2Cl_2, methanol, DMF, toluene, acetonitrile, benzene, toluene and hexane (spectroscopy grade) were purchased from Merck and used as such.

2.1.1.4 Solvents for Electrochemical measurement

Dichloromethane (AR grade) was purchased from Merck, India and dried with standard techniques before use.

2.1.2 Reagents

Pyrrole was purchased from Sisco research laboratories (SRL) and Spectrochem. Cuprous chloride, triethyl orthoformate, dimethyl oxalate, iminodiacetic acid, pentfluorobenzaldhyde, 2,6-difluorobenzaldhyde, 3,5-difluorobenzaldhyde, 2,5-dimethoxy-2,5-dihydrofuran, [bis(trifluoroacetoxy)iodo]benzene, trimethylsilyl bromide, triisopropylsilyl chloride, 1-triisopropylsilylpyrrole, chloranil, NaH, CaH_2, $LiOH.H_2O$, benzophenone, DDQ, trimethylsilylacetylene, N-iodosuccinimide, CuI, tetrabutylammonium fluoride,

tetrabutylammonium chloride, tetrabutylammonium bromide, 1(M) tetrabutylammonium fluoride in THF, 2,4-dinitrotoluene (DNT), 2,3-dimethyl-2,3-dinitrobutane (DMNB), $PdCl_2$, Pd/C (5%), $BF_3.OEt_2$, TFA, $Ni(acac)_2$ and $Pd(OAc)_2$ were purchased from Sigma-Aldrich® and used as such. THF, nitrobenzene and acetonitrile were purchased from Finar chemicals. GR grade toluene, acetic acid, 1,2-dichloroethane, benzyl alcohol, DMF, DCM, $CHCl_3$, DMSO, MeOH, diethyl ether, ethylene glycol and *i*-propanol were purchased from Merck/SRL/Finar/Avra. $TiCl_4$, Zn powder and sodium were purchased from Finar chemicals. Dimethyl sulphate and diethyl sulphate were purchased from Spectrochem, India. All the inorganic salts, mineral acids, hydroxylamine hydrochloride, potassium iodide, NaOH, $MgSO_4.7H_2O$, $KMnO_4$, K_2CO_3, Na_2SO_4, anhydrous $MgSO_4$, $Zn(OAc)_2.2H_2O$, KOH, $Na_2S_2O_3.5H_2O$, $NaHCO_3$, Nitromethane (NM), nitrobenzene (NB) and solvents used for the routine laboratory work, were purchased from Merck, India. *p*-TsOH, *o*-xylene and Raney Ni® on silica support were purchased from Avra, India. $FeCl_3$ and $NaHSO_3$ were purchased from Loba Chemie. $POCl_3$ was purchased from Chemlab, India. n-Butyllithium 1.6 (M) in hexane was purchased from Chempure, India. Mg-turnings, I_2, all alkyl bromides, phthalic anhydride, basic and neutral alumina were purchased from Sisco Research Laboratories. TNT, RDX and HMX were supplied by HEMRL, Pune, DRDO, India among them TNT was used after recrystallization. Octaethyporphyrin and ethyl 3,4-diethylpyrrole-2-carboxylate employed were synthesized by following reported procedure by my lab mate and generously gifted adequate quantity for our studies.[2]

2.2 Chromatography

Thin layer chromatography was performed on pre coated TLC Silica gel 60 F_{254} on aluminium sheet, purchased from Merck. Column chromatography was carried out on silica gel (100-200 mesh) purchased from Merck/SRL/Dessica, India.

2.3 Characterization and instrumentation

Nuclear magnetic resonance (NMR) spectra were obtained on Bruker 400 MHz and 500 MHz FT-NMR spectrometer operating at ambient temperature. In $CDCl_3$, TMS (δ = 0 ppm) was used as internal standard for ^1H NMR spectra and for other deuterated solvents, solvent residual peak was taken as standard. Similarly, for ^{13}C NMR spectra solvent peak was taken as standard for all deuterated solvent for calibration purpose.

Mass spectral determinations were carried out by Bruker Maxis HRMS by ESI techniques and LCMS were recorded by Shimadzu-LCMS-2010 mass spectrometer both by positive and negative ionization method.

Elemental analyses were obtained through Thermo Finnigan Flash EA 1112 analyzer. Melting points were determined by a Lab India MR-VIS^{+} visual melting point apparatus and uncorrected. IR spectra were recorded on NICOLET 5700 FT-IR spectrometer by either using KBr pellet or neat sample.

UV-Vis spectra were recorded on Perkin Elmer Lambda 35 and Lambda 750 UV-VIS-NIR spectrophotometer. Fluorescence spectra were recorded on Horiba Zobin Yovan Fluoromax-4 and Fluorolog-3-221 spectrofluorometer equipped with Hamamatsu H10330-75 TE cooled NIR detector working at -60 °C. For the observation of steady-state emission spectra in the near-infrared (NIR) region, a photomultiplier tube module (H10330-75, Hamamatsu), a lock-in amplifier (5210, EG&G) combined with a chopper and a CW He-Cd laser (Omnichrome 74, Melles Griot) for the 442 nm excitation were used. All steady-state measurements were carried out by using a quartz cuvette with a path length of 1 cm at ambient temperatures. Fluorescent quantum yield of compounds were measured by comparative actinommetry method developed by William et al. by using appropriate fluorescent standard.[3]

2.3.1 Fluorescent lifetime measurements

Fluorescence lifetime measurements were carried out using a time correlated single-photon counting (TCSPC) spectrometer (Horiba Jobin Yvon IBH). PicoBrite diode laser source (λ_{exc} 375 nm) was used as the excitation source and an MCP photomultiplier (Hamamatsu R3809U-50) as the detector. The pulse repetition rate of the laser source was 10 MHz. The width of the instrument response function, which was limited by the fwhm of the exciting pulse, was around 55 ps. The lamp profile was recorded by placing a scatterer (dilute solution of Ludox in water) in place of the sample. The time resolved emission decay profiles were collected at steady state emission spectrum maxima's. Decay curves were analyzed by nonlinear least-squares iteration procedure using IBH DAS6 (Version 2.2) decay analysis software. The quality of the fit was assessed by inspection of the χ^2 values and the distribution of the residuals.

2.3.2 Singlet oxygen quantum yield measurements

The steady-state luminescence of singlet oxygen of porphycene **1** and their M(II) complex was measured by using a Fluorolog-3-221 spectrofluorometer equipped with Hamamatsu H10330-75 TE cooled NIR detector working at -60 °C. Tetraphenylporphyrin (**H_2TPP**) was taken as standard (ϕ_Δ 0.7). All samples exhibit the emission bands ranging from 1240 to 1320 nm with the peak at about 1274 nm. The singlet oxygen quantum yields ϕ_Δ for all samples can be determined by using eq 1 (comparative actinometry method):[4]

$$\phi_\Delta = \phi_\Delta^{std} \frac{I}{I_{std}} \frac{1 - 10^{-A^{std}}}{1 - 10^{-A}} \dots\dots\dots\dots\dots\dots\dots\dots\dots\dots\dots\dots\dots\dots\dots\dots.. (1)$$

where ϕ_Δ^{std}(0.7) is the singlet oxygen quantum yield of **H_2TPP** as the standard sample in aerated toluene, I and I_{std} refer to the singlet oxygen emission intensities at the peaks for the tested sample and **H_2TPP**, respectively, and A and A^{std} stand for the ground-state absorbance of the tested sample and **H_2TPP** at the excited wavelength. Each sample was recorded for three times under identical condition and average value was taken to determine peak intensity.

2.3.3 Cyclic voltammetry and differencial pulse voltammetry measurements

Cyclic voltammetric (CV) and differential pulse voltammetric (DPV) measurements were carried out using Zahner Zennium Electrochemical Workstation and electrodes were purchased from CH Instruments Inc. All measurements were performed in dry dichloromethane under flow of nitrogen and 0.1 M tetrabutylammonium hexafluorophosphate ($TBAPF_6$) used as a supporting electrolyte. Platinum disc as working electrode, platinum wire as counter electrode and Ag/AgCl in 1(M) KCl or in 3(M) NaCl as reference electrode were used. Ferrocenium/Ferrocene, Fc^+/Fc couple was used as external reference for calibration. The redox potentials were referenced *vs.* SCE or Ag/AgCl. All cyclic voltammetric data were recorded at 50 mV/s scan rate.

2.3.4 Single crystal XRD measurements

Some of the crystallographic data were collected on BRUKER SMART-APEX CCD diffractometer. Mo-K_α (λ = 0.71073 Å) radiation was used to collect X-ray reflections from the single crystal. Data reduction was performed using Bruker SAINT[5] software. Intensities for absorption were corrected using SADABS[6] and refined using SHELXL-97[7] with

anisotropic displacement parameters for non-H atoms. Hydrogen atoms on O and N were experimentally located in difference electron density maps. All C−H atoms were fixed geometrically using HFIX command in SHELX-TL. A check of the final CIF file using PLATON[8] did not show any missed symmetry. Remaining other crystallographic data were collected on Oxford Gemini A Ultra diffractometer with dual sources. Mo-K_α (λ = 0.71073 Å) and Cu-Kα (λ = 1.54184 Å) radiations were used to collect the X-ray reflections of the crystal. Data reduction was performed using CrysAlisPro 171.33.55 software.[9] Structures were solved and refined using Olex2-1.0, with anisotropic displacement parameters for non-H atoms. Hydrogen atoms on N were located from the Fourier map in all of the crystal structures. All C–H atoms were fixed geometrically. Empirical absorption correction was done using spherical harmonics, implemented in SCALE3 ABSPACK scaling algorithm. A check of the final CIF file using PLATON[8] did not show any missed symmetry.

2.3.5 Anion binding and protonation studies

For anion binding and protonation studies, stock solution of host molecules was prepared in spectroscopic grade solvent in specific concentration. The stock solution of guests of specific concentration was prepared by using stock solution of host. So, in the course of titration addition of guest didn't affect the concentration of host i.e. we can avoid dilution error. The general procedure for the UV-Vis titration involved the sequential addition of guest solution using Hamilton micro-syringe to 3 mL stock solution of host in cuvette followed by collection of UV-Vis data.

Equilibrium constants for anion binding studies were calculated by using Connor equation[10] where [L] = [anion]. The resulting equation, of the form, $y = (B \times x /(Ka \times x + 1)) + y_o$, was nonlinearly fit using OriginPro 8.0, where x = [anion], y = absorption of the host after successive addition, y_o = initial absorption of the host. $B = \Delta\varepsilon \times b$, *Ka* = the equilibrium constant. The change in absorbance was calculated at a λ value where the maximal spectral change was observed.

For Job's Plot[11] stock solution of same concentrated host and guest were prepared in spectroscopic grade methanol. The absorbance was measure in each case with different host-guest ratio with equal volume (3 mL). Job's plots were drawn by plotting $\Delta A.X_{guest}$ *vs.* X_{guest}, where ΔA indicates change in absorption during titration and X_{guest} is the mole fraction of guest.

2.3.6 Solution phase binding study of nitrated explosives

All solutions of measurements in this study were prepared using spectroscopic grade solvents. UV-Visible spectra were recorded with slit width 1 nm. In Stern-Volmer (SV) measurements solution of porphyrins and their zinc derivatives were taken whose absorbance were less than 0.1, to avoid any self-aggregation in chloroform unless mentioned. In a typical steady–state fluorescence measurement, 3 mL host solution in chloroform was taken in fluorescence cuvette with 1 cm path-length and fluorescence spectra were recorded immediately after each micro-liter addition of nitro compounds (maximum 30 µL of guest solution was added to avoid volume error resulting from dilution).

To determine solution phase quenching of fluorescence, SV measurements were performed, which will provide quantitative and systematic comparisons. Most measurements were done by using steady-state fluorescence measurements and the Stern-Volmer equation employed is[12]

$$\frac{F_0}{F} = (1 + K_S[Q])(1 + K_D[Q]) \qquad (1)$$

$$\frac{F_0}{F} = 1 + K_D[Q] + K_S[Q] + K_D K_S[Q]^2$$

At low concentration of quencher we can ignore $K_S K_D[Q]^2$ term then,

$$\frac{F_0}{F} = 1 + (K_D + K_S)[Q]$$

More simply,

$$\frac{F_0}{F} = 1 + K_{SV}[Q] \ldots\ldots\ldots\ldots\ldots\ldots\ldots (2)$$

Where F_0 and F are fluorescent intensities before and after addition of quencher, [Q] is the concentration of quencher, K_S and K_D are static and collisional quenching constant respectively and K_{SV} generally called SV quenching constant which is the sum of static and collisional quenching constants. SV quenching constant is dependent only on concentration of quencher. So, if we plot F_0/F vs. concentration of quencher then we will get straight line with intercept one and slope of the line provides the magnitude of SV quenching constant.

2.3.7 Vapor phase sensing of nitrated explosives

Porphyrins (~ 2 mg) were dissolved in HPLC grade chloroform (5 mL) and quoted on quartz plate (12.5 × 37.5 × 1 mm dimension, purchased from Applied Optics Inc., Bangalore, India) by spin coating method at 700 rpm. Spin coated quartz plates were dried in vacuum for 12 h before measurements were carried out. In a typical vapor phase measurement, explosive particulates were placed on 20 mL glass container and some amount of cotton was placed to avoid direct contact with measured coated film. The containers with explosives were kept closed for 48 h before measurements in order to generate saturated vapor pressure inside the container. Vapor phase fluorescent quenching measurements were carried out in Fluorolog-3-221 by front face techniques and coated quartz plate was placed on solid sample holder. In typical fluorescent quenching measurement coated quartz film was placed on the explosive container for required time and after removing from container fluorescence was measured immediately.

2.3.8 Axial ligation measurements

Axial ligation of Zn(II) porphyrins were carried out by UV-Vis titrimetric method in spectroscopic grade toluene. For axial ligation studies, stock solution of pyridine was prepared in spectroscopic grade toluene at specific concentration, which in turn was prepared by using stock solution of Zn(II)porphyrin used for measurement. So, in the course of titration addition of guest didn't affect the concentration of host i.e. we can avoid dilution error. The general procedure for the UV-Vis titration involved the sequential addition of pyridine solution using Hamilton microsyringe to 3 mL stock solution of Zn(II) porphyrins in cuvette followed by collection of UV-Vis data. Hill equation is used for determination of binding constant.[13]

$$\ln\left[\frac{(A_0 - A)}{(A_0 - A_{inf})}\right] = \mathrm{n}ln[py] - lnK \ldots\ldots\ldots\ldots\ldots\ldots\ldots\ldots\ldots (3)$$

The plot of $\ln[(A_0\text{-}A)/(A\text{-}A_{inf})$ *vs.* ln[py] gives a straight line, whose slope (n) and intercept provides the binding stoichiometry and the binding constant (lnK), respectively. Where A_0, A and A_{inf} stand for absorbance at the wavelength where maximum change occurred and [py] is the concentration of pyridine.

2.3.9 Two photon absorption (TPA) measurements for porphyrins

Z-scan measurements[14] were performed using ~2 ps [FW(1/e^2)M], 800 nm pulses with a repetition rate of 1 kHz delivered by an amplified Ti:sapphire system (Legend, Coherent). The amplifier was seeded with pulses of duration ~15 fs (~50-60 nm, FWHM) from a tunable laser oscillator (Micra, Coherent). The transform limited nature of amplified pulses was confirmed from the product of bandwidth and pulse duration measurements performed using external auto-correlation experiments. A quartz cuvette (1-mm thick) containing the sample solution was traversed in the focusing geometry enabled by an achromat lens of 200 mm focal length. The beam waist ($2\omega_0$) at focal plane was estimated to be 60±4 μm (FW1/e^2M) with a corresponding Rayleigh range (Z_R) of 3.5±0.4 mm ensuring the validity of thin sample approximation. The Z-scan was performed over a distance of $10Z_R$ on a high-resolution linear translation stage (Newport ILS250PP) by recording the sample transmittance. A LabVIEW program was designed and used for automating the data acquisition of the Z-scan experiments. Typical energies in the range of 1-5μJ, corresponding to peak intensities in the range of 70–200 GW/cm^2, were used for all the experiments. The closed aperture scans were performed at peak intensities <50 GW/cm^2 to avoid contribution from higher order nonlinearities. The open aperture z-scan data have been fitted using the relation obtained by Sheik Bahae et al.[15] by time integration of sample transmittance assuming a Gaussian temporal profile. The two photon absorption fitting is done using the equation (1). Where T(z) is the normalized transmittance as a function of z, $q_0 = \alpha_2 l_{eff} I_0$, α_2 = 2PA coefficient, I_0 is the peak intensity at focus.

$$T(z, S = 1) = \frac{1}{\sqrt{\pi} q_0(z, 0)} \int_{-\infty}^{\infty} \ln\left[1 + q_0(z, 0) e^{-\tau^2}\right] d\tau \qquad (1)$$

Effective path lengths in the sample of length L for 2PA is given as $L_{eff} = \frac{1 - e^{-\alpha_0 L}}{\alpha_0}$,

$L'_{eff} = \frac{1 - e^{-2\alpha_0 L}}{2\alpha_0}$, α_0 = linear absorption coefficient.

2.3.10 Excited state life time study by femtosecond pump-probe at 600 nm for porphyrins

For degenerate pump probe measurements the amplified pulses (~40 fs) pumped an OPA (TOPAS-C; Light Conversion) delivering 600 nm pulses with duration of ~70 fs. The pump

to probe intensity ratio was ensured to be >10:1. The probe beam was delayed using an optical delay line and the change in probe transmittance was monitored using the combination of a sensitive silicon photodiode and lock-in amplifier (Signal Recovery 7265). The pump pulses were chopped at a frequency of 109 Hz which was the reference for the lock-in amplifier. The samples were placed in a 5-mm quartz cuvette to achieve better signal-to-noise ratio. The data was fitted using the equation given below containing triple exponentials.[16]

$$\frac{\Delta T(t)}{T} = y_0 + A_1 e^{-(t-t_0)/\tau_1} + A_2 e^{-(t-t_0)/\tau_2} + A_3 e^{-(t-t_0)/\tau_3}$$

Where ΔT(t) is the time dependent change in probe transmission.

2.3.11 Two photon absorption (TPA) measurements for porphycenes and stretched porphycenes

The two-photon absorption spectrum was measured in the NIR region using the open-aperture Z-scan method with 130 fs pulses from an optical parametric amplifier (Light Conversion, TOPAS) operating at a repetition rate of 1 kHz generated from a Ti:sapphire regenerative amplifier system (Spectra-Physics, Hurricane). After passing through a 10 cm focal length lens, the laser beam was focused and passed through a 1 mm quartz cell. Since the position of the sample cell could be controlled along the laser beam direction (z axis) using the motor controlled delay stage, the local power density within the sample cell could be simply controlled under constant laser intensity. The transmitted laser beam from the sample cell was then detected by the same photodiode as used for reference monitoring. The on-axis peak intensity of the incident pulses at the focal point, I_0, ranged from 40 to 60 GW cm^{-2}. For a Gaussian beam profile, the nonlinear absorption coefficient can be obtained by curve fitting of the observed open-aperture traces *T(z)* with the following equation:

$$T(z) = 1 - \frac{\beta I_0 (1 - e^{-\alpha_0 l})}{2\alpha_0 [1 + \left(\frac{z}{z_0}\right)^2]}$$

where α_0 is the linear absorption coefficient, l is the sample length, and z_0 is the diffraction length of the incident beam. After the nonlinear absorption coefficient has been obtained, the TPA cross section $\sigma^{(2)}$ of one solute molecule (in units of GM, where 1 GM = 10^{-50} cm^4 s photon^{-1} molecule^{-1}) can be determined by using the following relationship:

$$\beta = \frac{10^{-3}\sigma^{(2)}N_A d}{h\nu}$$

where N_A is the Avogadro constant, d is the concentration of the compound in solution, h is the Planck constant, and ν is the frequency of the incident laser beam.

2.3.12 Femtosecond transient absorption measurements

The femtosecond time-resolved transient absorption (fs-TA) spectrometer consists of an optical parametric amplifier (OPA; Palitra, Quantronix) pumped by a Ti:sapphire regenerative amplifier system (Integra-C, Quantronix) operating at 1 kHz repetition rate and an optical detection system. The generated OPA pulses have a pulse width of ~ 100 fs and an average power of 100 mW in the range 280-2700 nm, which are used as pump pulses. White light continuum (WLC) probe pulses were generated using a sapphire window (3 mm thick) by focusing a small portion of the fundamental 800 nm pulses which was picked off by a quartz plate before entering the OPA. The time delay between pump and probe beams was carefully controlled by making the pump beam travel along a variable optical delay (ILS250, Newport). Intensities of the spectrally dispersed WLC probe pulses are monitored by a High Speed spectrometer (Ultrafast Systems) for both visible and near-infrared measurements. To obtain the time-resolved transient absorption difference signal (ΔA) at a specific time, the pump pulses were chopped at 500 Hz and absorption spectra intensities were saved alternately with or without pump pulse. Typically, 4000 pulses excite the samples to obtain the fs-TA spectra at each delay time. The polarization angle between pump and probe beam was set at the magic angle (54.7°) using a Glan-laser polarizer with a half-wave retarder in order to prevent polarization-dependent signals. Cross-correlation *fwhm* in pump-probe experiments was less than 200 fs and chirp of WLC probe pulses was measured to be 800 fs in the 400-800 nm region. To minimize chirp, all reflection optics in the probe beam path and a quartz cell of 2 mm path length were used. After fs-TA experiments, the absorption spectra of all compounds were carefully examined to detect if there were artifacts due to degradation and photo-oxidation of samples. The three-dimensional data sets of ΔA versus time and wavelength were subjected to singular value decomposition and global fitting to obtain the kinetic time constants and their associated spectra using Surface Xplorer software (Ultrafast Systems).

2.4 Preparation of starting materials

2.4.1 Synthesis of 3,4-dialkoxypyrrole[17]

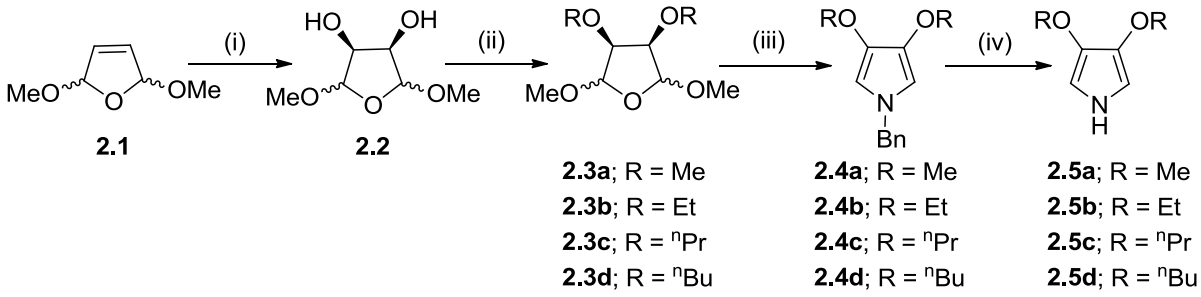

Scheme 2.1 Synthesis of 3,4-dialkoxypyrroles. Reagents and conditions: (i) $KMnO_4$, $MgSO_4$, -5 °C – 0 °C; (ii) (a) R = Me and Et; KOH, R_2SO_4, THF, Reflux, 24 h; (b) R = ^{n}Pr and ^{n}Bu, KOH, RBr, THF, reflux, 24 h; (iii) (a) R = Me and Et, H_2SO_4, H_2O, 80°C, 1 h and R = ^{n}Pr and ^{n}Bu, TFA, H_2O, 80 °C, 2 h; (b) $PhCH_2NH_2$. HCl, NaOAc, $CHCl_3$, RT, 24 h; (iv) Na, liqNH_3, THF, -78°C, 4 h.

2.4.1.1 3,4-Dihydroxy-2,5-dimethoxytetrahydrofuran (2.2)

A solution of 2,5-dimethoxy-2,5-dihydrofuran (**2.1**) (50 mL, 0.41 mol) in ethanol (410 mL) was placed in a two liter, round bottomed flask equipped with a mechanical stirrer, an addition funnel and a thermometer. The reaction was cooled to -5 °C and solution of $KMnO_4$ (65.14 g, 0.41 mol) and $MgSO_4.7H_2O$ (92.38 g, 0.37 mol) in water (1037 mL) was added dropwise slowly to maintain the internal temperature between -5 to 0 °C. The suspension was stirred at room temperature for 4 h, left standing overnight and filtered through a layer of silica gel. The filtrate was concentrated to 100 mL, and extracted with 1-butanol. The extracts was dried over anhydrous sodium sulphate and evaporated, to yield the desired compound **2.2** as pale yellow viscous oil. Yield obtained: 33.5g (50%), reported yield: 58%.

2.4.1.2 General procedure for synthesis of 3,4-dialkoxy-2,5-dimethoxytetrahydrofuran where R = Me and Et (2.3a and 2.3b)

A stirred mixture of **2.2** (30 g, 0.18 mol) and powdered potassium hydroxide (64.66 g, 1.15 mol) in THF (365 mL) was heated at reflux for 1 h. A solution of dimethyl sulphate (51.9 ml, 0.55 mol) in THF (210 mL) was added over 3 h and stirred at reflux condition for 16 h and the reaction was quenched with water (140 mL). After 1 h the mixture was further diluted with more water (840 mL) and extracted with diethyl ether first, and then with dichloromethane for three times. After removal of the solvent, the product **2.3a** was purified

by vacuum distillation at 90 °C under ~1 mmHg pressure. Yield obtained: 27.35 g (78%), reported yield: 90%.

3,4-Diethoxy-2,5-diethoxytetrahydrofuran (2.3b)

3,4-Dihydroxy-2,5-dimethoxytetrahydrofuran (**2.2**) (12.5 g, 76.14 mmol) and diethylsulphate (30 mL, 0.23 mol) were used for reaction. The product **2.3b** was purified by vacuum distillation at 110 °C under ~1 mmHg pressure. Yield: 13.75 g (80%), reported yield: 80%.

2.4.1.3 General procedure for synthesis of 3,4-dialkoxy-2,5-dimethoxytetrahydrofuran where R = ^{n}Pr and ^{n}Bu (2.3c and 2.3d)

A mixture of **2.2** (15 g, 91.37 mmol), KOH (25.64 g, 0.46 mol), n-propyl bromide (33.2 mL, 0.37 mol) and dry THF (40 mL) was heated under stirring for 24 h. Similar workup procedure as described for **2.3a** and **2.3b** was employed. The product was purified by fractional distillation under reduced pressure, to obtain isomeric mixture of 3,4-dipropoxy-2,5-dipropoxytetrahydrofuran (**2.3c**) (20.68 g) as colorless liquid and employed in the next step as such. Yield: 91%.

3,4-Dibutoxy-2,5-dimethoxytetrahydrofuran (2.3d)

3,4-Dihydroxy-2,5-dimethoxytetrahydrofuran (**2.2**) (10 g, 60.92 mmol) and n-butyl bromide (19.70 mL, 0.18 mol) were used for reaction. The product was purified by fractional distillation under reduce pressure, to yield isomeric mixture of 3,4-dibutoxy-2,5-dimethoxytetrahydrofuran (**2.3d**) (14.68 g) as colorless liquid and employed in the next step as such. Yield: 87%.

2.4.1.4 General Procedure for synthesis of N-benzyl-3,4-dialkoxypyrrole

General procedure for hydrolysis of 3,4-dialkoxy-2,5-dimethoxytetrahydrofuran (2.3a and 2.3b)

A solution of **2.3a** (30g, 0.16 mol) in 1M sulphuric acid (25.4 mL) was heated at 85 °C for 30 min during which time a MeOH/H_2O mixture (~7 mL) was distilled at maximum 85 °C distilled head temperature.

General procedure for hydrolysis of 3,4-dialkoxy-2,5-dialkoxytetrahydrofuran (2.3c and 2.3d)

The hydrolysis of water insoluble acetal **2.3c** (4.14 g, 16.65 mmol) was performed in a mixture of CF_3CO_2H (1.28 mL, 16.65 mmol), and H_2O (2.6 mL) for 90 min at 80 °C.

General procedure for synthesis of N-benzyl-3,4-dialkoxypyrroles (2.4a-d)

The residue obtained after hydrolysis was cooled to room temperature and added to a well stirred suspension of benzyl ammonium hydrochloride (112.07 g, 0.78 mol) in water (46.8 mL), sodium acetate (90.85 g, 1.11 mol) and chloroform (936 mL) and stirred for 17 h. The chloroform phase was washed with saturated aqueous sodium bicarbonate solution and passed through anhydrous Na_2SO_4. After removal of the solvent the residue was purified by column chromatography using 10% ethyl acetate in hexane as eluent to afford colorless crystalline product **2.4a** (24 g). Yield obtained: 71%, reported yield: 84%.

N-benzyl-3,4-diethoxypyrrole (2.4b)

3,4-Diethoxy-2,5-diethoxytetrahydrofuran **2.3b** (5 g, 22.70 mmol) was used for reaction. Crude product was purified by silica gel column chromatography by using EtOAc/hexane (5:95) as eluent to gives entitled compound **2.4b** (3.8 g) as colorless liquid. Yield obtained: 68%; ^{1}H NMR (400 MHz, $CDCl_3$), δ (ppm): 7.32-7.25 (m, 3H), 7.08 (d, 2H, *J* = 6.8 Hz), 4.84 (s, 2H), 3.90 (q, 4H, *J* = 6.8 Hz), 1.36 (t, 6H, *J* = 7.2 Hz); LCMS (ESI+): m/z: calculated for $C_{15}H_{20}NO_2$ ($M+H^+$): 246; found: 246.

N-benzyl-3,4-dipropoxypyrrole (2.4c)

3,4-Dipropoxy-2,5-dipropoxytetrahydrofuran **2.3c** (4.1 g, 16.65 mmol) was used for reaction. Crude product was purified by silica gel column chromatography by using hexane as eluent to give entitled compound **2.4c** (2 g) as light yellow liquid. Yield obtained: 44%; ^{1}H NMR (400 MHz, $CDCl_3$), δ (ppm): 7.30-7.24 (m, 3H), 7.08 (d, 2H, *J* = 6.8 Hz), 4.82 (s, 2H), 3.80 (t, 4H, *J* = 6.8 Hz), 1.76 (sex, 4H, *J* = 7.2 Hz), 0.98 (t, 6H, *J* = 7.6 Hz); ^{13}C NMR (100 MHz, $CDCl_3$), δ (ppm): 138.60, 137.15, 128.71, 127.61, 126.98, 104.30, 73.34, 54.11, 22.85, 10.57; LCMS (ESI+): m/z: calculated for $C_{17}H_{24}NO_2$ ($M+H^+$): 274; found: 274.

N-benzyl-3,4-dibutoxypyrrole (2.4d)

3,4-Dibutoxy-2,5-dipropoxytetrahydrofuran **2.3d** (5 g, 18.09 mmol) was used for reaction. Crude product was purified by silica gel column chromatography by using hexane as eluent to obtain the desired compound **2.4d** (3 g) as light yellow liquid. Yield obtained: 55%; ^{1}H NMR (400 MHz, $CDCl_3$), δ (ppm): 7.30-7.25 (m, 3H), 7.08 (d, 2H, *J* = 6.8 Hz), 4.83 (s, 2H), 3.83 (t, 4H, *J* = 6.8 Hz), 1.73 (quin, 4H, *J* = 8 Hz), 1.44 (sex, 4H, *J* = 7.6 Hz), 0.94 (t, 6H, *J* = 7.6 Hz); LCMS (ESI+): m/z: calculated for $C_{19}H_{28}NO_2$ ($M+H^+$): 302; found: 302.

2.4.1.5 General procedure for the synthesis of 3,4-dialkoxypyrrole (2.5a-d)

N-benzyl-3,4-dimethoxypyrrole (**2.4a**) (20 g, 0.09 mol) in anhydrous THF (100 mL) was added drop wise to a solution of sodium (4.44 g, 0.19 mol) in liquid ammonia (~600 mL) at -78 °C and reaction was allowed to run for 4 h. After the blue color faded, aqueous ammonium chloride was carefully added. Upon evaporation of ammonia, the aqueous phase was extracted with dichloromethane and passed through anhydrous Na_2SO_4. Subsequent evaporation of solvent under reduce pressure led to desired 3,4-dimethoxypyrrole **2.5a** (11.6 g) as colorless crystalline solid, which can be stored at -20 °C for months. Yield obtained: (99%), reported yield: 94%.

3,4-diethoxypyrrole (2.5b)

N-benzyl-3,4-diethoxypyrrole **2.4b** (1 g, 4.07 mmol) was used for reaction. Compound **2.5b** (500 mg) was obtained as white crystalline solid. Yield: 79%. Characterizations data matched exactly with previously reported compound.[18]

3,4-dipropoxypyrrole (2.5c)

N-benzyl-3,4-dipropoxypyrrole **2.4c** (1 g, 3.66 mmol) was used for reaction. Compound **2.5c** (545 mg) was obtained as greyish liquid. Yield: 81%; ^{1}H NMR (400 MHz, $CDCl_3$), δ (ppm): 7.08 (br s, 1H), 6.21 (d, 2H, *J* = 3.2 Hz), 3.83 (t, 4H, *J* = 8 Hz), 1.78 (sex, 4H, *J* = 7.2 Hz), 1.00 (t, 6H, *J* = 7.6 Hz); ^{13}C NMR (100 MHz, $CDCl_3$), δ (ppm): 137.39, 100.74, 73.15, 22.71, 10.49; LCMS (ESI+): m/z: calculated for $C_{10}H_{18}NO_2$ ($M+H^+$): 184; found: 184; Elemental Anal. Calcd for $C_{10}H_{17}NO_2$: C, 65.54; H, 9.35; N, 7.64. Found: C, 65.47; H, 9.31; N, 7.56.

3,4-dibutoxypyrrole (2.5d)

N-benzyl-3,4-dibutoxypyrrole **2.4d** (3 g, 9.95 mmol) was used for reaction. Compound **2.5d** (1.95 g) was obtained as colorless liquid. Yield: 93%; ^{1}H NMR (400 MHz, $CDCl_3$), δ (ppm): 7.04 (br s, 1H), 6.21 (d, 2H, *J* = 3.2 Hz) 3.87 (t, 4H, *J* = 6.8 Hz), 1.73 (quin, 4H, *J* = 8 Hz), 1.46 (sex, 4H, *J* = 7.6 Hz), 0.95 (t, 6H, *J* = 7.2 Hz); ^{13}C NMR (100 MHz, $CDCl_3$), δ (ppm): 137.68, 100.98, 71.50, 31.67, 19.34, 14.00; LCMS (ESI+): m/z: calculated for $C_{12}H_{22}NO_2$ ($M+H^+$): 212; found: 212; Elemental Anal. Calcd for $C_{12}H_{21}NO_2$: C, 68.21; H, 10.02; N, 6.63. Found C, 68.31; H, 10.12; N, 6.56.

2.4.2 Synthesis of dimethyl-3,4-dimethoxypyrrole-2,5-dicarboxylate (2.11)[18]

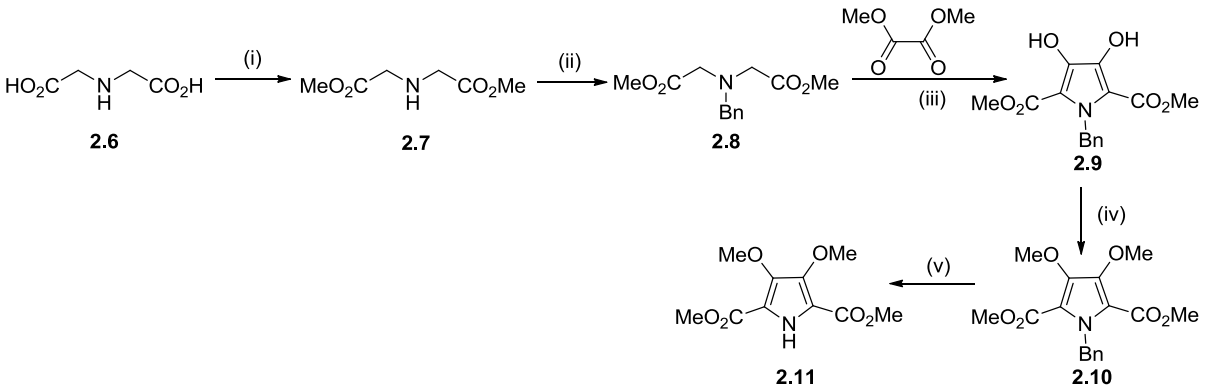

Scheme 2.2 Synthesis of dimethyl-3,4-dimethoxypyrrole-2,5-dicarboxylate. Reagents and conditions: (i) conc. H_2SO_4, MeOH, reflux, overnight. (ii) $BnNH_2$, $NaHCO_3$, DMF, 40 °C, 16 h. (iii) NaOMe, MeOH, reflux, 18 h, then AcOH. (iv) K_2CO_3, acetone, Me_2SO_4, reflux, 18 h. (v) TFA, anisole, conc. H_2SO_4, 90 °C, 30 min.

2.4.2.1 Synthesis of dimethyl iminodiacetate (2.7)[19]

Iminodiacetic acid (**2.6**) (70 g, 0.53 mol) was taken in dry MeOH (350 mL) and conc. H_2SO_4 (30 mL) was added dropwise to dissolve **2.6**. The reaction mixture was refluxed for overnight and after cooling, $CHCl_3$ (~250 mL) was added. Then the reaction mixture was neutralized with aqueous solution of sat. $NaHCO_3$. The $CHCl_3$ layer was separated and aqueous layer was extracted with $CHCl_3$ (~100 mL) for three times. Combined organic layer was passed through anhydrous Na_2SO_4 and evaporated under reduce pressure gives desired **2.7** (62.13 g) as pale yellow liquid. Yield obtained: 73%.

2.4.2.2 Synthesis of dimethyl-N-benzyliminodiacetate (2.8)

A mixture of dimethyl iminodiacetate (**2.7**) (62.14 g, 0.38 mol), benzyl bromide (45.8 mL, 0.39 mol) and $NaHCO_3$ (77.82 g, 0.93 mol) were taken in dry DMF (190mL). The reaction mixture was stirred at 40 °C until CO_2 evolution ceased (16 h). Then water (~200 mL) was added to the reaction mixture and extracted with toluene (3 ×~100 mL). The combined organic layer was passed through anhydrous Na_2SO_4 and evaporated under reduced pressure. The crude yellow oil was further purified by vacuum distillation to provide desired **2.8** (90.7 g) as colorless oil. Yield obtained: 95%, yield reported: 91%.

2.4.2.3 Synthesis of dimethyl 3,4-dihydroxy-N-benzylpyrrole-2,5-dicarboxylate (2.9)

Diemthyl N-benzyliminodiacetate (2.8) (90 g, 0.36 mol) and dimethyloxalate (42.36 g, 0.36 mol) were added to methoxide solution prepared from Na (17.95 g, 0.78 mol) and dry MeOH (200 mL) under nitrogen. The reaction mixture was stirred with mechanical stirrer at reflux temperature for 18 h. Glacial acetic acid was added to adjust the pH to 5 and mixture was poured into ice water (~1 L). The precipitate was filtered, washed with water and dried in air. The crude product was recrystallized from acetone to give desired **2.9** (52.89 g) as colorless crystalline solid. Yield obtained: 48%, reported yield: 58%.

2.4.2.4 Synthesis of dimethyl 3,4-dimethoxy-N-benzylpyrrole-2,5-dicarboxylate (2.10)

A mixture of **2.9** (16g, 52.40 mmol), dimethylsulphate (9.90 mL, 0.10 mol) and K_2CO_3 (36 g, 0.26 mol) were taken in dry acetone (650 mL) under nitrogen atmosphere. The reaction mixture was stirred vigorously with a heavy duty mechanical stirred under reflux condition for 18 h. After completion of reaction, cooled reaction mixture was filtered, washed with acetone and the filtrate was evaporated under reduce pressure. The crude reaction mixture was purified by silica gel column chromatography using EtOAc/hexane (2:8) as eluent to obtain the desired **2.10** (16.74 g) as colorless crystalline solid. Yield obtained: 96%, reported yield: 82%.

2.4.2.5 Synthesis of dimethyl 3,4-dimethoxy-N-benzylpyrrole-2,5-dicarboxylate (2.11)

A solution of **2.10** (20 g, 60 mmol), trifluoroacetic acid (72 mL), anisole (8.5 mL, 78 mmol) and 98% H_2SO_4 (2.2 mL) was heated at 90 °C for 30 min. After reaction, TFA was distilled under reduce pressure and can be used in further batches. The residue was dissolved in DCM

(~150 mL) and after placing on ice bath aq. $NaHCO_3$ (~400 mL) was added slowly to neutralize the solution. Then, DCM layer was separated and aqueous layer was extracted with DCM (4 × ~50 mL). Combined organic layer was passed through anhydrous Na_2SO_4 and concentrated in vacuum. The crude reaction mixture was washed with hexane to obtain a greyish solid. The crude product was further purified by silica gel column chromatography by using EtOAc/hexane (1:1) as eluent to obtain the desired **2.11** (11.76 g) as white crystalline solid. Yield obtained: 81%, reported yield: 71%.

2.4.3 Synthesis of 3,4-di(methylthio)pyrrole (2.16)[20]

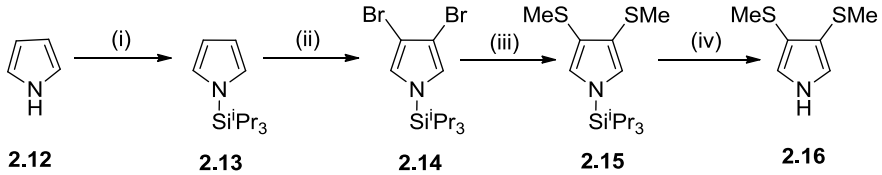

Scheme 2.3 Synthesis of 3,4-di(methylthio)pyrrole. Reagents and conditions: (i) NaH, THF, then $(^iPr)_3SiCl$, 0 °C, 1 h. (ii) NBS, THF, -78 °C, 1h. (iii) n-BuLi, THF, -78 °C, 8 h then Me_2S_2, 1 h. (iv) TBAF, THF, RT, 1 h.

2.4.3.1 Synthesis of N-triisopropylsilylpyrrole (2.13)[21]

Pyrrole (**2.12**) (5 ml, 72.07 mmol) was added slowly dropwise to a suspension of sodium hydride (60% dispersion in oil, 3.17 g, 79.27 mmol) in THF (125 mL) under nitrogen at 0 °C. The reaction mixture was allowed to stirred at same temperature for 1.5 h. Then, triisopropylsilyl chloride was added slowly at 0 °C and reaction mixture was allowed to stir for additional 1.5 h. Then reaction mixture was poured into ice-water and extracted with diethyl ether. Combined organic layer was washed with water and then with brine solution. Organic layer was passed through anhydrous Na_2SO_4 and evaporated under reduced pressure to obtain a yellow oily liquid. This compound was purified by fractional distillation at 80 °C under ~1mmHg to obtain the entitled compound **2.13** (15.76 g) as colorless liquid. Yield obtained: 97%.

2.4.3.2 Synthesis of 3,4-dibromo-N-triisopropylsilylpyrrole (2.14)[22]

N-triisopropylsilylpyrrole (**2.13**) (5 g, 22.38 mmol) in THF (25 mL) was cooled to -78 °C under nitrogen atmosphere and NBS (8 g, 44.94 mmol) in THF (100 mL) was added slowly over 1 h. After addition was over, reaction mixture was allowed to stir for additional 1 h and then allowed to warm to room temperature. Solvent was evaporated under reduced pressure,

washed with hexane for several time and filtered. Filtrate was evaporated to dryness under reduced pressure to get the crude product as pinkish white solid. The crude product was purified by silica gel column chromatography by using hexane as eluent to obtain the desired compound (**2.14**) along with some other mono and tribrominated product as white crystalline solid. Therefore, pure **2.14** (6.76 g) was obtained by recrystallization of above column chromatographed product with pentane at -20 °C, as white crystalline solid. Yield obtained: 79%, yield reported: 78%.

2.4.3.3 Synthesis of 3,4-di(methylthio)-N-triisopropylsilylpyrrole (2.15)[20]

A solution of n-BuLi in hexane (79 mL of 1.6 M, 0.126 mol) was added to a stirred solution of **2.14** (6 g, 15.73 mmol) in anhydrous THF (170 mL) at -78 °C under nitrogen atmosphere. The reaction mixture was stirred at -78 °C for 8 h and then Me_2S_2 (14.16 mL, 0.16 mol) was added and reaction mixture was left to reach room temperature and stirred for 30 min. The reaction mixture was quenched with water and extracted with DCM. The combined organic layer was washed with water and brine, dried over anhydrous Na_2SO_4. Organic layer was evaporated under reduced pressure and purified by column chromatography by using EtOAc/hexane (1:19) to provide entitled product **2.15** (4.55 g) as colorless liquid, which crystallized to colorless solid at low temperature. Yield obtained: 92%, yield reported: 76%.

2.4.3.4 Synthesis of 3,4-di(methylthio)pyrrole (2.16)[20]

A solution of **2.15** (4.55 g, 14.42 mmol) was taken in THF (30 mL) under nitrogen atmosphere. Then TBAF (15.9 mL of 1M solution in THF, 15.90 mmol) was added to the reaction mixture and allowed to stir for 1 h at room temperature. Water was added to the reaction mixture, extracted with diethyl ether and the organic layer was washed with water followed by brine and evaporated under reduced pressure and purified by silica gel column chromatography using EtOAc/hexane (1:9) as eluent to obtain the desired product **2.16** (1.93 g) as white crystalline solid and can be stored at -20 °C for months. Yield obtained: 84%, yield reported: quantitative.

2.4.4 Synthesis of 5,10,15,20-tetraphenylporphyrin (2.18)[23]

Freshly distilled pyrrole **2.12** (7.5 ml, 0.108 mol) and freshly distilled benzaldehyde **2.17** (10 mL, 0.089 mol) were taken in propanoic acid (360 mL). The reaction mixture was refluxed for 1 h and allowed to cool to room temperature. Then the reaction mixture was filtered by

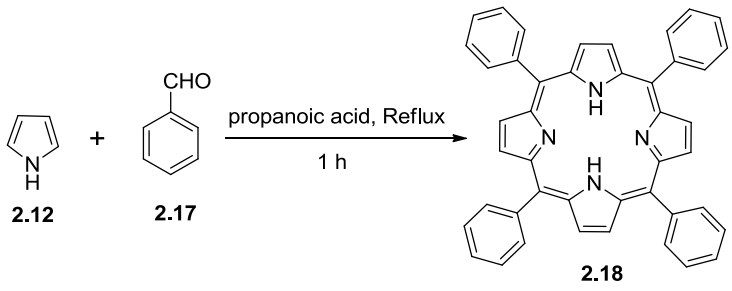

Scheme 2.4 Synthesis of 5,10,15,20-tetraphenylporphyrin.

suction filtration and washed with hot water followed by methanol to leave **2.18** as purple crystalline solid. Product was further purified by silica gel column chromatography by using $CHCl_3$ as eluent to yield pure **2.18** (2.92 g). Yield obtained: 19%, reported yield: 20%.

2.4.5 Synthesis of 5,10,15,20-tetraarylporphyrins (2.12-2.24)[24]

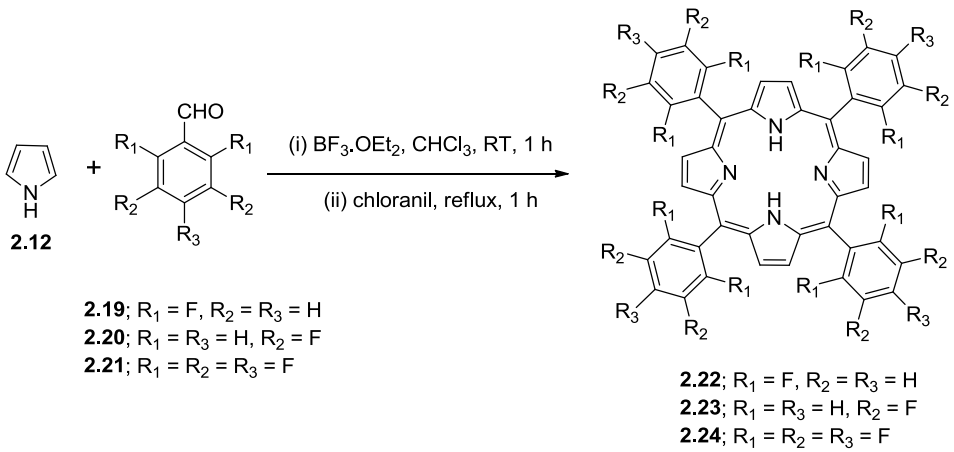

Scheme 2.5 Synthesis of *meso*-tetraarylporphyrins by Lindsey method.

General procedure for synthesis of tetraarylporphyrins

Pyrrole **2.12** (10 mmol) and arylaldhydes **2.19-2.21** (10 mmol) were taken in dry $CHCl_3$ (1 L) and purged with nitrogen for 30 min. Then $BF_3.OEt_2$ (3.3 mmol) was added and stirred at room temperature for 1 h. After that, *p*-chloranil (7.5 mmol) was added to the reaction mixture and refluxed for 1 h. The reaction mixture was quenched with triethylamine and solvent was evaporated under reduced pressure. Crude product was purified by silica gel column chromatography by using $CHCl_3$/hexane (1:1) as eluent to obtain pure porphyrins (**2.22-2.24**) as purple solid.

5,10,15,20-tetra(2,6-difluorophenyl)porphyrin (2.22)

2,6-Difluorobenzaldhyde (**2.19**) (228 µL, 2.1 mmol) and pyrrole (146 µL, 2.1 mmol) were used for reaction. Yield obtained: 135 mg (34%); reported yield: 46%.

5,10,15,20-tetra(3,5-difluorophenyl)porphyrin (2.23)

3,5-Difluorobenzaldhyde (**2.20**) (231 µL, 2.1 mmol) and pyrrole (146 µL, 2.1 mmol) were used for reaction. Yield obtained: 109 mg (27%).

5,10,15,20-tetra(pentafluorophenyl)porphyrin (2.24)

Pentafluorobenzaldhyde (**2.20**) (315 µL, 2.55 mmol) and pyrrole (177 µL, 2.55 mmol) were used for reaction. Yield obtained: 75 mg (12%); reported yield: 25%.

2.4.6 Synthesis of Zn(II)-5,10,15,20-tetraarylporphyrins (2.15-2.28)

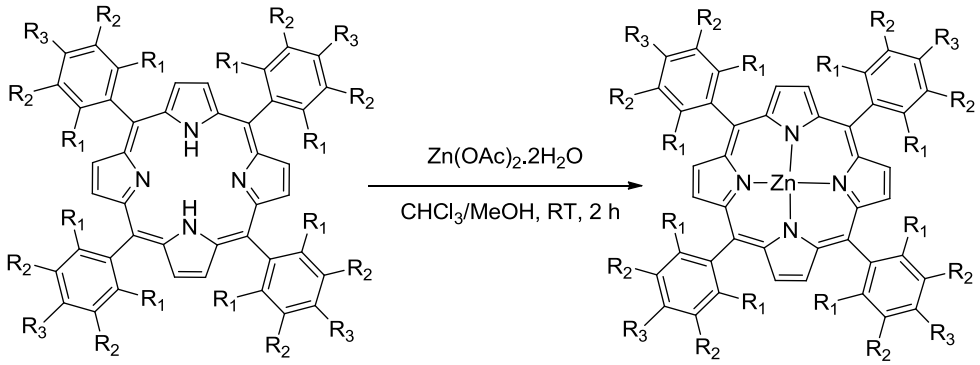

2.18; $R_1 = R_2 = R_3 = H$
2.22; $R_1 = F$, $R_2 = R_3 = H$
2.23; $R_1 = R_3 = H$, $R_2 = F$
2.24; $R_1 = R_2 = R_3 = F$

2.25; $R_1 = R_2 = R_3 = H$
2.26; $R_1 = F$, $R_2 = R_3 = H$
2.27; $R_1 = R_3 = H$, $R_2 = F$
2.28; $R_1 = R_2 = R_3 = F$

Scheme 2.6 Synthesis of Zn(II)tetraarylpophyrins.

General procedure for synthesis of Zn(II)-5,10,15,20-tetraarylporphyrins (2.15-2.28)

Porphyrins (1 eq.) were taken in $CHCl_3$ solution and $Zn(OAc)_2.2H_2O$ (10 eq.) solution in methanol was added. The reaction mixture was stirred for 2 h. Solvent was evaporated under reduce pressure and dissolved in $CHCl_3$, followed by washing with water. Organic layer was passed through anhydrous Na_2SO_4 and evaporated under reduced pressure. Crude product was purified by neutral alumina flash column by using $CHCl_3$/hexane solvent systems to obtain desired pure Zn(II)-porphyrins.

Zn(II)-5,10,15,20-tetraphenylporphyrin (2.25)

Porphyrin **2.18** (100 mg, 0.16 mmol) and $Zn(OAc)_2.2H_2O$ (357 mg, 1.6 mmol) were used for reaction and purified by using $CHCl_3$ as eluent. Yield obtained: 101 mg (93%).

Zn(II)-5,10,15,20-tetra(2,6-difluorophenyl)porphyrin (2.26)

Porphyrin **2.22** (69 mg, 0.09 mmol) and $Zn(OAc)_2.2H_2O$ (200 mg, 0.9 mmol) were used for reaction and purified by using $CHCl_3$/hexane (1:1) as eluent. Yield obtained: 74 mg (quant).

Zn(II)-5,10,15,20-tetra(3,5-difluorophenyl)porphyrin (2.27)

Porphyrin **2.23** (107 mg, 0.14 mmol) and $Zn(OAc)_2.2H_2O$ (310 mg, 1.4 mmol) were used for reaction and purified by using $CHCl_3$/hexane (1:1) as eluent. Yield obtained: 112 mg (97%).

Zn(II)-5,10,15,20-tetra(pentafluorophenyl)porphyrin (2.28)

Porphyrin **2.24** (24 mg, 0.025 mmol) and $Zn(OAc)_2.2H_2O$ (55 mg, 0.25 mmol) were used for reaction and purified by using $CHCl_3$/hexane (1:1) as eluent. Yield obtained: 24 mg (94%).

2.4.7 Synthesis of 2,3,7,8,12,13,17,18-octaalkoxyporphyrins[18]

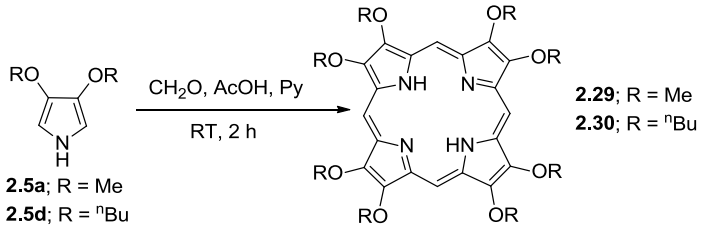

Scheme 2.7 Synthesis of octaalkoxyporphyrins.

General procedure for synthesis of octaalkoxyporphyrins

To a mixture of glacial AcOH (58 mL) and pyridine (18 mL), was added 37% aqueous formaldehyde (0.78 mL, 9.68 mmol) and dimethoxypyrrole (**2.5a**) (1.05 g, 8.26 mmol). A gentle stream of oxygen was passed through the reaction mixture for 2 h and stored uncovered for several days (3-7 days). Solvent was evaporated under reduced pressure and silica gel was added to make slurry, which was extracted continuously with hot toluene vapor by Soxhlet extraction technique for overnight. Toluene was evaporated and the crude product was purified by silica gel column chromatography using $CHCl_3$ as eluent to obtain pure

octamethoxyporphyrin (**2.29**) (130 mg) as purple crystalline solid. Yield obtained: 12%, reported yield: 20%.

2,3,7,8,12,13,17,18-octabutoxyporphyrin (2.30)

3,4-dibutoxypyrrole (2.5d) (450 mg, 2.13 mmol) and 37% HCHO (202 µL, 2.50 mmol) were used for reaction. The product was purified by $CHCl_3$/hexane (1:1) as eluent to obtain the titled compound **2.30** (65 mg) as reddish brown solid. Yield: 14%; m.p.: 141.5 °C; ^{1}H NMR (400 MHz, $CDCl_3$), δ (ppm): 10.08 (s, 4H), 4.98 (t, 16H, *J* = 6.4 Hz) 2.24 (quin, 16H, *J* = 3.2 Hz), 1.91 (sex, 16H, *J* = 7.6 Hz), 1.19 (t, 24H, *J* = 7.2 Hz), -4.41 (br s, 2H); ^{13}C NMR (100 MHz, $CDCl_3$), δ (ppm): 143.51, 94.51, 75.67, 32.83, 19.77, 14.29; HRMS (ESI+): m/z: calculated for $C_{52}H_{79}N_4O_8$ ($M+H^+$): 887.5892; found: 887.5898; Elemental Anal. Calcd for $C_{52}H_{78}N_4O_8$: C, 70.40; H, 8.86; N, 6.32. Found C, 70.56; H, 8.81; N, 6.25.

2.4.8 Synthesis of Zn(II)-2,3,7,8,12,13,17,18-octasubstitutedporphyrins

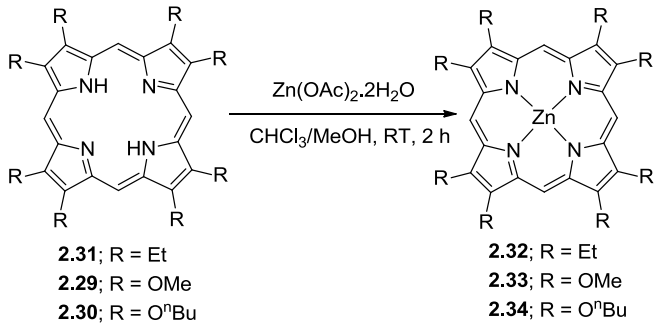

Scheme 2.8 Synthesis of Zn(II)-2,3,7,8,12,13,17,18-octasubstituted porphyrins.

These complexes were prepared following the same procedure for the synthesis of Zn(II)-5,10,15,20-tetraarylporphyrins described above.

Zn(II)-2,3,7,8,12,13,17,18-octaethylporphyrin (2.32)

Porphyrin **2.31** (100 mg, 0.19 mmol) and $Zn(OAc)_2.2H_2O$ (417 mg, 1.9 mmol) were used for reaction and purified by using $CHCl_3$ as eluent. Yield obtained: 105 mg (92%).

Zn(II)-2,3,7,8,12,13,17,18-octamethoxyporphyrin (2.33)

Porphyrin **2.29** (100 mg, 0.18 mmol) and $Zn(OAc)_2.2H_2O$ (399 mg, 1.8 mmol) were used for reaction and purified by using $CHCl_3$ in presence of 0.2% MeOH as eluent. Yield obtained: 85 mg (77%).

Zn(II)-2,3,7,8,12,13,17,18-octabutoxyporphyrin (2.34)

Porphyrin **2.30** (20 mg, 0.023 mmol) and $Zn(OAc)_2.2H_2O$ (99 mg, 0.45 mmol) were used for reaction and purified by using $CHCl_3$ in presence of 0.2% MeOH as eluent. Yield obtained: 16 mg (73%); m.p.: 158.6 °C; ^{1}H NMR (400 MHz, $CDCl_3$), δ (ppm): 10.12 (s, 4H), 4.99 (t, 16H, *J* = 6.4 Hz), 2.26 (quin, 16H, *J* = 4 Hz), 1.93 (sex, 16H, *J* = 7.6 Hz), 1.20 (t, 24H, *J* = 7.6 Hz); ^{13}C NMR (100 MHz, $CDCl_3$), δ (ppm): 144.37, 141.11, 95.31, 75.58, 32.91, 19.81, 14.32; HRMS (ESI+): m/z: calculated for $C_{52}H_{77}N_4O_8Zn$ ($M+H^+$): 949.5027; found: 949.5034; Elemental Anal. Calcd for $C_{52}H_{76}N_4O_8Zn$: C, 65.70; H, 8.06; N, 5.89. Found C, 65.87; H, 8.16; N, 5.81.

2.5 Summary

A brief account of various solvents, chemicals used in the synthesis and different spectrometers and other physical and computational methods employed for characterization in our investigation, is given in this chapter. Syntheses of the already reported compounds along with some new compounds by following reported procedure, which are employed as starting materials for the dissertation work, were also described here.

2.6 References

1. Armarego, W. L. F.; Chai, C. In *Purification of laboratory chemicals*; sixth edition, Elsevier, Burlington**, 2003**.
2. Sessler, J. L.; Mozaffari, A.; Johnson, M. R. *Org. Synth*. **1992**, *70*, 68.
3. Williams, A. T. R.; Winfield, S. A.; Miller, J. N. *Analyst* **1983**, *108*, 1067.
4. (a) Zhang, X. F.; Huang, J.; Xi, Q.; Wang, Y. *Aust. J. Chem.* **2010**, *63*, 1471. (b) Mathai, S.; Smith, T. A.; Ghiggino, K. P. *Photochem. Photobiol. Sci*. **2007**, *6*, 995.
5. SAINT, version 6.45 /8/6/03, Bruker AXS, **2003**.
6. Sheldrick, G. M. *SADABS*, Program for Empirical Absorption Correction of Area Detector Data, University of Göttingen, Germany, **1997**.
7. Sheldrick, G. M. *SHELXS-97* and *SHELXL-97*, Programs for the Solution and Refinement of Crystal Structures, University of Göttingen, Germany, **1997**.
8. (a) Spek, A. L. *PLATON*, *A Multipurpose Crystallographic Tool*, Utrecht University, Utrecht, The Netherlands, **2002**; (b) Spek, A. L. *J. Appl. Cryst.* **2003**, *36*, 7.
9. Oxford Diffraction (**2008**). CrysAlis CCD and CrysAlis RED. Versions 1.171.33.55. Oxford Diffraction Ltd, Yarnton, Oxfordshire, England.

10. K. A. Connors, *Binding Constants*, John Wiley & Sons: New York, **1987**, 148.
11. Z. D. Hill, P. MacCarthy, *J. Chem. Educ.* **1986**, *63*, 162.
12. Lakowicz, J. R. *Principle of Fluorescence Spectroscopy (3rd Edition)*, Publishers: Springers, **2006**, 282-283.
13. (a) Hunter, C. A.; Meah, M. N.; Senders, J. K. M. *J. Am. Chem. Soc*. **1990**, *112*, 5773. (b) Hill, A. V. *J. Physiol. London* **1910**, *40*, IV.
14. a) Kumar, R. S. S.; Rao, S. V.; Giribabu, L.; Rao, D. N. *Chem. Phys. Lett*. **2007**, *447*, 274. (b) Swain, D.; Singh, R.; Singh, V. K.; Krishna, N. V.; Giribabu, L.; Rao, S. V. *J. Mater. Chem. C* **2014**, *2*, 1711. (c) Sarma, T.; Panda, P. K.; Anusha, P. T.; Rao, S. V. *Org. Lett*. **2010**, *13*, 188. (d) Rao, S. V.; Prashant, T. S.; Sarma, T.; Panda, P. K.; Swain, D.; Tewari, S. P. *Chem. Phys. Lett*. **2011**, *514*, 98. (e) Anusha, P. T.; Swain, D.; Hamad, S.; Giribabu, L.; Prashant, T. S.; Tewari, S. P.; Rao, S. V. *J. Phys. Chem. C* **2012**, *116*, 17828. (f) Swain, D.; Anusha, P. T.; Sarma, T.; Panda, P. K.; Rao, S. V. *Chem. Phys. Lett*. **2013**, *580*, 73.
15. Sheik Bahae, M.; Said, A. A.; Wei, T. H.; Hagan, D. J.; Van Stryland, E. W. *IEEE J. Quant. Electron*. **1990**, *26*, 760.
16. (a) Anusha, P. T.; Swain, D.; Hamad, S.; Giribabu, L.; Prashant, T. S.; Tewari, S. P.; Rao, S. V. *J. Phys. Chem. C* **2012**, *116*, 17828. (b) Swain, D.; Anusha, P. T.; Sarma, T.; Panda, P. K.; Rao, S. V. *Chem. Phys. Lett*. **2013**, *580*, 73.
17. Merz, A.; Meyer, T. *Synthesis* **1999**, 94.
18. Merz, A.; Schropp, R.; Dötterl, *Synthesis* **1995**, 795.
19. Jongkees, A. *Recl. Trav. Chim. Pays-Bas*. **1908**, *27*, 287.
20. Sugiura, K.-i.; Ushiroda, K.; Johnson, M. T.; Miller, J. S.; Sakata, Y. *J. Mater. Chem*. **2000**, *10*, 2507.
21. Arikawa, Y.; Nishida, H.; Kurasawa, O.; Hasuoka, A.; Hirase, K.; Inatomi, N.; Hori, Y.; Matsukawa, J.; Imanishi, A.; Kondo, M.; Tarui, N.; Hamada, T.; Takagi. T.; Takeuchi, T.; Kajino, M. *J. Med. Chem*. **2012**, *55*, 4446.
22. (a) Bray, B. L.; Mathies, P. H.; Naef, R.; Solas, D. R.; Tidwell, T. T.; Artis, D. R.; Muchowski, J. M. *J. Org. Chem*. **1990**, *55*, 6317. (b) Shum, P. W.; Kozikowski, A. P. *Tetrahedron Lett*. **1990**, *31*, 6785.
23. Alder, A. D.; Longo, F. R.; Finarelli, J. D.; Goldmacher, J.; Assour, J.; Korsakoff, L. *J. Org. Chem*. **1967**, *32*, 476.
24. Lindsey, J. S.; Wagner, R. W. *J. Org. Chem*. **1989**, *54*, 828.

2.7 Representative NMR spectra

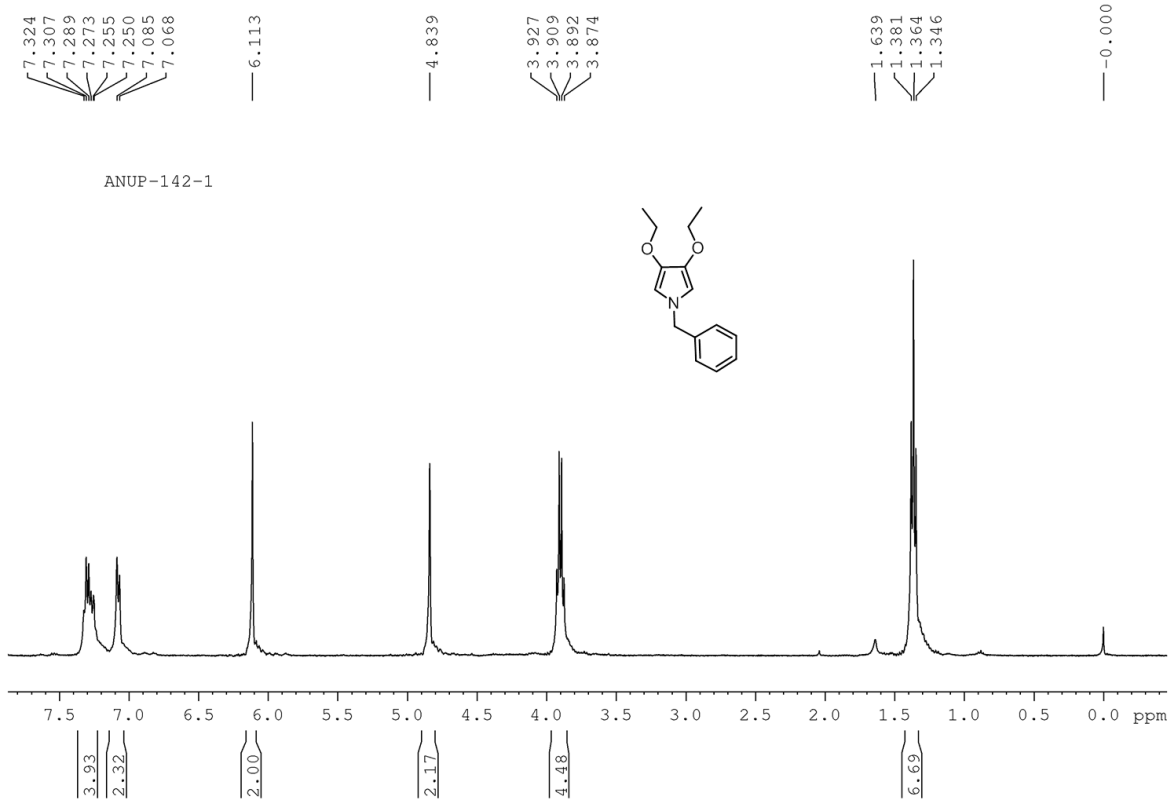

Figure 2.1 ^{1}H NMR spectrum of **2.4b** in $CDCl_3$.

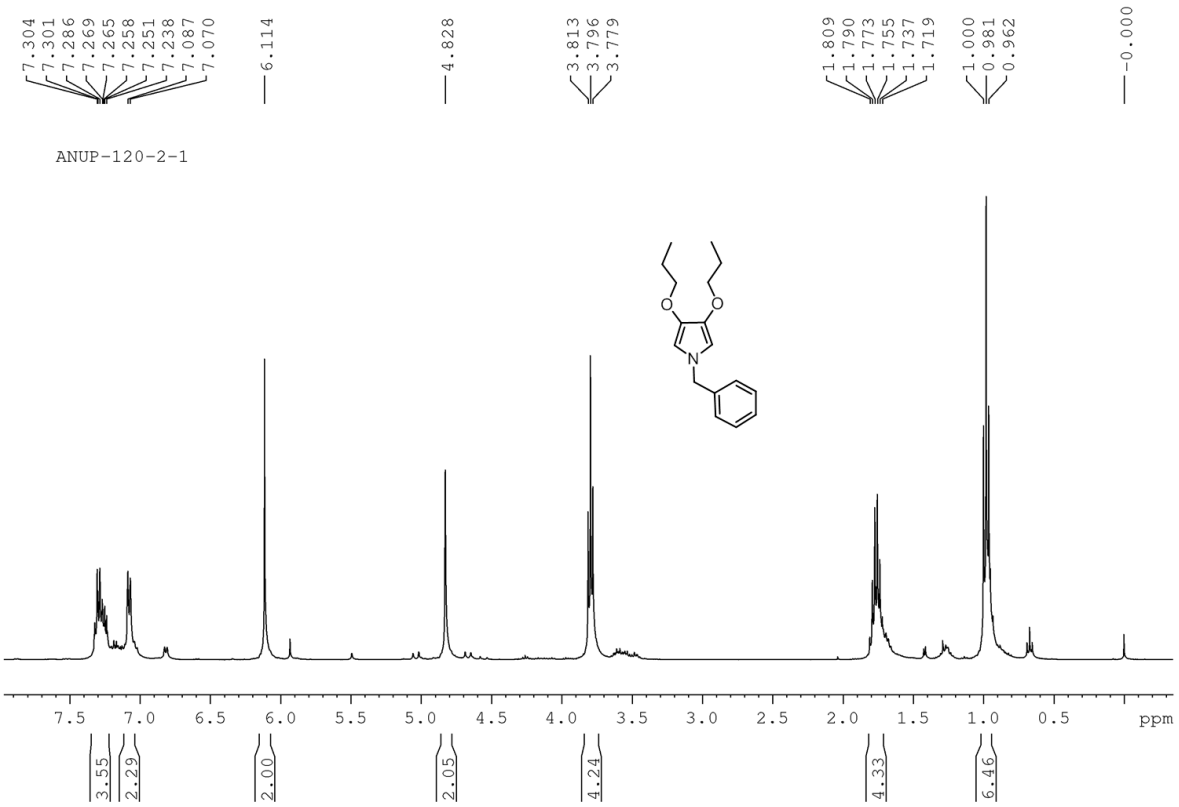

Figure 2.2 ^{1}H NMR spectrum of **2.4c** in $CDCl_3$.

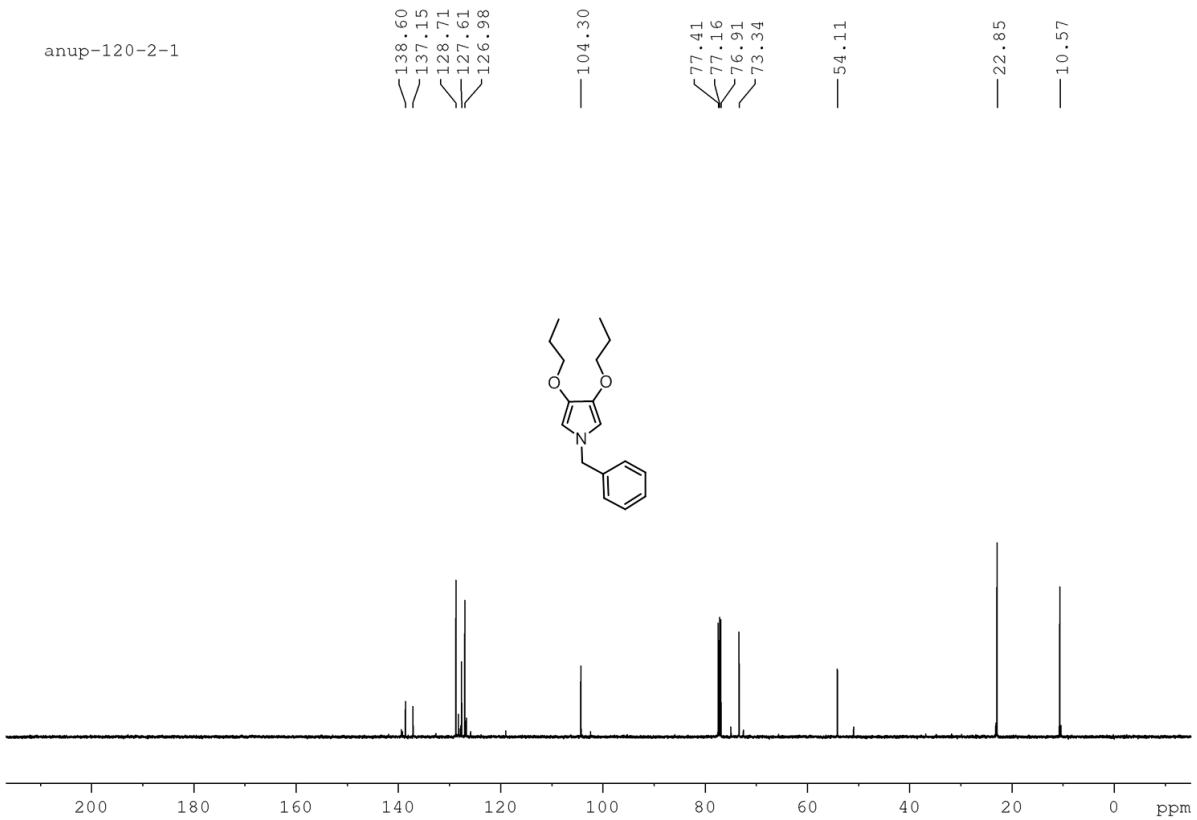

Figure 2.3 ^{13}C NMR spectrum of **2.4c** in $CDCl_3$.

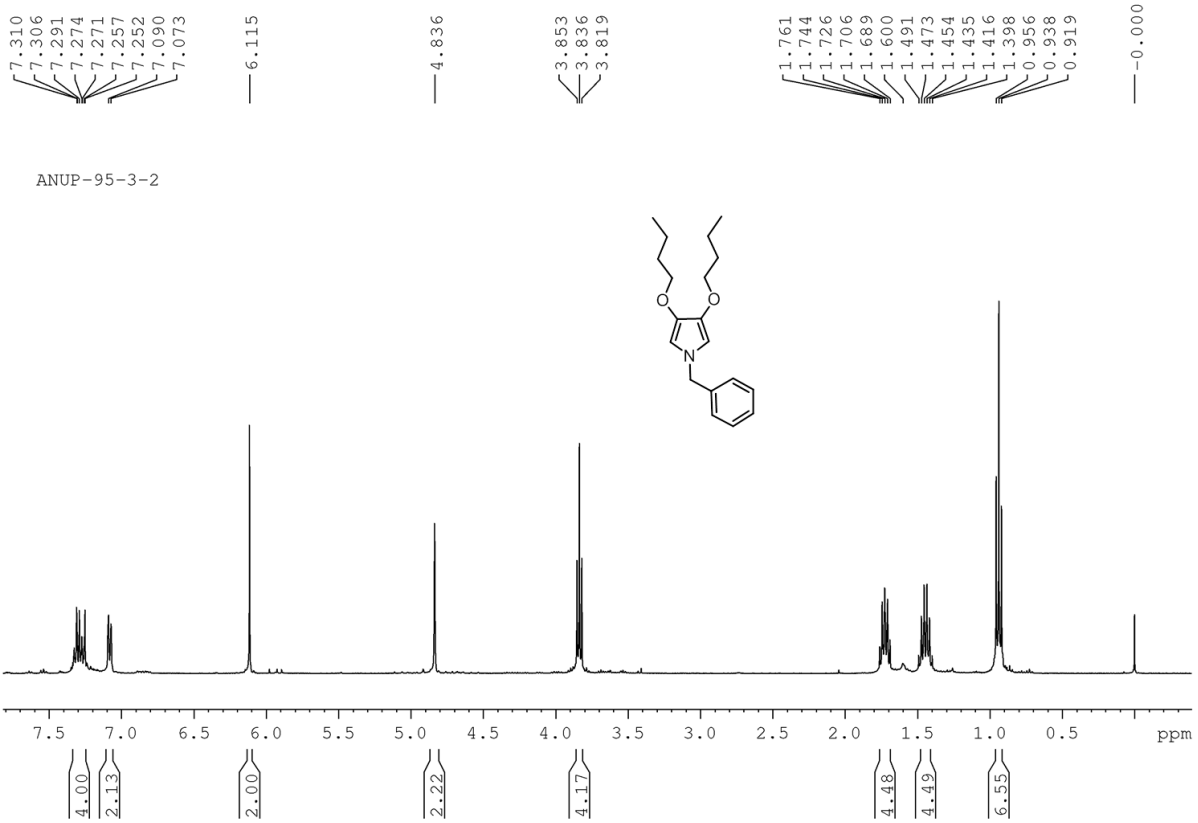

Figure 2.4 ^{1}H NMR spectrum of **2.4d** in $CDCl_3$.

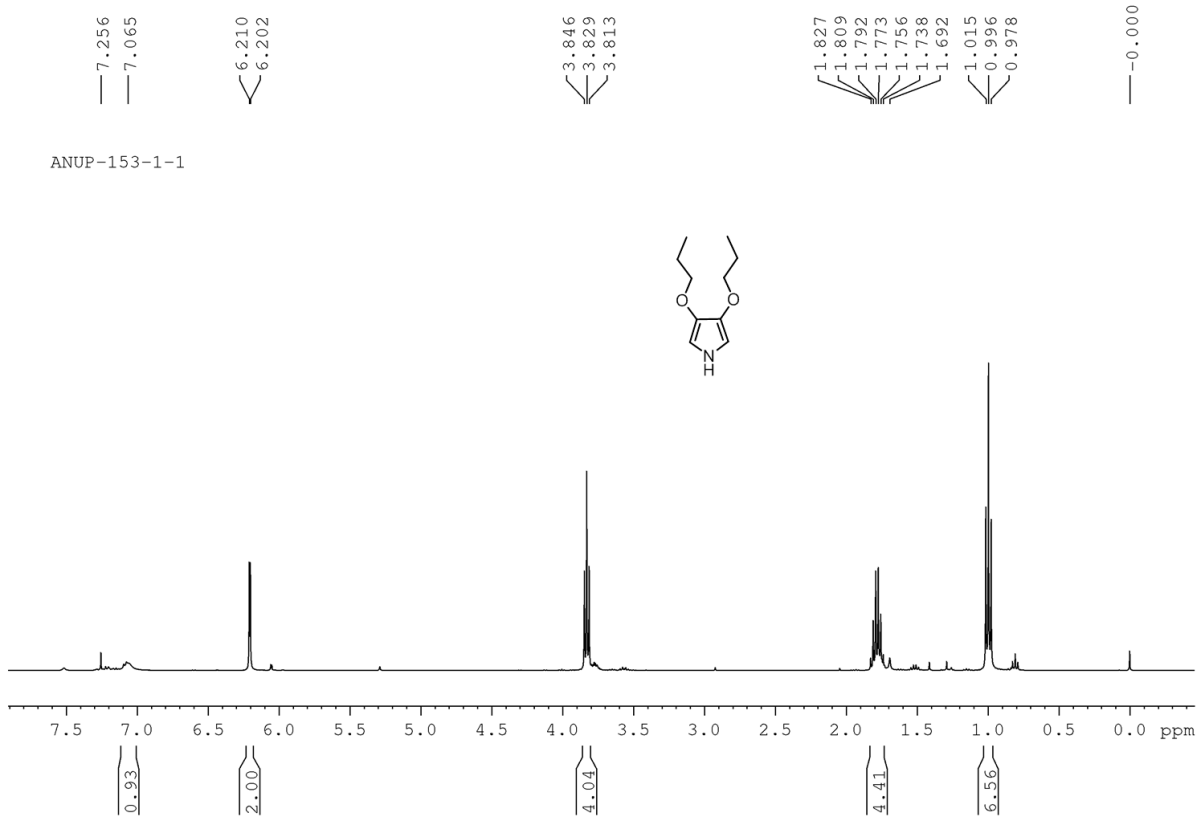

Figure 2.5 ^{1}H NMR spectrum of **2.5c** in $CDCl_3$.

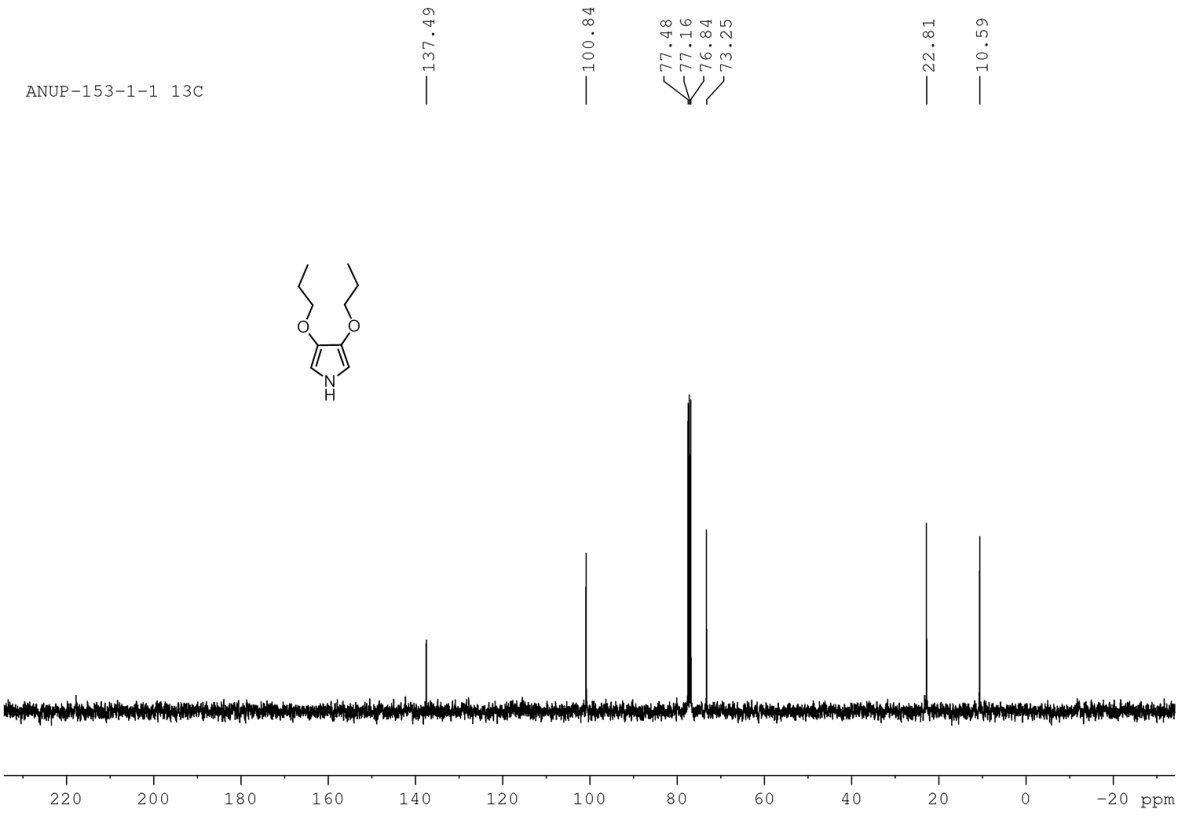

Figure 2.6 ^{13}C NMR spectrum of **2.5c** in $CDCl_3$.

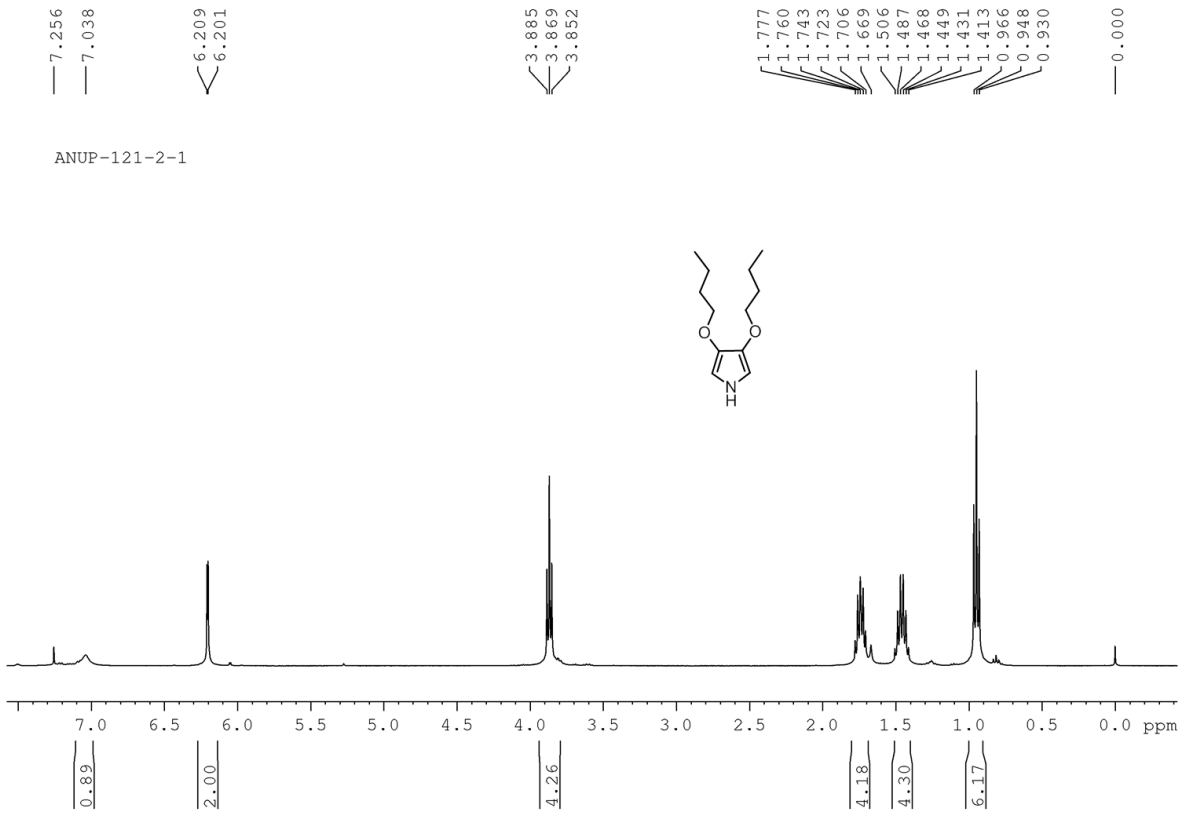

Figure 2.7 ^{1}H NMR spectrum of **2.5d** in $CDCl_3$.

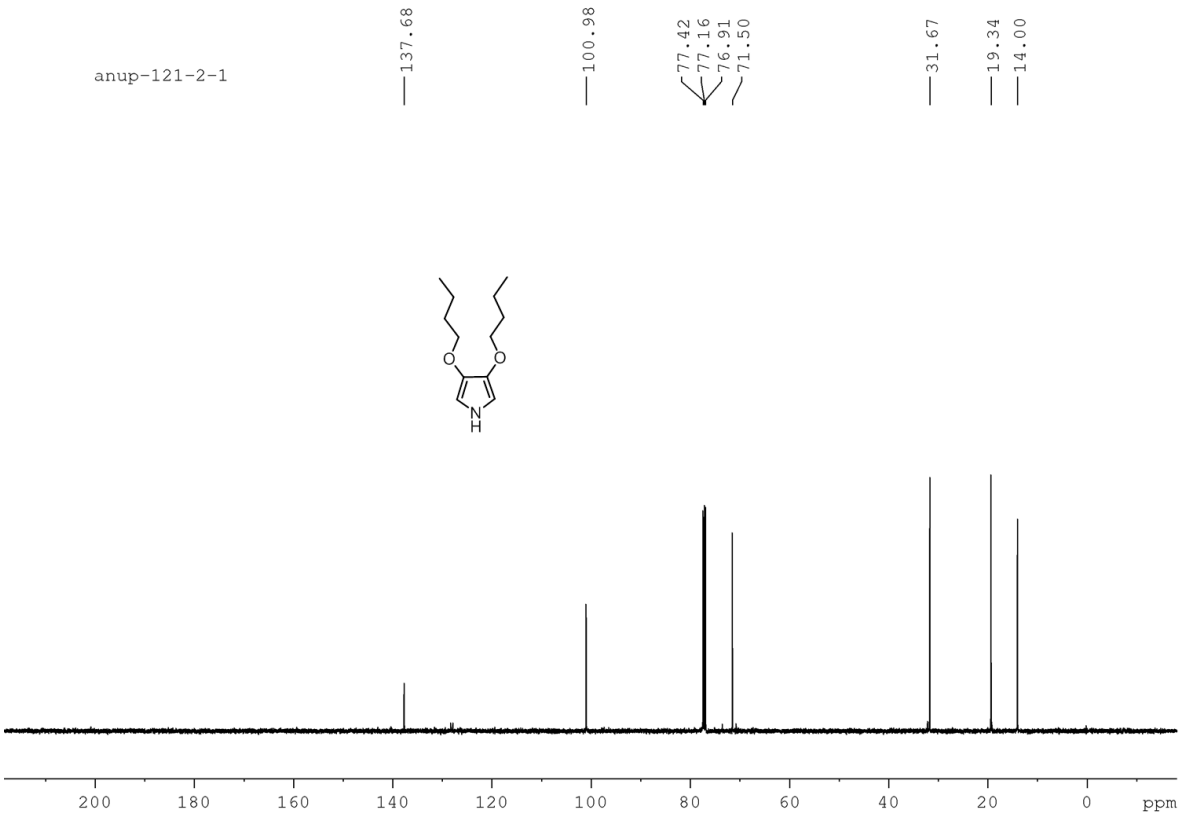

Figure 2.8 ^{13}C NMR spectrum of **2.5d** in $CDCl_3$.

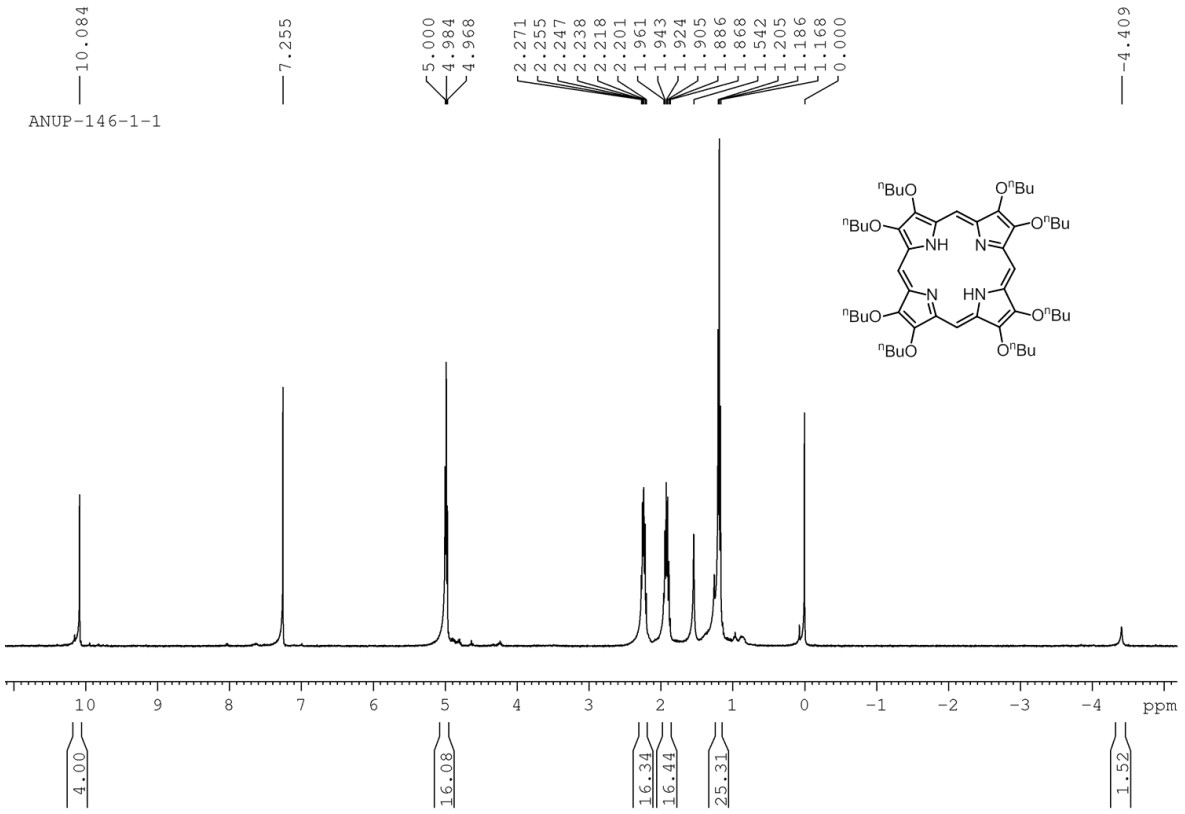

Figure 2.9 ^{1}H NMR spectrum of **2.30** in $CDCl_3$.

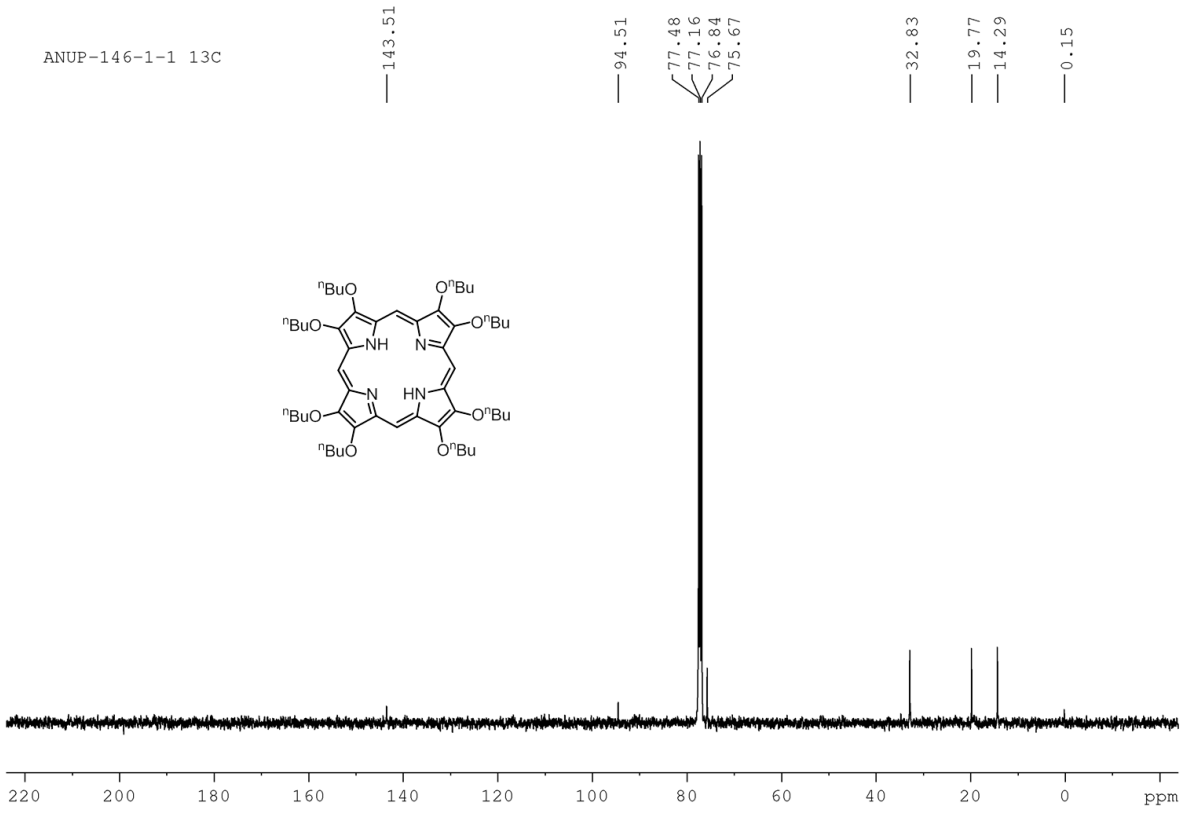

Figure 2.10 ^{13}C NMR spectrum of **2.30** in $CDCl_3$.

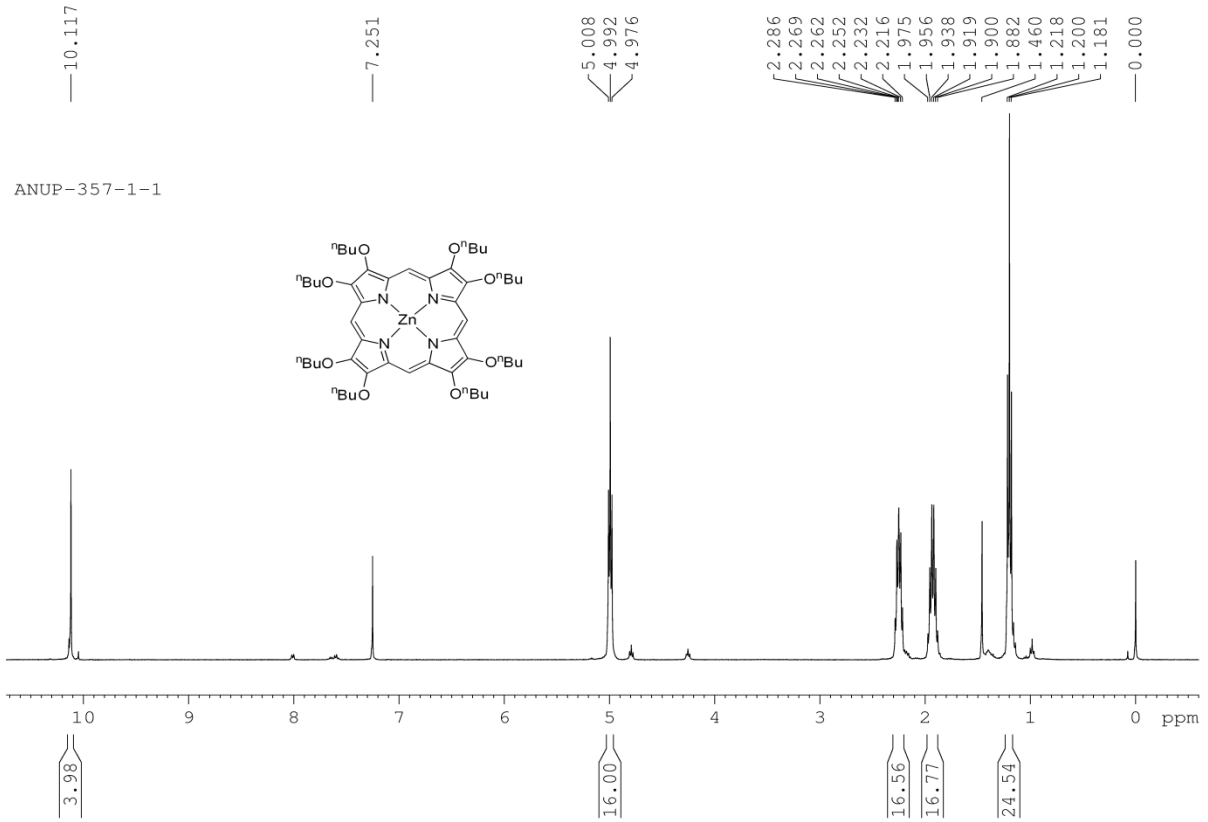

Figure 2.11 ^{1}H NMR spectrum of **2.34** in $CDCl_3$.

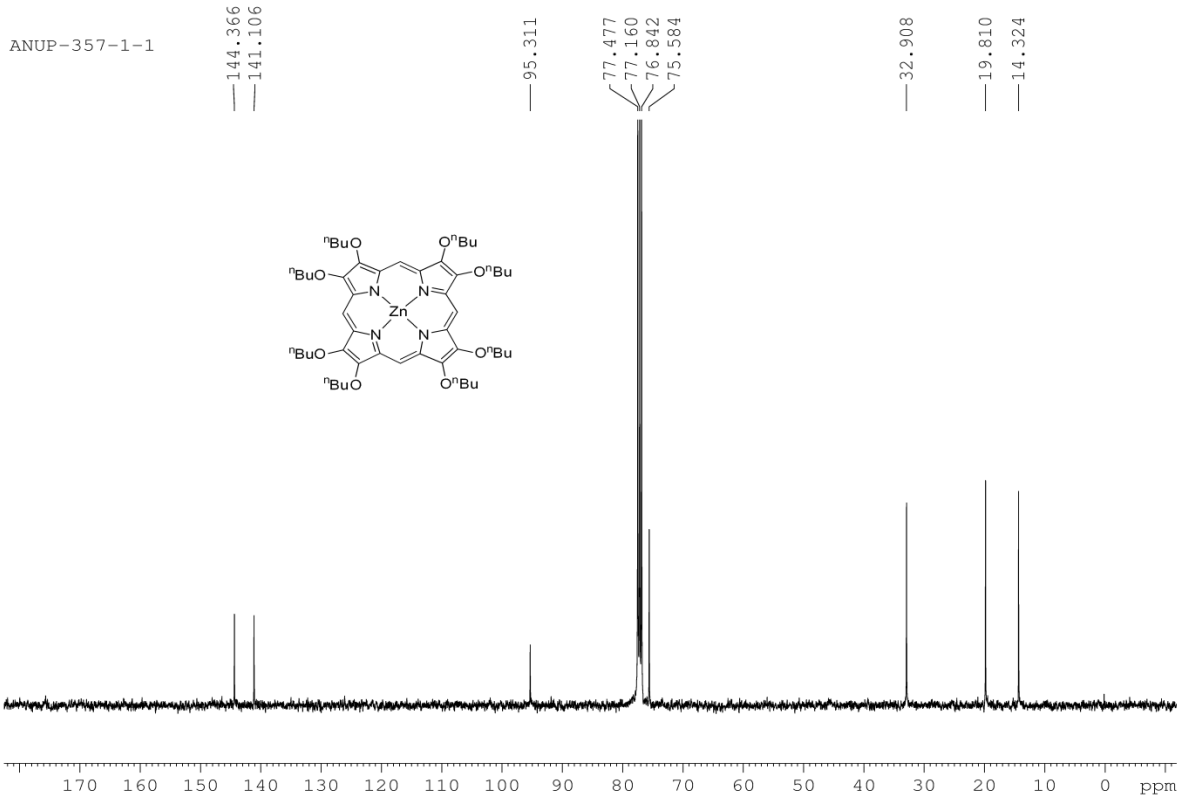

Figure 2.12 ^{13}C NMR spectrum of **2.34** in $CDCl_3$.

CHAPTER 3

Alkoxyporphyrins: Enhanced Sensitivity Towards Nitroexplosives

3.1 Introduction

Detection of explosive and its residues are crucial for homeland security, environmental cleanliness and military issues.[1] It is estimated that approximately 60 to 70 million mines are deployed worldwide and according to International Committee of the Red Cross that ~26,000 people are involved in landmine incident annually and ~40% of them are children.[2] Recently, use of modern explosives, cased in plastic make their detection much challenging, following conventional methods. Further, environmental cleaning of explosive residues is very important because of its prolonged toxicity effect on human.[3] Also, recent rise in global terror concern, has forced scientists to develop methods to detect explosives, which should be highly sensitive, low cost and convenient for field deployment.[4]

3.1.1 Current methodologies for explosive detection

There are many sensing methods to detect explosives, which has their own advantages, as well as, disadvantages, making them inappropriate for versatile application. For example, metal detectors are widely used for explosive detection, but modern day explosives are cased in plastic, rendering this method obsolete for their detection. Similarly, canines are most sensitive method to detect explosive residues because of its larger olfactory system[5] and suitable for field as well as fixed sites, such as airport, however dogs are surprisingly expensive to train and easily get fatigue, making widespread use challenging. Ionization mass-spectrometry (IMS) can be highly sensitive for detection and identification of explosive residue from cloth, skin and particular objects, but positive identification involves comparative analysis of laboratory standard and can target few specific explosive compounds only.[6] Other disadvantages with IMS are it requires careful instrumentation and limited portability, hindering its broader application. Backscattering X-ray screening provides high resolution images of luggage and persons to detect objects similar to bomb but unable to detect explosive residues and hence, has limited portability for field deployment. Infrared technologies have been developed to detect landmine; however poor specificity and false positive signal limit their broader use.[4a] Raman spectroscopy is promising for standoff detection of explosive by identifying specific vibrational characters, but it works best for white solids, however it takes longer time for analysis.[7] Colorimetric techniques are most popular for detection of explosive residues, dependent on the chemical reaction between explosive molecules and an indicator, which provides visual color change. Kits based on these statistics are available from many commercial source, but it requires higher amount of

explosive residues for optimal response and also their inability to detect explosive vapor signature, limit their applicability. Therefore, in present scenario development of effective method still remains as a challenging job for scientists.

3.1.2 Fluorescence quenching methodology

Fluorescence quenching method is opposite to colorimetric method because in presence of explosive, dimming of fluorescence intensity of fluorophore occurs. Generally, it involves photoinduced electron transfer from electron rich fluorophore to relatively electron deficient analyte. A simple MO diagram depicting how photo excited electron in SOMO* of

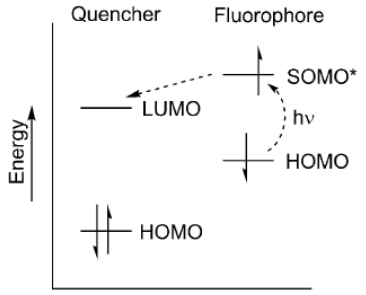

Figure 3.1 Energy level diagram for photoinduced electron transfer leading to fluorescence quenching.

fluorophore can donate to relatively low lying LUMO of electron deficient explosive molecule (Figure 3.1). This SOMO* and LUMO energy gap in vibrational relaxation level is the driving force for photoinduced electron transfer process. Fluorescence quenching methods have certain advantages compared to other conventional methods due to its fast real time response, requires very less amount of compound, reversibility, and ultra-low detection limit. Also, it can be encased with small handheld device, making it appropriate for field detection.

3.1.3 Type of explosives

Designing of sensor for explosives is dependent on their diverse nature, and hence poses challenge in their detection. For example, nitroaromatics like TNT, DNT and picric acid (PA) are challenging targets for vapor phase sensors, but their low vapor pressures (VP_{TNT} = 1 ppb) overcome by their adhesiveness to surface, therefore, making their sensing achievable. Also, electron poor nitro-aromatics effectively form π-π stacking interaction with electron rich fluorophore, thereby leading to their detection by fluorometric method. On the other hand, aliphatic nitro-organics, such as 2,3-dimethyl-2,3-dinitrobutane (DMNB), is legally used as taggent in plastic bonded explosives, exhibits high vapor pressure, which can be

detect by IMS and trained dog easily. Due to absence of aromatic ring in DMNB, it forms weak interaction with π-system of fluorophore, hence making its detection challenging by fluorescence quenching method. Similarly, absence of strong π-π stacking due to the lack of aromatic ring and low vapor pressure, make detection challenging by current method for

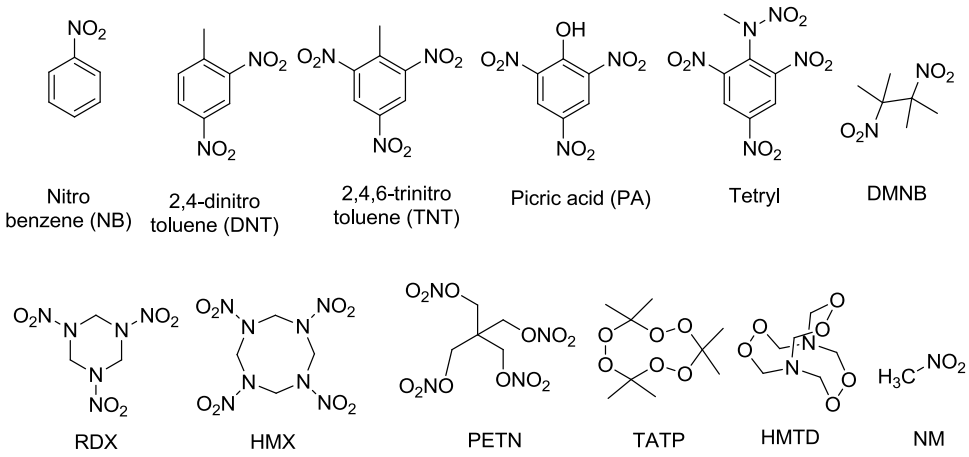

Figure 3.2 Compound of interest for explosive detection.

RDX, HMX and PETN, commonly used for military purpose. Organic peroxides like TATP and HMTD, are easily synthesized form inexpensive materials and are widely used for homemade explosives, highly sensitive to friction, temperature and more powerful than military explosives. Although lack of aromaticity make their detection challenging by fluorometric sensing method, but their strong oxidisable nature suggests electron transfer reaction may be a suitable approach for their sensing. Notably, most of the fluorescence quenching based sensors concentrate on TNT and its decomposition product DNT's vapor signature, because explosive compositions available worldwide, generally contains TNT.[1]

3.1.4 Conjugated organic polymer based fluorescence sensors

Most of the work on explosive sensing by fluorescent quenching assay was done on fluorescent conjugated polymer (**CP**) due to its enhanced sensitivity arising from effective exciton transfer, throughout the conjugated polymeric chain. For the sake of brevity, we will try to highlight some important achievement by organic polymers. Modified poly(phenyleneethynylene) (PPEs) and poly(phenylenevinylene) (PPVs) are most widely studied CP for explosive sensing, due to favorable π-π interaction with electron poor nitroaromatics and effective exciton transfer. The pioneering PPE for explosive detection was pentiptycene-derived phenylene-ethynylene polymers **3.1**.[8] The pentiptycene groups provide bulk to minimize self-quenching and increases porosity leading to higher selectivity towards

TNT. Similarly, triphenylene containing PPEs and dibenzochrysene based PPEs **3.2** exhibited higher sensitivity towards TNT arising from their longer excited state lifetime compared to

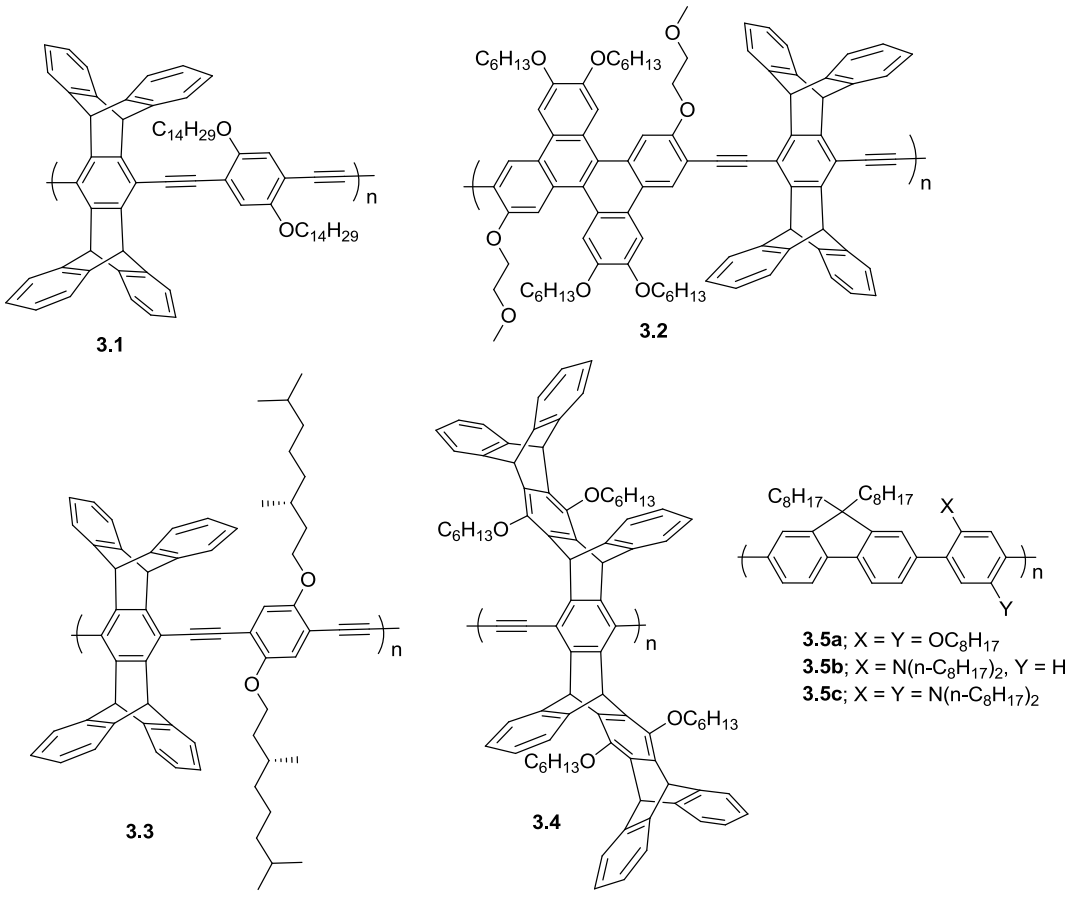

Figure 3.3 Conjugated polymers for explosive sensing.

PPEs.[9] Further, a copolymer consisting of bulky monomer and chiral monomers **3.3** exhibited high sensitivity owing to extension of exciton migration into 3D polymer chain.[10] A class of poly(*p*-phenylenebutadiynylenes) (PPD) **3.4** was utilized for explosive sensing, which revealed high sensitivity towards TNT in solution and solid state (50% in 1 sec), and can be attributed to the enhanced porosity arising from rigid 3D scaffold, leading to significant improvement in response time.[11] Polyphenylenes with twisted backbone (**3.5a-c**), were also used to increase sensitivity towards DMNB by increasing SOMO* energy levels with quenching efficiencies as high as K_{SV} = 9 M^{-1}.[12] Notably, the pentiptycene-conjugated polymer has been fabricated onto the tip of an optical fiber bundle as a semi-selective nitroaromatic sensor.[13] This sensor primarily detects the more volatile DNT vapor from land mine with fast response time (200 ms). Nomadics Inc. has fabricated and commercialized a landmine detector by employing this technology, currently in use by NATO force for field application.[14]

3.1.5 Conjugated inorganic polymer based fluorescence sensors

Polysilanes and polymetallols are highly fluorescent, most extensively studied among inorganic conjugated polymers.[4b] Polysilanes are highly fluorescent and involve σ-σ* delocalization along Si-Si chains confining conjugation along the chain, thus provides exciton migration similar to conjugated organic polymers.[4b] Structurally rigid fluoroalkylated polysilane **3.6**, shows high sensitivity both in solution (K_{SV} = 0.84-4.15 × 10^4 M^{-1} for PA, TNB, DNT and DNB) and thin films.[15] Exceptional sensitivity arises from polysilane

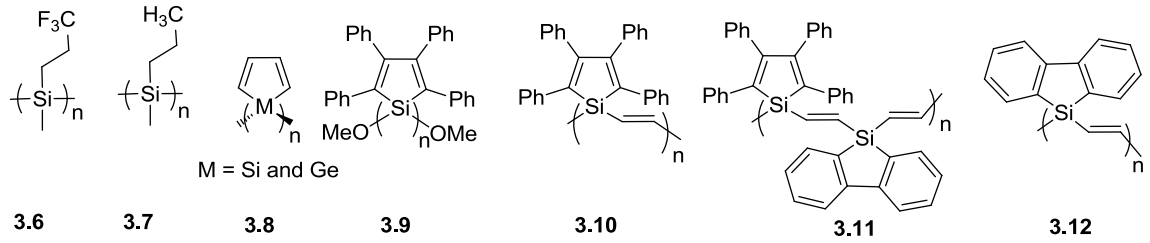

Figure 3.4 Inorganic conjugated polymers employed for explosive sensing.

endowed with hundreds of Si-atom and each of which capable of binding with quencher molecules. In addition, higher sensitivity observed for fluoro-alkylated analogue **3.6** compared to alkylated analogs **3.7**, due to additional fluorinated side chain capable of stabilizing the HOMO and LUMO, thus easing electron transfer process. Similar to ploysilanes, polymetallols are also highly fluorescent and capable of σ-σ* delocalization along polymer backbone. Fluorescence quenching was observed for polymetallols, both in solution and thin film with sensitivity upto 50 ppb of TNT after 1 min exposure.[16] Initial work on polytetraphenyl-1,1-silole **3.9** by Trogler and coworkers, involved high sensitivity towards TNT, DNT and NB (K_{SV} = 4 × 10^3 M^{-1}), even in presence of common environment pollutants, thereby reducing false positive alarm.[17] Further, the study of more extended conjugated polymer by replacing Si-Si bond with stronger Si-C bonds (silicon-vinylene functionalities) (**3.10**-**3.12**), indicates the latter retains almost all properties of polysilanes.[18] These molecules showed higher sensitivity towards TNT (K_{SV} ≈ 1 × 10^4 M^{-1}) compared to analogous polymetallols, which arise from stronger interaction of nitroaromatics with silicon center, leading to more efficient electron transfer in inner sphere. Finally, in order to test the possibility of applying these polymers in detection of explosives, polymer solution was spread on filter paper and dried. When irradiated with UV light, quenching leads to dark spot on the filter paper in presence of explosive analyte. They have reported detection limit by this method as low as 5 ng for TNT and PA and 10-20 ng for DNT. One of their studied polymer

could visually detect under UV light for RDX, HMX and Tetryl (200 pg), highlighting importance of this method.[19]

3.1.6 Single molecule based fluorescence sensors

Small molecule fluorophores have similar prospects for detection strategy, by virtue of simple synthesis, diverse pathway for fluorescence quenching and ability to detect wide range of explosive molecules. The principal difference between polymeric and small molecule based detection lies in the physical mechanism of fluorophore quenching and the absence of excitonic migration, leading to quenching of fluorescence in ratiometric manner. However,

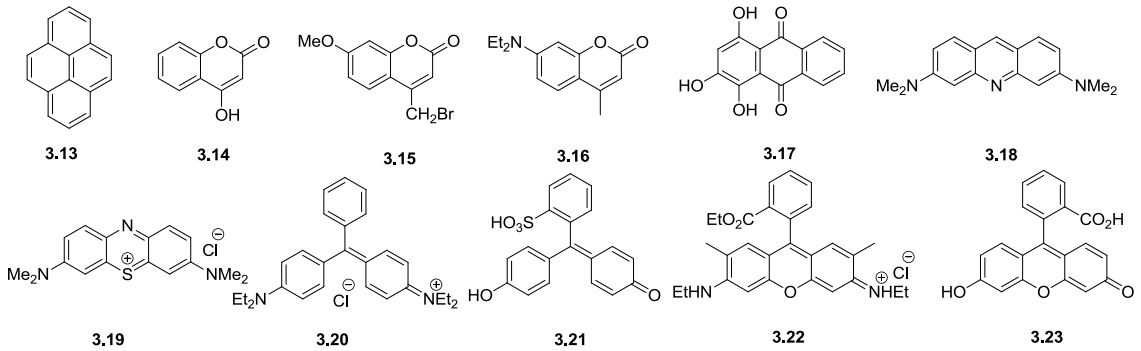

Figure 3.5 Some single molecule fluorophores studied by McGuffin and coworker.

fluorescence quenching of pyrene **3.13** is widely used to detect nitrated compounds but fluorophore with reduced toxicity and oxygen sensitivity would be more desirable. A series of organic fluorophores, including coumarins (**3.15-16**), purpurin **3.17**, acridine orange **3.18**, methylene blue **3.19**, rhodamine 6G **3.22**, malachite green **3.20**, phenol red **3.21** and fluorescein **3.23** were studied for their reduced toxicity compared to pyrene.[20] Fluorescence quenching efficiencies were studied with nitrobenzene and 4-nitrotoluene, showed comparable quenching efficiencies (K_{SV} = 50-140 M^{-1}) to that of pyrene (K_{SV} = 300 M^{-1}) and all fluorophores exhibited higher selectivity towards nitroaromatics, measured by Stern-Volmer constant ratio of common interferences, benzoic acid and nitrobenzene *vs* fluorophores (QS = $K_{SV(NT)}/K_{SV(BZA)}$). Notably, these fluorophores exhibited good fluorescence quenching towards nitromethane, with collisional quenching pathways predominating the quenching process. Mosoporous thin film in organically modified silica with bright pyrene **3.13** exhibits excimer emission for visual and rapid detection of nitroaromatics.[21] The enhanced sensitivity arises from more porous matrix of the modified silica. Inorganic fluorophore like Zn(salicylaldimine) complexes (**3.24-25**) exhibited modest quenching efficiencies towards DMNB and DNT (K_{SV} = 2-10 M^{-1}).[22] Also, unique quenching

responses of Zn(salicylaldimine) complexes led to their organization into a solution phase sensor array for discrimination of nitroaromatics.[23] The dipyrenylamidecalix[4]arene-[15]crown-5 (**3.26**) was used for colorimetric and fluorometric detection of nitrated

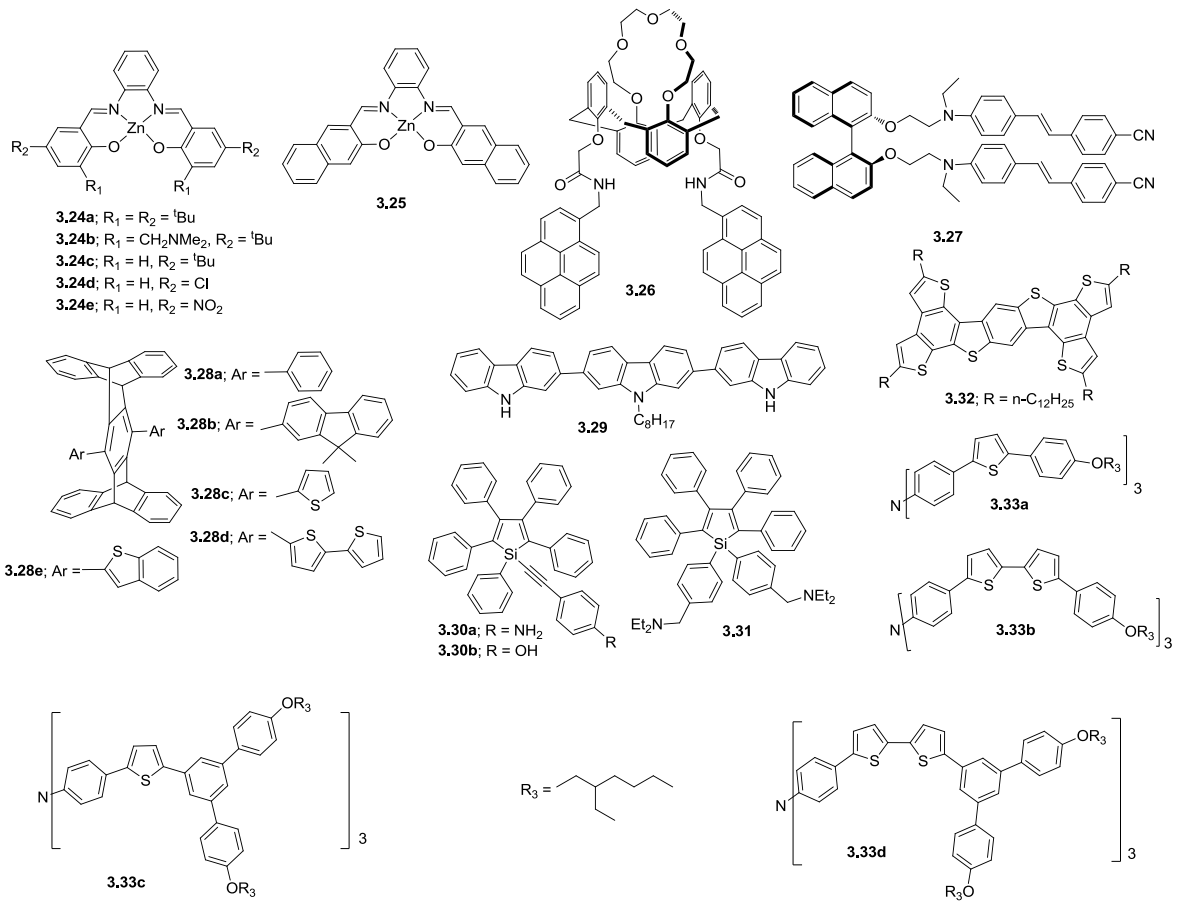

Figure 3.6 Examples of single molecule fluorophores for explosive sensing.

explosives, displayed higher quenching efficiencies for TNT and TNB with detection limit as low as 1 ppb, in acetonitrile solution.[24] Drop casted film of binapthyl derivative, functionalized with donor-acceptor substituted trans-stilbene **3.27** exhibited higher quenching efficiencies for DNT (91% quenching in 10 min) compared to TNT (72% quenching), owing to higher vapor pressure of former.[25] Also, a series of highly fluorescent 1,4-diarylpentiptycenes **3.28a-e** were also studied, which showed quenching of emission with the addition of NB, 2,4-DNT, TNT, 1-nitronaphthalene and DMNB both in DCM solution and embedded in polyurethane films towards explosive vapors.[26] A linear 2,7-linked carbazole trimer **3.29** was used to prepare nanofibrils, which form nanoporous entangled fibril networks.[27] The blue fluorescence of the film was efficiently quenched by TNT (70% in 60 sec) and DNT (50% in 10 sec) vapors. Further, the same sensing film can be recovered by heating at 50 °C in vacuum for 10 min, indicating its reusability and appropriateness for

onsite explosive detection. Similar to polysilole, terminal alkyne, 1-ethynylpentaphenylsiloles **3.30** showed aggregation (THF/H_2O 1:9) induced intense fluorescence at 500 nm, and the

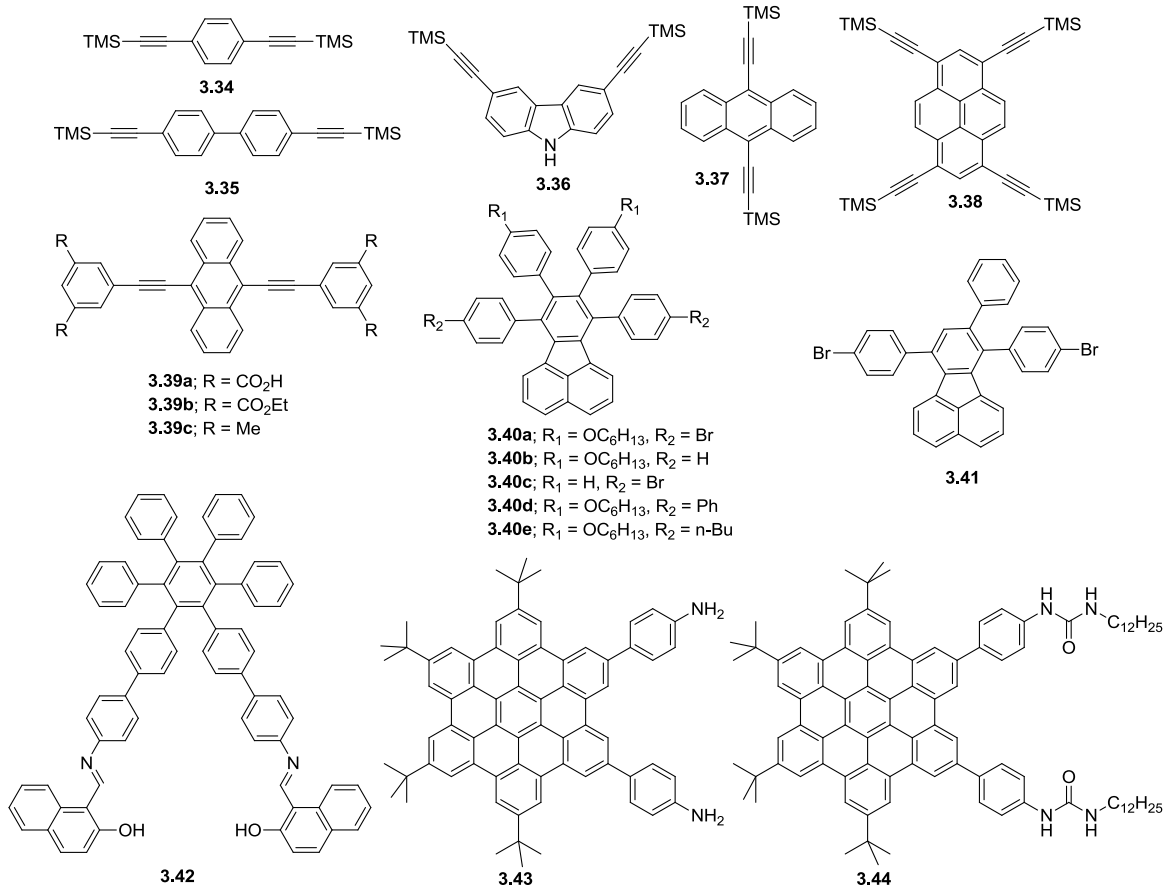

Figure 3.7 Single molecule fluorophores for explosive sensing.

emission intensity decreases upon addition of PA and weak quenching observed for DNT.[28] Similar, aggregation (THF/H_2O 1:100) induced fluorescence was also observed for silole derivative **3.31** and exhibited quenching of fluorescence with PA.[29] Planar benzothiophene compound **3.32** was employed to form 1D micro belt and 3D flower shape super nanostructures.[30] The 3D flower shape nanostructures, exhibited higher sensitivity towards DNT compared to 1D microbelt, arising from their larger surface area and highly porous network of 3D flower shape nanostructures. Branched fluorescent receptors containing thiophene unit in arm and triphenylamine centres **3.33a-d** were used for detection of 2,4-DNT, 1,4-DNB, DMNB and 4-NT and maximum quenching was observed for 1,4-DNB.[31] Also, time resolved study demonstrated that quenching is dominated by collisional interaction between dendrimer and nitro derivatives. A series of bulky trimethylsilylethynyl substituted fluorophores (**3.34-38**) to avoid self-quenching in solid state were studied, which showed sensitivity and selectivity towards nitroaromatics, both in solution and thin film.[32] Further,

hydrogen bond assisted supramolecular polymer of 9,10-bis(1,3-dicarboxylicphenyl-5-ethynyl)anthracene **3.39a** exhibited enhance sensitivity towards TNT and PA in solution and thin film.[33] Enhanced sensitivity of carboxylic analogues arise from the formation of supramolecular polymer through hydrogen bonding network compared to discrete analogues (**3.39b-c**), thus easing exciton migration throughout supramolecular polymer chain. Also, a series of fluoranthene molecules (**3.40-41**) were studied as promising materials for nitroaromatic detection. Solution phase fluorescence quenching study revealed 2-20 ppb and ~1.1 ppm level sensitivity for PA and TNT, respectively.[34] The vapor phase sensing showed fast detection of PA and contact based method on silica gel TLC plate ascertained femto gram level sensitivity for PA and TNT (~1.15 fg/cm^2). Aggregation induced emission of hexa-peri-hexabenzocoronenes (**3.43-44**) selectively detect PA in solution as well as in solid state and contact based method on filter paper strip proved attogram level sensitivity towards PA.[35] Self-assembled fluorescent nanorods of hexaphenylbenzene **3.42** in presence of cyanide ions exhibited colorimetric as well as fluorogenic sensing of TNT at attogram level with detection limit of 10.21 ppq.[36] Therefore, we can conclude that though initially thought that single molecule fluorophores can't perform better compare to polymers, due to absence of exciton transfer in discrete molecules; however, later developments showed that they can perform as much better sensor for nitroaromatics.

3.1.7 Porphyrin based fluorometric sensors

Exceptional photostability, ease in synthesis and easy functionalization makes porphyrins as one of the promising candidate for sensing application. A molecular imprinted polymer prepared from the mixture of porphyrin **3.45** with stoichiometric amount of TNT, styrene, divinylbenzene and radical initiator AIBN and washed with solvent to remove the TNT template, exhibited selective binding with TNT and TNB because it creates shape selective cavity appropriate for TNT.[37] Further, the physical properties of polymers like porosity, stability, rigidity, and hydrophilicity may be tuned by modulating appropriate functionalization of porphyrins, crosslinking agent and reaction conditions. This method would allow the specific recognition of explosive molecules. *Meso*-tetra(4-sulphonatophenyl)porphyrin **3.46** was studied for TNT detection in aqueous solution by absorbance and fluorescence quenching method.[38] The solution phase quenching constant was obtained 5.5×10^3 M^{-1} and able to detect TNT at as low as 200 ppb level. Porphyrin functionalized **3.47** silica nano-composite consisting of ordered micropores was used to detect TNT vapor and its sensitivity was nearly two time higher compared to conjugated

polymers.[39] Using this technique 55% and 97% quenching was observed after 10 sec and 2 min respectively. Further, same group has developed porphyrin and metalloporphyrin doped

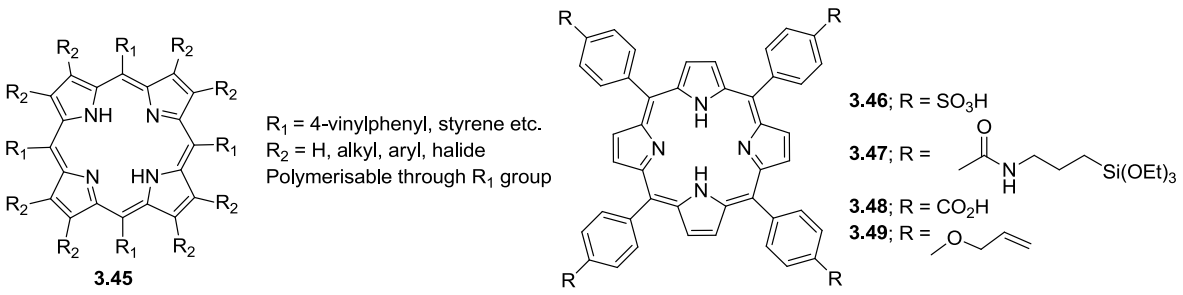

Figure 3.8 Porphyrin based sensors for explosive detection.

bimodal porous structure by using CTAB and polystyrene spheres as structure directing agent.[40] This porphyrin doped bimodal porous film showed 55% quenching of fluorescence in presence of saturated TNT vapor in 10 sec. These used films can be easily recovered by simple toluene washing, proves appropriate for sensory application. In another approach, the same group demonstrated the preparation of meso-structured porphyrin and metalloporphyrin doped silica film using surfactant of various sizes as structure directing group. Simply, by changing surfactant they could achieve hexagonal and wormlike meso structures, for comparison purpose they have also prepared amorphous material without template.[41] As expected, they observed worse performance for amorphous film and cadmium porphyrin doped wormlike meso-structure exhibited highest quenching efficiencies (60% in 10 sec) towards TNT vapor. Highest efficiency was observed for wormlike structure because of better diffusion of explosive vapor in 3D matrix. Also, based on sol-gel chemistry and electrospinning techniques, porphyrin doped **3.48** nano-composite fiber was studied for explosive detection and the performance primarily dependent on morphology and phase of aggregation of nanofiber used.[42] In this method, maximum 20% quenching of fluorescence was observed for TNT vapor in 60 sec with porous nanofiber with ~400 nm diameter. A template free sol-gel method was employed to prepare porphyrin doped and highly mesoporous (upto 74% porosity) organically modified silica (ORMOSIL) thin film for TNT sensing in vapor phase.[43] These robust ORMOSIL network exhibited fluorescence quenching with TNT (8.6% in 10 sec) and DNT vapor, the response of the film dependent on the thickness. Recently, a facile strategy was used to fabricate porphyrin doped **3.49** porous thin film on U-bent poly(methyl methacrylate) optical fiber by *in situ* "click" polymerization for explosive sensing.[44] This developed U-bent porous thin film exhibited high fluorescence

quenching towards TNT (37.5% in 30 sec), DNT and NB vapor. Also, this used fiber can be recovered easily by ultrasonic washing in isopropanol.

3.1.8 Miscellaneous explosive sensors

Due to limited space it is difficult to discuss all methods applied for sensing of explosive materials. Owing to our interest in single molecule fluorophores, we have tried to cover some significant achievements towards this approach. Other than the methods discussed above, molecular imprinted polymers,[45] coordination polymers,[46] quantum dots,[47] graphene,[48] nanoparticles,[49] and metal organic frameworks (MOFs)[50] were also employed for sensing of high energy materials. In this regards, Ajayaghosh and coworkers reported a fluoro substituted organogelator, which exhibited attogram level sensitivity towards TNT.[51] Also, Pradeep and coworkers reported anchoring of silver clusters embedded in bovine serum albumin onto silica coated gold mesoflower, for selective visual detection of TNT in zaptomolar level.[52]

3.2 Research goal

Keeping the above prospective in mind, we wish to investigate the effect of substituent in the periphery of porphyrin, as a single molecule fluorophore towards sensing of nitro explosives based high energy materials (HEMs). As porphyrins are endowed with several peripheral positions for selective modulation of their physico-chemical properties via suitable functionalization and various metal ions can also be incorporated into their core in order to manipulate their coordination behavior and emission characteristics, we envisaged a greater scope for this class of molecules and hence proposed to explore in detail the sensitivity of various porphyrinic systems towards several nitrated explosives in organic media.[53] In the present study, we used *meso*-tetraphenylporphyrin (H_2TPP) **3.50**, several of its *meso*-fluoroaryl substituted derivatives, β-octaethylporphyrin (H_2OEP), β-octamethoxyporphyrin (H_2OMP), β-octabutoxyporphyrin (H_2OBuP) and also their corresponding Zn(II)-derivatives as the fluorophores (Scheme 1). **3.58** and **3.59** were used as electron rich porphyrins, whereas the fluoroporphyrins, in spite of being relatively electron deficient compare to **3.50** (and hence were expected to interact weakly with the analytes), were used to see if there is any peripheral interaction between the fluorine atoms and the relatively electron rich components of the nitrated explosives, enhancing their efficiencies, as Fujiki's group reported an enhanced response towards TNT by some of the fluoro-substituted polysilanes.[15] The nitrated explosives used as analytes, consist of nitroaromatics, viz. nitrobenzene (NB),

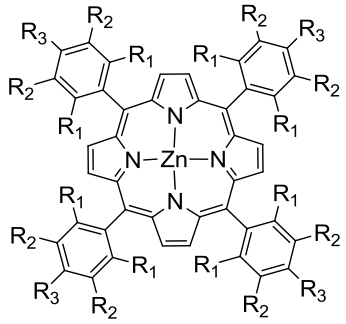

3.50; M = 2H, $R_1 = R_2 = R_3 = H$; H_2TPP
3.51; M = 2H, $R_1 = F$, $R_2 = R_3 = H$; $H_2T(2,6\text{-}F_2P)P$
3.52; M = 2H, $R_2 = F$, $R_1 = R_3 = H$; $H_2T(3,5\text{-}F_3P)P$
3.53; M = 2H, $R_1 = R_2 = R_3 = F$; H_2TF_5PP
3.54; M = Zn, $R_1 = R_2 = R_3 = H$; ZnTPP
3.55; M = Zn, $R_1 = F$, $R_2 = R_3 = H$; $ZnT(2,6\text{-}F_2P)P$
3.56; M = Zn, $R_2 = F$, $R_1 = R_3 = H$; $ZnT(3,5\text{-}F_3P)P$
3.57; M = Zn, $R_1 = R_2 = R_3 = F$; $ZnTF_5PP$

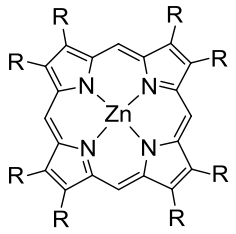

3.58; M = 2H, R = Et; H_2OEP
3.59; M = 2H, R = OMe; H_2OMP
3.60; M = 2H, R = O^nBu; H_2OBuP
3.61; M = Zn, R = Et; ZnOEP
3.62; M = Zn, R = OMe; ZnOMP
3.63; M = Zn, R = O^nBu; ZnOBuP

Scheme 3.1 Designed porphyrins and their Zn(II) -derivatives used for sensing studies.

1,3-dinitrobenzene (DNB), DNT, TNT, and alkylnitro compounds such as nitromethane (NM) and plastic explosive taggant DMNB, along with nitramines like RDX and HMX. Furthermore, we have used benzophenone along with benzonitrile as electron deficient and toluene as electron-rich controls of our experiments. Initially, we planned to investigate effect of substituents in solution state studies with nitro compounds. On the basis of solution state result, we wish to target few suitable porphyrins for vapor phase sensing studies and for future design of sensor molecules. In fact, the octabutoxyporphyrin and its Zn(II) derivative were designed on the basis of solution state studies, to evaluate the effect of alkyl group towards the sensing of nitro compounds both in solution and vapor states.

3.3 Materials and methods

Materials and methods including instrumentation used for quenching studies both in solution and vapor states were discussed in details in chapter 2 of this thesis.

3.4 Result and discussions

3.4.1 Synthesis of porphyrins

All porphyrins and their Zn(II)-derivatives (Scheme 3.1) were prepared using reported procedures, discussed in details in chapter 2 of this thesis and their structures were confirmed by standard spectral techniques. Though, octabutoxyporphyrin **3.60** and its Zn(II) derivative **3.63** were reported earlier by Ono and coworkers for possible implication in liquid crystalline application, but they have not provided any characterization information.[54] Therefore, we

synthesized it by employing the method reported by Merz and coworker.[55] The synthetic details along with characterization are discussed in chapter 2 of this thesis.

3.4.2 Photophysical properties of porphyrins

Table 3.1 Photophysical data for porphyrins (**3.50**-**3.63**) in chloroform at 25˚ C.

Porph.	UV-Vis nm (log ε)	(λ_{max}, nm)[b]	ϕ_f[a]
3.50	418 (5.72), 515 (4.30), 550 (3.89), 591 (3.73), 647 (3.62)	652, 716	0.11[c]
3.51	414 (5.51), 508 (4.28), 539 (3.44), 585 (3.78), 638 (2.77)	645, 711	0.069
3.52	416 (5.58), 512 (4.33), 545 (3.85), 587 (3.90), 642 (3.56)	649, 714	0.051
3.53	413 (5.57), 506 (4.40), 534 (3.32), 584 (3.88), 637 (2.75)	641, 709	0.052
3.54	423 (5.66), 533 (4.21), 593 (3.53)	603, 654	0.03[c]
3.55	421(5.64), 552 (4.27)	596, 649	0.026
3.56	422 (5.74), 553 (4.28), 592 (3.00)	603, 652	0.018
3.57	420 (5.59), 551 (4.15), 585 (1.81)	592, 647	0.018
3.58	400 (5.25), 498 (4.16), 534 (4.05), 566 (3.86), 620 (3.76)	622, 653, 688	0.13[c]
3.59	377 (5.19), 494 (3.98), 530 (4.09), 564 (3.76), 618 (3.78)	622, 647, 688	0.061[d]
3.60	383 (5.20), 500 (4.01), 534 (4.01), 565 (3.77), 619 (3.68)	622, 687	0.026
3.61	402 (5.56), 532 (4.32), 569 (4.46)	574, 628	0.045[c]
3.62	398 (5.34), 533 (4.24), 565 (4.29), 573 (4.33)	578, 632	0.031[d]
3.63	399 (5.38), 533 (4.22), 572 (4.32)	578, 632	0.04

[a] Fluorescence quantum yield, [b] Emission, [c] Quantum yield measured in benzene, taken from ref. 56; [d] Quantum yield measured in benzene, taken from ref. 57.

The UV-Vis and fluorescence spectral data for compounds (**3.50**-**3.63**) are reported in Table 3.1. Freebase porphyrins (**3.50**-**3.53** and **3.58**-**3.60**) display strong near-UV Soret absorption bands between 377–418 nm accompanied with four weaker Q-bands in the visible region (Figure 3.9), whereas the corresponding Zn(II)-porphyrin derivatives (**3.54**-**3.57** and **3.61**-**3.63**) possess strong Soret absorption bands between 398–423 nm with two characteristic weaker Q-bands (Figure 3.9). Porphyrins **3.50**-**3.63** show two emission bands (λ_{max} 574–714 nm) when excited at their Soret bands.

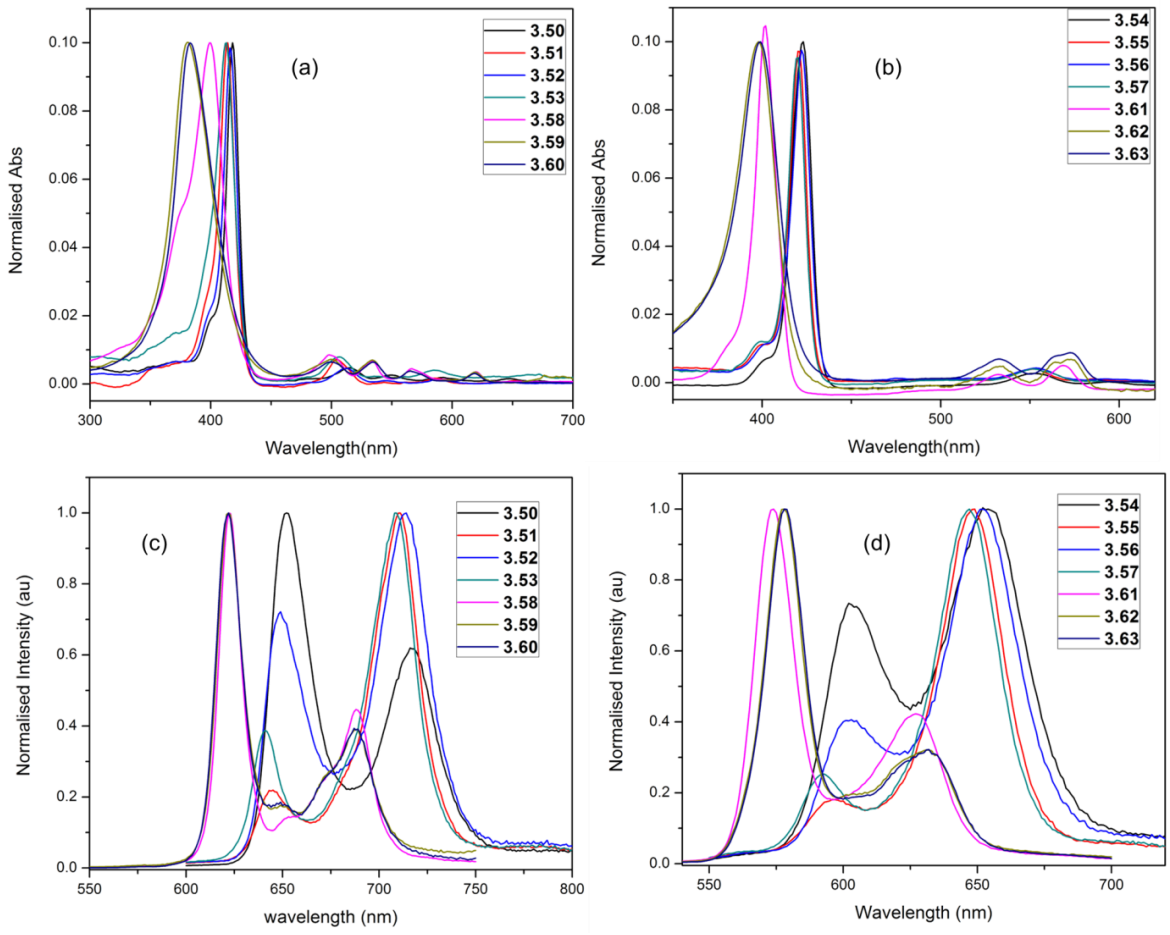

Figure 3.9 (a), (b) UV-Vis and (c), (d) fluorescence spectra of porphyrins used for sensing study.

3.4.3 Solution phase quenching studies

Quantitative evaluation of solution phase quenching of fluorescence was performed using the Stern–Volmer (SV) equation.[58] All compounds display varied degrees of quenching of fluorescence, upon successive addition of nitroaromatic compounds (Figure 3.10). However, no observable changes in peak maxima are noticed either in absorption (Figure 3.11) or in emission spectra; indicating a lack of strong interaction between porphyrin derivatives and nitroaromatics. Steady state SV plots of all sensing molecules display linearity (Figure 3.13) and are independent of the concentration of fluorophores (Figure 3.11). It is noteworthy to mention that electron rich porphyrins (**3.58**-**3.60**) and their Zn(II)-derivatives (**3.61**-**3.63**) show nonlinearity at higher concentrations of quencher, therefore, in these cases, titrations were performed at a lower concentration (10^{-4} M) to observe linear SV plots (Figure 3.13). Assuming that both static and dynamic quenching are occurring simultaneously at the higher concentrations, when the modified Stern–Volmer equation was applied,[58] the plot of (F_0/F - 1)/[Q] vs. [Q] again displayed nonlinearity (Figure 3.12). Therefore, we conclude that at

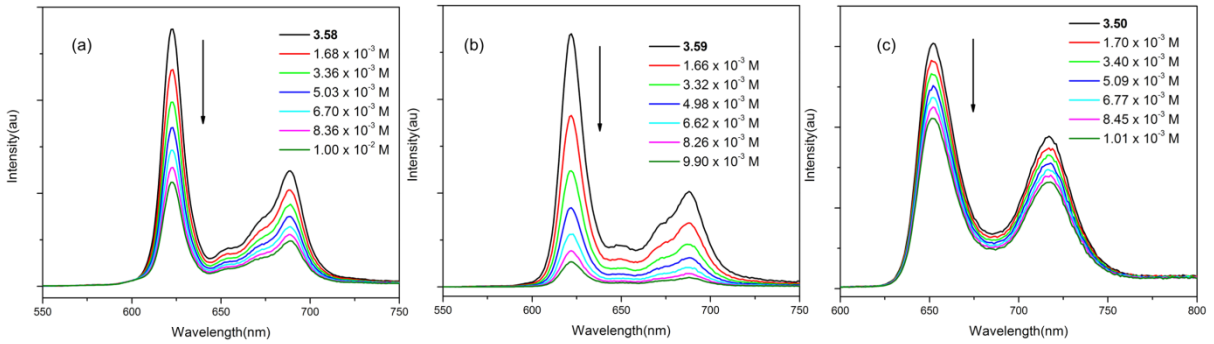

Figure 3.10 Quenching of fluorescence after successive addition of aliquots of (a) DNT to **3.58**, (b) TNT to **3.59** and (c) NB to **3.50** in chloroform at 25 °C.

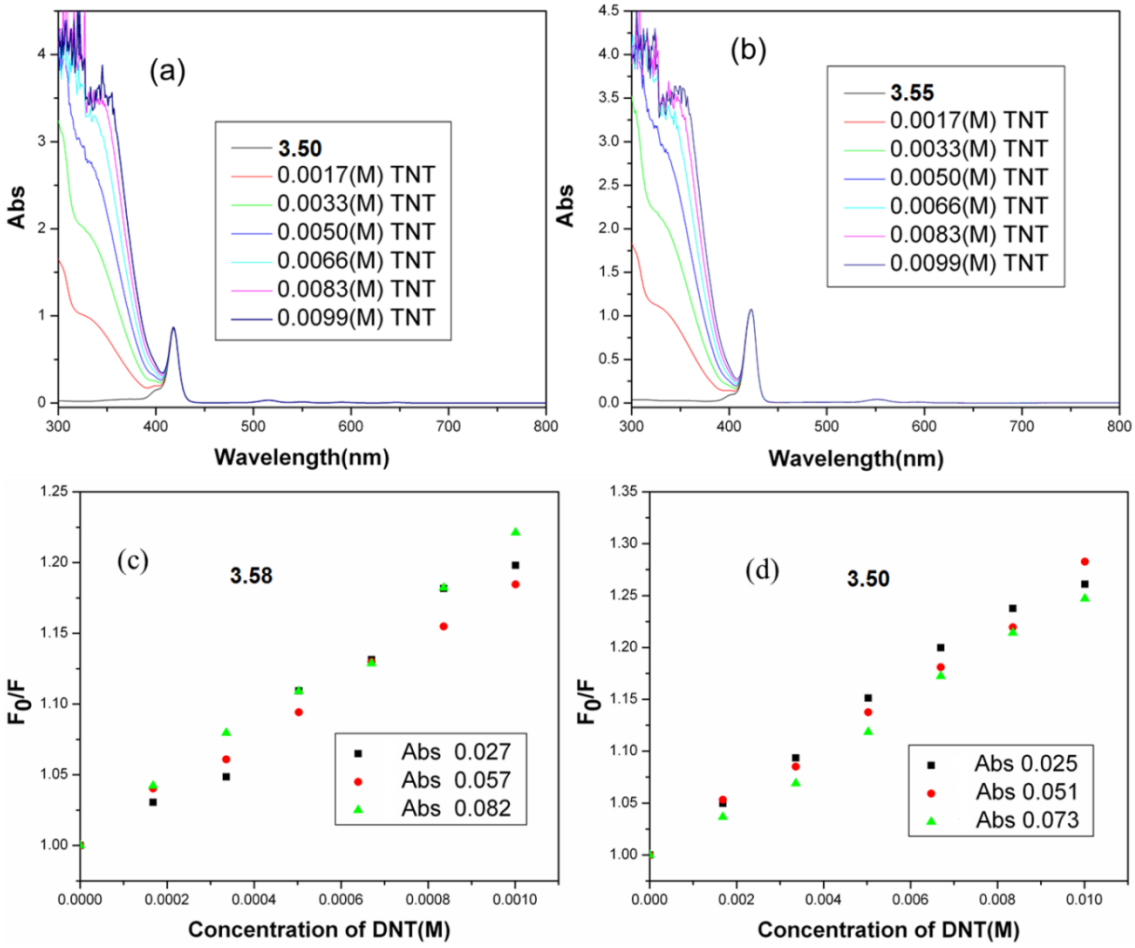

Figure 3.11 UV-Vis titration of (a) **3.50** and (b) **3.54** with successive addition of TNT in chloroform at 25˚C. Stern-Volmer plots for (c) **3.58** and (d) 3.**50** quenching experiments were done at different concentration of sensing molecule (mentioned in graph by OD), shows independent of concentration of host molecules.

higher concentrations fast quenching of fluorescence may result from aggregation and/or a quenching sphere of action between fluorophore and analyte molecules.[11] Best fit data of SV plots reveal moderate to good sensitivity of all porphyrin derivatives towards HEMs. K_{SV} for compounds **3.50**-**3.63** are summarized in Table 3.2. From the data it can be inferred that

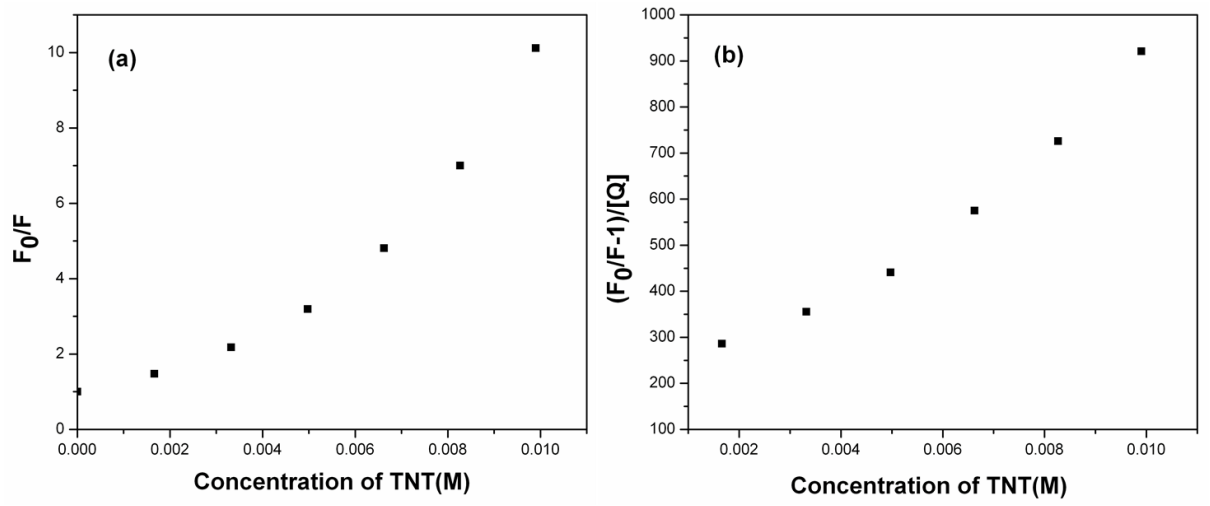

Figure 3.12 (a) Stern-Volmer plot for **10** with TNT at higher concentration showing nonlinearity and it is concave upward towards Y-axis shows static, collisional and other effects are presents simultaneously.

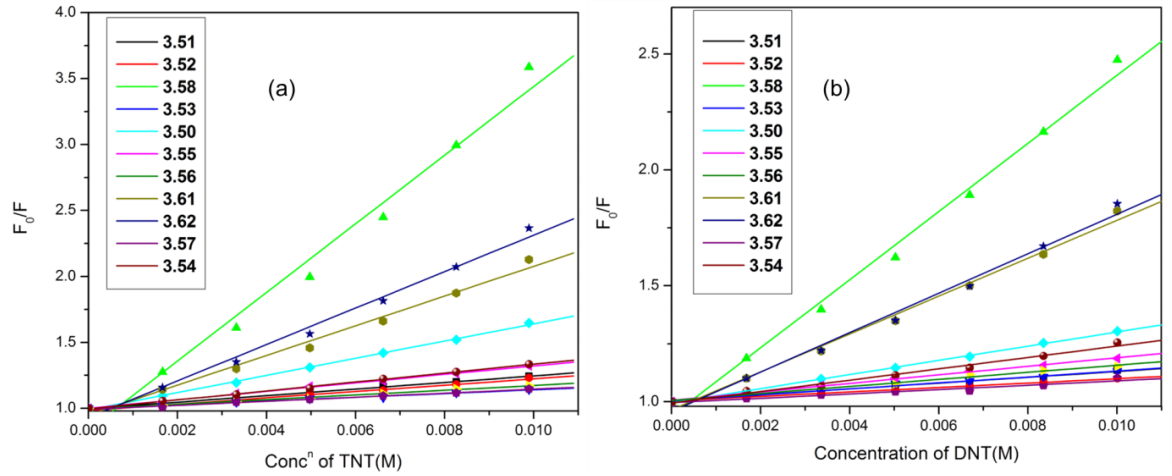

Figure 3.13 Stern–Volmer plots of sensing molecules for (a) TNT, and (b) DNT.

quenching of fluorescence is observed probably due to photo-excited electron transfer from electron rich porphyrins to electron deficient nitroaromatics. Among the sensing molecules **3.59** shows the highest K_{SV} for all nitroaromatics, which may arise from facile electron transfer from electron rich porphyrin (owing to the presence of eight electron donating methoxy groups at the β-positions of the porphyrin moiety) to electron deficient nitroaromatic entities.[59] Furthermore, as the number of nitro groups increases on the aromatic ring, their quenching efficiency concomitantly increases as a result of their increased electron deficient character, which facilitates the formation of a charge transfer complex with the porphyrins. Consequently, among the nitroaromatics, the decreasing order of K_{SV} is TNT > DNT ≈ DNB > NB. The presence of one additional binding site in Zn(II) porphyrins compared to freebase porphyrins led to the emergence of another mode of interaction between the

Table 3.2 S-V constants for porphyrins and their Zn(II)-derivatives in chloroform at 25˚C.

Porph	TNT	DNT	*m*-DNB	NB	DMNB	NM	RDX[#]	HMX[#]	BP
3.50	65	31	36	2.4	-	-	-	-	3.2
3.51	25	13	7	1.6	-	-	-	-	-
3.52	24	10	7	2.8	-	-	-	-	-
3.53	14	13	7	5.5	-	-	-	-	-
3.54	34	24	27	9	3.6	2.8	-	-	7.7
3.55	32	18	22	3	-	-	-	-	-
3.56	18	15	15	6.9	-	-	-	-	-
3.57	15	9	9	2.6	-	-	-	-	-
3.58	192	108	113	29	1.6	-	5.46	-	3.7
3.59	324	226	136	78	-	-	13.3	-	52
3.60	217	142	82	57	-	-	-	-	35
3.61	99	85	70	34	3.5	4.3	-	7.3	6.4
3.62	106	78	57	25	3.4	3.5	-	0.7	21
3.63	114	58	41	31	1.9	2.4	-	-	22

[#] For HMX and RDX, acetone and methanol were used as solvent, respectively.

metalloporphyrins and the nitroaromatics via the axial ligation of nitro group to the Zn, apart from the π–π stacking interactions. The decreasing order of quenching efficiency of the freebase porphyrins is **3.59** > **3.60** > **3.58** > **3.50** > **3.51** ≈ **3.52** ≈ **3.53** and for Zn(II)-porphyrins is **3.62** > **3.63** > **3.61** > **3.54** > **3.55** > **3.56** > **3.57** towards nitroaromatics. However, freebase porphyrins (**3.50**–**3.53**, **3.58**–**3.60**) were found to display better quenching ability than the Zn(II)-derivatives (**3.54**–**3.57**, **3.61**–**3.63**), which may be attributed to the depletion in electron density at the porphyrin core upon insertion of the Lewis acidic metal ion. Most importantly, octabutoxyporphyrin **3.60** and its Zn(II) derivatives **3.63** exhibit weaker quenching constant compare to octamethoxy analogue, though they are comparable in electron rich character. This may be attributed to the bulky butoxy groups at the periphery hindering effective excited state π–π donor acceptor interaction. Fluoroporphyrins (**3.51**–**3.54**) and their Zn(II)-derivatives (**3.56**–**3.57**) show poor response towards nitroaromatics as compared to nonfluorinated analogues due to their relatively electron deficient nature and hence we can conclude that here fluoro groups are not playing any additional role towards sensing, unlike the fluoro-substituted polysilanes.[15] Interestingly, in the case of the Zn(II)-derivatives of the electron deficient fluoroporphyrins, greater quenching was observed compared to their freebase analogues, which may be attributed to the additional interaction via axial ligation of the nitro group of the analyte to the metal ion. Another interesting point noticed is that in case of some porphyrins, DNT exhibits a greater quenching ability

compared to DNB, although DNB is relatively more electron deficient in nature. For example, while **3.50**, **3.55** and **3.58** shows the normal trend of DNB showing greater quenching constants compared to DNT, in the case of freebase fluoroporphyrins **3.51**–**3.53** this order is reversed, i.e. DNT shows greater K_{SV} constant compared to DNB. This may be attributed to a weak H-bonding type interaction between methyl hydrogen of DNT with fluoro groups at the porphyrin periphery, however for their corresponding zinc derivatives, owing to the reduced π-electron density at the porphyrin ring, this interaction becomes negligible. Furthermore, a marked difference was observed in the binding of DNT and DNB with **3.58** and **3.59**, where the latter displays an almost 1.66 times stronger affinity towards DNT compared to DNB. On the other hand, **3.59** and **3.60** shows a relatively higher affinity for DNB than DNT. This trend can be explained on the basis of a H-bonding type interaction between methyl hydrogen of DNT with oxygen of the methoxy groups at the porphyrin periphery and a similar trend was also observed for the Zn(II)-derivative of **3.59** and **3.60** (i.e. **3.62** and **3.63** respectively). The relatively higher preference of **3.61** to DNT than DNB may be attributed to better axial ligation of the relatively electron rich DNT to the Zn(II)-porphyrin moiety.

Among all the porphyrins **3.59** displays the highest binding affinity with TNT and the significantly greater magnitude of K_{SV} of **3.59** compared to **3.58**, may be attributed to the additional interaction between a methyl of TNT with porphyrin methoxy groups like in the case of DNT. The SV constant of 324 M^{-1} observed for **3.59** is better than all single molecule fluorophores reported so far except pyrene, which is toxic to the environment.[22,31,20] Poly(iptycenebutadiynylene) based conjugated polymers designed by Swager's group for detection of nitroaromatics, in comparison displayed relatively moderate K_{SV} (50–170 M^{-1}) for TNT where quenching of fluorescence was observed through exciton transfer over the entire polymer moiety, thereby creating an amplified sensory response compared to a single molecule fluorophore.[11] There are only few reports of single molecule fluorophores where higher K_{SV} values were observed.[32,33,60]

Among alkylnitro compounds we have studied DMNB (plastic explosive taggant) and nitromethane (rocket propellant). Unlike nitroaromatics, these alkylnitro compounds bind only weakly due to the lack of π–π stacking interactions. Here we observed that the zinc complexes of electron rich porphyrins (**3.61**–**3.63** and **3.54**) showing moderate K_{SV} may be due to axial ligation of nitro group to zinc and/or by a collisional quenching mechanism

(Table 3.2). The K_{SV} for DMNB is comparable to that reported previously.[31,61] A similar behavior was also noticed for nitromethane (Table 3.2).

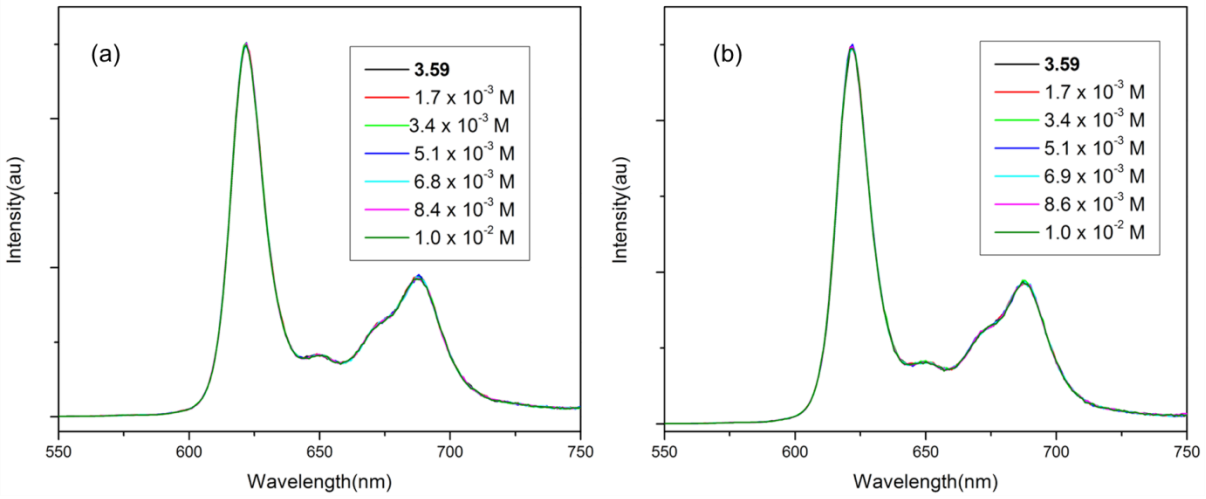

Figure 3.14 Fluorescence quenching experiments for **3.59** with successive addition of (a) benzonitrile (BN) and (b) toluene.

We have used HMX and RDX (high explosives) among the nitramines for our studies. Due to their poor solubility in chloroform, acetone and methanol were used as the solvents for titrations, respectively. There are only a few reports on sensing of RDX and HMX in the solution phase, the majority of them showing no quenching of fluorescence.[60,62] Trogler and coworkers reported hollow silica nanospheres containing a silafluorene-fluorene conjugated polymer for detection of RDX in aqueous solution[62a] and recently they have used organosilicon polymers for the separation and detection of RDX and HMX.[62b] However, McGuffin's group demonstrated that pyrene (in acetonitrile) possesses the highest affinity towards RDX and HMX.[60] In case of the porphyrins, only electron rich analogues **3.58**–**3.59** and **3.61**-**3.62** shows moderate interactions with RDX and HMX (Table 3.2).

The control experiments reveal only electron rich porphyrins (**3.50**, **3.58**-**3.60**) and their zinc(II)-derivatives (**3.54**, **3.61**-**3.63**) exhibit moderate quenching of fluorescence by benzophenone and the magnitudes are quite lower compared to all nitroaromatics (Table 3.2). Fluoroporphyrins and their zinc complexes did not display any quenching of fluorescence in the presence of benzophenone (BP). On the other hand, benzonitrile and toluene did not show any quenching of fluorescence with any of the studied porphyrin derivatives (Figure 3.14). Therefore, from the above control experiments we can conclude that some of our designed porphyrins are almost selective towards explosive molecules.

3.4.4 Solid phase fluorescence quenching studies

In view of field detection of explosive vapor, thin film based sensors are found more suitable in term of reusability, and can be converted into small opto-electronic device. Our much informative solution phase study concludes that electron rich porphyrins show better sensitivity towards nitroaromatics. Thus we targeted **3.50**, **3.58**, **3.59** and **3.60** and their Zn(II) complexes, to study the effect of substituents and the role of coordinated metal ion in the vapour phase sensing of HEMs, through fluorescence quenching study. As we observed best sensitivity towards TNT for porphyrin **3.59**, therefore, one of our objectives is to study analogous octabutoxyporphyrin **3.60**, to ascertain the effect of longer alkyl chains in sensing, as they may disrupt the π-π stacking interaction between the porphyrins in solid state to enhance porosity. For vapour phase sensing chloroform solution of porphyrins (~2 mg in 5 mL $CHCl_3$) were spin coated on quartz plate for fluorescence quenching studies. Spin coated film upon subjected to UV-Vis study, reveals bathochromically shifted relatively broad Soret band, accompanied by Q-bands. Fluorescence spectra of alkoxy analogues experience maximum change with high energy band becoming less intense and low energy band appearing relatively more intense, probably owing to self-aggregation in solid state.

Fluorescence measurements of prepared spin coated films were done by inserting prepared film into glass vial (20 mL) containing analytes of interest (kept in closed condition for 48 h to maintain saturated vapour pressure inside the vial before measurement) and cotton gauze to prevent direct contact with the quartz coated film. After exposure of quartz film for specific time fluorescence was measured immediately at particular excited wavelength (Soret band). We have used TNT, DNT, PA, NB and DMNB for vapour phase detection.

Table 3.3 Percentage of quenching of fluorescence of porphyrins after exposed to saturated vapour of explosive molecules for 60 sec.

Porphyrins	TNT	DNT	PA	NB	DMNB
3.50	17	20	22	15	10
3.58	28	24	26	12	16
3.59	46	49	26	40	45
3.60	38	54	40	73	32
3.54	6	17	13	24	12
3.61	15	14	6	3	3
3.62	30	32	32	62	27
3.63	56	48	29	39	28

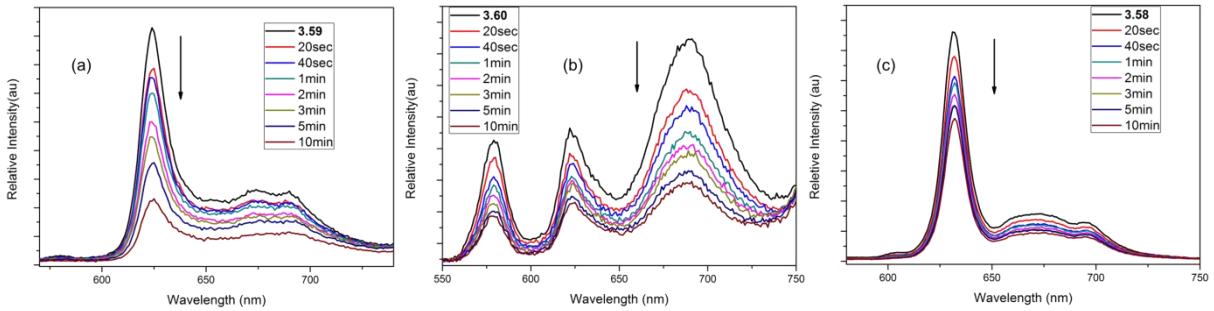

Figure 3.15 Quenching of fluorescence after exposed to saturated vapour of (a) TNT to thin film of **3.59**, (b) PA to the thin film of **3.60** and (c) DNT to the thin film of **3.58**.

As expected all porphyrins displayed quenching of fluorescence in presence of vapour of explosive analytes (Figure 3.15). Fluorescence quenching data of porphyrins after 60 sec exposure to explosive vapour are given in Table 3.3. We observed 38%, 54%, 40% and 73% of quenching of fluorescence with porphyrin **3.60** thin films after 1 min exposure to saturated vapour of TNT, DNT, PA and NB, respectively. Alkoxyporphyrins (**3.59**-**3.60** and **3.62**-**3.63**) exhibited higher quenching of fluorescence compared to non-alkoxy analogues probably due to their electron rich nature resulting in stronger donor and acceptor complexes. As expected, among alkoxyporphyrins best fluorescence quenching response is observed for octabutoxyporphyrin **3.60**. We know that in solid state quenching efficiencies dependent on (i) formation of effective donor acceptor complex, (ii) thickness of the film, (iii) porosity of the solid matrix, which allows effective diffusion of explosive vapour.[11] Though we have observed weaker affinity towards nitro-compounds in solution state, but higher affinity in solid state for porphyrin **3.60** may be attributed to the effective diffusion of explosive analyte created by bulky butoxy groups in periphery. Maximum quenching of fluorescence is observed for NB (73% in 1 min) with porphyrin **3.60**, probably due to its higher vapour pressure and relatively smaller size, resulting effective diffusion in porous solid matrix, and this could possibly predominates over electrostatic interaction. Futher, comparable efficiency is observed for TNT and DNT with porphyrins and might result from the combined effect of higher electrostatic interaction of TNT and higher vapour pressure of DNT. Despite relatively low vapour pressure of PA (40% in 1 min with **3.60**) we observed good quenching of fluorescence and no protonation of porphyrin films could be observed (no change in fluorescent peak maxima of porphyrins after exposure to PA vapour). This indicates that these films would act as PA sensor as well. Further, owing to the importance of DMNB, in view of its use as taggant for modern day plastic cased explosives, and as there are very few reports on fluorometric quenching based sensing of DMNB due to lack of its aromatic

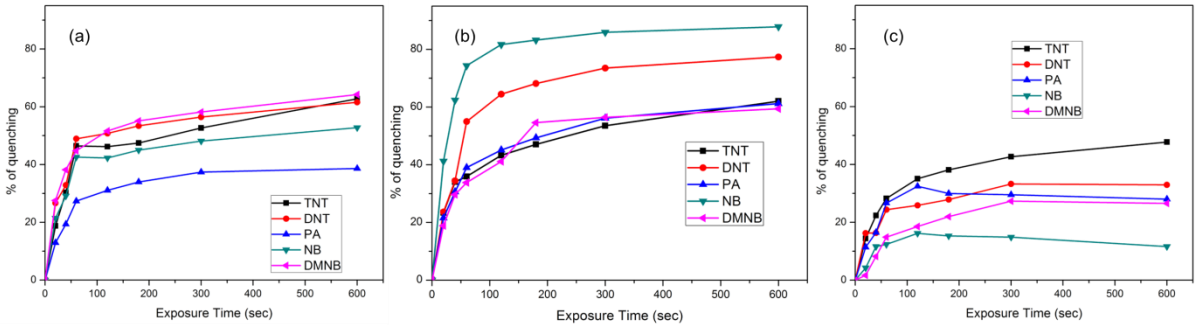

Figure 3.16 Quenching of fluorescence intensity of thin film of (a) **3.59**, (b) **3.60** and (c) **3.58** by nitrated explosive vapours with time.

character, we investigated this molecule as an analyte towards our targeted porphyrins Interestingly, we observed very good fluorescence quenching of alkoxyporphyrins in solid state in presence of DMNB vapour (best 45% with **3.59** in 1 min), which is quite comparable with nitroaromatic compounds, compared to non-alkoxylated porphyrins. Notably, all porphyrin thin films undergoes saturation in quenching of fluorescence after exposed to explosive molecules for ~2 min, indicating slower diffusion of explosive vapour into the core of thin film (Figure 3.16). The quenching of fluorescence observed for alkoxy analogues are more efficient towards TNT, compared to porphyrin doped on organically modified silica thin film reported by Bayindir and coworkers[43] and comparable with porphyrin doped mesoporous silica thin film reported by Li and coworkers.[39-42] Further, alkoxyporphyrins exhibits better sensitivity towards TNT vapour, compared to very recently reported porphyrin doped on the surface of U-bent poly(methylmethacrylate) optical fibre by click polymerisation techniques.[44] In addition, thin film of porphyrins after exposure to explosive vapour, display recovery of their quenched fluorescence slowly after keeping in air, indicating their possible reusability and hence seems appropriate for sensor application. Due to easy fabrication by simple spin coating compare to existing fabrication techniques, alkoxyporphyrins may emerge as better and versatile fluorescence quenching based explosive sensor for field application.

3.5 Conclusion

In conclusion, a series of porphyrins and their Zn(II)-derivatives endowed with both electron rich and electron deficient porphyrin cores were explored for the detection of nitrated energetic materials, by introducing appropriate substituents at the porphyrin periphery. The effect of substituents at the porphyrin periphery could be clearly observed in solution phase study with regard to their interactions with nitrated explosive molecules along with the effect

of the metal ion at its core. Significantly, as a single molecule fluorophore, some of these porphyrins display binding with HEMs that are either stronger or similar in magnitude to those displayed by conjugated polymeric fluorophore molecules. Preliminary, vapor phase fluorescence quenching study revealed good sensitivity towards not only nitroaromatics, but also, for plastic explosive taggant. Further, alkoxyporphyrins display better sensitivity towards explosive molecules compared to non-alkoxy analogues and sensitivities are comparable and in some cases better than previously reported porphyrins.[39-44] To the best of our knowledge, there are very few reports where good sensitivity was observed for both nitroaromatics and alkylnitro compounds, highlighting the importance of alkoxyporphyrins. Easy synthetic access along with simple fabrication techniques and good sensitivity towards a series of explosive molecules indicate alkoxporphyrins can act as versatile sensor for explosive detection. Currently, control experiments with common environmental pollutants, further detailed vapor phase studies, reusability of thin film of porphyrins are in progress in our laboratory.

3.6 References

1. Craznik, A. W. *Nature* **1998**, *394*, 417.
2. U.S. Department of State, "Hidden killers: the global demining crisis," U.S. Dept. State, Publ. 190 575, Washington, DC, **1998**.
3. Lima, D. R.; Bezerra, M. L.; Neves, E. B.; Moreira, F. R. *Rev. Environ. Health* **2011**, *26*, 101.
4. (a) Thomas III, S. W.; Joly, G. D.; Swager, T. M. *Chem. Rev*. **2007**, *107*, 1339. (b) Toal, S. J.; Trogler, W. C. *J. Mater. Chem*. **2006**, *16*, 2871. (c) Singh, S. *J. Hazard. Mater*. **2007**, *144*, 15. (d) Germain, M. E.; Knapp, M. J. *Chem. Soc. Rev*. **2009**, *38*, 2543. (e) Meaney, M. S.; McGuffin, V. L. *Anal. Bioanal. Chem*. **2008**, *391*, 2557. (f) Salinas, Y.; Martínez-Máñez, R.; Marcos, M. D.; Sancenón, F.; Costero, A. M.; Parra, M.; Gil, S. *Chem. Soc. Rev*. **2012**, *41*, 1261.
5. Yinon, J. *Anal. Chem*. **2003**, *75*, 99A.
6. Moore, D. S. *Rev. Sci. Instrum*. **2004**, *75*, 2499.
7. Moore, D. S.; Scharff, R. J. *Anal. Bioanal. Chem*. **2009**, *393*, 1571.
8. Yang, J. S.; Swager, T. M. *J. Am. Chem. Soc*. **1998**, *120*, 11864.
9. Yamaguchi, S.; Swager, T. M. *J. Am. Chem. Soc*. **2001**, *123*, 12087.
10. Zahn, S.; Swager, T. M. *Angew. Chem., Int. Ed*. **2002**, *41*, 4225.
11. Zhao, D.; Swager, T. M. *Macromolecules* **2005**, *38*, 9377.

12. Thomas, S. W.; Amara, J. P.; Bjork, R. E.; Swager, T. M. *Chem. Commun*. **2005**, 4572.
13. (a) Albert, K. J.; Myrick, M. L.; Brown, S. B.; James, D. L.; Milanovich, F. P.; Walt, D. R. *Environ. Sci. Technol*. **2001**, *35*, 3193. (b) Albert, K.; Walt, D. *Anal. Chem*. **2000**, *72*, 1947.
14. www.nomadics.com
15. Saxena, A.; Fujiki, M.; Rai, R.; Kwak, G. *Chem. Mater*. **2005**, *17*, 2181.
16. Sohn, H.; Calhoun, R. M.; Sailor, M. J.; Trogler, W. C. *Angew. Chem., Int. Ed*. **2001**, *40*, 2104.
17. Sohn, H.; Sailor, M. J.; Magde, D.; Trogler, W. C. *J. Am. Chem. Soc*. **2003**, *125*, 3821.
18. Sanchez, J. C.; DiPasquale, A. G.; Rheingold, A. L.; Trogler, W. C. *Chem. Mater*. **2007**, *19*, 6459.
19. Toal, S. J.; Sanchez, J. C.; Dugan, R. E.; Trogler, W. C. *J. Forensic Sci*. **2007**, *52*, 79.
20. Meaney, M. S.; McGuffin, V. L. *Anal. Chim. Acta* **2008**, *610*, 57.
21. Beyazkilic, P.; Yildirim, A.; Bayindir, M. *ACS Appl. Mater. Interfaces* **2014**, *6*, 4997.
22. Germain, M. E.; Vargo, T. R.; McClure, B.; Rack, J. J.; Van Patten, P. G.; Odoi, M.; Knapp, M. J. *Inorg. Chem*. **2008**, *47*, 6203.
23. Germain, M. E.; Knapp, M. J. *J. Am. Chem. Soc*. **2008**, *130*, 5422.
24. Lee, Y. H.; Liu, H.; Lee, J. Y.; Kim, S. H.; Kim, S. K.; Sessler, J. L.; Kim, Y.; Kim, J. S. *Chem.–Eur. J*. **2010,** *16*, 5895.
25. Vijayakumar, C.; Tobin, G.; Schmitt, W.; Kima, M.; Takeuchi, M. *Chem. Commun*. **2010**, *46*, 874.
26. Zyryanov, G. V.; Palacios, M. A.; Anzenbacher Jr, P. *Org. Lett*. **2008**, *10*, 3681.
27. Zhang, C.; Che, Y.; Yang, X.; Bunes, B. R.; Zang, L. *Chem. Commun*. **2010**, *46*, 5560.
28. Li, Z.; Dong, Q.; Lam, J. W. Y.; Sun, J.; Qin, A.; Haüßler, M.; Dong, Y. P.; Sung, H. H. Y.; William, I. D.; Sing Kwok, H.; Tang, B. Z. *Adv. Funct. Mater*. **2009**, *19*, 905.
29. Dong, Y.; Lam, J. W. Y.; Qin, A.; Li, Z.; Liu, J.; Sun, J.; Dong, Y.; Tang, B. Z. *Chem. Phys. Lett*. **2007**, *446*, 124.
30. Wang, L.; Zhou, Y.; Yan, J.; Wang, J.; Pei, J.; Cao, Y. *Langmuir* **2009**, *25*, 1306.
31. Olley, D. A.; Wren, E. J.; Vamvounis, G.; Fernee, M. J.; Wang, X.; Burn, P. L.; Meredith, P.; Shaw, P. E. *Chem. Mater*. **2011**, *23*, 789.
32. Shanmugaraju, S.; Joshi, S. A.; Mukherjee, P. S. *J. Mater. Chem*. **2011**, *21*, 9130.

33. Gole, B.; Shanmugaraju, S.; Bar, A. K.; Mukherjee, P. S. *Chem. Commun*. **2011**, *47*, 10046.
34. (a) Venkatramaiah, N.; Kumar, S.; Patil, S. *Chem. Commun*. **2012**, *48*, 5007. (b) Venkatramaiah, N.; Kumar, S.; Patil, S. *J. Phys. Chem. C* **2013**, *117*, 7236. (c) Venkatramaiah, N.; Kumar, S.; Patil, S. *Chem. –Eur. J*. **2012**, *18*, 14745.
35. Vij, B.; Bhalla, B.; Kumar, M. *ACS Appl. Mater. Interfaces* **2013**, *5*, 5373.
36. Bhalla, B.; Pramanik, S.; Kumar, M. *Chem. Commun*. **2013**, *49*, 895.
37. Murray, G. M.; Arnold, B. M.; Lawrence, D. S. *US Pat. Appl*. 2001077664, **2001**.
38. Rahman, M.; Harmon, H. J. *Spectrochim. Acta Part A* **2006**, *65*, 901.
39. Tao, S.; Shi, Z.; Li, G.; Li, P. *ChemPhysChem*. **2006**, *7*, 1902.
40. Tao, S.; Yin, J.; Li, G. *J. Mater. Chem*. **2008**, *18*, 4872.
41. (a) Tao, S.; Li, G.; Zhu, H. *J. Mater. Chem*. **2006**, *16*, 4521. (b) Tao, S.; Li, G. *Colloid Polym. Sci*. **2007**, *285*, 721.
42. Tao. S.; Li, G.; Yin, J. *J. Mater. Chem*. **2007**, *17*, 2730.
43. Yildirim, A.; Budunoglu, H.; Deniz, H.; Guler, M. O.; Bayindir, M. *ACS Appl. Mater. Interfaces* **2010**, *2*, 2892.
44. Ma, J.; Lv, L.; Zou, G.; Zhang, Q. *ACS Appl. Mater. Interfaces* **2015**, *7*, 241.
45. (a) Li, J.; Kenclig, C. E.; Nesterov, E. E. *J. Am. Chem. Soc*. **2007**, *129*, 15911. (b) Lu, W.; Xue, M.; Xu, Z.; Dong, X.; Xue, F.; Wang, F.; Wang, Q.; Meng, Z. *Curr. Org. Chem*. **2015**, *19*, 62. (c) Bunte, G.; Hürttlen, J.; Pontius, H.; Hartlieb, K.; Krause, H. *Anal. Chem. Acta* **2007**, *591*, 49. (d) McCluskey, A.; Holdsworth, C. I.; Bowyer, M. C. *Org. Biomol. Chem*. **2007**, *5*, 3233. (e) Bunte, G.; Heil, M.; Röseling, D.; Hürttlen, J.; Pontius, H.; Krause, H. *Propellants Explos. Pyrotech*. **2009**, *34*, 245. (f) Roseling, D.; Tuercke, T.; Krause, H.; Loebbecke, S. *Org. Process Res. Dev*. **2009**, *13*, 1007. (g) Stringer, R. C.; Gangopadhyay, S.; Grant, S. A. *Anal. Chem*. **2010**, *82*, 4015.
46. (a) Lan, A.; Li, K.; Wu, H.; Olson, D. H.; Emge, T. J.; Ki, W.; Hong, M.; Li, J. *Angew. Chem., Int. Ed*. **2009**, *48*, 2334. (b) Zhang, C.; Che, Y.; Zhang, Z.; Yang, X.; Zang, L. *Chem. Commun*. **2011**, *47*, 2336. (c) Xue, Y. -S.; He, Y.; Zhou, L.; Chen, F.-J.; Xu, Y.; Du, H.-B.; You, X.-Z.; Chen, B. *J. Mater. Chem. A* **2013**, *1*, 4525. (d) Zhang, C.; Che, Y.; Zhang, Z.; Yang, X.; Zang, L. *Chem. Commun*. **2011**, *47*, 2336.
47. (a) Xia, Y.; Song, L.; Zhu, C. *Anal. Chem*. **2011**, *83*, 1401. (b) Zhang, K.; Zhou, H.; Mei, Q.; Wang, S.; Guan, G.; Liu, R.; Zhang, J.; Zhang, Z. *J. Am. Chem. Soc*. **2011**, *133*, 8424. (c) Xia, Y.; Chen, H. *Anal. Chem*. **2014**, *86*, 11062. (d) Li, Z.; Wang, Y.; Ni, Y.; Kokot, S. *Spectrochem. Acta A* **2015**, *137*, 1213. (e) Wang, Y.; Ni, Y. *Anal.*

Chem. **2014**, *86*, 7463. (f) Swarnkar, A.; Shankar, G. S.; Nag, A. *Chem. Commun*. **2014**, *50*, 4743. (g) Carrillo-Carrión, C.; Simonet, B. M.; Valcárcel, M. *Anal. Chem. Acta* **2013**, *792*, 93. (h) Wang, Y.-q.; Zou, W.-s. *Talanta* **2011**, *85*, 469. (i) Freeman, R.; Willner, I. *Nano. Lett*. **2009**, *9*, 322. (j) Chen, Y.; Chen, Z.; He, Y.; Lin, H.; Sheng, P.; Liu, C.; Luo, S.; Cai, Q. *Nanotechnology* **2010**, *21*, 125502.

48. (a) Tang, L.; Feng, H.; Cheng, J.; Li, J. *Chem. Commun*. **2010**, *46*, 5882. (b) Robinson, J. T.; Perkins, F. K.; Snow, E. S.; Wei, Z.; Sheehan, P. E. *Nano. Lett*. **2008**, *8*, 3137. (c) Chen, T.-W.; Sheng, Z.-H.; Wang, K.; Wang, F.-B.; Xia, X.-H. *Chem. – Asian. J*. **2011**, *6*, 1210. (d) Ma, L.; Zhao, P.; Wu, W.; Niu, H.; Cai, J.; Lan, Y.; Bai, X.; Wang, W. *Polym. Chem*. **2013**, *4*, 4746. (e) Esfandiar, A.; Kybert, N. J.; Dattoli, E. N.; Han, G. H.; Lerner, M. B.; Akhavan, O.; Irajizad, A.; Johnson, A. T. C. *Appl. Phys. Lett*. **2013**, *103*, 183110. (f) Ray, P.; Pandey, S.; Rao, V. R. *J. Appl. Phys*. **2014**, *116*, 124902.
49. (a) Long, Y.; Chen, H.; Yang, Y.; Wang, H.; Yang, Y.; Li, N.; Li, K.; Pei, J.; Liu, F. *Macromolecules* **2009**, *42*, 6501. (b) Salinas, Y.; Climent, E.; Martínez-Máñez, R.; Sancenón, F.; Dolores Marcos, M.; Soto, J.; Costero, A. M.; Gil, S.; Parra, M.; de Diego, A. P. *Chem. Commun*. **2011**, *47*, 11885.
50. (a) Gong, Y.-N.; Huang, Y.-L.; Jiang, L.; Lu, T.-B. *Inorg. Chem*. **2014**, *53*, 9457. (b) Gole, B.; Bar, A. K.; Mukherjee, P. S. *Chem. –Eur. J*. **2014**, *20*, 13321. (c) Hu, Z.; Deibert, B. J.; Li, J. *Chem. Soc. Rev*. **2014**, *43*, 5815. (d) Gole, B.; Bar, A. K.; Mukherjee, P. S. *Chem. –Eur. J*. **2014**, *20*, 2276. (e) Banerjee, D.; Hu, Z.; Li, J. *Dalton Trans*. **2014**, *43*, 10668. (f) Gong, Y.-N.; Jiang, L.; Lu, T.-B. *Chem. Commun*. **2013**, *49*, 11113. (g) Nagarkar, S. S.; Joarder, B.; Chaudhari, A. K.; Mukherjee, S.; Ghosh, S. K. *Angew. Chem. Int. Ed*. **2013**, *52*, 2881. (h) Pramanik, S.; Zhang, C.; Zhang, X.; Emge, T. J.; Li, J. *J. Am. Chem. Soc*. **2011**, *133*, 4153. (i) Xu, H.; Liu, F.; Cui, Y.; Chen, B.; Qian, G. *Chem. Commun*. **2011**, *47*, 3153. (j) Zhou, X.; Li, H.; Xiao, H.; Li, L.; Zhao, Q.; Yang, T.; Zou, J.; Huang, W. *Dalton Trans*. **2013**, *42*, 5718.
51. Kartha, K. K.; Babu, S. S.; Srinivasan, S.; Ajayaghosh , A. *J. Am. Chem. Soc*. **2012**, *134*, 4834.
52. Mathew, A.; Sajanlal, P. R.; Pradeep, T. *Angew. Chem., Int. Ed*. **2012**, *51*, 9596.
53. Rana, A.; Panda, P. K. *RSC Adv*. **2012**, *2*, 12164.
54. Murashima, T.; Wakamori, N.; Uchihara, Y.; Ogawa, T.; Uno, H.; Ono, N. *Mol. Cryst. Liq. Cryst*. **1996**, *278*, 165.

55. (a) Merz, A.; Meyer, T. *Synthesis* **1999**, 94. (b) Merz, A.; Schropp, R.; Dötterl, E. *Synthesis* **1995**, 795.
56. Ohno, O.; Kaizu, Y.; Kobayashi, H. *J. Chem. Phys*. **1985**, *82*, 1779.
57. Rana, A.; Panda, P. K. *Tetrahedron Lett*. **2011**, *52*, 2697.
58. Lakowicz, J. R. *Principle of Fluorescence Spectroscopy (3rd Edition), Publishers: Springer* **2006**, 282.
59. Chandrashekar, T. K.; Krishnan, V. *Inorg. Chem*. **1981**, *20*, 2782.
60. Goodpaster, J. V.; McGuffin, V. L. *Anal. Chem*. **2001**, *73*, 2004.
61. Germain, M. E.; Vargo, T. R.; Khalifah, P. G.; Knapp, M. J. *Inorg. Chem*. **2007**, *46*, 4422.
62. (a) Yang, J.; Aschemeyer, S.; Martinez, H. P.; Trogler, W. C. *Chem. Commun*. **2010**, *46*, 6804. (b) Martinez, H. P.; Grant, C. D.; Reynolds, J. G.; Trogler, W. C. *J. Mater. Chem*. **2012**, *22*, 2908. (c) Jian, C.; Seitz, W. R. *Anal. Chim. Acta* **1990**, *237*, 265. (d) Ponnu, A.; Anslyn, E. V. *Supramol. Chem*. **2010**, *22*, 65.

CHAPTER 4

3,8,13,18-Tetrachloro-2,7,12,17-tetramethoxyporphyrin: Synthesis, Characterisation and NLO Studies

4.1 Introduction

Porphyrins are a class of important biological pigments, endowed with rich photophysical properties owing to the 22π-electron aromatic system, of which 18π-electrons are in conjugation.[1] Porphyrins are most widely studied compounds in chemistry and ~10,000 papers on porphyrins were published in last five years. This is not too astounding in terms of their stability, photophysical and optical properties, chemical versatility and conformational flexibility along with biological relevance to respiration, photosynthesis, medicine and as permeating cofactors in biochemistry marked them as research individual par excellence.[2] Further, the properties of this macrocyclic tetrapyrrolic system can be easily modulated via substitution at one or more of the peripheral *meso*- and/or β-positions.[1] Also the macrocycle acts as a very good ligand, binding to most of the metal ions in the periodic table along with several metalloids and nonmetals.[1] Among the porphyrins, β-substituted porphyrins are unique, owing to their close structural resemblance to naturally occurring porphyrins. Apart from their use as synthetic model for mimicking in vivo systems, they could also be

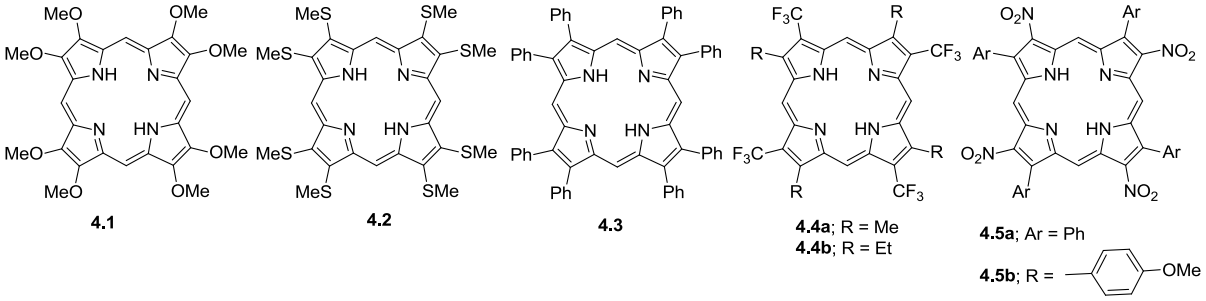

Scheme 4.1: Some of the specially designed β-octasubstituted porphyrins

functionalized using various electron donating and/or withdrawing substituents to achieve interesting properties. In this regard there are very few reports containing substituents other than alkyl groups at all of their β-positions (Scheme 4.1).[3] In particular, pyrroles containing simultaneous one electron donating and one electron withdrawing substituents at their adjacent β-pyrrole positions are rare.[4] These types of molecules may possess interesting nonlinear optical properties owing to this special arrangement of multiple donor and acceptor substituents.

4.1.1 Scrambling of porphyrin

Though porphyrin endowed with donor acceptor groups at β-position have wider scope in terms of application, but it suffers serious limitation during synthesis i.e. “scrambling”, which resulted in formation of mixture of regio-isomers instead of desired product.[1] In general

porphyrins are synthesized by condensation of pyrrolic precursors in presence of acid or Lewis acid followed by oxidation. This exchange process generally observed in polypyrranes (Scheme 4.2) during condensation and is proposed to proceed by the fragmentation of

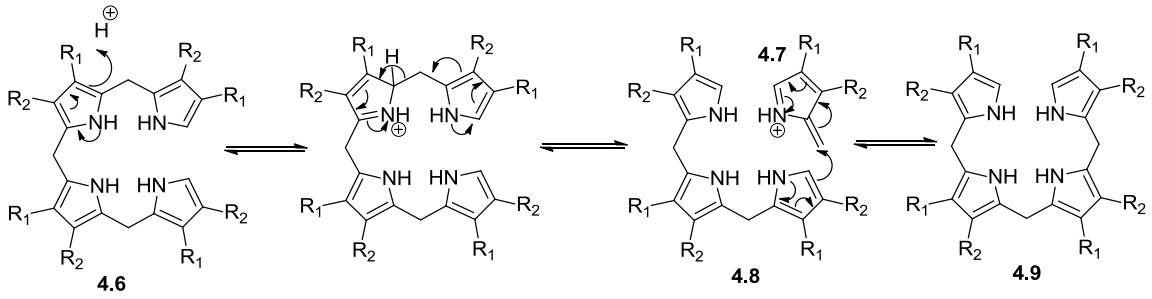

Scheme 4.2 Proposed pathways towards scrambling during acid catalyzed condensation.

polypyrrane (**4.6**) to pyrrolic (**4.8**) and azafulvene components (**4.7**). Later recombination of these fragments can form a new polypyrranes (**4.9**) that can't be formed by direct condensation, thereby, ultimately leads to a scrambled mixture of porphyrins. Though it is very difficult to control scrambling but several attempts have been made to control it. In this regard, Smith and coworkers developed the condensation of 2,5-bis-(N,N-dimethylamino-methyl)pyrroles (**4.10**) with 2,5-diunsubstituted pyrroles (**4.11**) under neutral condition in

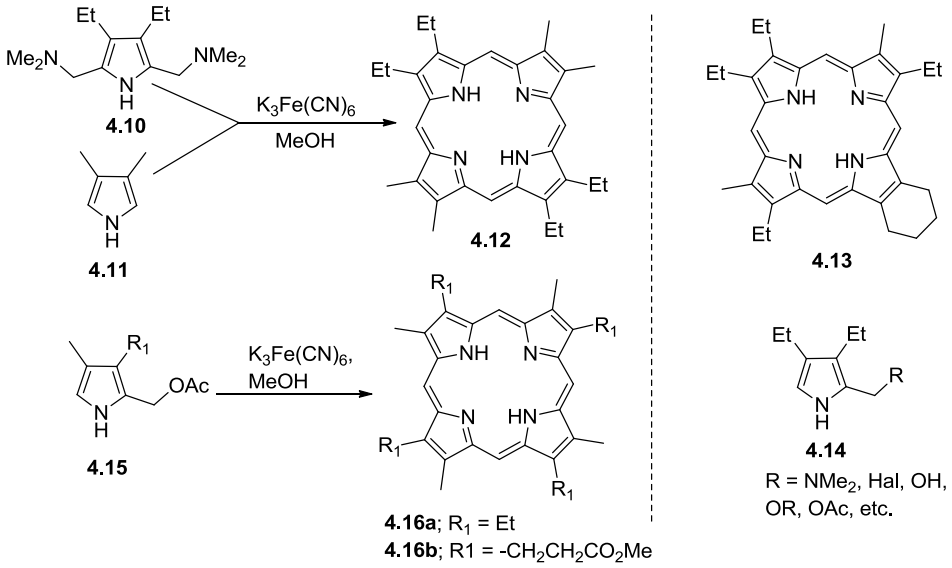

Scheme 4.3 Synthesis of "type-I" β-substituted porphyrins.

presence of $K_3[Fe(CN)_6]$ as oxidant to obtain unscrambled porphyrins in good yield (Scheme 4.3).[5] They further extended this method to synthesize unsymmetrical porphyrins (**4.13**) by [3+1] condensation of tripyrrane and 2,5-bis-(N,N-dimethylaminomethyl)pyrroles (**4.10**).[6] Further, this method works well with the cyclo tetramerisation of monopyrrole (**4.14**), where

2-position substituted with a carbon bearing good leaving group with 3- and 4-substituents are different, resulted with only "type-I" porphyrin (**4.16**).[7] Later, Lindsey and coworkers studied the mechanistic details by using different acids along with different additives for the [2+2] McDonald type condensation of a 5-substituted dipyrromethane and an aldehyde for the synthesis of meso aryl substituted *trans*-A_2B_2porphyrins.[8] They employed laser desorption mass spectrometry (LDMS) method enabled rapid screening of the degree of scrambling as a function of acid catalyst, reagent concentration, reagent stoichiometry, solvent, salts and temperature. They have identified two conditions which gave little or no scrambling: (1) condensation at 10 mM in acetonitrile at 0 °C with $BF_3.OEt_2$ catalyst with NH_4Cl as additive followed by oxidation with DDQ, and (2) condensation at 0.1 M in DMSO at 100 °C in presence of NH_4Cl followed by air oxidation. Further, they also examined 17 different acid catalysts for condensation of dipyrromethane carbinols towards the synthesis of meso substituted porphyrins and found that four acids ($InCl_3$, $Sc(OTf)_3$, $Yb(OTf)_3$ and $Dy(OTf)_3$) works best in terms of suppressing scrambling and decreasing acidolysis.[9]

4.2 Research goal

Here, we report the first synthesis of type-I 3,8,13,18-tetrachloro-2,7,12,17-tetramethoxy-porphyrin **4.17**.[10] This molecule is unique, in the sense that it contains an electron donating methoxy and electron withdrawing chloro group on the adjacent β-positions of each pyrrole moiety. This could be achieved due to the unprecedented synthesis of 3-chloro-4-methoxy-pyrrole-2-aldehyde **4.19** from exhaustive formylation of 3,4-dimethoxypyrrole **4.18**.[11] Further, the basis of design in most of these systems for better NLO response is to have suitable donor and acceptor functionalities at the periphery of aromatic porphyrin ring or extended multi-porphyrinic systems.[12] In this regard, monomeric porphyrin units were also studied as either reference for designing more accomplished systems or as standalone systems to gain understanding about their NLO response. We envisaged β-octasubstituted porphyrins which could be synthesized quite conveniently, could possibly, emerge as attractive target systems. Therefore, we wish to synthesize porphyrin **4.17** along with its Zn(II) and Ni(II) complexes, to evaluates the effect of donor-acceptor substituents on β-pyrrolic moieties and effect of M(II) ion in the complexes towards their third order NLO properties.[13] Further, we evaluated the third order NLO response for analogous β-octamethoxyporphyrin **4.1** along with its Zn(II) complex, which is endowed with all eight electron donating methoxy groups at their β-positions for comparison.

4.3 Results and discussions

4.3.1 Synthesis of porphyrins

4.3.1.1 Exhaustive formylation of 3,4-dialkoxypyrroles

Owing to the electron rich character of 3,4-dimethoxypyrrole and hence higher reactivity, we presumed that by exhaustive formylation it may be possible to obtain the 2,5-dialdehyde derivative **4.20** in a single step that can be employed as a useful building block in porphyrinoid synthesis. However, when **4.18** was subjected to Vilsmeier–Haack formylation

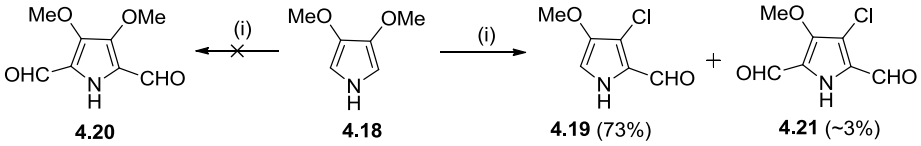

Scheme 4.4 Exhaustive formylation of 3,4-dimethoxypyrrole **4.18**. Reagents and conditions: (i) $POCl_3$/DMF (5 eqv), DCE, reflux, 8 h.

with five equivalents of DMF–$POCl_3$ we obtained two fractions after column chromatography, the first being a very minor fraction followed by the major fraction (Scheme 4.4). ^{1}H NMR spectra and mass analysis of neither fraction matched with **4.20**, it revealed some interesting facts, for example ^{1}H NMR spectra of both fractions display resonances corresponding to aldehyde groups (further confirmed from IR stretching bands at 1677 and 1633 cm^{-1} for first fraction and 1637 cm^{-1} for second fraction). Moreover, first fraction

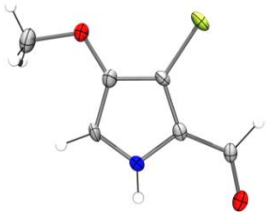

Figure 4.1 Molecular structure of **4.19** scaled in 35% probability level. Color code: C, grey; H, white; N, blue; Cl, yellow green.

possessed two very close lying resonances at 9.86 and 9.87 ppm for aldehyde protons and the intensity ratio of CHO:NH:α-CH:OMe protons in ^{1}H NMR is 2:1:0:3 and the corresponding ratio for the second fraction is 1:1:1:3. The above data clearly indicate the asymmetric nature of both the products along with only mono formylation in the second fraction. Mass spectra reveal peaks at 186 and 160 for the two fractions. As Vilsmeier reagent sometimes leads to chlorination,[14] we assumed one of the β-substituents as chlorine. When we tried to reinterpret our data, excellent agreement was observed. This was further confirmed by elemental

analysis. However, accurate regiochemistry could be unequivocally assigned from the solid state structure obtained from the single crystal of the second fraction via XRD analysis (Figure 4.1). Subsequently, the first fraction was assigned as the structure **4.21** (~3%) and the major fraction as **4.19** (73%). The formation of **4.19** could be explained on the basis of the following mechanism (Scheme 4.5) that also explains the formation of **4.21** upon the use of

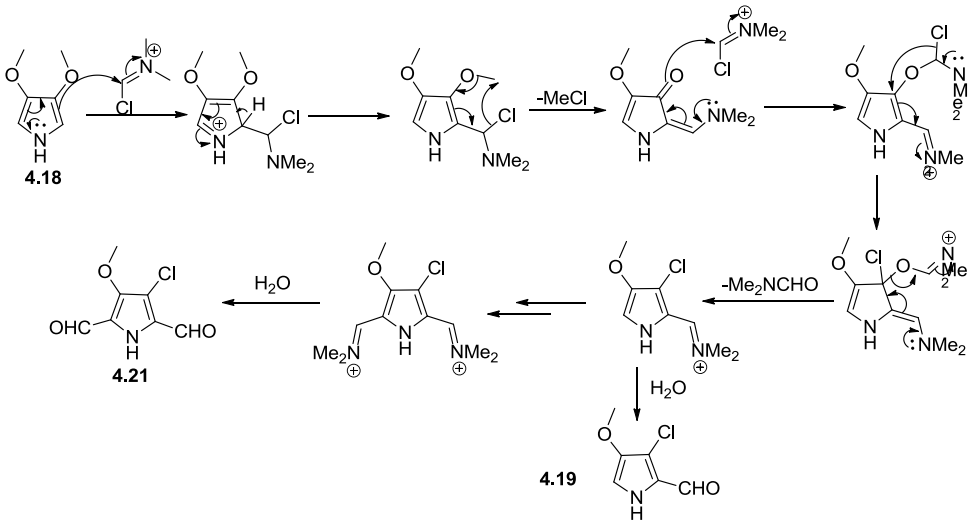

Scheme 4.5 Proposed mechanism for the formation of **4.19** and **4.21** from **4.18**

excess Vilsmeier reagent. Further increase of reaction time or increase of Vilsmeier reagent to 10–20 equiv. only reduced the yield of **4.19**. Also decreasing Vilsmeier reagents (< 5 equiv) not only decreased the yield of **4.19** but also led to the formation of 3,4-dimethoxypyrrole-2-aldehyde as a byproduct.

To evaluate further applicability of this unusual transformation we performed Vilsmeier–Haack formylation of **4.18**, where Vilsmeier reagent prepared form PBr_3 and DMF (5 equiv)

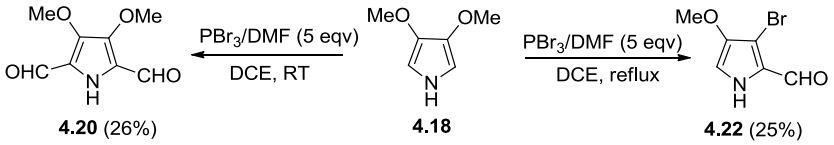

Scheme 4.6 Exhaustive formylation of 3,4-dimethoxypyrrole using PBr_3/DMF.

in DCE led to formation of desired 3-bromo-4-methoxypyrrole-2-aldehyde (**4.22**) in 25% yield under reflux condition (Scheme 4.6). Relatively, poor yield may be resulted from poor solubility of Vilsmeier reagent (PBr_3/DMF) in DCE and longer reaction time (40 h). Further, using DMF though solubility issue of Vilsmeier reagent could be taken care, however we could not observed the formation of **4.22**. On the other hand, when we performed the reaction

at room temperature (2 days) in DCE, it led to formation of 3,4-dimethoxypyrrole-2,5-dialdhyde (**4.20**) in 26% yield, indicating demethoxylation and halogenation at 3-position of pyrrole occurs under reflux condition.

We also performed exhaustive formylation of other 3,4-dialkoxypyrroles (ethoxy, propoxy and butoxy) using $POCl_3$/DMF as Vilsmeier reagent to evaluate the effect of alkoxy groups (Scheme 4.7). Under identical condition, with corresponding 3,4-dialkoxypyrrole (**4.23a-c**), described in scheme 4.4, we could not able to observed chlorinated product, instead only

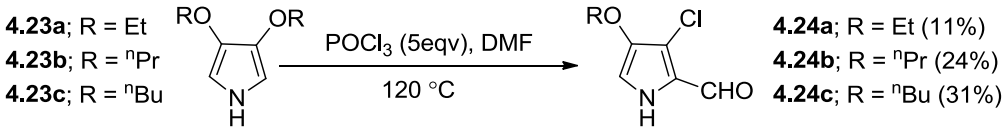

Scheme 4.7 Exhaustive formylation of 3,4-dialkoxypyrroles (**4.23a-c)**

corresponding monoformylated products were isolated. However, at higher temperature i.e. formlylation of **4.23a-c** in DMF at 120 °C (8 h) led to formation of corresponding 3-chloro-4-alkoxypyrrole-2-aldehydes (**4.24a-c**) in 11%, 24% and 31% respectively. Therefore, requirement of relatively higher temperature proves our presumption for the proposed mechanism (Scheme 4.5), and relatively low yield for higher alkoxypyrroles compared to methoxy analogue, may be attributed to difficulty in elimination of heavier alkyl halide and thereby hindering the progress of the reaction in forward direction.

4.3.1.2 Synthesis of 3,8,13,18-tetrachloro-2,7,12,17-tetramethoxyporphyrin (4.17) and its metallo-derivatives

Sodium borohydride reduction of **4.19** yielded the hydroxymethyl derivative **4.25**, which was directly used in the next step after work up. Refluxing **4.25** in acetic acid led to the formation of the desired tetrachlorotetramethoxyporphyrin in 48% yield, *albeit*, as a mixture of regio-isomers. In order to obtain the type I porphyrin derivative **4.17** in pure form, we checked the reactivity of **4.25** following various literature procedures, using different acid catalysts *viz.* $BF_3.OEt_2$,[15] TFA,[8] and *p*-TsOH[4] (Figure 4.2). The minimum scrambling was observed in case of TFA. Further, use of 48% HBr in ethanol[16] and $K_3[Fe(CN)_6]$ in acetic acid[17] also led to scrambled product only. Therefore, further optimization of reaction condition was performed by modulating the time and equivalents of TFA (Figure 4.2), which led us to the optimal condition to obtain pure **4.17** in 5.8% yield using 0.1 equiv of TFA for 15 min. Subsequent reaction under neutral condition using methanol as solvent and $K_3[Fe(CN)_6]$ as oxidant[5-7]

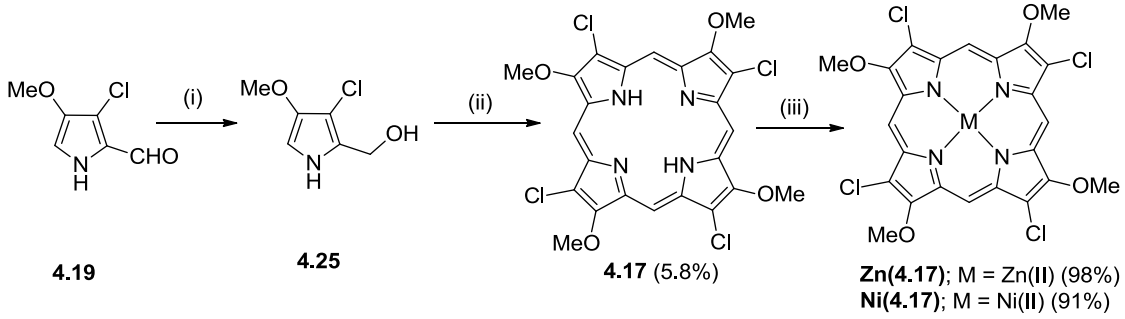

Scheme 4.8 Synthesis of porphyrin **4.17** and its metallo-derivatives. Reagents and conditions: (i) $NaBH_4$, MeOH, 4 h, RT; (ii) (a) TFA (0.1 equiv), $CHCl_3$, 15 min, (b) DDQ, 1 h; (iii) (a) M = Zn(II): $Zn(OAc)_2$, MeOH, $CHCl_3$, 8 h, reflux; (b) M = Ni(II): $Ni(acac)_2$, *o*-xylene, 4 h, reflux.

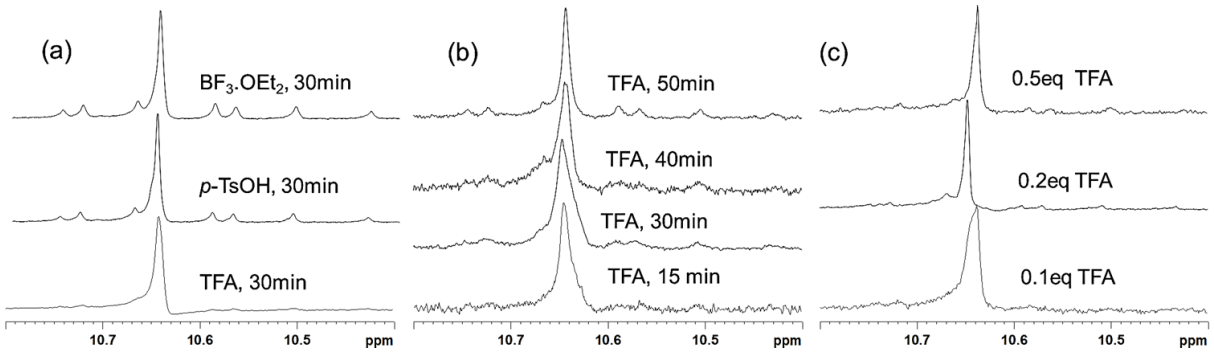

Figure 4.2 Acid catalyzed scrambling study toward formation of **4.17** using ^{1}H NMR (*meso* protons part) (a) using different acid catalysts (b) using 0.1 equiv TFA with time and (c) using different concentration of TFA reaction run for 30 min.

produced the desired pure porphyrin derivative with slightly reduced yield (4.5%). Metallation of **4.17** using various metal(II) salts *viz.* Zn(II) and Ni(II) led to the successful insertion of metal onto the porphyrin core (confirmed by UV-Vis study). The products were characterized using ^{1}H NMR, ^{13}C NMR, UV-Vis, mass spectra, and elemental analysis.

4.3.2 ^{1}H NMR studies

The effect of four chloro groups at the β-positions could be clearly observed by the downfield shift of the NH resonance form -4.41 (in case of **4.1**) to -4.13 ppm (Table 4.1). Similarly, the methoxy protons appear at 4.99 (**4.1**; 4.79) ppm. However, the shift is minimal in case of the meso-Hs. This may be attributed to the cancellation of dipole owing to the symmetrical disposition of the four chloro substituents at the porphyrin periphery. Further, similar type of observation was also reported for **4.5a-b**.[4a] However, due to poor solubility, **Ni(4.17)** could not be characterized by ^{1}H NMR spectroscopy.

4.3.3 Photophysical properties

The UV–visible spectra for compounds **4.17**, **Zn(4.17)** and **Ni(4.17)** are presented in Figure 4.3a and the spectra data in Table 4.1. Freebase porphyrin **4.17** displayed strong near-UV Soret absorption band at 383 nm, accompanied with four weaker Q-bands in the visible

Table 4.1 Ground state photophysical studies of the porphyrins in chloroform at 25 °C.

Porphyrins	UV-Vis (nm, log ε)	λ_{max} (Fl) nm (ϕ)[a]	τ_f (ns)[b]
4.17	383 (4.85), 502 (3.80), 539 (3.81), 571 (3.60), 626 (3.64)	629, 659, 696 (0.045)	4.54
4.1	377 (5.19), 494 (3.98), 530 (4.09), 564 (3.76), 618 (3.78)	622, 647, 688 (0.061)[c]	3.77
Zn(4.17)	409 (5.02), 540 (3.99), 579 (4.03)	584, 638 (0.032)	0.17, 1.18
Zn(4.1)	398 (5.34), 533 (4.24), 565 (4.29), 573 (4.33)	578, 632 (0.031)[c]	0.17, 1.32
Ni(4.17)	391 (5.06), 519 (3.88), 558 (4.34)	---	---

[a] for fluorescence quantum yield measurements - H_2OEP (ϕ_f 0.13) for freebase porphyrins and Zn(II)OEP (ϕ_f 0.045) for Zn(II) complexes were used as reference, [b] fluorescence lifetime, [c] fluorescence quantum yield measured in benzene.

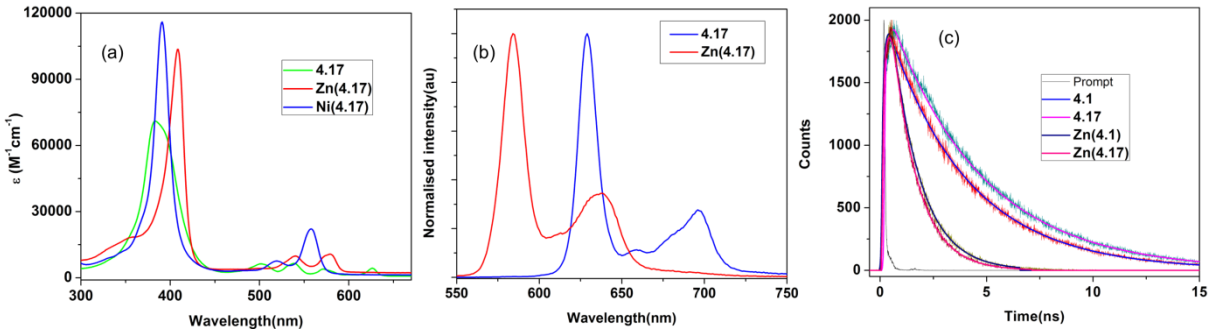

Figure 4.3 (a) UV-Vis spectra, (b) Fluorescence spectra and (c) fluorescence decay profiles of porphyrins.

region, whereas the Zn(II)-complexes of **4.17** i.e. **Zn(4.17)** and **Ni(4.17)** derivatives possess strong Soret absorption bands at 409 nm and 391 nm, respectively, with two characteristic weaker Q-bands in the visible spectral region (519-579 nm). The porphyrins **4.17** and **Zn(4.17)** emit in the red regions with emission maxima at 629 and 584 nm, respectively. There is a marginal red shift in UV-Vis spectra of **4.17** along with Zn(II) and Ni(II) complexes compare to porphyrin **4.1**, probably due to high symmetry in structure which nullifies the electron withdrawing effect of chloro groups. Except for Ni(II)-derivative (which did not fluoresce), the emission spectra of the other porphyrins are presented in Figure 4.3b. These porphyrins display two prominent emission peaks, with **Zn(4.17)** at 575 and 630 nm,

which are blue shifted compared to the freebase porphyrin, i.e. **4.17** that displayed two peaks near 625 and 680 nm. Similar to UV-Vis spectra, we also observed slightly red shifted emission maxima for **4.17** and **Zn(4.17)** compared to corresponding octamethoxy analogue (**4.1** and **Zn(4.1)**). The fluorescence lifetime data of **4.1**, **4.17**, and their Zn(II) derivatives are

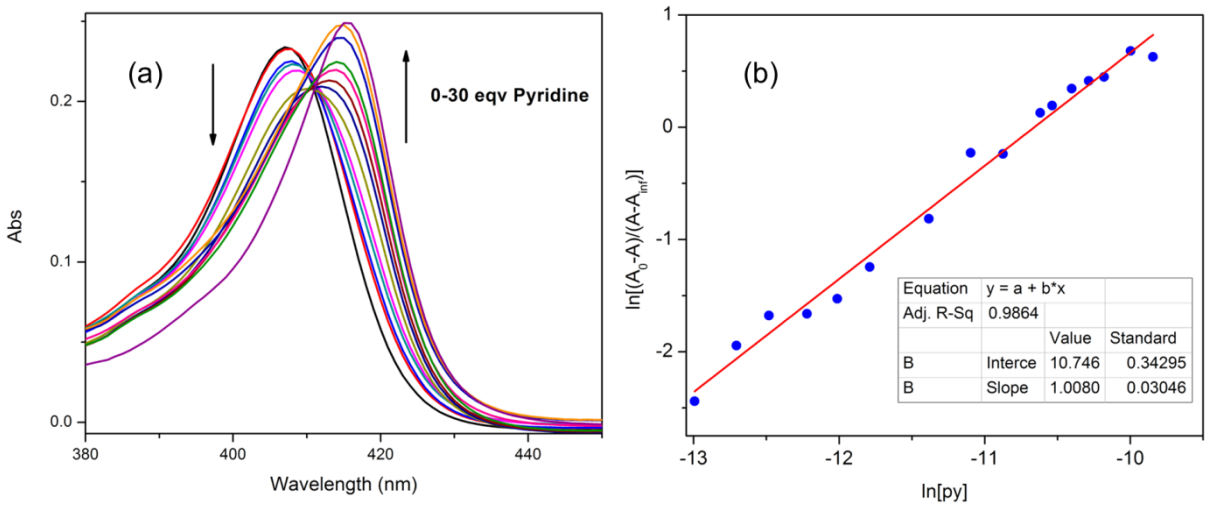

Figure 4.4 (a) UV-Vis spectral change of **Zn(4.17)** with addition of pyridine. (b) Hill plot for axial ligation of pyridine with **Zn(4.17).** Hill plot showing 1:1 binding of **Zn(4.17)** with pyridine. In this plot A_0, A and A_{inf} stands for absorbance at 407 nm of **Zn(4.17)**, partially ligated complex, completely ligated complex, [py] indicates the molar concentration of pyridine.

tabulated in Table 4.1, whereas their life time decay profiles are depicted in Figure 4.3c. Freebase porphyrins **4.1** and **4.17** both demonstrated shorter lifetimes of 3.77 and 4.54 ns, respectively, compared to its octaethyl analogue.[18] Whereas, Zn(II) complexes of **4.1** and **4.17** exhibited dual lifetimes, however, relatively shorter compared to their freebase analogues. The reduced singlet life time of these molecules may be attributed to efficient deactivation by oxygen and/or chloro groups present at the periphery.

Although the effect of chloro groups could not be observed prominently in the absorption and emission spectra, but the relative decrease in basicity of the porphyrin could be observed from the increase in affinity of **Zn(4.17)** towards pyridine, using toluene as a non-coordinating solvent (ln K = 10.75, K = 4.66×10^4 M^{-1}) with 1:1 binding stoichiometry (Figure 4.4).[19] Whereas **Zn(4.1)** owing to its greater basicity didn't show any affinity toward pyridine, instead could only interact with much stronger bases like piperidine as axial ligand.[20]

4.3.4 Molecular structure analysis

The solid state structure obtained via single crystal (obtained by sublimation at 290 °C and ~0.001 mmHg) X-ray diffraction study revealed a planar macrocyclic framework according

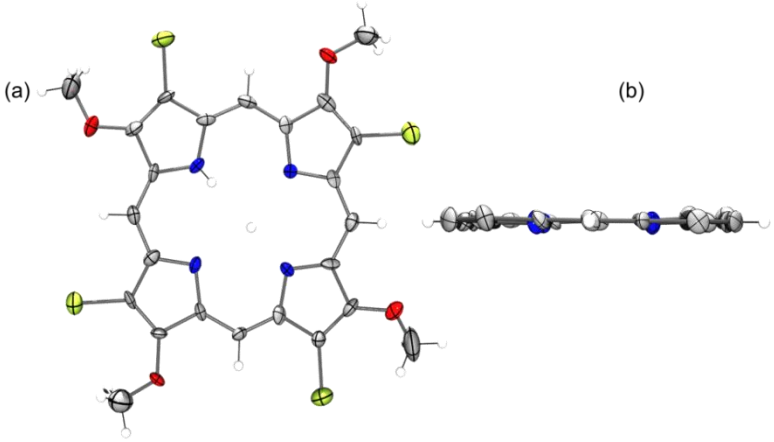

Figure 4.5 Molecular structure of **4.17** scaled in 35% probability level (a) front view and (b) side view. In side view methoxy and chloro groups are omitted for clarity. Color code: C, grey; H, white; N, blue; Cl, yellow green.

to our expectation on the basic of the spectroscopic data obtained (Figure 4.5). The maximum displacements of imino N from mean plane drawn through macrocyclic core is 0.055 Å. Similar to other β-substituted porphyrins, it adopts near square type core.

4.3.5 Two photon absorption (TPA) studies

The two photon absorption studies for porphyrins were carried out in collaboration with S. Venugopal Rao's research group at ACRHEM, University of Hyderabad. The NLO coefficients (β) and absorption cross-sections (σ_2) were extracted from the open aperture data presented in Figure 4.6a while n_2 was calculated from the closed aperture data presented in Figure 4.6b using the Sheik–Bahae formulation.[21] Table 4.2 depicts the n_2 values of the molecules investigated indicating a positive non-linearity (magnitude of $\sim 10^{-16}$ cm^2/W). TPA coefficients were obtained from experimental data and the magnitudes were $\sim 10^{-11}$cm/W. TPA cross-sections (σ_2) were also estimated from TPA coefficients and the magnitudes were in the range of 10^3–10^4 GM. The complete summary of NLO coefficients and cross-sections along with third order NLO susceptibilities are presented in Table 4.2. The effect of introduction of electron withdrawing chloro-groups to an electron rich porphyrin core, which imparts a donor-acceptor characteristic to the resultant macrocycles, could be clearly noticed in these porphyrins, with large enhancement in σ_2 values in case of porphyrin **4.17** and its

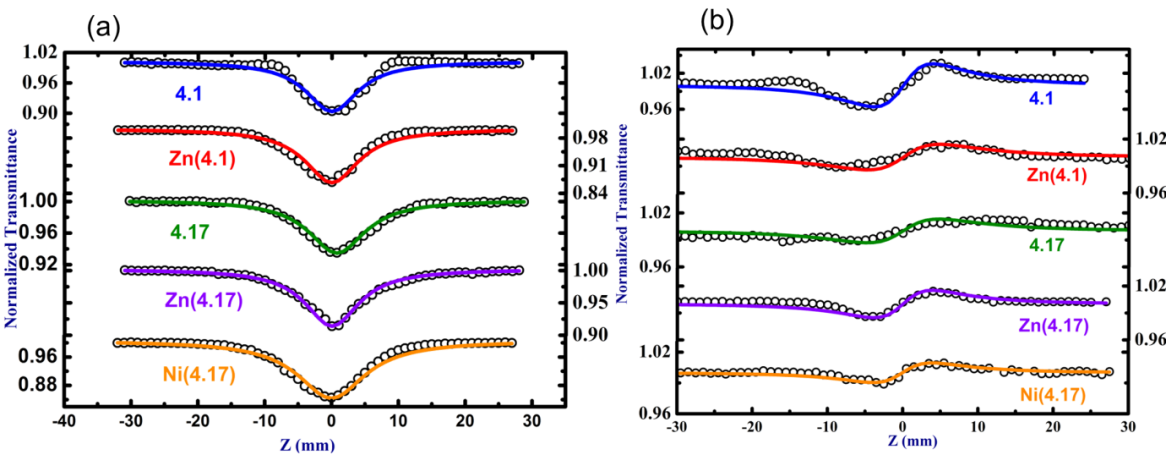

Figure 4.6 (a) Open aperture data for porphyrins. The data were recorded at 800 nm in chloroform with a peak intensity of ~100–200 GW/cm^2. (b) Closed aperture data for porphyrins. The data were recorded at 800 nm in chloroform with a peak intensity of <50 GW/cm^2. For clarity the tick labels for two samples are indicated on right axes.

Table 4.2 Summary of NLO coefficients, cross-sections of various porphyrin derivatives studied using ~2 ps, 1 kHz pulses

Porphyrins	n_2 **(cm^2/W) × 10^{-16}**	β **(cm/W) ×10^{-11}**	σ_{2PA} **(GM)**	**Re$\lvert\chi^{(3)}\rvert$ (esu) × 10^{-14}**	**Im$\lvert\chi^{(3)}\rvert$ (esu) × 10^{-22}**	**$\lvert\chi^{(3)}\rvert$ (esu) × 10^{-14}**	**$\lvert\chi^{(3)}\rvert$ (m^2/V^2) × 10^{-22}**
4.1	2.90	2.85	1960	1.52	0.95	1.80	2.50
Zn(4.1)	1.20	4.20	4000	0.63	1.40	1.52	2.10
4.17	1.10	1.85	6440	0.57	0.61	0.85	1.20
Zn(4.17)	1.25	2.50	14740	0.65	0.83	1.06	1.50
Ni(4.17)	0.80	5.20	53690	0.41	1.74	1.80	2.50

metallo-derivatives (containing four electron donating methoxy and four electron withdrawing chloro-groups), as compared to porphyrin **4.1** and its metallo-derivatives (containing only eight electron donating methoxy groups). The largest σ_2 value was obtained for **Ni(4.17)** (~5 × 10^4 GM). Interestingly, Zn(II) and Ni(II) complexes of **4.17** demonstrated strong 2PA coefficients and cross-sections compared to freebase itself which, probably, could be attributed to the effect of central metal ion.[12b] Porphyrin **4.1** and **Zn(4.1)** exhibited nearly twice the nonlinear absorption coefficient (β), when compared to that of **4.17** and **Zn(4.17)**. However, the n_2 value of porphyrin **4.1** was stronger compared to **4.17** molecule and metal derivative of **4.1**, i.e. **Zn(4.1)**. The closed aperture scans were performed with peak intensities <50 GW/cm^2 where we expect minimal contribution from nonlinear absorption and higher order nonlinearities. The NLO coefficients presented here are expected to encompass

predominant contributions from electronic motion since the studies were performed with ~2 ps pulses. However, detailed studies with using techniques such as degenerate four wave mixing have to be performed to separate contribution from other kind of nonlinearities such as molecular orientation.[22] The solvent contribution was negligible and was confirmed through open aperture data of solvent alone. In one of our earlier studies we had investigated the fs (~40 fs) NLO properties of some representative molecules and recorded n_2 values of $\sim 10^{-17}$cm^2/W and β values of 10^{-13}cm/W (solvent contribution was minimal).[23] These n_2 values truly represent the electronic nonlinearity.

4.3.6 Femto-second pump-probe experiments

Figure 4.7 depicts the pump-probe data of porphyrin **4.1**, **Zn(4.1)**, and **4.17** obtained at 600 nm using ~70 fs pulses. The data was fitted using the equation given below containing triple exponentials.[24]

$$\frac{\Delta T(t)}{T} = y_0 + A_1 e^{-(t-t_0)/\tau_1} + A_2 e^{-(t-t_0)/\tau_2} + A_3 e^{-(t-t_0)/\tau_3}$$

where $\Delta T(t)$ is the time dependent change in probe transmission. We attempted fitting the

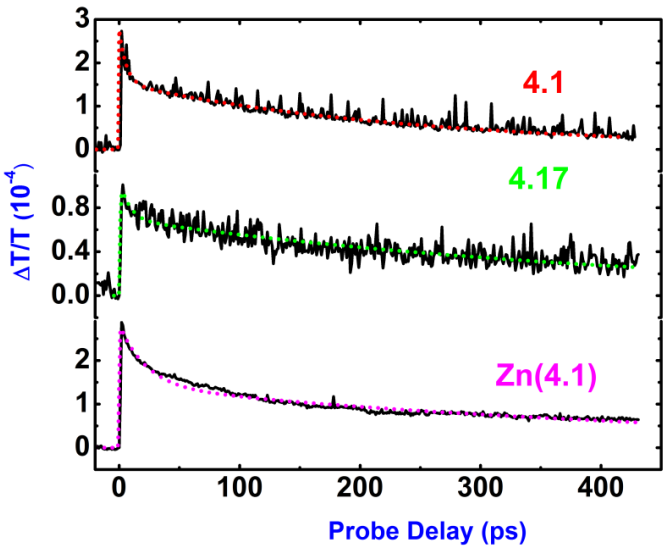

Figure 4.7 Pump-probe data (wriggly line) and the theoretical fits (dotted lines) for porphyrins recorded at 600 nm in chloroform.

data using two exponentials[24b] but the fits were poor, especially at the initial time scales (<30 ps). The three lifetimes obtained (τ_1, τ_2, and τ_3) are summarized in Table 4.3. Before assigning the lifetimes observed from our pump-probe data we thoroughly investigated the literature on similar porphyrins and their dynamics. Ha-Thi et al. studied ultrafast dynamics

of copper(II)tetraphenylporphyrin (CuTPP), copper(II)octaethylporphyrin (CuOEP), and the freebase tetraphenylporphyrin (H_2TPP) in the gas phase.[25] The first two molecules exhibited a sequential four-step decay ending on a slow evolution in the nanosecond range $^2S_2 \rightarrow {}^2CT \rightarrow {}^2T \rightarrow {}^2$ground state. For the free-base case, the first ultrafast time constant of ~110 fs was attributed to an extremely rapid S_2–S_1 internal conversion. Okhrimenko et al. measured a slow component with lifetime of ~690 ps in a Ni(II)porphyrin derivative, which was independent of probe wavelength. This process was established to be an electronic deactivation from the metal $d_{x^2-y^2}$ excited state to its d_{z^2} ground state.[22] Three lifetimes were observed in the studies of Ni(II)TPPF, Ni(II)TNPP, and Ni(II)TPrF_7P.[26] The fastest lifetime

Table 4.3 Fluorescence lifetimes and non-radiative lifetimes of various porphyrin derivatives studied using ~70 fs pulses

Porphyrins	Fluorescence lifetime (τ_f) (ns)	Lifetime 1 (τ_1) (ps)	Lifetime 2 (τ_2) (ps)	Lifetime 3 (τ_3) (ps)
4.1	3.77	0.6	6.0	250
Zn(4.1)	0.17, 1.32	0.3	22.0	480
4.17	4.54	0.6	8.0	430

(<1.2 ps) was assigned to ($\pi\pi^*$) → (d,d) transition while the intermediate lifetime (of few ps) was assigned to vibrational relaxation within the (d,d) states and the longest lifetime of 450-690 ps was assigned to the (d,d) → ground state transition. In the present case we do not expect participation of any 'd' states since there are no unfilled 'd' orbitals in our systems. In the case of **Ni(4.17)** we can possibly expect such states but the pump-probe data of this molecule has not been presented here (due to poor solubility). Furthermore, there is also no possibility of any charge transfer (CT) states existing in our molecules. Dogan et al. investigated the pump-probe dynamics of 5,10,15,20-tetrakis(4-hydroxyphenyl)porphyrin with different central metal ions (Zn^{2+}, Ni^{2+}, Co^{2+}, Fe^{3+}) using 532 nm excitation and observed three components in the data.[27] They attributed the observed three lifetimes to ($S_2 \rightarrow S_1$), ($S_1 \rightarrow$ ISC), ($T_1 \rightarrow S_0$) transitions for filled 'd' shell metal and free base porphyrins, on the other hand those were attributed to ($S_2 \rightarrow S_1$), ($S_1 \rightarrow$ d), (d → S_0) for unfilled 'd' shell metal porphyrins. Yoon et al. investigated several highly symmetric expanded porphyrins and observed singlet excited state lifetime varying from 0.7 ps to 560 ps.[28] Zewail's group studied ultra-fast dynamics in freebase/Zn(II) tetraphenylporphyrins and from the detailed transient

absorption data they assigned the lifetimes of (a) 100–200 fs for intramolecular vibrational energy redistribution (b) 1.4 ps for vibrational redistribution caused by elastic collision with solvent molecules and (c) 10–20 ps for thermal equilibration by energy exchange with solvent.[29] Howe and Zhang studied two phthalocyanine molecules and observed two lifetimes (10 ps and 370/460 ps) which they assigned to internal conversion from S_2 to S_1 (possibly including vibrational relaxation within S_1) and S_1 to S_0 non-radiative transitions.[30]

Figure 4.8 shows a typical energy level diagram considering the various absorption peaks for the molecules investigated. We propose the following mechanisms of de-excitation and based on that the observed three different lifetimes can possibly be assigned to specific processes. The shortest lifetime (τ_1) of 300–600 fs could be attributed to the internal conversion (IC) from S_2 states to the highest lying S_1 states. The shorter lifetime (τ_2) could, possibly, be attributed to vibrational relaxation within the S_1 states manifold. The longest lifetime, probably, has strong component from the non-radiative relaxation from S_1 state to the ground state. The other two plausible contributions to τ_3 are (a) from the radiative lifetime (S_1 to S_0)

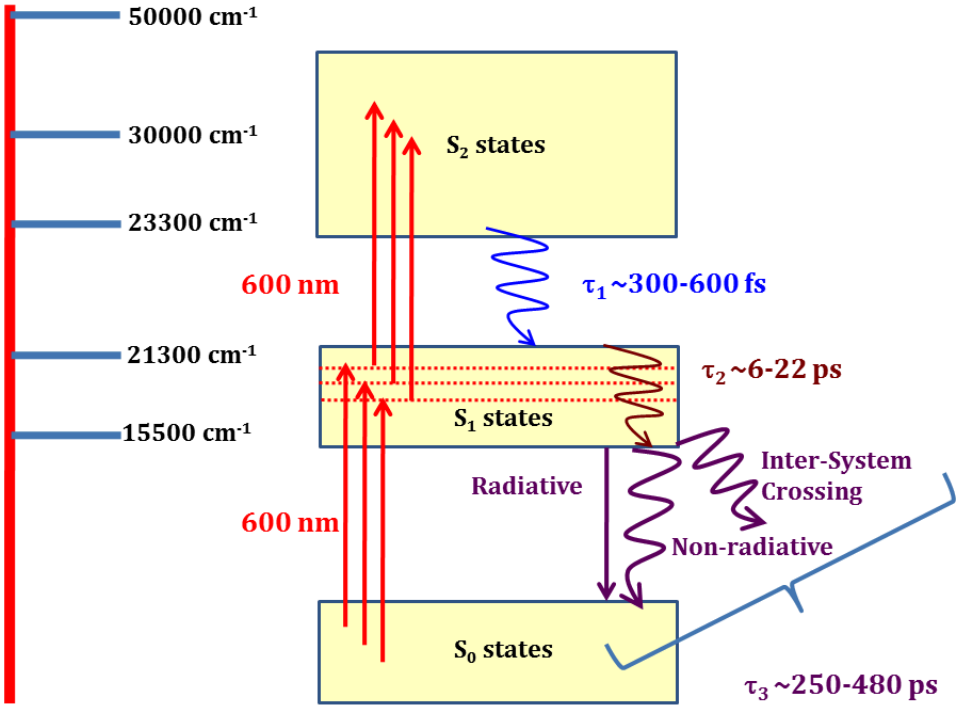

Figure 4.8 Simplified energy level diagram explaining the observed pump-probe dynamics using possible de-excitation mechanisms.

and (b) intersystem crossing (S_1 to T_1).[30] However, magnitude of the former can be considered to be negligible since the fluorescence quantum yields of these molecules are typically < 6% while the intersystem crossing component, though occur on similar time

scales or shorter, cannot be quantified from the present studies. Moreover, it was reported in similar molecules that in the absence of interaction between porphyrin macrocycle π orbitals and metal ion 'd' orbitals intersystem crossing rates will typically be in the ns time scales.[27] Furthermore, there could be a longer component (of few ns) in the pump-probe data since the bleaching has not recovered fully (Figure 4.7) and this possibly could reflect the radiative lifetime. Due to limitations in our delay stage we could not record the signal beyond 600 ps. However, detailed transient absorption data (using white light probe) is essential to exactly identify the origin of the observed three lifetimes. The important point we try to convey is that these molecules possess fast lifetimes and can be tailored with structural modifications, which is essential to arrive at potentially device capable molecules. The lifetimes observed in the present studies are similar to the ones measured in porphycenes, recently investigated by our group.[31]

4.4 Conclusion

In conclusion, we have demonstrated the synthesis and characterization of 3,8,13,18-tetrachloro-2,7,12,17-tetramethoxyporphyrin (**4.17**), which could be achieved owing to the unexpected synthesis of 3-chloro-4-methoxypyrrole-2-aldehyde (**4.19**) during exhaustive formylation of 3,4-dimethoxypyrrole (**4.18**). Selective chlorination of pyrrole at 3 or 4-position is much challenging, as it requires expensive catalytic condition but due to higher reactivity of 3,4-dimethoxypyrrole (**4.18**) we are able to achieve this by simple Vilsmeier-Haack formylation condition. We have extended this methodology towards synthesis of 3-bromo-4-methoxypyrrole-2-aldehyde (**4.22**) successfully. Also, requirement of longer alkyl substituents are much necessary in terms of enhanced solubility for further investigation as we have faced in the current studies. Therefore, we adapted this methods for higher 3,4-alkoxypyrroles (**4.23a-c**), to obtain the corresponding 3-chloro-4-alkoxypyrrole-2-aldehydes (**4.24a-c**) in moderate yield, employing higher temperature compared to methoxy analogue. Further, we have observed that by careful control of reaction condition we can suppress scrambling of porphyrin, which is one of the major obstacles for synthesis of unsymmetric porphyrins.

Also, we performed detailed studies for extracting the NLO coefficients and absorption cross-sections for above mentioned porphyrins along with their octamethoxy analogues. Fluorescence lifetimes measured for these molecules indicated radiative lifetime of ~0.17-4.54 ns. NLO coefficients and cross-sections retrieved from ps Z-scan technique were ~1.85-

5.2 × 10^{-11} cm^2/W and ~2000-54,000 GM, respectively. As expected, we have observed higher TPA absorption for chloromethoxy analogues, which arise from the presence of sequential electron donating and electron withdrawing substituents. The magnitudes of nonlinear refractive indices were ~0.8-2.9 × 10^{-16} cm^2/W. NLO measurements performed with ~40 fs pulses revealed the electronic contribution to the nonlinearity. Ultrafast decay dynamics were also investigated using fs degenerate pump-probe technique and three lifetimes observed were assigned to different de-excitation mechanisms.

The presence of multiple chloro groups makes this porphyrin an attractive candidate for catalysis and also as a potential photosensitizer for PDT. Recently, it is observed that the presence of halogens, in particular fluorine and chlorine reduces the porphyrin aggregation and enhances photocurrent generation, thereby, making them attractive materials for photovoltaics.[32] Presently, our efforts is on towards the synthesis of 3,8,13,18-tetrachloro-2,7,12,17-tetraalkoxyporphyrins, endowed with higher alkoxy groups and evaluate their possible potential applications.

4.5 Experimental details

General procedure for synthesis of 3-halo-4-alkoxypyrrole-2-aldehyde: To DMF (13.4 mL, 173 mmol) under nitrogen atmosphere $POCl_3$ (14.7 mL, 157 mmol) was added dropwise maintaining the temperature between 0-5 °C and then 1,2-dichloroethane (70 mL) was added to it. A solution of 3,4-dimethoxypyrrole (4 g, 31.5 mmol) in 1,2-dichloroethane (70 mL) was added dropwise, keeping temperature below 5 °C. After completion of addition, the reaction mixture was refluxed for 8 h, cooled to room temperature, and sat. NaOAc (64.5 g, 0.79 mol) was added to quench the reaction and the reaction mixture was refluxed for additional 2 h. After regular work-up, the crude product was purified by silica gel column using EtOAc/hexane (2:8) as eluent. Two fractions were collected. The minor first fraction gives **4.21**, as white crystalline product. The second major fraction yields **4.19**, as white crystalline solid.

3-Chloro-4-methoxypyrrole-2,5-dialdehyde (4.21): Yield: 168 mg (3%); m.p.:122° C; IR (neat): *ν* (cm^{-1}) 3108, 1677, 1633; ^{1}H NMR (400 MHz, $CDCl_3$), δ (ppm): 9.87 (s, 1H), 9.86 (s, 1H), 4.14 (s, 3H); ^{13}C NMR (100 MHz, $CDCl_3$), δ (ppm): 179.21, 178.63, 150.06, 128.54, 123.51, 111.72, 62.45; LCMS m/z calcd for $C_7H_6NO_3Cl$ 187, found (negative ionization) 186

(M^--1); Elemental Anal. Calcd for $C_7H_6NO_3Cl$: C, 44.82; H, 3.22; N,7.47. Found C, 44.65; H, 3.22; N, 7.61.

3-Chloro-4-methoxypyrrole-2-aldehyde (4.19): Yield: 3.7 g (73%); m.p.:172 °C; IR (neat): *v* (cm^{-1}) 3126, 1637; ^{1}H NMR (400 MHz, $CDCl_3$), δ (ppm): 9.61 (s, 1H), 9.26 (br s, 1H), 6.72 (d, 1H, *J* =1.4 Hz), 3.83 (s, 1H); ^{13}C NMR (100 MHz, $CDCl_3$), δ (ppm): 177.72, 145.76, 125.54, 111.48, 109.46, 58.94; LCMS m/z calcd for $C_6H_6NO_2Cl$ 159, found: 160 (M+1); Elemental Anal. Calcd for $C_6H_6ClNO_2$: C, 45.16; H, 3.79; N, 8.78. Found C, 45.26; H, 3.68; N, 8.78.

3-bromo-4-methoxypyrrole-2-aldehyde (4.22): Vilsmeier reagent was prepared from PBr_3 (554 µL, 5.90 mmol) and DMF (502 µL, 6.49 mmol). After addition of 3,4-dimethoxypyrrole (**4.18**) (150 mg, 1.18 mmol) in DCE (15 mL) reaction mixture was refluxed for 24 h. Yield: 59 mg (25%); m.p.: 170 °C; IR (neat): *v* (cm^{-1}) 3122, 1630; ^{1}H NMR (400 MHz, $CDCl_3$), δ (ppm): 9.62 (s, 1H), 9.16 (br s, 1H), 6.72 (d, 1H, *J* = 3.6 Hz), 3.83 (s, 3H); ^{13}C NMR (100 MHz, $CDCl_3$), δ (ppm): 177.84, 145.89, 125.67, 111.64, 109.68, 59.08 ; LCMS (ESI+): m/z: calculated for $C_6H_7BrNO_2$ (M^+): 204; found: 204; Elemental Anal. Calcd for $C_6H_6BrNO_2$: C, 35.32; H, 2.96; N, 6.87. Found C, 35.41; H, 2.89; N, 6.91.

3,4-dimethoxypyrrole-2,5-dialdehyde (4.20): Same procedure and scale followed as discussed for **4.22** but reaction mixture was run at room temperature for 48 h. Yield: 55 mg (26%). Spectral data are exactly matching with data previously reported by Sessler and coworkers.[33]

3-chloro-4-ethoxypyrrole-2-aldehyde (4.24a): After addition of 3,4-diethoxypyrrole (**4.23a**) (50 mg, 0.32 mmol) in DMF (5 mL) reaction mixture was run at 120 °C for 48 h. Yield: 6 mg (11%); m.p.: 161.7 °C; ^{1}H NMR (400 MHz, $CDCl_3$), δ (ppm): 9.60 (s, 1H), 9.23 (br s, 1H), 6.72 (t, 1H, *J* = 1.6 Hz), 4.01 (q, 2H, *J* = 6.8 Hz), 1.42 (t, 3H, *J* = 7.2 Hz); HRMS (ESI+): m/z: calculated for $C_7H_9ClNO_2$ ($M+H^+$): 174.0316; found: 174.0301.

3-chloro-4-propoxypyrrole-2-aldehyde (4.24b): After addition of 3,4-dipropoxypyrrole (**4.23b**) (50 mg, 0.27 mmol) in DMF (5 mL) reaction mixture was heated at 120 °C for 8 h. Yield: 12 mg (24%); m.p.: 121.8 °C; ^{1}H NMR (400 MHz, $CDCl_3$), δ (ppm): 9.95 (br s, 1H), 9.58 (s, 1H), 6.77 (t, 1H, *J* = 1.8 Hz), 3.90 (t, 2H, *J* = 6.8 Hz), 1.81 (sex, 2H, *J* = 7.6 Hz), 1.03 (t, 3H, *J* = 7.2 Hz); ^{13}C NMR (100 MHz, $CDCl_3$), δ (ppm): 177.81, 144.91, 125.46, 112.57,

111.32, 73.91, 22.70, 10.45; HRMS (ESI+): m/z: calculated for $C_8H_{11}ClNO_2$ ($M+H^+$): 188.0473; found: 188.0481.

3-chloro-4-butoxypyrrole-2-aldehyde (4.24c): After addition of 3,4-dibutoxypyrrole (**4.23c**) (50 mg, 0.24 mmol) in DMF (2 mL) reaction mixture was heated at 120 °C for 8 h. Yield: 15 mg (31%); m.p.: 109.3 °C; ^{1}H NMR (400 MHz, $CDCl_3$), δ (ppm): 9.61 (s, 1H), 9.02 (br s, 1H), 6.71 (t, 1H, *J* = 2.4 Hz), 3.93 (t, 2H, *J* = 6.8 Hz), 1.77 (quin, 2H, *J* = 6.4 Hz), 1.49 (sex, 2H, *J* = 7.6 Hz), 0.98 (t, 3H, *J* = 7.2 Hz); ^{13}C NMR (100 MHz, $CDCl_3$), δ (ppm): 177.80, 144.95, 125.46, 112.55, 111.27, 72.15, 31.40, 19.20, 13.94; HRMS (ESI+): m/z: calculated for $C_9H_{13}ClNO_2$ ($M+H^+$): 202.0629; found: 202.0635.

(3-chloro-4-methoxy-1H-pyrrol-2-yl)methanol (4.25): To **4.19** (500 mg, 3.14 mmol) in methanol (30 mL), under nitrogen atmosphere, $NaBH_4$ (2.38 g, 62.80 mmol) was added portion wise. After addition was complete the reaction mixture was stirred at room temperature for 4 h and then quenched with water. After regular work-up, **4.25** was obtained as colorless oil and was used in the next step without further purification. This oil turned brown when kept outside. ^{1}H NMR (400 MHz, $CDCl_3$), δ (ppm): 7.89 (br s, 1H), 6.29 (s, 1H), 4.61 (s, 2H), 3.76 (s, 3H).

3,8,13,18-tetrachloro-2,7,12,17-tetramethoxyporphyrin (**4.17):** To **4.25** (3.14 mmol, assuming 100% conversion in second step) obtained from the above reaction in chloroform (125 mL), under nitrogen atmosphere. TFA (24 µL, 0.314 mmol) was added with vigorous stirring, and the stirring was continued for 15 min. During this time, reaction mixture turned brown. The reaction mixture was quenched with the addition of excess triethylamine. The resultant reaction mixture was oxidized with DDQ (445 mg, 1.96 mmol) and the mixture was stirred for additional 1 h. Then the reaction mixture was evaporated to dryness and the black residue was dissolved in methanol and filtered to remove unreacted DDQ and other polymeric impurities. The resultant product was purified by silica gel column using chloroform as eluent. The first fraction (red color) was collected and evaporation of solvent yielded the desired type I pure porphyrin **4.17** as brown powder. Yield: 26 mg (6%); m.p.: > 300 °C; ^{1}H NMR (500 MHz, $CDCl_3$), δ (ppm): 10.14 (s, 4H), 4.99 (s, 12H), -4.13 (br s, 2H); ^{1}H NMR (400 MHz, $CDCl_3$ + TFA), δ (ppm): 10.64 (s, 4H), 5.1(s, 12H); ^{13}C NMR (100 MHz, $CDCl_3$ + TFA), δ (ppm): 154.70, 139.50, 134.78, 115.50, 112.67, 61.55; LCMS m/z Calcd for $C_{24}H_{18}N_4O_4Cl_4$ 568, found 569 (M+1); Elemental Anal. Calcd for $C_{24}H_{18}N_4O_4Cl_4$: C, 50.73; H, 3.19; N, 9.86. Found: C, 50.59; H, 3.25; N, 9.75.

Zn(II)-3,8,13,18-tetrachloro-2,7,12,17-tetramethoxyporphyrin (Zn(4.17)): To **4.17** (12 mg, 0.021 mmol) in chloroform (150 mL), $Zn(OAc)_2.2H_2O$ (46 mg, 0.21 mmol) in methanol was added and the resulting mixture was refluxed under stirring condition for 8 h, while color of the solution changed to bright pink. After aqueous work-up and subsequent washing of the product with methanol, the desired product was obtained as brown powder. Yield: 13 mg (98%); m.p.: >300 °C; ^{1}H NMR (400 MHz, $CDCl_3$), δ (ppm): 10.11 (s, 4H), 4.96 (s, 12H); LCMS m/z Calcd for $C_{24}H_{16}N_4O_4Zn$ 631.63, found 632.55 (M+1); Elemental Anal. Calcd for $C_{24}H_{16}N_4O_4Zn$: C, 45.64; H, 2.55; N, 8.87. Found: C, 45.52; H, 2.41; N, 8.71.

Ni(II)-3,8,13,18-tetrachloro-2,7,12,17-tetramethoxyporphyrin (Ni(4.17)): To **4.17** (12 mg, 0.021 mmol) in *o*-xylene (100 mL), $Ni(acac)_2$ (54 mg, 0.21 mmol) was added under nitrogen atmosphere and refluxed for 4 h. After cooling, the reaction mixture was evaporated to dryness under reduced pressure. The residue was washed with methanol several times to remove the impurities and the residue was dried under vacuum to obtain the desired product as pink color powder 12 mg (91%); m.p.: >300 °C; LCMS m/z Calcd for $C_{24}H_{16}N_4O_4Ni$ 624.91, found 625 (M^-); Elemental Anal. Calcd for $C_{24}H_{16}N_4O_4Ni$: C, 46.13; H, 2.58; N, 8.97. Found: C, 46.21; H, 2.51; N, 8.85.

4.6 Crystallographic Details

Crystallographic data for **4.19** was collected on BRUKER SMART-APEX CCD diffractometer. Mo−Kα (λ = 0.71073 Å) radiation was used to collect X-ray reflections on the single crystal. Crystallographic data for **4.17** was collected on Oxford Gemini A Ultra diffractometer with dual source. Mo-Kα (λ = 0.71073 Å) radiation was used to collect the X-ray reflections of the crystal.

Pertinent crystallographic data collection and refinement parameter are shown in the following tables:

Crystal Data	4.17	4.19
CCDC No.	816866	812392
Formula unit	$C_{24}H_{18}Cl_4N_4O_4$	$C_6H_6ClNO_2$
Formula Weight	568.22	159.57
Crystal system	Monoclinic	Monoclinic
T [K]	293(2)	298(2)
a [Å]	8.106(15)	8.527(4)
b [Å]	13.177(3)	7.396(3)
c [Å]	22.720(4)	11.155(5)
α [°]	90	90
β [°]	105.140(16)	92.963(7)
γ [°]	90	90
volume [$Å^3$]	2342.7(8)	702.6(5)
Space group	P 21/c	P 21/c
Z′	1	1
Z	4	4
D_{calc} [$g.cm^{-3}$]	1.679	1.509
μ/mm^{-1}	0.548	0.476
Reflns collected	8371	5272
Unique reflns	4004	1344
Obs. reflns	1101	1222
R(int)	0.1027	0.0599
R_1 [$I > 2\sigma(I)$],	0.0588(1101)	0.1158(1222)
wR_2	0.0509(4004)	0.2757(1344)
GOF	0.684	1.426

4.7 References

1. Kadish, K. M.; Smith, K. M.; Guilard, R. *The Porphyrin Handbook*; Academic Press: San Diego, **2000**, *Vol. 1-9*.
2. Senge, M. O. *Chem. Commun*. **2011**, *47*, 1943.
3. (a) Merz, A.; Scropp, R.; Dotterl, E. *Synthesis* **1995**, 795. (b) Senge, M. O.; Flögel, O.; Senge, K. R. *J. Porphyrin Phthalocyanines* **2001**, *5*, 503. (c) Sugiura, K.; Ravikumar, M.; Chandrashekar, T. K.; Sakata, Y. *Chem. Lett*. **1997**, *26*, 291. (d) Ono,

N.; Maruyama, K. *Chem. Lett*. **1988**, *17*, 1511. (e) Takeda, J.; Ohya, T.; Sato, M. *Chem. Pharm. Bull*. **1990**, *38*, 264. (f) Takeda, J.; Sato, M. *Chem. Lett*. **1994**, *23*, 2233.

4. (a) Ono, N.; Muratani, E.; Fumoto, Y.; Ogawa, T.; Tazima, K. *J. Chem Soc., Perkin Trans. I* **1998**, 3819. (b) Ono, N.; Kawamura, H.; Maruyama, K. *Bull. Chem. Soc. Jpn*. **1989**, *62*, 3386. (c) Aoyagi, K.; Toi, H.; Aoyama, Y.; Ogoshi, H. *Chem. Lett*. **1988**, *17*, 1891. (d) Onda, H.; Toi, H.; Aoyama, Y.; Ogoshi, H. *Tetrahedron Lett*. **1985**, *26*, 4221. (e) Homma, M.; Aoyagi, K.; Aoyama, Y.; Ogoshi, H. *Tetrahedron Lett*. **1983**, *24*, 4343.
5. Nguyen, L. T.; Senge, M. O.; Smith, K. M. *Tetrahedron Lett*. **1994**, *35*, 7581.
6. Nguyen, L. T.; Senge, M. O.; Smith, K. M. *J. Org. Chem*. **1996**, *61*, 998.
7. Nguyen, L. T.; Smith, K. M. *Tetrahedron Lett*. **1996**, *37*, 7177.
8. Littler, B. J.; Ciringh, Y.; Lindsey, J. S. *J. Org. Chem*. **1999**, *64*, 2864.
9. Geier III, G. R.; Callinan, J. B.; Rao, P. D.; Lindsey, J. S. *J. Porphyrins Phthalocyanines* **2001**, *5*, 810.
10. Rana, A.; Panda, P. K. *Tetrahedron Lett*. **2011**, *52*, 2697.
11. Merz, A.; Meyer, T. *Synthesis* **1999**, 94.
12. (a) Pawlicki, M.; Collins, H. A.; Denning, R. G.; Anderson, H. L. *Angew. Chem. Int. Ed*. **2009**, *48*, 3244. (b) Senge, M. O.; Fazekas, M.; Notaras, E. G. A.; Blau, W. J.; Zawadzka, M.; Locos, O. B.; Mhuircheartaigh, E. M. N. *Adv. Mater*. **2007**, *19*, 2737.
13. Swain, D.; Rana, A.; Panda, P. K.; Rao, S. V. *Chem. Phys. Lett*. **2014**, *610-611*, 310.
14. (a) Johnson, A. W.; Oldfield, D. *J. Chem. Soc. (C)* **1966**, 794. (b) Brahma, S.; Ray, J. K. *Tetrahedron* **2008**, *64*, 2883.
15. Lindsey, J. S.; Wagner, R. W. *J. Org. Chem*. **1989**, *54*, 828.
16. Syrbu, S. A.; Lyubimova, T. V.; Semeikin, A. S. *Chem. Heterocycl. Compd*. **2004**, *40*, 1262.
17. Momenteau, M.; Mispelter, J.; Loock, B.; Lhoste, J. M. *Can. J. Chem*. **1978**, *56*, 2598.
18. Ohno, O.; Kaizu, Y.; Kobayashi, H. *J. Chem. Phys*. **1985**, *82*, 1779.
19. (a) Hunter, C. A.; Meah, M. N.; Senders, J. K. M. *J. Am. Chem. Soc*. **1990**, *112*, 5773. (b) Hill, A. V. *J. Physiol. London* **1910**, *40*, IV.
20. Panda, P. K. Ph.D. Dissertation, Indian Institute of Science, Bangalore, India, **2002**.
21. Sheik Bahae, M.; Said, A. A.; Wei, T. H.; Hagan, D. J.; Van Stryland, E. W. *IEEE J. Quant. Electron*. **1990**, *26*, 760.

22. Okhrimenko, A. N. (PhD. thesis), Bowling Green State University, USA, **2005**.
23. Swain, D.; Rana, A.; Panda, P. K.; Rao, S. V. *Proc. SPIE* **2012**, *8258*, 82581B.
24. (a) Anusha, P. T.; Swain, D.; Hamad, S.; Giribabu, L.; Prashant, T. S.; Tewari, S. P.; Rao, S. V. *J. Phys. Chem. C* **2012**, *116*, 17828. (b) Swain, D.; Anusha, P. T.; Sarma, T.; Panda, P. K.; Rao, S. V. *Chem. Phys. Lett*. **2013**, *580*, 73.
25. Ha-Thi, M.-H.; Shafizadeh, N.; Poisson, L.; Soep, B. *J. Phys. Chem. A* **2013**, *117*, 8111.
26. (a) Eom, H. S.; Jeoung, S. C.; Kim, D.; Ha, J.-H.; Kim, Y.-R. *J. Phys. Chem. A* **1997**, *101*, 3661. (b) Rodriguez, J.; Kirmaier, C.; Holten, D. *J. Am. Chem. Soc*. **1989**, *111*, 6500. (c) Rodriguez, J.; Holten, D. *J. Chem. Phys*. **1990**, *92*, 5944.
27. Dogan, N.; Dumanogullari, F. M.; Hayvali, M.; Yilmaz, H.; Kurum, U.; Yaglioglu, H. G.; Elmali, A. *Chem. Phys. Lett*. **2011**, *508*, 265.
28. Yoon, Z. S.; Kwon, J. H.; Yoon, M.-C.; Koh, M. K.; Noh, S. B.; Sessler, J. L.; Lee, J. T.; Seidel, D.; Aguilar, A.; Shimizu, S.; Suzuki, M.; Osuka, A.; Kim, D. *J. Am. Chem. Soc*. **2006**, *128*, 14128.
29. (a) Baskin, J. S.; Yu, H.-Z.; Zewail, A. H. *J. Phys. Chem. A* **2002**, *106*, 9837. (b) Yu, H.-Z.; Baskin, J. S.; Zewail, A. H. *J. Phys. Chem. A* **2002**, *106*, 9845.
30. Howe, L.; Zhang, J. Z. *J. Phys. Chem. A* **1997**, *101*, 3207.
31. Rao, S. V.; Prashant, T. S.; Sarma, T.; Panda, P. K.; Swain, D.; Tewari, S. P. *Chem. Phys. Lett*. **2011**, *514*, 98.
32. Wróbel, D.; Siejak, A.; Siejak, P. *Sol. Energy Mater. Sol. Cells* **2010**, *94*, 492.
33. Sessler, J. L.; Callaway, W.; Dudek, S. P.; Date, R. W.; Lynch, V.; Bruce, D. W. *Chem. Commun*. **2003**, 2422.

4.8 Representative NMR spectra

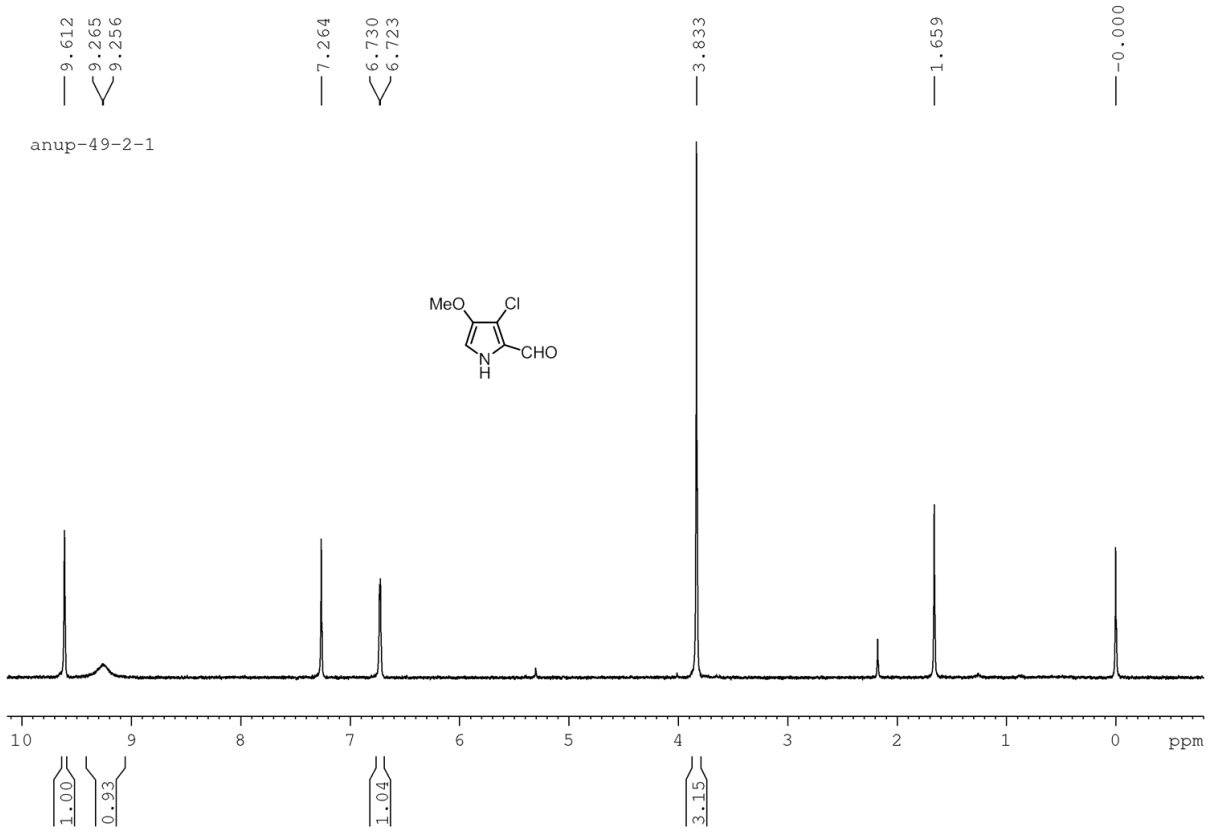

Figure 4.9 ^{1}H NMR spectrum of **4.19** in $CDCl_3$.

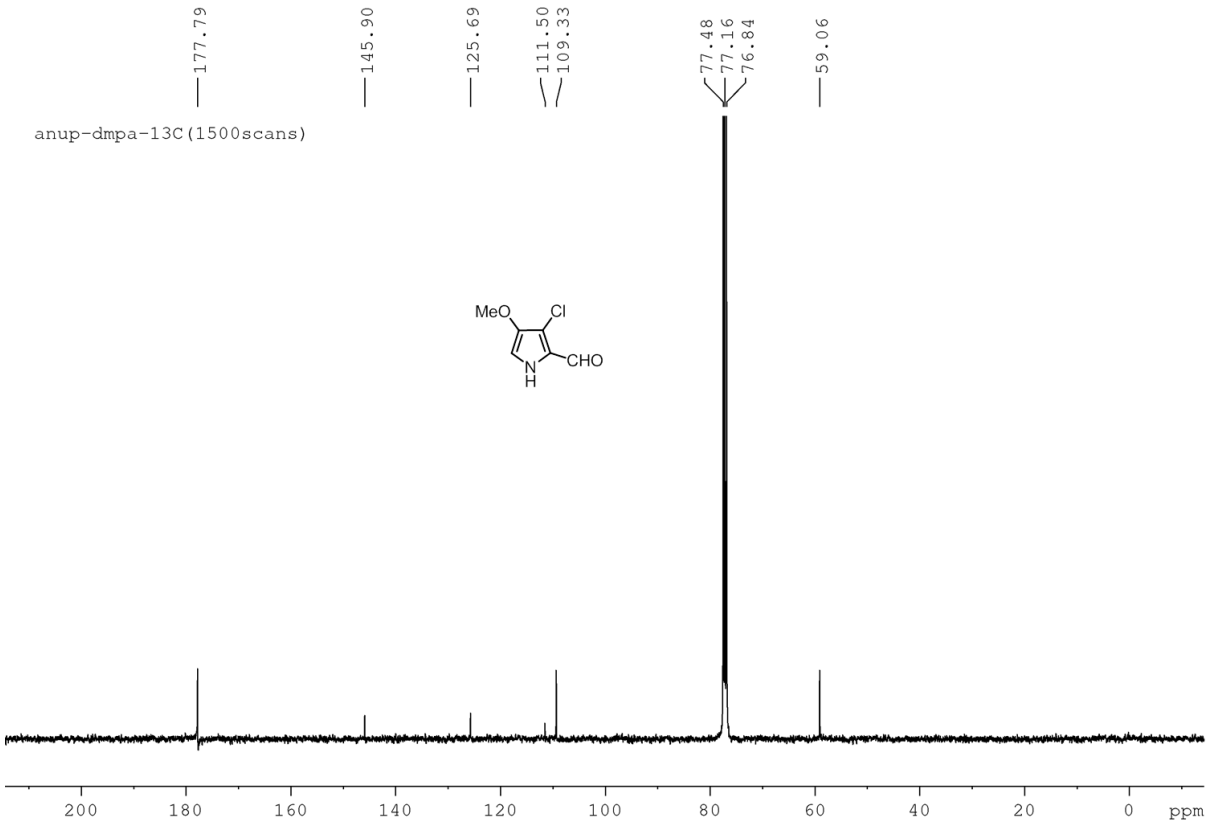

Figure 4.10 ^{13}C NMR spectrum of **4.19** in $CDCl_3$.

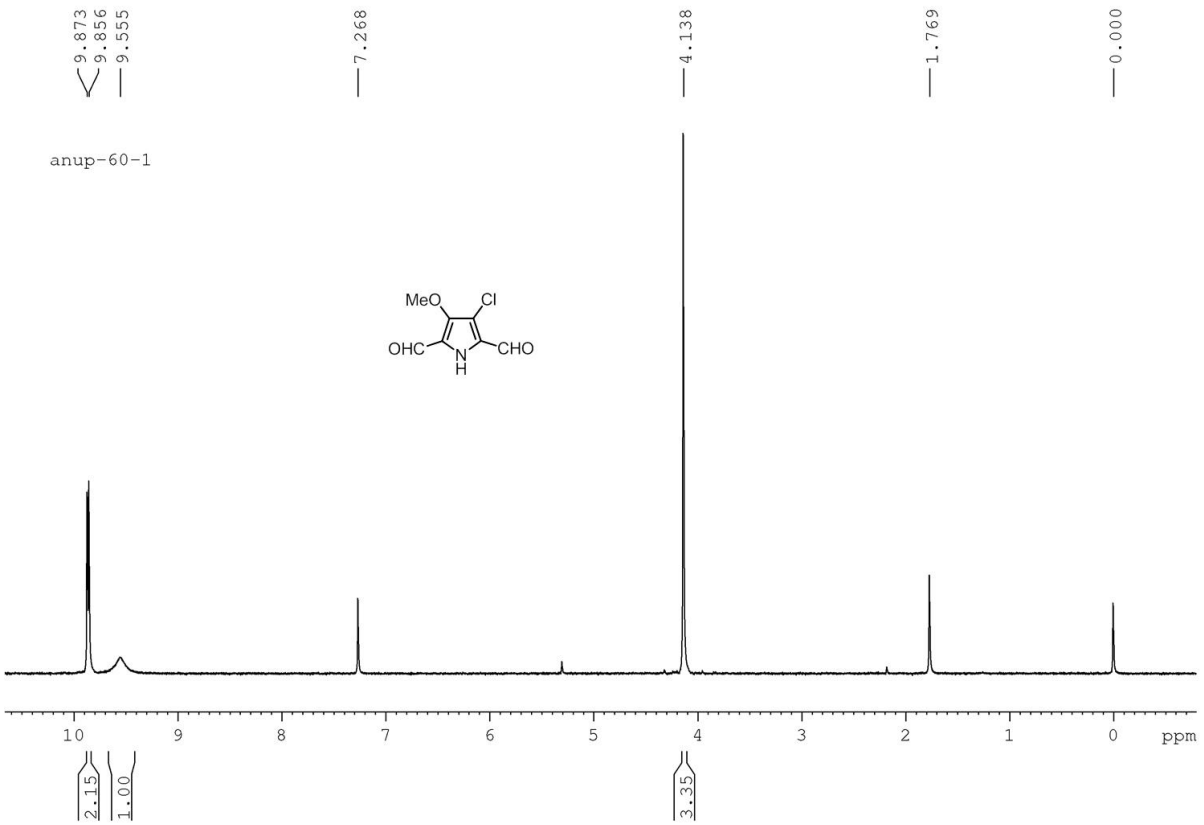

Figure 4.11 ^{1}H NMR spectrum of **4.21** in $CDCl_3$.

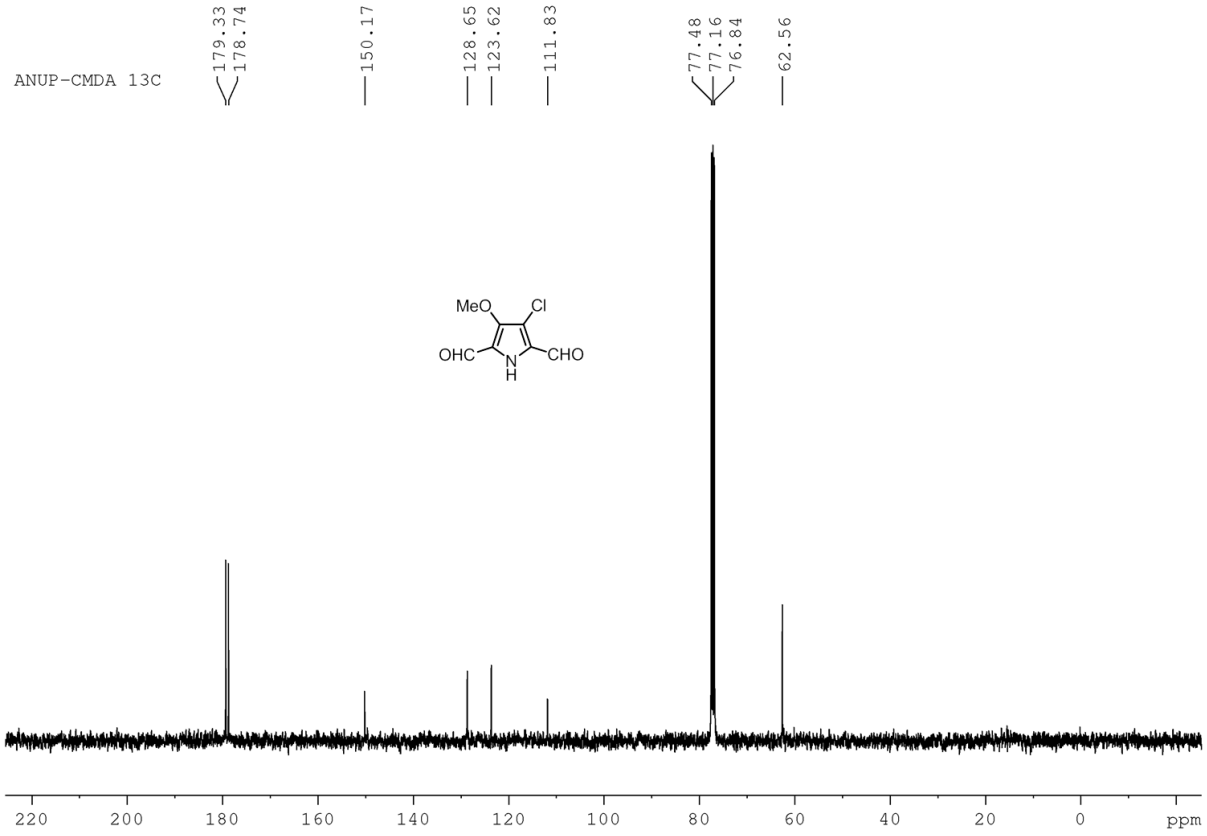

Figure 4.12 ^{13}C NMR spectrum of **4.21** in $CDCl_3$.

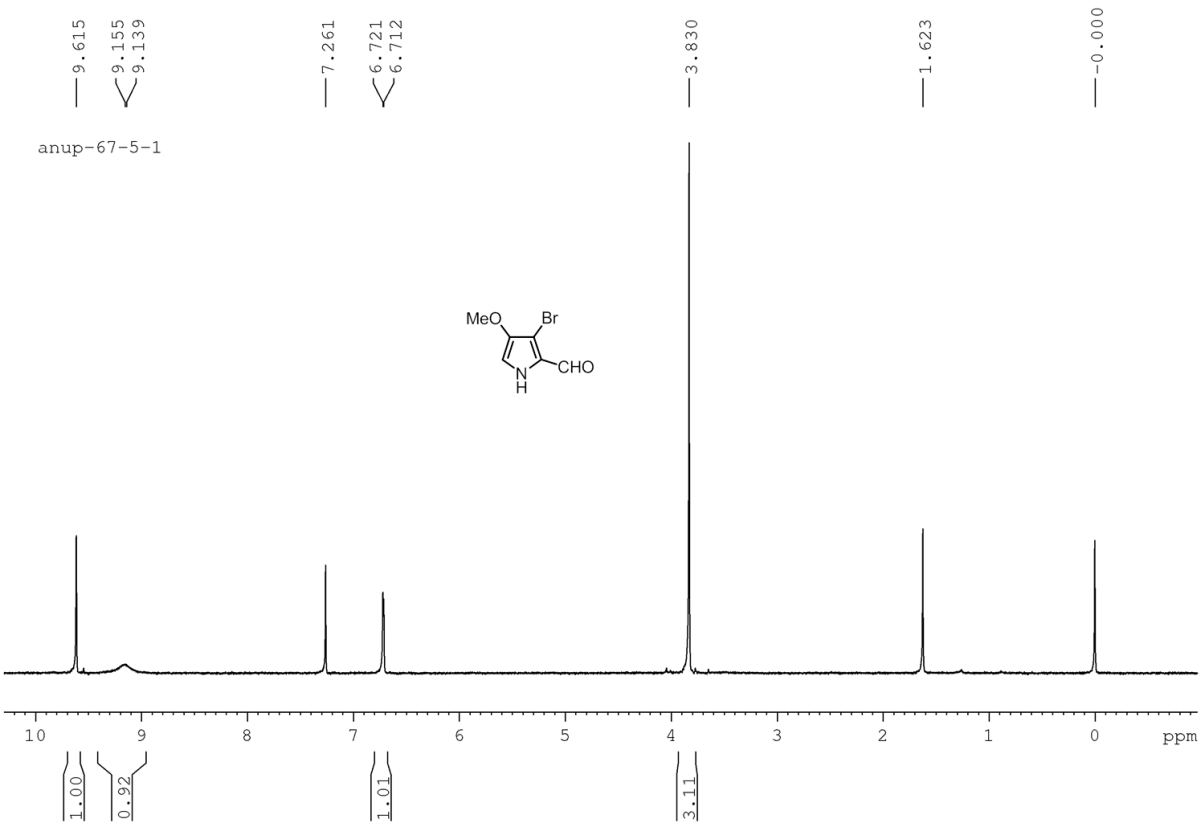

Figure 4.13 ^{1}H NMR spectrum of **4.22** in $CDCl_3$.

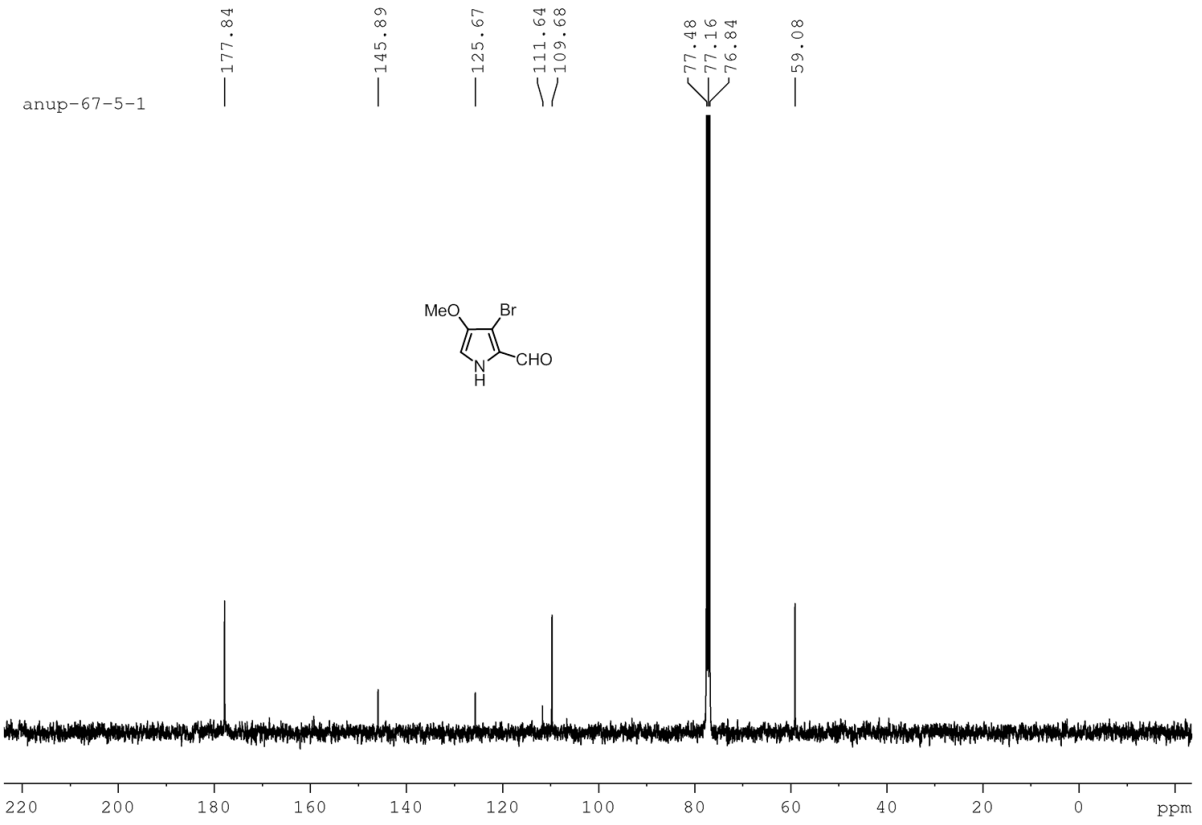

Figure 4.14 ^{13}C NMR spectrum of **4.22** in $CDCl_3$.

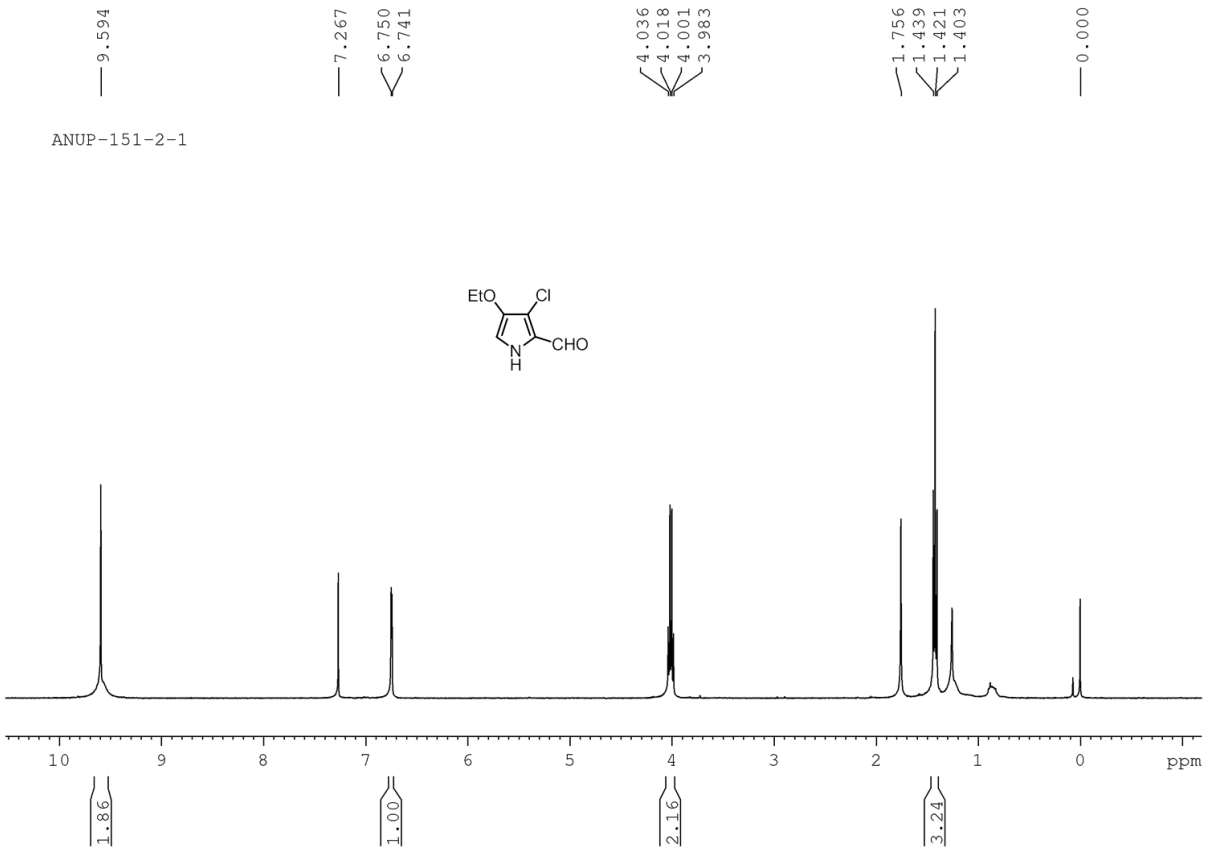

Figure 4.15 ^{1}H NMR spectrum of **4.24a** in $CDCl_3$.

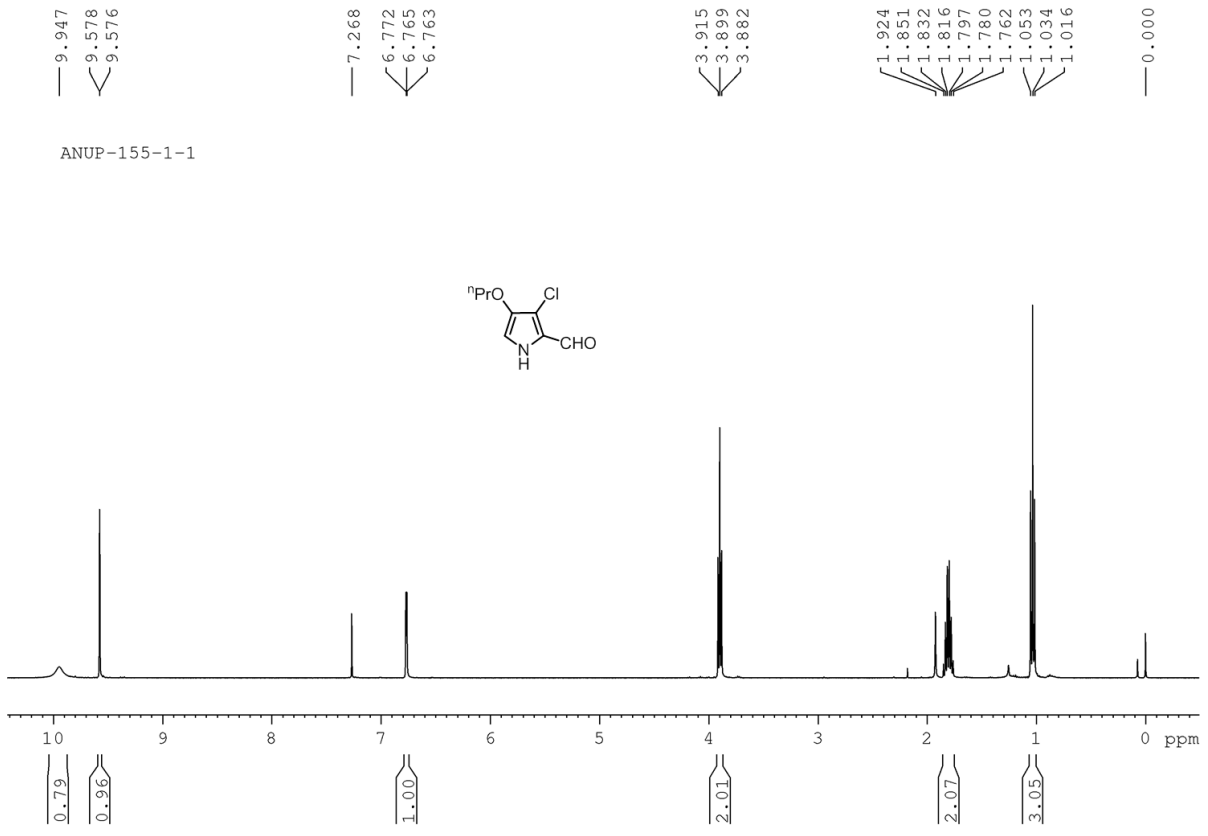

Figure 4.16 ^{1}H NMR spectrum of **4.24b** in $CDCl_3$.

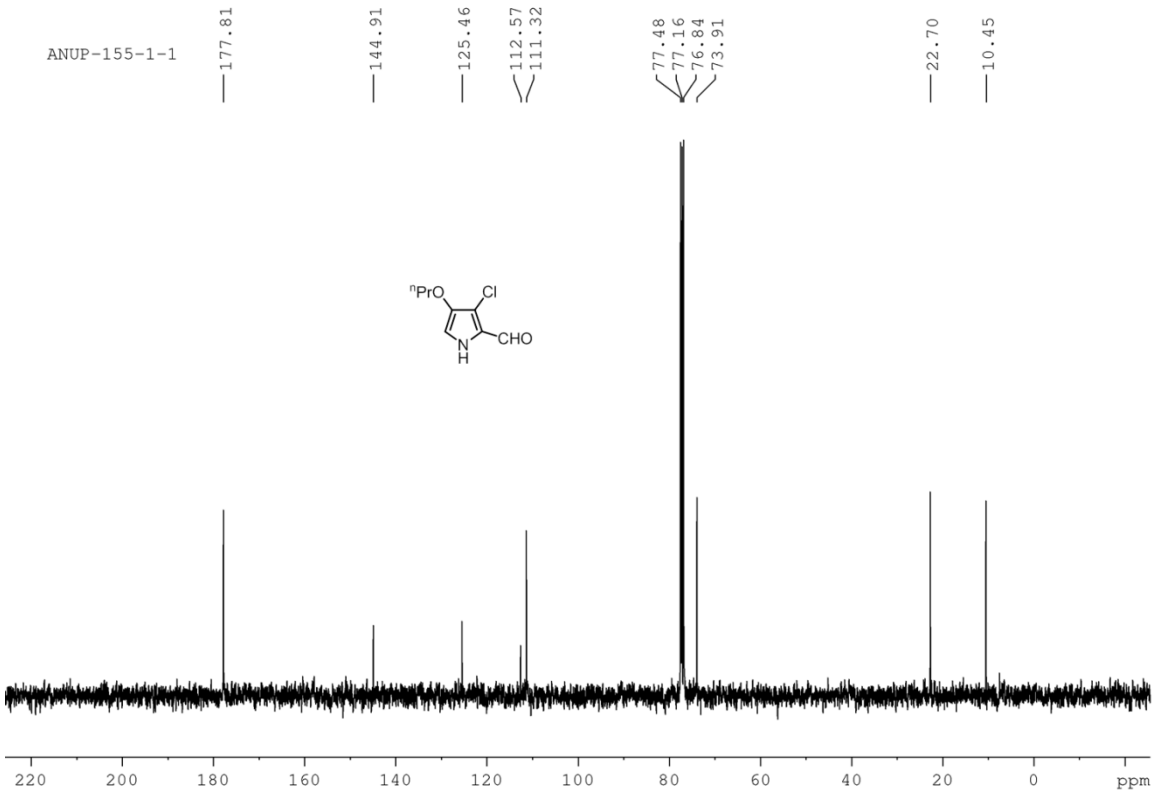

Figure 4.17 ^{13}C NMR spectrum of **4.24b** in $CDCl_3$.

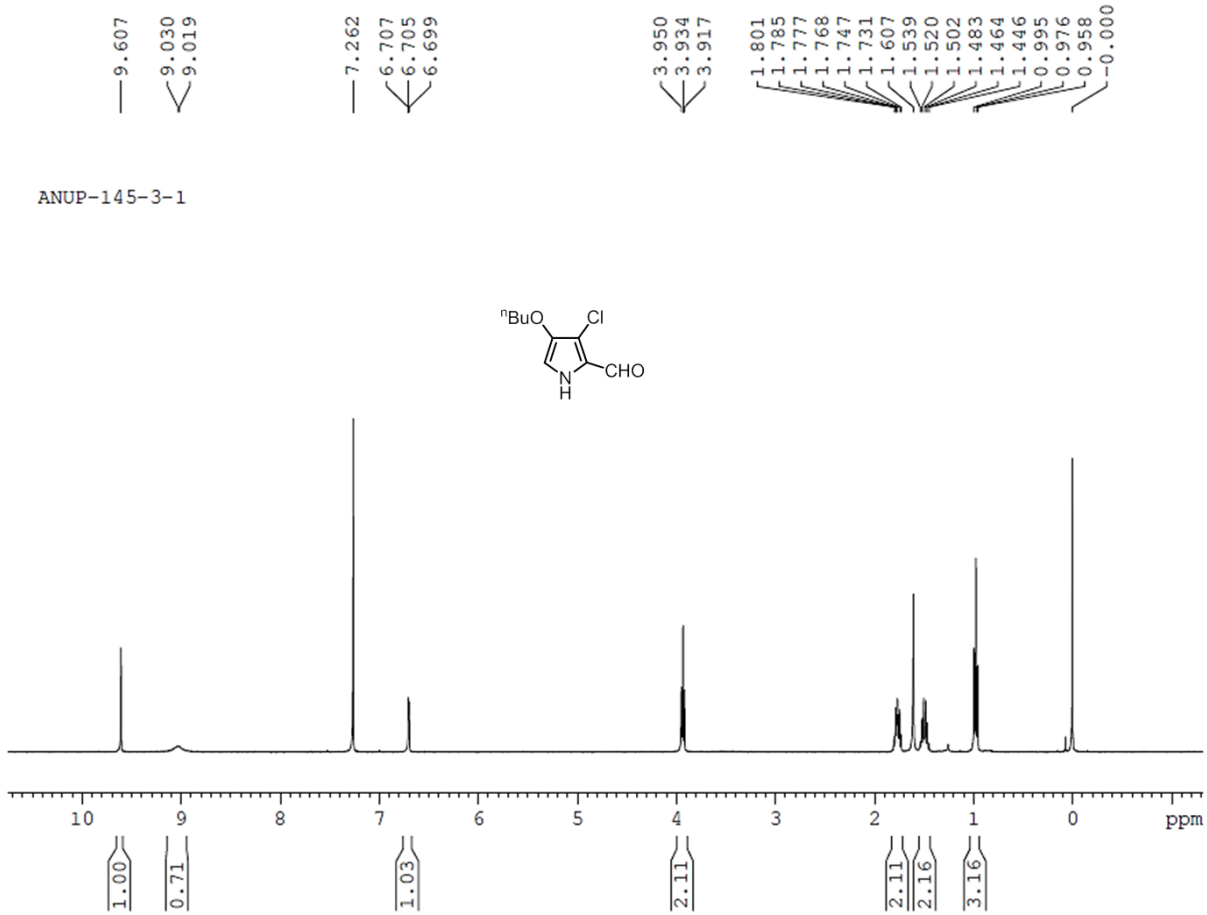

Figure 4.18 ^{1}H NMR spectrum of **4.24c** in $CDCl_3$.

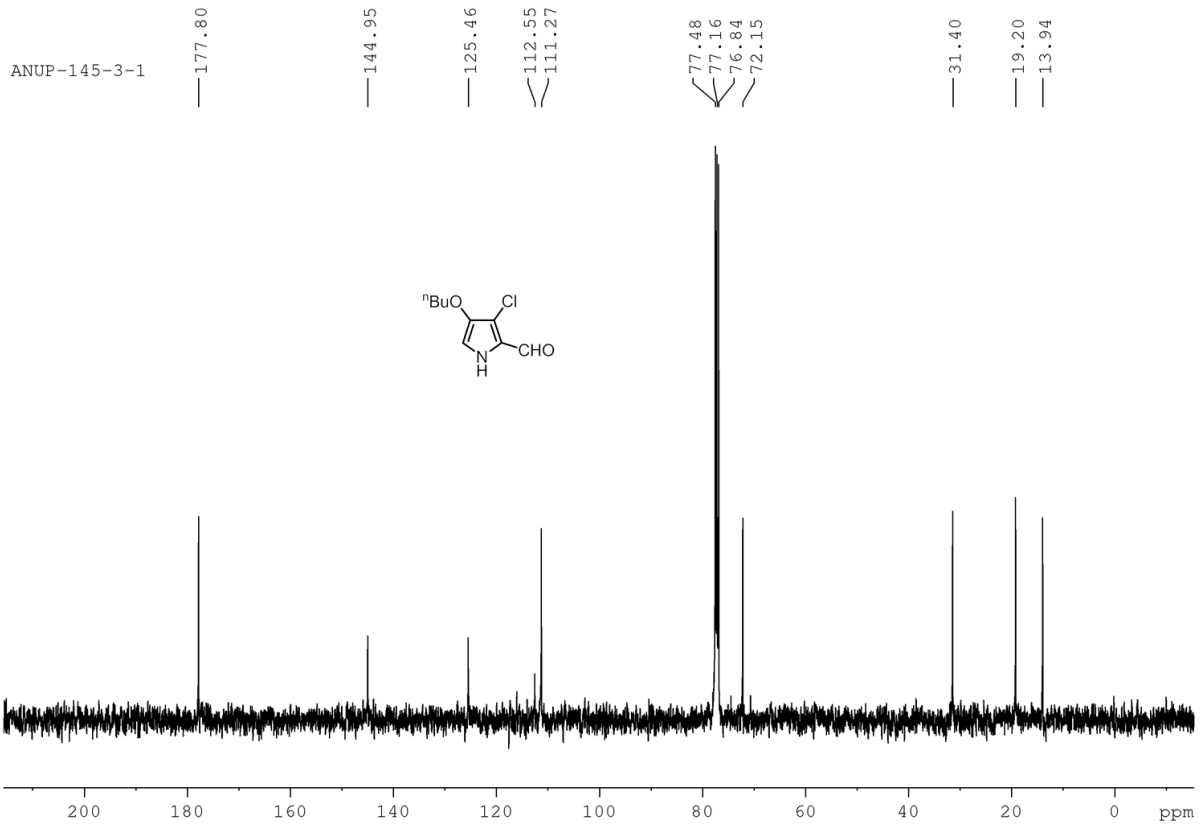

Figure 4.19 ^{13}C NMR spectrum of **4.24c** in $CDCl_3$.

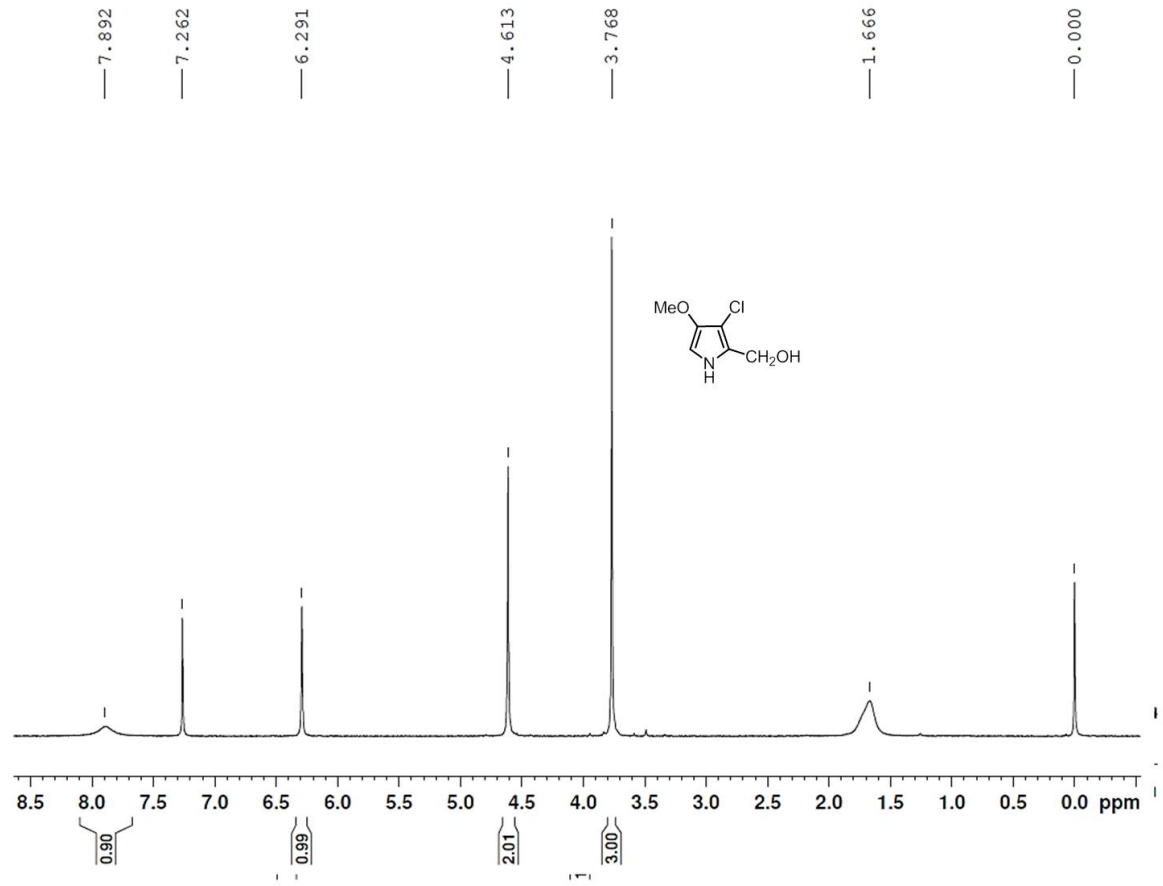

Figure 4.20 ^{1}H NMR spectrum of **4.25** in $CDCl_3$.

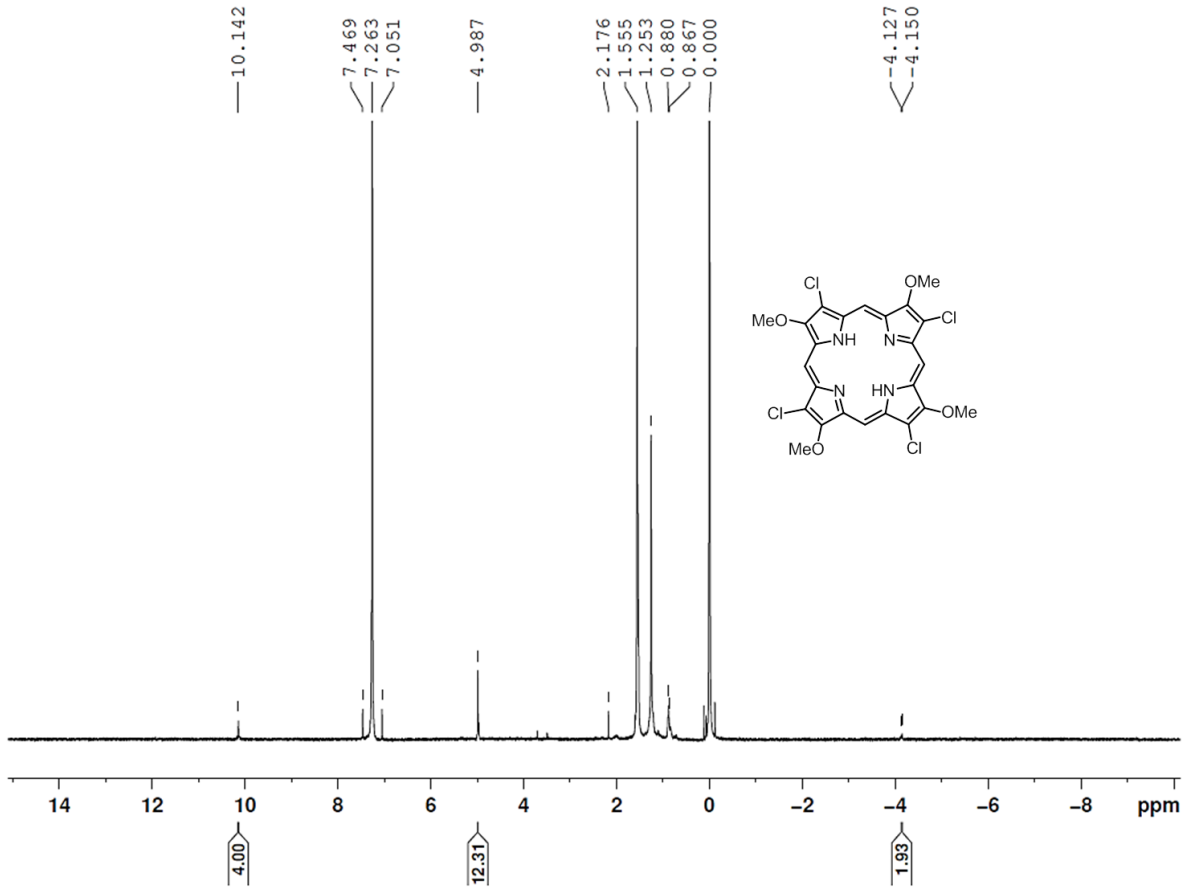

Figure 4.21 ^{1}H NMR spectrum of **4.17** in $CDCl_3$.

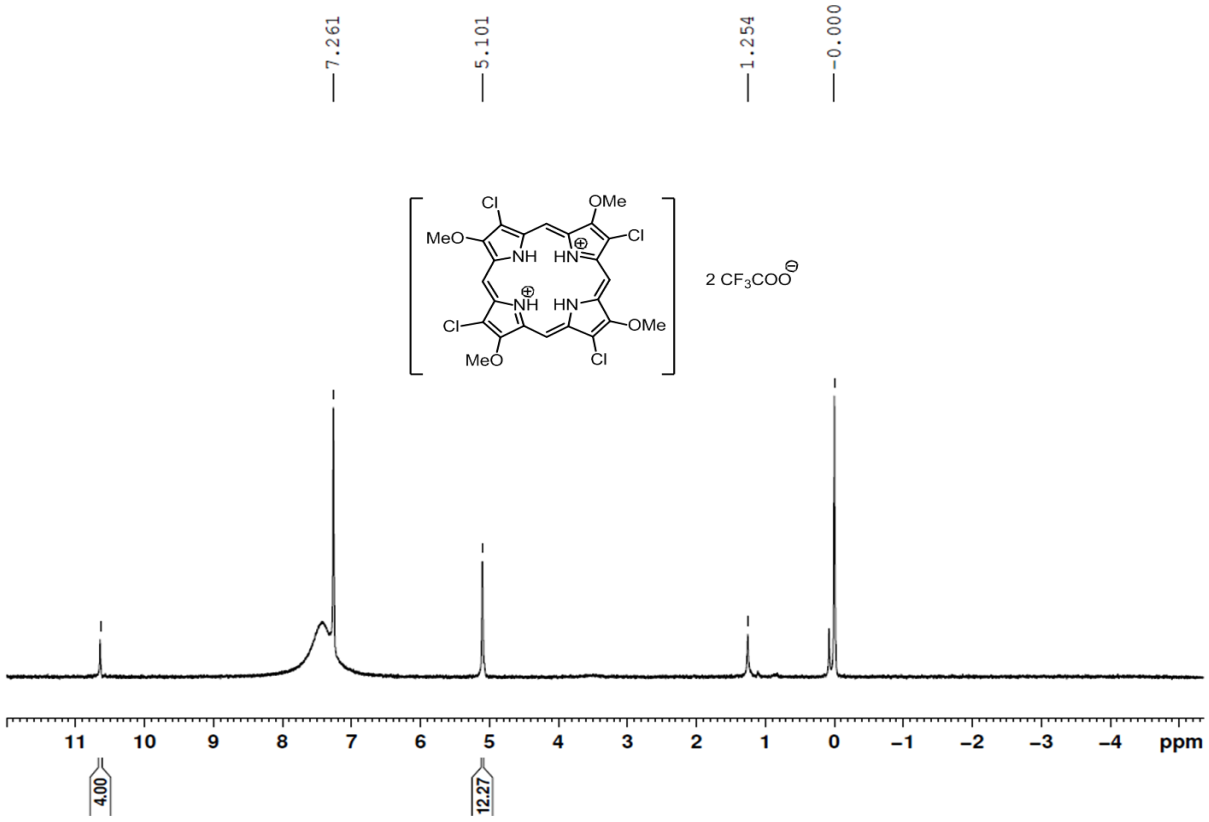

Figure 4.22 ^{1}H NMR spectrum of **4.17** in $CDCl_3$ in presence of TFA.

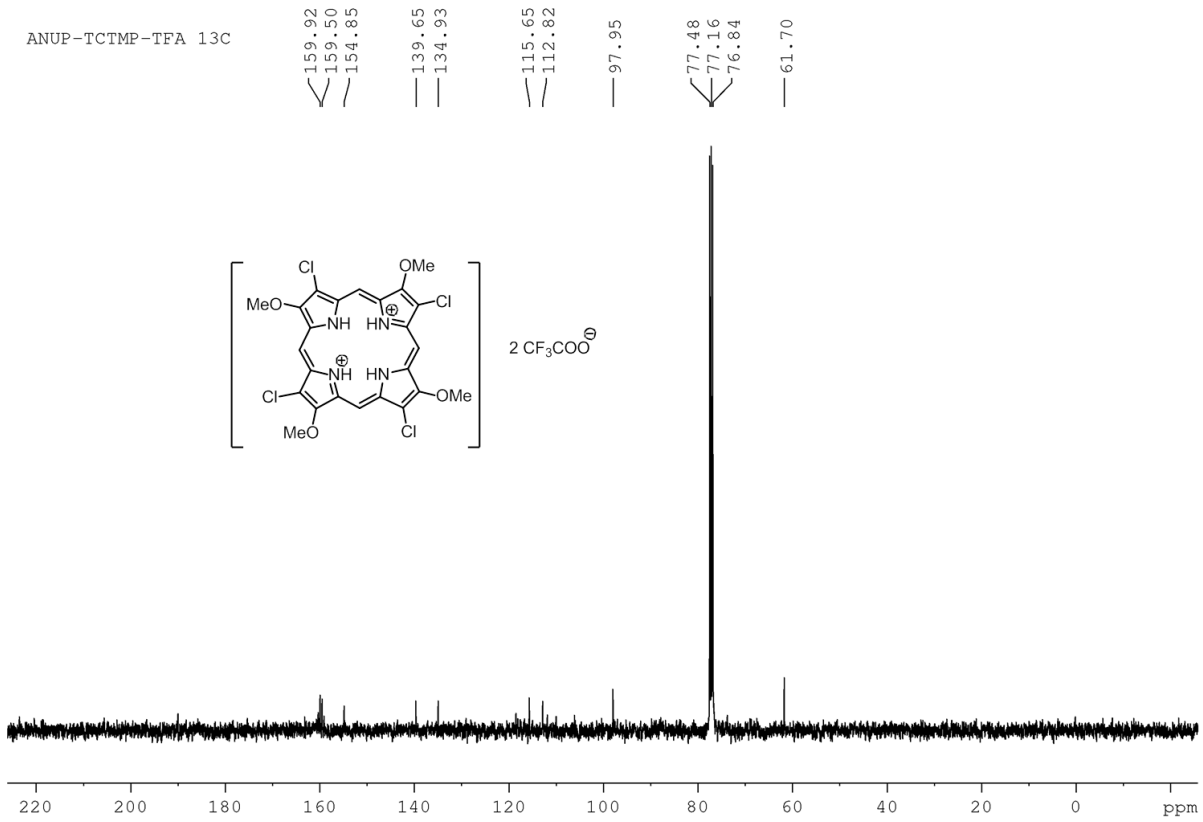

Figure 4.23 ^{13}C NMR spectrum of **4.17** in $CDCl_3$ in presence of TFA.

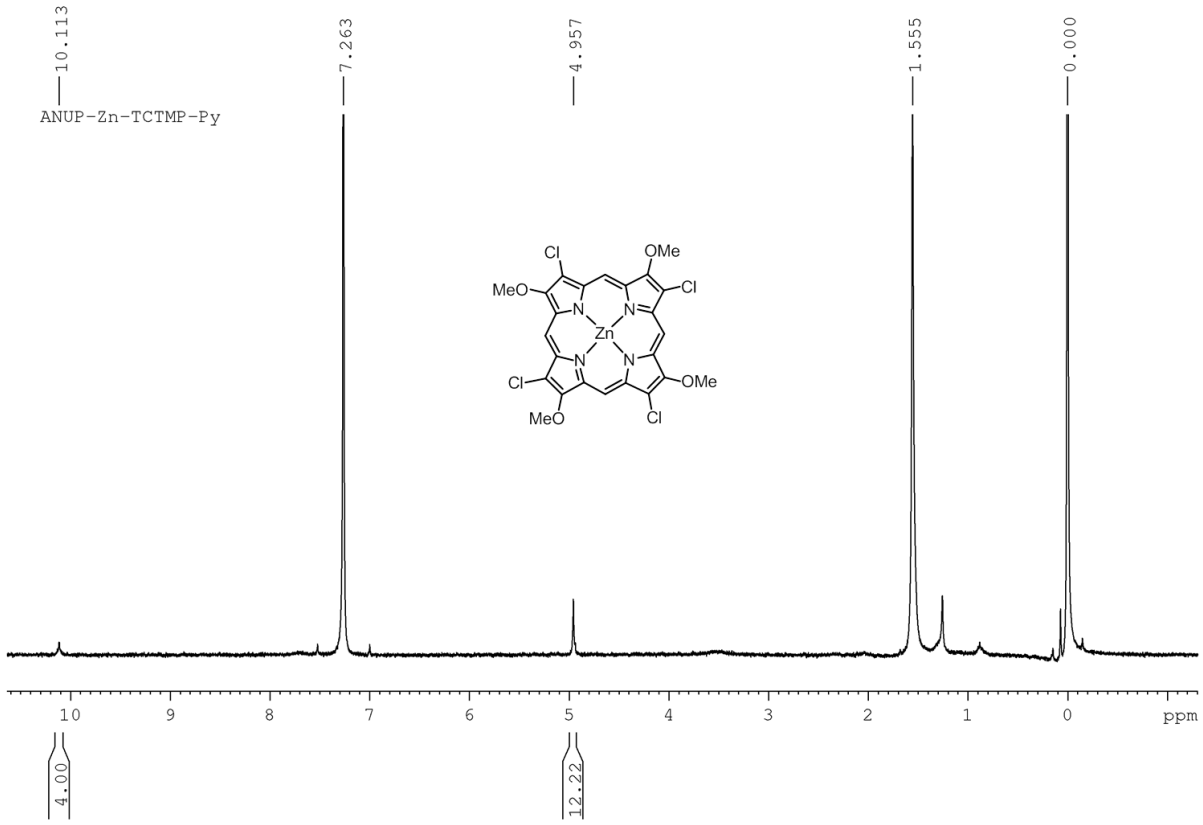

Figure 4.24 ^{1}H NMR spectrum of **Zn(4.17)** in $CDCl_3$.

CHAPTER 5

β-Methoxyporphycenes: Potential Photosensitizers for Photodynamic Therapy (PDT)

5.1 Introduction

5.1.1 Background

Porphycene, the first constitutional isomer of much revered porphyrin, was first introduced by renowned annulene chemist E. Vogel in 1986.[1] This could be obtained by reshuffling of *meso*-methine carbons of porphyrin, where two bipyrrolic moieties are connected through the

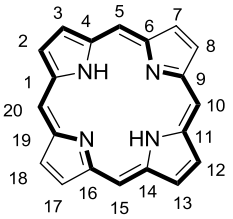

5.1
Porphyrin

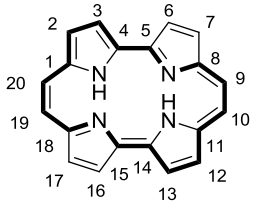

5.2
Porphycene

two meso like carbon atoms on each side through α-positions and found to be the most stable isomer of porphyrin. The trivial name "porphycene" originated from resemblance of its features to both porphyrin and acene. According to Franck's systematic approach porphycene can be referred as [18]porphyrin-(2.0.2.0).[2]

The diatropic ring current in ^{1}H NMR spectra of porphycenes revealed aromatic nature of these macrocycles. In general, the external *meso* and β-pyrrolic protons resonate at 9.62-9.21 ppm, however the internal imino proton resonate at 0.6-9 ppm (for porphyrins -3 to -5 ppm) dependent on position and type of substituent present at periphery. The unusually large downfield shift of imino protons can be explained by strong NH···N hydrogen bonding. Further, ^{1}H NMR spectra also revealed the D_{2h} symmetry of porphycene. Unlike porphyrin, absence of NH stretching frequency (3300-3360 cm^{-1}) in IR spectrum further proved NH···N hydrogen bonding interaction.[3]

Similarly, UV-Vis spectra of porphycenes, are quite similar to porphyrins with subtle differences. For example, the spectra in general consist of a strong Soret band at 350-450 nm and three Q-types bands at 500-750 nm range. In contrast to porphyrins, the lower symmetry of porphycene led to more intense (~20 times) lowest energy band, making them efficient photosensitizer for photo dynamic therapy (PDT).[4] Also, fluorescence spectra and quantum yield of porphycenes strongly dependent on the type of substituents and their relative positions.

One of the major differences between tetrapyrrolic porphycene and porphyrin systems pertains to the effect of peripheral alkyl substituents on the geometry of the ring skeleton and hence on the shape and size of N_4 core.[5] If we examine the patterns A, B and C of

symmetrical tetraalkyl substitution of porphycene i.e., the 9,10,19,20-, 2,7,12,17- and 3,6,13,16-tetraalkyl porphycene respectively (Figure 5.1). Substitution at 2,7,12,17-position (pattern B) do not affect the ring skeleton noticeably, compare to parent porphycene, but alkyl substitution at 9,10,19,20 (type A) and 3,6,13,16 (type C), the presence of α,α′-bipyrrole and cisoid CHCH structural moieties give rise to considerable non-bonding repulsion, which

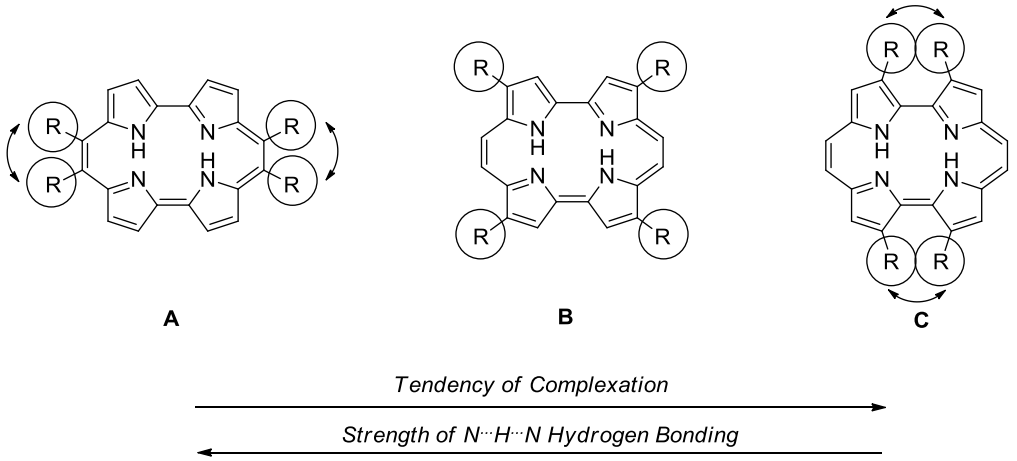

Figure 5.1 Non-bonding interactions of alkyl substituents in symmetrical tetraalkylporphycenes.

influence the shape of the N_4-core remarkably. On a closer scrutiny of substituent patterns of A, B, and C, it become discernible that the shape of N_4 core changes from rectangular to almost square, from A to C. These unusual steric aspects of alkylated porphycenes, according to which the strength of N-H···N hydrogen bonding and as a consequence the tendency for metal complexation are inversely related to, in the series, are indicated by arrows in Figure 5.1.

The difference in shapes of N_4-core, inability to direct N-atoms towards metal ion linearly, besides strong intra-core N-H···N hydrogen bonding interaction, makes complexation of porphycenes less facile than that of porphyrins. Still, a wide range of stable mono, di, tri and tetravalent metal complexes of porphycenes are currently known. Among them, Co(II), Ni(II), Cu(II), Zn(II), Pt(II) and Pd(II) complexes are most widely studied.[2]

Porphycenes exhibits two one electron reduction and two one electron oxidations steps, which are similar to bacteriochlorins, a tetrapyrrolic macrocycles, which possesses D_{2h} symmetry in analogy to porphycene.[2] In general, for porphycene the HOMO-LUMO (separation between first oxidation and reduction waves) gap is found to be 1.85±0.15 V, which is much smaller compared to porphyrins (2.25±0.15 V), and linked to decrease of molecular symmetry, which is further supported by smaller difference in first and second reduction steps (0.35±0.07 V) compared to porphyrins (0.42±0.05 V). Also, HOMO-LUMO

gap in porphycene complexes is quite sensitive to peripheral substituents along with the size and electronegativity of coordinated metal cations. Though significant substituent effects were observed, the nature of these effects was neither linear (in a Hammett σ sense) nor additive and this trend is in contrast to porphyrins (where linear effect of reduction potentials was observed). The non-additivity of substituent effects in porphycene, not only originated from lower symmetry, but also, accompanied with a significant contribution from steric effect, in particular for highly substituted derivatives.

Porphycene gains much attention due to its unique intense absorption in red region; making it one of the best photosensitizer for photodynamic therapy (PDT).[4] Also, porphycenes are studied widely in the field of catalysis[6], material chemistry[7], protein mimicry[8], nonlinear optical studies[9] and most recently for dye sensitized solar cell application[10]. Notably, recent study on dinapthoporphycenes show good third order nonlinear optical response with laser intensity dependent multiphoton absorption.[9a-b] Further, NH-tautomerism, the double hydrogen transfer study and excited state photodynamics make this molecule an object of great fundamental interest.[11] In this regard, very recently Grill & co-worker demonstrated how to control the hydrogen transfer in a single porphycene molecule.[12]

5.1.2 Synthesis of porphycenes

Porphycene was first synthesized by McMurry coupling of bipyrrole dialdehyde led to the formation of 20π-dihydroporphycene, which undergoes spontaneous oxidation in presence of oxygen to form unsubstituted porphycene **5.2** in 2% yield (Scheme 5.1).[1] Thereafter, McMurry coupling method remains the most widely accepted protocol for synthesis of porphycene till now. However, recently, Srinivasan and coworker developed an acid catalyzed oxidative coupling of bipyrrolylethane (Scheme 5.2)[13] and very recently, Ravikanth and coworkers further modified the synthesis of bipyrrolylethene, enabling the synthesis of various meso-aryl porphycenes (**5.14a-f**).[14] Therefore, till now majority of effort are directed towards the synthesis of bipyrrolyl precursor (bipyrrole dialdehyde) for the synthesis of porphycene.

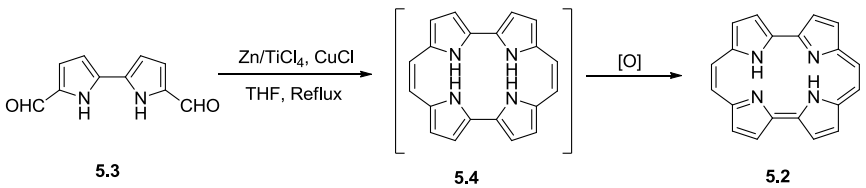

Scheme 5.1 Vogel's first synthesis of porphycene.

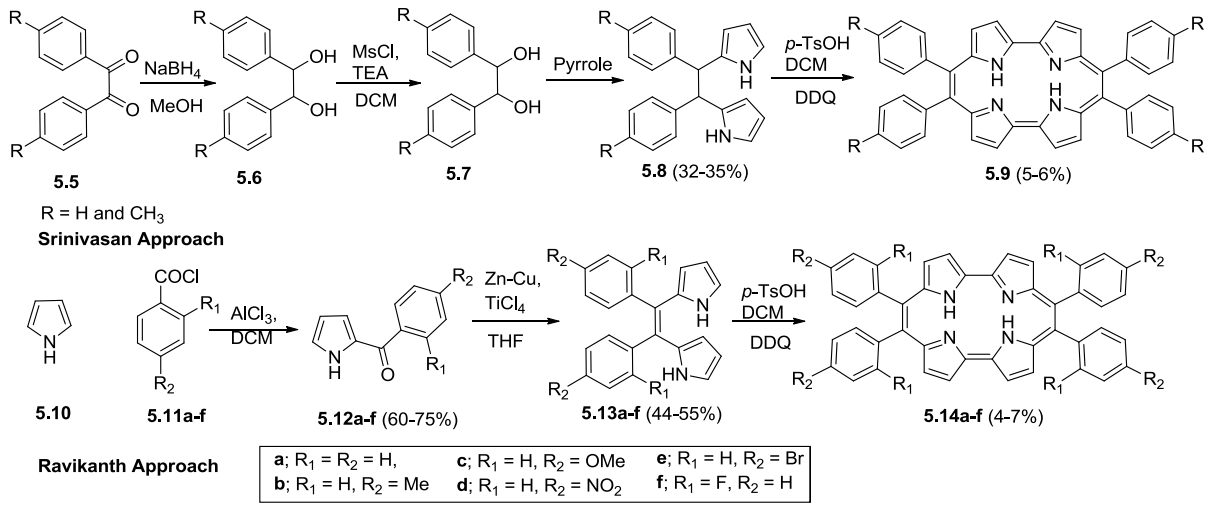

Scheme 5.2 Synthesis of meso aryl substituted porphycenes by acid catalyzed condensation method.

5.1.2.1 Synthesis of bipyrrole dialdehyde

The most widely acceptable and conventional method for synthesis of 2,2′-bipyrroles, is the Ullmann coupling[15] of iodopyrroles (Scheme 5.3). This method provides synthetic flexibility and can incorporate a wide range of substituents in β-position of pyrrole. After coupling, the resulted tetraester is subjected to deprotection, followed by formylation led to

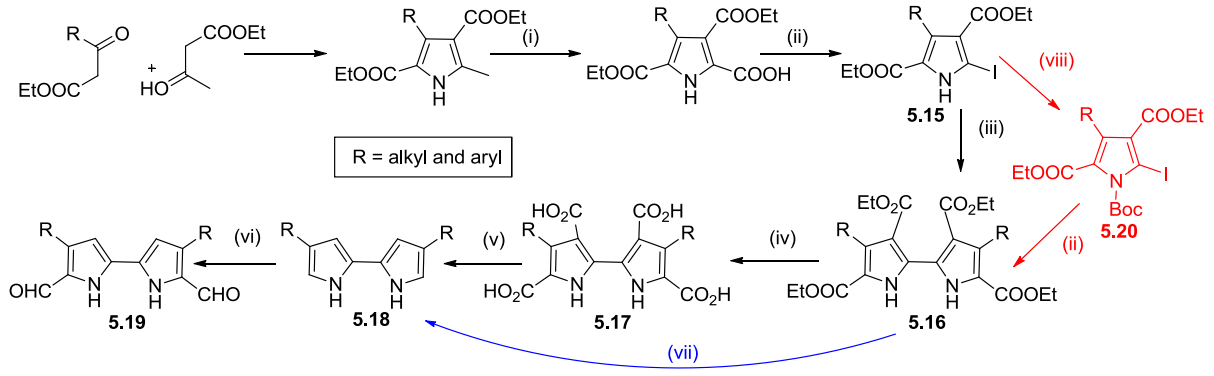

Scheme 5.3 Synthesis of bipyrrole dialdehyde by conventional Ullmann coupling method. Reagents and conditions: (i) Br_2, SO_2Cl_2, AcOH/HCOOH, 0 °C; (ii) KI/I_2, EtOH/H_2O, 75 °C; (iii) Cu, DMF, 20 °C; (iv) NaOH, EtOH/H_2O, reflux; (v) Sublimation; (vi) $POCl_3$, DMF, DCE, reflux; (vii) NaOH, ethylene glycol, reflux; (viii) $(Boc)_2O$, DMAP, DCM, RT.

formation of desired bipyrrole dialdehyde **5.19**. Sessler and coworker improved the yield of Ullmann coupling (Scheme 5.3), by introducing protection/deprotection using t-butoxycarbonyl (Boc) group (modification denoted by red color).[16] Further, Nonell and coworkers modified decarboxylation steps by avoiding sublimation steps, they have synthesized 2,2′-bipyrrole **5.18** in a single step by the treatment of tetraester derivative with

NaOH/ethylene glycol at reflux condition (Scheme 5.3 modification denoted by blue color).[17] The elimination of sublimation step enabled the scaling up of the synthesis. However, the synthesis of bipyrrole dialdehyde by conventional Ullmann coupling method requires multiple steps.

Another remarkable modification made by Nonell and coworkers to avoid unstable bipyrrole intermediate (Scheme 5.4).[18] They used two orthogonal carboxylic ester **5.22** enable selective debenzylation of two benzyl ester situated at β-pyrrolic position and subsequent

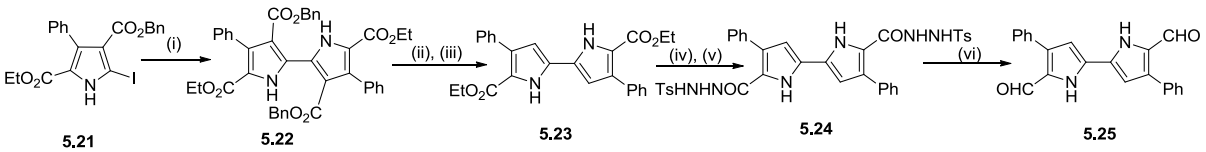

Scheme 5.4 Non decarboxylative synthesis of diphenylbipyrroledialdehyde. Reagents and conditions (yield in parenthesis): (i) Cu, DMF, 23 °C, 20 h (89%); (ii) Pd/C, $HCOOH/HCOONH_4$, reflux, 4 h (100%); (iii) ethylene glycol, 170 °C, 5 h (93%); (iv) NH_2NH_2, EtOH, reflux, 48 h, (93%); (v) TsCl, pyridine, 23 °C, 1 h (96%); (vi) diethylene glycol, Na_2CO_3, 170 °C (92%).

decarboxylation by heating in ethylene glycol provides bipyrrole diester **5.23**. Then bipyrrole diester was converted into ditosylhydrazide bipyrrole **5.24** which was subject to MacFayden-Stevens reaction sequence to yield desired bipyrrole dialdehyde **5.25**. However, the main disadvantage of this method was the additional number of steps.

Borrell and coworkers reported a new strategy by using masked bipyrrole precursor **5.26** blocked at 3 and 3′ positions (Scheme 5.5).[19] Thus it can be readily halogenated in the remaining positions, then pyrrolic nitrogen was protected with SEM ([β-(trimethylsilyl)-

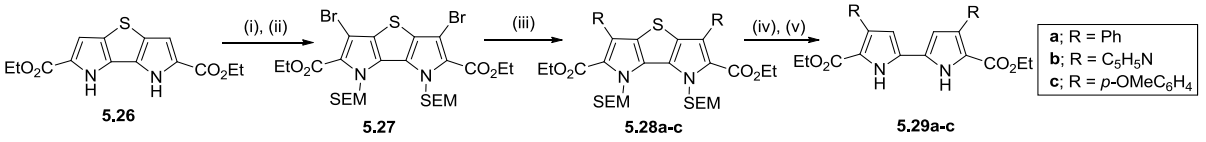

Scheme 5.5 Reagents and conditions: (i) Br_2, AcOH/ AcOEt; (ii) SEMCl, NaH, THF; (iii) $RB(OH)_2$, $Pd(PPh_3)_4$, Na_2CO_3, 1,4-dioxane; (iv) Ni Raney, EtOH; (v) TBAF (1 M in THF), 1,4-dioxane.

ethoxy]methyl) group. The resulting dibrominated compound **5.27** can be further substituted by employing Suzuki coupling, followed by removal of sulfur atom by Raney Ni® desulfuration reaction and subsequent deprotection of SEM with tetrabutylammonium fluoride (TBAF) led to formation of 4,4′-disubstituted bipyrrole esters (**5.29a-c**). Although

this route offers flexibility in term of introduction of different substituent at 4,4′-position but inefficient in terms of step economy due to expensive multistep synthesis.

In order to avoid multistep synthesis of porphycene, Sánchez-García and coworkers developed one pot synthesis of 2,2′-substituted bipyrrole (Scheme 5.6).[20] In this method,

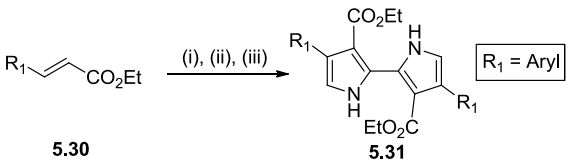

Scheme 5.6 One pot synthesis of bipyrrole diesters. Reagents and conditions: (i) TOSMIC, n-BuLi; (ii) n-BuLi, Me_3SnCl; (iii) $Cu(NO_3)_2.2H_2O$.

cinnamic esters **5.30** were treated with *p*-toluenesulphonylmethylisocyanide (TOSMIC) to generate respective pyrroles , which were then subjected to stannylation followed by *in-situ* oxidative coupling with $Cu(NO_3)_2$ to form the desired bipyrrole diesters **5.31**. Notably, this procedure can reduce the synthesis of porphycene by five steps compared to conventional Ullmann coupling methodology.

Towards the synthesis of bipyrroledialdehyde contribution of Smith and coworkers was notable (Scheme 5.7).[21] They used modified mild Ullmann coupling strategy by using Pd/C and Zn powder in water and toluene biphasic medium of 3,4-disubstituted-5-iodo pyrrole

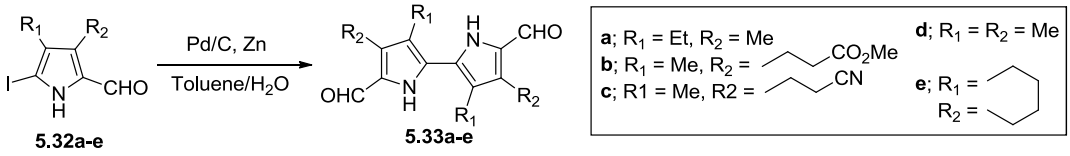

Scheme 5.7 Pd-catalysed Ullmann coupling for synthesis of bipyrrole dialdehyde.

aldehydes (**5.32a-e**) to corresponding bipyrrole dialdehydes (**5.33a-e**) at room temperature. More interestingly, they were able to control deiodination (acetone/H_2O) and coupling (toluene/H_2O) by simply changing solvent medium. This mild reaction condition works well not only with ester but also aldehyde substituents and also provides better yield with electron rich pyrroles.

5.1.2.2 β- and *meso*-substituted porphycene

Soon after the synthesis of unsubstituted porphycene, Vogel and coworkers realized that it suffers poor solubility similar to porphine. This led them to synthesized corresponding tetra-

n-propyl derivative **5.34**, which display good solubility in organic solvent, and was developed in anticipation that it would play vibrant role similar to octaethylporphyrin in porphyrin chemistry.[22] It was synthesized by McMurry coupling of bipyrrole dialdehyde by using low valent titanium reagent followed by oxidation in air. This generalized methodology can be used to synthesize a series of β-substituted porphycenes from their corresponding bipyrrole dialdehydes. The UV-vis spectrum of porphycene **5.34** is similar to its unsubstituted analogue with low energy Q-band at 633 nm. The ^{1}H NMR spectrum revealed that NH protons resonate at 3.04 ppm, indicative of strong NH···N hydrogen bonding interactions. Solid state structural analysis revealed that core of the macrocycle is planar in nature and N_4 core form rectangular shape in analogy to parent porphycene. Subsequently, Vogel and coworkers

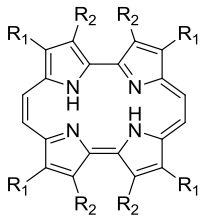

5.34; R_1 = ^{n}Pr, R_2 = H
5.35; R_1 = Et, R_2 = H
5.36; R_1 = Me, R_2 = H
5.37; R_1 = ^{t}Bu, R_2 = H
5.38; R_1 = Ph, R_2 = H
5.39; R_1 = $(CH_2)_2OMe$, R_2 = H
5.40; R_1 = $(CH_2)_2OEt$, R_2 = H
5.41; R_1 = Et, R_2 = Me
5.42; R_1 = R_2 = Et
5.43; R_1 = R_2 = Me
5.44; R_1 = Et, R_2 = CF_3

Scheme 5.8 β-substituted porphycenes.

introduced β-octaethylporphycene **5.42**, whose crystal structure revealed slight twist along α-α′-link of bipyrrole units, arising from non-bonding interactions of ethyl groups at 3,6- and 13,16- positions.[23] These unfavorable interactions enforced the N_4 core of macrocycles to adopt square shape and can form stable coordination complexes with several metal cations. Recently, Hayashi and coworkers introduced 2,7,12,17-tetraethyl-3,6,13,16-tetra(trifluoromethyl)porphycene **5.44**, which displays a large red shifted absorption at 719 nm.[24] This molecule displayed a great deal of distortion in the porphycene core due to non-bonding interaction between bulky CF_3 groups at inner β-positions and found to be nonfluorescent. Further, its electron deficient nonplanar structural feature, enabled them to isolate the reduced 20π-dihyrdoporphycene derivative, which can be further oxidized and reduced reversibly by using appropriate oxidizing and reducing agents.[25]

Vogel and coworkers also introduced *meso*-substituted porphycenes **5.47a-c** (Scheme 5.9), which can be synthesized by McMurry coupling of diacylated bipyrroles followed by oxidation with DDQ.[5] More interestingly, they were able to isolate 20π-electron intermediates **5.46a-c** as colorless solid and X-ray structure of **5.46c** revealed cyclophane type structure in solid state. This finding conclude that the interaction between *meso*-alkyl substituents lead to slowdown of the rate of pyrrole ring rotation and hence, prevent the

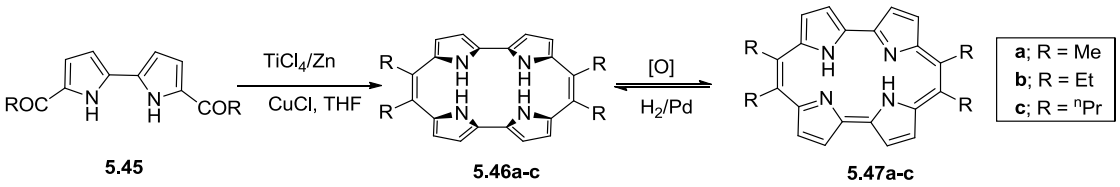

Scheme 5.9 *meso*-substituted porphycenes.

molecule to adopt planar form required for spontaneous oxidation. The X-ray structure of porphycene **5.47c** revealed planar conformation, but unfavorable interaction between meso alkyl groups leads to shorter opposite N-N distance (2.5 Å vs 2.6Å) and hence geometry of N_4 core becomes distinctly rectangular. Due to strong NH···N hydrogen bonding interaction, the NH protons resonate in low field region of ^{1}H NMR spectrum (6.82 ppm). Recently, Srinivasan and coworkers[13] and Ravikanth and coworkers[14] also reported a series of *meso*-aryl substituted porphycenes (**5.9** and **5.14a-f**) exhibiting strong fluorescence.

Recently, Yamada and coworkers introduced first dodecasubstituted porphycenes by using bicyclo[2.2.2]octadiene (BCOD) fused pyrrole as building block.[26] Conventional McMurry

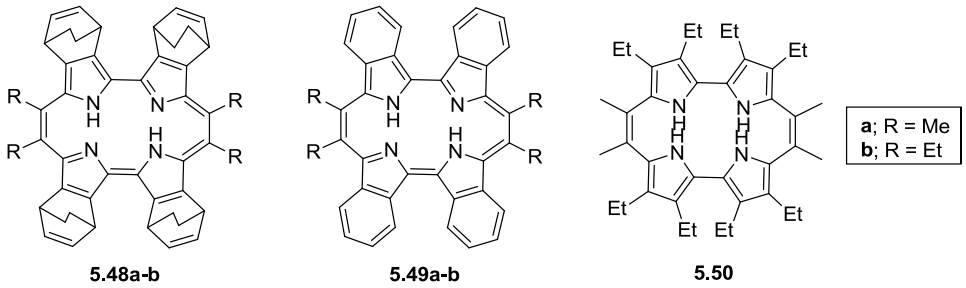

Scheme 5.10 Dodecasubstituted porphycenes.

coupling of acylated BCOD fused bipyrrole led to formation of corresponding *meso*-tetraalkyl BCOD fused porphycenes which was further converted to corresponding tetrabenzoporphcenes by heating at 220 °C under vacuum. The molecular structure of dodecasubstituted porphycene reveals saddle type structure with rectangular N_4 core. However, the synthesis of dodecaalkylsubstituted porphycene remains unsuccessful, and ended up with the formation of 20π-dihydroporphycene, which could not be oxidized with DDQ.

5.1.2.3 Heteroporphycenes

Vogel and coworkers also introduced the first heteroporphycene, the tetraoxaporphycene dication **5.51**, which was synthesized from McMurry coupling of bifurandialdehyde leading

to formation of 20π-intermediate, which could be further oxidized to desired porphycene diperchlorate salt, with bromine and 70% perchloric acid.[27] Interestingly, 20π-intermediate

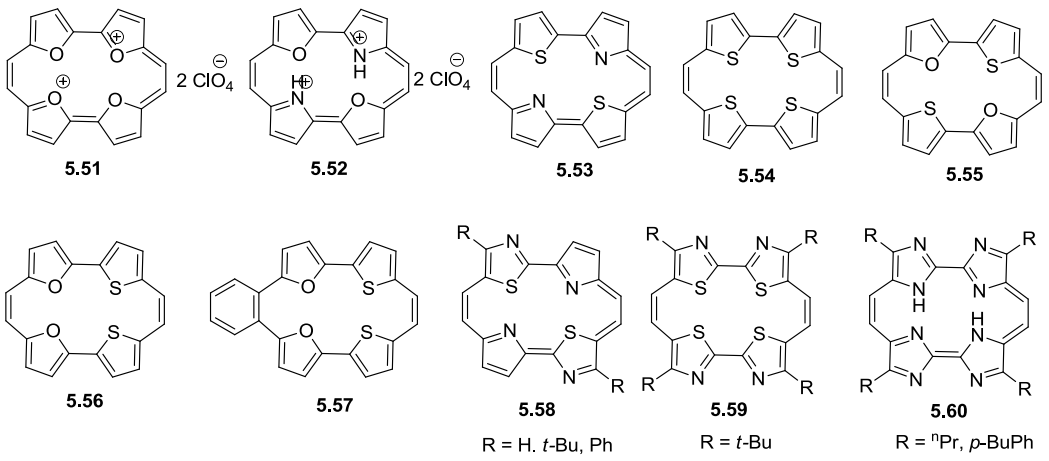

Scheme 5.11 Heteroporphycenes.

exhibits paratropic ring current in ^{1}H NMR spectrum and X-ray structure show planar core. Further, the 18π-aromatic character of tetraoxaporphycene dication is confirmed by ^{1}H NMR, UV-Vis spectrum and solid state structural analysis. Again, Vogel and coworkers reported dioxaporphycene **5.52**, by McMurry coupling of corresponding bipyrrole dialdehyde, via the formation of isolable 20π-intermediate, which was oxidized to desired porphycene by using the mixture of conc. HNO_3 and 75% $HClO_4$.[28] Neidlein and coworkers reported dithiaporphycene analogue **5.53** by McMurrry coupling followed by oxidation with DDQ and its solid state structure reveals planar core.[29] Further, Merz and coworkers[30] and Cava and coworkers[31] independently attempted to synthesize tetrathiaporphycene **5.54** by McMurry coupling of dithiophene dialdehyde to obtain only the 20π intermediate, but failed to oxidize it to the desired porphycene, either chemically or electrochemically. Interestingly, the 20π intermediate undergoes a reversible two electron reduction, may be ascribed to the formation of 22π aromatic dianion species. The spectro-electrochemistry study of the reduced product exhibits two absorption bands at 477 and 700 nm, revealing aromatic nature of this species. Mixed furan-thiophene dihydroporphycenes (**5.55-57**) were reported by Dai et al. but could not be aromatized.[32] Again, Neidlein and coworkers described the synthesis of dithiazoleporphycene **5.58**, whose aromatic nature was proved by ^{1}H NMR and UV-Vis spectral patterns.[33] However, they have also reported tetrathia analogue **5.59**, which could not be aromatized.[34] Recently, Nonell and Sessler independently reported imidacene **5.60** containing 1,3-imidazole building block.[35] However, Sessler group reported tetraalkyl analogue, on the other hand Nonell group reported the corresponding tetraaryl counterpart.

The tetraarylimidacene **5.60**, shows 100 nm red shift in UV-Vis spectrum compare to tetraphenylporphycene **5.38**, which can be ascribed to the introduction of four additional N-atoms.

5.1.2.4 *π*-Extended porphycenes

The π-extended porphycene is one of the least explored classes, probably owing to synthetic difficulties associated with the desired building blocks. First true π-extended porphycene reported by Vogel and coworkers, dibenzoporphycene **5.61** by McMurry coupling of benzobipyrrole dialdehyde followed by DDQ oxidation, however synthetic details of this molecule is not reported in public domain.[36] Yamada and coworkers reported tetrabenzofused porphycene **5.62** by McMurry coupling of BCOD fused bipyrrole dialdehyde to provide the corresponding BCOD fused porphycene, which was subjected to retro Diels-Alder reaction at 220 °C under vacuum, to provide the desired porphycene.[37] They have also reported dibenzoporphycene **5.63** by mixed McMurry coupling of BCOD fused bipyrrole and

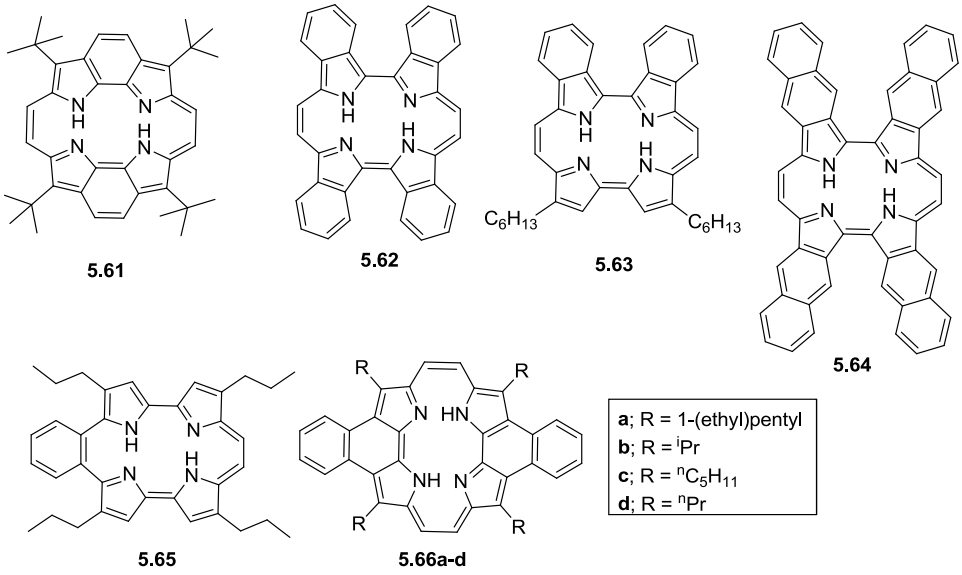

Scheme 5.12 π-extended porphycenes.

alkylated bipyrrole dialdehydes. The result of π-extension clearly reflected in the absorption spectrum of tetrabenzoporphycene **5.62**, which undergoes substantial red shift compared to β-alkylated porphycenes. It exhibited B-band at 434 nm and lowest energy Q-band at 670 nm. Further, red shift in absorption was observed for tetrabenzo fused dodecasubstituted porphycenes (**5.49a-b**) (B-band at ~450 nm and lowest energy Q-band at ~740 nm).[26] Again, they reported tetranapthoporphycene **5.64** by employing same methodology discussed above, which however exhibits much lower solubility compare to tetrabenzoporphycene **5.62**, and

hence could not be analysed by ^{1}H NMR spectroscopy.[38] The *meso*-fused benzotetrapropyl-porphycene **5.65** was obtained by electrocyclisation and spontaneous dehydrogenation of less symmetric side product obtained from the McMurry coupling of monovinylogousbipyrrole dialdehyde.[39] Very recently, our group[9a] and Sessler group[40] independently reported the synthesis of dinaphthoporphycenes (**5.66a-d**) by McMurry coupling of naphthobipyrrole dialdehydes. The fusion of bipyrrole with naphthalene clearly reflected in bathochromic shift of both B-band (~400 nm) and lowest energy Q-band (~715 nm) in absorption spectra of the dinaphthoporphycenes and further, they exhibit laser intensity dependent strong two and three photon absorption.

5.1.2.5 Functionalisation and reactivity of porphycenes

Functionalisation of porphycene is important for advanced application purpose. In this regard, Vogel and coworkers found that catalytic hydrogenation of porphycene led to the formation of partial reduced product **5.68**, analoguous to chlorin.[41] Similar product was also

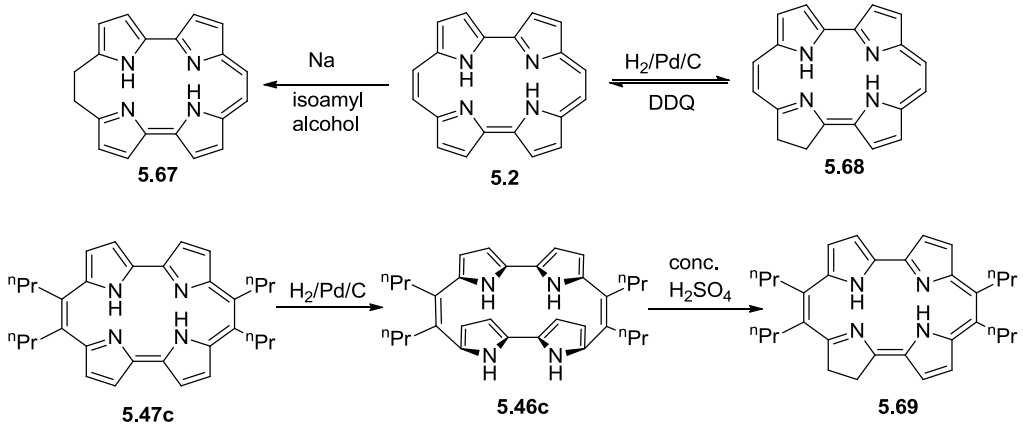

Scheme 5.13 Reduction of porphycenes

obtained during the McMurry coupling of bipyrrole dialdehyde, as side product and could be re-oxidised by using DDQ. Also, Vogel and coworkers found that the treatment of porphycene with Na metal in *iso*-amyl alcohol leads to the formation of 9,10-dihydroporphycene **5.67**.[41] Similarly, catalytic hydrogenation of porphycene **5.47c** by using H_2/Pd/C led to the formation of cyclophane type intermediate **5.46c** which could be further converted to 2,3-dihydroporphycene **5.69** by using catalytic amount of conc. H_2SO_4.[42]

Halogenation of alkylated porphycene provides upto tetra substituted species and among them tetrahalogenated species **5.71** can be easily isolated.[43] Mono bromination and iodination products **5.72** of tetrapropylporphycene **5.34** could be achieved selectively on solid

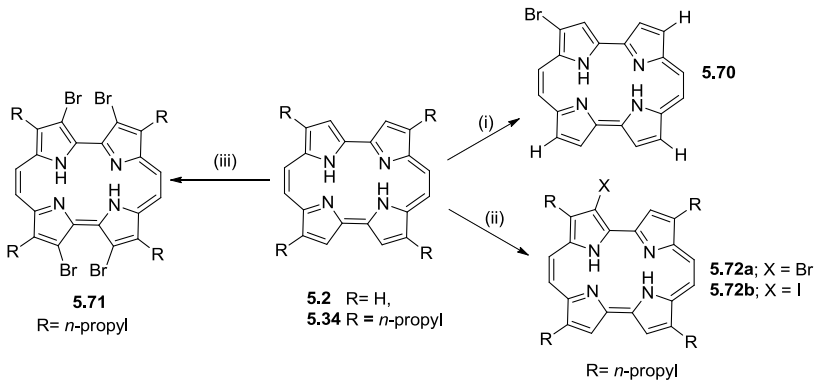

Scheme 5.14 Halogenation of porphycenes: (i) NBS, $CHCl_3$, (ii) (X = Br) Amberlyst A-26, bromoform, CH_2Cl_2, AcOH, 0 °C. (X = I) I_2, 0 °C. (iii) Br_2, CCl_4, $NaOAc/H_2O$.

support,[43a] however, in case of unsubstituted porphycene halogenation exclusively takes place at 2-position e.g. **5.70**.

Sulfonation of porphycene can be achieved with fuming H_2SO_4 leading to formation of mono-, di- and tri-sulfonated porphycenes (**5.73a-d**)[44] and sodium salts of these sulfonated salts are water soluble and hence should be useful for biological application. Further,

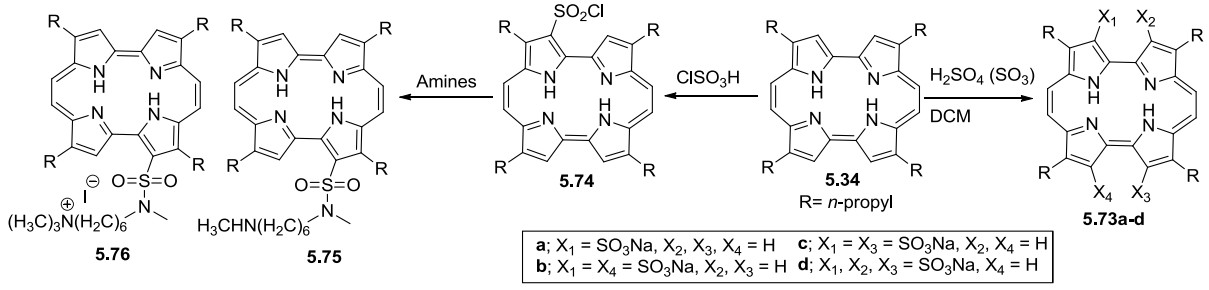

Scheme 5.15 Sulfonation of porphycene.

treatment of porphycene with sulphonyl chloride led to formation of 3-sulphonylchloride porphycene **5.74**, which can be further converted to sulfonamides (**5.75-76**) with the treatment of appropriate amines.[45] These water soluble sulfonamides act as an effective mitochondrial localizer.[45]

Further, nitration of porphycene by using $AgNO_3$/AcOH in DCM takes place selectively at 9-position to obtained **5.77**, which can be further reduced to amine **5.78**.[46] Similarly, acyloxylation takes place at 9-position, leading to formation of acyloxy derivative **5.79**, which subsequently could be converted to 9-hydroxyporphycene **5.80** upon hydrolysis.[46a] These 9-substituted porphycenes are important precursors for further substitution; increased water solubility and bathochromic shift in absorption, make them useful to study as photosensitizer for PDT.[47]

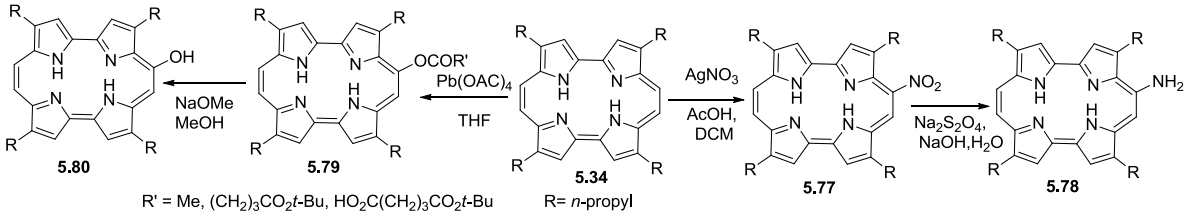

Scheme 5.16 Nitration and acyloxytion of porphycene.

Goetz and coworkers used 2,7,12,17-tetramethoxyethylporphycene **5.39**, to carry out an array of appropriate peripheral substitutions for PDT application.[48] The methoxy functional group can be easily deprotected using BBr_3 to afford corresponding alcohol **5.81**, which in turn can further transformed into different functional groups viz. mesylate (**5.82**), cyano (**5.83**) and carboxylate (**5.84**).[47] Further, in presence of boric acid, BBr_3 led to formation of

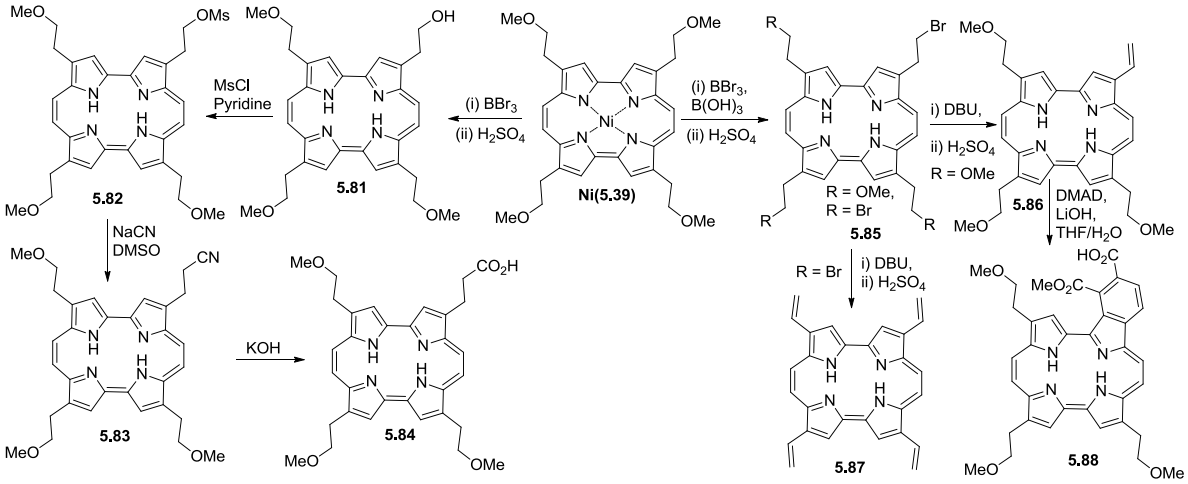

Scheme 5.17 Functional group interconversion in porphycenes.

mono-, di-, tri- and tetra-brominated products **5.85**. This can be further converted to vinylporphycene **5.87** in presence of DBU.[47] Again, Diels-Alder reaction of mono-vinylated porphycene **5.86** with dimethylacetylenedicarboxylate (DMAD) led to formation of mono-benzoporphycene **5.88**, which is studied widely as potential photosensitizer for PDT.[48,49]

5.1.3 Porphycene and photodynamic therapy (PDT)

The photodynamic action induces cell death by the combined effect of efficient photosensitizer, visible light and molecular oxygen. The photodynamic therapy is an important therapeutic solution for treatment of various types of cancer. The advantage of PDT lies on the low systematic toxicity and high tumor selectivity. An ideal photosensitizer should be a chemically well-defined entity and synthetically affordable, should be nontoxic

but highly phototoxic and should display high tumor selectivity.[4] It should exhibit high absorption coefficient in biological transparent window (600-900 nm) and efficiently generate active form of oxygen (i.e. singlet oxygen) in presence of light. Lastly, it should have good pharmacokinetics to be cleared rapidly from body to prevent post treatment long lasting skin photosensitivity.[4] Towards these aspects porphycene scores over porphyrin, due to it lower symmetry, it possess higher absorption coefficient ($\lambda > 600$ nm, $\varepsilon > 50000$ $M^{-1}cm^{-1}$) in 600-800 nm regions appropriate for PDT.[4] The photobiology and photophysical

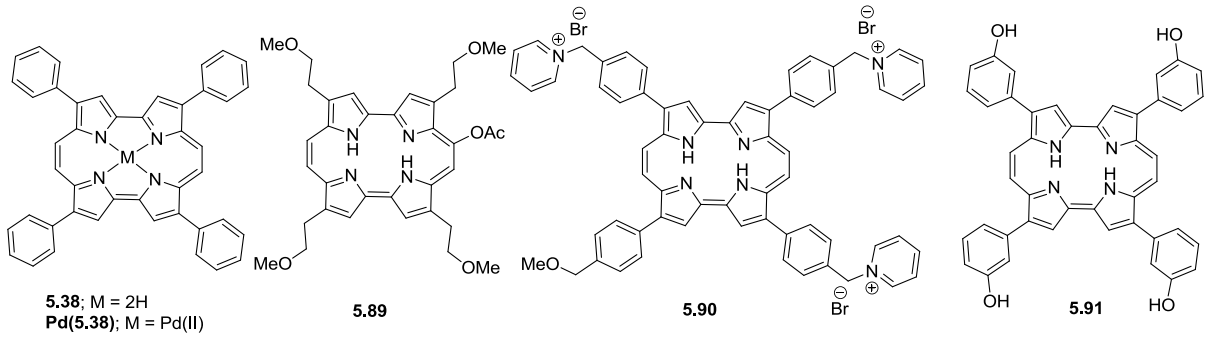

Scheme 5.18 Porphycenes studied for photodynamic therapy.

properties of porphycenes make them exceptional candidates as photosensitizer, showing fast cell uptake and varied subcellular localization.[4] In this regards, several 2,7,12,17-tetraalkyl-substituted porphycenes (methyl, ethyl, n-propyl, methoxyethyl), as well as tetraphenyl derivatives and its Pd(II) complex (**5.38** and **Pd(5.38)**) were studied for photo induced cell damage *in vitro*, as well as *in vivo*.[4] PDT of cultured cells with **5.38** and its **Pd(5.38)** complexes induced cytoskeletal change, mitotic blockage and dose dependent apoptotic and necrotic cell death.[50] Goetz and coworkers[48] studied 2,7,12,17-tetramethoxyethylporphycene **5.39** and its peripherally substituted derivatives were incorporated into small unilamellar liposomes and incubated into SSK2 murine fibrosarcoma cells. Incorporation of methoxy groups leads to very fast cellular uptake time ((0.14 ± 0.04) to (14 ± 4) h) and LD_{50} concentration was as low as (8.5 ± 2.8) × 10^{-9} M for porphycene **5.39**. These porphycenes were found to be 17-220 times photodynamically more active, compare to currently clinically approved photosensitizer Photofrin®. Notably, 9-actetoxy-2,7,12,17-tetramethoxyethyl-porphycene **5.89**, where presence of methoxy group increases cellular uptake and acetoxy group increases solubility and hydrophilicity, can be applied topically, is in Phase II preclinical trial with Glaxo Dermatology and Cytopharm for topical photodynamic therapy against psoriasis vulgaris and superfacial non-melanoma skin cancer.[51] Further, Nonell and coworkers introduced first tricationic porphycene **5.90** for antimicrobial photodynamic

therapy against gram positive and gram negative bacteria.[52] Very recently, they have introduced porphycene analogue of clinically approved temoporfin (Foscan®), temocene **5.91** for PDT.[53] However, it displays lower photodynamic activity towards HeLa cells compare to temoporfin, but exhibits higher photostability, lower dark toxicity and mitochondrial localization.

5.2 Research goal

Therefore, keeping the recent developments in porphycene chemistry in mind, we proposed to develop some novel porphycene molecules, which may find potential application as photosensitizer for PDT. In this regard, we found that the presence of methoxy groups (**5.39**) has significant advantages over the nonmethoxylated analogues such as **5.34**; first, it enhances cell localization, probably owing to the greater hydrophilicity it imparts, and second, it can be subsequently deprotected to hydroxy and further substituted with long alkyl, alkoxy, or sugar moieties or different salts in order to modulate the lipophilicity of the resultant macrocycle.[48] Also, we found that presence of halogen group in the periphery of porphycene enhances triplet conversion and hence, singlet oxygen quantum yield. This led us to explore the possible synthesis of β-octamethoxyporphycene **5.92** along with their M(II)

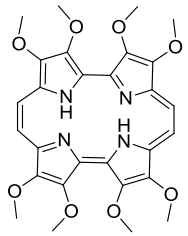

5.92

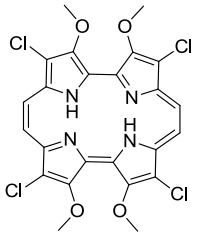

5.93

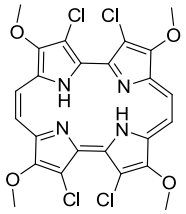

5.94

complexes, which has potential application as a photosensitizer (PS) in PDT.[54] Further, unanticipated synthesis of 3-chloro-4-methoxypyrrole-2-aldehyde,[55] led us to explore the synthesis of two positional isomer of β-terachlorotetramethoxyporphycenes (**5.93** and **5.94**) along with their M(II) complexes to evaluates the effect of chloro groups in their photophysical properties compared to octamethoxy analogue along with positional substituent effect. Also, we observed that lengthy multistep synthesis of porphycenes is one of the major drawbacks to explore its novel properties. Therefore, one of our objectives was to synthesize porphycenes in shortest possible pathway to overcome related problems. Another aspect of our interest is to see if the effect of substituents at the 3,6- and 13,16-positions and their consequence on its structure, photophysical and electrochemical properties.

5.3 Results and discussions

5.3.1 Synthesis of porphycenes

As we have designed to synthesize porphycene by conventional McMurry coupling of bipyrrole dialdehyde, therefore our focus was zeroed on the synthesis of bipyrrole dialdehyde. In chapter 3, we have discussed about the synthesis of 3,4-dimethoxypyrrole-2-aldehyde **5.95** and 3-chloro-4-methoxypyrrole-2-aldehyde **5.96**. Both the aldehydes were subjected to iodination using N-iodosuccinimide (NIS), to obtain the corresponding 5-iodo-compounds (**5.97-98**) in good yield. Further Ullmann coupling of these iodo compounds (**5.97-98**) led to formation of deiodinated products (**5.95-96**) exclusively, instead of desired bipyrrole dialdehydes (**5.99-100**) probably due to electron rich nature of these pyrrole

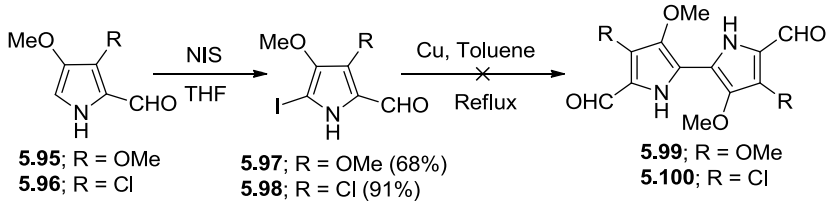

Scheme 5.19 Ullmann coupling methodology towards the synthesis of bipyrrole dialdehydes.

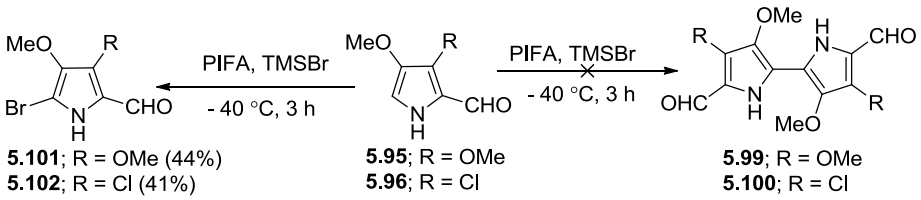

Scheme 5.20 Kita's methodology towards the synthesis of bipyrrole dialdehydes.

aldehydes. Recently, Kita and coworkers reported oxidative coupling of electron rich pyrroles to corresponding bipyrroles in good yield.[56] As we know the 3,4-dimethoxypyrrole is highly reactive and hence relatively less stable, therefore we tried oxidative coupling reaction on both the pyrrole aldehydes (**5.95-96**). The oxidative coupling of aldehydes **5.95-96** by using [bis(trifluoroacetoxy)iodo]benzene (PIFA) as oxidant and trimethylsilyl bromide (TMSBr) as Lewis acid at -40 °C provided non-fluorescent white crystalline products in good yield. Further characterization of these compounds led us to identify these compounds as 5-bromo-pyrrole aldehydes (**5.101-102**), instead of the desired bipyrroledialdehydes, which was further confirmed by bromination of the pyrrolealdehydes with N-bromosuccinimide (NBS). Therefore, it was difficult to synthesize our targeted materials by conventional approach.

Hence our focus shifted to the synthesis of tetramethoxybipyrroledialdehyde **5.99**, in order to synthesize the desired β-octamethoxyporphycene **5.92**.

5.3.1.1 Synthesis of β-octamethoxyporphycene 5.92

The key to our target was the precursor diformyl derivative of tetramethoxy-2,2′-bipyrrole **5.99**. Modified Pd-catalyzed Ullmann coupling of iodopyrrole **5.97**, following Smith's strategy, led to desired bipyrrole **5.99** in poor yield (14%).[21] Therefore, we decided to explore

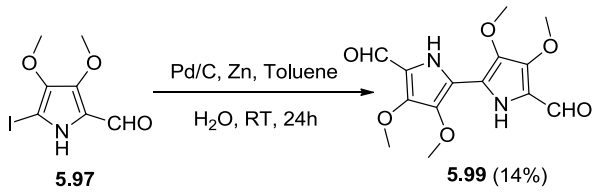

Scheme 5.21 Pd-catalyzed modified Ullmann Coupling synthetic pathway for the synthesis of **5.99**.

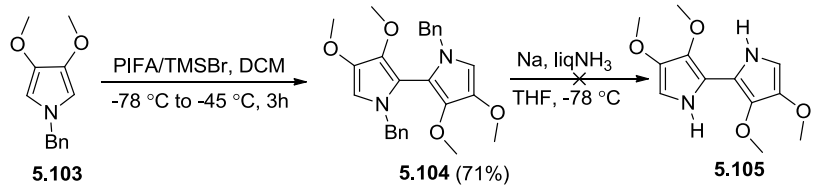

Scheme 5.22 PIFA/TMSBr coupling of N-benzyl-3,4-dimethoxypyrrole towards synthesis of **5.99**.

the synthesis of bipyrrole directly from the pyrrole itself using hypervalent iodine mediated Lewis acid catalyzed coupling reactions with PIFA as an oxidant and TMSBr as a Lewis acid reported by Kita's group.[56] Owing to the high reactivity of the 3,4-dimethoxypyrrole **5.106**,[57] initially we used the corresponding N-benzyl derivative **5.103** (which happens to be the precursor for pyrrole **5.106**), as our starting material. This led to the successful isolation of the doubly N-protected 2,2′-bipyrrole **5.104** in good yield (71%), whose structure was further confirmed by X-ray diffraction (XRD) analysis (Figure 5.2). Subsequent debenzylation using Na/liq NH_3, however, led to decomposition of the desired product **5.105**. Therefore, we decided to explore the PIFA-TMSBr coupling of 3,4-dimethoxypyrrole **1.506** itself. As expected, we could notice the formation of the product at -45 °C; however, the compound undergoes decomposition during the purification. In order to avoid this, we subjected the reaction mixture to Vilsmeier-Haack formylation, immediately after the workup process. Finally this led us to the desired product **5.99** (two-step yield 39%; Scheme 5.23), whose structure was confirmed by XRD analysis (Figure 5.2). McMurry coupling of the dialdehyde **5.99** using $TiCl_4$/Zn finally resulted in the formation of the desired octamethoxyporphycene

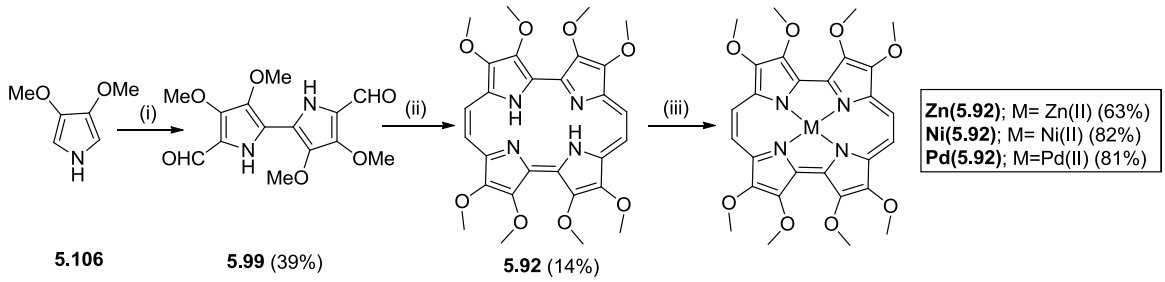

Scheme 5.23 Synthesis of β-octamethoxyporphycene and its M(II) derivatives. Reagents and conditions: (i) (a) PIFA, TMSBr, DCM, -78 °C to -45 °C, 3 h; (b) $POCl_3$, DMF, DCE, reflux, 2 h; (ii) Zn, $TiCl_4$, CuCl, THF, reflux, 1 h; (iii) **Zn1**: $Zn(OAc)_2.2H_2O$, $CHCl_3$/MeOH, reflux, 4 h; **Ni1**: $Ni(acac)_2$, o-xylene, reflux, 4 h; **Pd1**: $Pd(OAc)_2$, AcOH, reflux, 7 h.

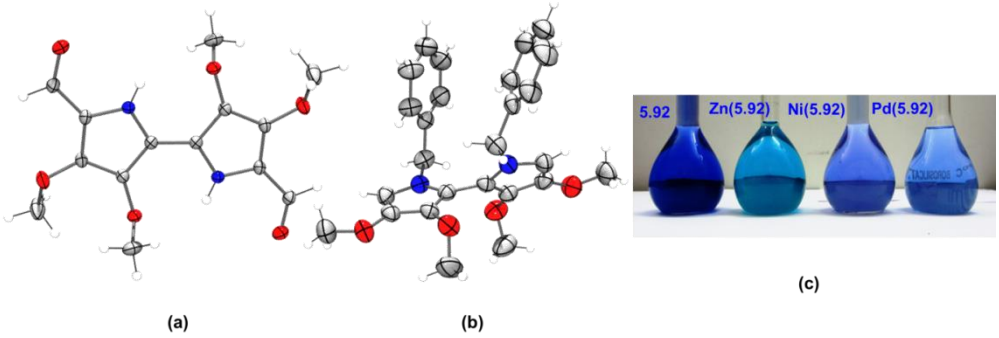

Figure 5.2 Molecular structure of (a) **5.99** and (b) **5.104** drawn at 35% probability level (color code: grey: C, blue: N, red: O, white: H.). (c) Solubility of porphycene (**5.92**) and their M(II) complexes in methanol.

5.92 in 14% yield (Scheme 5.23). Here the porphycene could be synthesized in only three steps from the constituent pyrrole derivative, making it the shortest route to β-substituted porphycenes. Further, this strategy emerged as more efficient compared to the traditional iodination and Ullmann coupling route (also not possible in this case) to bipyrrole synthesis (where in many occasions BOC protection is essential for enhanced yield). The freebase porphycene could be further converted to its Zn(II)-, Ni(II)- and Pd(II)- complexes. All of the porphycene derivatives were characterized following standard spectroscopic techniques. Further, the solid state structures of the freebase **5.92**, **Zn(5.92)**, and **Pd(5.92)** could be ascertained by XRD analyses. These porphycenes show good lipophilicity and hydrophilicity, displaying good solubility in all organic solvents ranging from hexane to methanol (Figure 5.2c).

5.3.1.2 Synthesis of β-tetrachlorotetramethoxyporphycenes (5.93 and 5.94)

We reported that the exhaustive Vilsmeier-Haack formylation of 3,4-dimethoxypyrrole **5.106** led to unexpected formation of 3-chloro-4-methoxypyrrole-2-aldehyde **5.96** in good yield in

chapter 3.[55] Therefore, for the synthesis of the desired precursor 4-chloro-3-methoxypyrrole-2-aldehyde **5.111**, we employed **5.96** as the starting material (Scheme 5.24). The aldehyde

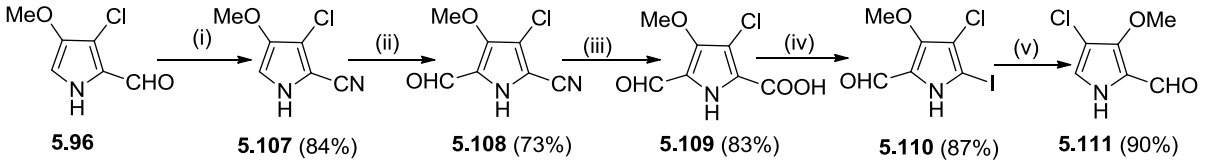

Scheme 5.24 Synthesis of 4-chloro-3-methoxypyrrole-2-aldehyde **5.111**. Reagent and conditions: (i) (a) $NH_2OH.HCl$, Et_3N, DCE, 60 °C 2 h; (b) Phthalic anhydride, reflux, 24 h; (ii) $POCl_3$, DMF, DCE, reflux, 1 h; (iii) NaOH, H_2O, reflux, 48 h; (iv) I_2, KI, $NaHCO_3$, DCE, H_2O, 80 °C, 1.5 h; (v) 5% Pd/C (4 mol%), Zn, H_2 (1atm), RT, 18 h.

group of **5.96** was converted to oxime with $NH_2OH.HCl$ in presence of triethylamine, followed by dehydration of oxime with phthalic anhydride under reflux condition provided the desired 3-chloro-4-methoxypyrrole-2-nitrile **5.107** in 84% overall yield.[58] The Vilsmeier-Haack formylation of **5.107** afforded the 3-chloro-5-formyl-4-methoxypyrrole-2-nitrile **5.108** in 73% yield, whose structure was further confirmed by single crystal XRD (Figure 5.3). Subsequently, hydrolysis of **5.108** with aqueous NaOH under reflux condition led to the formation of 3-chloro-5-formyl-4-methoxypyrrole-2-carboxylic acid **5.109** in 83% yield. However, our repeated effort towards deprotection of the carboxylic acid of **5.109** under all standard conditions failed. Therefore, we were forced to change our strategy to employ decarboxylative iodination followed by de-iodination to obtain the desired de-carboxylated product. So, iodination of **5.109** with $KI_3/NaHCO_3$ at 80 °C resulted in the formation of 4-chloro-5-iodo-3-methoxypyrrole-2-aldehyde **5.110** in 87% yield and subsequent, de-iodination of **5.110** by the method developed by Smith group[21] using catalytic amount of Pd/C with activated Zn in aqueous acetone, fortunately led to the formation of desired 4-chloro-3-methoxypyrrole-2-aldehyde **5.111** in 90% yield, whose structure was unequivocally confirmed by single crystal XRD (Figure 5.3).

With both the pyrrolic precursors in hand, we proceeded to perform oxidative coupling to synthesize the bipyrroles (Scheme 5.25). As the aldehyde group is expected to hinder the oxidative coupling reaction, therefore, it was protected with ethyl-2-cyanoacetate by Knoevenagel condensation, in presence of triethylamine to form the cyanoacrylate protectedpyrroles **5.112** and **5.113** in 94 and 97% yields, respectively.[59] Scholl oxidation of **5.112** and **5.113** with $FeCl_3$ using TFA as solvent, led to the formation of corresponding bipyrroles,[60] and without further characterization, the cyanoacrylate groups were deprotected

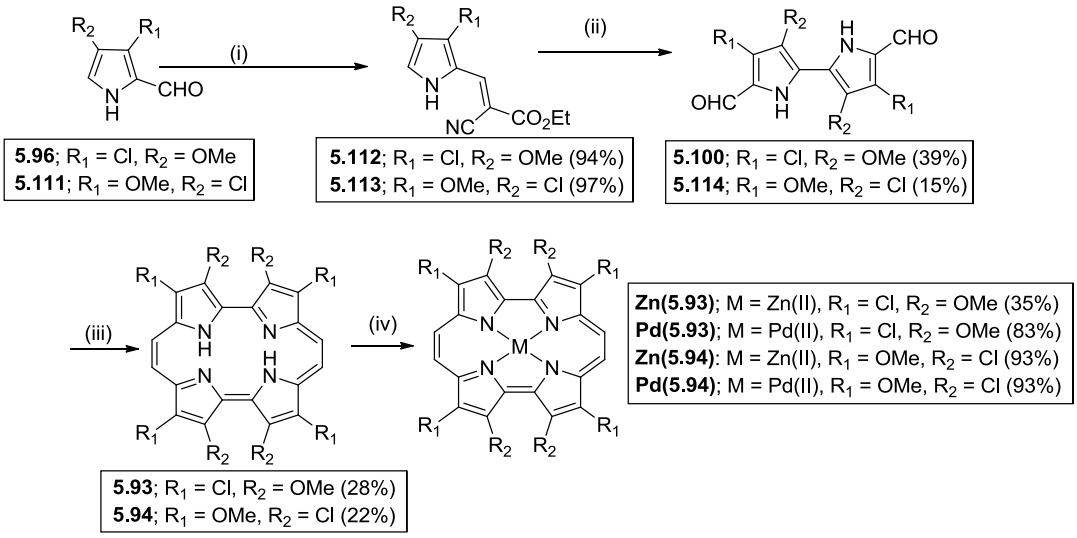

Scheme 5.25 Synthesis of β-tetrachlorotetramethoxyporphycenes. Reagents and conditions: (i) ethylcyano-acetate, NEt_3, Toluene, reflux, 4 h; (ii) (a) $FeCl_3$, TFA, RT, 24 h. (b) NaOH, H_2O, reflux, 3 h; (iii) Zn, $TiCl_4$, CuCl, THF, Reflux, 1 h; (iv) for Zn(II) complex $Zn(OAc)_2$, $CHCl_3$, MeOH, reflux 4 h and for Pd(II) complex $Pd(OAc)_2$, DCE, AcOH, reflux, 4 h.

by refluxing in 3M NaOH to afford the desired bipyrroledialdehydes **5.100** and **5.114** in 39% and 15% yields, respectively in two steps. Interestingly, our previously developed oxidative coupling of **5.112** by using PIFA and $BF_3.OEt_2$ at -40 °C, followed by deprotection as mentioned above provided the desired **5.100** in comparable yield.[54,56] However, synthesis of **5.114** under identical condition resulted in failure, indicating probably PIFA is not sufficiently strong to activate α-position of pyrrole **5.113**, due to presence of deactivating chloro group at the adjacent β-position compare to activating methoxy group in **5.112**.[61] Further, the structure of **5.100** was confirmed by single crystal XRD technique (Figure 5.3). Most interestingly, molecular structure of bipyrroledialdehyde **5.100** exists in the unusual cis conformation.

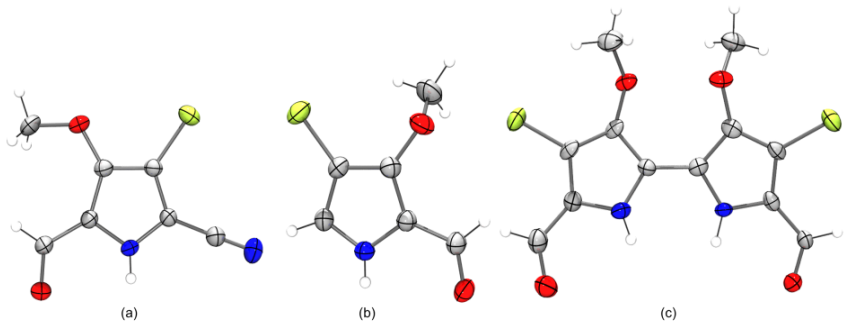

Figure 5.3 Molecular structures of (a) **5.108**, (b) **5.111** and (c) **5.100** scaled in 35% probability level. Color code: C, grey; H, white; N, blue; O, red; chlorine, yellow green.

Finally, McMurry coupling of **5.100** and **5.114** with low valent Ti generated from Zn/$TiCl_4$, in presence of CuCl under reflux condition, followed by aerial oxidation provided the desired porphycenes **5.93** and **5.94** in 28 and 22% yields, respectively. Both the freebase porphycenes were further converted to their corresponding Zn(II) and Pd(II) complexes. All the compounds were well characterized by standard spectroscopic techniques.

5.3.2 ^{1}H NMR studies

The ^{1}H NMR spectrum of octamethoxyporphycene **5.92** reveals the *meso* protons and imino protons resonating at 9.66 and 0.36 ppm. In comparison to analogous octaethylporphycene **5.42**, the *meso* protons (9.48 ppm) are shifted downfield by 0.18 ppm, whereas the NH signal (0.65 ppm) is shifted upfield by about 0.3 ppm[23], which may be attributed to the presence of eight electron-donating methoxy groups at the porphycene periphery.

Similarly, the ^{1}H NMR spectra of free base tetrachlorotetramethoxyporphycenes **5.93** and **5.94** consist of *meso* protons resonating at 9.80 and 9.65 ppm and inner imino protons at 0.98 and 0.16 ppm, respectively. Though very marginal difference was observed in *meso* proton resonances, however, significant upfield shift could be noticed in imino proton signals for **5.94** compare to **5.93** (by 0.82 ppm). This may arise from greater nonbonding interactions between four bulky chloro substituents at 3,6- and 13,16- positions compare to O's of methoxy substituents. This could be further confirmed by comparison of ^{1}H NMR spectrum of analogous octamethoxyporphycene **5.92** imino protons with that of **5.93** (0.36 vs 0.98 ppm), where the marginal down field shift in case of latter could be attributed to the four electron withdrawing chloro groups.

5.3.3 UV-Vis and fluorescence properties of porphycenes

The UV-Vis spectra of porphycene **5.92** and its metallo derivatives were recorded in chloroform (Figure 5.4 and Table 5.1). Porphycene **5.92** shows one characteristic intense Soret band at 382 nm and three weaker Q-bands at 557, 599, and 636 nm. The lowest energy band is 29 and 21 nm blue-shifted compared to octaethylporphycene **5.42** and etioporphycene **5.41**, respectively,[23] which may be attributed to an increase in HOMO-LUMO energy difference due to the presence of electron-rich methoxy groups at its periphery. The UV-Vis spectra of metalloporphycenes **Zn(5.92)**, **Ni(5.92)**, and **Pd(5.92)** show red-shifted Soret bands at 388-390 nm compared to freebase porphycene **5.92** and also display one Q-band between 590 and 618 nm. Further, compound **5.92** displays very weak emission ($\phi_f < 10^{-4}$),

whereas insertion of zinc led to a substantial enhancement in the emission (ϕ_f of **Zn(5.92)** 0.025; Figure 5.4b) with an intense band at 632 nm accompanied by a weaker lower energy band (689 nm). Both porphycene **5.92** and its Zn(II)-derivative show relatively weaker

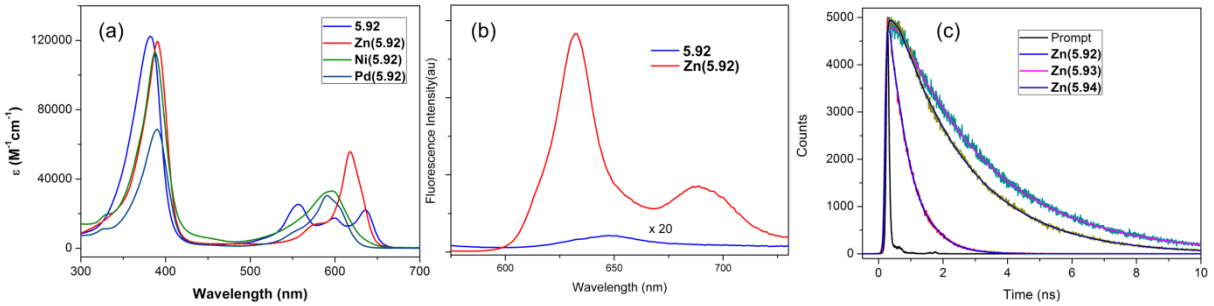

Figure 5.4 (a) UV-Vis, (b) fluorescence spectra of octamethoxyporphycenes. (c) Fluorescence decay profile of porphycenes.

Table 5.1 Comparative photophysical data of porphycenes.

	UV-Vis (in $CHCl_3$)	Emission			
Comp.	**λ_{max} in nm (log ε)**	**λ_{max} (nm)**[a]	**(ϕ_f)**[b]	**(τ_f) (ns)**[c]	**(ϕ_Δ)**[d]
5.92	382 (5.09), 557 (4.40), 599 (4.24), 636 (4.34)	649	<0.0001	---	---
Zn(5.92)	390 (5.08), 618 (4.75)	632, 689	0.025	0.6	0.12
Ni(5.92)	388 (5.05), 596 (4.52)	---	---	---	---
Pd(5.92)	390 (4.84), 590 (4.48)	---	---	---	0.73
5.93	376 (5.16), 384 (5.14), 565 (4.58), 608 (4.35), 647 (4.52)	655, 717	0.00071	---	---
Zn(5.93)	391 (5.24), 588 (4.33), 638 (4.90)	645, 706	0.17	2.9	0.73
Pd(5.93)	389 (4.94), 561 (4.14), 606 (4.70)	---	---	---	0.86
5.94	385 (5.13), 572 (4.52), 625 (4.31), 664 (4.46)	676	0.00075	---	---
Zn(5.94)	391(4.90), 604 (4.14), 638 (4.61)	654, 711	0.16	2.4	0.57
Pd(5.94)	391(4.93), 603 (4.64), 624 (4.55)	---	---	---	0.83
Pd(5.42)	310 (3.93), 390 (4.99), 566 (4.09), 603 (4.61), 618 (4.61)	---	---	---	0.89
Zn(5.42)	375 (4.89), 393 (5.21), 590 (4.34), 638 (4.97)[e]	660[e]	0.05[e]	3.2[e]	0.68

[a] Fluorescence in $CHCl_3$, [b] fluorescence quantum yield, [c] fluorescence lifetime, [d] singlet oxygen quantum yield, [e] data taken from ref 23, for **(ϕ_f)** measurement **H_2TPP** in benzene (ϕ_f 0.11) was taken as reference.

emission compared to **5.42** and its Zn(II)-complex (**Zn(5.42)**); with **Zn(5.92)** possessing relatively shorter fluorescence lifetime (0.6 ns; Figure 5.4c) compared to analogous **Zn(5.42)** (3.2 ns).[62]

The UV-Vis spectra of **5.93** in $CHCl_3$ consists of split Soret bands at 376 and 384 nm, along with three Q-type bands at 565, 608 and 647 nm, whereas **5.94** displays Soret band at 385 nm and Q-type bands at 572, 625 and 664 nm (Figure 5.5). The lowest energy band is 11 and 28 nm red shifted respectively for **5.93** and **5.94** compared to octamethoxy analogue **5.92**,

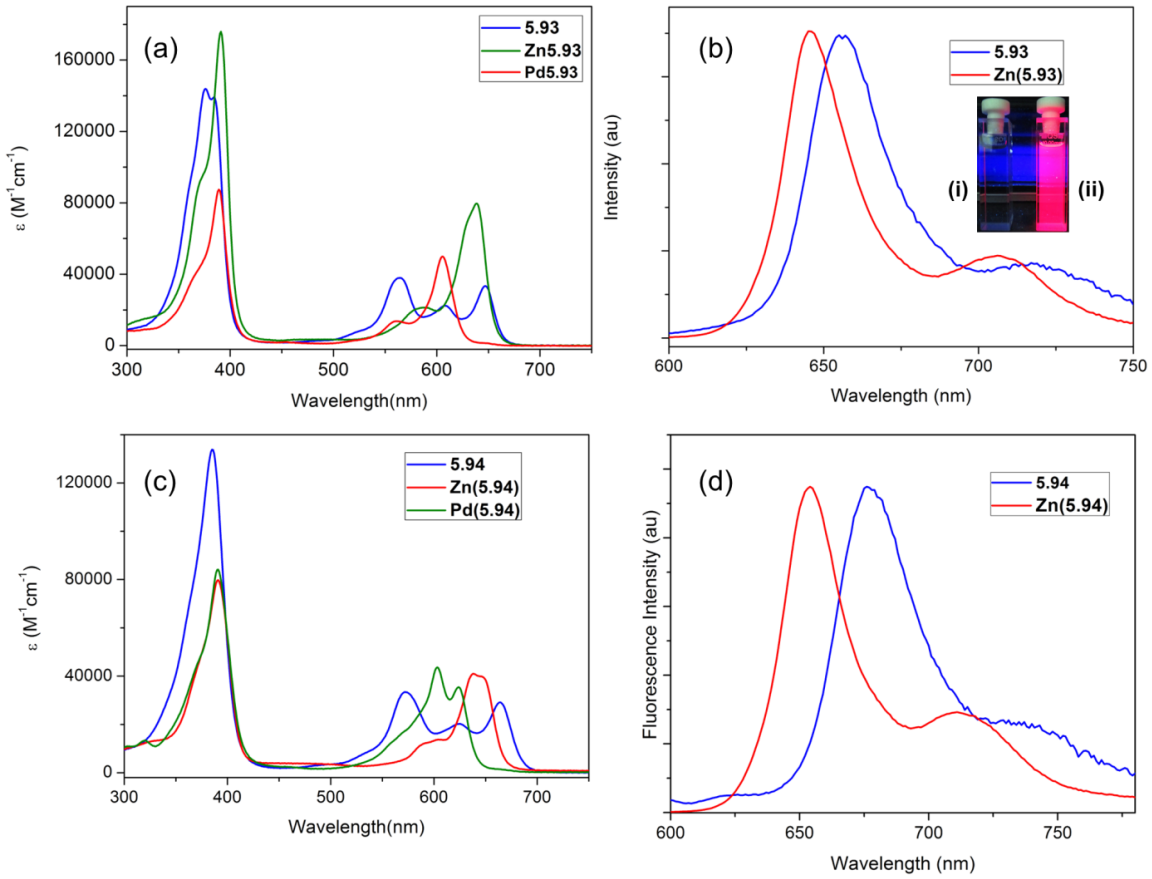

Figure 5.5 (a), (c) UV-Vis, (b), (d) fluorescence spectra of tetrachlorotetramethoxyporphycenes. In inset of Figure (b) depicting the fluorescence of (i) **5.93** and (ii) **Zn(5.93)** upon exposure to UV light (356 nm).

indicating electron deficient nature of these porphycenes. Further, between them, while there is hardly any change in the absorption of the Soret band, on the other hand the lowest energy band for **5.94** is 17 nm red shifted compare to **5.93** and this may be attributed to the greater non-bonding interaction between relatively bulky chloro groups at 3,6- and 13,16- positions. This clearly reflects the positional effect of substituents for porphycenes **5.93** and **5.94**. Again, Zn(II) and Pd(II) complexes of **5.93** and **5.94** consist of red shifted Soret band at 389-391 nm and blue shifted Q-bands at 606-638 nm compared to corresponding freebase porphycenes. Notably, here also the positional effect of substituents could be clearly observed in these isomers; first of all lowest energy bands of complexes of **5.94** red shifted compare to **5.93** and consist of split Q-bands for complexes of **5.94**, the latter trend is also observed for complexes of octaethyl analogue **5.42**.[23] Interestingly, the split Soret bands observed in

freebase porphycene **5.93**, merged into one (with a prominent shoulder on the higher energy side), upon complexation with metal ions, indicating greater symmetry due to lack of NH-tautomerization.

The freebase porphycenes **5.93** and **5.94** are weakly emissive (ϕ_f for **5.93** and **5.94**: 0.0007) with emission maxima at 655 and 676 nm, respectively (Figure 5.5). Similar to other octasubstituted porphycenes, complexation with Zn(II) leads to substantial enhancement in emission for both **Zn(5.93)** and **Zn(5.94)** (ϕ_f for **Zn(5.93)**, 0.17 and **Zn(5.94)**, 0.16) with emission maxima at 645 and 654 nm respectively (Figure 5.5). More strikingly, replacement of four methoxy group of octamethoxy analogue **Zn(5.92)**, with chloro groups [**Zn(5.93)** and **Zn(5.94)**] leads to enhancement of fluorescence, indicating electron donating methoxy groups probably act as quencher of fluorescence through enhanced internal charge transfer (ICT). This is again reflected in the longer fluorescence lifetime observed for chloromethoxy analogues (τ_f for **Zn(5.93)**: 2.9 ns and **Zn(5.94)**: 2.2 ns) (Figure 5.4) compared to octamethoxy analogue **Zn(5.92)** (τ_f 0.6 ns).

5.3.4 X-ray crystal structure analysis

Molecular structure of porphycenes **5.92**, **Pd(5.92)** and **Zn(5.92)** were unequivocally characterized in the solid state by X-ray crystallographic analysis (Figure 5.6). All porphycenes display planar macrocyclic core, and the observed planarity is more compared to **5.42**. For example, the mean deviation of nitrogen atoms from the mean plane of porphycene **5.92** (excluding the methoxy substituents) is only 0.021 Å (0.27 Å for **5.42**).[23] This probably

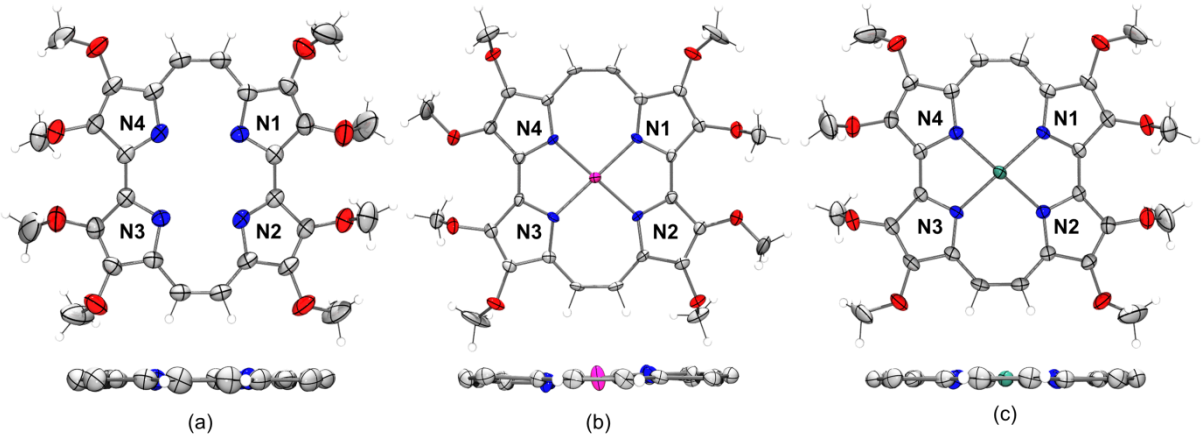

Figure 5.6 X-ray crystal structure of (a) **5.92**, (b) **Zn(5.92)**, and (c) **Pd(5.92)** (above front view and below side view) drawn in 35% probability level. In side views methoxy groups are omitted for clarity. Color code: C, gray; N, blue; O, red; H, white; Zn, pink; Pd, green.

resulted from the reduced van der Waals repulsion between 3,6- and 13,16- substituents, by replacing the ethyl groups with less bulky methoxy groups in **5.42**. However, these repulsive interactions are still strong enough to enforce a square-type core for porphycene **5.92** (N1-N2 2.741 Å and N2-N3 2.758 Å), as observed in case of **5.41-42**.[23] Among the metalloporphycenes, the deviation is relatively more in the case of **Zn(5.92)** (±0.083 Å) than **Pd(5.92)** (±0.034 Å). As expected, metal insertion in the macrocyclic core led to a change in geometry from square to rectangular type (**Pd(5.92)** N1-N2 2.575 Å, N2-N3 3.009 Å and **Zn(5.92)** N1-N2 2.613 Å, N2-N3 3.024 Å).

The crystal structures of **5.93** and **5.94** along with their axially pyridine ligated complexes, **Zn(5.93)** and **Zn(5.94)** were characterized by XRD techniques (Figure 5.7). The molecular structure of **5.93** and **5.94** displays planar configuration (maximum displacement of N from mean plane drawn through macrocyclic core, 0.053 and 0.032 Å for **5.93** and **5.94** respectively). In contrast to tetrabromotetrapropylporphycene **5.71**, the presence of chloro groups at 3,6- and 13,16- positions in **5.94** didn't exert any distortion on macrocyclic core. Also, crystal packing structures of **5.93** and **5.94** (Figure 5.8) display strong face to face π-π stacking, with interplanar distance of 3.42 and 3.49 Å between the two porphycene units for **5.93** and **5.94**, respectively and corresponding centroid-centroid distance of 3.95 and 4.13 Å, respectively. In analogy to other octasubstituted porphycenes, **5.94** retains square type core (N1-N2: 2.78 Å, N2-N3: 2.715 Å and N1-N2: 2.727 Å, N2-N3: 2.761 Å for **5.93** and **5.94** respectively). In contrast to **5.94**, the core of **5.93,** is comparatively more rectangular in nature and whereas, unexpectedly core is relatively expanded towards N2-N3 and contracted towards N1-N2 for **5.94**, despite the presence of inner chloro groups. This could be explained by in plane nonbonding repulsion of chloro groups at 3,6- and 13,16- positions, however, for **5.93** it is reverse. Also, N2-N3 distance is higher for **5.94**, which is further supported by comparative upfield shift of imino protons in ^{1}H NMR resulting from relatively weak N-H$^{\cdots}$N H-bonding interaction. Further, we can conclude that the distinctive substitution effects on absorption and emission properties of **5.93** and **5.94** arises from the in plane non-bonding interaction at 3,6- and 13,16-positions and the resultant change in core size. **Zn(5.93).Py** and **Zn(5.94).Py** (Py denotes pyridine) display rectangular core as noticed in other octasubstituted porphycenes. The axial coordination with pyridine led to Zn ion residing above the plane of the macrocycle in both cases and the displacement of Zn from mean plane drawn through four core N-atoms is 0.53 and 0.36 Å, respectively for **Zn(5.93).Py** and **Zn(5.94).Py**. The average Zn-N distance is 2.04 Å for both structures. Interestingly, the axial ligation of Zn

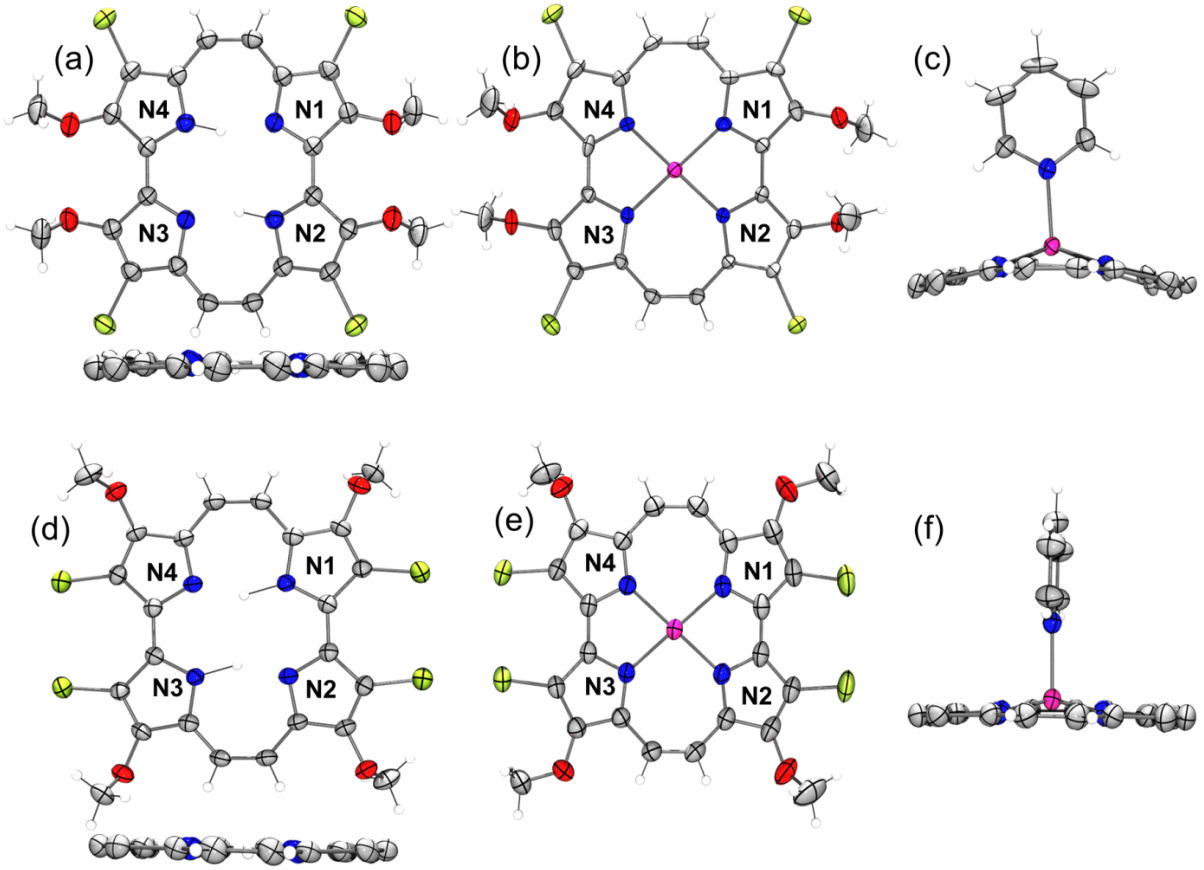

Figure 5.7 Molecular structure of (a) **5.93** (above front and below side view) (d) **5.94** (above front and below side view) (b) **Zn(5.93).Py** front view, (c) **Zn(5.93).Py** side view, (e) **Zn(5.94).Py** front view and (f) **Zn(5.94).Py** side view, scaled in 35% probability level. Pyridine from all front views of Zn(II) complexes and chloro, methoxy groups from all side views are removed for clarity. Color code: C, grey; N, blue; O, red; Cl, yellow green; H, white; Zn, pink.

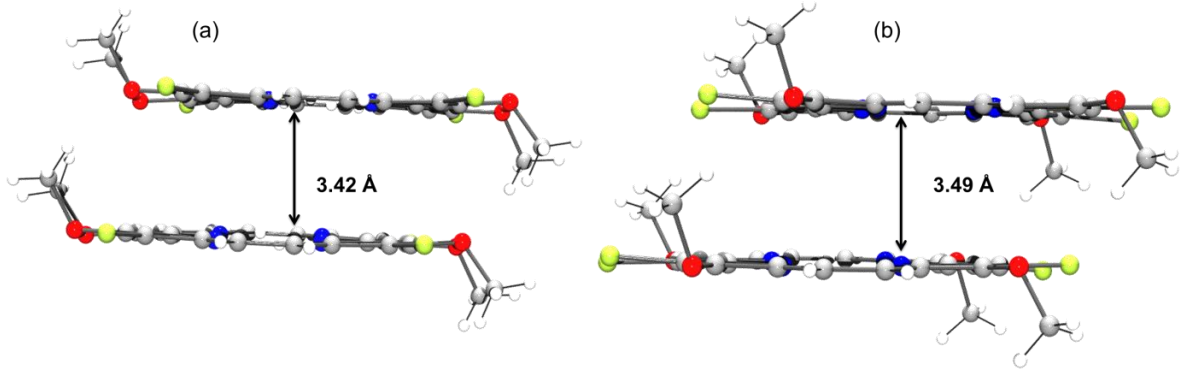

Figure 5.8 Distinctive π-π-stacking diagrams of (a) **5.93** and (b) **5.94**. Color code: C, grey; N, blue; O, red; Cl, yellow green; H, white.

with pyridine, lead to elevation of Zn along with deformation of core of the macrocycle in case of **Zn(5.93).Py** to result in a cone shape formation, but in contrast, for **Zn(5.94).Py** only elevation of Zn is observed but core of macrocycle remains almost planar, a trend which is

also observed for **Zn(5.42).Py**.[23] The degree of displacement can be measured by the displacement of β-C's from mean plane drawn through four imino nitrogens and the maximum displacement observed for β-C's is 0.72 and 0.17 Å for **Zn(5.93).Py** and **Zn(5.94).Py**, respectively, clearly reflects the distortion of core in **Zn(5.93).Py**. Also, displacement of imino Ns from the mean plane drawn through macrocycle (methoxy, chloro, pyridine and Zn excluded) is 0.22 and 0.04 Å, respectively for **Zn(5.93).Py** and **Zn(5.94).Py** indicating a relatively more planar core for **Zn(5.94).Py**. These attributes clearly demonstrate the positional effect of substituents, even in case of the metallo-derivatives where **Zn(5.93).Py** adopts a cone shape form and **Zn(5.94).Py** adopts a planar structure, probably the presence of four chloro group at 3,6- and 13,16- positions hindering the core deformation owing to reduced non-bonding interactions.

5.3.5 Electrochemical studies of porphycenes

Redox potentials of porphycene **5.92** and its metallo-derivatives were determined by cyclic voltammetry (CV) and differential pulse voltammetry (DPV) in dichloromethane (Figure 5.9). These porphycenes display typical two ring oxidation and two ring reduction potentials. A closer inspection of the voltammogram of **5.92** reveals reversibility for the second ring reduction potential only, and further the absence of the clear reduction waves in the oxidation

Table 5.2 Comparative Oxidation and Reduction Potentials (in V vs SCE) for Porphycenes and their M(II) Complexes

Porphycenes	Reduction	Oxidation	HOMO-LUMO (ΔE)
5.92	-1.29, -1.11[a]	+0.78,[a] +1.15[a]	1.89
Zn(5.92)	-1.38, -1.13[a]	+0.60, +0.75	1.73
Ni(5.92)	-1.45, -1.19	+0.71, +1.17	1.90
Pd(5.92)	-1.36, -1.13[a]	+0.77, +1.28	1.90
5.93	-0.81, -0.60	+1.15[a], +1.29[a]	1.75
5.94	-0.73, -0.56	+1.16[a], +1.39[a]	1.72
Zn(5.93)	-1.20[a], -0.89	+0.99, +1.23	1.88
Zn(5.94)	-0.89, -0.83	+0.96, +1.11[a]	1.79
5.42[b]	-1.26, -0.94	+0.87, +1.10	1.81
Zn(5.42)[b]	-1.38, -1.09	+0.64, +0.78	1.73
Ni(5.42)[b]	-1.46, -1.06	+0.81, +1.12	1.87
Pd(5.42)	-1.46[a], -1.04	+0.88, +1.30	1.92

[a]Measured by DPV. [b]Taken from ref 63.

half indicates the unstable nature of both the cation radical and the dication of porphycene **5.92**. Redox potentials of **5.92** and its M(II) complexes are summarized vs SCE in Table 5.2.

All metalloporphycenes show two reversible ring oxidation potentials (stabilized by the presence of Lewis acidic metal ions) and two reduction potentials. The relatively electron-rich characters of the octamethoxyporphycene **5.92** and its metal complexes, in comparison to their octaethyl analogue **5.42** and its metal complexes, are clearly reflected in their redox potentials (Table 5.2), in particular in their corresponding first oxidation (less positive potential) and reduction (more negative potential) potentials.[63] In addition, the HOMO−LUMO energy gap of **5.92** and its M(II)-derivatives was evaluated from the difference between the first oxidation and first reduction potentials. The energy gap of **5.92** ($\Delta E = E_{ox1} - E_{red1}$ = 1.89 V) is slightly higher than that of **5.42** (1.81 V), which is attributed to the presence of strong electron-donating methoxy groups and again clearly reflected in the blue shift of Q-bands in the absorption spectrum.

The electrochemical properties of porphycene **5.93**, **5.94** and their Zn(II) complexes were characterized by cyclic voltammetry (CV) and differential pulse voltammetry (DPV) in CH_2Cl_2 using tetrabutylammonium hexafluorophosphate as supporting electrolyte (Figure 5.8 and Table 5.2). The electrochemical measurement for Pd(II) complexes couldn't be performed due to their poor solubility in organic solvents. The results of electrochemical studies are summarized in Table 5.2. These porphycenes and their Zn(II) complexes display typical two one electron reduction and two one electron oxidation potentials. Introduction of four chloro group by replacing methoxy group of **5.92** leads to more positive oxidation and reduction potentials observed. The first reduction potential is 0.51 and 0.55 V more positive and similarly first oxidation potential is 0.37 and 0.38 V more positive, respectively for **5.93**

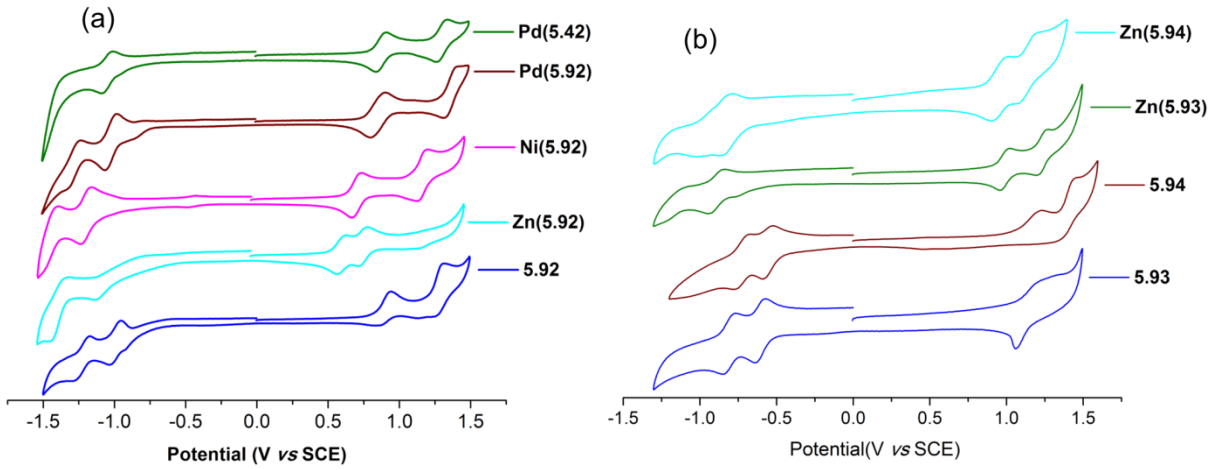

Figure 5.9 Cyclic voltammogram (CV) of porphycenes at 50 mV/sec scan rate. In Figure (b) for increasing solubility of Zn(II) complexes ~50 µL THF was added.

and **5.94** compare to octamethoxy analogue **5.92**,[54] confirming the relatively more electron deficient nature of both the macrocycles. Also, the more positive change in reduction potential compare to oxidation potential proves that LUMO is more stabilize compare to HOMO, upon introduction of four chloro groups. Similar to first oxidation and reduction potential there is a significant change in second reduction potential in **5.93** and **5.94** compared to **5.92**, over second oxidation potential where change in minimal. Surprisingly, the positional effect of substituents on the redox potentials of these porphycenes are found to be minimal, in particular for the first oxidation and reduction potentials, whereas that in case of the second oxidation and reduction potential is comparatively more significant. Further, all Zn(II) complexes (**Zn(5.93)** and **Zn(5.94)**) show more positive reduction potential and oxidation potentials compared to analogous **Zn(5.92)**. The HOMO-LUMO gap for porphycene **5.93** and **5.94** found to be 1.75 and 1.72 V, respectively, which is 0.14 and 0.17 V lower compare to **5.92**, clearly reflected in the relatively red shifted lower energy bands in UV-Vis spectra of **5.93** and **5.94**.

5.3.6 Singlet oxygen generation efficiencies of porphycenes

In photodynamic therapy, an efficient photosensitizer is one that converts molecular oxygen to singlet oxygen ($^1O_2$) most effectively, in the presence of light, which is responsible for subsequent death of the cancerous cells. So keeping this in mind, we have measured steady state luminescence spectra of singlet oxygen for **5.92** and its metallo-derivatives in aerated toluene. Among them, **Zn(5.92)** and **Pd(5.92)** show emission bands ranging from 1240 to 1320 nm with maxima at about 1278 nm, when excited at 600 nm (Figure 5.10). Singlet oxygen quantum yield of **Zn(5.92)** and **Pd(5.92)** was evaluated by comparative actinometry

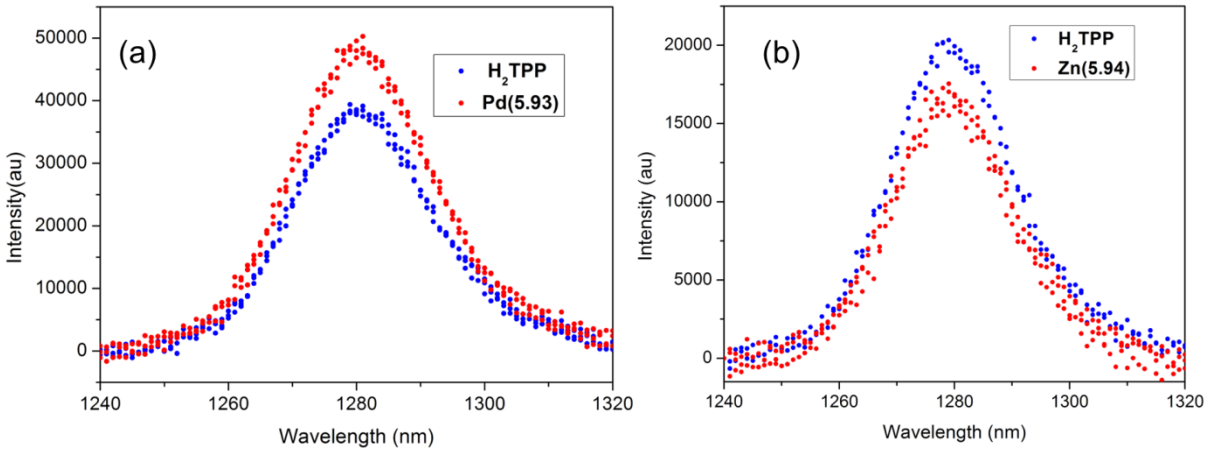

Figure 5.10 Singlet oxygen emission of optically matched aerated toluene solution of (a) **Pd(5.93)** and (b) **Zn(5.94)** (λ_{exc} ~600-620 nm).

method by using tetraphenylporphyrin (H_2TPP) as reference (ϕ_Δ 0.7) in aerated toluene.[64] The singlet oxygen quantum yields obtained for **Zn(5.92)** and **Pd(5.92)** are 0.12 and 0.73, respectively. Although not very high (up to 0.95) as noticed in case of bromo-substituted porphycenes (owing to expected heavy atom effect of bromine),[64a] still it is comparable to that observed in the case of 2,7,12,17-tetraphenylporphycenatopalladium(II) **Pd(5.38)** (0.78).[64c] Analogous measurement for **Zn(5.42)** and **Pd(5.42)** display singlet oxygen quantum yields of 0.68 and 0.89, respectively. Interestingly, in case of octaethylporphycene, the effect of the heavy atom is marginal (Zn *vs* Pd), whereas that in case of their methoxy analogues is quite substantial. This indicates the higher intersystem crossing (ISC) noticed in the case of **Zn(5.42)**[62] is not a general phenomenon in porphycenes. Further, like its strong dependence on nature of substituents at the periphery,[65] it also depends on the nature of the metal ion at the core, and further detailed photophysical study may elaborate on this aspect. Free base **5.92** didn't show any singlet oxygen emission like **5.42**, probably due to lack of efficient ISC.[62]

Unlike **5.71**[64a], freebase porphycenes **5.93** and **5.94** could not able to produce singlet oxygen, indicating probably chloro groups can't effectively enhance triplet population, a key requirement for singlet oxygen generation. However, upon complexation we could observe singlet oxygen generation, with ϕ_Δ for **Zn(5.93)** and **Zn(5.94)**, 0.73 and 0.57 respectively and ϕ_Δ for **Pd(5.93)** and **Pd(5.94)**, 0.86 and 0.83, respectively. There is a substantial enhancement in singlet oxygen quantum yield by replacing four methoxy groups of analogous metal complexes of **5.92** with chloro groups, indicating methoxy groups probably acted as triplet state quencher. Further, we observed remarkable difference in singlet oxygen generation efficiencies by simply changing substituents positions to conclude that there is a remarkable effect exerted by substituents and also their position on porphycene periphery dictates it's singlet oxygen generation ability.

5.4 Conclusion

In conclusion, PIFA-TMSBr coupling of 3,4-dimethoxypyrrole to corresponding bipyrrole enabled us to synthesize octamethoxyporphycene **5.92** for the first time, which happens to be the most efficient route toward the synthesis of β-substituted porphycenes. Also, we have synthesized two positional isomers of β-tetrachlorotetramethoxyporphycenes. In fact, they belong to the first example of chloro-substituted porphycenes. The oxidative coupling of protected pyrrole aldehydes enable us to synthesize bipyrrole dialdehydes in three steps from

the corresponding pyrrole aldehydes and by using this strategy, we can avoid unstable α-free bipyrrole intermediates. Further, we have studies positional effects of substituents in porphycene for the first time and probably due to α-α′ fused bipyrrolic units and lower symmetry compare to porphyrin; there is a significant positional effect on photophysical, structure and electrochemical properties in porphycene. The presence of methoxy groups led to an increase in their hydrophilicity (these porphycenes display good solubility in methanol). Photosensitizers based on the Pd(II)-porphyrinoids display promising results in clinical trials.[66] In this regard, Zn(II) and Pd(II) complexes of all studied porphycenes effectively generate singlet oxygen, along with its expected higher cell viability (owing to the presence of methoxy groups), may emerge as promising photosensitizers for photo-oxidation, DNA cleavage, and PDT. Our current effort is on to widen the current methodology towards synthesis of novel porphycenes along with possible exploration of PDT activity of currently developed porphycene complexes.

5.5 Experimental details

3,4-dimethoxy-5-iodopyrrole-2-aldehyde (5.97): 3,4-dimethoxypyrrole-2-aldehyde (**5.95**) (2 g, 12.9 mmol) was taken in THF (50 mL) under nitrogen atmosphere. Then, N-iodosuccinimide (3.05 g, 13.5 mmol) was added at -30 °C and reaction mixture was allowed to run at that temperature for 2 h. After completion of reaction, reaction mixture was quenched by addition of sodium bicarbonate solution, organic layer was separated and aqueous layer was extracted with diethyl ether. The combined organic layer was washed with aqueous sodium thiosulphate followed by brine solution and passed through anhydrous Na_2SO_4 and evaporated to dryness under reduced pressure. Crude product was purified by silica gel column using EtOAc/hexane (2:8) as eluent to obtain **5.97** (2.70 g) as crystalline white solid. Yield: 68%; m.p.: 98 °C; IR (KBr): ν (cm^{-1}) 3175, 1604; ^{1}H NMR (400 MHz, $CDCl_3$), δ (ppm): 9.34 (s, 1H), 9.20 (br s,1H), 4.05 (s, 3H), 3.84 (s, 3H); ^{13}C NMR (100 MHz, $CDCl_3$), δ (ppm): 174.96, 146.35, 140.65, 123.85, 73.06, 62.65, 61.30; HRMS (ESI+): m/z: Calcd for $C_7H_9INO_3$ ($M+H^+$): 281.9622; found: 281.9627.

3-chloro-4-dimethoxy-5-iodopyrrole-2-aldehyde (5.98): Same procedure was followed as described for **5.97**. 3 g (18.8 mmol) of 3-chloro-4-methoxypyrrole-2-aldehyde (**5.96**) was taken and crude product was purified by column chromatography using EtOAc/hexane (1:9) as eluent to yield **5.98** (4.89 g) as white crystalline solid. Yield: 91%; m.p.: 115 °C; IR (KBr): ν (cm^{-1}) 3189, 1647; ^{1}H NMR ($CDCl_3$, 400 MHz), δ (ppm): 9.78 (br s, 1H), 9.39 (s, 1H), 3.90

(s, 3H); ^{13}C NMR ($CDCl_3$, 100 MHz), δ (ppm): 175.96, 147.53, 129.96, 114.73, 70.99, 62.37; HRMS (ESI+): m/z: Calcd for $C_6H_6ClINO_2$ ($M+H^+$): 285.9126; found: 285.9135.

3,4-dimethoxy-5-bromopyrrole-2-aldehyde (5.101): To a stirred solution of 2-formyl-3,4-dimethoxypyrrole (**5.95**) (1 g, 6.44 mmol) in DCM, PIFA and TMSBr were quickly added at -78 °C. The reaction mixture was then stirred for 3 h, while the reaction temperature was maintained below -40 °C. After the reaction is completed, saturated aqueous sodium bicarbonate was added to the mixture, and then stirred for an additional 10 min. at ambient temperature. The organic layer was separated and the aqueous phase was extracted with DCM. The combined extract was dried with sodium sulphate and evaporated to dryness. The residue was purified by column chromatography using EtOAc/hexane (3:7) as eluent to provide product **5.101** (667 mg) as white crystalline solid. Yield: 44%; m.p.: 118 °C; IR (KBr): ν (cm^{-1}) 3160, 1640; ^{1}H NMR ($CDCl_3$, 400 MHz), δ (ppm): 9.77 (br s, 1H), 9.41 (s, 1H), 4.07 (s, 3H), 3.85 (s, 3H); ^{13}C NMR ($CDCl_3$, 100MHz), δ (ppm):174.97, 146.99, 135.58, 119.68, 103.99, 62.31, 61.09; HRMS (ESI+): m/z: calculated for $C_7H_9NO_3Br$ ($M+H^+$): 233.9760; found: 233.9767; Elemental analysis Calcd for $C_7H_8NO_3Br$: C, 35.92; H, 3.45; N, 5.98. Found: C, 35.87; H, 3.41; N, 6.12.

3-chloro-4-methoxy-5-bromopyrrole-2-aldehyde (5.102): Same procedure described for **5.101** was followed. 3-chloro-4-methoxypyrrole-2-aldehyde (**5.96**) (500mg, 3.13mmol) was used for reaction and product was purified by column chromatography using EtOAc/hexane (3:7) as eluent to obtain the product **5.101** (308 mg) as white crystalline solid. Yield: 41%; m. p.: 140 °C; IR (KBr): ν (cm^{-1}) 3200, 1651; ^{1}H NMR ($CDCl_3$, 400 MHz), δ (ppm): 9.52 (s, 1H), 9.40 (br s, 1H), 3.90 (s, 3H); ^{13}C NMR ($CDCl_3$, 100 MHz), δ (ppm): 176.29, 142.62, 125.97, 116.21, 103.07, 62.17; HRMS (ESI+): m/z: calculated for $C_6H_6NO_2BrCl$ ($M+H^+$): 237.9265; found: 237.9270; Elemental analysis Calcd for $C_6H_5NO_2BrCl$: C, 30.22; H, 2.11; N, 5.87. Found: C, 30.29; H, 2.18; N, 5.81.

3,3′,4,4′-tetramethoxy-2,2′-bipyrrole-5,5′-dialdehyde (5.99) by Pd-catalysed modified Ullmann coupling reaction : A mixture of 5% Pd-C (14 mg) and activated zinc dust (70 mg, 1.1 mg-atom) was placed under nitrogen. Then, 4 mL of toluene/water (1:1) was added and the mixture was stirred at room temperature under argon for 15 min. 3,4-dimethoxy-5-iodopyrrole-2-aldehyde **5.97** (100 mg, 0.36 mmol) in toluene (6 mL) was added through a syringe. Finally, distilled water (6 mL) was added and the mixture was stirred vigorously at room temperature under nitrogen for 24 h. The reaction was stopped by adding CH_2Cl_2 (40

mL) to the mixture and it was sonicated to form two layers. After the aqueous layer was removed, the remaining solution was filtered through Celite, which was washed three times with CH_2Cl_2. The organic solvents were collected and dried over anhydrous Na_2SO_4 and evaporated under reduced pressure. The pure target compound was separated using a silica gel column eluted with EtOAc/ hexane (3:7) as brown crystalline solid **5.99** (8 mg), along with 3,4-dimethoxypyrrole-2-aldehyde **5.95** (42 mg). Yield: 14%; m.p.: 195-196 °C; IR (KBr): ν (cm^{-1}) 3441, 1621; ^{1}H NMR (400 MHz, $CDCl_3$), δ (ppm): 9.62 (s, 2H), 9.10 (br s, 2H), 4.06 (s, 6H), 4.00 (s, 6H); ^{13}C NMR (100 MHz, $CDCl_3$), δ (ppm): 175.61, 145.85, 134.84, 119.26, 118.26, 62.59, 61.37; UV-Vis data, λ_{max} nm (log ε): 400 (4.60); Fluorescence data (λ_{max} nm): 440; ϕ_f : 0.67; HRMS (ESI+): m/z: calculated for $C_{14}H_{17}N_2O_6$ ($M+H^+$): 309.1087; found: 309.1086.

N,N′-dibenzyl-3,3′,4,4′-tetramethoxy-2,2′-bipyrrole (5.104): To a stirred solution of N-benzyl-3,4-dimethoxypyrrole (**5.103)** (4 g, 18.4 mmol) in CH_2Cl_2 (200 mL), PIFA (3.96 g, 9.2 mmol) and TMSBr (2.42 mL, 18.4 mmol) were quickly added at –78 °C under nitrogen. The reaction mixture was stirred for 3 h, while the temperature was maintained below –45 °C. Subsequently, the reaction was quenched with saturated aqueous $NaHCO_3$ (ca. 200 mL), and then stirred for an additional 10 min at ambient temperature. The organic layer was separated and the aqueous phase was extracted with CH_2Cl_2 .The combined extract was dried with Na_2SO_4 and evaporated to dryness and the crude reaction mixture was purified by silica gel column using EtOAc/hexane (1:9) as eluent to obtain **5.104** (2.83 g) as white crystalline solid. Yield: 71%; m.p.: 95 – 96 °C; ^{1}H NMR (400 MHz, $CDCl_3$), δ (ppm): 7.22 - 7.20 (m, 6H), 6.95 - 6.93 (m, 4H), 4.58 (q, 4H, *J* = 13.3), 3.70 (s, 6H), 3.67 (s, 6H); ^{13}C NMR (100 MHz, $CDCl_3$), δ (ppm): 139.43, 138.33, 135.15, 128.44, 127.68, 127.31, 109.38, 102.54, 60.73, 58.16, 50.71; HRMS (ESI+): m/z: calculated for $C_{26}H_{29}N_2O_4$ ($M+H^+$): 433.2122; found: 433.2127.

3,3′,4,4′-tetramethoxy-2,2′-bipyrrole-5,5′-dialdehyde (5.99): To a stirred solution of 3,4-dimethoxypyrrole **5.106** (2 g, 15.7 mmol) in CH_2Cl_2 (200 mL), PIFA (3.38 g, 7.87 mmol) and TMSBr (2.08 mL, 15.7 mmol) were quickly added at –78 °C under nitrogen. The reaction mixture was stirred for 3 h, while the temperature was maintained below –45 °C. After the completion of the reaction, saturated aqueous $NaHCO_3$ (ca. 150 mL) was added to the mixture, and then stirred for an additional 10 min at ambient temperature. The organic layer was separated and the aqueous phase was extracted with CH_2Cl_2 as quickly as possible

(Because color of the reaction mixture changes from colorless to green to black tar under ambient condition). The combined extract was dried with Na_2SO_4 and evaporated to dryness and the crude reaction mixture was used immediately for formylation without further purification. Crude reaction mixture dissolved in DCE (70 mL), was rapidly added to ice cooled stirred Vilsmeier-Haack formylating mixture prepared from $POCl_3$ (7.3 mL, 78.6 mmol) and DMF (6.7 mL, 86.5 mmol) in DCE (70 mL) under nitrogen atmosphere. After addition was over ice-bath was replaced with oil bath and the reaction mixture was refluxed for 2 h and then cooled on ice bath and Na_2CO_3 (41.7 g, 0.39 mol) in water (200 mL) added carefully and refluxed for additional 2 h. After cooling the reaction mixture to room temperature, organic layer was separated and water layer was extracted with DCM for three times. Combined organic layer was passed through anhydrous Na_2SO_4 and evaporated to dryness, resulting in black solid. Crude reaction mixture was purified by silica gel column chromatography using EtOAc/Hexane (3:7) as eluent to obtain compound **5.99** (951 mg) as brown crystalline needles. Yield: 39%.

2,3,6,7,12,13,16,17-octamethoxyporphycene (5.92): To a slurry of low-valent titanium reagent, generated by reduction of titanium tetrachloride (2.67 mL, 24.32 mmol) in dry THF (180 mL) with activated zinc (3.18 g) and CuCl (481mg, 4.86 mmol) by refluxing for 2 h, a solution of **5.99** (300 mg, 0.97 mmol) in dry THF (120 mL) was added dropwise slowly over 2 h under refluxing condition with vigorous stirring. The reaction mixture was heated under reflux for an additional 1 h and then hydrolyzed by slow addition of 10% aqueous sodium carbonate (ca. 100 mL) to the ice cooled reaction mixture and filtered through celite to remove the excess metal, washed with diethyl ether and organic layer was separated. Organic layer was evaporated to dryness under reduce pressure. Resulting crude reaction mixture was dissolved in DCM (50 mL), washed with water, and the organic layer was passed through anhydrous sodium sulphate and evaporated to dryness under reduce pressure. The crude reaction mixture was purified by silica gel column chromatography using EtOAc/hexane (3:7) as eluent to yield the desired porphycene **5.92** as blue purple crystalline solid (37 mg). Yield: 14%; m.p.: 297-298 °C; ^{1}H NMR (400 MHz, $CDCl_3$), δ (ppm): 9.66 (s, 4H), 4.77 (s, 12H), 4.64 (s, 12H), 0.36 (s, 2H); ^{13}C NMR (100 MHz, $CDCl_3$), δ (ppm): 146.86, 143.32, 134.66, 126.77, 108.48, 64.33, 62.42; UV-Vis data in $CHCl_3$, λ_{max} nm (log ε): 382 (5.09), 557 (4.40), 599 (4.24), 636 (4.34); Fluorescence in $CHCl_3$, (λ_{exc} 382 nm) nm: 651; HRMS (ESI+): m/z: calculated for $C_{28}H_{31}N_4O_8$ ($M+H^+$): 551.2142; found: 551.2142.

2,3,6,7,12,13,16,17-octamethoxyporphycenato zinc(II) (Zn(5.92)): To a stirred solution of **5.92** (10 mg, 0.018 mmol) in chloroform (10 mL) under nitrogen, $Zn(OAc)_2.2H_2O$ (40 mg, 0.18 mmol) was added and reaction mixture was refluxed for 4 h. The reaction mixture was evaporated to dryness, re-dissolved in chloroform, washed with water and evaporated under reduced pressure. Crude product was finally purified by activated neutral alumina column using chloroform as eluent to obtain **Zn(5.92)** (7 mg) as purple solid. Yield: 63%; m.p.: >300 °C; ^{1}H NMR (400 MHz, $CDCl_3$), δ (ppm): 9.65 (s, 4H), 4.76 (s, 12H), 4.64 (s, 12H); ^{13}C NMR (125MHz, $CDCl_3$), δ (ppm): 146.83, 143.32, 134.65, 126.75, 108.47, 64.31, 62.43; UV-Vis data in $CHCl_3$, λ_{max} nm (log ε): 390 (5.08), 618 (4.75); Fluorescence in $CHCl_3$, (λ_{exc} 382 nm) nm: 631, 686; ϕ_f: 0.025; HRMS (ESI+): m/z: calculated for $C_{28}H_{29}N_4O_8Zn$ ($M+H^+$): 613.2177; found: 613.2176.

2,3,6,7,12,13,16,17-octamethoxyporphycenato nickel(II) (Ni(5.92)): To a stirred solution of **5.92** (10 mg, 0.018 mmol), $Ni(acac)_2$ (93 mg, 0.36mmol) in *o*-xylene was added and refluxed for 4 h. After reaction mixture was cooled to room temperature, *o*-xylene was evaporated under reduced pressure and crude compound was purified by silica gel column chromatography using chloroform as eluent to obtain **Ni(5.92)** (9 mg) as purple crystalline solid. Yield: 82%; m.p.: >300 °C; ^{1}H NMR (400 MHz, $CDCl_3$), δ (ppm): 9.42 (s, 4H), 4.70 (s, 12H), 4.58 (s, 12H); ^{13}C NMR (125 MHz, $CDCl_3$), δ (ppm): 147.41, 140.39, 138.14, 135.52, 105.01, 64.02, 62.47; UV-Vis data in $CHCl_3$, λ_{max} nm (log ε): 388 (5.05), 596 (4.52); HRMS (ESI+): m/z: calculated for $C_{28}H_{29}N_4O_8Ni$ ($M+H^+$): 607.1339; found: 607.1331.

2,3,6,7,12,13,16,17-octamethoxyporphycenato palladium(II) (Pd(5.92)): To a stirred solution of **5.92** (25 mg, 0.045 mmol), $Pd(OAC)_2$ (101 mg, 0.45 mmol) in AcOH (20 mL) was added and refluxed for 7 h. After reaction was over, solvent was evaporated under reduced pressure and purified by silica gel column using chloroform as eluent to obtain **Pd(5.92)** (24 mg) as purple solid. Yield: 81%; m.p.: >300 °C; ^{1}H NMR (400 MHz, $CDCl_3$), δ (ppm): 9.58 (s, 4H), 4.77 (s, 12H), 4.67 (s, 12H); ^{13}C NMR (125 MHz, $CDCl_3$), δ (ppm): 147.36, 140.26, 137.41, 136.13, 104.27, 64.16, 62.53; UV-Vis data in $CHCl_3$, λ_{max} nm (log ε): 390 (4.84), 590 (4.48); HRMS (ESI+): m/z: calcd for $C_{28}H_{29}N_4O_8Pd$ ($M+H^+$): 655.1020; found: 655.1047.

2,3,6,7,12,13,16,17-octaethylporphycenato palladium(II) (Pd(5.42)): To a stirred solution of **5.42** (10 mg, 0.019 mmol) and $Pd(OAC)_2$ (43 mg, 0.19 mmol) in glacial acetic acid (10 mL) was refluxed for 7 h. After reaction was over, solvent was evaporated under reduce

pressure and purified by silica gel column using chloroform/hexane (1:1) as eluent to obtain **Pd(5.42)** (10 mg) as purple solid. Yield: 83%; m.p.: 293 - 294 °C; ^{1}H NMR (400 MHz, $CDCl_3$), δ (ppm): 9.66 (s, 4H), 4.05 (q, 4H, J = 7.6 Hz), 3.99 (q, 4H, *J* = 7.6 Hz), 1.85 (t, 12H, *J* = 7.4 Hz), 1.77 (t, 12H, *J* = 7.4 Hz); ^{13}C NMR (100 MHz, $CDCl_3$), δ (ppm): 146.75, 144.06, 143.89, 136.01, 106.34, 20.94, 20.11, 18.83, 18.51; UV-Vis data, λ_{max} nm (log ε): 310 (3.93), 390 (4.99), 566 (4.09), 603 (4.61), 618 (4.61); HRMS (ESI+): m/z: calcd for $C_{36}H_{45}N_4Pd$ ($M+H^+$): 639.2674; found: 639.2679.

3-Chloro-4-methoxypyrrole-2-nitrile (5.107): 3-Chloro-4-methoxypyrrole-2-aldehyde (**5.96**) (3 g, 18.81 mmol) and triethylamine (7.9 mL, 56.40 mmol) were taken in dry DCE (150 mL) under nitrogen atmosphere. Hydroxylamine hydrochloride (1.57 g, 22.57 mmol) was added to the reaction mixture and stirred at 60 °C for 2 h. Then, phthalic anhydride (5.57 g, 37.62 mmol) was added in small portion wise and the reaction mixture was stirred at reflux condition for 24 h and allowed to reach to room temperature and washed twice with saturated aqueous $NaHCO_3$ to remove phthalic acid. Aqueous layer was extracted three times with DCM (~150 ml × 3), combined organic layer was passed through anhydrous Na_2SO_4 and evaporated under reduced pressure to dryness. Crude product was washed with DCM, filtered, washed with DCM until filtrate become colorless leaving the entitled product **5.107** as white crystalline solid. Additional amount of compound obtained by purifying filtrate by silica gel column chromatography using EtOAc/hexane (3:7) as eluent (2.46 g, combined yield). Yield: 84%; m.p.: 209.8 °C; IR (neat): ν (cm^{-1}) 3299, 3122, 2217; ^{1}H NMR (400 MHz, DMSO-d_6), δ (ppm): 12.27 (br s, 1H), 7.00 (s, 1H), 3.71 (s, 3H); ^{13}C NMR (100 MHz, DMSO-d_6), δ (ppm): 143.67, 112.64, 108.47, 108.00, 96.57, 58.48; HRMS (ESI+): m/z: calculated for $C_6H_6N_2OCl$ ($M+H^+$): 157.0163; found: 157.0177; Elemental analysis Calcd for $C_5H_5N_2OCl$: C, 46.03; H, 3.22; N, 17.89. Found: C, 46.12; H, 3.28; N, 17.81.

3-Chloro-5-formyl-4-methoxypyrrole-2-nitrile (5.108): 3-Chloro-4-methoxypyrrole-2-nitrile (**5.107**) (2 g, 12.77 mmol) was taken in DCE (140 mL) and DMF (9 mL) was added under nitrogen atmosphere and reaction mixture was allowed to reflux to dissolve **5.107** completely. Under reflux condition $POCl_3$ (3.6 mL, 38.31 mmol) was added dropwise and stirred under reflux condition for 1 h. Then reaction mixture was cooled on ice bath and NaOAc (15.71 g, 0.19 mole) in water (100 mL) added carefully and the reaction mixture was refluxed for additional 2 h. After cooling to room temperature organic layer was separated and water layer was extracted with DCM for three times. Combined organic layer was washed with aqueous $NaHCO_3$ solution. Then, organic layer was passed through anhydrous

Na_2SO_4 and evaporated to dryness. Crude reaction mixture was purified by silica gel column chromatography using EtOAc/Hexane (2:8) as eluent to obtain compound **5.108** (1.73 g) as white crystalline solid. Yield: 73%; m.p.: 138.6 °C; IR (neat): ν (cm^{-1}) 3221, 2232, 1628; ^{1}H NMR (400 MHz, $CDCl_3$), δ (ppm): 10.62 (br s, 1H), 9.75 (s, 1H), 4.14 (s, 3H); ^{13}C NMR (100 MHz, $CDCl_3$), δ (ppm): 177.81, 150.03, 123.37, 112.85, 110.52, 106.35, 62.33; HRMS (ESI+): m/z: calculated for $C_7H_6N_2O_2Cl$ ($M+H^+$): 185.0112; found: 185.0109; Elemental analysis Calcd for $C_7H_5N_2O_2Cl$: C, 45.55; H, 2.73; N, 15.18. Found: C, 45.63; H, 2.71; N, 15.07.

4-Chloro-5-formyl-3-methoxypyrrole-2-carboxylic acid (5.109): 3-Chloro-5-formyl-4-methoxypyrrole-2-nitrile (**5.108**) (2 g, 10.84 mmol) and NaOH (4.33 g, 0.108 mole) were taken in H_2O (60 mL) and the reaction mixture was refluxed for 48 h. After completion of hydrolysis, reaction mixture was placed on an ice bath and acidified with conc. HCl to pH 1 to result precipitation of the desired compound as white solid. Precipitate was filtered, washed with ice water and dried under vacuum to find the entitled compound (**5.109).4H_2O** (2.47 g) as white powdery solid. Yield: 83%; m.p.: 226.2 °C (dec); IR (neat): ν (cm^{-1}) 2948, 1718, 1688, 1643, 1614; ^{1}H NMR (400 MHz, DMSO-d_6), δ (ppm): 13.56 (br, s, 1H), 12.76 (br s, 1H), 9.69 (s, 3H), 3.93 (s, 3H); ^{13}C NMR (100 MHz, DMSO-d_6), δ (ppm): 179.26, 160.07, 148.01, 122.28, 121.82, 108.03, 62.23; HRMS (ESI+): m/z: calculated for $C_7H_7NO_4Cl$ ($M+H^+$): 204.0058; found: 204.0067; Elemental analysis Calcd for $C_7H_6NO_4Cl.4H_2O$: C, 30.50; H, 5.12; N, 5.08. Found: C, 30.68; H, 5.03; N, 5.16.

4-Chloro-5-iodo-3-methoxypyrrole-2-aldehyde (5.110): Sodium bicarbonate (835 mg, 9.94 mmol) in water (15 mL) was added to 4-chloro-5-formyl-3-methoxypyrrole-2-carboxylic acid (**5.109**) (830 mg, 3.01 mmol) at room temperature under nitrogen atmosphere. After **5.109** was dissolved completely, DCE (40 mL) was added to the reaction mixture and temperature raised to 80 °C. Then, iodine (802 mg, 3.16 mmol) and KI (1.05 g, 6.32 mmol) dissolved in water (40 mL) was added dropwise over 30 min and allowed to stir for additional 1 h at same temperature. The reaction mixture was cooled to room temperature and excess sodium thiosulphate was added in small portions to remove excess iodine and stirred for 10 min. The reaction mixture was taken in a separatory funnel and organic layer was collected. Organic layer was passed through anhydrous Na_2SO_4 and evaporated to dryness under reduced pressure. Crude reaction mixture was purified by silica gel column chromatography using EtOAc/hexane (2:8) as eluent to provide entitled **5.110** (750 mg) as white crystalline solid. Yield: 87%; m.p.: 128.6 °C; IR (neat): ν (cm^{-1}) 3381, 3221, 1616; ^{1}H NMR (400 MHz,

$CDCl_3$), δ (ppm): 9.87 (br s, 1H), 9.42 (s, 1H), 4.09 (s, 3H); ^{13}C NMR (100 MHz, $CDCl_3$), δ (ppm): 175.19, 151.07, 125.28, 111.89, 81.00, 62.29; HRMS (ESI+): m/z: calculated for $C_6H_5NO_2ClNa$ ($M+Na^+$): 307.8946; found: 307.8944; Elemental analysis Calcd for $C_6H_5NO_2ClI$: C, 25.24; H, 1.77; N, 4.91. Found: C, 25.36; H, 1.71; N, 4.98.

4-Chloro-3-methoxypyrrole-2-aldehyde (5.111): Activated Zinc (1.20 g), 4-chloro-5-iodo-3-methoxypyrrole-2-aldehyde (**5.110**) (1.75g, 6.13 mmol) and 5% Pd/C (490 mg) were taken in acetone/water (140/140 mL) under nitrogen atmosphere and reaction mixture was allowed to stir vigorously at room temperature for 18 h. The reaction mixture was quenched with DCM (~150 mL), organic layer was separated and aqueous layer washed with DCM (~50 mL) for three times. Combined organic layer was passed through celite and washed with DCM for three times. Organic layer was passed through anhydrous Na_2SO_4 and evaporated to dryness under reduced pressure. Crude reaction mixture was purified by silica gel column chromatography using EtOAc/hexane (3:7) as eluent to obtain the product **5.111** (879 mg) as white crystalline solid. Yield: 90%; m.p.: 133.4 °C; IR (neat): ν (cm^{-1}) 3077, 1621; ^1H NMR (400 MHz, $CDCl_3$), δ (ppm): 9.62 (s, 1H), 9.39 (br s, 1H), 6.95 (d, 1H, *J* = 3.6 Hz), 4.09 (s, 3H); ^{13}C NMR (100 MHz, $CDCl_3$), δ (ppm): 176.63, 151.69, 123.54, 120.83, 104.46, 62.25; HRMS (ESI+): m/z: calculated for $C_6H_5NO_2Cl$ ($M+H^+$): 160.0160; found: 160.0160; Elemental analysis Calcd for $C_6H_6NO_2Cl$: C, 45.16; H, 3.79; N, 8.78. Found: C, 45.23; H, 3.84; N, 8.65.

General procedure for synthesis of ethyl 3-(3,4-disubstituted-pyrrol-2-yl)-2-cyanoacrylate (5.112-5.113): 3-Chloro-4-methoxypyrrole-2-aldehyde (**5.96**) (2 g, 25.06 mmol) was taken in toluene (60 mL) under nitrogen. Subsequently, ethyl-2-cyanoacetate (2.9 mL, 27.57 mmol) and triethylamine (3.5 mL, 25.06 mmol) were added and allowed the reaction mixture to stir at reflux condition for 4 h. The reaction mixture was allowed to cool to room temperature and kept at -20 °C for 2 h to result the precipitation of compound as yellow fibrous solid. The reaction mixture was filtered and washed with cold hexane, leaving the entitled compound **5.112** (3 g) as yellow fibrous solid.

Ethyl 3-(3-chloro-4-methoxypyrrol-2-yl)-2-cyanoacrylate (5.112): Yield: 94%; m.p.: 181.1 °C; IR (neat): ν (cm^{-1}) 3391, 2215, 1694; ^1H NMR (400 MHz, $CDCl_3$), δ (ppm): 9.47 (br s, 1H), 8.07 (s, 1H), 6.81 (d, 1H, *J* = 3.6 Hz), 4.35 (d, 2H, *J* = 7.2 Hz), 3.85 (s, 3H), 1.38 (t, 3H, *J* = 6.8 Hz); ^{13}C NMR (100 MHz, $CDCl_3$), δ (ppm): 162.97, 146.52, 138.40, 121.39, 118.60, 113.19, 110.84, 93.22, 62.40, 58.90, 14.36; HRMS (ESI+): m/z: calculated for

$C_{11}H_{11}N_2O_3ClNa$ ($M+Na^+$): 277.0350; found: 277.0354; Elemental analysis Calcd for $C_{11}H_{11}N_2O_3Cl$: C, 51.88; H, 4.35; N, 11.00. Found: C, 51.76; H, 4.43; N, 10.85.

Ethyl 3-(4-chloro-3-methoxypyrrol-2-yl)-2-cyanoacrylate (5.113): 4-Chloro-3-methoxypyrrole-2-carbaldehyde (**5.111**) (850 mg, 5.33 mmol) was taken for reaction. After reaction was over, it was allowed to come to room temperature and kept at -20 °C for 2 h to result the precipitation of compound. The reaction mixture was filtered and washed with cold hexane to leave the entitled compound **5.113** as reddish yellow solid. Filtrate was evaporated under reduced pressure and washed with methanol to result another crop of compound and finally methanol washed part was purified by silica gel column chromatography by using EtOAc/hexane (2:8) as eluent to obtain **5.113** as yellow crystalline solid. Combined yield: 1.32 g (97%); m.p.: 154.2 °C; IR (neat): ν (cm^{-1}) 3358, 2215, 1693; ^1H NMR (400 MHz, $CDCl_3$), δ (ppm): 9.46 (br s, 1H), 8.04 (s, 1H), 7.05 (d, 1H, *J* = 3.6 Hz), 4.33 (d, 2H, *J* = 6.8 Hz), 4.07 (s, 3H), 1.37 (t, 3H, *J* = 7.2 Hz); ^{13}C NMR (100 MHz, $CDCl_3$), δ (ppm): 163.46, 151.61, 137.71, 125.46, 119.05, 116.52, 105.37, 90.38, 62.16, 61.93, 14.41; HRMS (ESI+): m/z: calculated for $C_{11}H_{11}N_2O_3ClNa$ ($M+Na^+$): 277.0350; found: 277.0348. Elemental analysis Calcd for $C_{11}H_{11}N_2O_3Cl$: C, 51.88; H, 4.35; N, 11.00. Found: C, 51.76; H, 4.28; N, 11.07.

General procedure for synthesis of 3,3'-disubsituted-4,4'-disubstituted-[2,2'-bipyrrole]-5,5'-dialdehyde (5.100 and 5.114): Ethyl 3-(3-chloro-4-methoxypyrrol-2-yl)-2-cyanoacrylate (**5.112**) (500 mg, 1.96 mmol) and $FeCl_3$ (954 mg, 5.88 mmol) were taken in trifluoroacetic acid (TFA) (15 mL) and stirred at room temperature for 24 h. The reaction mixture was evaporated under reduced pressure, residue was dissolved in acetone and passed through anhydrous K_2CO_3 and followed by washing with acetone and chloroform, until color of solution becomes colorless. Combined organic layer was evaporated under reduced pressure and subjected to silica gel column chromatography using $CHCl_3$ as eluent. The orange fluorescent fraction was collected and evaporated to obtain the oxidatively coupled product as purple crystalline solid. This compound was used directly for hydrolysis without further characterization. Compound obtained in the previous step was subjected to hydrolysis with aqueous 3M NaOH (6 mL) under reflux condition for 3 h. The reaction mixture was placed on ice bath, diluted with water (~50 mL) and neutralized with conc. HCl to result in precipitation of compound as bright golden yellow fibrous solid. Precipitated compound was filtered, washed with water and subjected to silica gel column chromatography using

EtOAc/hexane (2:8) as eluent to obtain the desired dialdehyde **5.100** (122 mg) as golden yellow fibrous solid.

4,4'-dichloro-3,3'-dimethoxy-[2,2'-bipyrrole]-5,5'-dialdehyde (5.100): Yield: 122 mg (39%); m.p.: 233.4 °C; IR (neat): ν (cm^{-1}) 3277, 1655; ^{1}H NMR (400 MHz, $CDCl_3$), δ (ppm): 9.64 (s, 2H), 9.51 (br s, 2H), 4.11 (s, 6H); ^{13}C NMR (100 MHz, $CDCl_3$), δ(ppm): 176.55, 141.49, 125.11, 117.72, 113.71, 61.68; UV-Vis data in $CHCl_3$, λ_{max} nm (log ε): 397 (4.57); Fluorescence in $CHCl_3$ λ_{max} nm : 450; Fluorescence quantum yield in $CHCl_3$ (ϕ_f): 0.77; HRMS (ESI+): m/z: calculated for $C_{12}H_{11}N_2O_4Cl_2$ ($M+H^+$): 317.0090; found: 317.0098.

3,3'-dichloro-4,4'-dimethoxy-[2,2'-bipyrrole]-5,5'-dialdehyde (5.114): Ethyl 3-(4-chloro-3-methoxypyrrol-2-yl)-2-cyanoacrylate (**5.113**) (500 mg, 1.96 mmol) was taken for reaction and purified by silica gel column chromatography using EtOAc/hexane (3:7) as eluent to obtain **5.114** (48 mg) as light yellow solid. Yield: 15%; m.p.: 259.3 °C; IR (neat): ν (cm^{-1}) 3193, 1655; ^{1}H NMR (400 MHz, DMSO-d_6), δ (ppm): 12.30 (br s, 2H), 9.68 (s, 2H), 4.04 (s, 6H); ^{13}C NMR (100 MHz, $CDCl_3$), δ (ppm): 176.97, 149.94, 123.14, 121.08, 103.75, 62.40; UV-Vis data in $CHCl_3$, λ_{max} nm (log ε): 365 (4.56), 384 (4.57); Fluorescence in $CHCl_3$ λ_{max} nm: 402, 422; Fluorescence quantum yield in $CHCl_3$ (ϕ_f): 0.08; HRMS (ESI+): m/z: calculated for $C_{12}H_{11}N_2O_4Cl_2$ ($M+H^+$): 317.0090; found: 317.0063; Elemental analysis Calcd for $C_{12}H_{10}N_2O_4Cl_2$: C, 45.45; H, 3.18; N, 8.83. Found: C, 45.38; H, 3.26; N, 8.72.

General procedure for synthesis of β-tetrachlorotetramethoxyporphycenes (5.93-94): To a slurry of low-valent titanium reagent, generated by reduction of titanium tetrachloride (1.73 mL, 15.75 mmol) in dry THF (100 mL) with activated zinc (2.06 g) and CuCl (481mg, 4.86 mmol) by refluxing for 3 h, a solution of **5.100** (200 mg, 0.63 mmol) in dry THF (100 mL) was added dropwise slowly over 3 h under reflux condition with vigorous stirring. The reaction mixture was heated under reflux for an additional 1 h and then hydrolyzed by slow addition of 10% aqueous sodium carbonate (ca. 100 mL) to the ice cooled reaction mixture. The reaction mixture was filtered through celite to remove the excess metal, washed with $CHCl_3$ until color of the filtrate become colorless and organic layer was separated. Organic layer was passed through anhydrous sodium sulphate and evaporated to dryness under reduce pressure. The crude reaction mixture was purified by silica gel column chromatography using $CHCl_3$ as eluent to yield the desired porphycenes **5.93** as blue purple crystalline solid (51 mg).

2,7,12,17-tetrachloro-3,6,13,16-tetramethoxyporphycene (5.93): Yield: 28%; m.p.: >300 °C; ^{1}H NMR (500 MHz, $CDCl_3$), δ (ppm): 9.80 (s, 4H), 4.78 (s, 12H), 0.98 (br s, 2H); UV-Vis data in $CHCl_3$, λ_{max} nm (log ε): 376 (5.16), 384 (5.14), 565 (4.58), 608 (4.35), 647 (4.52); Fluorescence in $CHCl_3$ in nm, (λ_{exc} 382 nm): 655, 717; Fluorescence quantum yield in $CHCl_3$ (ϕ_f): 0.00071; HRMS (ESI+): m/z: calculated for $C_{24}H_{19}N_4O_4Cl_4$ ($M+H^+$): 567.0155; found: 567.0165.

3,6,13,16-tetrachloro-2,7,12,17-tetramethoxyporphycene (5.94): 3,3'-dichloro-4,4'-dimethoxy-[2,2'-bipyrrole]-5,5'-dialdehyde (**5.114**) (60 mg, 0.19 mmol) and THF (50 mL + 50 mL) were taken and **5.114** in THF (50 mL) was added dropwise over 3 h. Yield: 12 mg (22%); m.p.: >300 °C; ^{1}H NMR (400 MHz, $CDCl_3$), δ (ppm): 9.65 (s, 4H), 4.82 (s, 12H), 0.16 (br s, 2H); UV-Vis data in $CHCl_3$, λ_{max} nm (log ε): 385 (5.13), 572 (4.52), 625 (4.31), 664 (4.46); Fluorescence in $CHCl_3$ nm, (λ_{exc} 572 nm): 676; Fluorescence quantum yield in $CHCl_3$ (ϕ_f): 0.00075; HRMS (ESI+): m/z: calculated for $C_{24}H_{19}N_4O_4Cl_4$ ($M+H^+$): 567.0155; found: 567.0160; Elemental analysis Calcd for $C_{24}H_{18}N_4O_4Cl_4$: C, 50.73; H, 3.19; N, 9.86. Found: C, 50.65; H, 3.26; N, 9.78.

General procedure for synthesis of β-tetrachlorotetramethoxyporphycenato zinc(II) complexes (Zn(5.93)-(5.94)): 2,7,12,17-Tetrachloro-3,6,13,16-tetramethoxyporphycene (**5.93**) (10 mg, 0.018 mmol) and $Zn(OAc)_2.2H_2O$ (77 mg, 0.35 mmol) were taken in mixture of $CHCl_3$/MeOH (1:1, 40 mL) under nitrogen. The reaction mixture was refluxed for 4 h and solvent was evaporated under reduced pressure. Residue was purified by activated neutral alumina column chromatography using $CHCl_3$/MeOH (49:1) as eluent to provide **Zn(5.93)** (4 mg) as blue purple solid.

2,7,12,17-tetrachloro-3,6,13,16-tetramethoxyporphycenato zinc(II) (Zn(5.93)): Yield: 35%; m.p.: >300 °C; ^{1}H NMR (400 MHz, $CDCl_3$ in presence of small amount of CD_3OD), δ (ppm): 9.84 (s, 4H), 4.79 (s, 12H); UV-Vis data, λ_{max} nm (log ε): 391 (5.24), 588 (4.33), 638 (4.90); Fluorescence in $CHCl_3$ in nm, (λ_{exc} 390 nm): 645, 706; Fluorescence quantum yield in $CHCl_3$ (ϕ_f): 0.17; HRMS (ESI+): m/z: calculated for $C_{24}H_{17}N_4O_4Cl_4Zn$ ($M+H^+$): 628.9290; found: 628.9299.

3,6,13,16-tetrachloro-2,7,12,17-tetramethoxyporphycenato zinc(II) (Zn(5.94)): 5 mg of **5.94** was taken for reaction. After reaction was over, solvent was evaporated under reduced pressure. Residue was dissolved in $CHCl_3$, washed with water and chloroform layer was

passed through anhydrous Na_2SO_4. Solvent was evaporated under reduced pressure to obtain **Zn(5.94)** (5.2 mg) as purple solid. Yield: 93%; m.p.: > 300 °C; ^{1}H NMR (400 MHz, $CDCl_3$ in presence of small amount of CD_3OD), δ (ppm): 9.73 (s, 4H), 4.77 (s, 12H); UV-Vis data in $CHCl_3$, λ_{max} nm (log ε): 391(4.90), 604 (4.14), 638 (4.61); Fluorescence in $CHCl_3$ in nm, (λ_{exc} 390 nm): 654, 711; Fluorescence quantum yield in $CHCl_3$ (ϕ_f): 0.16; HRMS (ESI+): m/z: calculated for $C_{24}H_{16}N_4O_4Cl_4ZnNa$ ($M+Na^+$): 650.9109; found: 650.9115; Elemental analysis Calcd for $C_{24}H_{16}N_4O_4Cl_4Zn$: C, 45.64; H, 2.55; N, 8.87. Found: C, 45.58; H, 2.61; N, 8.76.

General procedure for synthesis of β-tetrachlorotetramethoxyporphycenato palladium(II) complexes (Pd(5.93-94)): 2,7,12,17-Tetrachloro-3,6,13,16-tetramethoxyporphycene (**5.93**) (10 mg, 0.018 mmol) and $Pd(OAc)_2$ (40 mg, 0.18 mmol) were taken in equimolar mixture of AcOH/DCE (40 mL) and stirred under reflux condition for 4 h. The solvent was evaporated under reduced pressure and residue was washed with diethyl ether to remove unreacted $Pd(OAc)_2$. Then, residue was dissolved in $CHCl_3$ under reflux condition, filtered and washed repeatedly with hot $CHCl_3$ until color of the filtrate became colorless. Combined solvent was evaporated under reduce pressure to obtain the desired compound **Pd(5.93)** (10.1 mg) as purple solid.

2,7,12,17-tetrachloro-3,6,13,16-tetramethoxyporphycenato palladium(II) (Pd(5.93)): Yield: 83%; m.p.: > 300 °C; UV-Vis data in $CHCl_3$, λ_{max} nm (log ε): 389 (4.94), 561 (4.14), 606 (4.70); HRMS (ESI+): m/z: calculated for $C_{24}H_{16}N_4O_4Cl_4PdNa$ ($M+Na^+$): 692.8853; found: 692.8853.

3,6,13,16-tetrachloro-2,7,12,17-tetramethoxyporphycenato palladium(II) (Pd(5.94)): 4 mg of **5.94** was used for reaction. Yield: 4.4 mg (93%); m.p.: > 300 °C; UV-Vis data in $CHCl_3$, λ_{max} nm (log ε): 391 (4.93), 603 (4.64), 624 (4.55); LCMS (ESI-): m/z: calculated for $C_{24}H_{17}N_4O_4Cl_4Pd$ (M-H): 671; found: 671; Elemental analysis Calcd for $C_{24}H_{16}N_4O_4Cl_4Pd$: C, 42.85; H, 2.40; N, 8.33. Found: C, 42.68; H, 2.32; N, 8.41.

4.6 Crystallographic Details

Crystallographic data for **5.92, 5.99, 5.100**, **5.108, 5.111** and **Zn(5.92)** were collected on BRUKER SMART-APEX CCD diffractometer. Mo−Kα (λ = 0.71073 Å) radiation was used to collect X-ray reflections on the single crystal. Crystallographic data for **5.104**, **Pd(5.92)** and **Zn(5.93).Py** were collected on Oxford Gemini A Ultra diffractometer with dual source. Mo-Kα (λ = 0.71073 Å) radiation was used to collect the X-ray reflections of the crystal.

Crystallographic data for **5.93**, **5.94**, and **Zn(5.94).Py** were also collected on Oxford Gemini A Ultra diffractometer where Cu-Kα (λ = 1.54184 Å) radiation was used to collect the X-ray reflections of the crystal.

Pertinent crystallographic data collection and refinement parameter are shown in the following tables:

Crystal Data	**5.99**	**5.100**	**5.108**	**5.111**
CCDC No.	950091			
Formula unit	$C_{14}H_{16}N_2O_6$	$C_{12}H_{10}N_2O_4Cl_2$	$C_7H_5N_2O_2Cl$	$C_6H_6NO_2Cl$
Formula Weight	308.29	317.12	184.58	159.57
Crystal system	Triclinic	Monoclinic	Triclinic	Monoclinic
T [K]	298(2)	298(2)	298(2)	298(2)
a [Å]	4.379(4)	4.859(8)	6.037(2)	12.132(3)
b [Å]	8.588(8)	20.457(4)	8.101(3)	6.7332(17)
c [Å]	9.945(9)	14.700(3)	9.222(3)	8.752(2)
α [°]	77.220(14)	90.00	70.622(5)	90.00
β [°]	82.897(15)	97.600(3)	74.480(5)	91.331(4)
γ [°]	85.329(14)	90.00	85.612(5)	90.00
volume [$Å^3$]	361.4(5)	1337.2(4)	409.9(3)	714.8(3)
Space group	P 21/c	P 21/n	P-1	P 21/c
Z´	0.5	1	1	1
Z	2	4	2	4
D_{calc} [$g.cm^{-3}$]	1.417	1.575	1.495	1.483
μ/mm^{-1}	0.112	0.499	0.422	0.467
Reflns collected	3963	13757	4234	7062
Unique reflns	1666	2644	1612	1422
Obs. reflns	1141	2587	1553	1359
R(int)	0.0375	0.0582	0.0244	0.0334
R_1 [$I > 2\sigma(I)$],	0.0759(1141)	0.1507(2587)	0.0714(1553)	0.0520(1359)
wR_2	0.1914(1666)	0.2669(2644)	0.1610(1612)	0.1286(1442)
GOF	1.121	1.507	1.367	1.233

Crystal Data	5.92	Zn(5.92)	Pd(5.92)	5.104
CCDC No.	950087	950088	950089	950090
Formula unit	$C_{28}H_{30}N_4O_9$	$C_{28}H_{28}N_4O_8Zn$	$C_{28}H_{28}N_4O_8Pd$	$C_{26}H_{28}N_2O_4$
Formula Weight	566.56	613.91	654.94	432.50
Crystal system	Orthorhombic	Orthorhombic	Orthorhombic	Monoclinic
T [K]	298(2)	298(2)	293(2)	293(2)
a [Å]	13.867(2)	11.6106(9)	14.1047(6)	12.3046(7)
b [Å]	12.856(2)	9.0413(7)	12.6047(5)	10.5352(6)
c [Å]	15.535(2)	24.953(2)	15.5260(7)	18.0332(14)
α [°]	90.00	90.00	90.00	90.00
β [°]	90.00	90.00	90.00	90.359(5)
γ [°]	90.00	90.00	90.00	90.00
volume [$Å^3$]	2769.6(7)	2619.4(4)	2760.3(2)	2337.6(3)
Space group	Pbca	Pbca	Pbca	P 21/n
Z′	0.5	0.5	0.5	1
Z	4	4	4	4
D_{calc} [$g.cm^{-3}$]	1.359	1.557	1.576	1.229
μ/mm^{-1}	0.103	0.998	0.730	0.083
Reflns collected	26946	23410	11683	10552
Unique reflns	2724	2323	2720	5336
Obs. reflns	1501	2267	1515	2018
R(int)	0.0730	0.0419	0.0429	0.0462
R_1 [$I > 2\sigma(I)$],	0.0881(1501)	0.1037(2267)	0.0354(1515)	0.0648(2018)
wR_2	0.3191(2724)	0.1953(2323)	0.1086(2720)	0.1498(5336)
GOF	1.049	1.367	0.914	0.963

Crystal Data	5.93	5.94	Zn(5.93).Py	Zn(5.94).Py
CCDC No.				
Formula unit	$C_{24}H_{18}N_4O_4Cl_4$	$C_{24}H_{18}N_4O_4Cl_4$	$C_{29}H_{21}N_5O_4Cl_4Zn$	$C_{29}H_{21}N_5O_4Cl_4Zn$
Formula Weight	568.22	568.22	710.68	710.68
Crystal system	Monoclinic	Monoclinic	Monoclinic	Monoclinic
T [K]	293(2)	293(2)	293(2)	293(2)
a [Å]	3.9469(2)	4.1263(3)	14.0391(19)	10.7037(5)
b [Å]	27.0301(15)	23.8718(19)	14.1663(13)	17.9473(9)
c [Å]	10.9065(5)	11.9867(6)	15.990(2)	15.8353(7)
α [°]	90.00	90.00	90.00	90.00
β [°]	98.544(5)	98.803(5)	113.950(16)	106.927(5)
γ [°]	90.00	90.00	90.00	90.00
volume [$Å^3$]	1150.65(11)	1161.18(17)	2906.2(6)	2910.2(2)
Space group	P 21/c	P 21/c	P 21/c	P 21/c
Z´	0.5	0.5	1	1
Z	2	2	4	4
D_{calc} [$g.cm^{-3}$]	1.640	1.617	1.624	1.622
μ/mm^{-1}	5.047	4.977	1.259	4.941
Reflns collected	3733	4043	10492	11867
Unique reflns	1961	2190	4964	5521
Obs. reflns	1455	1355	2576	3903
R(int)	0.0523	0.0365	0.0851	0.0355
R_1 [$I > 2\sigma(I)$],	0.0744(1455)	0.0781(1355)	0.0672(2576)	0.0535(3903)
wR_2	0.2799(1961)	0.2632(4043)	0.1038(4964)	0.1617(5521)
GOF	1.132	1.104	0.949	1.024

4.7 References

1. Vogel, E.; Kocher, M.; Schmickler, H.; Lex, J. *Angew. Chem., Int. Ed. Engl*. **1986**, *25*, 257.
2. Gosmann, M.; Franck, B. *Angew. Chem. Int. Ed. Engl*. **1986**, *25*, 1100.
3. (a) Sessler, J. L.; Gebauer, A.; Vogel, E. *Porphyrin Handb*. **2000**, *2*, 1. (b) Sánchez-García, D.; Sessler, J. L. *Chem. Soc. Rev*. **2008**, *37*, 215.

4. Stockert, J. C.; Cañete, M.; Juarranz, A.; Villanueva, A.; Horobin, R. W.; Borrell, J. I.; Teixidó, J.; Nonell, S. *Curr. Med. Chem*. **2007**, *14*, 997.
5. Vogel, E.; Köcher, M.; Lex, J.; Ermer, O. *Isr. J. Chem*. **1989**, *29*, 257.
6. (a) Hayashi, T.; Okazaki, K.; Urakawa, N.; Shimakoshi, H.; Sessler, J. L.; Vogel, E.; Hisaeda, Y. *Organometallics* **2001**, *20*, 3074. (b) Lo, W.-C.; Che, C.-M.; Cheng, K.-F.; Mak, T. C. W. *Chem. Commun*. **1997**, 1205.
7. (a) Barbe, J.-M.; Richard, P.; Aukauloo, M. A.; Lecomte, C.; Petit, P.; Guilard, R. *J. Chem. Soc., Chem. Commun*. **1994**, 2757. (b) Brenner, W.; Malig, J.; Costa, R. D.; Guldi, D. M.; Jux, N. *Adv. Mater*. **2013**, *25*, 2314. (c) Costa, R. D.; Malig, J.; Brenner, W.; Jux, N.; Guldi, D. M. *Adv. Mater*. **2013**, *25*, 2600.
8. (a) Matsuo, T.; Dejima, H.; Hirota, S.; Murata, D.; Sato, H.; Ikegami, T.; Hori, H.; Hisaeda, Y.; Hayashi, T. *J. Am. Chem. Soc*. **2004**, *126*, 16007. (b) Hayashi, T.; Murata, D.; Makino, M.; Sugimoto, H.; Matsuo, T.; Sato, H.; Shiro, Y.; Hisaeda, Y. *Inorg. Chem*. **2006**, *45*, 10530.
9. (a) Sarma, T.; Panda, P. K.; Anusha, P. T.; Rao, S. V. *Org. Lett*. **2011**, *13*, 188. (b) Rao, S. V.; Prashant, T. S.; Swain, D.; Sarma, T.; Panda, P. K.; Tewari, S. P. *Chem. Phys. Lett*. **2011**, *514*, 98. (c) Arnbjerg, J.; Jiménez-Benzo, A.; Paterson, M. J.; Nonell, S.; Borell, J. I.; Christiansen, O.; Ogilby, P. R. *J. Am. Chem. Soc*. **2007**, *129*, 5188. (d) Kim, K. K.; Sung, Y. M.; Matsuo, T.; Hayashi, T.; Kim, D. *Chem. –Eur. J*. **2011**, *17*, 7882.
10. (a) Feihl, S.; Costa, R. D.; Brenner, W.; Margraf, J. T.; Casillas, R.; Langmar, O.; Browa, A.; Shubina, T. E.; Clark, T.; Jux, N.; Guldi, D. M. *Chem. Commun*. **2014**, *50*, 11339. (b) Saeki, H.; Kurimoto, O.; Nakaoka, H.; Misaki, M.; Kuzuhara, D.; Yamada, H.; Ishida, K.; Ueda, Y. *J. Mater. Chem. C* **2014**, *2*, 5357.
11. (a) Berman, A.; Michaeli, A.; Feitelson, J.; Bowman, M. K.; Norris, J. R.; Levanon, H.; Vogel, E.; Koch, P. *J. Phys. Chem.* **1992**, *96*, 3041. (b) Gil, M.; Dobkowski, J.; Wiosna-Sałyga, G.; Urbańska, N.; Fita, P.; Radzewicz, C.; Pietraszkiewicz, M.; Borowicz, P.; Marks, D.; Glasbeek, M.; Waluk, J. *J. Am. Chem. Soc.* **2010**, *132*, 13472. (c) Fita, P.; Radzewicz, C.; Waluk, J. *J. Phys. Chem. A* **2008**, *112*, 10753. (d) Piwoński, H.; Sokołowski, A.; Kijak, M.; Nonell, S.; Waluk, J. *J. Phys. Chem. Lett.* **2013**, *4*, 3967. (e) Ciąćka, P.; Listkowski, A.; Kijak, M.; Nonell, S.; Kuzuhara, D.; Yamada, H.; Radzewicz, C.; Waluk, J. *J. Phys. Chem. B* **2015**, *119*, 2292.
12. Kumagai, T.; Hanke, F.; Gawinkowski, S.; Sharp, J.; Kotsis, K.; Waluk, J.; Persson, M.; Grill, L. *Nature Chem.* **2014**, *6*, 41.

13. Anju, K. S.; Ramakrishnan, S.; Thomas, A. P.; Suresh, E.; Srinivasan, A. *Org. Lett*. **2008**, *10*, 5545.
14. Ganapathi, E.; Chatterjee, T.; Ravikanth, M. *Eur. J. Org. Chem*. **2014**, 6701.
15. Fanta, P. E. *Chem. Rev*. **1964**, *64*, 613.
16. Sessler, J. L.; Hoehner, M. C. *Synlett* **1994**, 211.
17. Nonell, S.; Bou, N.; Borrell, J.; Teixidó, J.; Villanueva, A.; Juarranz, A.; Cañete, M. *Tetrahedron Lett.* **1995**, *36*, 3405.
18. Gavalda, A.; Borrell, J. I.; Teixidó, J.; Nonell, S.; Arad, O.; Grau, R.; Cañete, M.; Juarranz, A.; Villanueva, A.; Stockert, J. C. *J. Porphyrins Phthalocyanines* **2001**, *5*, 846.
19. Arad, O.; Morros, J.; Batllori, X.; Teixidó, J.; Nonell, S.; Borrell, J. I. *Org. Lett.* **2006**, *8*, 847.
20. Sánchez-García, D.; Borrell, J. I.; Nonell, S. *Org. Lett.* **2009**, *11*, 77.
21. (a) Jiao, L.; Hao, E.; Vincente, G. H.; Smith, K. M. *J. Org. Chem*. **2007**, *72*, 8119. (b) Jiao, L.; Hao, E.; Fronczek, F. R.; Vicente, M. G. H.; Smith, K. M. *J. Porphyrins Phthalocyanines* **2011**, *15*, 433.
22. Vogel, E.; Balci, M.; Pramod, K.; Koch, P.; Lex, J.; Ermer, O. *Angew. Chem. Int. Ed. Engl*. **1987**, *26*, 928.
23. Vogel, E.; Koch, P.; Hou, X.-L.; Lex, J.; Lausmann, M.; Kisters, M.; Aukauloo, M. A.; Richard, P.; Guilard, R. *Angew. Chem. Int. Ed. Engl*. **1993**, *32*, 1600.
24. Hayashi, T.; Nakashima, Y.; Ito, K.; Ikegami, T.; Aritome, I.; Suzuki, A.; Hisaeda, Y. *Org. Lett*. **2003**, *5*, 2845.
25. Matsuo, T.; Ito, K.; Kanehisa, N.; Hayashi, T. *Org. Lett*. **2007**, *9*, 5303.
26. Kuzuhara, D.; Yamada, H.; Yano, K.; Okujima, T.; Mori, S.; Uno, H. *Chem. –Eur. J*. **2011**, *17*, 3376.
27. Vogel, E.; Sicken, M.; Röhrig, P.; Schmickler, H.; Lex, J.; Ermer, O. *Angew. Chem. Int. Ed. Engl*. **1988**, *27*, 411.
28. Cöln, D. Ph. D. Dissertation, University of Cologne, Federal Republic of Germany, **1991**.
29. Munno, G. D.; Lucchesini, F.; Neidlein, R. *Tetrahedron* **1993**, *49*, 6863.
30. Ellinger, F.; Gieren, A.; Hübner, T.; Lex, J.; Lucchesini, F.; Merz, A.; Neidlein, R.; Salbeck, J. *Monatsh. Chem*. **1993**, *124*, 931.
31. Hu, Z.; Atwood, J. L.; Cava, M. P. *J. Org. Chem*. **1994**, *59*, 8071.
32. Dai, W.-M.; Mak, W. L. *Tetrahedron Lett*. **2000**, *41*, 10277.

33. Nüssbaumer, T.; Krieger, C.; Neidlein, R. *Eur. J. Org. Chem.* **2000**, *13*, 2449.
34. Nüssbaumer, T.; Neidlein, R. *Helv. Chim. Acta* **2000**, *83*, 1161.
35. (a) Sargent, A. L.; Hawkins, I. C.; Allen, W. E.; Liu, H.; Sessler, J. L.; Fowler, C. J. *Chem. Eur. J.* **2003**, *9*, 3065. (b) Nonell, S.; Borrell, J. I.; Borrós, S.; Colominas, C.; Rey, O.; Rubio, N.; Sánchez-García, D.; Teixidó, J. *Eur. J. Org. Chem*. **2003**, *9*, 1635.
36. Vogel, E. *Pure Appl. Chem.* **1993**, *65*, 143.
37. Kuzuhara, D.; Mack, J.; Yamada, H.; Okujima, T.; Ono, N.; Kobayashi, N. *Chem.-Eur. J.* **2009**, *15*, 10060.
38. Kuzuhara, D.; Yamada, H.; Mori, S.; Okujima, T.; Uno, H. *J. Porphyrins Phthalocyanines* **2011**, *15*, 930.
39. Dietrich, H.-J. *PhD Thesis*, University of Cologne, **1994**.
40. Roznyatovskiy, V.; Lynch, V.; Sessler, J. L. *Org. Lett*. **2010**, *12*, 4424.
41. Vogel, E.; Köcher, M.; Balci, M.; Teichler, I.; Lex, J.; Schmickler, H.; Ermer, O. *Angew. Che. Int. Ed. Engl*. **1987**, *26*, 931.
42. Vogel, E.; Grigat, I.; Köcher, M.; Lex, J. *Angew. Chem. Int. Ed. Engl*. **1989**, *28*, 1655.
43. (a) Will, S.; Rahbar, A.; Schmickler, H.; Lex, J.; Vogel, E. *Angew. Chem., Int. Ed. Engl.* **1990**, *29*, 1390. (b) Aritome, I.; Shimakoshi, H.; Hisaeda, Y. *Acta Crystallogr., Sect. C: Cryst. Struct. Commun.* **2002**, *58*, o563. c) Vogel, E.; Koch, P. A.; Rahbar, A.; Cross, A. D. *US Pat.* 5 244 671, **1993**.
44. Baba, T.; Shimakoshi, H.; Hisaeda, Y. *Tetrahedron Lett*. **2004**, *45*, 5973.
45. Mak, N.-K.; Kok, T.-W.; Wong, R. N.-S.; Lam, S.-W.; Lau, Y.-K.; Leung, W.-N.; Cheung, N.-H.; Huang, D. P.; Yeung, L.-L.; Chang, C. K. *J. Biomed. Sci*. **2003**, *10*, 418.
46. (a) Vogel, E.; Mueller, M.; Halpern, O.; Cross, A. D. *US Pat.* 5 637 608, **1997**. (b) Porter, H. K. *Org. React*. **1973**, *20*, 455.
47. Vogel, E.; Richert, C.; Benninghaus, T.; Muller, M.; Cross, A. D. *US Pat.* 5 179 120, **1993**.
48. Richert, C.; Wessels, J. M.; Müller, M.; Kisters, M.; Benninghaus, T.; Goetz, A. E. *J. Med. Chem.* **1994**, *37*, 2797.
49. Pandey, R. K. *J. Porphyrins Phthalocyanines* **2000**, *4*, 368.
50. (a) Cañete, M.; Ortiz, A.; Juarranz, A.; Villanueva, A.; Nonell, S.; Borrell, J. I.; Teixidó, J.; Stockert, J. C. *Anti-Cancer Drug Des*. **2000**, *15*, 143. (b) Cañete, M.; Ortega, C.; Gavaldá, A.; Cristóbal, J.; Juarranz, A.; Nonell, S.; Teixidó, J.; Borrell, J. I.; Villanueva, A.; Rello, S.; Stockert, J. C. *Int. J. Oncol*. **2004**, *24*, 1221.

51. (a) Sternberg, E. D.; Dolphin, D.; Brückner, C. *Tetrahedron*, **1998**, *54*, 4151. (b) Karrer, S.; Abels, C.; Szeimies, R. M.; Bäumler, W.; Hohenleutner, U.; Goetz, A. E.; Landthaler, M. *Proc. SPIE*, **1995**, *2625*, 278.
52. Ragàs, X.; Sánchez-García, D.; Ruiz-González, R.; Dai, T.; Agut, M.; Hamblin, M. R.; Nonell, S. *J. Med. Chem.* **2010**, *53*, 7796.
53. García-Díaz, M.; Sánchez-García, D.; Soriano, J.; Sagristà, M. L.; Mora, M.; Villanueva, Á.; Stockert, J. C.; Cañate, M.; Nonell, S. *Med. Chem. Commun*. **2011**, *2*, 616.
54. Rana, A.; Panda, P. K. *Org. Lett*. **2014**, *16*, 78.
55. Rana, A.; Panda, P. K. *Tetrahedron Lett*. **2011**, *52*, 2697.
56. Dohi, T.; Morimoto, K.; Maruyama, A.; Kita, Y. *Org. Lett*. **2006**, *8*, 2007.
57. (a) Merz, A.; Scropp, R.; Dotterl, E. *Synthesis* **1995**, 795. (b) Merz, A.; Meyer, T. *Synthesis* **1999**, 94.
58. Mazat, C.; Gade, L. H. *Chem. –Eur. J*. **2002**, *8*, 4308.
59. Paine III, J. B.; Dolphin, D. *J. Org. chem*. **1988**, *53*, 2787.
60. Falk, H.; Flödl, H. *Monatsh. Chem*. **1988**, *119*, 247.
61. Grzybowski, M.; Skonieczny, K.; Butenschön, H.; Gryko, D. T. *Angew. Chem. Int. Ed*. **2013**, *52*, 9900.
62. Berman, A.; Michaeli, A.; Feitelson, J.; Bowman, M. K.; Norris, J. R.; Levanon, H.; Vogel, E.; Koch, P. *J. Phys. Chem*. **1992**, *96*, 3041.
63. Gisselbrecht, J. P.; Gross, M.; Köcher, M.; Lausmann, M.; Vogel, E. *J. Am. Chem. Soc*. **1990**, *112*, 8618.
64. (a) Shimakoshi, H.; Baba, T.; Iseki, Y.; Aritome, I.; Endo, A.; Adachi, C.; Hisaeda, Y. *Chem. Commun*. **2008**, 2882. (b) Shao, W.; Wang, H.; He, S.; Shi, L.; Peng, K.; Lin, Y.; Zhang, L.; Ji, L.; Liu, H. *J. Phys. Chem. B* **2012**, *116*, 14228. (c) Rubio, N.; Prat, F.; Bou, N.; Borrell, J. I.; Teixidó, J.; Vollanueva, Á.; Juarranz, Á.; Cañete, M.; Stockert, J. C.; Nonell, S. *New J. Chem*. **2005**, *29*, 378.
65. Levanon, H.; Toporowicz, M.; Ofir, H.; Fessenden, R. W.; Das, P. K.; Vogel, E.; Köcher, M.; Promod, K. *J. Phys. Chem*. **1988**, *92*, 2429.
66. Ethirajan, M.; Chen, Y.; Joshi, P.; Pandey, R. K. *Chem. Soc. Rev*. **2011**, *40*, 340.

4.8 Representative NMR spectra

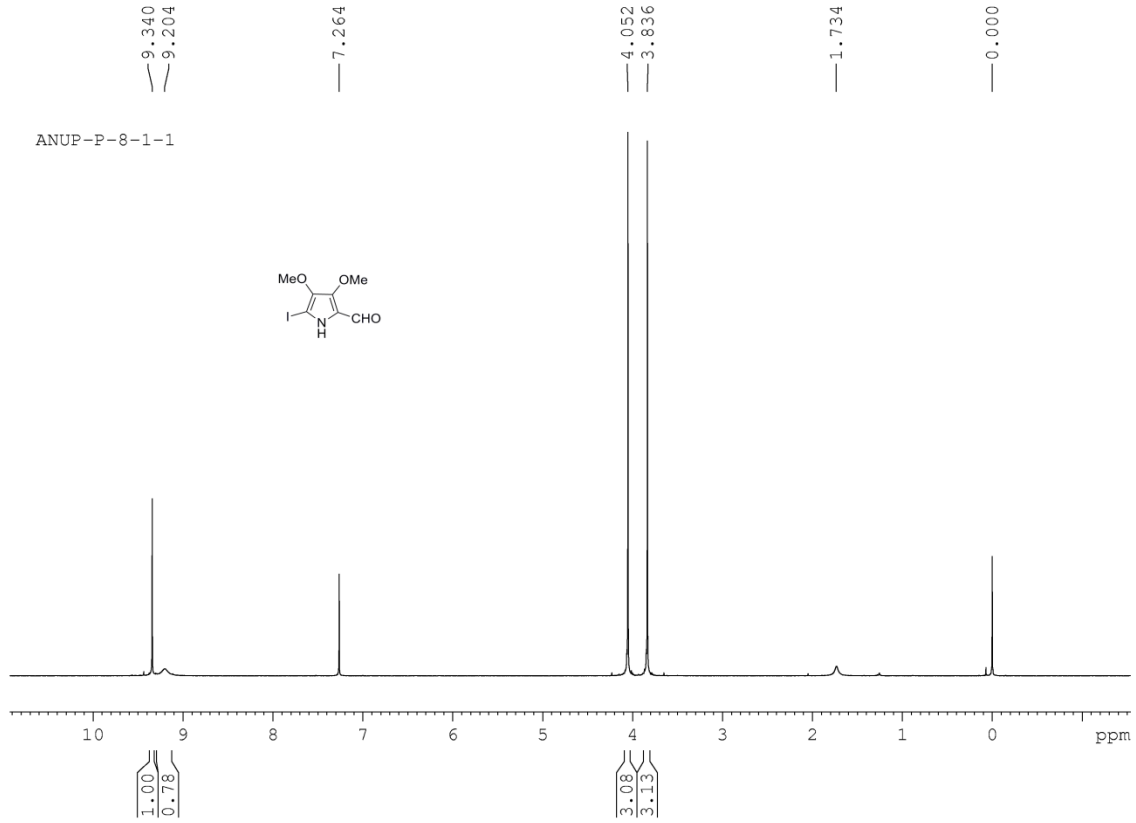

Figure 5.11 ^{1}H NMR spectrum of **5.97** in $CDCl_3$.

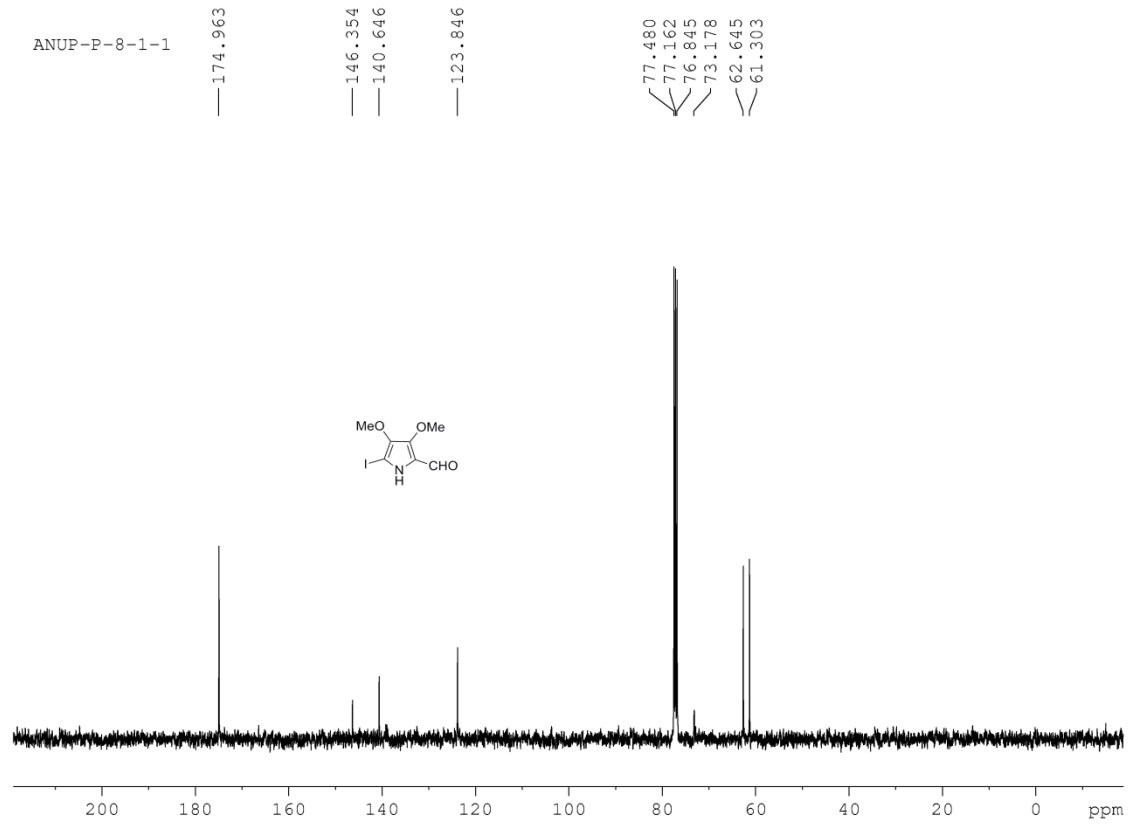

Figure 5.12 ^{13}C NMR spectrum of **5.97** in $CDCl_3$.

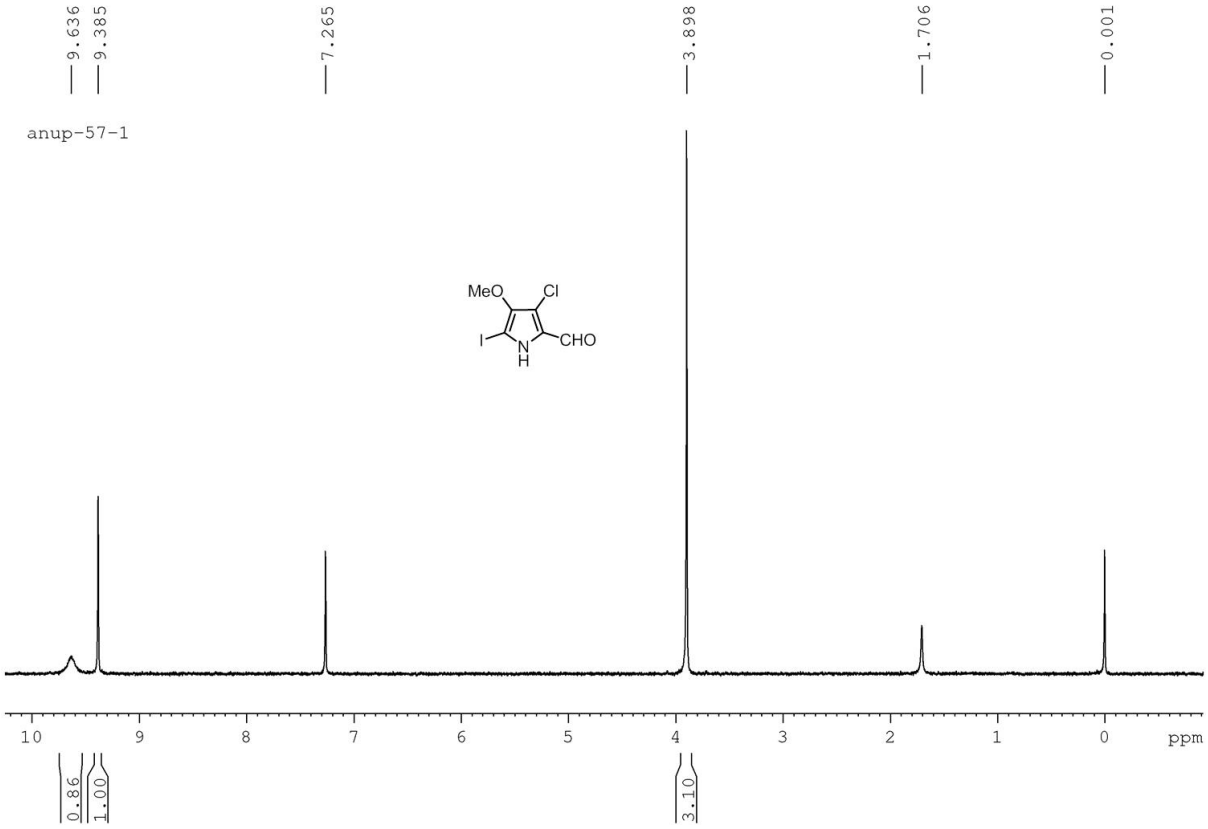

Figure 5.13 ^{1}H NMR spectrum of **5.98** in $CDCl_3$.

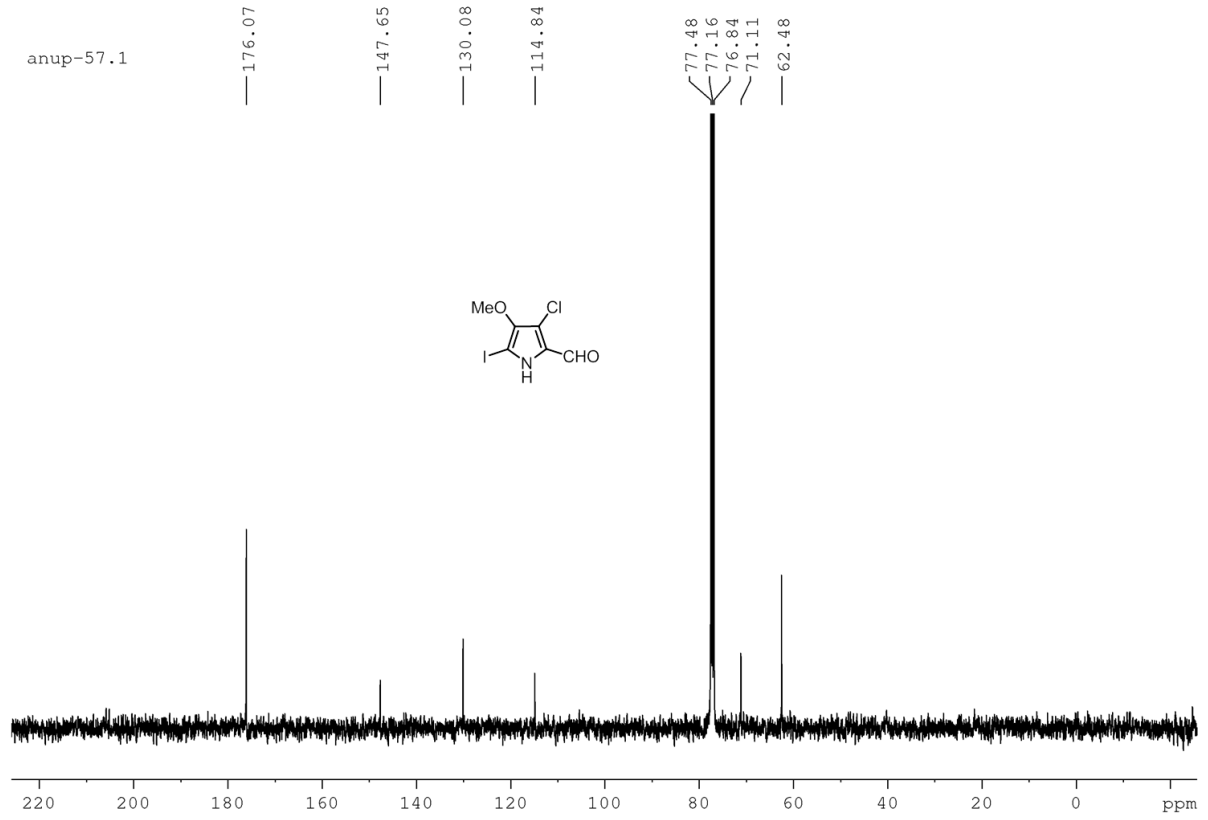

Figure 5.14 ^{13}C NMR spectrum of **5.98** in $CDCl_3$.

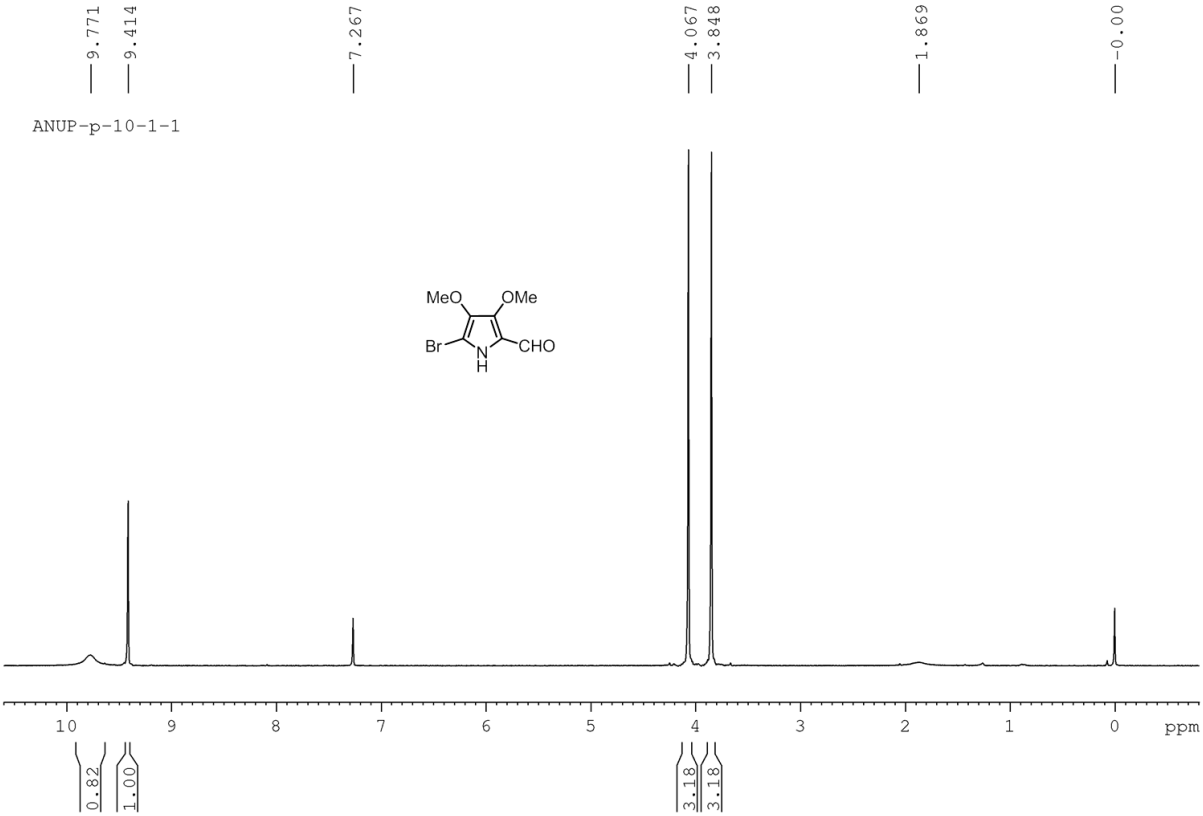

Figure 5.15 ^{1}H NMR spectrum of **5.101** in $CDCl_3$.

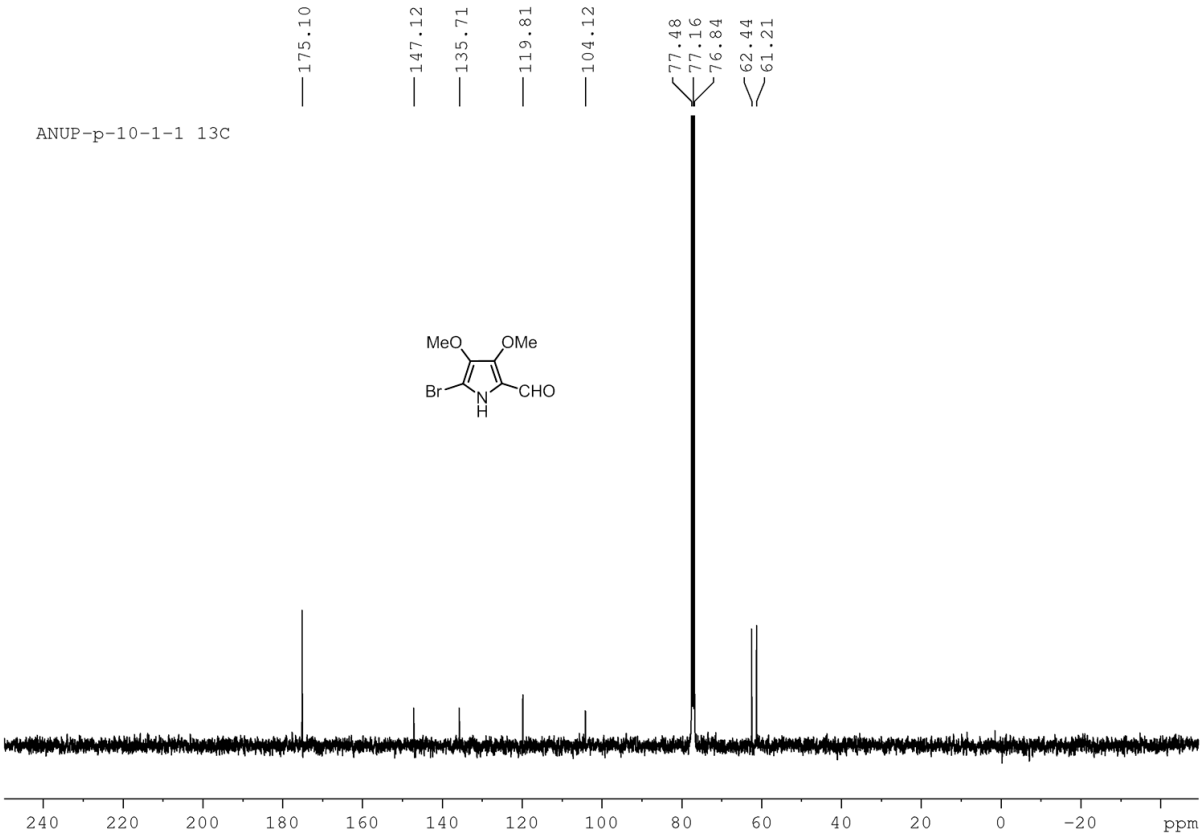

Figure 5.16 ^{13}C NMR spectrum of **5.101** in $CDCl_3$.

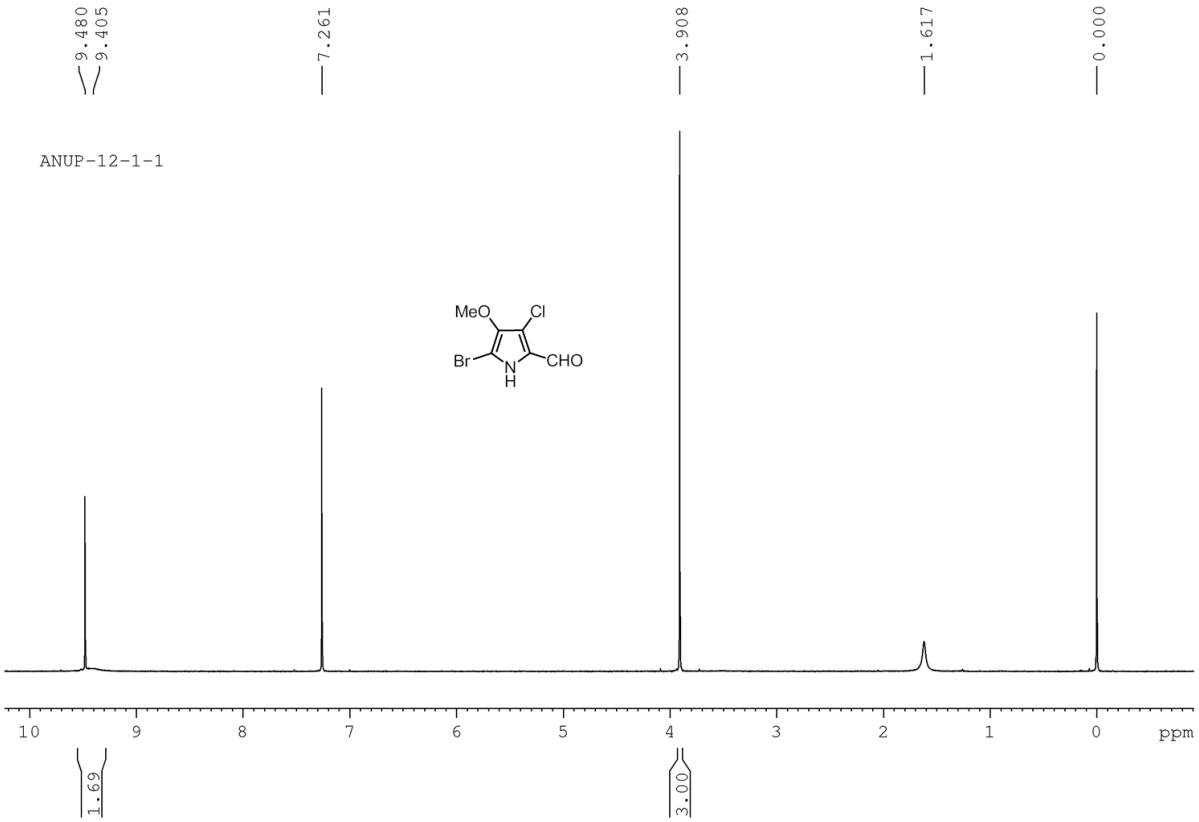

Figure 5.17 ^{1}H NMR spectrum of **5.102** in $CDCl_3$.

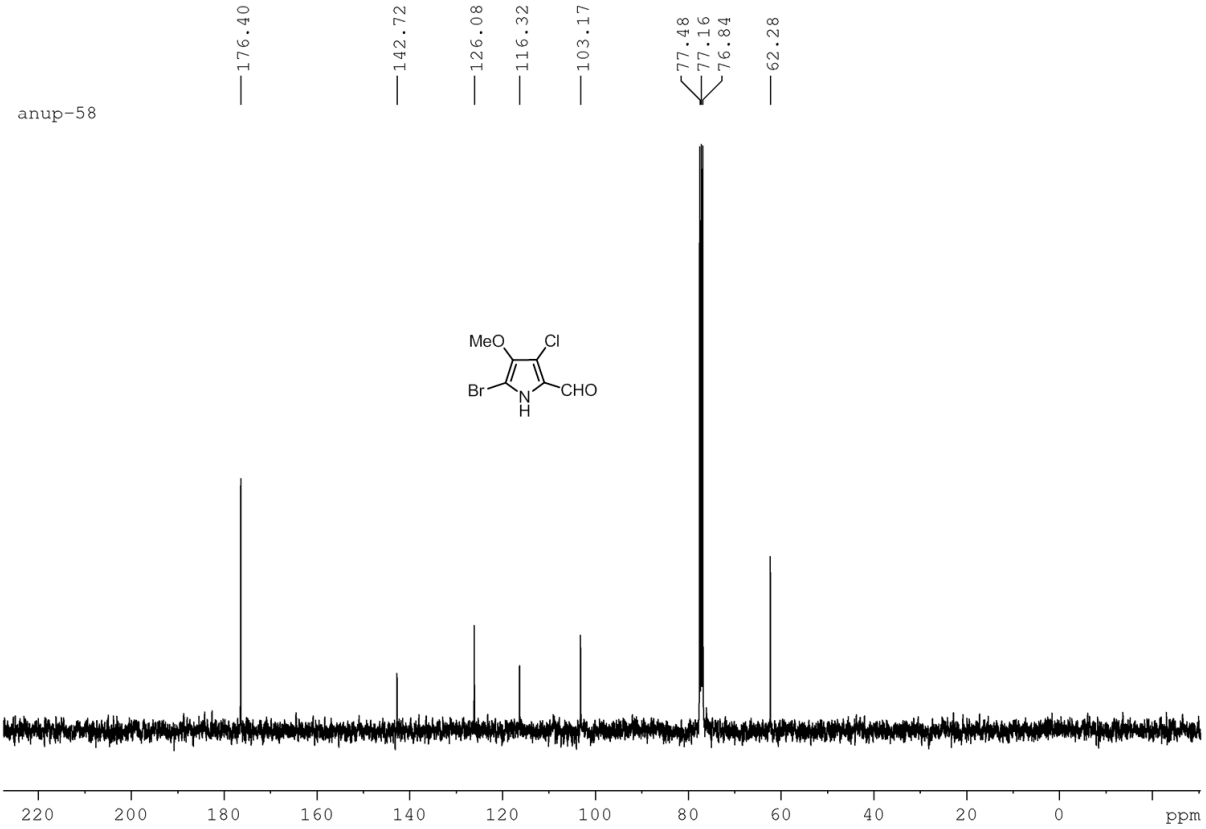

Figure 5.18 ^{13}C NMR spectrum of **5.102** in $CDCl_3$.

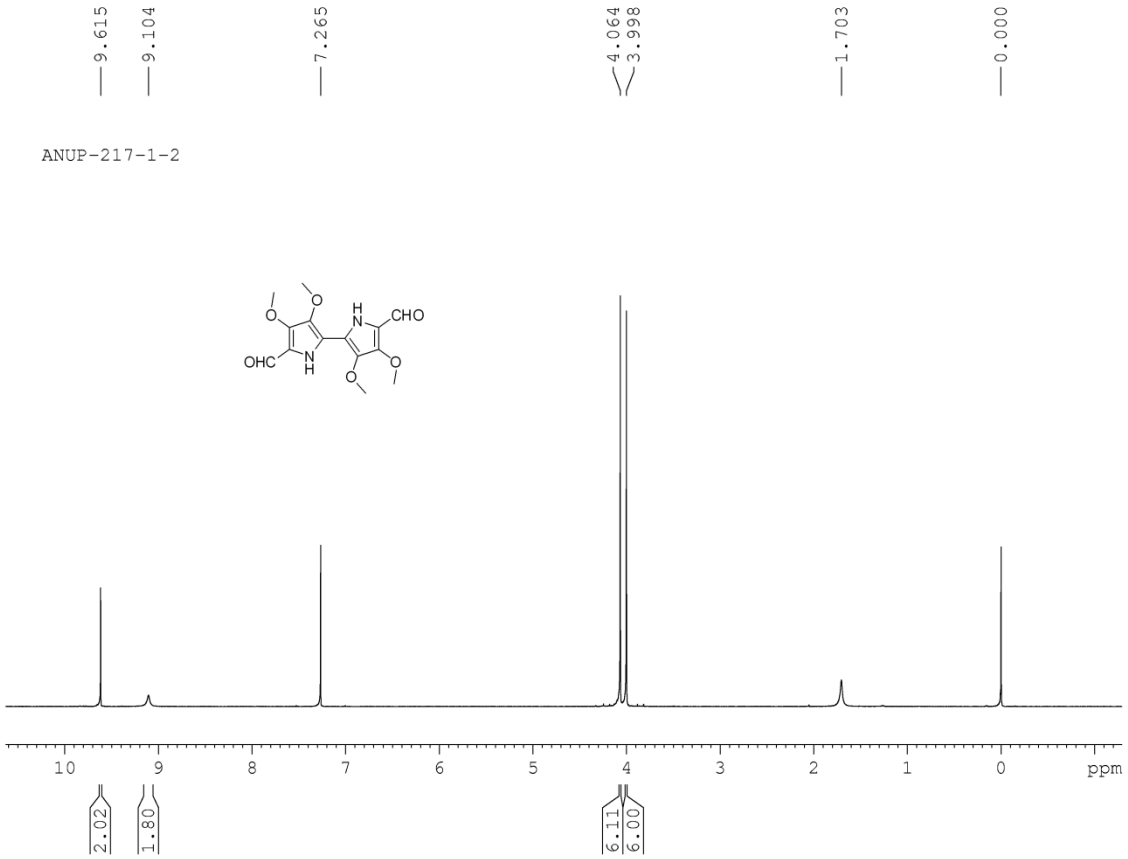

Figure 5.19 ^{1}H NMR spectrum of **5.99** in $CDCl_3$.

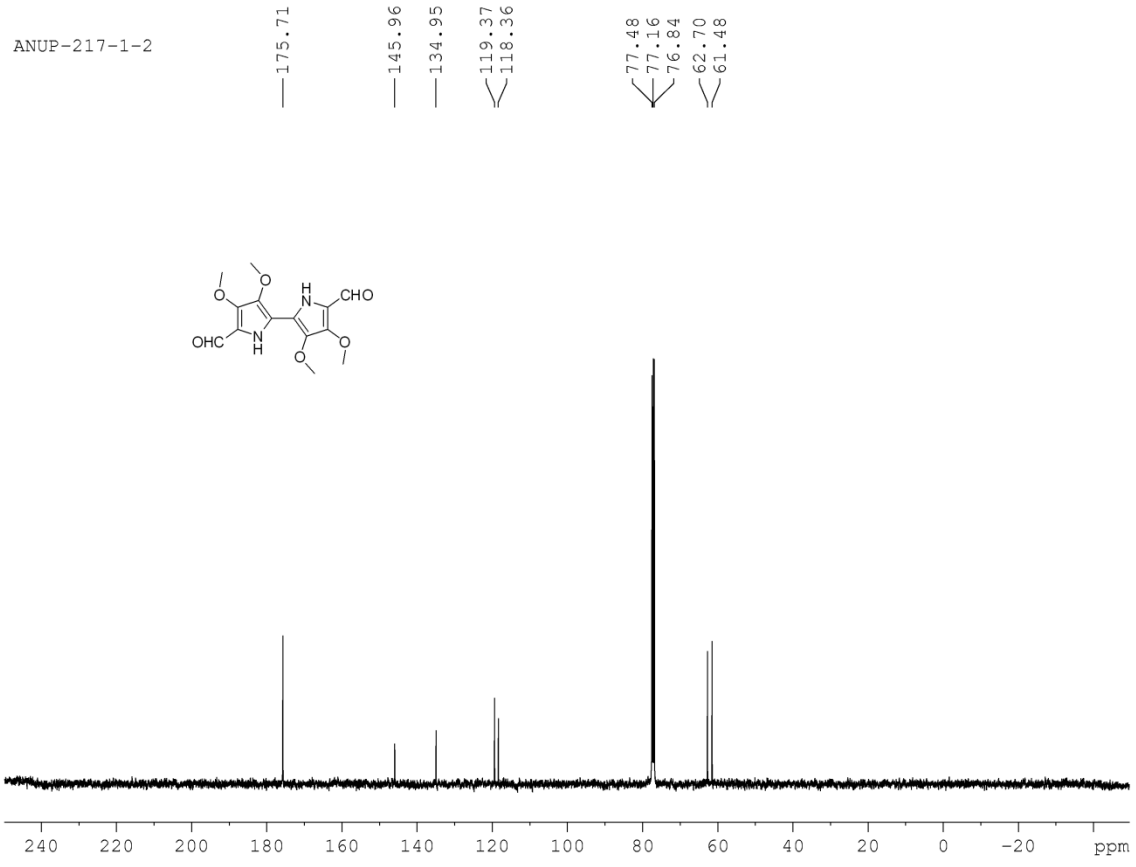

Figure 5.20 ^{13}C NMR spectrum of **5.99** in $CDCl_3$.

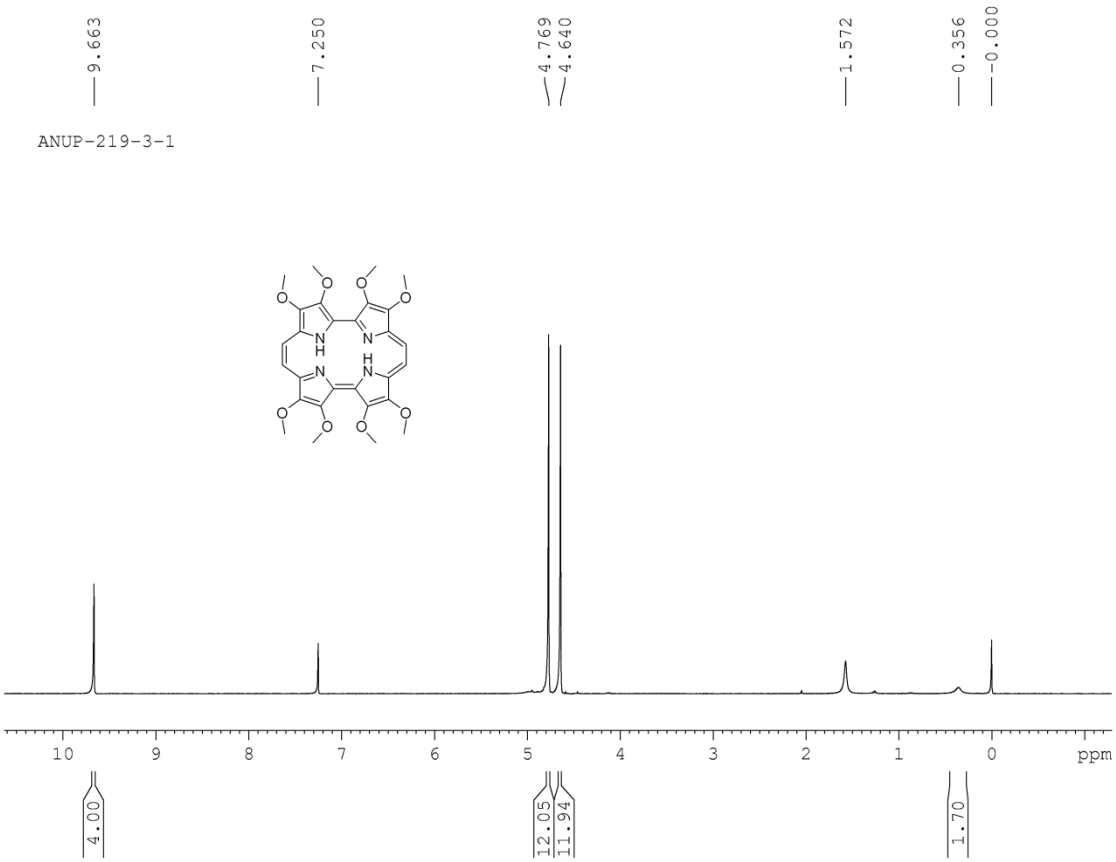

Figure 5.21 ^{1}H NMR spectrum of **5.92** in $CDCl_3$.

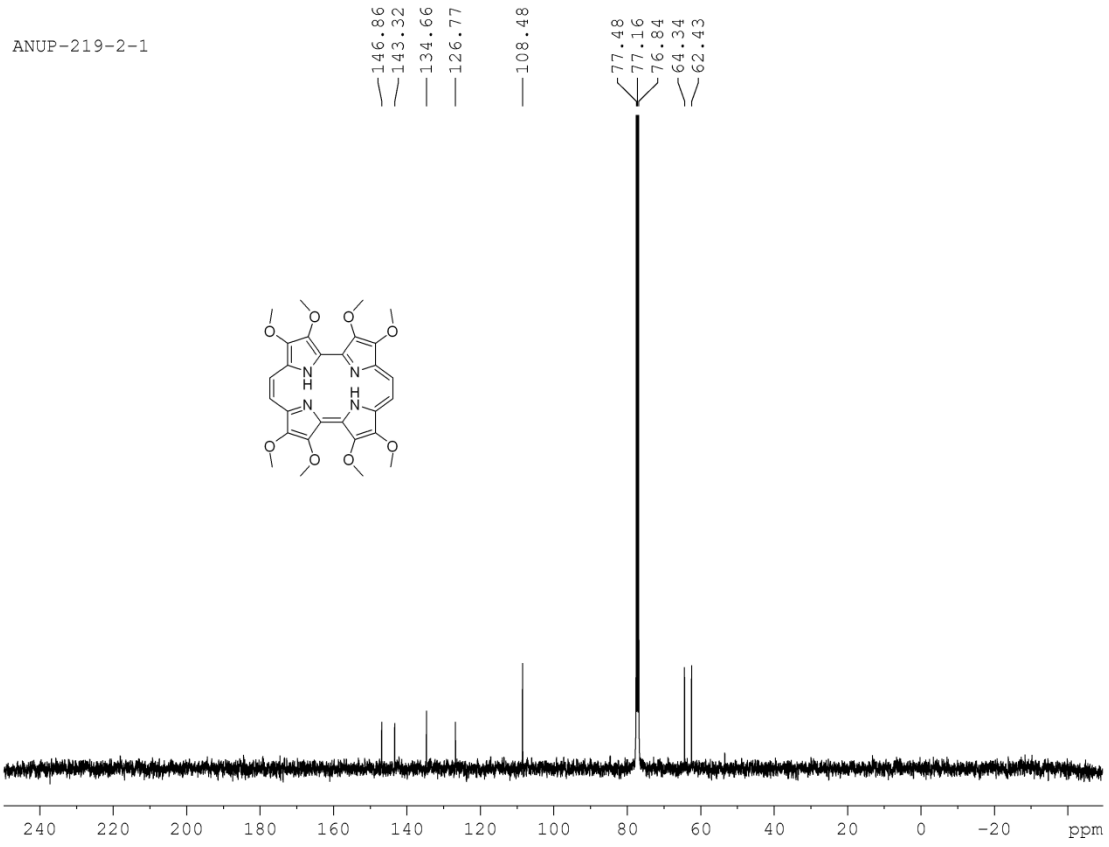

Figure 5.22 ^{13}C NMR spectrum of **5.92** in $CDCl_3$.

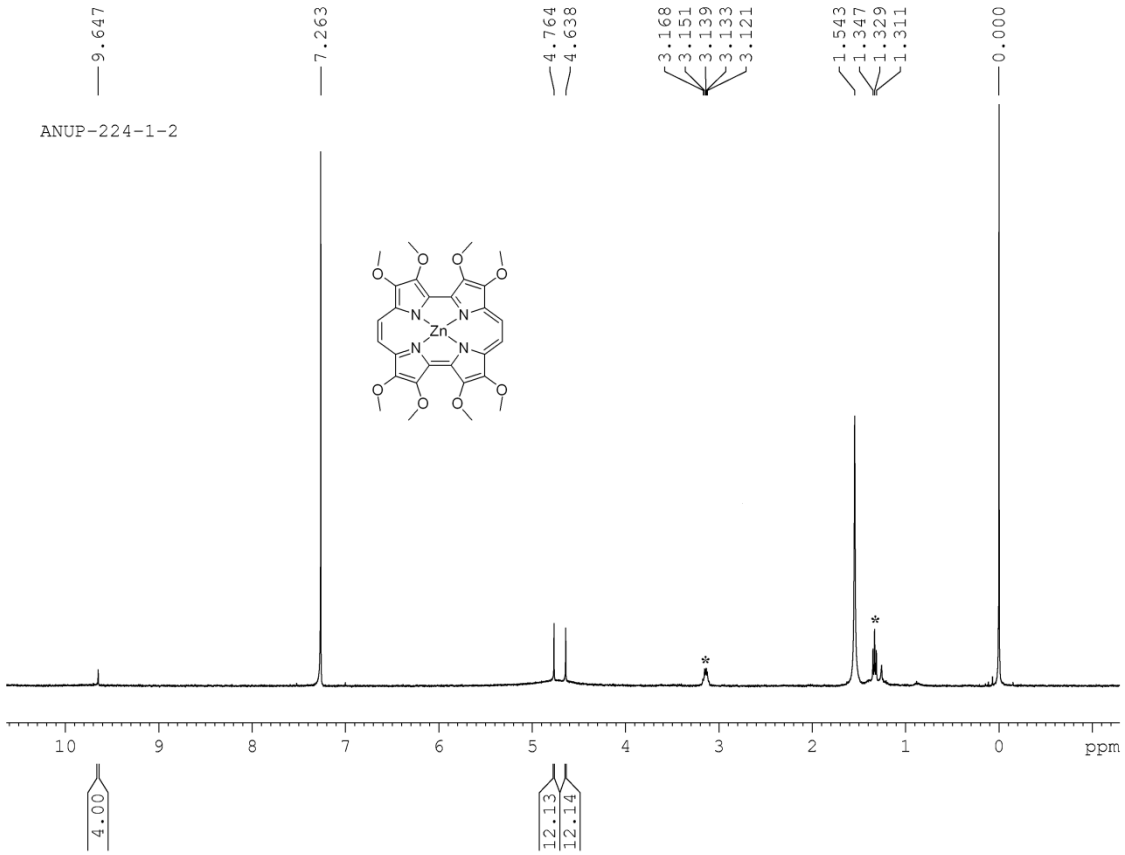

Figure 5.23 ^{1}H NMR spectrum of **Zn(5.92)** in $CDCl_3$. * represents peaks for NEt_3.

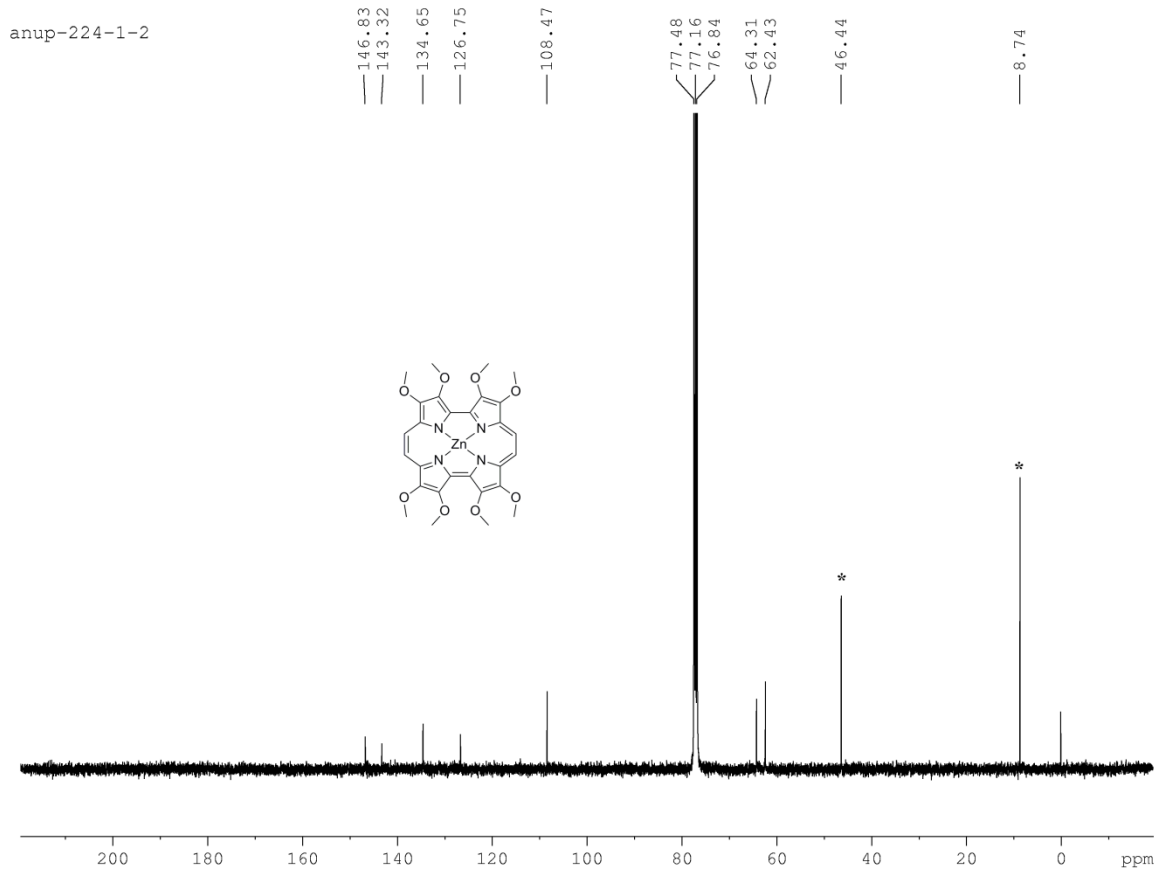

Figure 5.24 ^{13}C NMR spectrum of **Zn(5.92)** in $CDCl_3$. * represents peaks for NEt_3.

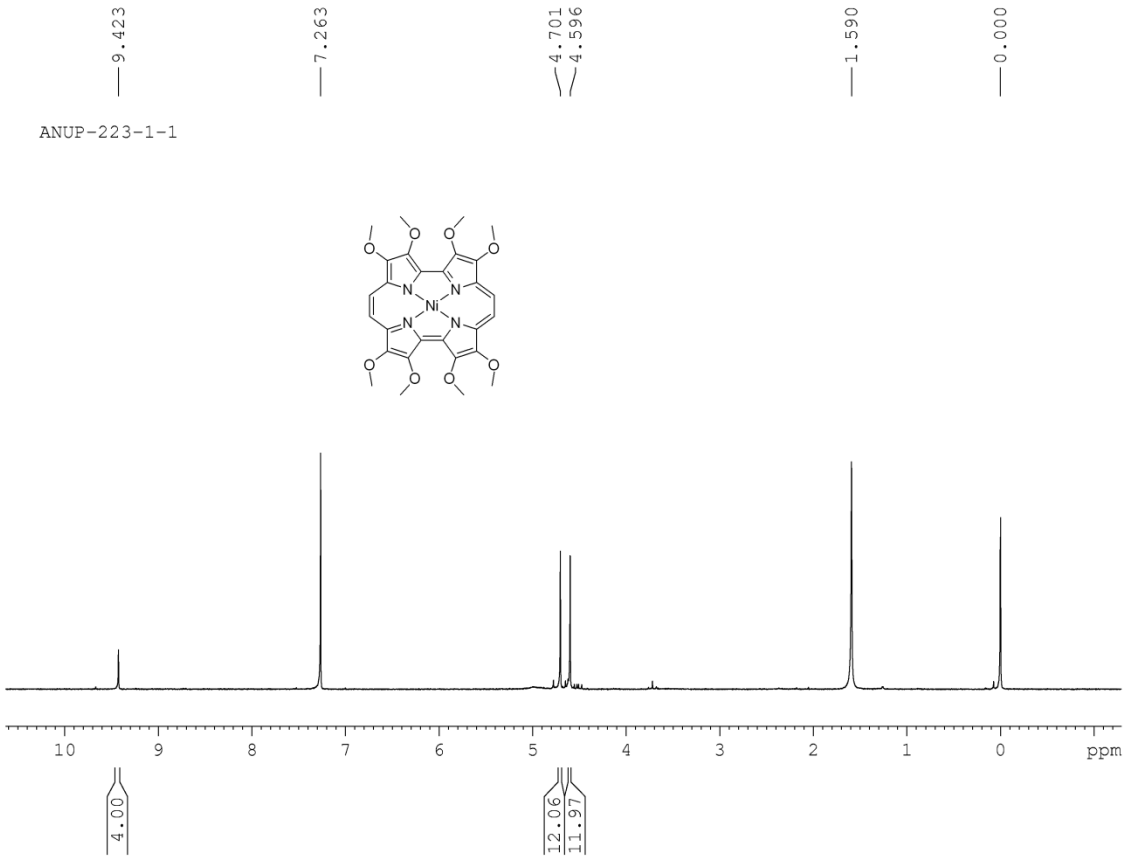

Figure 5.25 ^{1}H NMR spectrum of **Ni(5.92)** in $CDCl_3$.

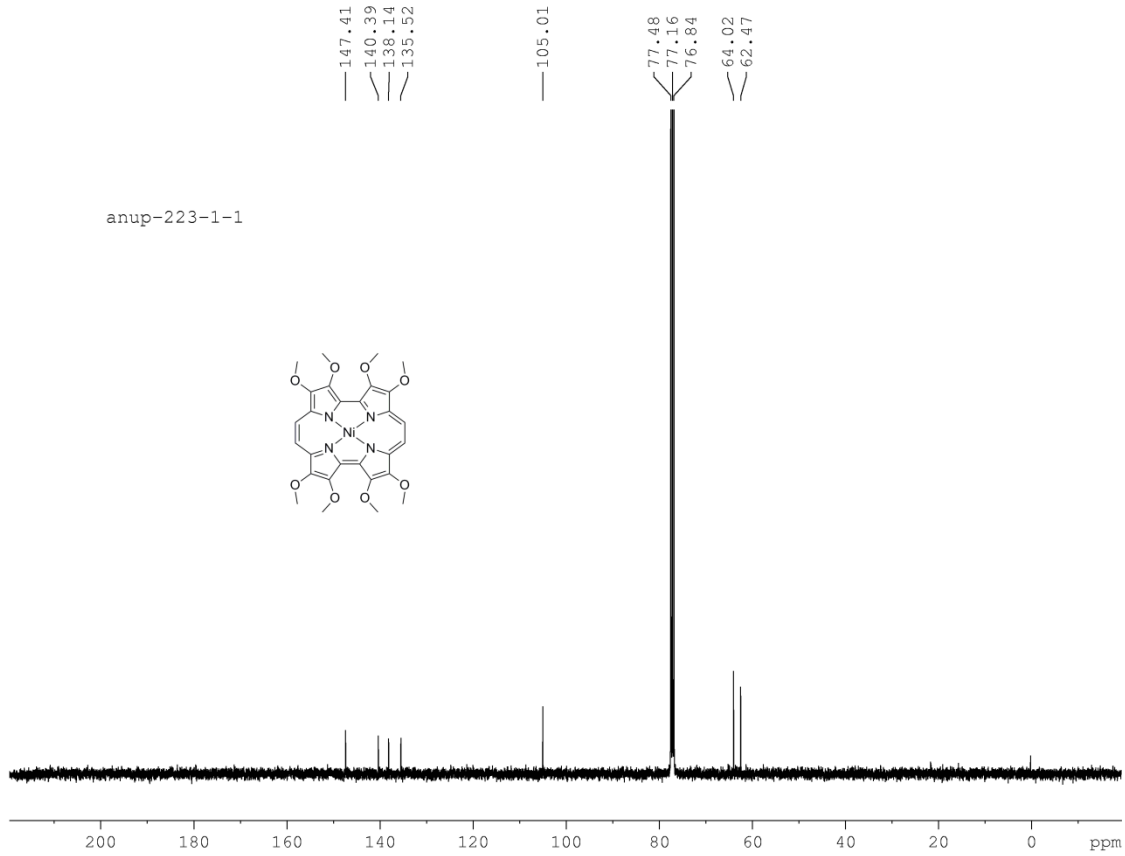

Figure 5.26 ^{13}C NMR spectrum of **Ni(5.92)** in $CDCl_3$.

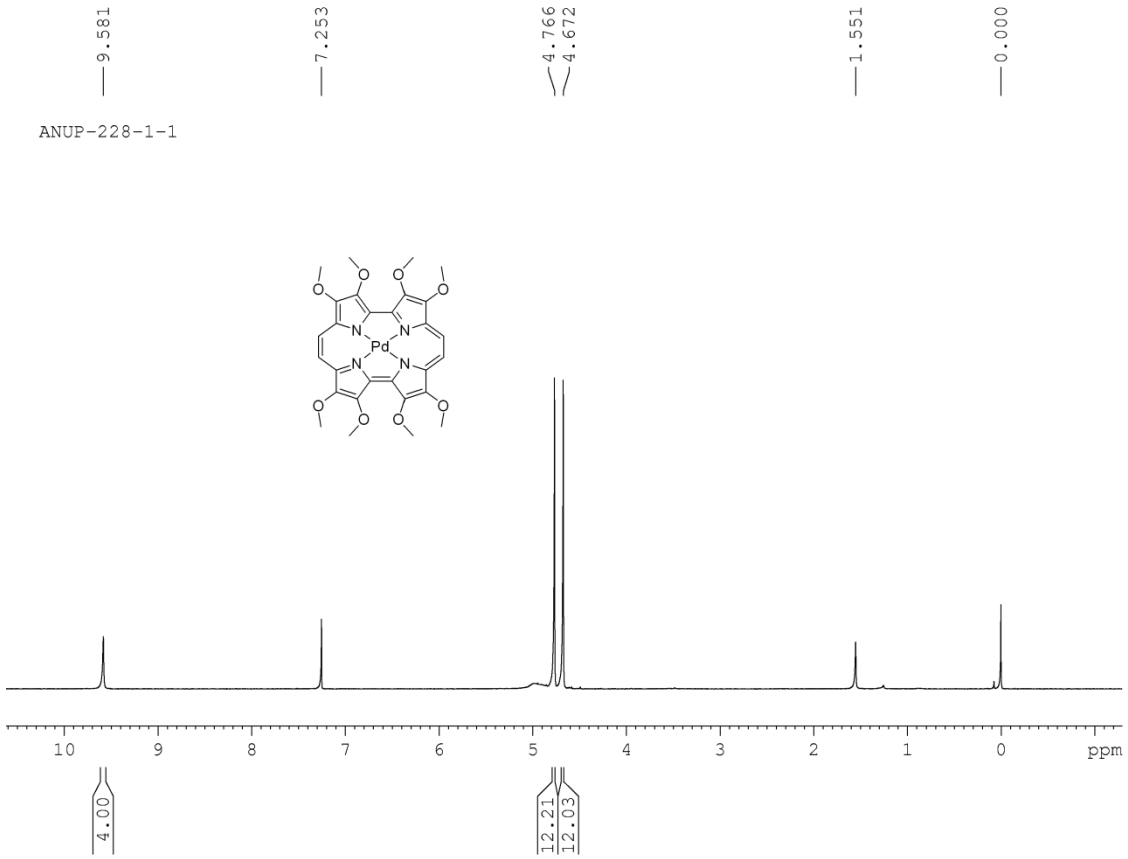

Figure 5.27 ^{1}H NMR spectrum of **Pd(5.92)** in $CDCl_3$.

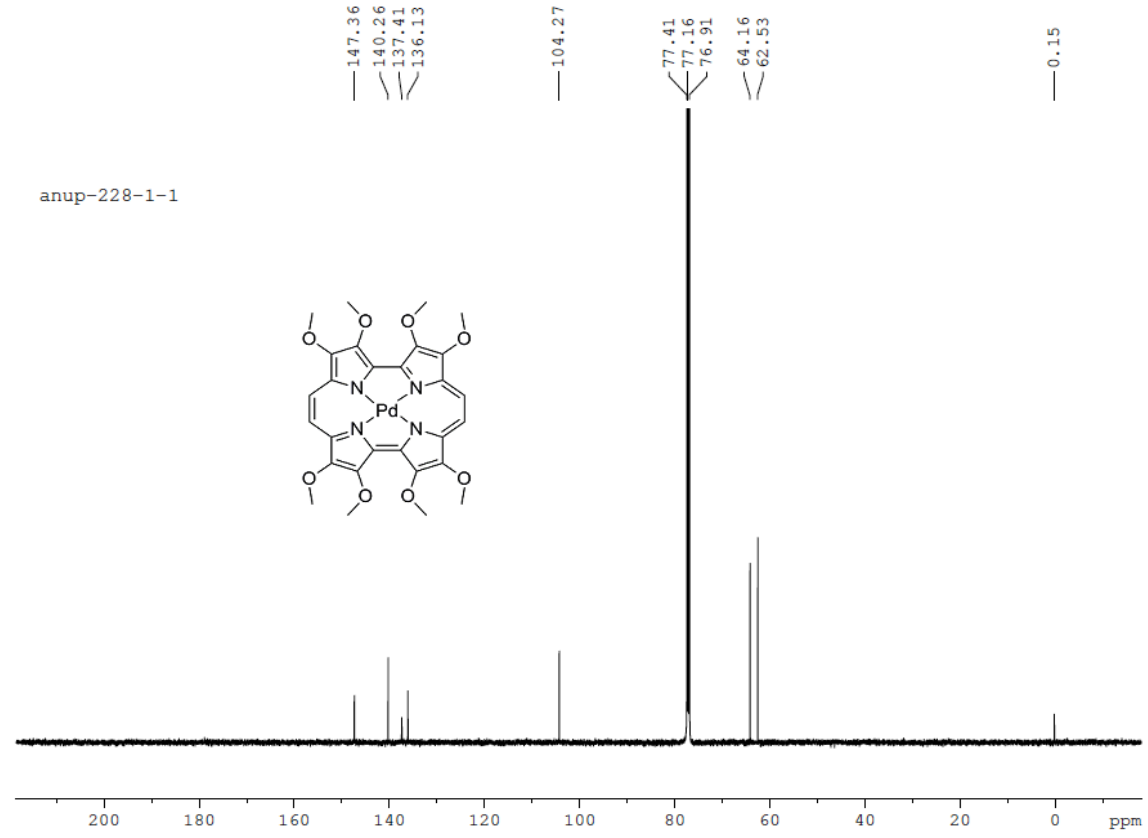

Figure 5.28 ^{13}C NMR spectrum of **Pd(5.92)** in $CDCl_3$.

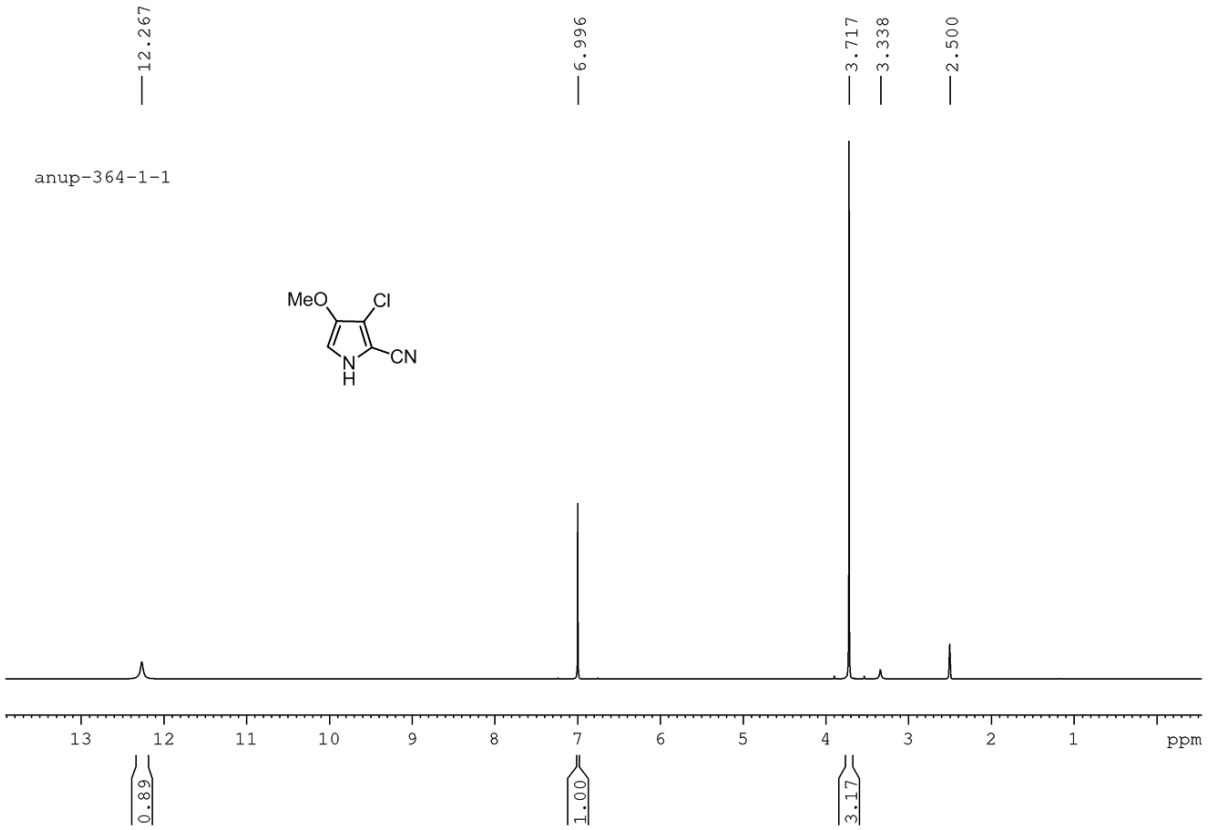

Figure 5.29 ^{1}H NMR spectrum of **5.107** in DMSO-d_6.

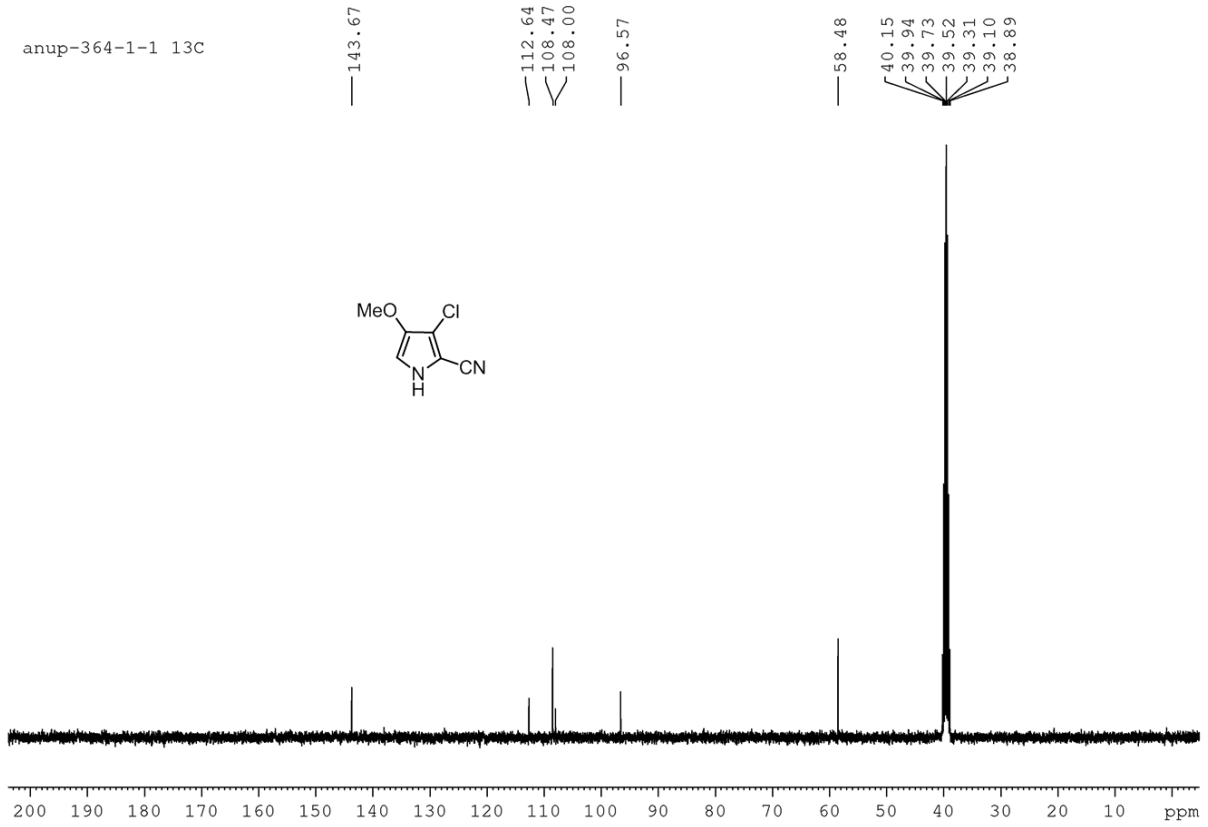

Figure 5.30 ^{13}C NMR spectrum of **5.107** in DMSO-d_6.

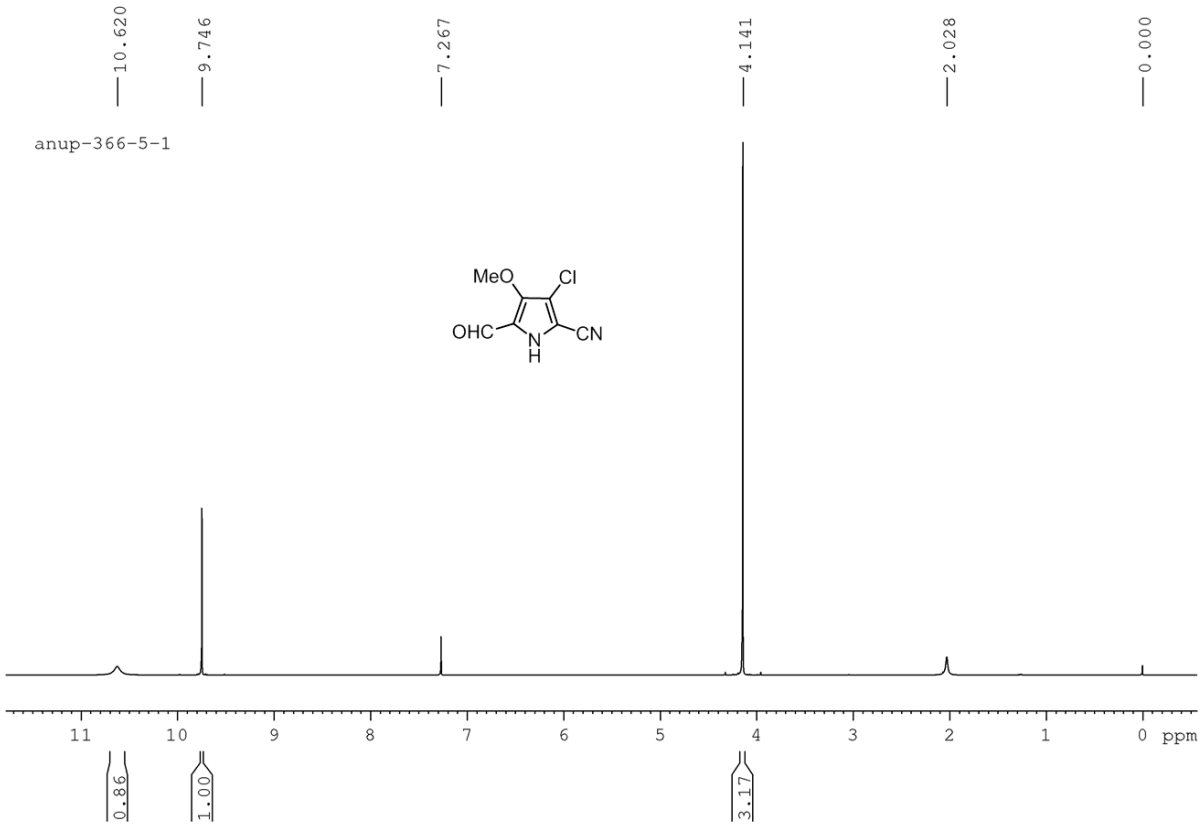

Figure 5.31 ^{1}H NMR spectrum of **5.108** in $CDCl_3$.

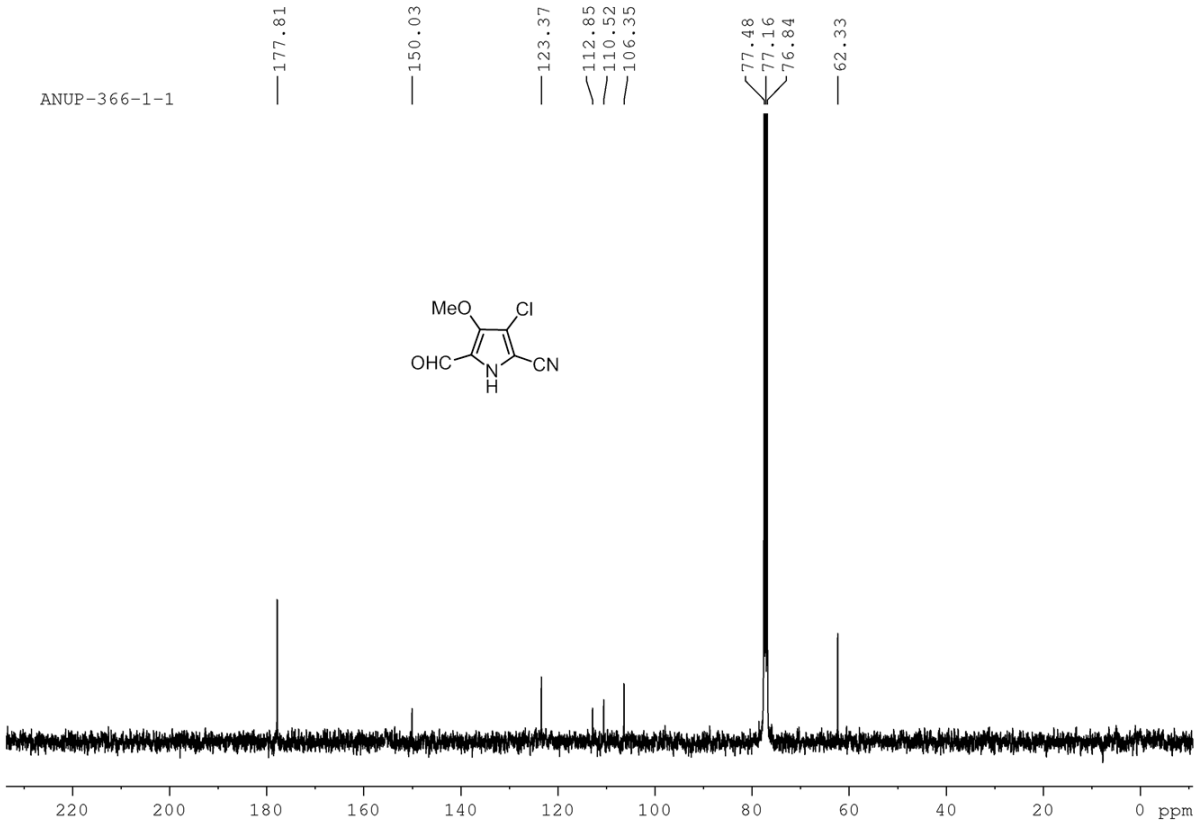

Figure 5.32 ^{13}C NMR spectrum of **5.108** in $CDCl_3$.

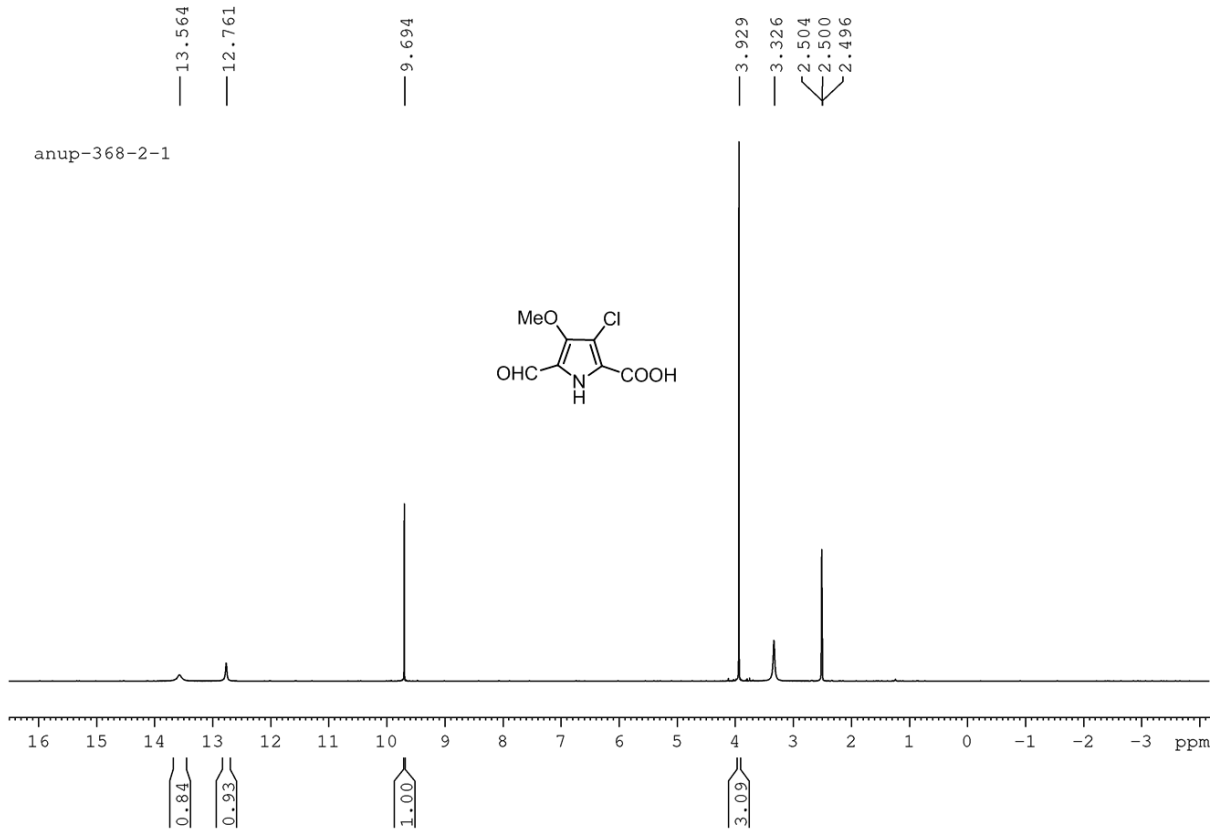

Figure 5.33 ^{1}H NMR spectrum of **5.109** in DMSO-d_6.

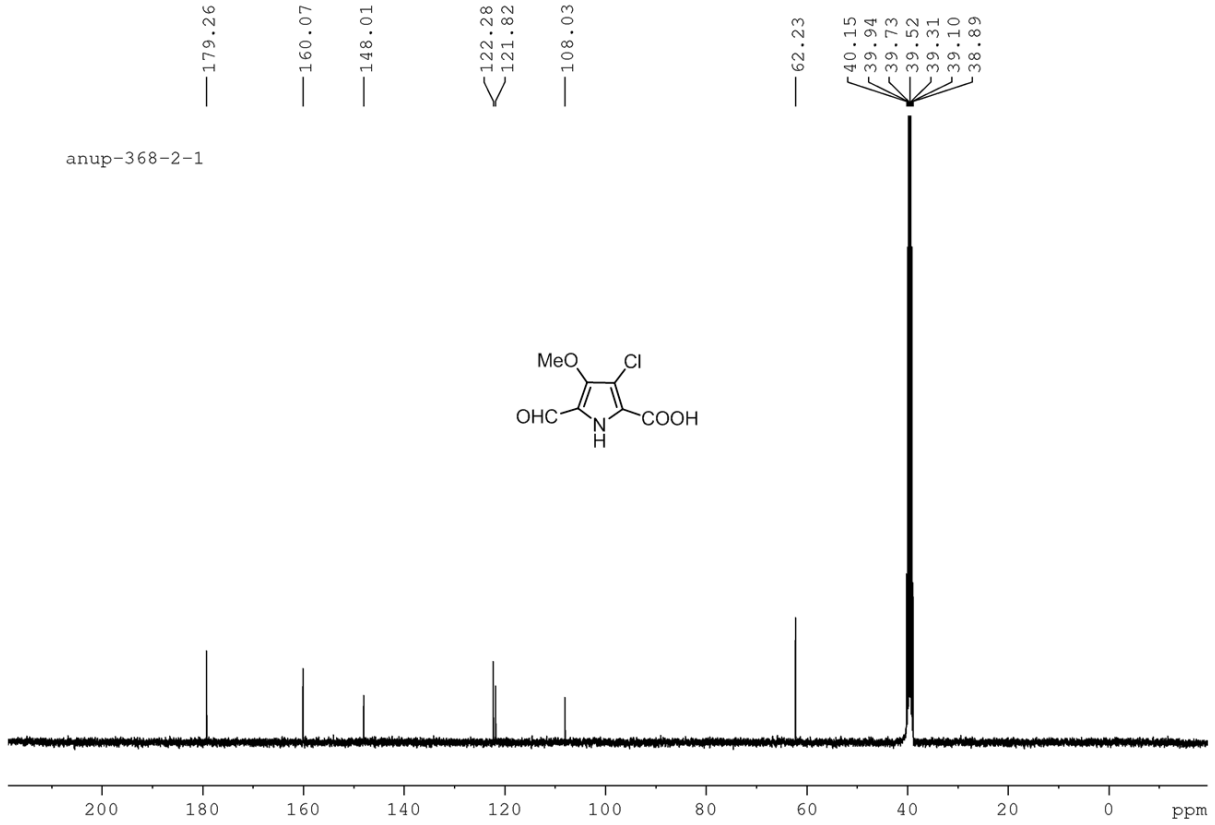

Figure 5.34 ^{13}C NMR spectrum of **5.109** in DMSO-d_6.

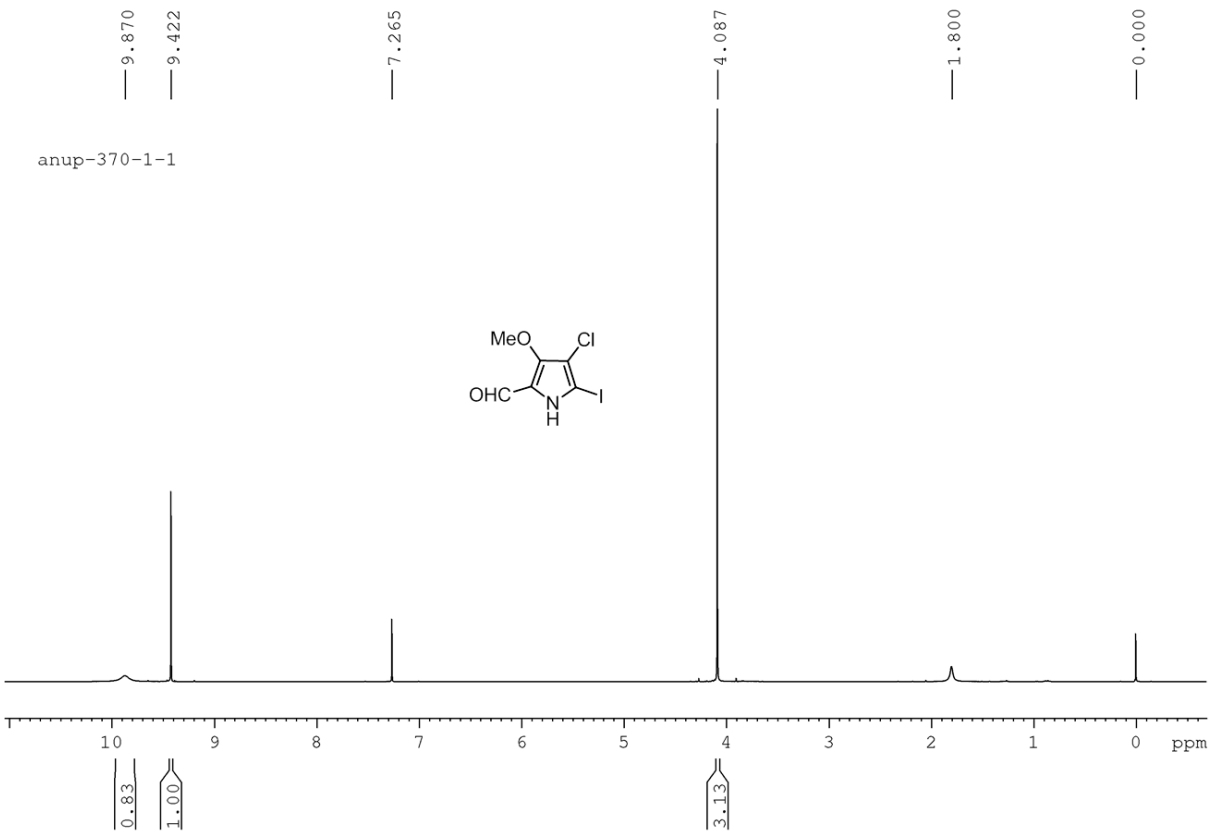

Figure 5.35 ^{1}H NMR spectrum of **5.110** in $CDCl_3$.

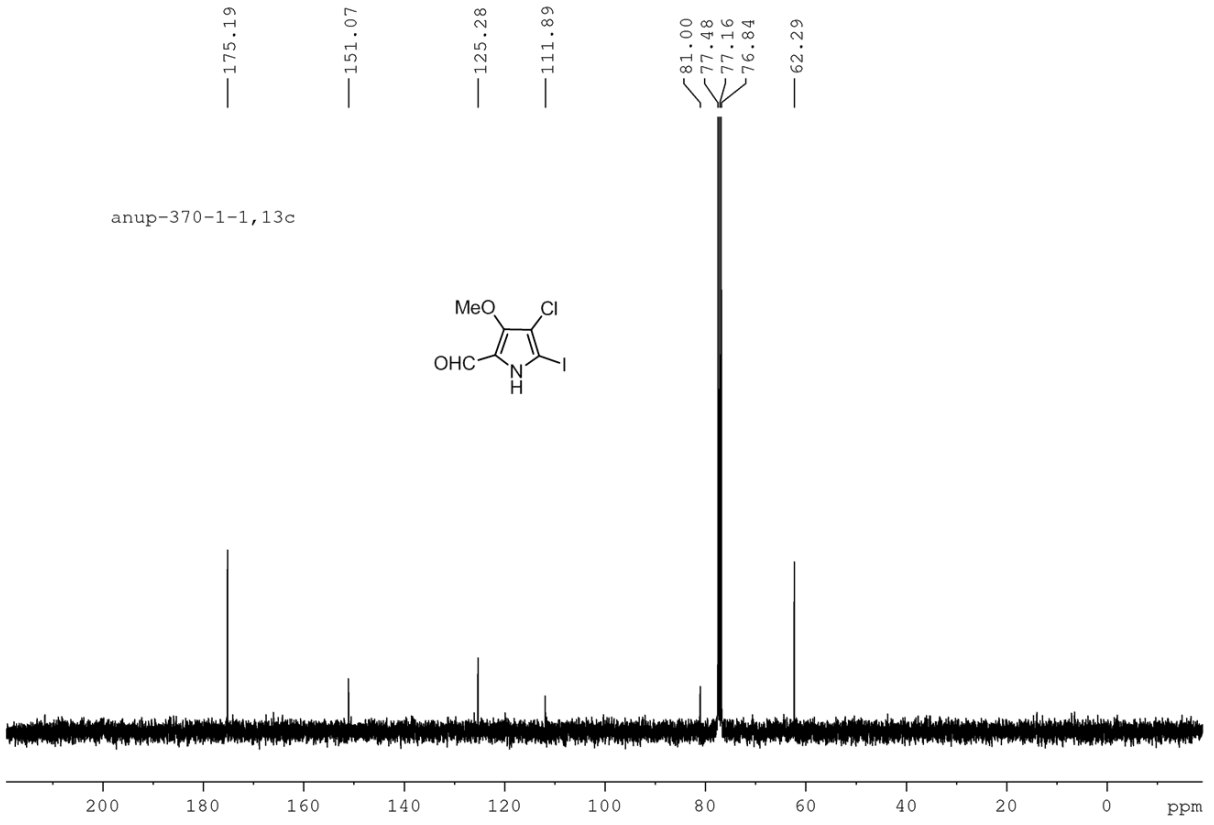

Figure 5.36 ^{13}C NMR spectrum of **5.110** in $CDCl_3$.

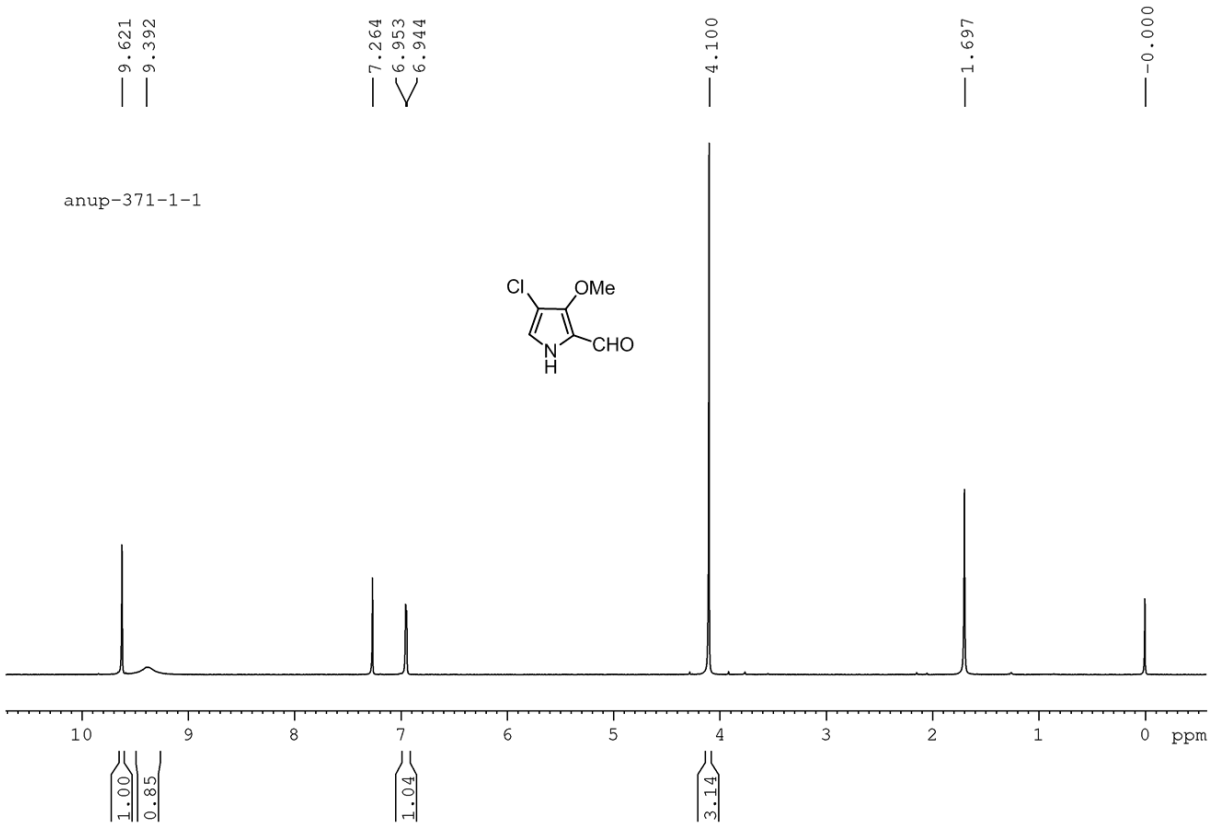

Figure 5.37 ^{1}H NMR spectrum of **5.111** in $CDCl_3$.

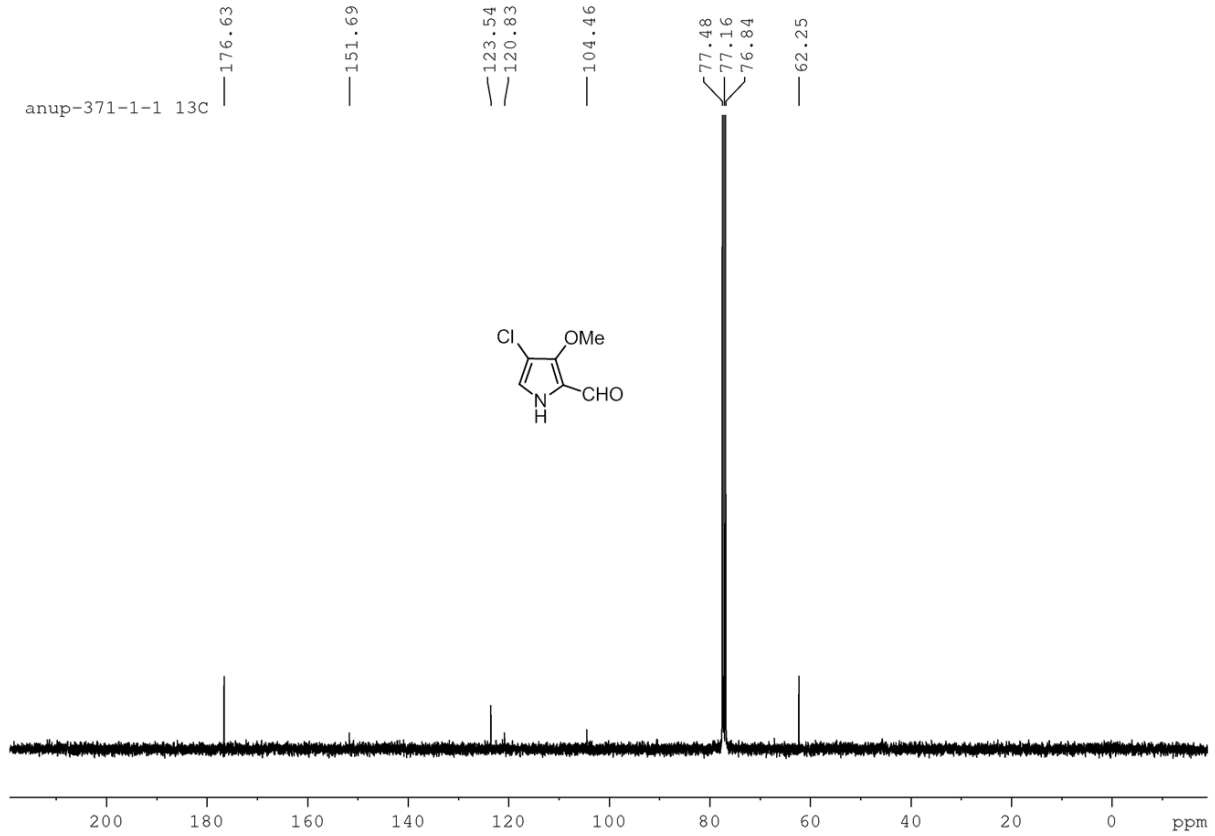

Figure 5.38 ^{13}C NMR spectrum of **5.111** in $CDCl_3$.

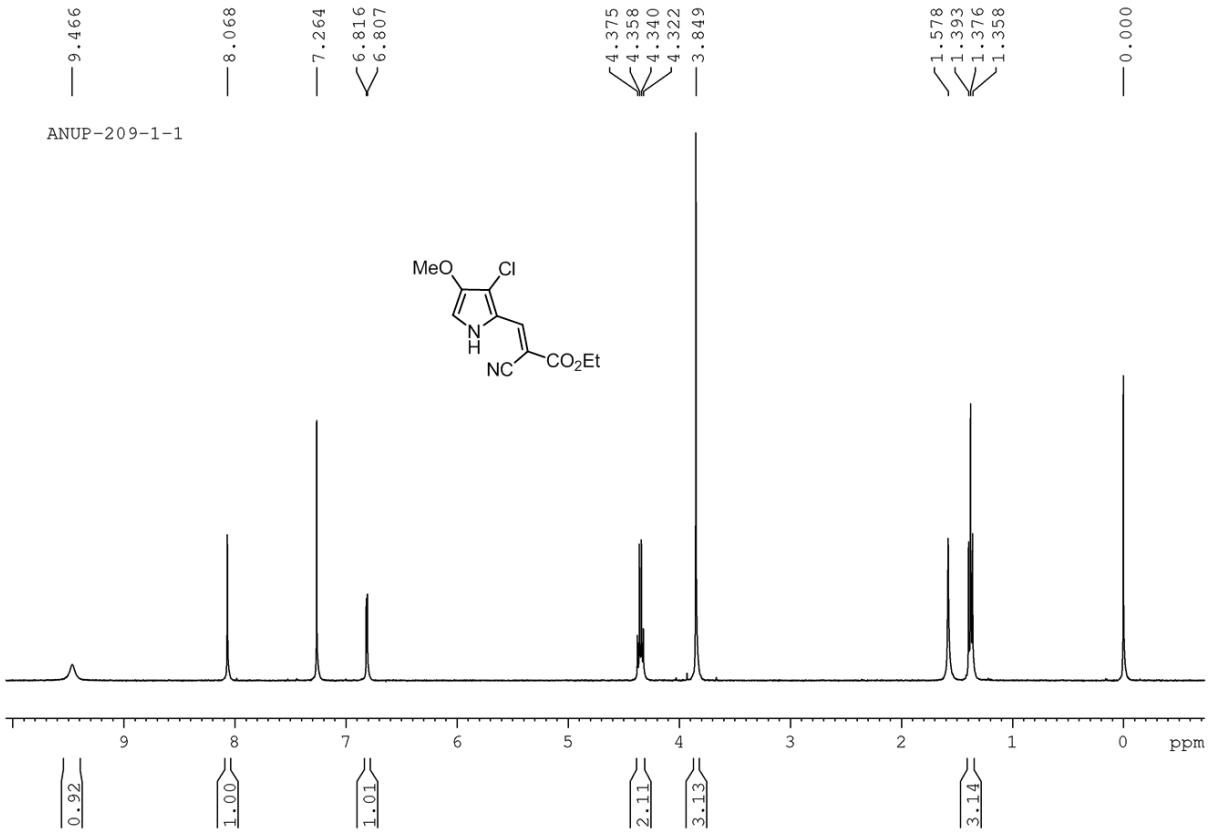

Figure 5.39 ^{1}H NMR spectrum of **5.112** in $CDCl_3$.

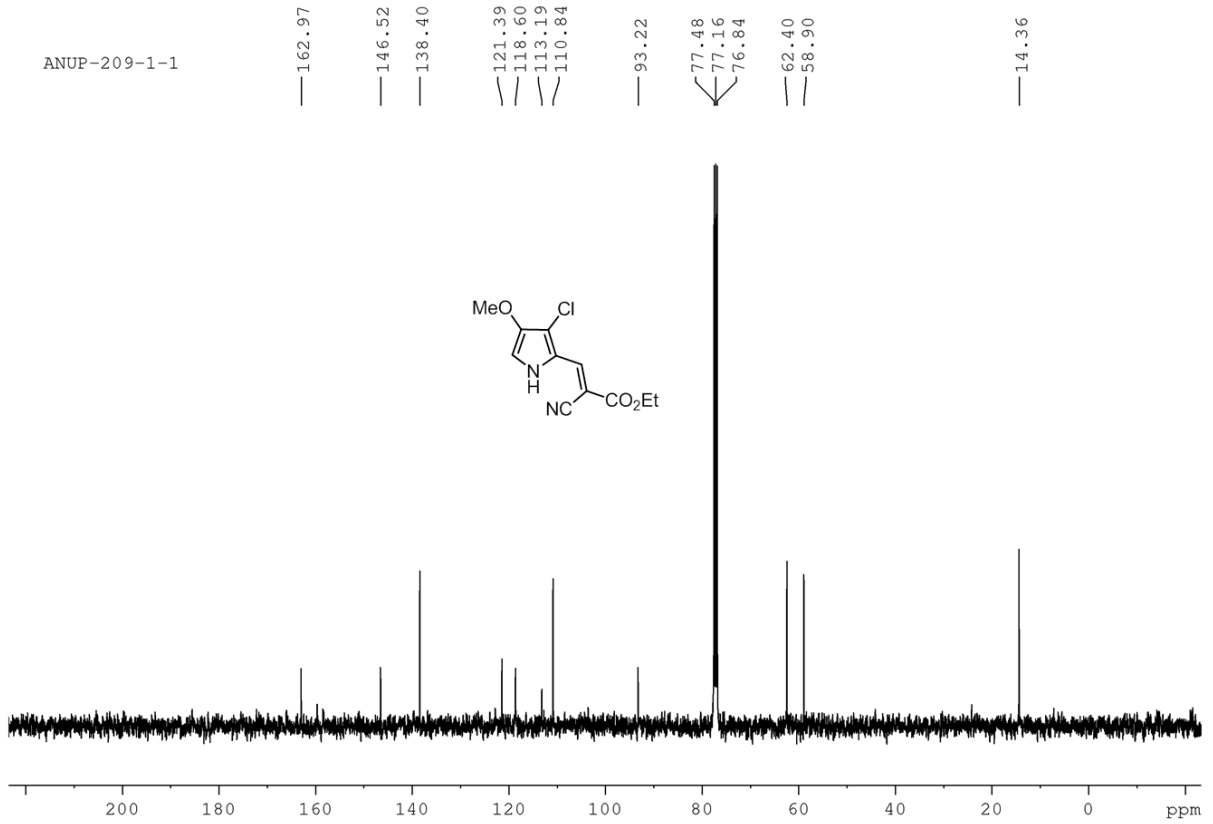

Figure 5.40 ^{13}C NMR spectrum of **5.112** in $CDCl_3$.

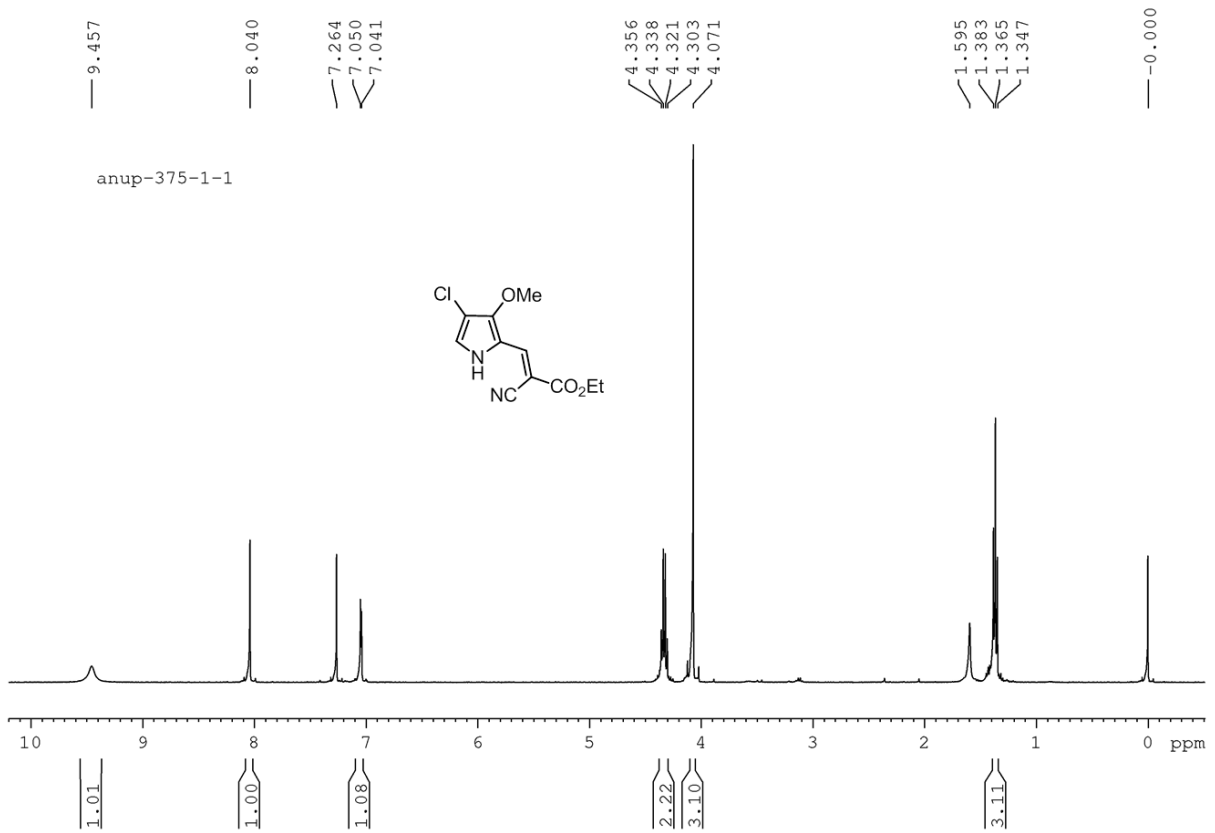

Figure 5.41 ^{1}H NMR spectrum of **5.113** in $CDCl_3$.

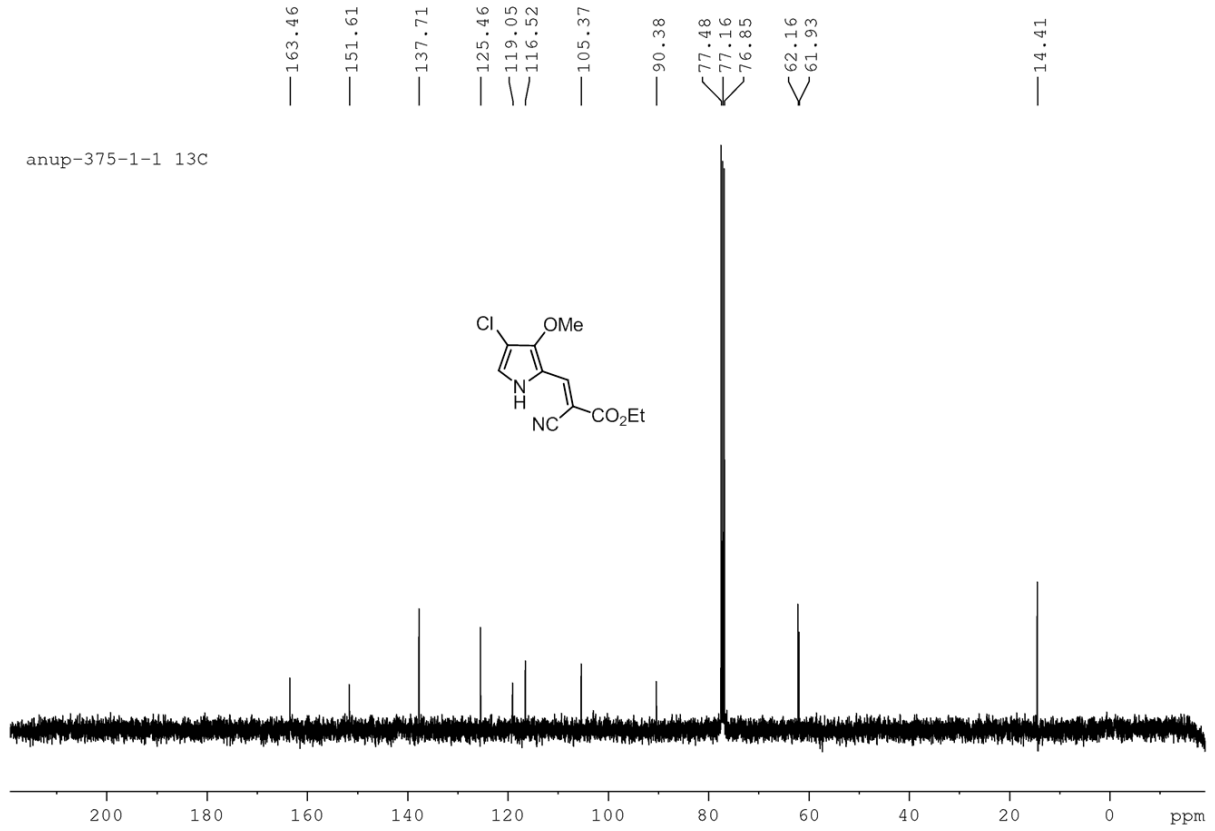

Figure 5.42 ^{13}C NMR spectrum of **5.113** in $CDCl_3$.

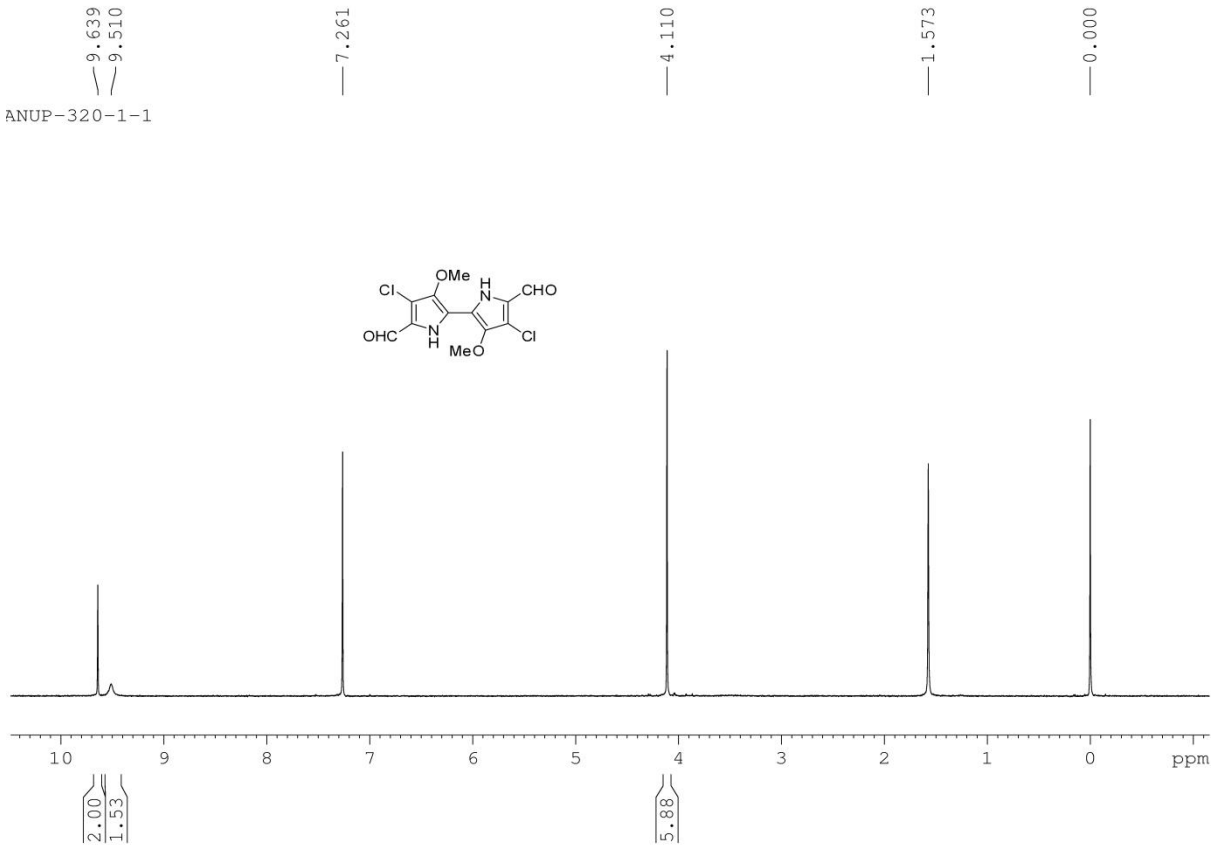

Figure 5.43 ^{1}H NMR spectrum of **5.100** in $CDCl_3$.

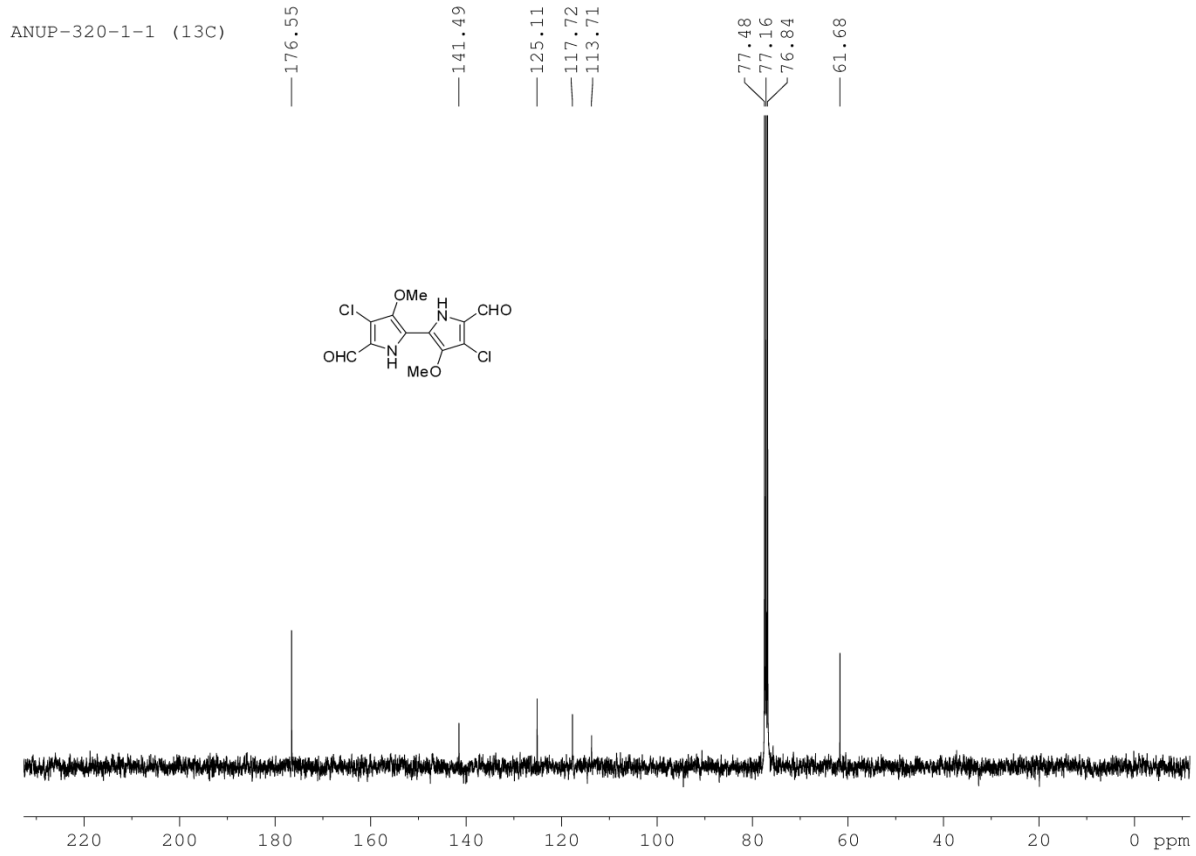

Figure 5.44 ^{13}C NMR spectrum of **5.100** in $CDCl_3$.

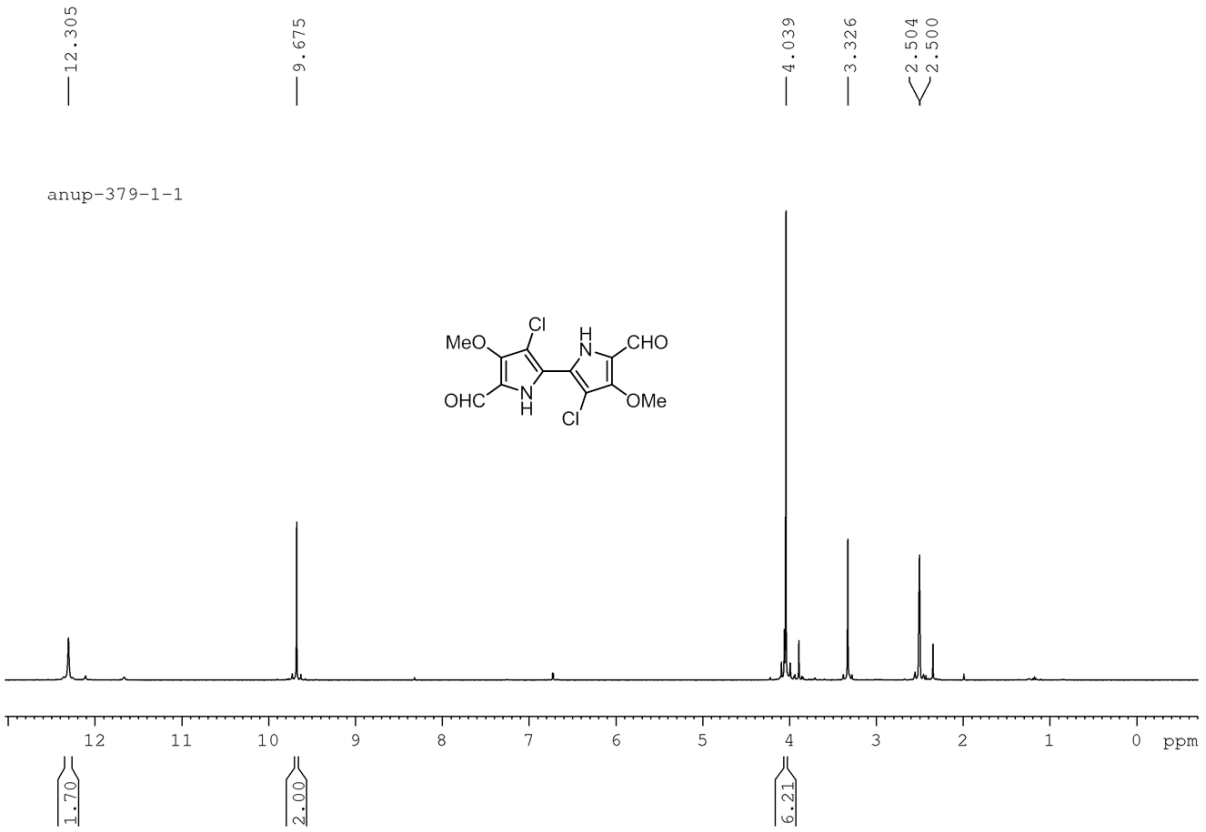

Figure 5.45 ^{1}H NMR spectrum of **5.114** in DMSO-d_6.

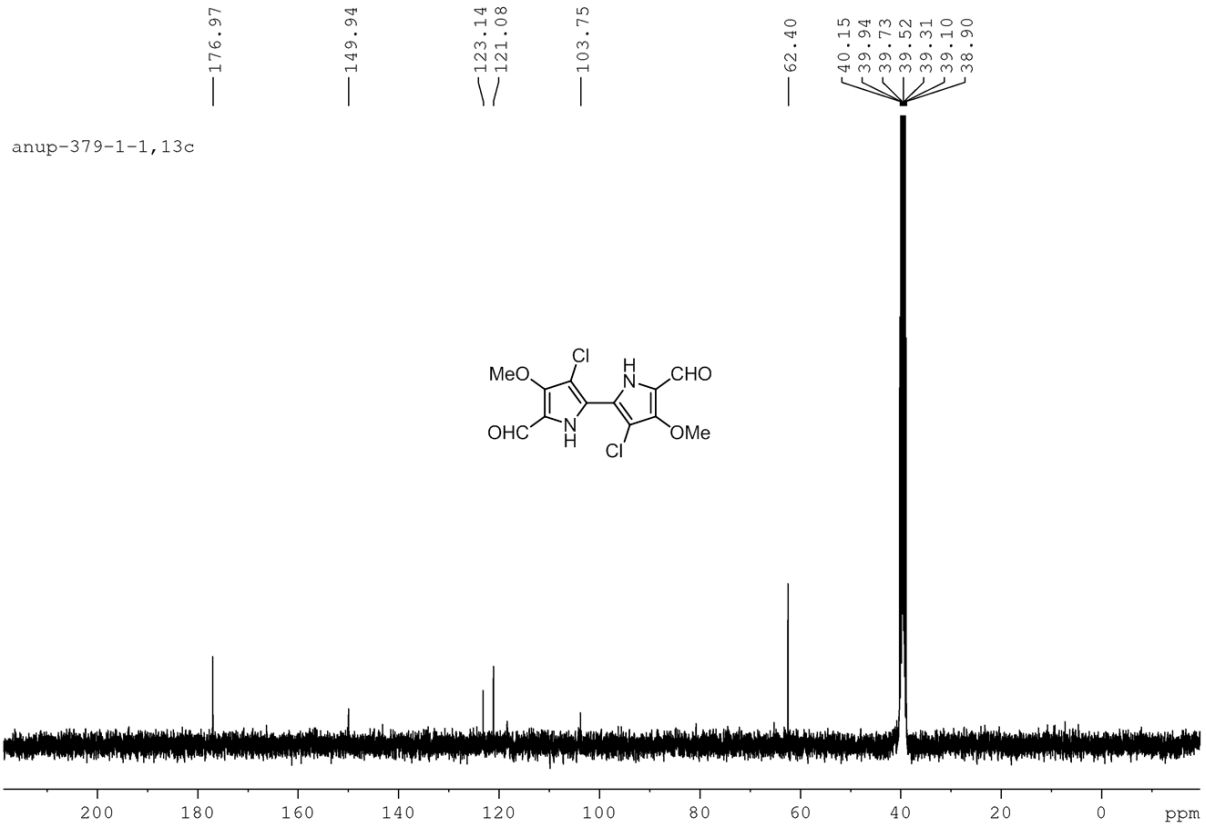

Figure 5.46 ^{13}C NMR spectrum of **5.114** in DMSO-d_6.

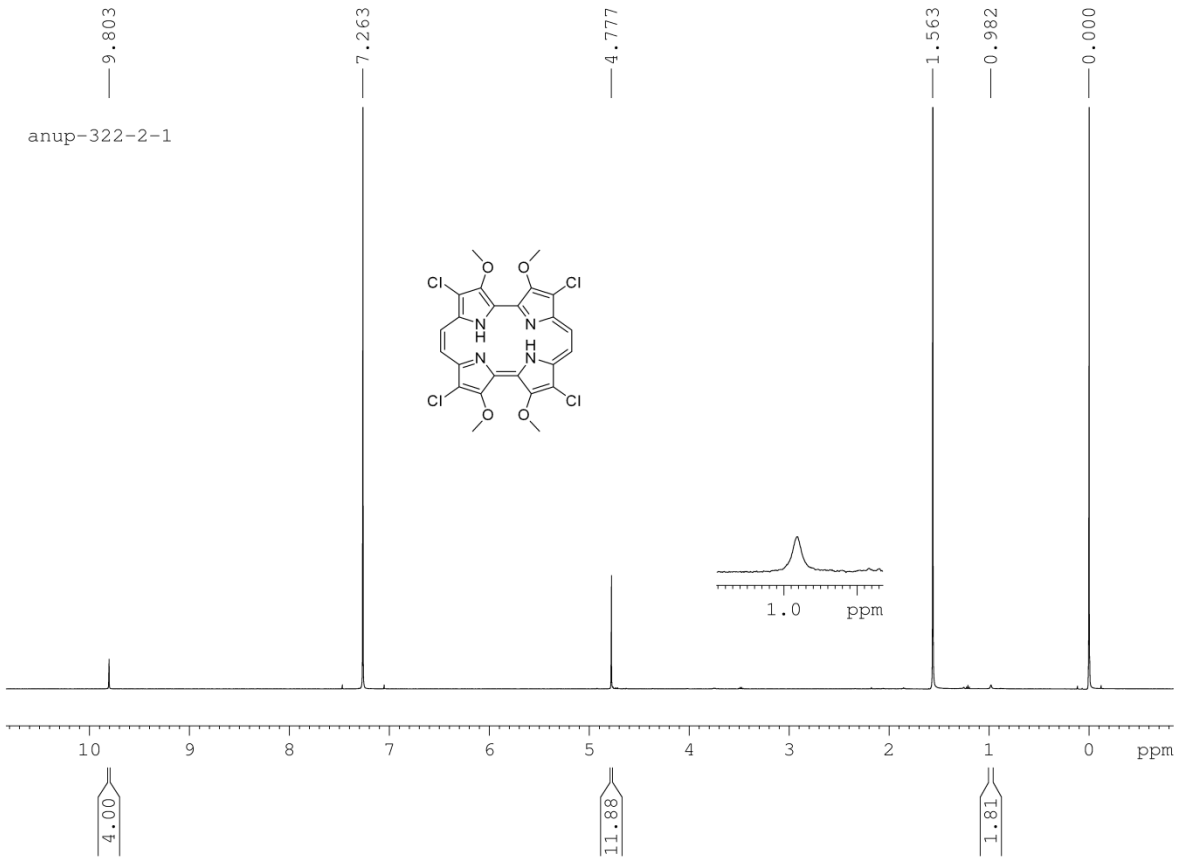

Figure 5.47 ^{1}H NMR spectrum of **5.93** in $CDCl_3$.

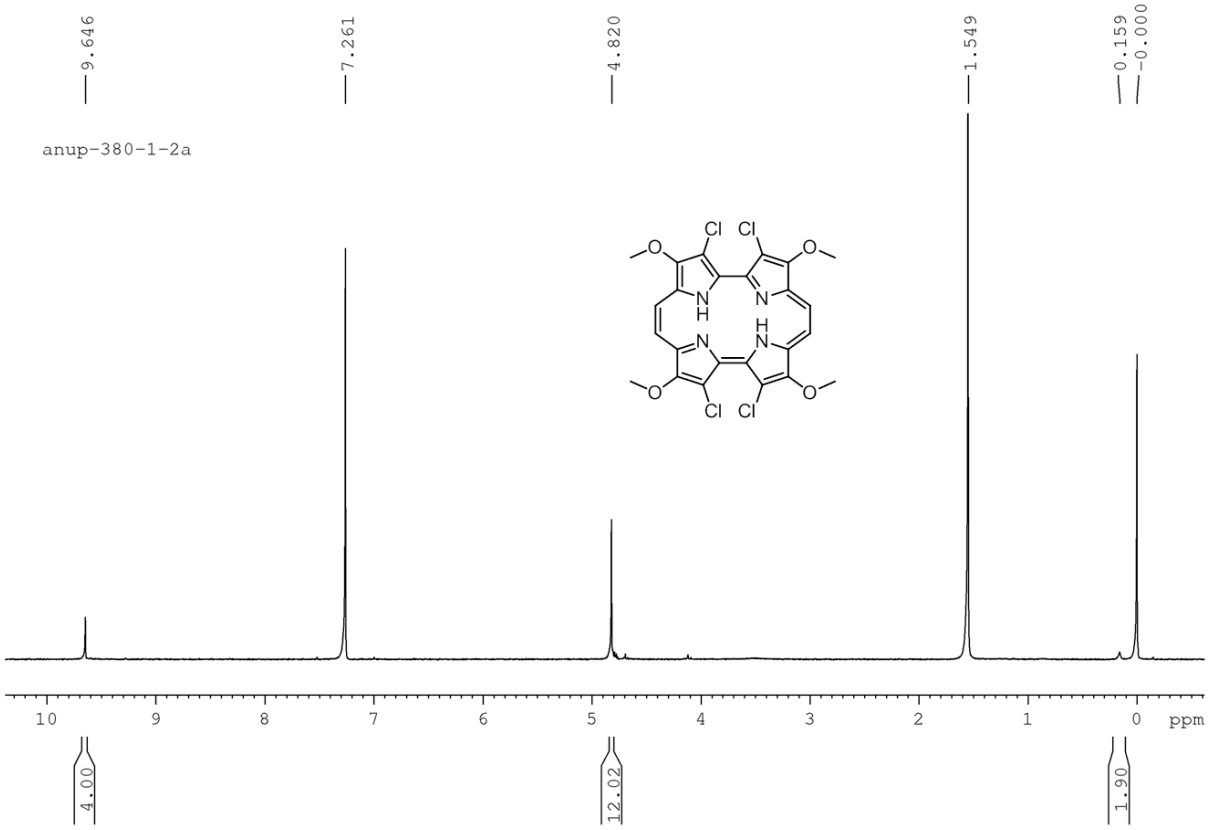

Figure 5.48 ^{1}H NMR spectrum of **5.94** in $CDCl_3$.

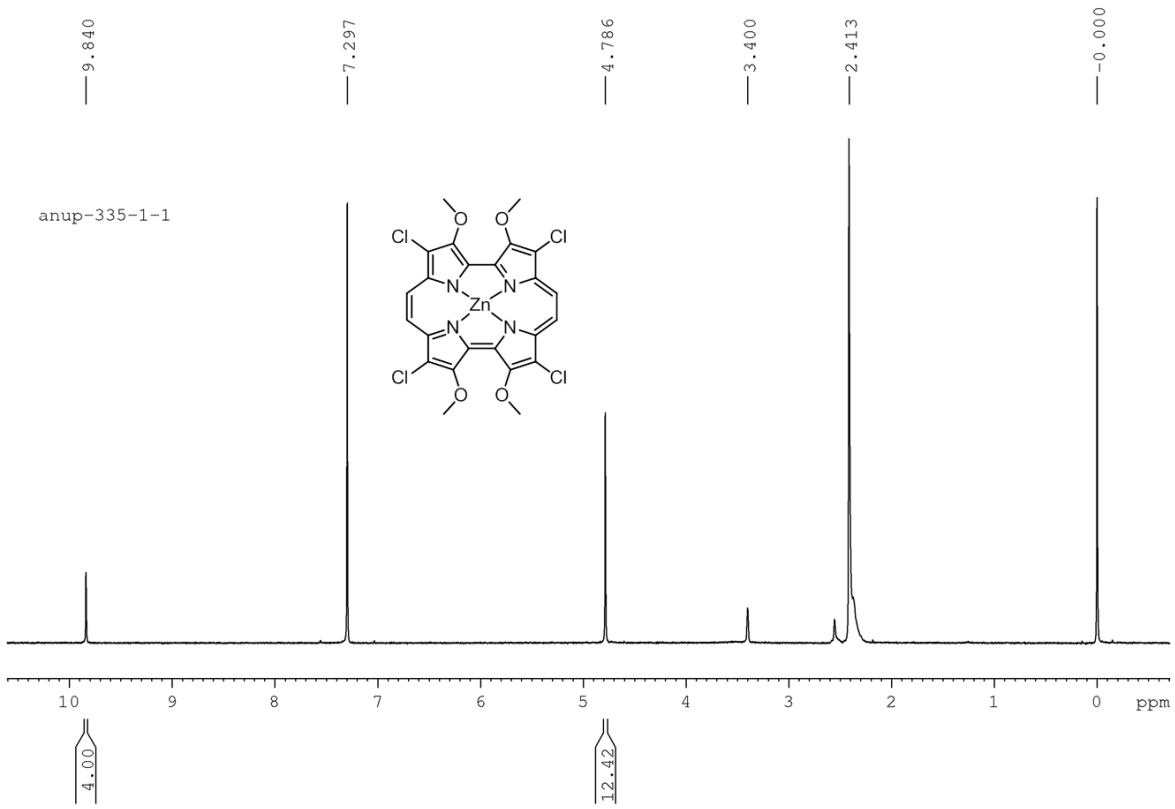

Figure 5.49 ^{1}H NMR spectrum of **Zn(5.93)** in $CDCl_3$ in presence of small amount of MeOH-d_4.

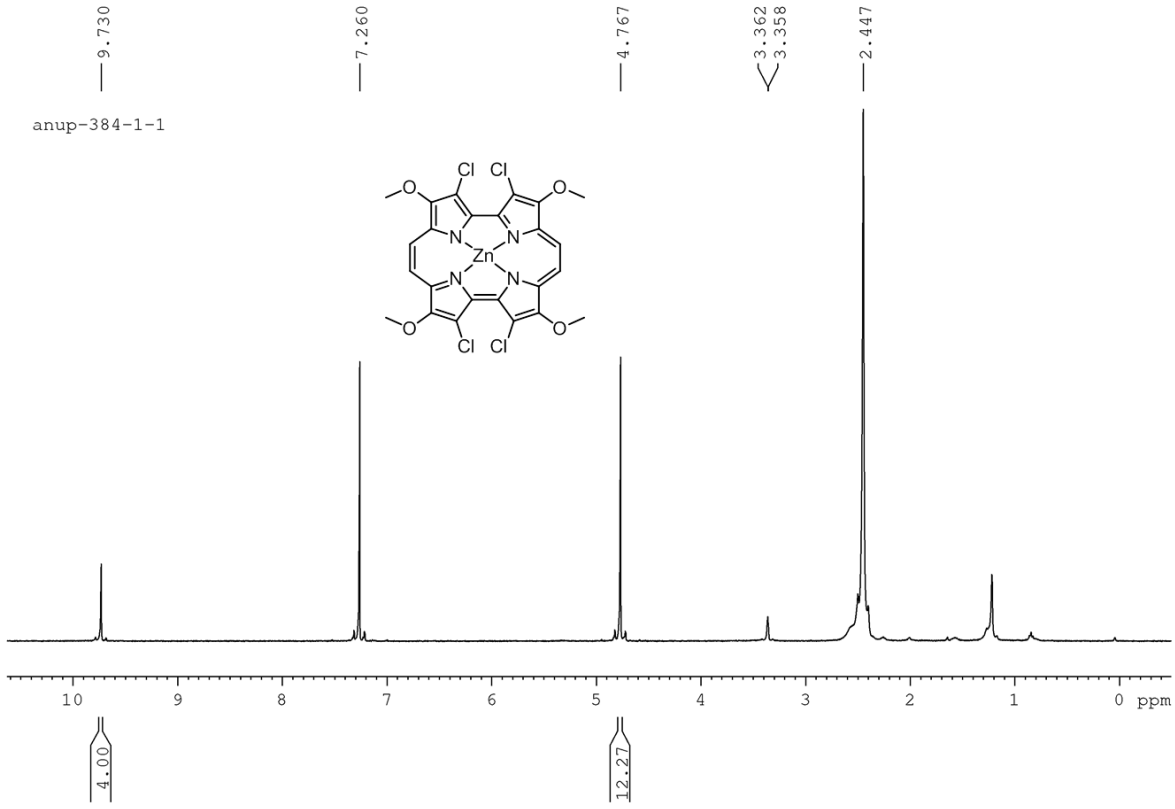

Figure 5.50 ^{1}H NMR spectrum of **Zn(5.94)** in $CDCl_3$ in presence of small amount of MeOH-d_4.

CHAPTER 6

β-Octa(methylthio)porphycenes: Synthesis, Characterisation and NLO Studies

6.1 Introduction

In the previous chapter we have introduced a detailed overview about porphycenes and as this chapter also deals with porphycene, therefore, a brief introduction focused on the goal of our work will be provided.

Porphycene is the first abiotic constitutional isomer of the much revered, naturally occurring pigment, porphyrin to be reported by Vogel.[1] Owing to the reduced symmetry, this macrocycle displays enhanced absorption in the red region. Initially, this drew wide attention of researchers to explore its potential utility as an effective photosensitizer for photodynamic therapy.[2] However, exploration of its potential as nonlinear optical (NLO) materials, is still in infancy stage due to difficulties associated with the synthesis of appropriately substituted porphycenes and their further substitution ability.[2,3] Recent study on dinapthoporphycenes

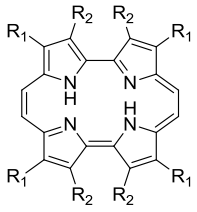

6.2; $R_1 = R_2 = Et$
6.3; $R_1 = R_2 = OMe$
6.4; $R_1 = Et$, $R_2 = CF_3$

shows good third order NLO response with laser intensity dependent multiphoton absorption.[3a-b] Further, the trifluoromethyl (CF_3)-substituted porphycene **6.4**[4] displays relatively less two-photon absorption (TPA) cross section compared to the etioporphycene.[3d] Interestingly, porphyrins containing similarly electron-donating (OMe) and withdrawing substituents (Cl) on adjacent β-pyrrolic positions display higher TPA cross section compared to the porphyrins endowed with all electron-donating substituents at their β-positions.[5] As the structure and photophysical properties of porphycenes are more sensitive to effect of substituents compared to porphyrins, therefore we wish to explore if this trait can be extended to their NLO properties.

6.2 Research goal

Based on the above discussion, we wish to synthesize the first porphycene with all electron withdrawing substituents at its β-positions, namely β-octakis(methylthio)porphycene **6.1** (Scheme 6.1), to see the effect of electron withdrawing substituents on the third order NLO properties of porphycene macrocycle, along with the effect of heteroatoms at the macrocyclic periphery. Separately, SMe group acts not only as good protecting group, but can also be used as a good leaving group for S_NAr and catalytic organic transformations, and hence may

enhance the scope for further substitution on porphycene periphery.[6] Herein, we report the synthesis of the desired porphycene **6.1** and explored its structure, complexation and photophysical properties including their excited state studies. Further, the third order NLO response of the freebase porphycene along with its Ni(II)-complex were explored at wavelengths where their one photon absorption (OPA) is minimal and compared with those of the corresponding β-octaethyl **6.2**[7] and β-octamethoxy **6.3**[8] analogues to evaluate the substituent effect.

6.3 Result and Discussions

6.3.1 Synthesis of porphycene

The synthesis of porphycene **6.1** was achieved by modifying the previously developed method in our group (Scheme 6.1).[8] Briefly, oxidative coupling of 3,4-di(methylthio)pyrrole **6.5**[9] with hypervalent iodine(III) reagent, [bis(trifluoroacetoxy)iodo]benzene (PIFA) as oxidant and TMSBr as Lewis acid at -40 °C led to the formation of desired bipyrrole **6.6** in very poor yield, probably due to the relatively electron deficient nature of **6.5** than 3,4-dimethoxypyrrole.[8,10] In order to activate the electron deficient pyrrole **6.5**, we performed PIFA coupling with a relatively strong Lewis acid (BF_3.OEt) under the same reaction condition, to obtain the desired bipyrrole **6.6** in 34% yield. Unlike, tetramethoxy-2,2'-

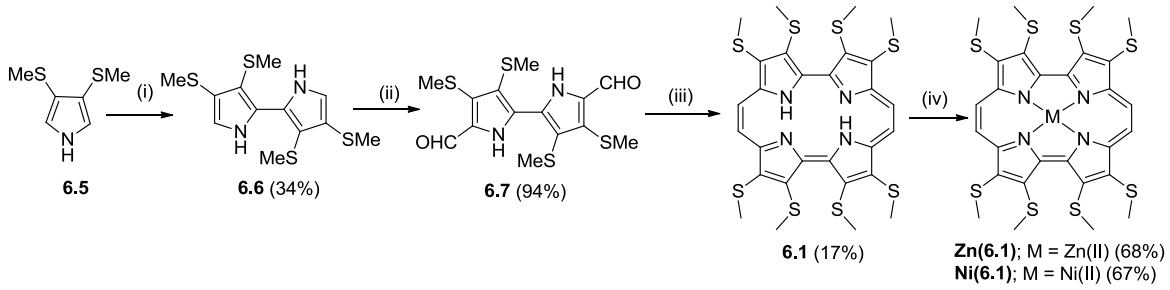

Scheme 6.1 Synthesis of β-octa(methylthio)porphycenes. Reagents and conditions: (i) PIFA, $BF_3.OEt_2$, DCM, -78 °C to -40 °C, 3 h; (ii) $POCl_3$, DMF, DCE, reflux, 4 h; (iii) (a) Zn, $TiCl_4$, CuCl, THF, reflux, 1 h. (b) DDQ, $CHCl_3$, RT, 1 h; (iv) For **Zn(6.1)** ($Zn(OAc)_2$, $CHCl_3$, MeOH, reflux 4 h, and for **Ni(6.1)** ($Ni(acac)_2$, *o*-xylene, reflux, 4 h.

bipyrrole[8], bipyrrole **6.6** found to be quite stable and hence can be purified by silica gel column chromatography and stored at -20 °C for months. The bipyrrole **6.6** was subjected to Vilsmeier Haack formylation to provide the dialdehyde **6.7** in 94% yields, whose structure was further confirmed by X-ray crystallography (Figure 6.1). Finally, McMurry coupling of **6.7** with Zn/$TiCl_4$ in presence of CuCl, under reflux condition provided the

dihydroporphycene as the coupling product, which undergoes slow oxidation under ambient condition, probably indicating the electron deficient nature of the desired porphycene **6.1**. Therefore, after McMurry coupling followed by usual workup, the resultant yellow orange residue was dissolved in $CHCl_3$ and subjected to oxidation with 2,3-dichloro-5,6-dicyano-1,4-benzoquinone (DDQ) at room temperature, which finally led to the desired porphycene **6.1** in 17% yield. The freebase porphycene was further converted to its Zn(II) and Ni(II) complexes in 68 and 67% yield, respectively. Notably, the **Zn(6.1)** complex undergoes demetallation slowly in solution indicating its labile nature. All the compounds were characterized by standard spectroscopic techniques.

6.3.2 ^{1}H NMR studies

The ^{1}H NMR spectrum of **6.1** displays meso protons at 9.68 ppm, which is about 0.31 ppm downfield shifted compared to porphycene **6.4** (9.37 ppm) and this trend is again observed in case of the imino protons resonating at 2.98 ppm for **6.1**, which is 0.65 ppm downfield shifted compare to **6.4** (2.33 ppm), indicating the electron deficient nature of former.[4]

6.3.3 Solid state structural studies

The solid state structure of porphycene **6.1** could also be unequivocally elucidated by single crystal X-ray diffraction analysis (Figure 6.1). It clearly reveals replacement of eight oxygen atoms of **6.3** with relatively bulkier sulphur atoms, leads to twisting of pyrrole moieties along Cα-Cα´ axis of bipyrrole units in molecular structure. Similar to porphycene **6.4**, saddle

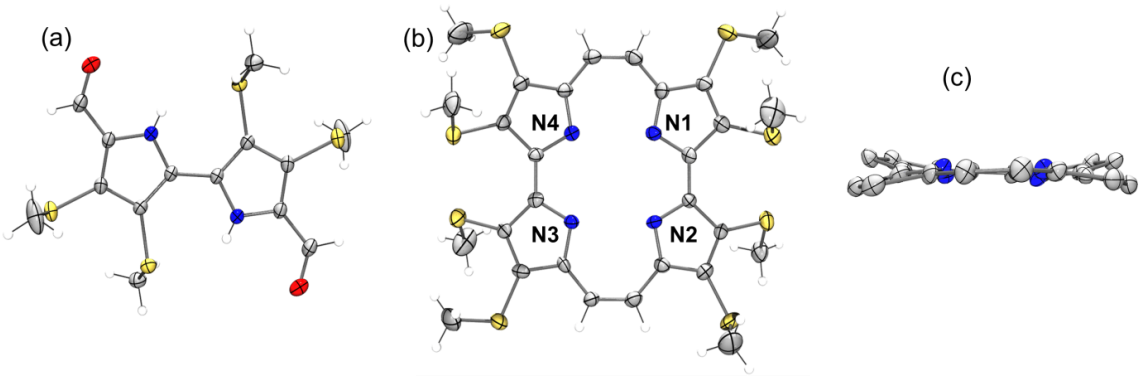

Figure 6.1 Molecular structure of (a) **6.7**, (b) front view of **6.1** and (c) side view of **6.1** drawn in 35% probability level. In side view, all hydrogen atoms and methylthio groups were removed for clarity. Colour code: C, grey; H, white; N, blue; O, red; S, yellow.

distorted structure is observed for **6.1**, arising from lone pair-lone pair repulsion between adjacent bulkier sulphur atoms at 3,6- and 13,16-positions. The average torsion angle

between the two adjacent pyrroles along the Cα-Cα′ axis of bipyrrole is 24.10°, which is less compared to porphycene **6.4** (29.50°).[4] The degree of distortion can also be measured by displacement of β-C's of the pyrrolic moieties from the mean plane drawn through four core nitrogens and the maximum displacement observed in **6.1** is 0.544 Å, which is again much lower compared to that of **6.4** (0.976 Å).[4] These data clearly reflected lesser nonbonding interaction between the SMe substituents at the inner β-positions compared to the CF_3 units in **6.4**, hence making it relatively more planar. The core of porphycene **6.1** exhibits near square type geometry like other β-octa-substituted analogues.

6.3.4 Absorption and emission properties

The UV-Vis absorption spectrum (Figure 6.2) of porphycene **6.1** in $CHCl_3$ reveals striking difference from those of other β-octa-substituted porphycenes reported so far, consisting of a split Soret band (i.e. the shoulder at higher-energy side more obvious) with absorption maxima at 411 nm and three merged Q-bands. Moreover, unlike other similarly substituted porphycenes, the band at the middle of the three sub-structure of the Q-band shows the

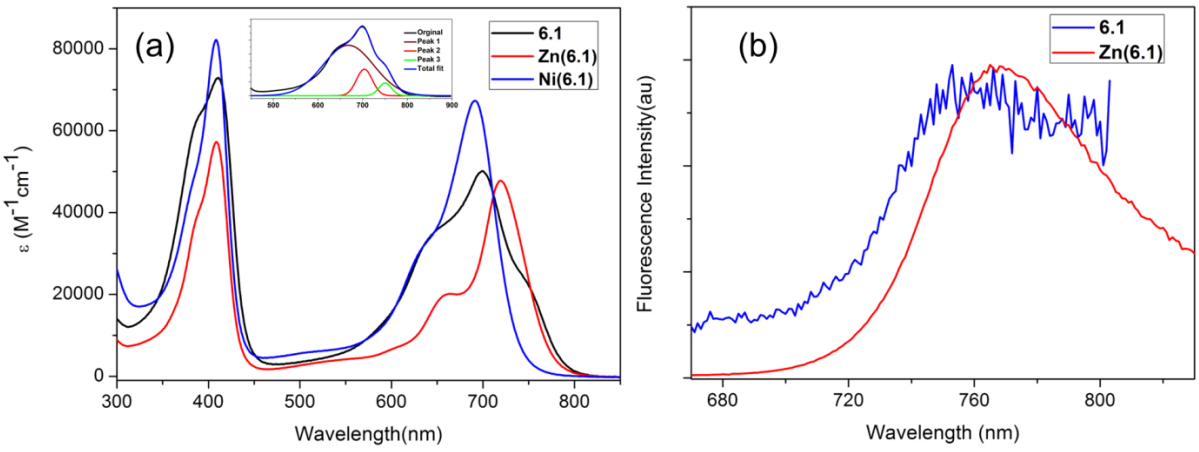

Figure 6.2 (a) The UV-Vis absorption spectra of **6.1**, **Zn(6.1)** and **Ni(6.1)** and (b) Fluorescence spectra of **6.1** and **Zn(6.1)**. In figure (a) inset contains the Gaussian deconvolution of the Q-bands of **6.1** in $CHCl_3$ at 25 °C.

maximum intensity. This unusual type of Q-bands originates from the rhodifying effect induced by eight electron-deficient methylthio groups.[9a] The lowest-energy band appeared at ~750 nm (deconvoluted; shown in the inset of Figure 6.2a), which is ~26 nm red shifted compared to porphycenes **6.4**, clearly indicating the more electron deficient nature of **6.1**.[4] Further, macrocycle **6.1** displays a very intense Q-band (Q-band/Soret maxima 0.69), which has not been noticed previously in other freebase porphycenes. This highlights the unique substituent effect in **6.1** with all electron deficient substituents and may partly be attributed to

Table 6.1 Photophysical properties of porphycenes in chloroform at 25 °C

Porphycenes	UV-Vis λ_{max} nm (log ε)	Emission λ_{max} (nm)
6.1	411 (4.86), 699 (4.70)	754
Zn(6.1)	409 (4.75), 664 (4.30), 719 (4.68)	765
Ni(6.1)	408 (4.91), 691 (4.83)	---

S···S interactions. Notably, the Soret band of **6.1** is red shifted compared to other β-octasubstituted porphycenes, again reflecting on its electron deficient behaviour.[4,8,11] The UV-Vis absorption spectra of **Zn(6.1)** and **Ni(6.1)** display slightly blue shifted Soret bands (409 and 408 nm, respectively) compared to **6.1** and blue shifted Q-bands (719 and 691 nm, respectively). Similar to freebase porphycene **6.1**, intense Q-bands were also observed for both **Zn(6.1)** and **Ni(6.1)** (Q-band /Soret maxima for **Zn(6.1)**, 0.83 and **Ni(6.1)**, 0.82). Porphycene **6.1** and its Zn(II) derivative display very weak emission with maxima at 754 and 765 nm, respectively (Figure 6.2). Although all these molecules possess intense absorption in the NIR region, only **Zn(6.1)** could convert molecular oxygen to reactive singlet oxygen in aerated toluene solution, albeit with very poor efficiency (ϕ_Δ 0.04), thereby indicating their inability to act as photosensitiser.

6.3.5 Two photon absorption studies

The two photon absorption studies were done in collaboration with Prof. Dongho Kim Group at Yonsei University, Korea. It has widely been established that the most important factor that contributes to the enhancement of two-photon absorption (TPA) is the extension of π-conjugation. Another effective factor that is proposed to enhance TPA is charge-transfer interactions.[12] In this context, β-octaethyl, β-octamethoxy and β-octamethylthio analogues were employed to examine the effect of charge-transfer interactions on TPA property[13] by the Z-scan technique, in toluene from 1200 to 1500 nm, where the contribution from OPA is negligible (Figure 6.3-4). The TPA profiles revealed spectral features that are in good agreement with the band structure of the lowest one-photon absorption band. The maximum TPA cross-sections of porphycenes **6.1**, **6.2** and **6.3** were measured to be 370, 110 and 230 GM at 1400, 1300 and 1200 nm, respectively. The maximum TPA cross-sections of their corresponding Ni(II)complexes i.e. **Ni(6.1)**, **Ni(6.2)** and **Ni(6.3)**, were measured to be 270, 130 and 210 GM at 1400, 1200 and 1200 nm, respectively. The octamethoxyporphycenes **6.3** and **Ni(6.3)** display larger TPA cross-section compared to corresponding octaethyl analogues, probably owing to facile internal charge transfer ability of methoxy groups. On the other

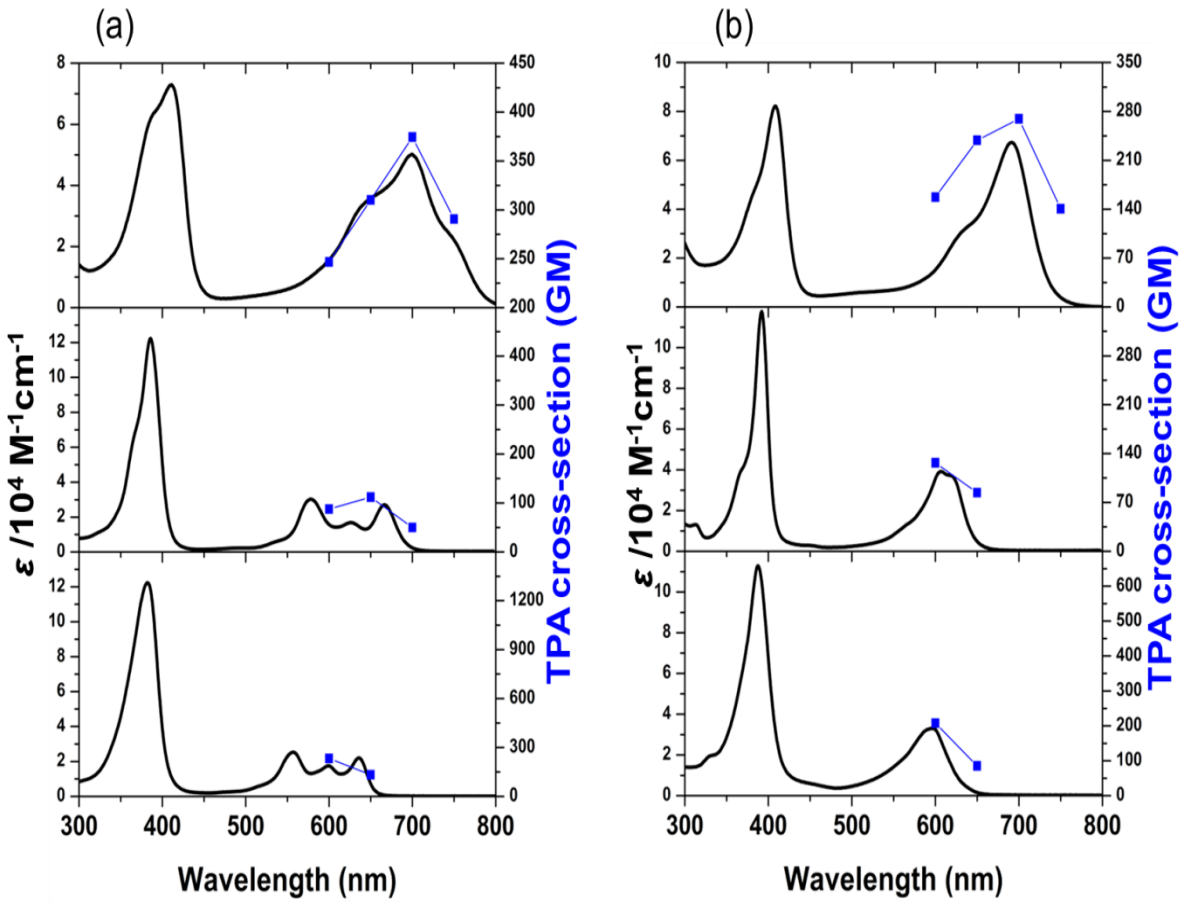

Figure 6.3 OPA (solid line) and TPA (point line) of (a) freebase porphycenes and (b) their corresponding Ni(II)-complexes: **6.1**, **Ni(6.1)** (top), **6.2**, **Ni(6.2)** (middle) and **6.3**, **Ni(6.3)** (bottom) in toluene. The TPA spectra are displayed at $\lambda_{ex}/2$ for comparison with the OPA spectra.

hand, owing to their electron-deficient character porphycenes **6.1** and its Ni(II)complex are expected to possess smaller TPA cross-sections than other porphycene analogues.[14] However, these electron deficient molecules (**6.1** and **Ni(6.1)**) display larger TPA cross-section than other porphycene analogues. It is known that the number of π-electrons and/or the molecular geometry associated with the static and dynamic polarizability are the determining factors in controlling NLO response in simple molecules.[15] Therefore, these unexpected results may be attributed to the heavy atom effect of the S atoms in the methylthio substituents and their greater polarizability in the excited state.[16] Notably, all studied octasubstituted porphycenes have much higher TPA cross-section values compare to previously reported 2,7,12,17-tetraphenylporphycene (14 GM at 1100 nm) at similar wavelength region.[3c]

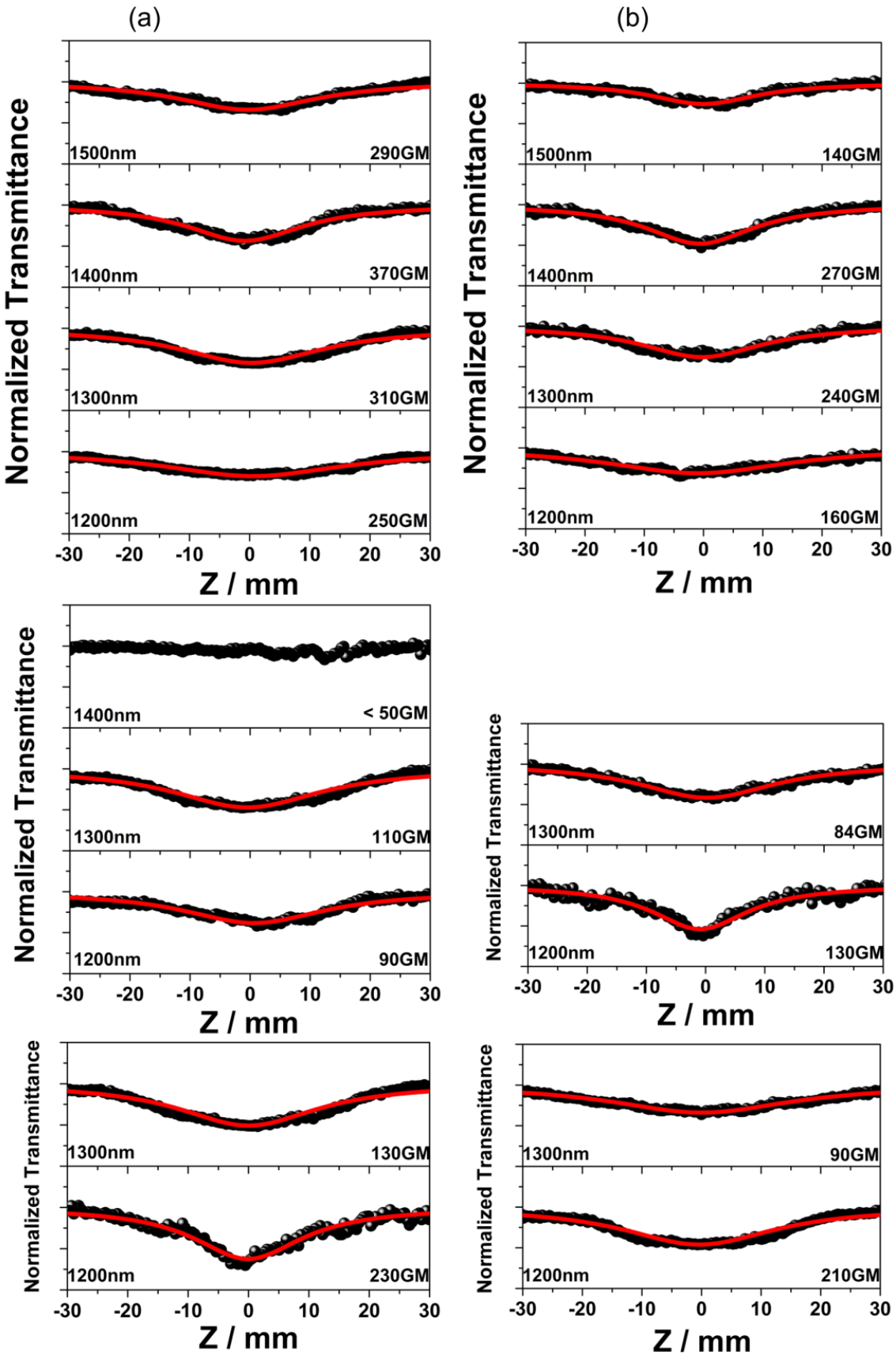

Figure 6.4 (a) Open aperture Z-scan curve of **6.1** (top), **6.2** (middle) and **6.3** (bottom). (b) Open aperture Z-scan curve of **Ni(6.1)** (top), **Ni(6.2)** (middle) and **Ni(6.3)** (bottom).

6.3.6 Femto second transient absorption studies

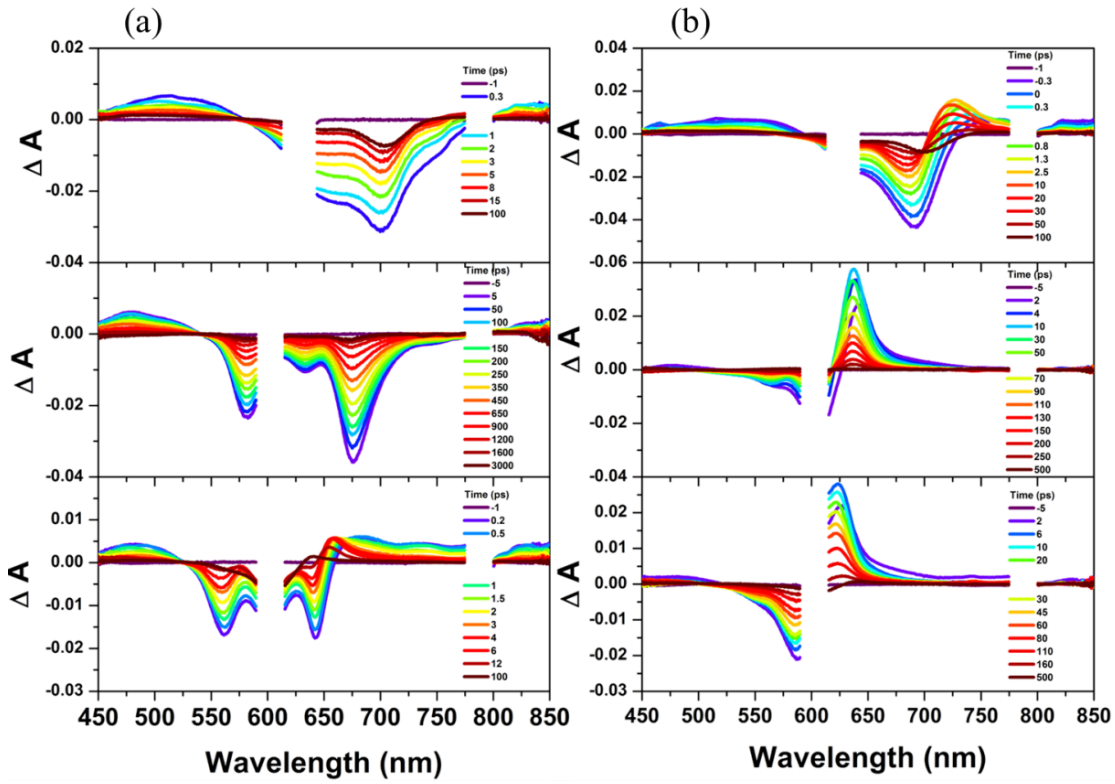

Figure 6.5 TA spectra of (a) **6.1** (top), **6.2** (middle) and **6.3** (bottom), and (b) **Ni(6.1)** (top), **Ni(6.2)** (middle), and **Ni(6.3)** (bottom) in toluene obtained with photoexcitation at 630 nm (top), 600 nm (middle) and 600 nm (bottom), respectively.

The excited-state dynamics of porphycenes **6.1**, **6.2**, **6.3**, and their Ni(II) complexes were probed via femtosecond transient absorption (TA) study (Figure 6.5-7), done in collaboration with Prof. Kim Group. The TA spectra of these compounds exhibited ground state bleaching signals whose spectral features correspond to their ground-state absorption bands. In the case of porphycene **6.2**, we could observe a single exponential decay time component (450 ps) that might be ascribed to the singlet excited state lifetime. In contrast to β-octaethylporphycene **6.2**, we could observe an additional long time residual in **6.1** and **6.3**, which might be ascribed to the excited triplet state. Therefore, we can assume that the fast time component of **6.1** (3.5 ps) and **6.3** (2.0 ps) might be originating from the combination of the intersystem crossing from the singlet excited-state to the triplet excited-state and relaxation of singlet excited-state. In the Ni(II) porphycenes, we can find a slight difference in the excited-state absorptions. As compared to the freebase porphycenes, the Ni(II)-derivatives show prominent excited state absorption bands at 700-750 nm (**Ni(6.1)**) and 600-650 nm (**Ni(6.2)** and **Ni(6.3)**). This particular feature most likely comes from the presence of a low-lying metal

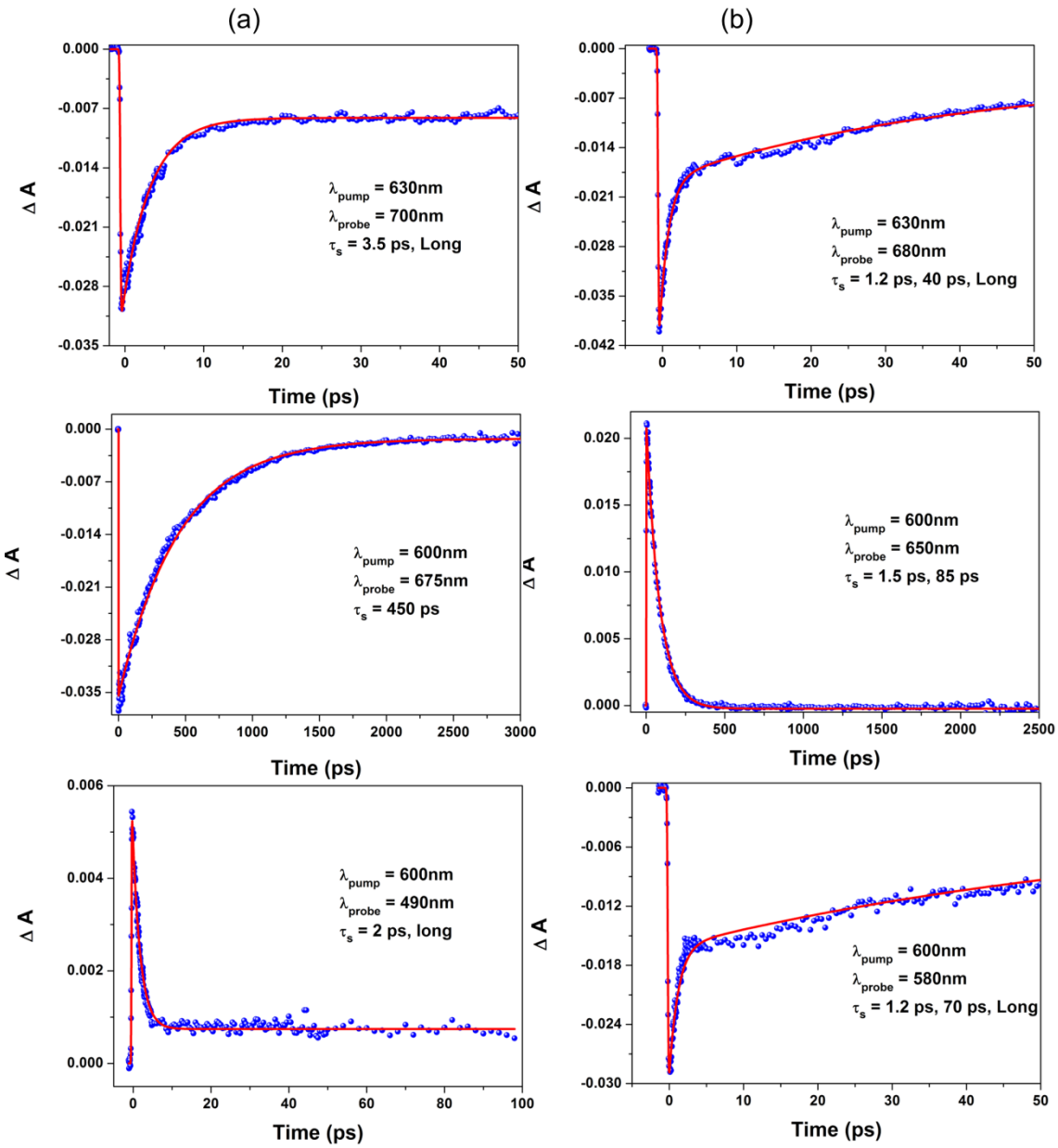

Figure 6.6 (a) The decay profiles of **6.1** (top), **6.2** (middle) and **6.3** (bottom). (b) The decay profiles of **Ni(6.1)** (top), **Ni(6.2)** (middle) and **Ni(6.3)** (bottom).

excited (d,d) state in Ni(II) complexes.[17] In the case of porphycene **Ni(6.2)**, the two time components (1.5 ps and 85 ps) can be explained by the transition from the high-lying singlet exited-state to the low-lying metal excited (d,d) state and relaxation from the low-lying metal excited (d,d) state to the singlet ground state. From this analysis, we can identify the origin of dynamics in the **Ni(6.1)** and **Ni(6.3)**, which possess two time components and long time residual in the decay profiles. In analogy to **Ni(6.2)**, we can assume that the fast time component of 1.2 ps might be ascribed to the transition to the low-lying metal excited state in **Ni(6.1)** and **Ni(6.3)**, whereas their corresponding 40 and 70 ps time components can be

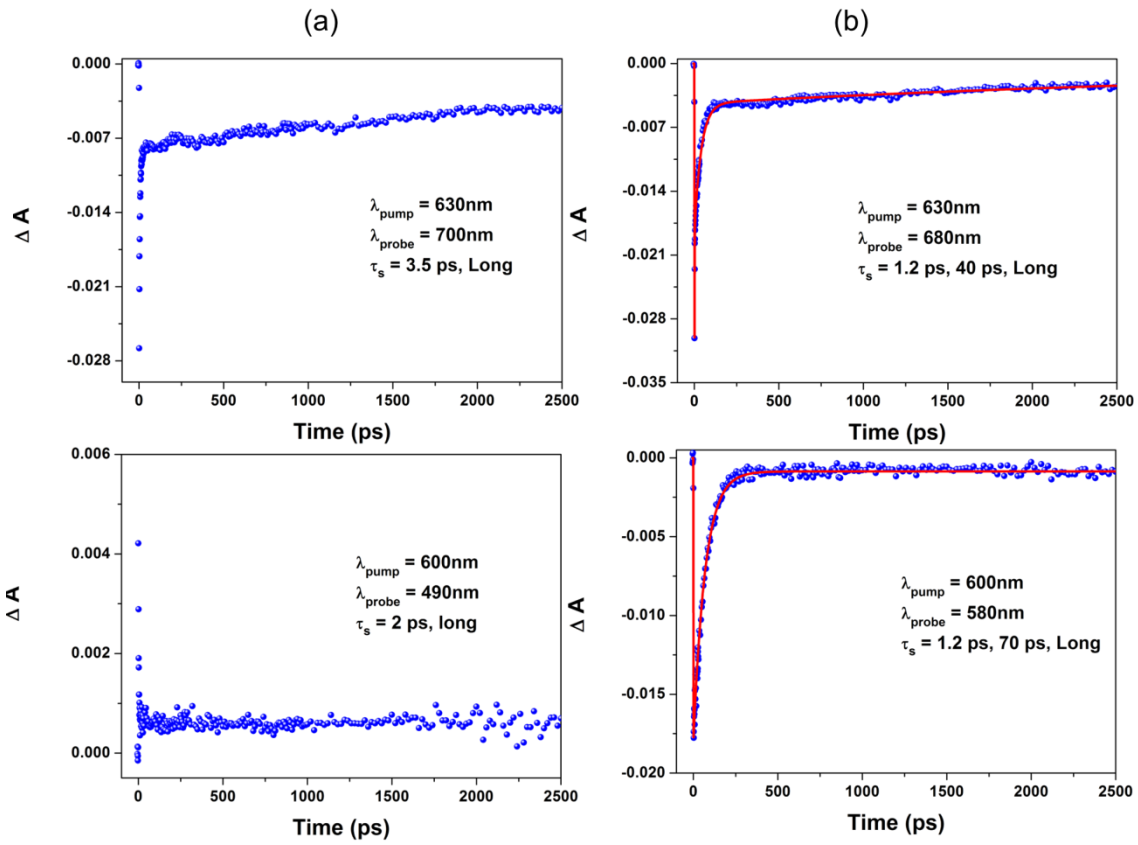

Figure 6.7 (a) The decay profiles of **6.1** (top) and **6.3** (bottom) on long delay. (b) The decay profiles of **Ni(6.1)** (top) and **Ni(6.3)** (bottom) on long delay.

explained by the relaxation from the low-lying metal excited (d,d) state to the singlet ground state. Additionally, the long time residual in the **Ni(6.1)** and **Ni(6.3)** might be ascribed to the excited triplet state, similar to **6.1** and **6.3**.

6.3.7 Electrochemical studies

The redox potential of porphycene **6.1** and its metallo-derivatives were determined by cyclic voltammetry (CV) and differential pulse voltammetry (DPV) techniques in dichloromethane solution, using tetrabutylammonium hexafluorophosphate as supporting electrolyte (Figure 6.8 and table 6.1). All porphycenes displays typical two reversible or/and quasi-reversible one electron reductions and two reversible or/and quasi-reversible one electron oxidations. The porphycene **6.1** shows first reduction potential at -0.43 V and first oxidation potential at +1.09 V, which is 0.68 V and 0.31 V more positive respectively, compare to analogous **6.3** clearly revealing its more electron deficient nature.[8] Also, there is a drastic change in first reduction potential compare to the first oxidation potential, upon introduction of electron withdrawing substituents, indicating greater stabilization of its LUMO. All metal complexes

Table 6.1 Redox potentials (in V vs SCE) for porphycenes and their M(II) complexes

Porphycenes	Reduction	Oxidation	HOMO-LUMO (V)
6.1	-0.54[a], -0.43[a]	+1.09[a], +1.25[a]	1.52
Zn(6.1)	-0.93[a], -0.68	+0.90 [a], +0.98[a]	1.58
Ni(6.1)	-0.68[a], -0.55[a]	+1.01, +1.30	1.56
6.4[b]	-1.29, -1.11	+0.78, +1.15	1.89
Zn(6.4)[b]	-1.38, -1.13	+0.60, +0.75	1.73
Ni(6.4)[b]	-1.45, -1.19	+0.71, +1.17	1.90

[a] measured by DPV and [b] taken from ref 8.

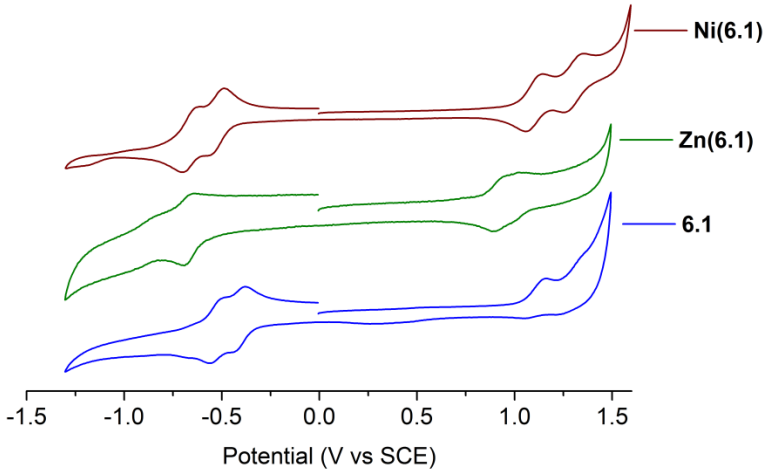

Figure 6.8 Cyclic voltammograms of **6.1**, **Zn(6.1)**, and **Ni(6.1)** in dichloromethane at 25 °C (scan rate 50 mV/s).

of porphycene **6.1** display two reversible oxidation and two reversible reduction potentials. Similar to freebase porphycene **6.1,** analogous trend was observed in oxidation and reduction potentials for **Zn(6.1)** and **Ni(6.1)** complexes when compared to their corresponding octamethoxy analogues (Table 1).[8] The HOMO-LUMO gap (ΔE) for porphycene **6.1** is 1.52 V, which is 0.37 V lower compare to **6.3** clearly reflecting in the observed red shifted low energy band in UV-Vis spectrum.[8] The ΔE for porphycene **6.1** is marginally higher (0.08 V) compare to that of porphycene **6.4,** which again can be attributed to its lesser degree of distortion than **6.4**.[4]

6.3.8 Synthesis of unsubstituted porphycene

Porphycene **6.1** could be further converted to the parent unsubstituted porphycene **6.8** (Scheme 6.2), via deprotection using Raney Ni®/H_2 at room temperature, followed by oxidation with DDQ, in 61% yield. Synthesis of this porphycene was initially reported by Vogel and coworker and suffers from very poor yield.[1] Whereas, recently only Waluk and

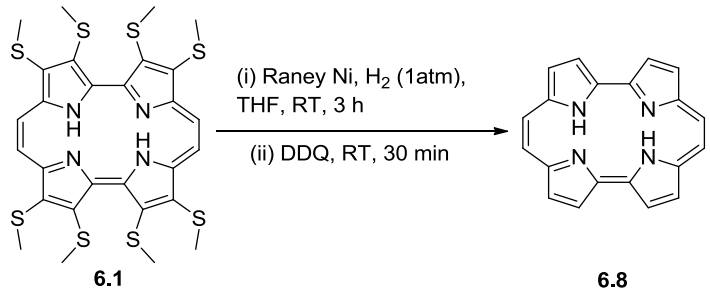

Scheme 6.2 Synthesis of unsubstituted porphycene **6.8**

coworkers could improve the yield (65%) by deprotection of tert-butyl groups of 2,7,12,17-tetra-tert-butylporphycene upon heating at very high temperature (200 °C) under strong acidic condition.[18]

6.4 Conclusion

In conclusion, we have synthesized the first porphycene endowed with all electron-deficient substituents at their β-positions, namely octamethylthioporphycene efficiently by employing oxidative coupling of 3,4-di(methylthio)pyrrole. Current methodology, using $BF_3.OEt_2$ we can enhance the oxidative power of PIFA to enable efficient synthesis of electron deficient bipyrroles, directly from their constituent pyrroles in single step. The third order nonlinear optical studies for freebase porphycenes and their Ni(II) complexes were done for β-octasubstituted porphycenes and revealed that the modulation of substituent at periphery varies NLO response and highest TPA cross-section was observed for porphycene **6.1** (370 GM at 1400 nm). Further, owing to its mild deprotection ability, methylthio groups can be employed towards the synthesis of novel functionalized porphycenes and currently our efforts are underway in this direction.

6.5 Experimental details

3,3',4,4'-tetrakis(methylthio)-2,2'-bipyrrole (6.6): To a stirred solution of 3,4-di(methylthio)pyrrole (**6.5)** (800 mg, 5.02 mmol) in dry CH_2Cl_2 (80 mL), PIFA (1.08 g, 2.51 mmol) and $BF_3.OEt_2$ (620 μL, 5.02 mmol) were quickly added at –78 °C under nitrogen. The reaction mixture was stirred for 3 h, while the temperature was maintained below – 40 °C. Subsequently, saturated aqueous $NaHCO_3$ (ca. 100 mL) was added to quench the reaction, and then stirred for an additional 10 min at ambient temperature. The organic layer was separated and the aqueous phase was extracted with CH_2Cl_2. The combined organic extract was dried with anhydrous Na_2SO_4 and evaporated to dryness under reduced pressure. The

crude reaction mixture was purified by silica gel column using EtOAc/hexane (1:9) as eluent to obtain the desired **6.6** (272 mg) as white crystalline solid. Yield: 34%; m.p.: 170.7 °C; ^{1}H NMR (400 MHz, $CDCl_3$), δ (ppm): 10.99 (br s, 2H), 6.84 (d, 2H, *J* = 2.8 Hz), 2.41 (s, 6H), 2.37 (s, 6H); ^{13}C NMR (100 MHz, $CDCl_3$), δ (ppm):127.74, 121.10, 119.51, 110.79, 20.67, 19.94; HRMS (ESI+): m/z: calculated for $C_{12}H_{17}N_2S_4$ ($M+H^+$): 317.0269; found: 317.0273.

3,3',4,4'-tetrakis(methylthio)-[2,2'-bipyrrole]-5,5'-dialdehyde (6.7): 3,3',4,4'-tetrakis-(methylthio)-2,2'-bipyrrole (**6.6**) (500 mg, 1.58 mmol) in dry DCE (15 mL) was rapidly added to ice cooled stirred Vilsmeier-Haack formylating mixture prepared from freshly distilled $POCl_3$ (737 µL, 7.91 mmol) and dry DMF (700 µL, 8.69 mmol) in dry DCE (10 mL) under nitrogen atmosphere. After addition was over ice-bath was replaced with oil bath and the reaction mixture was refluxed for 4 h. Then the reaction mixture was cooled on ice bath and sat. NaOAc (3.24 g, 39.5 mmol) in water (20 mL) added carefully and refluxed the reaction mixture for additional 2 h, resulting in precipitation of the product **6.7** as yellow fibrous crystalline solid. After cooling to room temperature, the reaction mixture was filtered, washed with water to leave the desired compound as yellow crystalline solid and some additional compound was also obtained from the evaporation of DCE layer under reduced pressure. Yield: 552 mg (93%); m.p.: 264 °C; IR (neat): ν (cm^{-1}) 3266, 1644; ^{1}H NMR (400 MHz, $CDCl_3$), δ (ppm): 11.81 (br s, 2H), 9.91 (s, 2H), 2.53 (s, 6H), 2.47 (s, 6H); ^{13}C NMR (100 MHz, $CDCl_3$), δ (ppm): 179.00, 132.95, 132.79, 130.45, 119.15, 20.81, 20.28; UV-Vis data in $CHCl_3$, λ_{max} nm (log ε): 370 (4.32), 388 (4.38); Fluorescence in $CHCl_3$ λ_{max} nm : 450; Fluorescence quantum yield in $CHCl_3$ (ϕ_f): 0.08; HRMS (ESI+): m/z: calculated for $C_{14}H_{17}N_2O_2S_4$ ($M+H^+$): 373.0167; found: 373.0177. Elemental analysis Calcd for $C_{14}H_{17}N_2O_2S_4$: C, 45.13; H, 4.33; N, 7.52. Found: C, 45.26; H, 4.26; N, 7.58.

2,3,6,7,12,13,16,17-octa(methylthio)porphycene (6.1): To a slurry of low-valent titanium reagent, generated by reduction of titanium tetrachloride (1.48 mL, 13.5 mmol) in dry THF (180 mL) with activated zinc (1.77 g) and CuCl (268 mg, 1.35 mmol) by refluxing for 3 h, a solution of **6.8** (200 mg, 0.54 mmol) in dry THF (120 mL) was added dropwise slowly over 2 h, under reflux condition with vigorous stirring. The reaction mixture was heated under reflux for an additional 1 h and then hydrolyzed by slow addition of 10% aqueous sodium carbonate (ca. 100 mL) to the ice cooled reaction mixture and filtered through celite to remove the excess metal, washed with chloroform. The organic layer was separated and was evaporated to dryness under reduced pressure. Resulting crude reaction mixture was dissolved in DCM

(50 mL), washed with water, organic layer was passed through anhydrous sodium sulphate and evaporated to dryness under reduced pressure. Unoxidised crude reaction mixture was dissolved in $CHCl_3$ (100 mL), DDQ (62 mg, 0.27 mmol) was added to it and stirred at room temperature for 1 h. Then, solvent was evaporated under reduced pressure. The crude reaction mixture was purified by silica gel column chromatography using $CHCl_3$ as eluent and the greenish-blue fraction was collected to yield the desired porphycene **6.1** (31 mg) as blue purple crystalline solid. Yield: 17%; m.p.: > 300 °C; ^{1}H NMR (400 MHz, $CDCl_3$), δ (ppm): 9.68 (s, 4H), 3.08 (s, 12H), 2.98 (s, 2H), 2.65 (s, 12H); ^{13}C NMR (100 MHz, $CDCl_3$), δ (ppm): 144.94, 141.70, 138.63, 135.46, 114.07, 20.08, 20.01; UV-Vis data in $CHCl_3$, λ_{max} nm (log ε): 411 (4.86), 699 (4.70); HRMS (ESI+): m/z: calculated for $C_{28}H_{31}N_4S_8$ ($M+H^+$): 679.0309; found: 679.0313. Elemental analysis Calcd for $C_{28}H_{30}N_4S_8$: C, 49.52; H, 4.45; N, 8.25. Found: C, 49.63; H, 4.51; N, 8.16.

Zn(II) 2,3,6,7,12,13,16,17-octa(methylthio)porphycene (Zn(6.1)): To a stirred solution of **6.1** (10 mg, 0.015 mmol) in chloroform (10 mL) under nitrogen atmosphere, $Zn(OAc)_2.2H_2O$ (65 mg, 0.30 mmol) in methanol (10 mL) was added and reaction mixture was refluxed for 4 h. Then the reaction mixture was cooled and evaporated to dryness, re-dissolved in chloroform, washed with water, and the $CHCl_3$ layer was passed through anhydrous Na_2SO_4 and evaporated under reduce pressure. Crude product was finally purified by activated neutral alumina flash column using chloroform/ methanol (99:1) as eluent to obtain **Zn(6.1)** (7.6 mg) as purple solid. Yield: 68%; m.p.: 99 °C; ^{1}H NMR (400 MHz, $CDCl_3$), δ (ppm): 9.94 (s, 4H), 3.01 (s, 12H), 2.81 (s, 12H); ^{13}C NMR (125 MHz, $CDCl_3$), δ (ppm):145.65, 145.58, 143.02, 113.78, 20.88, 20.74; UV-Vis data, λ_{max} nm (log ε): 409 (4.75), 664 (4.30), 719 (4.68); HRMS (ESI+): m/z: calculated for $C_{28}H_{28}N_4S_8ZnNa$ ($M+Na^+$): 762.9263; found: 762.9268. Elemental analysis Calcd for $C_{28}H_{28}N_4S_8Zn$: C, 45.30; H, 3.80; N, 7.55. Found: C, 45.26; H, 3.72; N, 7.65.

Ni(II) 2,3,6,7,12,13,16,17-octa(methylthio)porphycene (Ni(6.1)): To a stirred solution of **6.1** (10 mg, 0.015 mmol), $Ni(acac)_2$ (77 mg, 0.30 mmol) in *o*-xylene (10 mL) was added and refluxed for 4 h. After reaction mixture was cooled to room temperature, *o*-xylene was evaporated under reduced pressure and crude compound was purified by silica gel column chromatography using chloroform/hexane (1:1) as eluent to obtain **Ni(6.1)** (7.3 mg) as purple crystalline solid. Yield: 67%; m.p.: 205.5 °C; ^{1}H NMR (400 MHz, $CDCl_3$), δ (ppm): 9.76 (s, 4H), 2.95 (s, 12H), 2.79 (s, 12H); ^{13}C NMR (125 MHz, $CDCl_3$), δ (ppm): 147.37, 146.58, 145.24, 135.26, 111.61, 21.19, 21.11; UV-Vis data, λ_{max} nm (log ε): 408 (4.91), 691 (4.83);

HRMS (ESI+): m/z: calculated for $C_{28}H_{28}N_4S_8NiNa$ ($M+Na^+$): 756.9325; found: 756.9339. Elemental analysis Calcd for $C_{28}H_{28}N_4S_8Ni$: C, 45.71; H, 3.84; N, 7.61. Found: C, 45.86; H, 3.81; N, 7.73.

Porphycene (6.8): Porphycene **6.1** (5 mg, 0.0073 mmol) and Raney Ni® (~500 mg, slurry in water) were taken in THF (10 mL) under hydrogen atmosphere (1 atm, hydrogen balloon). The reaction mixture was stirred for 3 h at room temperature. Subsequently, the reaction mixture was passed through celite and washed with chloroform (3 × 10 mL). Combined organic layer was passed through anhydrous Na_2SO_4 and taken in a conical flask; DDQ (5 mg, 0.0219 mmol) was added and stirred for additional 30 min. Then reaction mixture was evaporated under reduce pressure and purified by silica gel column chromatography by using EtOAc/hexane (1:9) as eluent to obtain the desired product porphycene **6.8** (1.4 mg) as blue purple crystalline solid. Yield: 61%; ^{1}H NMR (400 MHz, $CDCl_3$), δ (ppm): 9.84 (s, 4H), 9.68 (d, 4H, *J* = 3.2 Hz), 9.25 (d, 4H, *J* = 3.2 Hz), 3.17 (br s, 2H).

4.6 Crystallographic Details

Crystallographic data for **6.1** was collected on Oxford Gemini A Ultra diffractometer with dual source and Mo-Kα (λ = 0.71073 Å) radiation was used to collect the X-ray reflections of the crystal. Crystallographic data for **6.7** was collected on Oxford Gemini A Ultra diffractometer with dual source and Cu-Kα (λ = 0.71073 Å) radiation was used to collect the X-ray reflections of the crystal.

Pertinent crystallographic data collection and refinement parameter are shown in the following tables:

Crystal Data	6.7	6.1
CCDC No.	1052053	1052052
Formula unit	$C_{14}H_{16}N_2O_2S_4$	$C_{28}H_{28}N_4OS_8$
Formula Weight	372.53	693.02
Crystal system	Monoclinic	Monoclinic
T [K]	293(2)	293(2)
a [Å]	4.9180(19)	8.8402(17)
b [Å]	8.5807(4)	14.927(3)
c [Å]	19.8851(8)	23.777(5)
α [°]	90.00	90.00
β [°]	97.072(4)	96.92(2)
γ [°]	90.00	90.00
volume [$Å^3$]	832.76(6)	3114.9(11)
Space group	P 21/c	P 21/n
Z′	0.5	1
Z	2	4
D_{calc} [$g.cm^{-3}$]	1.486	1.478
μ/mm^{-1}	5.308	0.604
Reflns collected	2899	12561
Unique reflns	1577	5515
Obs. reflns	1465	2574
R(int)	0.0175	0.0800
R_1 [$I > 2\sigma(I)$],	0.0412(1465)	0.0752(2574)
wR_2	0.1119(1577)	0.1793(5515)
GOF	1.040	0.985

6.7 References

1. Vogel, E.; Kocher, M.; Schmickler, H.; Lex, J. *Angew. Chem. Int. Ed. Engl*. **1986**, *25*, 257.
2. (a) Stockert, J. C.; Cañete, M.; Juarranz, A.; Villanueva, A.; Horobin, R. W.; Borrell, J. I.; Teixidó, J.; Nonell, S. *Curr. Med. Chem*. **2007**, *14*, 997. (b) Sánchez-García, D.; Sessler, J. L. *Chem. Soc. Rev*. **2008**, *37*, 215.

3. (a) Sarma, T.; Panda, P. K.; Anusha, P. T.; Rao, S. V. *Org. Lett*. **2011**, *13*, 188. (b) Rao, S. V.; Prashant, T. S.; Swain, D.; Sarma, T.; Panda, P. K.; Tewari, S. P. *Chem. Phys. Lett*. **2011**, *514*, 98. (c) Arnbjerg, J.; Jiménez-Benzo, A.; Paterson, M. J.; Nonell, S.; Borell, J. I.; Christiansen, O.; Ogilby, P. R. *J. Am. Chem. Soc*. **2007**, *129*, 5188. (d) Kim, K. K.; Sung, Y. M.; Matsuo, T.; Hayashi, T.; Kim, D. *Chem. –Eur. J*. **2011**, *17*, 7882.
4. Hayashi, T.; Nakashima, Y.; Ito, K.; Ikegami, T.; Aritome, I.; Suzuki, A.; Hisaeda, Y. *Org. Lett*. **2003**, *5*, 2845.
5. Swain, D.; Rana, A.; Panda, P. K.; Rao, S. V. *Chem. Phys. Lett*. **2014**, *610-611*, 310.
6. (a) Thamyongkit, P.; Bhise, A. D.; Taniguchi, M.; Lindsey, J. S. *J. Org. Chem*. **2006**, *71*, 903. (b) Martinez-Gonzalez, M. R.; Urías-Benavides, A.; Alvarado-Martinez, E.; Lopez, J. C.; Gómez, A. M.; Rio, M. D.; Garcia, I.; Costela, A.; Bañuelos, J.; Arbeloa; T.; Arbeloa, I. L.; Peña-Carbrera, E. *Eur. J. Org. Chem*. **2014**, 5659. (c) Pan, F.; Shi, Z.-J. *ACS Catal*. **2014**, *4*, 280. (d) Higashino, T.; Rodríguez-Morgade, M. S.; Osuka, A.; Torres, T. *Chem. –Eur. J*. **2013**, *19*, 10353.
7. Vogel, E.; Koch, P.; Hou, X.-L.; Lex, J.; Lausmann, M.; Kisters, M.; Aukauloo, M. A.; Richard, P.; Guilard, R. *Angew. Chem., Int. Ed. Engl*. **1993**, *32*, 1600.
8. Rana, A.; Panda, P. K. *Org. Lett*. **2014**, *16*, 78.
9. (a) Sugiura, K.-i.; Kumar, M. R.; Chandrashekar, T. K.; Sakata, Y. *Chem. Lett*. **1997**, *26*, 291; (b) Sugiura, K.-i.; Ushiroda, K.; Johnson, M. T.; Miller, J. S.; Sakata, Y. *J. Mater. Chem*. **2000**, *10*, 2507.
10. Dohi, T.; Morimoto, K.; Maruyama, A.; Kita, Y. *Org. Lett*. **2006**, *8*, 2007.
11. Stępień, M.; Donnio, B.; Sessler, J. L. *Chem. –Eur. J*. **2007**, *13*, 6853.
12. (a) Kim, K. S.; Noh, S. B.; Katsuda, T.; Ito, S.; Osuka, A.; Kim, D. *Chem. Commun*. **2007**, *24*, 2479. (b) Albota, M.; Beljonne, D.; Brédas, J.-L.; Ehrlich, J. E.; Fu, J.-Y.; Heikal, A. A.; Hess, S. E.; Kogej, T.; Levin, M. D.; Marder, S. E.; McCord-Maughon, D.; Perry, J. W.; Röckel, H.; Rumi, M.; Subramaniam, G.; Webb, W. W.; Wu, X.-L.; Xu, C. *Science* **1998**, *281*, 1653.
13. Tanaka, T.; Lee, B. S.; Aratani, N.; Yoon, M.-C.; Kim, D.; Osuka, A. *Chem. –Eur. J*. **2011**, *17*, 14400.
14. Mori, H.; Tanaka, T.; Aratani, N.; Lee, B. S.; Kim, P.; Kim, D.; Osuka, A. *Chem. –Asian J*. **2012**, *7*, 1811.

15. Yoon, Z. S.; Kwon, J. H.; Yoon, M.-C.; Koh, M. K.; Noh, S. B.; Sessler, J. L.; Lee, J. T.; Seidel, D.; Aguilar, A.; Shimizu, S.; Suzuki, M.; Osuka, A.; Kim. D. *J. Am. Chem. Soc*. **2006**, *128*, 14128.
16. (a) Andreu, R.; Blesa, M. J.; Carrasquer, L.; Garín, J.; Orduna, J.; Villacampa, B.; Alcalá, R.; Casado, J.; Delgado, M. C. R.; Navarrete, L.; Allain, M. *J. Am. Chem. Soc*. **2005**, *127*, 8835. (b) Bui, T.-T.; Iordache, A.; Chen, Z.; Roznyatovsky, V. M.; Saint-Aman, E.; Lim, J. M.; Lee, B. S.; Ghosh, S.; Moutet, J.-C.; Sessler, J. L.; Kim, D.; Bucher, C. *Chem. –Eur. J*. **2012**, *18*, 5853. (c) Rath, H.; Prabhuraja, V.; Chandrashekar, T. K.; Nag, A.; Goswami, D.; Joshi, B. S. *Org. Lett*. **2006**, *8*, 2325.
17. Eom, H. S.; Jeoung, S. C.; Kim, D.; Ha, J.-H.; Kim, Y. R. *J. Phys. Chem. A* **1997**, *101*, 3661.
18. Urbańska, N.; Pietraszkiewicz, M.; Waluk, J. *J. Porphyrins Phthalocyanines* **2007**, *11*, 596.

6.8 Representative NMR spectra

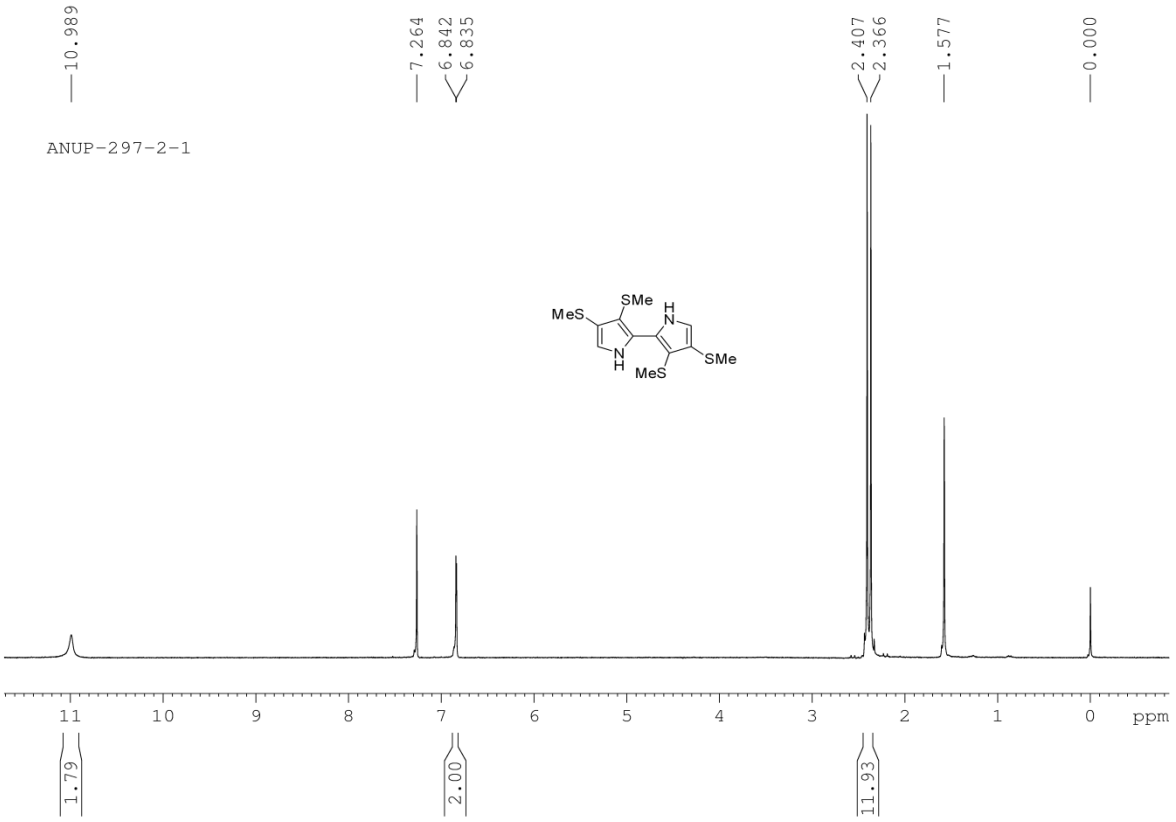

Figure 6.9 ^{1}H NMR spectrum of **6.6** in $CDCl_3$.

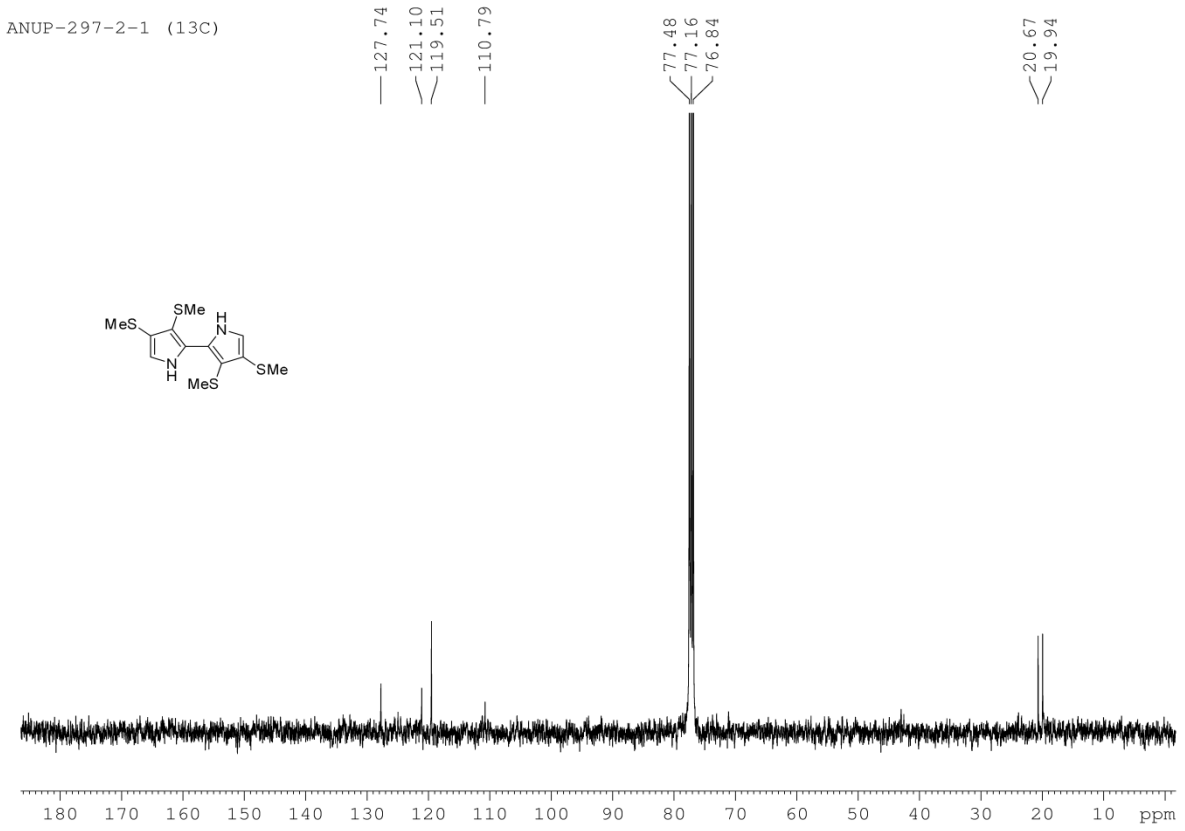

Figure 6.10 ^{13}C NMR spectrum of **6.6** in $CDCl_3$.

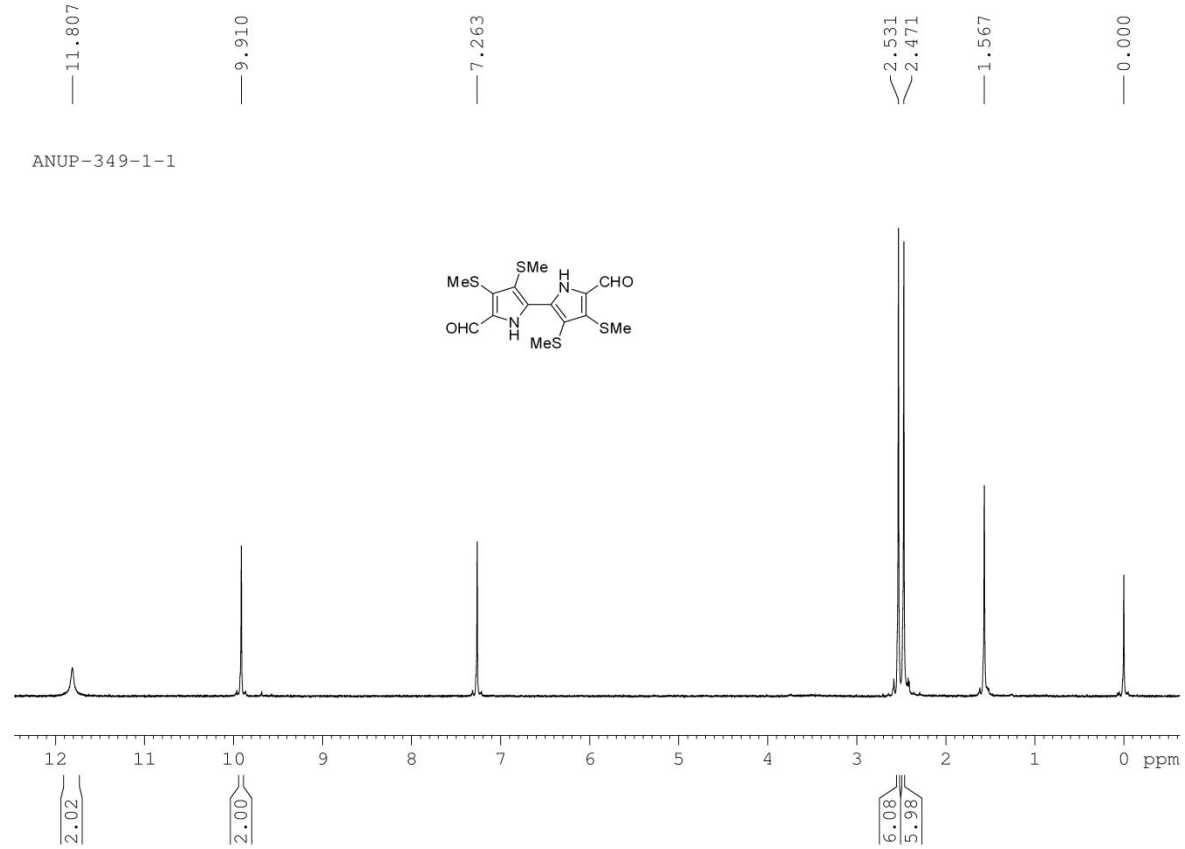

Figure 6.11 ^{1}H NMR spectrum of **6.7** in $CDCl_3$.

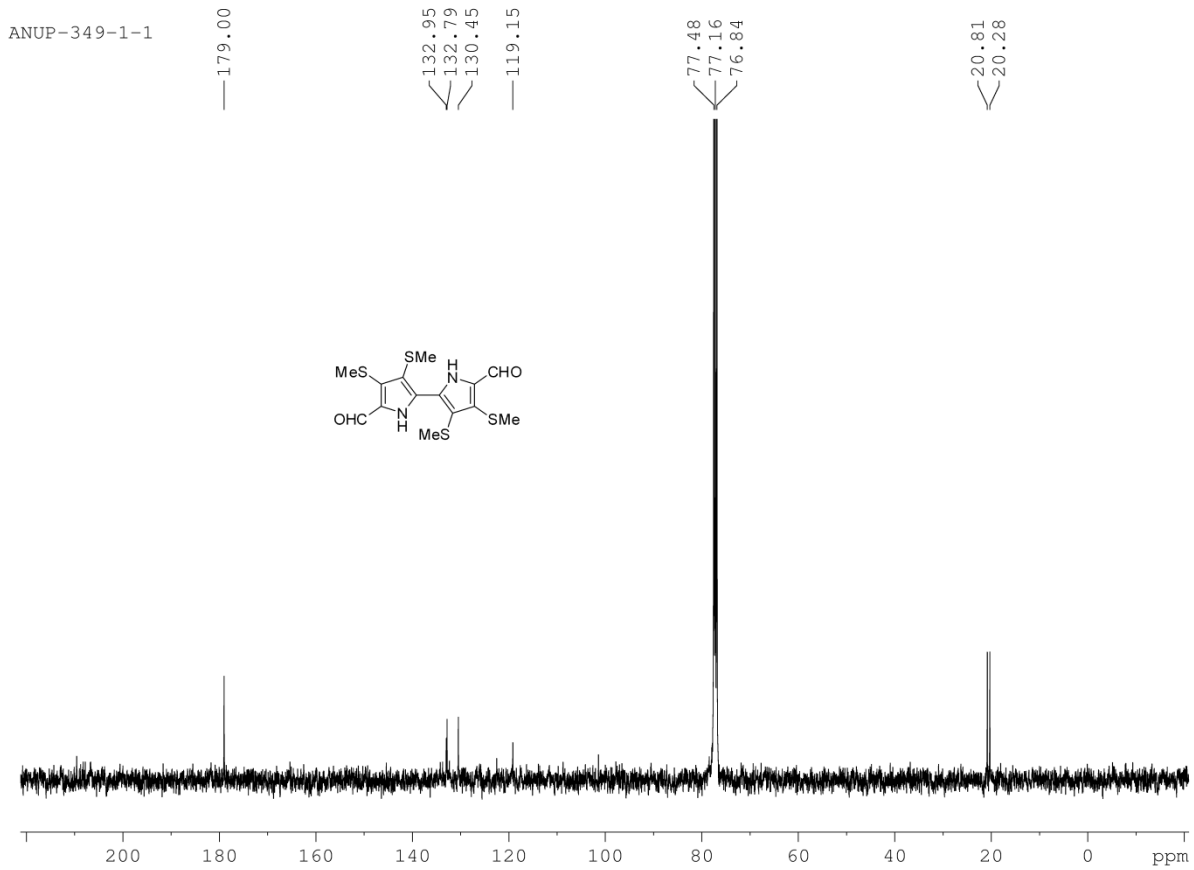

Figure 6.12 ^{13}C NMR spectrum of **6.7** in $CDCl_3$.

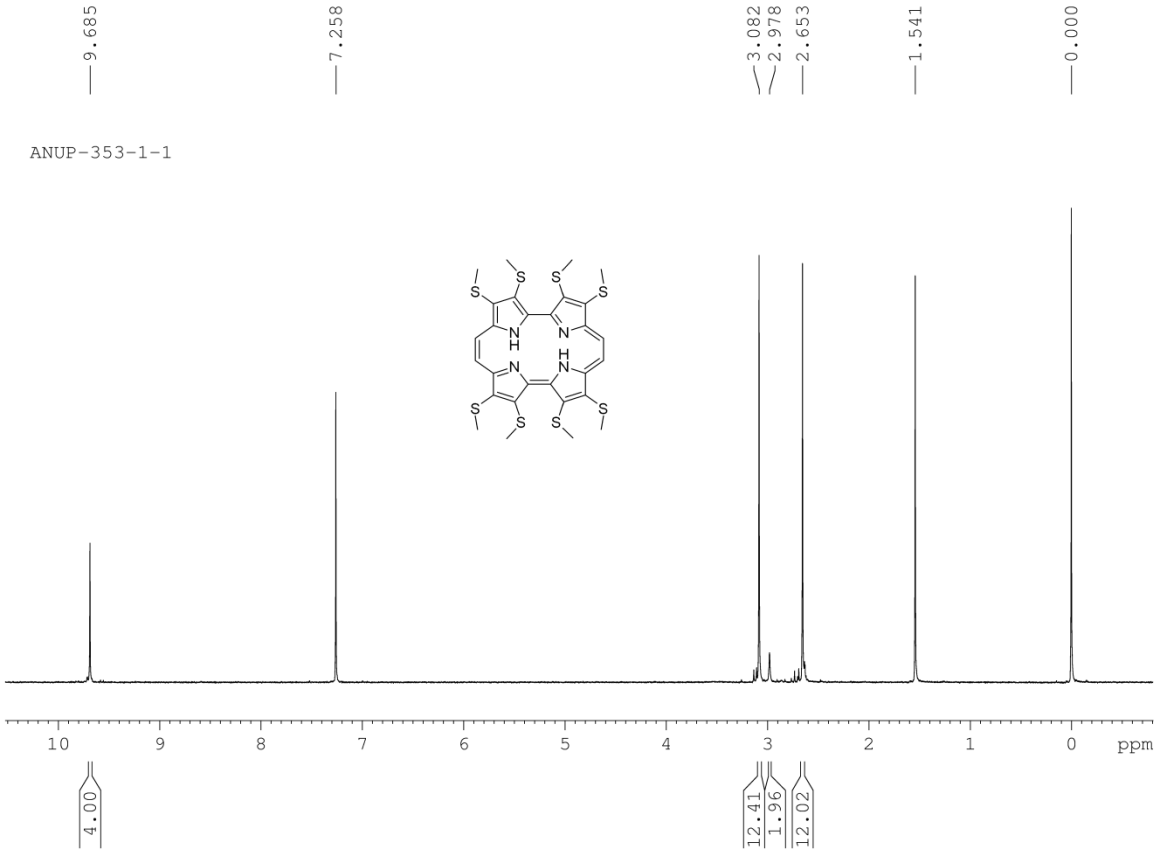

Figure 6.13 ^{1}H NMR spectrum of **6.1** in $CDCl_3$.

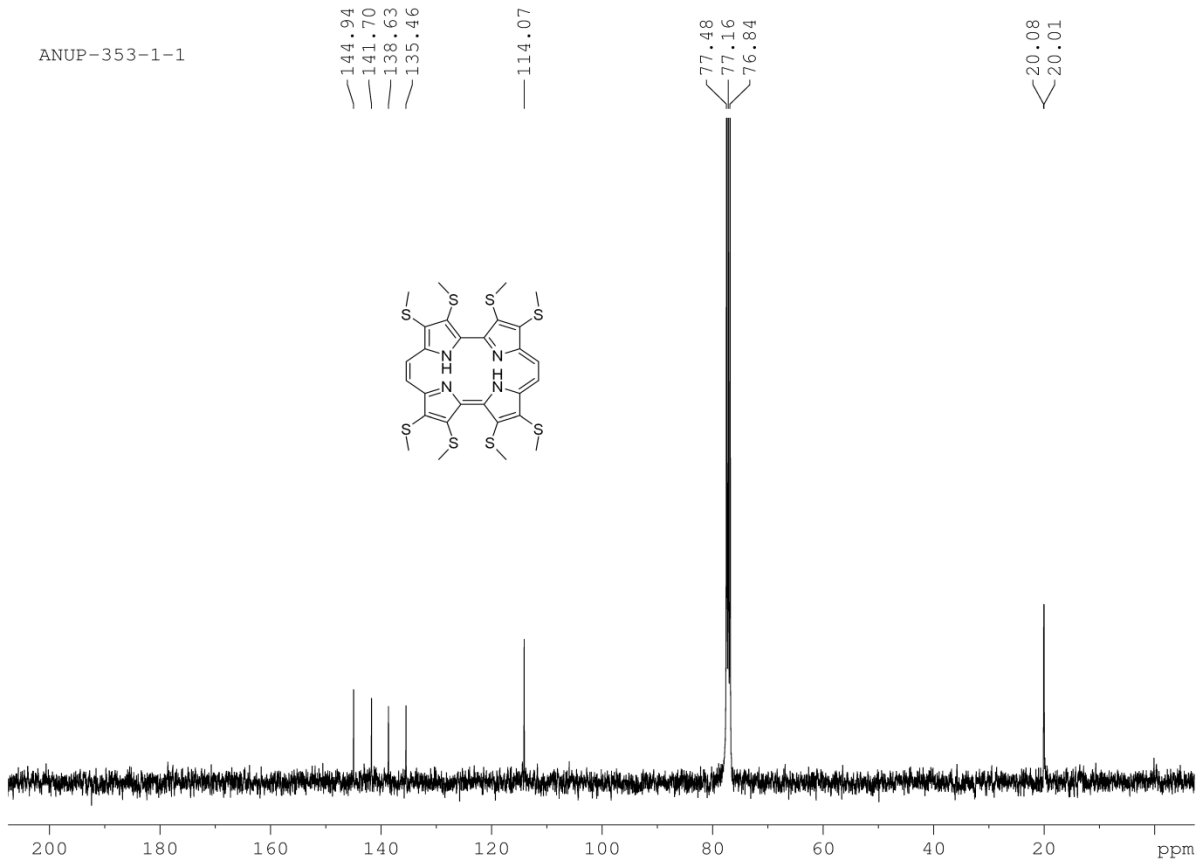

Figure 6.14 ^{13}C NMR spectrum of **6.1** in $CDCl_3$.

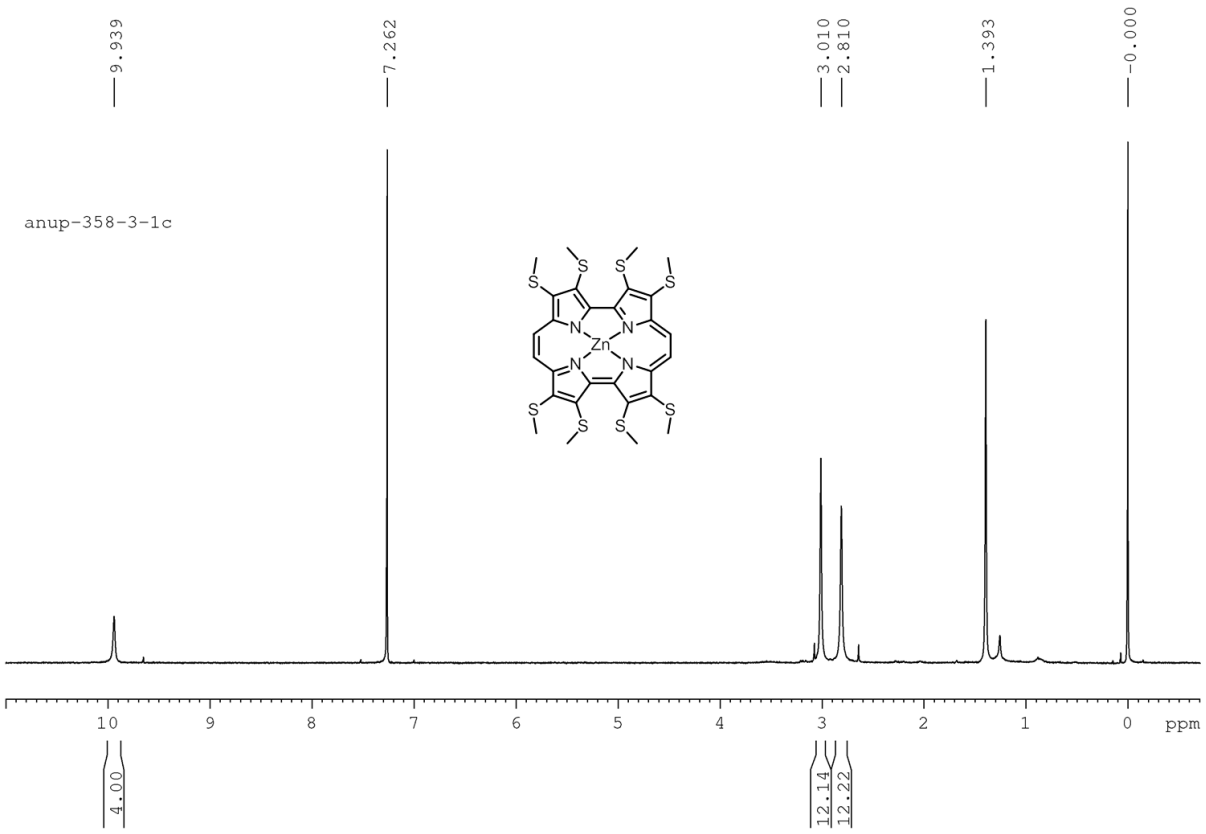

Figure 6.15 ^{1}H NMR spectrum of **Zn(6.1)** in $CDCl_3$.

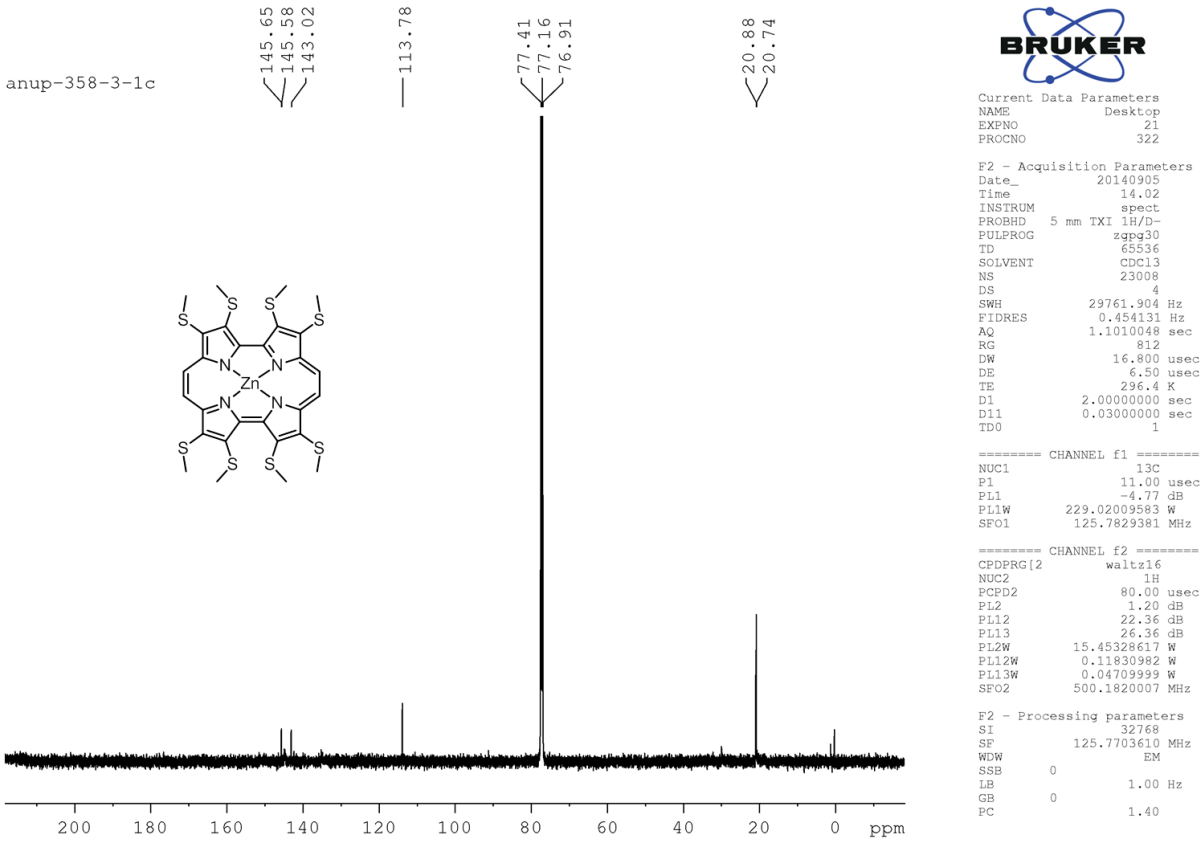

Figure 6.16 ^{13}C NMR spectrum of **Zn(6.1)** in $CDCl_3$.

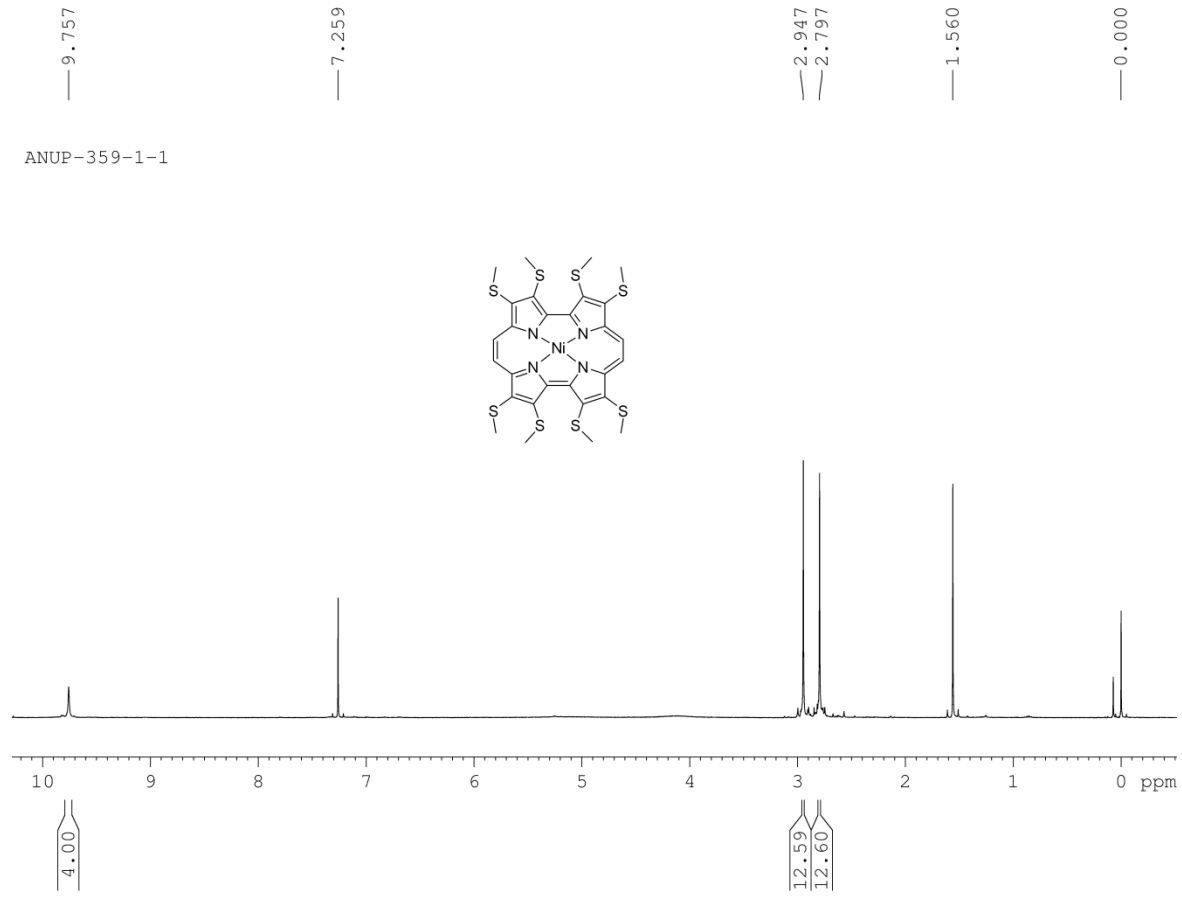

Figure 6.17 ^{1}H NMR spectrum of **Ni(6.1)** in $CDCl_3$.

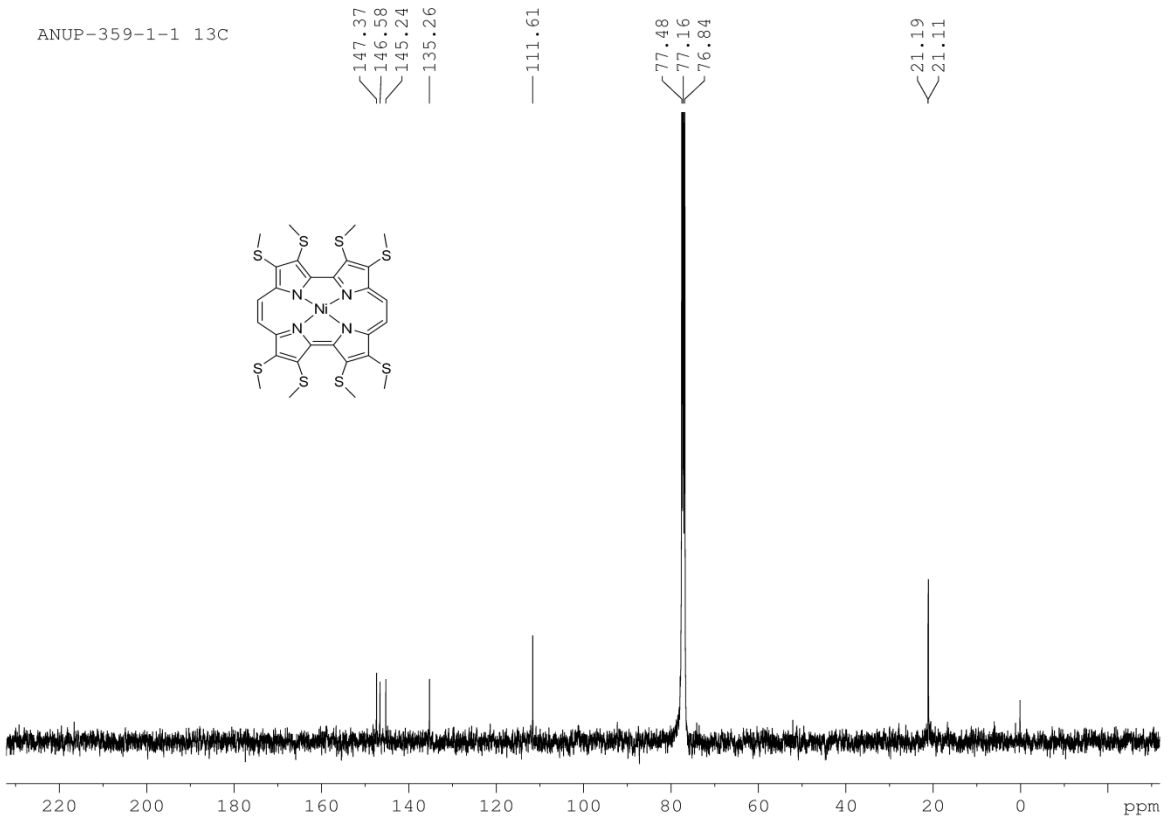

Figure 6.18 ^{13}C NMR spectrum of **Ni(6.1)** in $CDCl_3$.

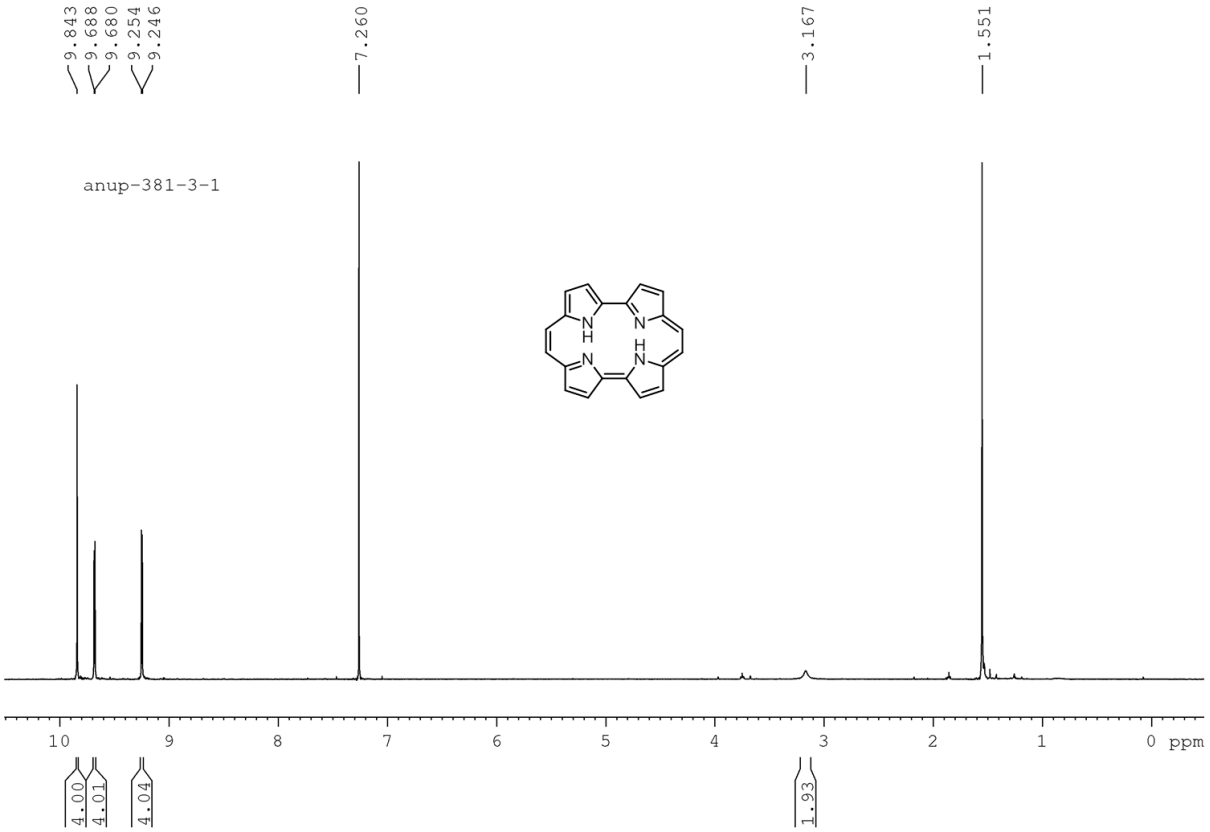

Figure 6.19 ^{13}C NMR spectrum of **6.8** in $CDCl_3$.

CHAPTER 7

β-Methoxy Substituted Stretched Porphycenes: Synthesis, Characterisation and NLO Studies

7.1 Introduction

Expanded porphyrins belong to a class of conjugated porphyrins endowed with a larger central core having more than 16 atoms.[1] As a result of core expansion, these expanded porphyrins display electronic structures that are quite similar to porphyrins in general; most often however produce systems with novel spectral and electronic features, and unprecedented coordination ability (towards both cations and anions) and structural features, including nonplanar "figure-eight" motifs.[1] Technically, we can produce an expanded porphyrin by two ways. The first way is to retain the number of pyrroles at four and then introduce additional bridging atoms (C or N) and the second way is to induct additional five member heterocycles either by keeping constant, decreasing or increasing number of bridging atoms. In this chapter we will discuss about the expanded porphyrins arising from the first strategy.

7.1.1 Vinylogous porphyrins

First of this kind of expanded porphyrin reported by Berger and LeGoff by the introduction of vinylogous porphyrin, [22]porphyrin-(3.1.3.1) (**7.1**), coined the name as "platyrin".[2] The ^{1}H NMR spectrum of platyrin revealed diamagnetic ring current with internal *meso* like proton and outer *meso* protons resonate at -8.97 and 16.15 ppm, supporting the aromatic nature of this macrocycle. The UV-Vis spectrum revealed Soret like bands at 477 nm (log ε = 5.60) for freebase and protonated salts with TFA. Though it was found to form complexes with Ni(II) and Cu(II), however insolubility and unstable nature deterred them to further explore the coordination behaviour. Later, Franck and coworkers reported 22π-bisvinylogous porphyrin **7.5** by acid catalysed condensation approach and found to be aromatic in nature as revealed by ^{1}H NMR and UV-Vis features similar to platyrin.[3] Besides, solid state structure of **7.5** found to be planar and further proved its aromatic nature. Soon after successful synthesis of platyrin, LeGoff and Weaver introduced tetravinylogous porphyrin analogue [26]porphyrin-(5.1.5.1) **7.2**.[4] However, UV-Vis and ^{1}H NMR features proved aromatic nature of this system, but low stability of both freebase and protonated form prohibited them from any further analysis. Again, in 1993, Franck and coworkers reported first stable [26]porphyrin-(5.1.5.1) **7.6** by acid catalysed condensation method.[5] The UV-Vis spectrum of **7.6** shows strong Soret type band at 510-520 nm region and increased stability allowed them to characterise structure by X-ray crystallography, which revealed planar and aromatic nature of this macrocycle. Further, Franck and coworkers introduced a different type of

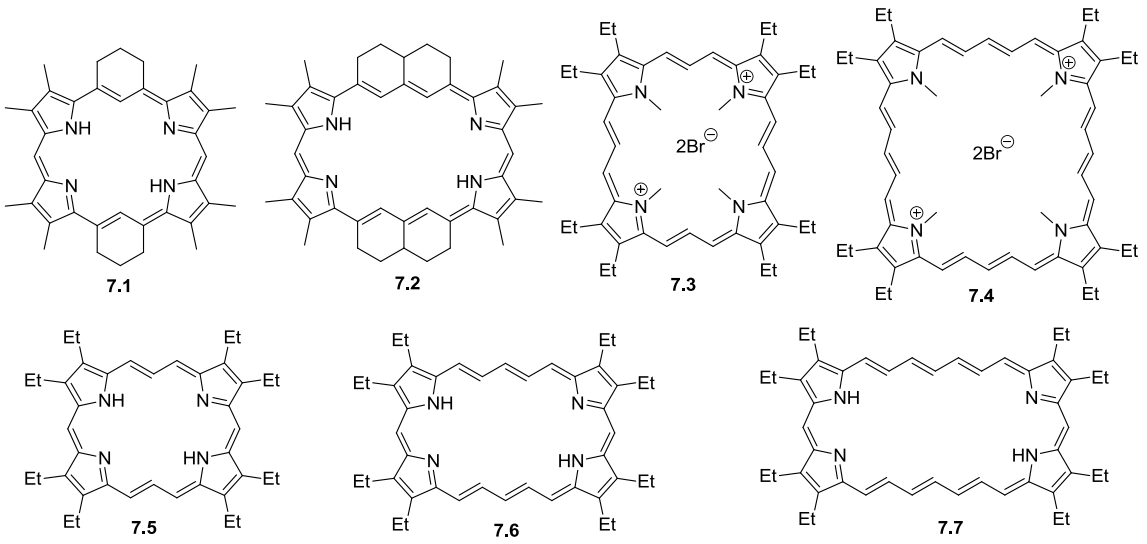

Figure 7.1 Vinylogous porphyrins.

tetravinylogous porphyrin known as [26]porphyrin-(3.3.3.3) **7.3** synthesized by acid catalysed condensation of N-methylpyrrolevinylalcohol followed by oxidation with bromine.[6] The UV-Vis spectrum of **7.3** revealed Soret type band at 547 nm with record molar extinction coefficient (909600 $M^{-1}cm^{-1}$) and large difference in chemical shift of external and internal meso protons, proved its planar and aromatic character. However, they couldn't obtain solid state data to support this conclusion. Further reduction of **7.3** with potassium in THF at -78 °C, led to formation of 28π antiaromatic species and under similar reaction condition at room temperature for 5 days provides a 30π-aromatic species, proved by ^{1}H NMR chemical shift and UV-Vis absorption spectral feature. Again, Franck and coworkers reported the synthesis of hexavinylogous porphyrin namely, [30]porphyrin-(7.1.7.1) **7.7**.[7] The difference in chemical shift in *meso* type internal and external protons was found to be 23.7 ppm. However, this value is marginally smaller compare to [26]porphyrin-(5.1.5.1) **7.3**, but still large enough to be considered as an aromatic macrocycle. The largest aromatic expanded porphyrin, [34]porphyrin-(5.5.5.5) **7.4** was synthesized by acid catalysed condensation of N-methylpyrrolebisvinylalcohol and subsequent oxidation with bromine to afford the desired product.[8] Although its solid state structure is yet to be characterised by X-ray diffraction, however large difference (31.5 ppm) in the chemical shift of inner and outer meso protons proved its aromatic nature.

7.1.2 Stretched Porphycenes

Soon after the synthesis of first stable porphyrin isomer i.e. porphycene, Vogel and coworkers reported the synthesis of first example of stretched porphycene, the

[22]tetradehydroporphyrin-(2.2.2.2) **7.8**, also called stretched porphycene, was synthesized by McMurry coupling of diformyldipyrrryldimethyne using low-valent Ti reagent followed by spontaneous oxidation led to the formation of desire product along with two other reduced macrocycles, namely, [22]porphyrin-(2.2.2.2) **7.10** and [22]didehydroporphyrin-(2.2.2.2) **7.11**.[9] The reduced products **7.10-11** probably resulted from the strongly reducing condition associated with McMurry coupling. Further the reduced products could be independently synthesized from **7.8** by partial hydrogenation using Lindlar catalyst.[10-11] The ^{1}H NMR

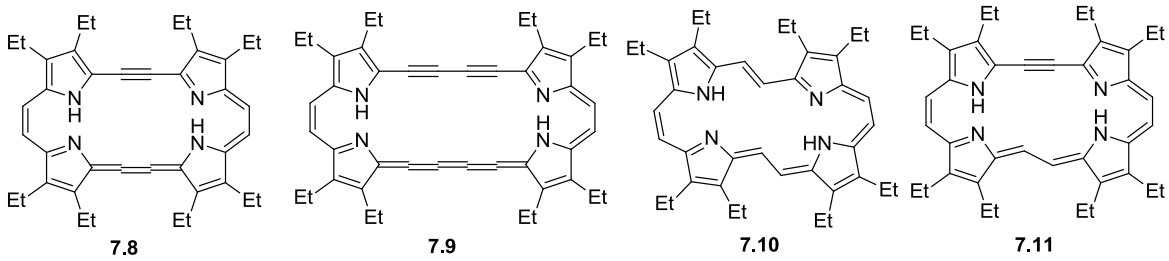

Figure 7.2 Stretched porphycenes stretched along bipyrrole unit of porphycene.

spectra of these molecules (**7.8**, **7.10**-**11**) were found to exhibit the upfield and downfield shift for imino protons and external *meso* protons, respectively, a characteristic feature of aromatic compounds. The UV-Vis spectrum of **7.8** revealed split Soret- and Q-type bands at 400-450 nm and 650-800 nm, respectively. Similarly, compound **7.10** exhibits strong split Soret band at 440/460 nm and a set of Q-bands at 672-790 nm range.[10] The X-ray crystal structure of compound **7.10** reveals a *cis-trans-cis-trans* arrangement and planarity of this macrocycle. Further, Vogel and coworkers described an alternative method to the synthesis of [22]porphyrin-(2.2.2.2) **7.10** by McMurry coupling of 2,5-diformylpyrrole, albeit in very poor yield.[10] The both stretched porphycenes were able to form mono and bis [$Rh(CO)_2$] complexes when treated with di-μ-chlorobis[dicarbonylrhodium(I)].[12] In similar approach, Vogel and coworkers reported [26]octadehydroporphyrin-(2.4.2.4) **7.9** by McMurry coupling of diformyldipyrrolyltetramethyne followed by aerial oxidation.[13] The diactylene-cumuleneporphycene **7.9** displays ^{1}H NMR spectrum similar to its monoacetylene-cumulene porphycene analogue **7.8**, but there is a significant bathochromic shift for both Soret and Q-type band in UV-Vis absorption spectrum due to comparatively larger π-conjugation pathway. Although all of these stretched porphycenes (**7.8**-**10**) display strong absorption and fluorescence in NIR region (700-900 nm), however not able to generate singlet oxygen efficiently, limiting their applicability as photosensitizer for PDT, due to low lying triplet state.[13]

The stretching along the *meso* position of porphycene resulted [22]porphyrin-(4.0.4.0) **7.12** analogue synthesized by McMurry coupling of a formyl-vinylogous-formylbipyrrole and subsequent air oxidation.[6] This reaction led to the formation of an alternative coupling

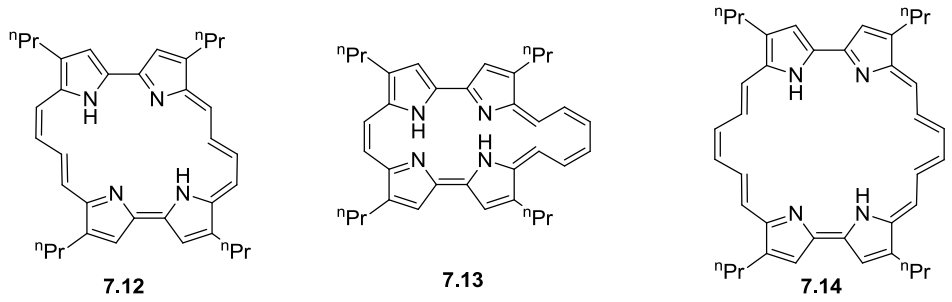

Figure 7.3 Stretched porphycenes stretched along *meso* position of porphycene.

byproduct namely [22]porphyrin-(6.0.2.0) **7.13**.[6] Like other stretched porphycenes [22]porphyrin-(4.0.4.0) **7.12** could be converted to stable Rh(I) complex when treated with di-μ-chlorobis[dicarbonylrhodium(I)].[6] Further, Vogel and coworkers introduced [26]porphyrin-(6.0.6.0) **7.14** by McMurry coupling of bisvinylogous formylbipyrrole.[6,14] The assignment of ^{1}H NMR signals was possible after protonation of this macrocycle and UV-Vis spectral features indicate that this macrocycle is aromatic in protonated state. Also, **7.14** could be further converted to Rh(I) complex upon treatment with di-μ-chlorobis-[dicarbonylrhodium(I)].[6]

7.2 Research goal

Therefore, from the above prospective we can conclude that though stretched porphycenes possess interesting photophysical properties compare to other expanded porphyrins, however this field is hardly explored in term of synthesis and potential applicability. In this regard, we

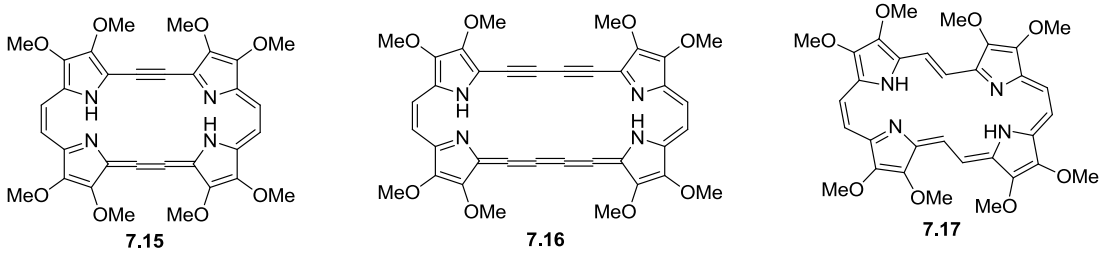

wish to synthesize two new acetylene-cumulene porphyrinoids with 22π and 26π aromatic conjugation pathways (**7.15-16**) and a new [22]porphyrin-(2.2.2.2) **7.17** derived from 3,4-dimethoxypyrrole. Also, one of our objectives is to improve the synthetic methodology, which will enable easy access to these molecules. Further, we know that expanded porphyrins

have gained much interest owing to their enhanced third order nonlinear optical (NLO) properties and interesting excited state photodynamics.[15] Therefore, we would like to investigate the third order NLO properties of these molecules along with previously reported corresponding octaethyl analogues to evaluate the substituent effect. Further, we have seen that the properties of porphycenes are much sensitive to the position and type of substituent and therefore, would like to explore if it could be extended to stretched porphycenes. In this regard, we would like to investigate the effect of substituents in stretched porphycenes on their structure, photophysical and electrochemical properties.

7.3 Results and discussion

7.3.1 Synthesis of expanded porphycenes

Synthesis of 22π and 26π aromatic acetylene-cumulene was achieved by McMurry coupling of the corresponding mono and diacetylenic bipyrroledialdehydes,[9] which in turn were synthesized following the improvised methods in literature, starting from the iodopyrrole aldehydes **7.18a-c**[16] (Scheme 7.1). Briefly, Sonogashira coupling of **7.18a-c** with trimethylsilylacetylene in the presence of bis(triphenylphosphine)palladium(II)dichloride [$PdCl_2(PPh_3)_2$] and cuprous iodide (CuI) led to trimethylsilylactylinic pyrrole aldehydes **7.19a**, **7.19b** and **7.19c** in 87, 88 and 78% yields, respectively. Subsequent deprotection of trimethylsilyl group with tetrabutylammonium fluoride provided the acetylene pyrrole derivatives **7.20a-c** quantitatively at room temperature.[17] Sonogashira coupling of **7.20a**, **7.20b** and **7.20c** with **7.18a**, **7.18b** and **7.18c**, respectively led to the successful synthesis of acetylene-bridged bipyrroledialdehydes **7.21a**, **7.21b** and **7.21c** in 62, 89 and 70% yields, respectively.[17] To improve the yield of the desired product, we employed the modified Glaser-Hay coupling protocol, where oxidative coupling of **7.20a-c** in the presence of catalytic amount of $PdCl_2(PPh_3)_2$ and CuI in presence of base, under oxygen atmosphere led to the desired diacetylene-bridged bipyrroledialdhydes **7.22a**, **7.22b** and **7.22c** with 94, 95 and 80% yields, respectively at room temperature. McMurry coupling of **7.21b** using standard procedure i.e. $Zn/TiCl_4$ in the presence of CuCl under reflux condition followed by oxidation in air provided the desired β-octamethoxymonoacetylene-cumuleneporphycene**7.15** in very poor yield with reduced β-octamethoxy[22]porphyrin-(2.2.2.2) **7.17** as the major product.[9] As the 3,4-dimethoxypyrrole analogue is a highly activated system, therefore, we performed the McMurry coupling reaction by slow addition of **7.21b** at room temperature and this modification led to the formation of the desired **7.15** as the major product and reduced

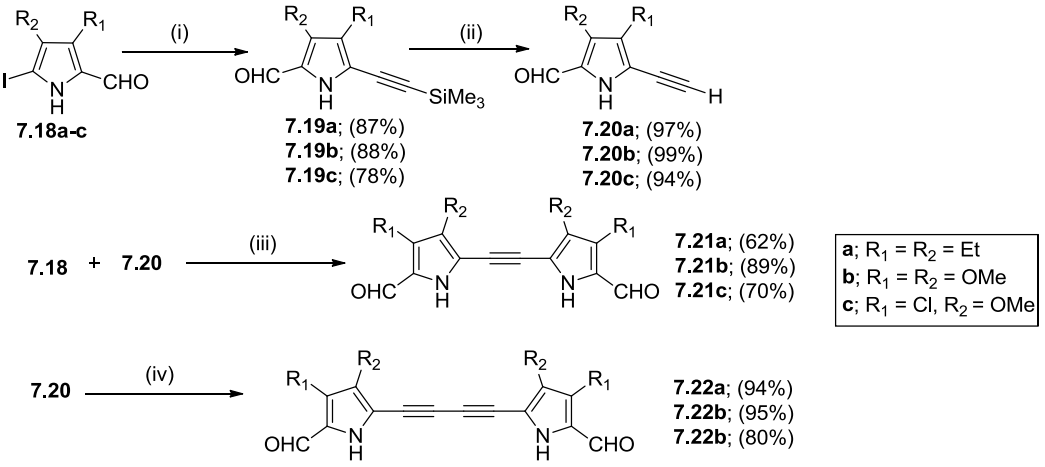

Scheme 7.1 Reagent and conditions: (i) $Pd(PPh_3)_2Cl_2$ (4 mol%), CuI (8 mol%), THF, 50 °C; (ii) TBAF, THF, RT; (iii) $Pd(PPh_3)_2Cl_2$ (4 mol%), CuI (8 mol%), THF, reflux; (iv) $Pd(PPh_3)_2Cl_2$ (5 mol%), CuI (10 mol%), O_2, THF, RT.

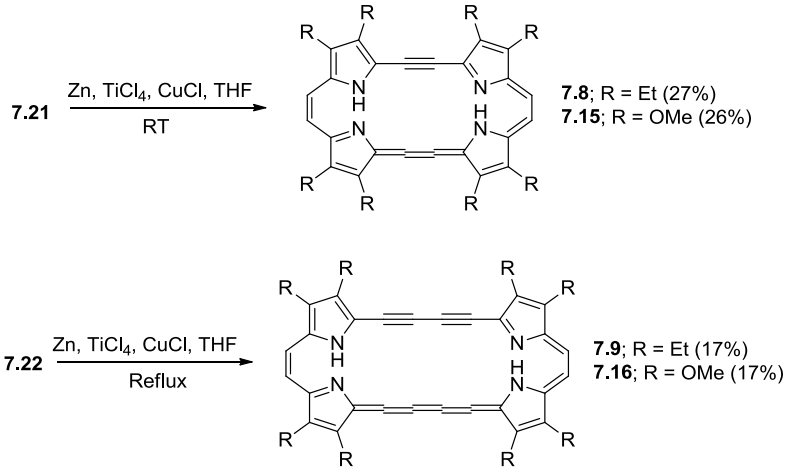

Scheme 7.2 Synthesis of acetylene-cumuleneporphycenes.

products as minor component. It was difficult to purify the mixture of product by column chromatography, however, pure compound **7.15** could be obtained in 26% yield (Scheme 7.2) by simple washing with hexane and chloroform mixture (1:1). On the other hand, McMurry coupling of **7.21c** under identical condition yielded corresponding mono acetylene-cumulene porphycene (detected by UV-Vis spectrum of reaction mixture), but due to poor solubility we couldn't isolate the entitled compound from reaction mixture. Interestingly, McMurry coupling of **7.21a** in the same manner resulted in the exclusive formation of the desired β-octaethylmonoacetylene-cumuleneporphycene **7.8** without any additional reduced products. The yield of this reaction (27%) was much higher compared to that reported by Vogel (18%).[9] Syntheses of β-octasubstituted diacetylene-cumuleneporphycenes (**7.9** and **7.16**) were achieved by McMurry coupling of diacetylene-bridged bipyrroledialdhydes (**7.22a-b**)

under reflux condition, however, again **7.22a-b** were added much slowly than reported by Vogel's group, which led to the formation of compounds **7.9** and **7.16** both in 17% yields, again the former could be isolated in much improved yield than reported (9%).[13] Once again we couldn't isolate McMurry coupling product of **7.22c** due to poor solubility.

Monoacetylene-cumuleneporphycenes (**7.8** and **7.15**) were reduced with Pd/C in presence of 1 atm hydrogen gas followed by oxidation with DDQ to [22]porphyrins-(2.2.2.2) (**7.10** and **7.17**) in good to reasonable yields (Scheme 7.3). Octamethoxy-substituted acetylene-

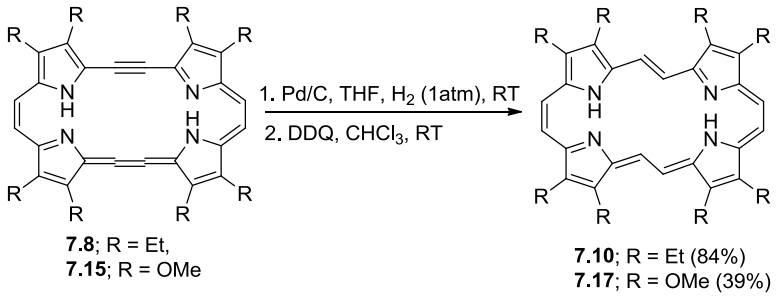

Scheme 7.3 Synthesis of [22]porphyrins-(2.2.2.2).

cumulene porphycene (**7.15**) undergoes a relatively slow reduction (48 h) compared to the octaethyl analogue (20 h). Our method shows an advantage over Vogel's method using Lindlar catalyst (35% yield),[10] as reflected in the improved yield of **7.10**. A moderate yield for **7.17** may be attributed to the longer reaction time. We could also synthesize **7.17** in 1.4% yield by reductive McMurry coupling of 3,4-dimethoxypyrrole-2,5-dialdehyde[18] as the only non-polymeric product.[10]

7.3.2 ^{1}H NMR analysis of expanded porphycenes

The macrocycles revealed aromatic features in the ^{1}H NMR spectra as the outer *meso* protons are downfield shifted and inner NH protons are upfield shifted. ^{1}H NMR spectrum of **7.15** indicates the *meso* protons are marginally perturbed, whereas the NH protons are significantly upfield shifted (0.86 ppm), in comparison to the octaethyl analogue **7.8** (2.19 ppm). This may be attributed to the increased electron density in the aromatic core of **7.15** due to the enhanced electron donating ability of methoxy substitutents at its periphery. A similar trend is also observed for diacetylene-cumulene porphycene analogues, where the NH protons are 1.19 ppm upfield shifted for the methoxy analogue (0.77 ppm for **7.16** vs 1.96 ppm for **7.9**). Similar to the octaethyl analogue **7.10**, the octamethoxy[22]porphyrin-(2.2.2.2) **7.17** displays downfield shifted outer *meso*-Hs at C-5, 11 and 12, whereas the inner *meso*-H

at C-6 is upfield shifted. For example, in **7.17**, H-5 protons are 0.21 ppm downfield shifted (11.98 ppm for **7.17** vs 11.77 ppm for **7.10**), H-6 protons are 0.5 ppm upfield shifted (-7.97 ppm for **7.17** vs -7.47 ppm for **7.10**) and the NH protons are 0.5 ppm upfield shifted (0.83 ppm for **7.17** vs 1.33 ppm for **7.10**), which clearly indicates a stronger substituent effect for this class of macrocycles than the acetylene-cumulene type macrocycles.

7.3.3 Structural analysis of expanded porphycenes

Molecular structures of **7.15** and **7.17** were characterised by X-ray crystallography (Figure 7.4). The crystal structure of expanded porphycene **7.15** possess a near planar macrocyclic

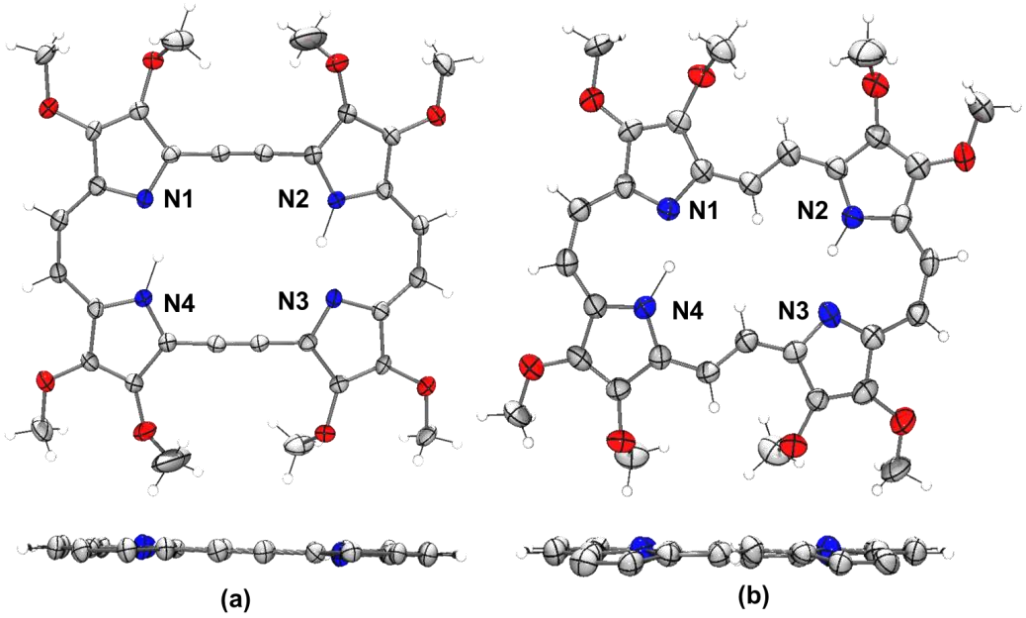

Figure 7.4 X-ray crystal structure of (a) **7.15** and (b) **7.17** (top: front view, bottom: side view) scaled in 35% probability level. In side views the methoxy groups are omitted for clarity. Color code: C, gray; N, blue; O, red; H, white.

core with mean deviation of 0.05 Å for the nitrogens from the average macrocyclic plane. The structure of the acetylene-cumulene bridge $C_{sp}{}^2C_{sp}C_{sp}C_{sp}{}^2$ appears equivalent on both sides of **7.15**, suggesting that **7.15** exist in the form of a resonance hybrid. Nitrogens of **7.15** form a rectangular core like **7.8**, with N1···N2 and N2···N3 distances of 5.355 and 2.608 Å, respectively. The X-ray crystal structure analysis of **7.17** confirms the *cis*, *trans*, *cis*, *trans* configuration of the compound, however the core of this macrocycle is slightly more distorted with mean deviation of nitrogens from mean ring plane 0.087 Å than **7.10** (0.05 Å)[10]. The four nitrogen atoms of **7.17** define a near-parallelogram type core geometry (N1-N2-N3 = 77.9°, N1-N4-N3 = 77.8°).

7.3.4 Absorption and emission properties

The UV-Vis absorption and fluorescence spectra of compounds **7.8-10** and **7.15-17** were recorded in chloroform at room temperature (Figure 7.5 and Table 7.1). The introduction of acetylene spacers into the bipyrrolic units of the octamethoxyporphycene[16] gives rise to a

Table 7.1 Photophysical data for stretched porphycenes

Comp. Name	UV-Vis λ_{max} in nm, (log ε) in chloroform	Fluorescence λ_{max} (nm) in toluene	ϕ_f
7.8	407 (5.29), 440 (4.90), 679 (4.60), 726 (4.88), 768 (4.91)	782, 864	0.12±0.08[a]
7.9	449 (5.18), 496 (5.01), 841 (5.00), 889 (5.03)	904	< 0.1[a]
7.10	442 (5.29), 466 (4.98), 674 (4.56), 728 (4.23), 791 (4.71)	804, 906	0.08±0.08[a]
7.15	411 (4.97), 445 (4.65), 672 (4.29), 714 (4.54), 758 (4.41)	---	---
7.16	456 (5.10), 500 (4.87), 832 (4.86), 884 (4.76)	---	---
7.17	442 (5.26), 467 (4.96), 665 (4.50), 708 (4.10), 774 (4.57)	784, 886	0.0095[b]

[a] Taken from ref 13 [b] Fluorescence quantum yield of **7.17** in chloroform was measured by using **H_2TPP** in toluene (ϕ_f 0.11) as reference.

huge change in the UV-Vis absorption spectra. Both the split Soret bands and Q-bands are bathochromically shifted for **7.15** and **7.16** as compared to the octamethoxyporphycene, due to the increased conjugation pathway (22π and 26π *vs* 18π-system). Addition of two acetylene spacers to methoxy-substituted bipyrrole resulted in a red-shift of the lowest-energy band from 636 nm to 758 nm, and further red-shift to 884 nm upon addition of two more acetylene spacers. The UV-Vis absorption spectra of **7.15** and **7.16** show marginal change in absorption maxima compared to their ethyl analogues.[9,13] However, there is a discernible difference in the spectral patterns, in particular in the Q-band region, where the methoxy-derivatives display the 2nd band as the most intense one among the three, whereas for the ethyl analogues, the lowest energy band is the most intense one. Again the effect of substituents is more apparent in the case of [22]porphyrin-(2.2.2.2), with the absorption spectrum of **7.17** showing the lowest-energy Q-band about 17 nm blue-shifted compared with that of **7.10**.[10] We could not detect any fluorescence for **7.15** and **7.17**. Also compared to **7.10**, the stretched porphycene **7.17** exhibits weaker fluorescence, with λ_{max} at 779 nm (ϕ_f 0.0095). These results support that in case of the methoxy-substituted macrocycles intramolecular charge transfer (ICT) is more facile. Additionally, we can assume that

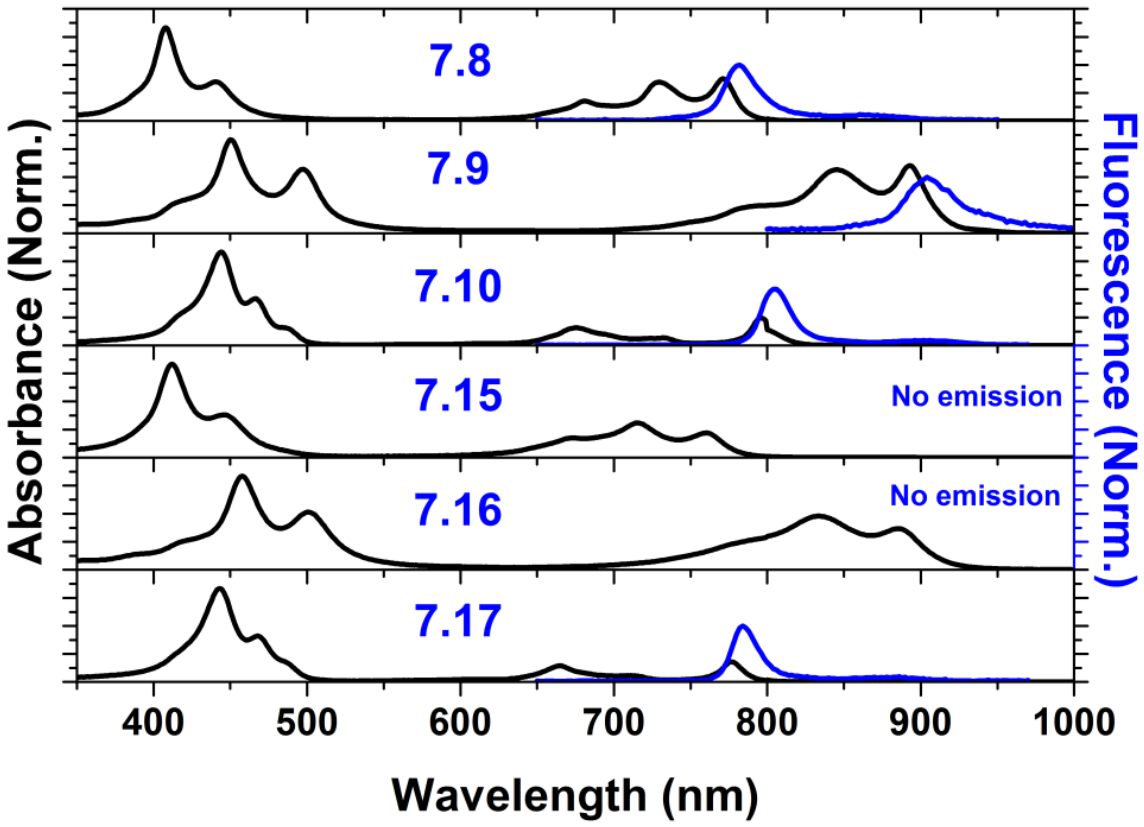

Figure 7.5 Normalized UV-Vis absorption (black lines) and fluorescence spectra (blue lines) of stretched porphycenes.

acetylene-cumulene porphyrinoids are endowed with stronger ICT character than β-octamethoxy[22]porphyrin-(2.2.2.2).

7.3.5 Two-photon absorption studies

The two photon absorption studies were carried out in collaboration with Prof. Kim's group. Two-photon absorption (TPA) is a third-order NLO phenomenon, whose probability of occurrence is closely related to π-electron behaviour. Recent theoretical and experimental studies have indicated that ICT character could lead to an enhancement of the TPA cross-section.[19] In this context, to investigate the effect of ICT character, TPA measurements for methoxy-derivatives of the stretched porphycenes **7.15-17** were performed and compared with that of the ethyl analogues **7.8-10** by the Z-scan technique in toluene at 1300-1900 nm, where the contribution from one-photon absorption (OPA) is negligible (Figure 7.6-7). The TPA profiles revealed spectral features that are in a good agreement with those of the lowest one-photon absorption band. The maximum TPA cross-sections of **7.8**, **7.9** and **7.10** were measured to be 580, 770 and 370 GM at 1400, 1700 and 1300 nm, respectively. Meanwhile, the maximum TPA cross-sections of **7.15**, **7.16** and **7.17**, were measured to be 640, 830 and

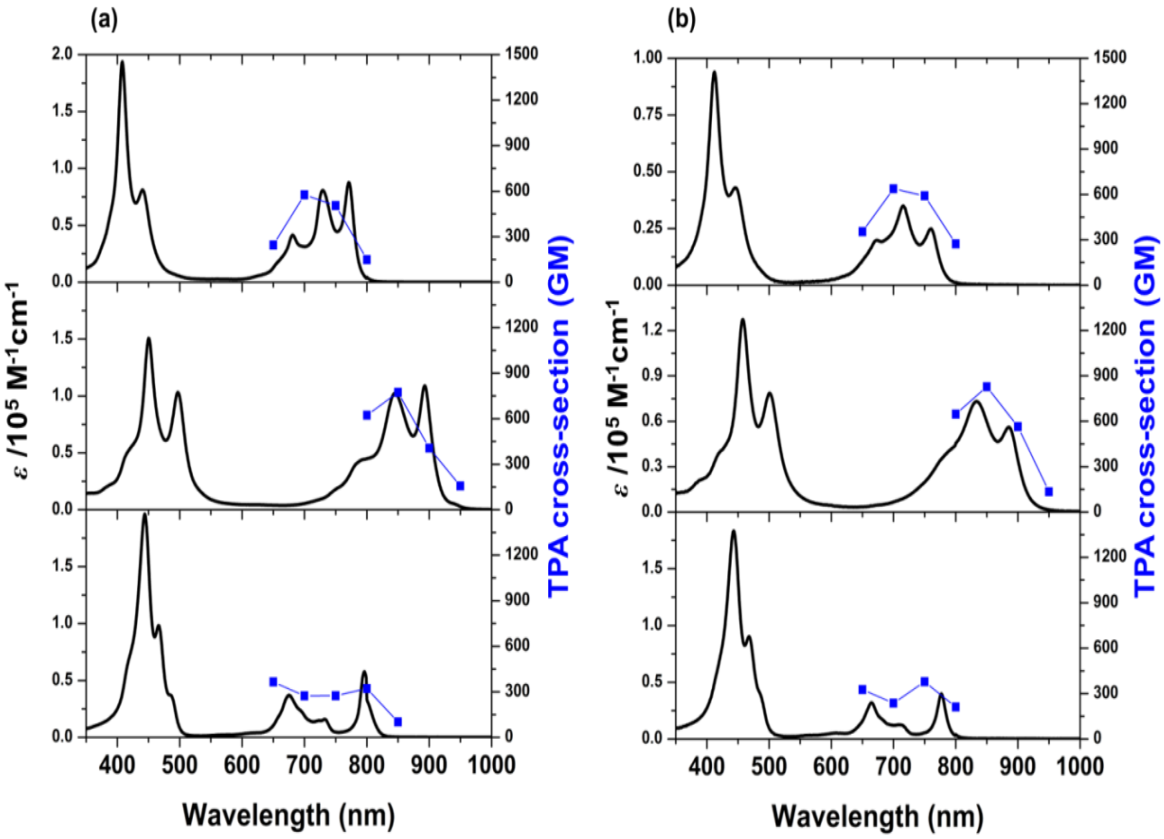

Figure 7.6 OPA (solid line) and TPA spectra (point-line) of (a) **7.8** (top), **7.9** (middle) and **7.10** (bottom) (b) **7.15** (top), **7.16** (middle) and **7.17** (bottom) in toluene. The TPA spectra are plotted at $\lambda_{ex}/2$ for comparison with the OPA spectra.

380 GM at 1400, 1700 and 1500 nm, respectively. Based on the observed trends, we can conclude that the TPA cross-sections of methoxy analogues are larger than those of the ethyl analogues due to facile ICT character. Further, we have observed higher TPA cross-section for 26π-acetylene-cumulene porphycenes compared to corresponding 22π-acetylene-cumulene porphycenes due to the more extended π-conjugated network for the former. Additionally, the TPA cross-sections of isoelectronic [22]porphyrins-(2.2.2.2) are smaller than those of 22π-acetylene-cumulene porphyrinoids. Here we note that TPA cross-section is closely related to the conformational flexibility in the π-conjugated network.[20] As we can see that acetylene-cumulene porphyrinoids are much rigid and tend to be more effectively conjugated compared to [22]porphyrins-(2.2.2.2) with vinylinic linker, which is known to undergo an isodynamic transformation involving rotation around *trans* –CH=CH– bonds,[10] leading to relatively low TPA cross-section. Interestingly, expansion of aromaticity could be clearly noticed for all the expanded porphycenes as compared to their porphycene analogues.[21]

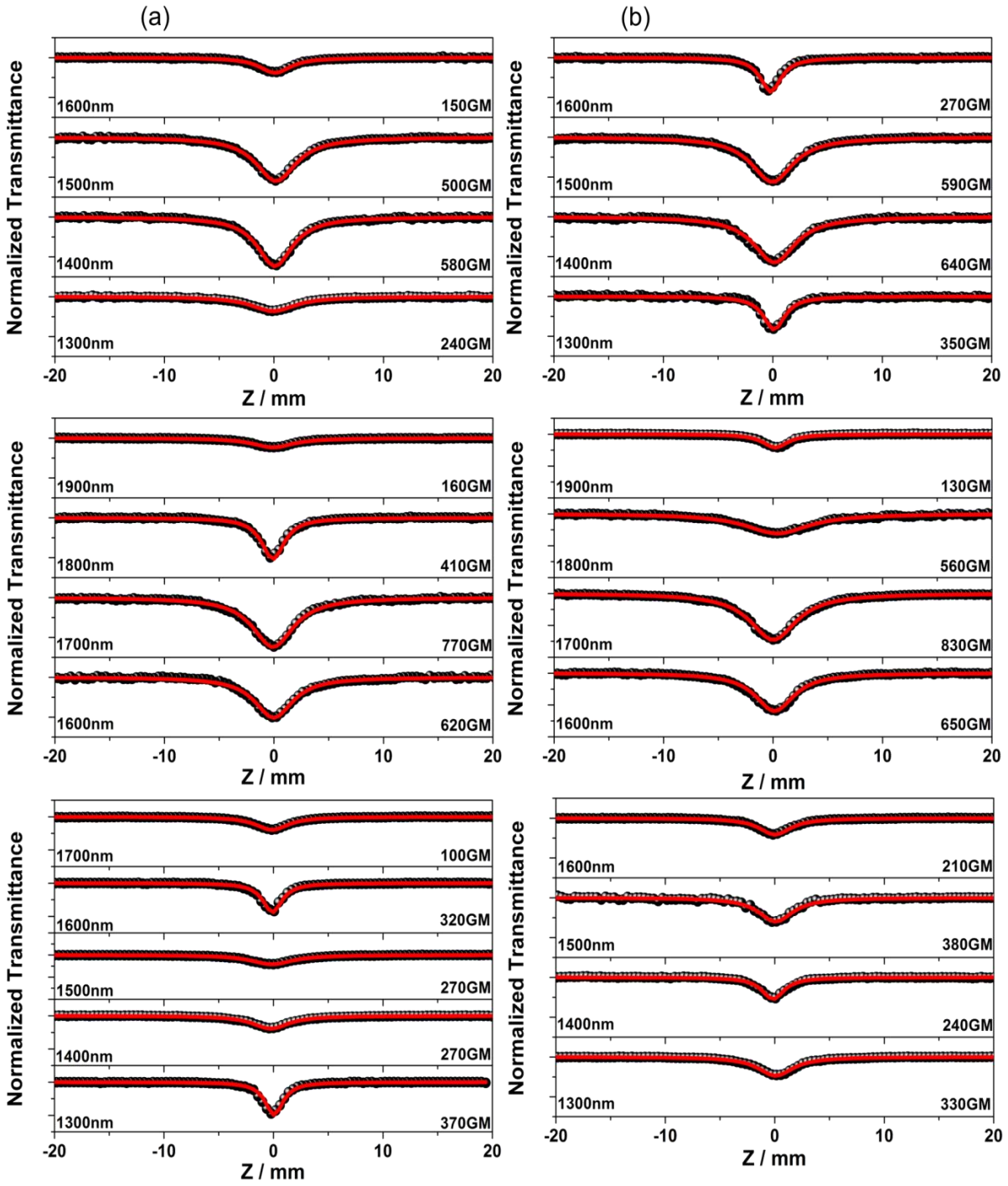

Figure 7.7 (a) Open aperture Z-scan curves of **7.8** (top), **7.9** (middle) and **7.10** (bottom). (b) Open aperture Z-scan curves of **7.15** (top), **7.16** (middle) and **7.17** (bottom).

7.3.6 Femtosecond transient absorption studies

The femtosecond transient absorption (TA) studies were carried out also in collaboration with Prof. Kim's group. To examine the excited-state dynamics of **7.8-10** and **7.15-17**, we have measured TA spectra of these compounds (Figure 7.8). The TA spectra exhibited ground

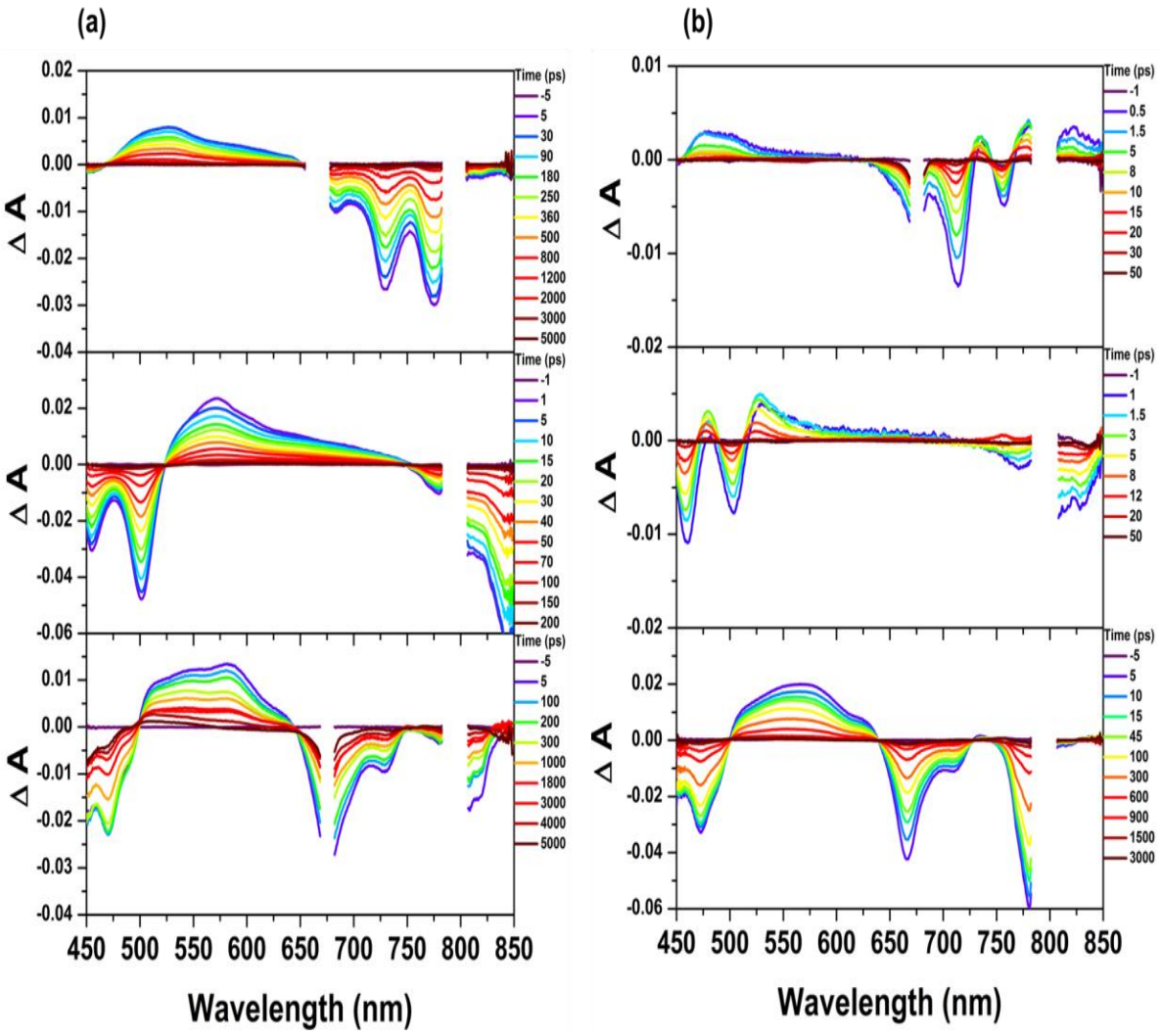

Figure 7.8 (a) TA spectra of **7.8** (top), **7.9** (middle) and **7.10** (bottom) and (b) TA spectra of **7.15** (top), **7.16** (middle), and **7.17** (bottom) in toluene obtained with photoexcitation at 670 nm (top), 830 nm (middle) and 670 nm (bottom), respectively.

state bleaching signals, whose spectral features correspond to their ground-state absorption bands. The fitted time components of the ethyl analogues are 630, 36 and 2000 ps for **7.8**, **7.9** and **7.10**, respectively (Figure 7.9). These results are in good agreement with those reported in previous work.[13] Also, the decay times of methoxy analogues are 11, 7.3 and 370 ps for **7.15**, **7.16** and **7.17**, respectively (Figure 7.9). Compared to the ethyl analogues, the methoxy derivatives exhibit significantly shorter excited-state lifetimes. This feature could be attributed to the ICT character from the methoxy substituent to the porphyrinoid core. As the time-resolution of the TA set-up used is ~150 fs, we can assume that the timescale of the ICT process lies within few hundred femtoseconds, which hinders the direct observation of the ICT process in the spectra.

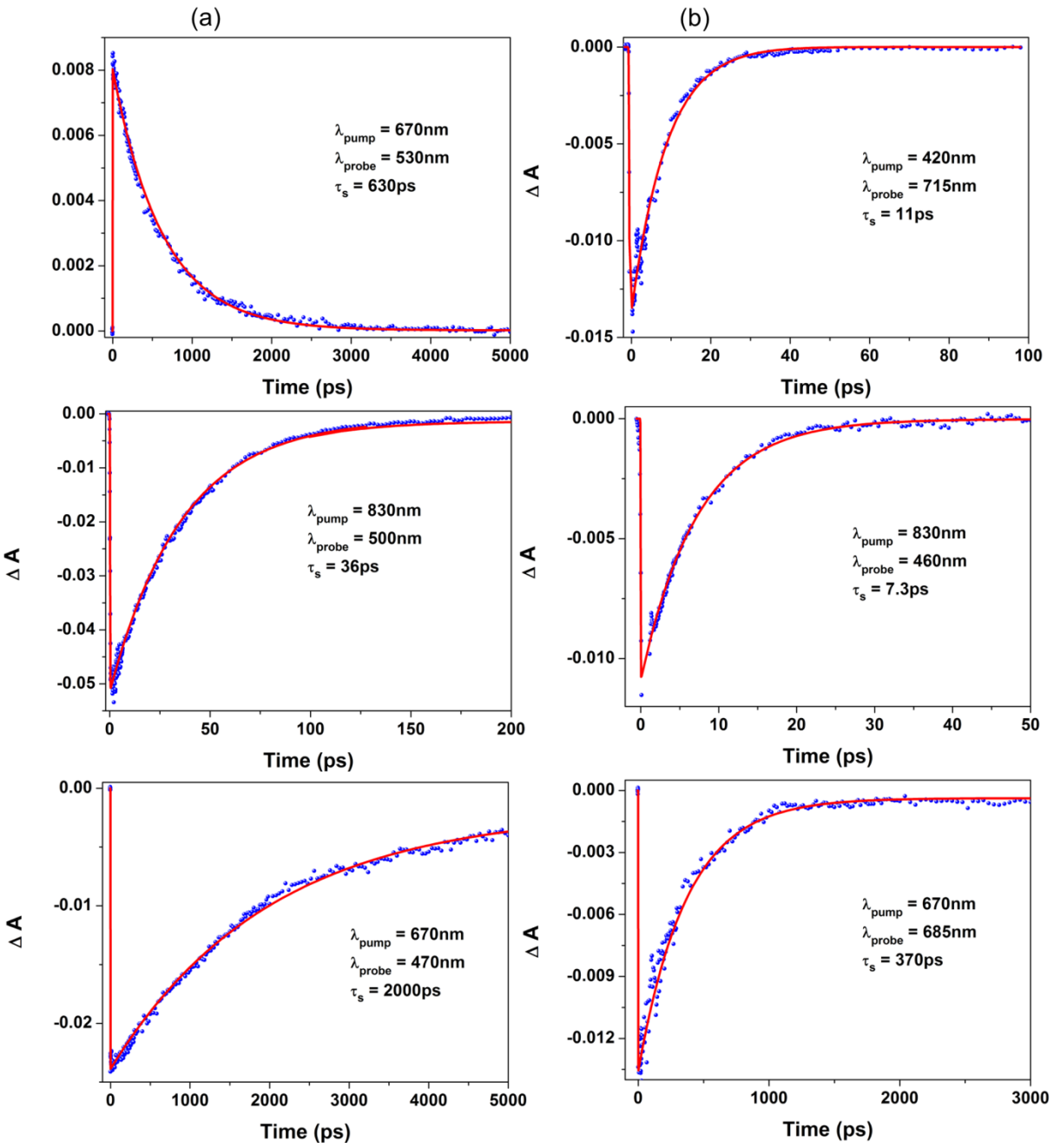

Figure 7.9 (a) The decay profiles of **7.8** (top), **7.9** (middle) and **7.10** (bottom). (b) The decay profiles of **7.15** (top), **7.16** (middle) and **7.17** (bottom) in toluene.

7.3.7 Electrochemical studies

The redox potentials of all expanded porphycenes were analysed by cyclic voltammetry (CV) and differential pulse voltammetry (DPV) in dichloromethane. Similar to β-octamethoxyporphycene,[16] all expanded porphycenes show two reversible reductions and two reversible or quasi-reversible oxidations. Oxidation and reduction potentials referenced *vs* Ag/AgCl for all expanded porphycenes are summarised in Table 7.2. The first oxidation

Table 7.2 Redox Potentials for Expanded Porphycenes (in V *vs* Ag/AgCl)

Comp Name	Reduction	Oxidation	HOMO-LUMO (V)
7.8[a]	-0.88, -0.57	+0.80, +1.09	1.37
7.9[a]	-0.49, -0.30	+0.72, +0.98	1.02
7.10[a]	-1.02, -0.87	+0.67, ---	1.54
7.15	-0.76, -0.58	+0.74[b], +1.10[b]	1.32
7.16	-0.46[b], -0.33[b]	+0.68[b], +0.92[b]	1.02
7.17	-1.05, -0.89	+0.62, +1.02	1.52

[a] taken from ref 22, [b] measured by DPV

potentials for octamethoxy-substituted expanded porphycenes appeared at +0.74, +0.68 and +0.62 V and the first reduction potentials were observed at -0.58, -0.33 and -0.89 V for **7.15**, **7.16** and **7.17**, respectively. Due to the presence of electron rich methoxy groups at their periphery the first oxidation and the first reduction potential are less positive and more negative, respectively, for these expanded porphycenes, indicating the more electron rich nature of these macrocycles as compared to the ethyl-substituted analogues. Interestingly, the

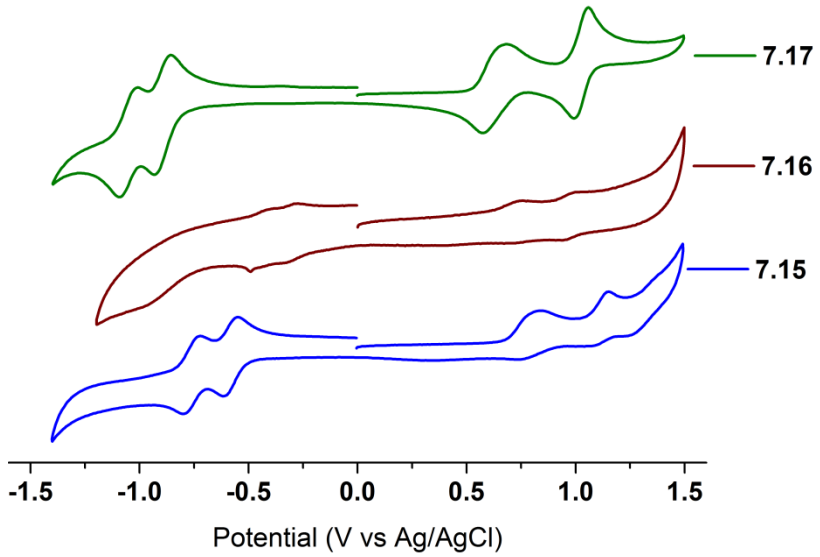

Figure 7.10 Cyclic voltammograms of **7.15-17** in dichloromethane at 25 °C (scan rate 50 mV/s).

change in the oxidation and reduction potential is very marginal as observed in the corresponding porphycenes (β-ethyl and β-methoxy analogues),[16,23] probably owing to the absence of distortion between adjacent pyrrolic moieties of bipyrrole units, by inserting acetylinic and vinylinic spacers (arising from the van der Waals repulsion between their inner β-substituents). Upon extension of the conjugation pathway from 22π to 26π, the changes in the first oxidation potentials were less obvious, compared to the first reduction potential,

which may be attributed to the minimal perturbation in the energy levels of HOMO than LUMO, for these molecules, indicating that the extension of conjugation leads to greater stabilization of the LUMO.[22] The HOMO-LUMO energy gaps of all methoxy substituted expanded porphycenes ($\Delta E = E_{ox1} - E_{red1}$) were almost similar to those of ethyl analogues, which is further supported by the minimal change observed in the lowest-energy Q-bands in their absorption spectra.

7.4 Conclusion

In conclusion, we have synthesized β-octamethoxy acetylene-cumulene porphycenes and [22]porphyrin-(2.2.2.2) along with their octaethyl congeners by employing modified synthetic protocol with higher yields. The substituent effect is found to be more severe in the case of [22]porphyrin-(2.2.2.2) than acetylene-cumulene bridged porphycenes as noticed from their absorption spectra. The dominant ICT character of methoxy groups could be noticed through enhanced TPA cross-sections for the methoxy-substituted macrocycles compared to their ethyl analogues. Most importantly the expansion of π-conjugation network both by introduction of meso methine group and pyrrole moieties behaves similarly towards NLO response. The NLO properties of studied expanded porphycenes are dominated not only by π-conjugated network, but also conformation flexibility plays an important role. The ICT property of methoxy groups led to much shorter excited state lifetimes for methoxy analogues. The electrochemical studies revealed that the first oxidation and reduction became less positive and more negative, respectively, complying with the electron rich character of these octamethoxy-expanded porphycenes.

7.5 Experimental details

3,4-diethylpyrrole-2-aldehyde: 3,4-Diethylpyrrole (3.8 g, 3.08 mmol) in DCE (10 mL) was added slowly to ice cooled stirred Vilsmeier-Haack reagent prepared from $POCl_3$ (3.5 mL, 37.01 mmol) and DMF (2.9 mL, 37.01 mmol) in DCE (40 mL) under nitrogen atmosphere. After addition was over, ice-bath was replaced with oil bath and the reaction mixture was refluxed for 2 h. Then reaction mixture was cooled on ice bath and NaOAc (15.2 g, 0.19 mol) in water (70 mL) added carefully and further refluxed for additional 2 h. After cooling the reaction mixture to room temperature organic layer was separated and aqueous layer was extracted with DCM for three times. Combined organic layer was washed with aqueous sodium bicarbonate solution and passed through anhydrous Na_2SO_4 and evaporated to dryness. Crude reaction mixture was purified by silica gel column chromatography using

EtOAc/Hexane (2:8) as eluent to obtain entitled compound (4.58 g) as light yellow liquid, which solidified at low temperature to light yellow crystalline solid. Yield: 98%. All characterization data matched with previously reported compound.[24]

3,4-ethyl-5-iodo-pyrrole-2-aldehyde (7.18a): 3,4-Diethylpyrrole-2-aldehyde (2 g, 13.2 mmol) was taken in THF (50 mL) under nitrogen atmosphere. Then, N-iodosuccinimide (3.05 g, 13.5 mmol) was added and reaction mixture was allowed to run at room temperature for 2 h. After completion of reaction, it was quenched by addition of sodium bicarbonate solution, organic layer was extracted and aqueous layer was extracted with diethyl ether. The combined organic layer was passed through anhydrous Na_2SO_4 and evaporated to dryness under reduced pressure. Crude product was purified by silica gel column using EtOAc/hexane (2:8) as eluent to afford **10a** (3.25 g) as white crystalline solid. Yield: 89%. All characterization data matched with previously reported compound.[9]

General procedure for synthesis of 3,4-disubstituted-5-((trimethylsilyl)ethynyl)pyrrole-2-aldehyde (7.19a-c): 3,4-Dimethoxy-5-iodopyrrole-2-aldehyde (**7.18b**) (1 g, 3.56 mmol), $Pd(PPh_3)_2Cl_2$ (100 mg, 0.14 mmol) and CuI (54 mg, 0.28 mmol) were taken in THF (16 mL) under nitrogen atmosphere. Subsequently, triethylamine (3 mL, 21.36 mmol) and trimethylsilylacetylene (755 μL, 5.34 mmol) were added. The homogeneous reaction mixture was stirred at 50 °C for 1 h. Reaction mixture was washed with water and extracted with diethyl ether for three times. Combined organic layer was passed through anhydrous Na_2SO_4 and evaporated to dryness under reduced pressure. Crude product was purified by silica gel column chromatography using EtOAc/hexane (1:9) as eluent to obtain 3,4-dimethoxy-5-((trimethylsilyl)ethynyl)-pyrrole-2-aldehyde (**7.19b**) (787 mg) as white crystalline solid.

3,4-dimethoxy-5-((trimethylsilyl)ethynyl)pyrrole-2-aldehyde (7.19b): Yield: 787 mg (88%); m.p.: 85.5 °C; IR (KBr): ν (cm^{-1}) 3216, 2148, 1638; ^{1}H NMR (400 MHz, $CDCl_3$), δ (ppm): 9.53 (s, 1H), 8.44 (br, s, 1H), 4.02 (s, 3H), 3.97 (s, 3H), 0.25 (s, 9H); ^{13}C NMR (100 MHz, $CDCl_3$), δ (ppm): 176.14, 144.75, 140.98, 119.16, 110.10, 104.22, 93.89, 61.34, -0.30; HRMS (ESI+): m/z: calculated for $C_{12}H_{18}NO_3Si$ ($M+H^+$): 252.1050; found: 252.1055.

3,4-diethyl-5-((trimethylsilyl)ethynyl)-pyrrole-2-aldehyde (7.19a): 3,4-Diethylpyrrole-2-aldehyde (**7.18a**) (2 g, 7.21 mmol) was taken for reaction. Yield: 1.56 g (87%); reported yield: 90%. All data are matched with previously reported compound.[13]

3-chloro-4-methoxy-5-((trimethylsilyl)ethynyl)pyrrole-2-aldehyde (7.19c): 3-Chloro-4-methoxypyrrole-2-aldehyde (**7.18c**) (2 g, 7.01 mmol) was taken for reaction. Yield: 1.4 g (78%); m.p.: 106.5 °C; IR (neat): ν (cm^{-1}) 3236, 2151, 1647; ^{1}H NMR (400 MHz, $CDCl_3$), δ (ppm): 9.57 (s, 1H), 9.02 (br s, 1H), 4.05 (s, 3H), 0.25 (s, 9H); ^{13}C NMR (100 MHz, $CDCl_3$), δ (ppm): 176.90, 147.66, 125.01, 112.97, 108.71, 104.90, 93.15, 60.99, -0.32; HRMS (ESI+): m/z: calculated for $C_{11}H_{15}NO_2SiCl$ ($M+H^+$): 256.0555; found: 256.0559.

General procedure for synthesis of 5-ethynyl-3,4-disubstituted pyrrole-2-aldehyde (7.20a-c): 3,4-Dimethoxy-5-((trimethylsilyl)ethynyl)pyrrole-2-aldehyde (**7.19b**) (1 g, 3.98 mmol) was taken in THF (20 mL) under nitrogen atmosphere and 1 M TBAF (4.4 mL, 4.40 mmol) in THF was added. Reaction mixture was stirred at room temperature for 1 h and then water was added to the reaction mixture and extracted with diethylether for three times. The combined organic layer was passed through anhydrous Na_2SO_4 and evaporated to dryness under reduced pressure. Crude product was purified by silica gel column chromatography using EtOAc/hexane (2:8) as eluent to yield 5-ethynyl-3,4-dimethoxypyrrole-2-aldehyde **(7.20b)** (705 mg) as white crystalline solid.

5-ethynyl-3,4-dimethoxypyrrole-2-aldehyde (7.20b): Yield: 705 mg (99%); m.p.: 93.8 °C; IR (KBr): ν (cm^{-1}) 3277, 3216, 2104, 1633; ^{1}H NMR (400 MHz, $CDCl_3$), δ (ppm): 9.54 (s, 1H), 9.24 (br s, 1H), 4.03 (s, 3H), 3.97 (s, 3H), 3.54 (s, 1H); ^{13}C NMR (100 MHz, $CDCl_3$), δ (ppm): 176.44, 145.01, 141.44, 119.44, 109.28, 85.72, 73.47, 61.58, 61.45; HRMS (ESI+): m/z: calculated for $C_9H_{10}NO_3$ ($M+H^+$): 180.0655; found: 180.0660.

5-Ethynyl-3,4-diethylpyrrole-2-aldehyde (7.20a): 3,4-diethyl-5-((trimethylsilyl)ethynyl)-pyrrole-2-aldehyde (**7.19b**) (1.5 g, 6.06 mmol) was taken for reaction. Yield: 1.03 g (97%). All data ~~are~~ matched with previously reported compound.[13]

5-ethynyl-3-chloro-4-methoxypyrrole-2-aldehyde (7.20c): 3-Chloro-4-methoxy-5-((trimethylsilyl)ethynyl)pyrrole-2-aldehyde (**7.19c**) (1.6 g, 6.26 mmol) was used for reaction. Yield: 1.08 g (94%); m.p.: 149.2 °C; IR (KBr): ν (cm^{-1}) 3208, 2115, 1638; ^{1}H NMR (400 MHz, $CDCl_3$), δ (ppm): 9.59 (s, 1H), 9.45 (br s, 1H), 4.05 (s, 3H), 3.56 (s, 1H); ^{13}C NMR (100 MHz, $CDCl_3$), δ (ppm): 177.23, 148.06, 125.29, 113.27, 107.97, 86.19, 72.82, 61.24; HRMS (ESI+): m/z: calculated for $C_8H_7NO_3Cl$ ($M+H^+$): 184.0163; found: 180.0163.

General Procedure for synthesis of 5,5'-(ethyne-1,2-diyl)bis(3,4-disubstituted pyrrole-2-aldehyde) (7.21a-c): 3,4-Dimethoxy-5-iodopyrrole-2-aldehyde (**7.18b**) (600 mg, 2.13

mmol), 5-ethynyl-3,4-dimethoxypyrrole-2-aldehyde **(7.20b)** (389 mg, 2.17 mmol), $Pd(PPh_3)_2Cl_2$ (30 mg, 0.043 mmol) and CuI (16 mg, 0.086 mmol) were taken under argon atmosphere. THF (24 mL) and triethylamine (1.8 mL, 12.78 mmol) were purged with argon for 20 min and then transfer to the reaction flask via cannula. Subsequently, the reaction mixture was heated at 60 °C for 3 h, cooled and was evaporated to dryness under reduced pressure. Crude product was purified by silica gel column chromatography using EtOAc/hexane (1:1) as eluent to provide 5,5'-(ethyne-1,2-diyl)bis(3,4-dimethoxypyrrole-2-aldehyde) **(7.21b)** (629 mg) as brownish yellow powdery solid.

5,5'-(ethyne-1,2-diyl)bis(3,4-dimethoxypyrrole-2-aldehyde) (7.21b): Yield: 629 mg (89%); m.p.: 255 °C (dec); IR (KBr): ν (cm^{-1}) 3183, 1622; ^{1}H NMR (400 MHz, DMSO-d_6), δ (ppm): 12.04 (br s, 2H), 9.48 (s, 2H), 3.94 (s, 6H), 3.90 (s, 6H); ^{13}C NMR (100 MHz, DMSO-d_6), δ (ppm): 176.18, 143.48, 140.57, 119.99, 108.33, 86.27, 61.40, 61.36; HRMS (ESI+): m/z: calculated for $C_{16}H_{17}N_2O_6$ ($M+H^+$): 333.1081; found: 333.1084.

5,5'-(ethyne-1,2-diyl)bis(3,4-diethylpyrrole-2-aldehyde) (7.21a): 3,4-Diethyl-5-iodopyrrole-2-aldehyde(**7.18a**) (1 g, 3.61 mmol), 5-ethynyl-3,4-diethylpyrrole-2-aldehyde **(7.20a)** (664 mg, 3.79 mmol) were taken and reaction was run for 16 hour at 60 °C. Yield of **7.21a**: 720 mg (62%). All data matched with previously reported compound.[9]

5,5'-(ethyne-1,2-diyl)bis(3-chloro-4-methoxypyrrole-2-aldehyde) (7.21c): 300 mg (1.05 mmol) of **7.18c** and 197 mg (1.07 mmol) of **7.20c** were used for reaction and reaction mixture was refluxed for 12 h. Yield: 250 mg (70%); m.p.: > 300 °C (dec); IR (neat): ν (cm^{-1}) 3317, 1635; ^{1}H NMR (400MHz, DMSO-d_6), δ (ppm): 12.89 (br s, 2H), 9.55 (s, 2H), 3.99 (s, 6H); ^{13}C NMR (100MHz, DMSO-d_6), δ (ppm): 177.32, 147.11, 125.67, 109.98, 107.10, 85.85, 61.11; HRMS (ESI+): m/z: calculated for $C_{14}H_{11}N_2O_4Cl_2$ ($M+H^+$): 341.0090; found: 341.0093.

General procedure for synthesis of 5,5'-(buta-1,3-diyne-1,4-diyl)bis(3,4-disubstituted pyrrole-2-aldehyde) (7.22a-c): 5-Ethynyl-3,4-dimethoxypyrrole-2-aldehyde **(7.20b)** (300 mg, 1.67 mmol), $Pd(PPh_3)_2Cl_2$ (59 mg, 0.083 mmol), CuI (32 mg, 0.167 mmol) and triethylamine (1.4 mL, 10.02 mmol) were taken in THF (18 mL). Reaction mixture was bubbled with oxygen for 1 h at room temperature. Reaction mixture was evaporated to dryness under reduced pressure. Crude product was purified by silica gel column chromatography using EtOAc/hexane (3:7) as eluent to obtain 5,5'-(buta-1,3-diyne-1,4-diyl)bis(3,4-dimethoxypyrrole-2-aldehyde) **(7.22b)** (284 mg) as yellow powdery solid.

5,5'-(buta-1,3-diyne-1,4-diyl)bis(3,4-dimethoxypyrrole-2-aldehyde) (7.22b): Yield: 284 mg (95%); m.p.: 207.7 °C; IR (KBr): ν (cm^{-1}) 3205, 2142, 1627; ^{1}H NMR (400 MHz, DMSO-d_6), δ (ppm): 12.09 (br s, 2H), 9.50 (s, 2H), 3.94 (s, 6H), 3.87 (s, 6H); ^{13}C NMR (100 MHz, DMSO-d_6), δ (ppm): 176.63, 142.99, 142.78, 120.96, 106.79, 80.36, 75.13, 61.68, 61.37; HRMS (ESI+): m/z: calculated for $C_{18}H_{17}N_2O_6$ ($M+H^+$): 357.1081; found: 357.1086.

5,5'-(buta-1,3-diyne-1,4-diyl)bis(3,4-diethylpyrrole-2-aldehyde) (7.22a): 5-Ethynyl-3,4-diethylpyrrole-2-aldehyde **(7.20a)** (400 mg, 2.28 mmol) was taken for reaction. Yield of **7.22a**: 372 mg (94%). All data matched with previously reported compound.[13]

5,5'-(buta-1,3-diyne-1,4-diyl)bis(3-chloro-4-methoxypyrrole-2-aldehyde) (7.22c): 100 mg (0.55 mmol) of **7.20c** was used for reaction. Yield: 80 mg (80%); m.p.: > 300 °C; IR (neat): ν (cm^{-1}) 3224, 2356, 1637; ^{1}H NMR (400 MHz, DMSO-d_6), δ (ppm): 12.94 (br s, 2H), 9.56 (s, 2H), 3.97 (s, 6H); ^{13}C NMR (100 MHz, DMSO-d_6), δ (ppm): 177.57, 149.22, 126.37, 109.56, 106.03, 80.39, 74.60, 61.11; HRMS (ESI+): m/z: calculated for $C_{16}H_{11}N_2O_4Cl_2$ ($M+H^+$): 365.0090; found: 365.0097.

General procedure for synthesis of 2,3,8,9,14,15,20,21-octasubstituted-5,6,17,18-tetradehydro-[22]porphyrins-(2.2.2.2) or 2,3,8,9,14,15,20,21-octasubstituted-monoacetylene-cumuleneporphycenes (7.8 and 7.15): A slurry of activated zinc (1.57 g) and copper(I)chloride (237 mg, 2.4 mmol) were taken in THF (100 mL) under nitrogen atmosphere and $TiCl_4$ (1.32 mL, 12 mmol) was added slowly. The reaction mixture was then refluxed for 3 h with vigorous stirring and then the slurry was allowed to cool to room temperature. 5,5'-(Ethyne-1,2-diyl)bis(3,4-dimethoxypyrrole-2-aldehyde) **(7.21b)** (200 mg, 0.60 mmol) in THF (100 mL) was added slowly over 5 h at room temperature with vigorous stirring. The reaction mixture was continued for an additional 2 h and then hydrolyzed by slow addition of 10% aqueous sodium carbonate (ca. 100 mL) to the ice cooled reaction mixture. Subsequently, chloroform (~100 mL) was added to the reaction mixture and allowed to stir at room temperature for additional 2 h. Reaction mixture was filtered through celite, organic layer was separated and then celite portion was taken in a beaker and washed with chloroform repeatedly until washings became colorless. Combined organic layer was passed through anhydrous Na_2SO_4 and evaporated to dryness under reduced pressure. Crude reaction mixture was purified with methanol/chloroform (1:99) to obtain mixture of **7.15** with acetylenic dihydro and tetrahydro (**7.17**) reduced products. The mixture of product was washed with chloroform/hexane (1:1), filtered and washed with same solution until filtrate

became colorless, to leave pure **7.15** (47 mg) as blue crystalline solid. Filtrate was evaporated to dryness under reduce pressure, which could be further reduced to tetrahydro product (**7.17**) in good yield by using 20 mol% Pd/C at 1 atm H_2 pressure.

2,3,8,9,14,15,20,21-octamethoxy-5,6,17,18-tetradehydro-[22]porphyrin-(2.2.2.2) (7.15): Yield: 47 mg (26%); m.p.: > 300 °C; IR (KBr): ν (cm^{-1}) 2066; ^{1}H NMR (500 MHz, $CDCl_3$), δ (ppm): 10.05 (s, 4H), 5.34 (s, 12H), 4.92 (s, 12H), 0.86 (s, 2H); UV-Vis data in $CHCl_3$, λ_{max} nm (log ε): 411 (4.97), 445 (4.65), 672 (4.29), 714 (4.54), 758 (4.41); HRMS (ESI+): m/z: calculated for $C_{32}H_{31}N_4O_8$ ($M+H^+$): 599.2136; found: 599.2142.

2,3,8,9,14,15,20,21-octaethyl-5,6,17,18-tetradehydro-[22]porphyrin-(2.2.2.2) (7.8): 5,5'-(Ethyne-1,2-diyl)bis(3,4-diethylpyrrole-2-aldehyde) **(7.21a)** (200 mg, 0.62 mmol) was taken for reaction. Crude reaction mixture was purified by silica gel column chromatography using chloroform/hexane (1:1) as eluent yields **7.8** (48 mg) as blue crystalline solid. Yield: 48 mg (27%); ^{1}H NMR (400 MHz, $CDCl_3$), δ (ppm): 10.00 (s, 4H), 4.46 (q, 8H, *J* = 7.6 Hz), 4.12 (q, 8H, *J* = 7.6 Hz), 2.25 (t, 12H, *J* = 7.6 Hz), 2.19 (s, 2H), 1.94 (t, 12H, *J* = 7.6 Hz); UV-Vis data in $CHCl_3$, λ_{max} nm (log ε): 407 (5.29), 440 (4.90), 679 (4.60), 726 (4.88), 768 (4.91).

General procedure for synthesis of 2,3,10,11,16,17,24,25-octasubstituted-5,6,7,8,19,20,21,22-tetradehydro-[26]porphyrin-(2.4.2.4) or 2,3,10,11,16,17,24,25-octasubstituted diacetylene-cumuleneporphycenes (7.9 and 7.16): A slurry of activated zinc (1.46 g) and copper(I)chloride (221 mg, 2.24 mmol) were taken in THF (100 mL) under nitrogen atmosphere and $TiCl_4$ (1.23 mL, 11.2 mmol) was added slowly. The reaction mixture was refluxed for 3 h with vigorous stirring. 5,5'-(Buta-1,3-diyne-1,4-diyl)bis(3,4-dimethoxypyrrole-2-aldehyde) **(7.22b)** (200 mg, 0.56 mmol) in THF (100 mL) was added slowly over 2 h with vigorous stirring. The reaction mixture was heated under reflux for an additional 2 h and then hydrolyzed by slow addition of 10% aqueous sodium carbonate (ca. 100 mL) to the ice cooled reaction mixture. Subsequently, chloroform (~100 mL) was added to the reaction mixture and allowed to stir at room temperature for additional 2 h. Reaction mixture was filtered through celite, organic layer was separated and then celite portion was taken in a beaker and washed with chloroform repeatedly until washings became colorless. Combined organic layer was passed through anhydrous Na_2SO_4 and evaporated to dryness under reduced pressure. Crude reaction mixture was purified by silica gel column chromatography using methanol/chloroform (1:99) as eluent provides mixture of **7.16** with some impurities. The mixture of product was washed with chloroform/hexane (1:1), filtered

and washed with same solution until filtrate becomes colorless, to obtain pure **7.16** (30 mg) as shiny green crystalline solid.

2,3,10,11,16,17,24,25-octamethoxy-5,6,7,8,19,20,21,22-tetradehydro-[26]porphyrin-(2.4.2.4) (7.16): Yield: 30 mg (17%); m.p.: > 300 °C; IR (KBr): ν (cm^{-1}) 2016; ^{1}H NMR (500 MHz, $CDCl_3$), δ (ppm): 10.15 (s, 4H), 5.42 (s, 12H), 4.96 (s, 12H), 0.77 (s, 2H); UV-Vis data in $CHCl_3$, λ_{max} nm (log ε): 456 (5.10), 500 (4.87), 832 (4.86), 884 (4.76); HRMS (ESI+): m/z: calculated for $C_{36}H_{31}N_4O_8$ ($M+H^+$): 647.2136; found: 647.2145.

2,3,10,11,16,17,24,25-octaethyl-5,6,7,8,19,20,21,22-tetradehydro-[26]porphyrin-(2.4.2.4) (7.9): 5,5'-(Buta-1,3-diyne-1,4-diyl)bis(3,4-diethylpyrrole-2-aldehyde) **(7.22a)** (200 mg, 0.57 mmol) was taken for reaction. Crude reaction mixture was purified by silica gel column chromatography using chloroform/hexane (1:1) as eluent to obtain pure **7.22a** (30 mg) as blue crystalline solid. Yield: 30 mg (17%); ^{1}H NMR (400 MHz, $CDCl_3$), δ (ppm): 10.09 (s, 4H), 4.57 (q, 8H, *J* = 7.6 Hz), 4.15 (q, 8H, *J* = 7.6 Hz), 2.30 (t, 12H, *J* = 7.6 Hz), 1.98 (t, 12H, *J* = 7.6 Hz), 1.96 (s, 2H); UV-Vis data in $CHCl_3$, λ_{max} nm (log ε): 449 (5.18), 496 (5.01), 841 (5.00), 889 (5.03).

General procedure for synthesis of 2,3,8,9,14,15,20,21-octasubstituted[22]porphyrin-(2.2.2.2) (7.10 and **7.17):** 2,3,8,9,14,15,20,21-Octamethoxy-5,6,17,18-tetradehydro-[22]porphyrin(2.2.2.2) (**7.15**) (10 mg, 0.017 mmol) and 5% Pd/C (7 mg) were taken in THF (30 mL) under blanket of hydrogen (1 atm, hydrogen balloon). Progress of the reaction was checked with UV-Vis spectroscopy by drawing small amount aliquot from reaction mixture. After completion of the reaction (~ 48 h), hydrogen balloon was removed and the reaction mixture was diluted with chloroform. Subsequently, DDQ (12 mg, 0.051 mmol) was added and stirred for another 30 min. The reaction mixture was passed through celite and washed with chloroform. Combined organic layer was evaporated to dryness under reduced pressure and purified by silica gel column chromatography using chloroform as eluent to afford desired product **7.17** (4 mg) as blue crystalline solid.

2,3,8,9,14,15,20,21-octamethoxy[22]porphyrin-(2.2.2.2) (7.17): Yield: 4 mg (39%); m.p.: 260.9 °C; ^{1}H NMR (400 MHz, $CDCl_3$), δ (ppm): 11.98 (d, 2H, *J* = 14.8 Hz), 9.90 (d, 2H, *J* = 11.2 Hz), 9.84 (d, 2H, *J* = 11.2 Hz), 5.05 (s, 6H), 4.93 (s, 6H), 4.87 (s, 6H), 4.82 (s, 6H), 0.83 (s, 2H), -7.97 (d, 2H, *J* = 14.8 Hz) ; ^{13}C NMR (100 MHz, $CDCl_3$), δ (ppm): 145.91, 144.97, 143.12, 142.89, 139.40, 138.77, 131.95, 131.72, 114.48, 112.79, 109.26, 106.55, 63.61, 63.55, 63.51, 62.10; UV-Vis data in $CHCl_3$, λ_{max} nm (log ε): 442 (5.26), 467 (4.96),

665 (4.50), 708 (4.10), 774 (4.57); Fluorescence λ_{max} in nm: 779 (λ_{exc} 442 nm); Fluorescence quantum yield: 0.0095; HRMS (ESI+): m/z: calculated for $C_{32}H_{35}N_4O_8$ ($M+H^+$): 603.2449; found: 603.2454.

2,3,8,9,14,15,20,21-octaethyl[22]porphyrin-(2.2.2.2) (7.10): 2,3,8,9,14,15,20,21-Octaethyl-5,6,17,18-tetradehydro-[22]porphyrin(2.2.2.2) **7.8** (20 mg, 0.034 mmol) and 5% Pd/C (16 mg) were taken in THF (30 mL) under blanket of hydrogen (1 atm). Reaction was run for 20 h. Crude product was purified by silica gel column chromatography using chloroform/hexane (1:1) as eluent to afford desired product **7.10** (17 mg) as blue crystalline solid. Yield: 17 mg (84%); ^{1}H NMR (400 MHz, $CDCl_3$), δ (ppm): 11.77 (d, 2H, *J* = 15.2 Hz), 9.93 (d, 2H, *J* = 11.2 Hz), 9.88 (d, 2H, *J* = 11.2 Hz), 4.68 (q, 4H, *J* = 7.6 Hz), 4.24 (q, 4H, *J* = 7.6 Hz), 4.14 (q, 4H, *J* = 7.6 Hz), 4.09 (q, 4H, *J* = 7.6 Hz), 2.27 (t, 6H, *J* = 7.6 Hz), 2.06 (t, 6H, *J* = 7.6 Hz), 1.93 (t, 6H, *J* = 7.6 Hz), 1.91 (t, 6H, *J* = 7.6 Hz), 1.33 (s, 2H), -7.47 (d, 2H, *J* = 15.2 Hz); UV-Vis data in $CHCl_3$, λ_{max} nm (log ε): 442 (5.29), 466 (4.98), 674 (4.56), 728 (4.23), 791 (4.71).

Synthesis of 2,3,8,9,14,15,20,21-octamethoxy[22]porphyrin-(2.2.2.2) (7.17) by McMurry coupling of 3,4-dimethoxypyrrole-2,5-dialdehyde: A slurry of activated zinc (3.59 g) and copper(I)chloride (544 mg, 5.5 mmol) were taken in THF (100 mL) under nitrogen atmosphere and $TiCl_4$ (1.23 mL, 11.2 mmol) was added slowly. The reaction mixture was refluxed for 3 h with vigorous stirring. 3,4-dimethoxypyrrole-2,5-dialdehyde (200 mg, 1.09 mmol) in THF (50 mL) was added slowly over 2 h with vigorous stirring under reflux condition. The reaction was continued for an additional 1 h, cooled and hydrolyzed by slow addition of 10% aqueous sodium carbonate (ca. 100 mL) to the ice cooled reaction mixture. The reaction mixture was allowed to stir at room temperature for another 2 h, filtered through celite and washed with chloroform. Organic layer was separated and aqueous layer was extracted twice with chloroform. Combined organic layer was passed through anhydrous Na_2SO_4 and evaporated to dryness under reduced pressure. Crude reaction mixture was purified by silica gel column chromatography using chloroform as eluent to provide pure **7.17** (2.4 mg) as blue crystalline solid. Yield: 2.4 mg (1.4%).

7.6 Crystallographic details

Crystallographic data for **7.17** was collected on Oxford Gemini A Ultra diffractometer with dual source. Mo-Kα (λ = 0.71073 Å) radiation was used to collect the X-ray reflections of the crystal. Crystallographic data for **7.15** was collected on BRUKER SMART-APEX CCD

diffractometer. Mo-Kα (λ = 0.71073 Å) radiation was used to collect X-ray reflections on the single crystal. Relevant crystallographic data collection and refinement parameters are shown in the following table:

Crystal Data	**7.15**	**7.17**
CCDC No.	1051706	1051707
Formula unit	$C_{32}H_{30}N_4O_8$	$C_{32}H_{34}N_4O_8$
Formula Weight	598.60	602.63
Crystal system	Triclinic	Monoclinic
T [K]	298(2)	293(2)
a [Å]	6.659(5)	9.2798(12)
b [Å]	14.335(16)	22.731(13)
c [Å]	17.013(13)	16.745(4)
α [°]	65.12(3)	90.00
β [°]	84.49(7)	101.57(2)
γ [°]	77.42(9)	90.00
volume [$Å^3$]	1438(2)	2840.4(9)
Space group	P -1	P 21/n
Z′	0.5	1
Z	2	4
D_{calc} [$g.cm^{-3}$]	1.383	1.409
μ/mm^{-1}	0.101	0.102
Reflns collected	13346	17590
Unique reflns	5200	4710
Obs. reflns	2854	1412
R(int)	0.0572	0.1484
R_1 [I > 2σ(I)],	0.0814(2854)	0.0669(1412)
wR_2	0.2167(5200)	0.1171(4710)
GOF	0.995	0.872

7.7 References

1. (a) The Porphyrin Handbook, **2000**, *2*, 55. (b) Sessler, J. L.; Seidel, D. *Angew. Chem. Int. Ed.* **2003**, *42*, 5134.

2. Berger, R. A.; LeGoff, E. *Tetrahedron Lett.* **1978**, *19*, 4225.
3. (a) König, H.; Eickmeier, C.; Möller, M.; Rodewald, U.; Franck, B. *Angew. Chem. Int. Ed. Engl*. **1991**, *29*, 1393. (b) Beckmann, S.; Wessel, T.; Franck, B.; Hönle, W.; Borrmann, H.; Schnering, H.-G. *Angew. Chem. Int. Ed. Engl*. **1991**, *29*, 1395. (c) Gosmann, M.; Vogt, A.; Franck, B. *Liebigs Ann. Chem*. **1990**, 163.
4. LeGoff, E.; Weaver, O. G. *J. Org. Chem*. **1987**, *52*, 710.
5. Wessel, T.; Franck, B.; Möller, M.; Rodewald, U.; Läge, M. *Angew. Chem. Int. Ed. Engl*. **1993**, *32*, 1148.
6. Dietrich. H.-J. Ph. D. dissertation, University of Cologne, **1994**.
7. Eickmeier, C.; Franck, B. *Angew. Chem. Int. Ed. Engl*. **1997**, *36*, 2213.
8. Knübel, G.; Franck, B. *Angew. Chem. Int. Ed. Engl*. **1988**, *27*, 1170.
9. Jux, N.; Koch, P.; Schimickler, H.; Lex, J.; Vogel, E. *Angew. Chem. Int. Ed. Engl*. **1990**, *29*, 1385.
10. Vogel, E.; Jux, N.; Rodriguez-Val, E.; Lex, J.; Schmickler, H. *Angew. Chem. Int. Ed. Engl*. **1990**, *29*, 1387.
11. Rodriguez-Val, E. Ph. D. dissertation, University of Cologne, **1994**.
12. Jux, N. Ph. D. dissertation, University of Cologne, **1994**.
13. Mártire, D. O.; Jux, N.; Aramendía, P. F.; Negri, R. M.; Lex, J.; Braslavsky, S. E.; Schaffner, K.; Vogel, E. *J. Am. Chem. Soc.* **1992**, *114*, 9969.
14. Vogel, E. *Pure. Appl. Chem*. **1993**, *65*, 143.
15. (a) Lim, J. M.; Yoon, Z. S.; Shin, J.-Y, Kim, K. S.; Yoon, M.-C.; Kim, D. *Chem. Commun.* **2009**, 261. (b) Shin, J.-Y.; Kim, K. S.; Yoon, M.-C.; Lim, J. M.; Yoon, Z. S.; Osuka, A.; Kim, D. *Chem. Soc. Rev.* **2010**, *39*, 2751. (c) Gokulnath, S.; Chandrashekar, T. K. *J. Chem. Sci.* **2008**, *120*, 137. (d) Pawlicki, M.; Collins, H. A.; Denning, R. G.; Anderson, H. L. *Angew. Chem. Int. Ed.* **2009**, *48*, 3244. (e) Rath, H.; Sankar, J.; PrabhuRaja, V.; Chandrashekar, T. K.; Nag, A.; Goswami, D. *J. Am. Chem. Soc.* **2005**, *127*, 11608.
16. Rana, A.; Panda, P. K. *Org. Lett.* **2014**, *16*, 78.
17. Cho, D. H.; Lee, J. H.; Kim, B. H. *J. Org. Chem.* **1999**, *64*, 8048.
18. Sessler, J. L.; Callaway, W.; Dudek, S. P.; Date, R. W.; Lynch, V.; Bruce, D. W. *Chem. Commun.* **2003**, 2422.
19. Albota, M.; Beljonne, D.; Brédas, J.-L.; Ehrlich, J. E.; Fu, J.-Y.; Heikal, A. A.; Hess, S. E.; Kogej, T.; Levin, M. D.; Marder, S. E.; McCord-Maughon, D.; Perry, J. W.;

Röckel, H.; Rumi, M.; Subramaniam, G.; Webb, W. W.; Wu, X.-L.; Xu, C. *Science*. **1998**, *281*, 1653.

20. (a) Drobizhev, M.; Meng, F.; Rebane, A.; Stepanenko, Y.; Nickel, E.; Spangler, C. W.; *J. Phys. Chem. B* **2006**, *110*, 9802. (b) Frampton, M. J.; Akdas, H.; Cowley, A. R.; Rogers, J. E.; Slagle, J. E.; Fleitz, P. A.; Drobizhev, M.; Rebane, A.; Anderson, H. L. *Org. Lett*. **2005**, *7*, 5365. (c) Ahn, T. K.; Kim, K. S.; Kim, D. Y.; Noh, S. B.; Aratani, N.; Ikeda, C.; Osuka, A.; Kim, D. *J. Am. Chem. Soc*. **2006**, *128*, 1700.
21. Rana, A.; Lee, S.; Kim, D.; Panda, P. K. *Chem. Commun*. **2015**, DOI: 10.1039/C5CC02279G.
22. Bernard, C.; Gisselbrecht, J. P.; Gross, M.; Jux, N.; Vogel, E. *J. Electroanal. Chem.* **1995**, *381*, 159.
23. Gisselbrecht, J. P.; Gross, M.; Kócher, M.; Lausmann, M.; Vogel, E. *J. Am. Chem. Soc*. **1990**, *112*, 8618.
24. Kancharla, P.; Reynolds, K. A. *Tetrahedron* **2013**, *69*, 8375.

7.8 Representative NMR spectra

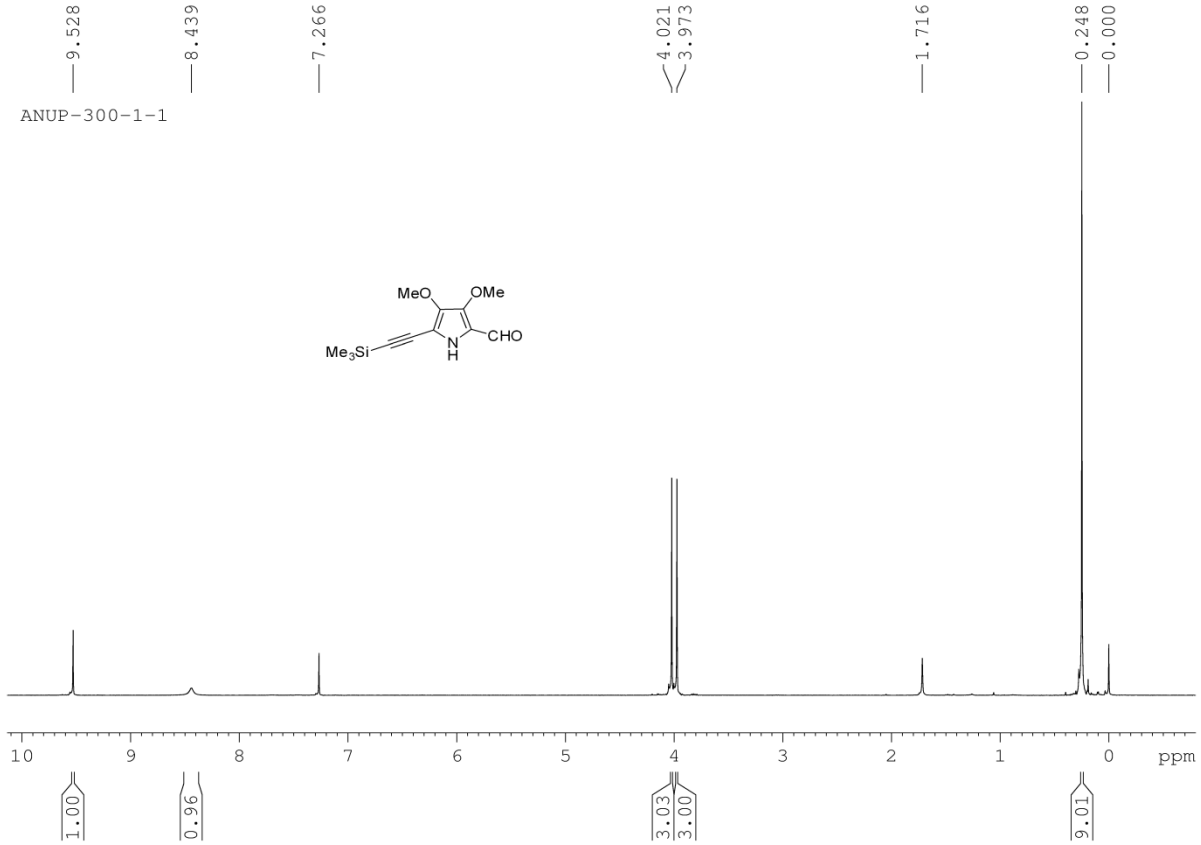

Figure 7.11 ^{1}H NMR spectrum of **7.19b** in $CDCl_3$.

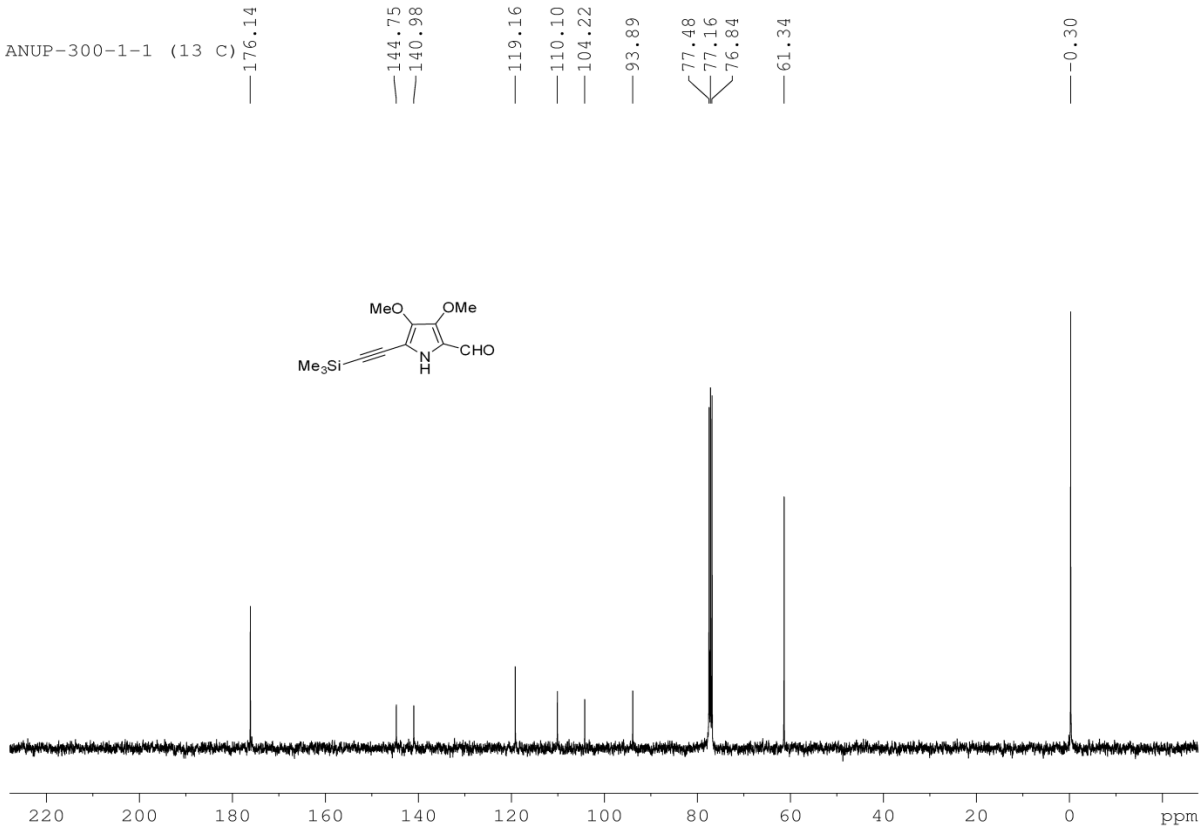

Figure 7.12 ^{13}C NMR spectrum of **7.19b** in $CDCl_3$.

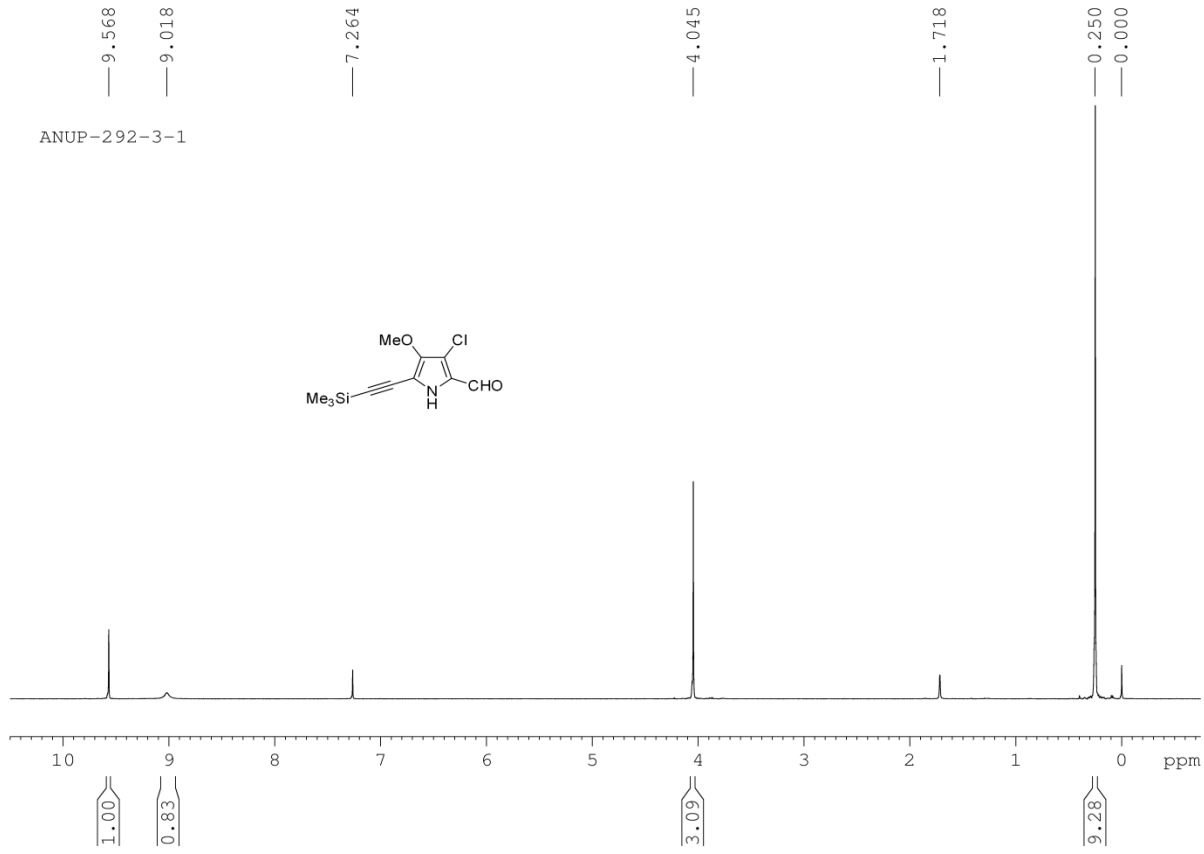

Figure 7.13 ^{1}H NMR spectrum of **7.19c** in $CDCl_3$.

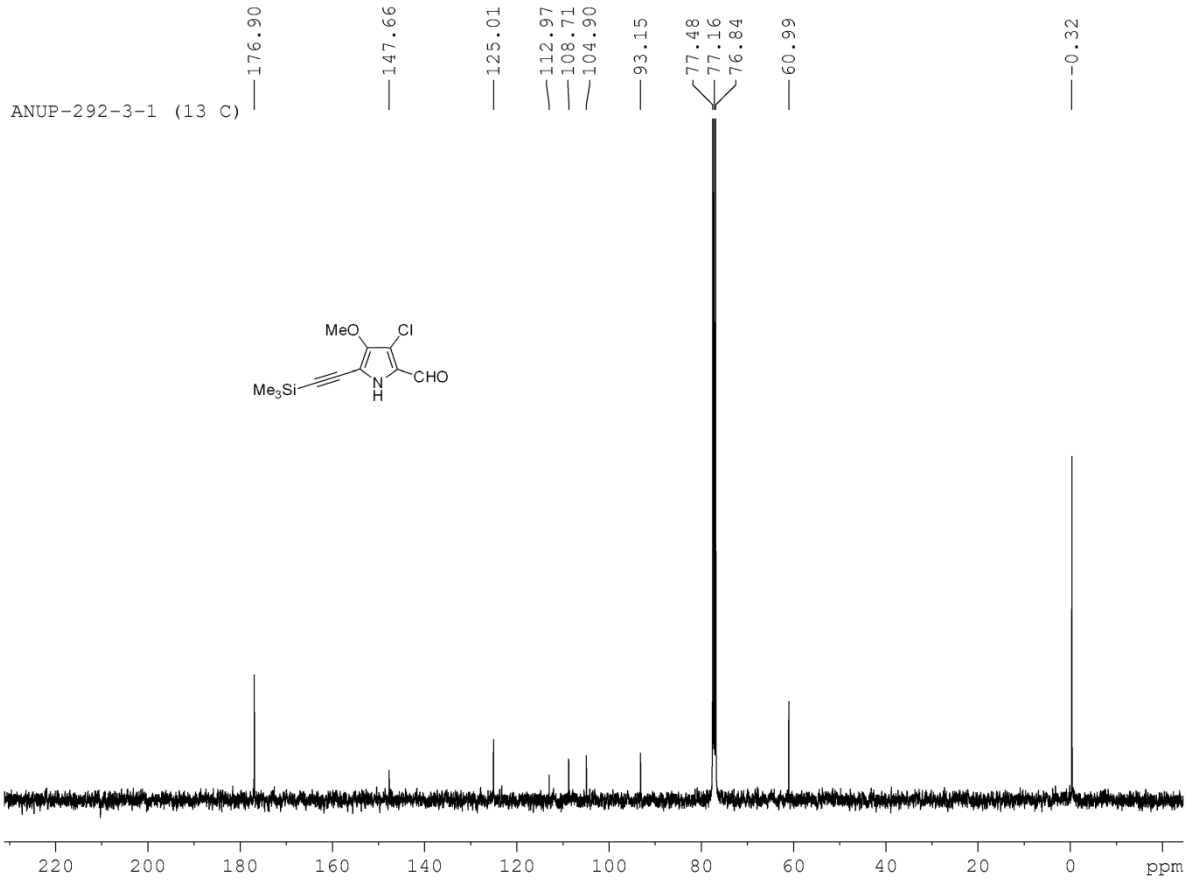

Figure 7.14 ^{13}C NMR spectrum of **7.19c** in $CDCl_3$.

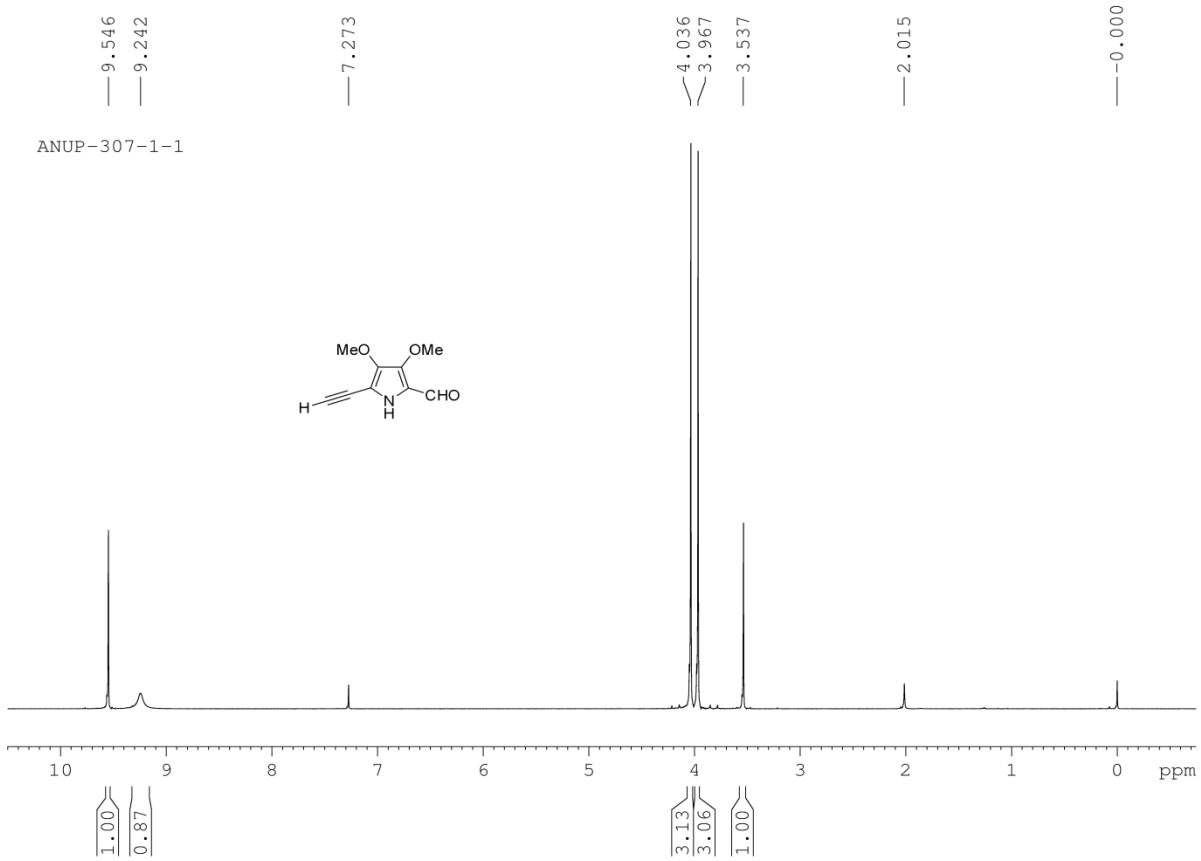

Figure 7.15 ^{1}H NMR spectrum of **7.20b** in $CDCl_3$.

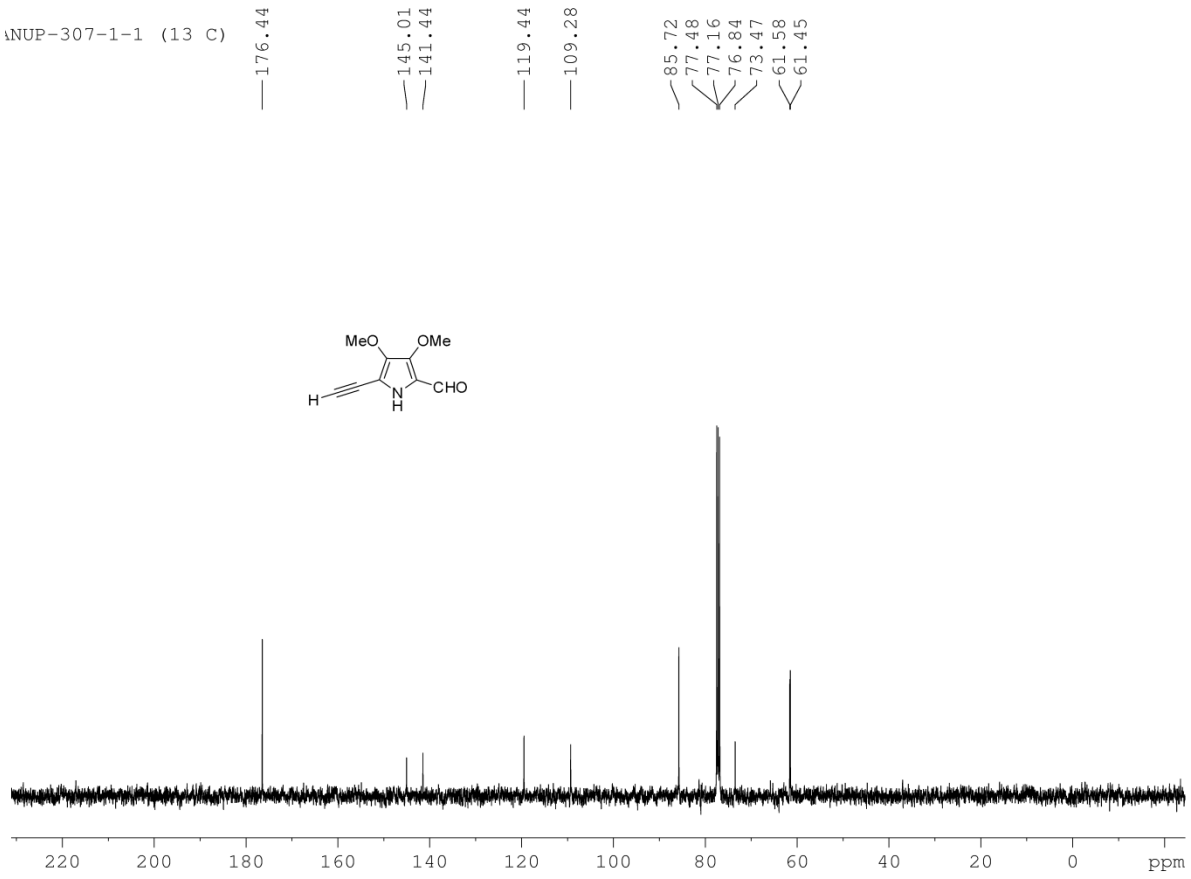

Figure 7.16 ^{1}C NMR spectrum of **7.20b** in $CDCl_3$.

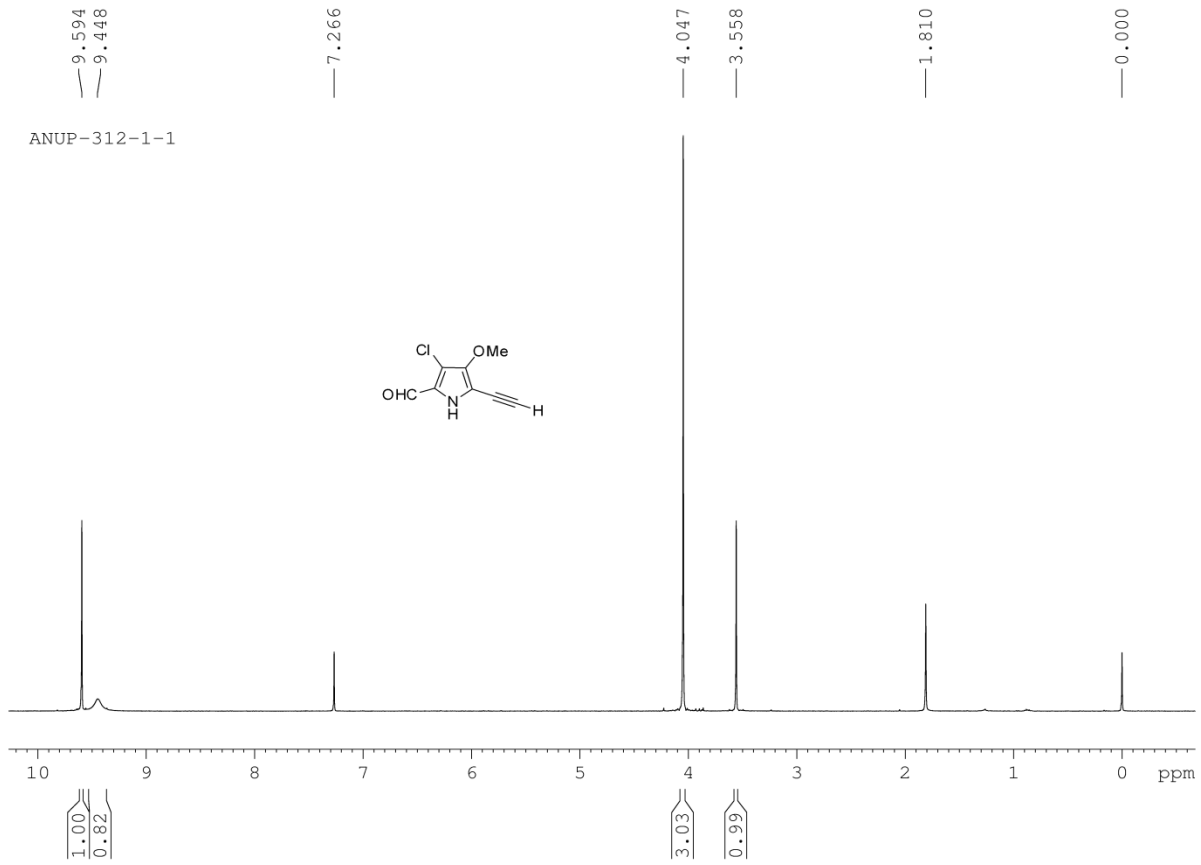

Figure 7.17 ^{1}H NMR spectrum of **7.20c** in $CDCl_3$.

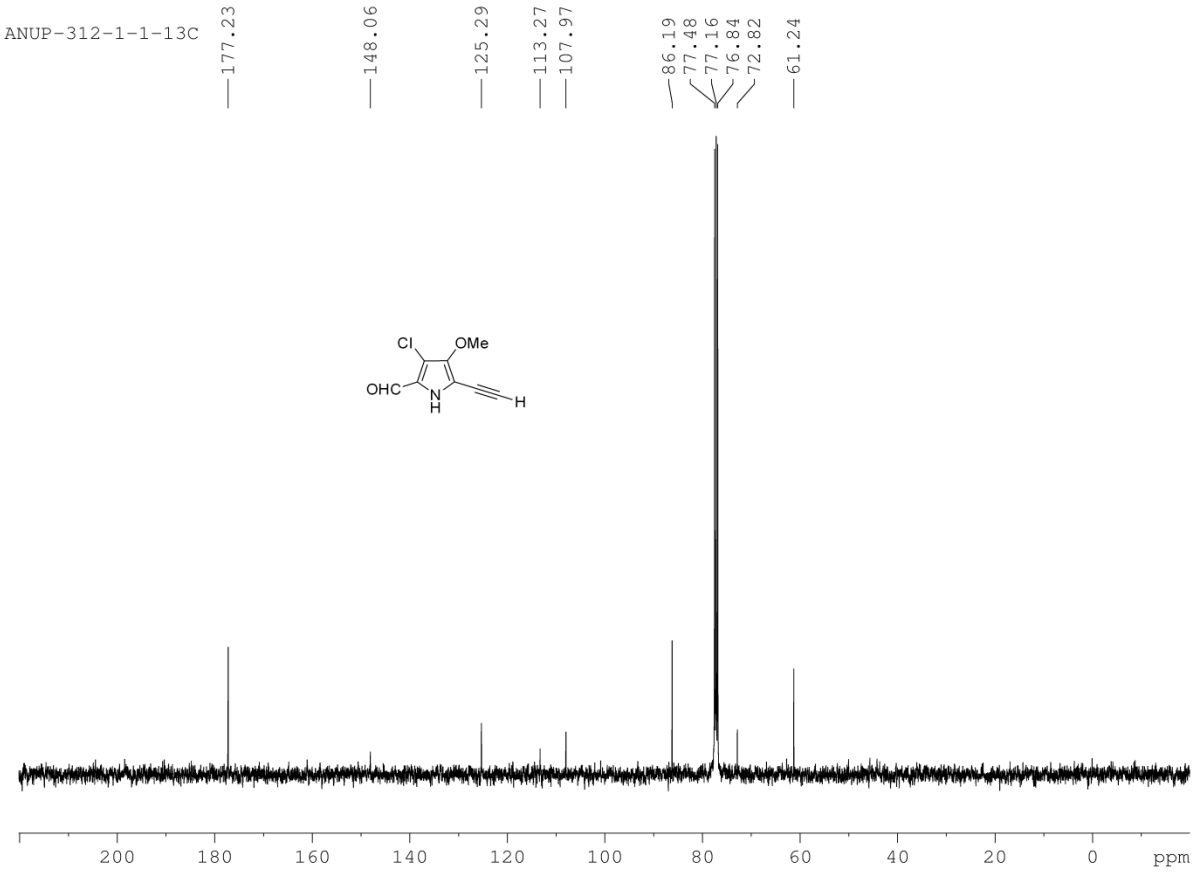

Figure 7.18 ^{13}C NMR spectrum of **7.20c** in $CDCl_3$.

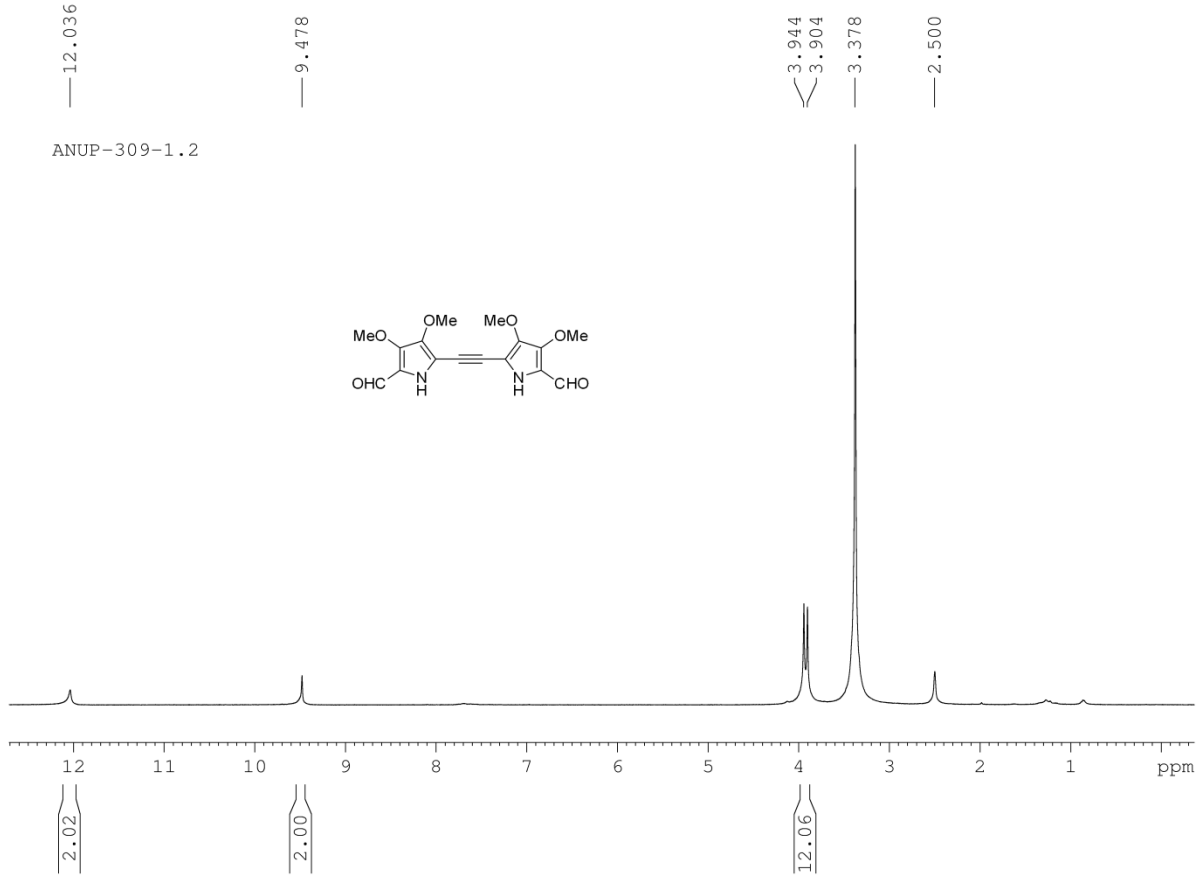

Figure 7.19 ^{1}H NMR spectrum of **7.21b** in DMSO-d_6.

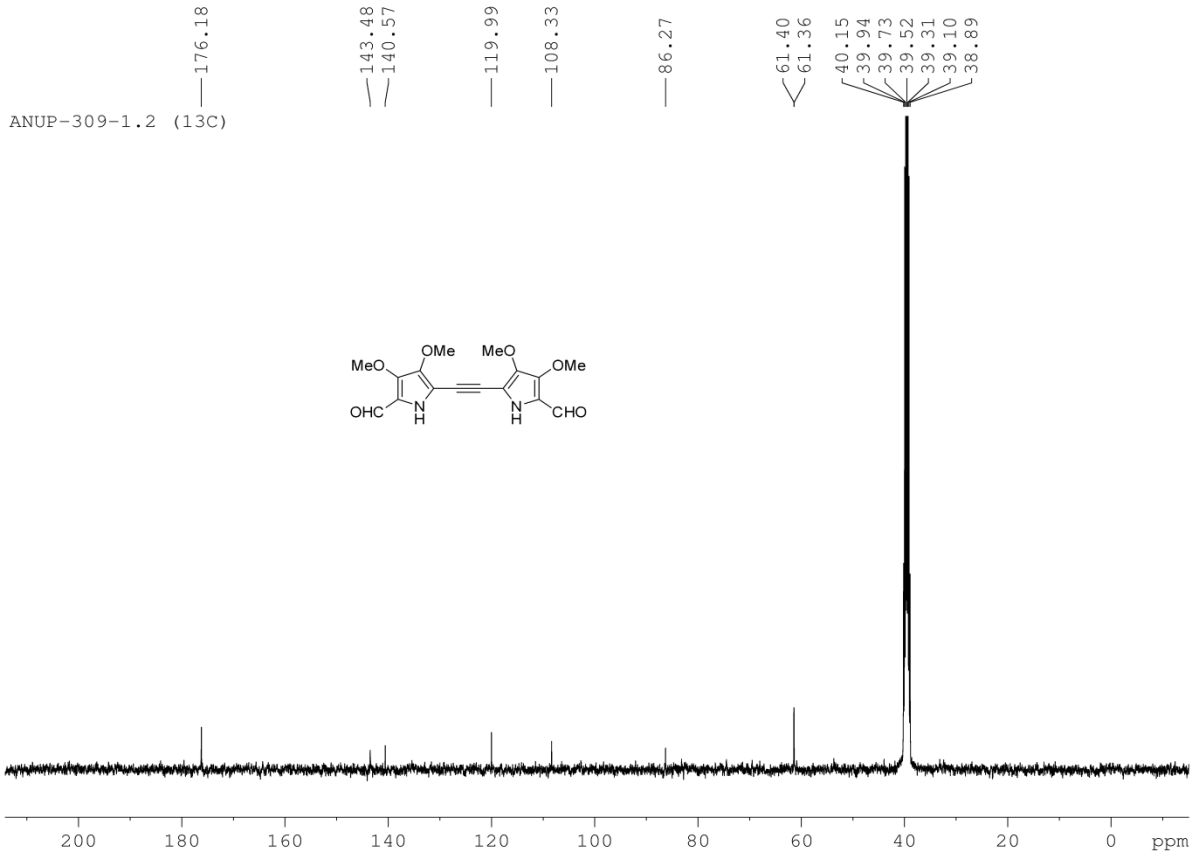

Figure 7.20 ^{13}C NMR spectrum of **7.21b** in DMSO-d_6.

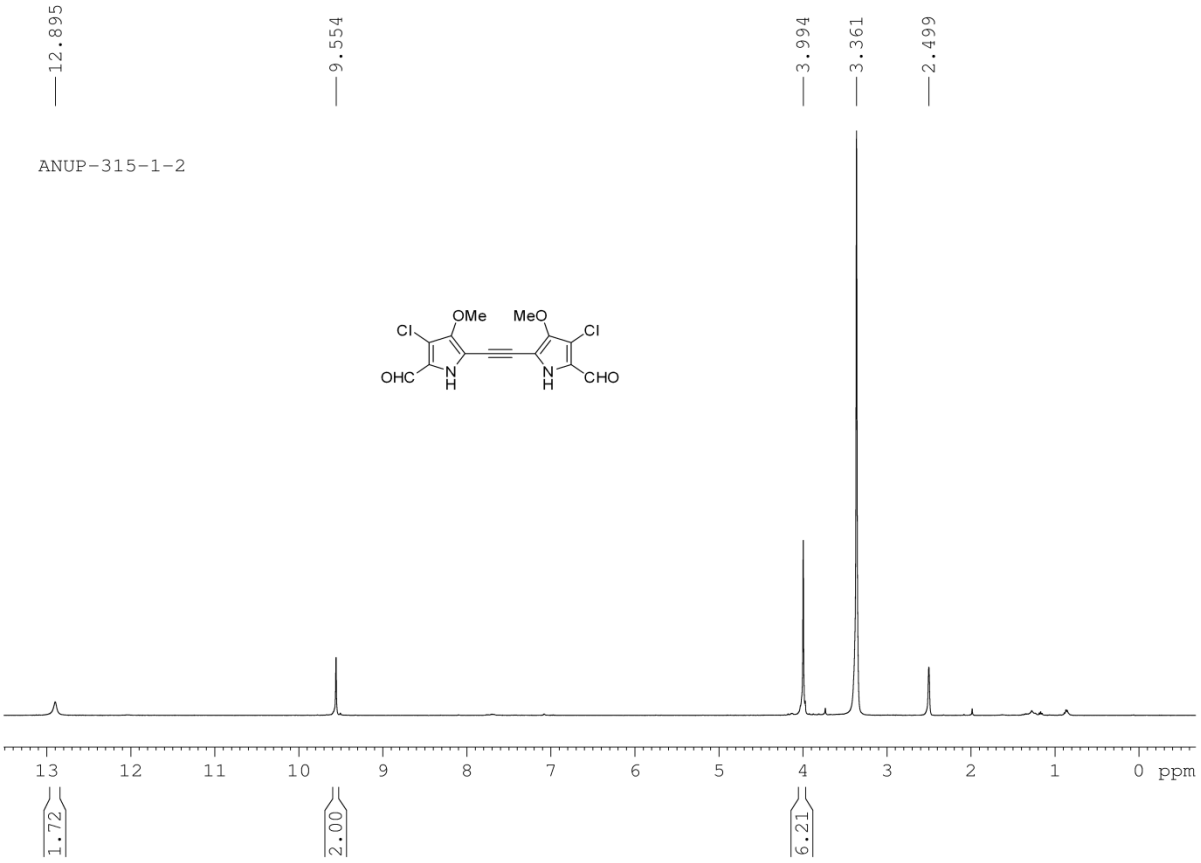

Figure 7.21 ^{1}H NMR spectrum of **7.21c** in DMSO-d_6.

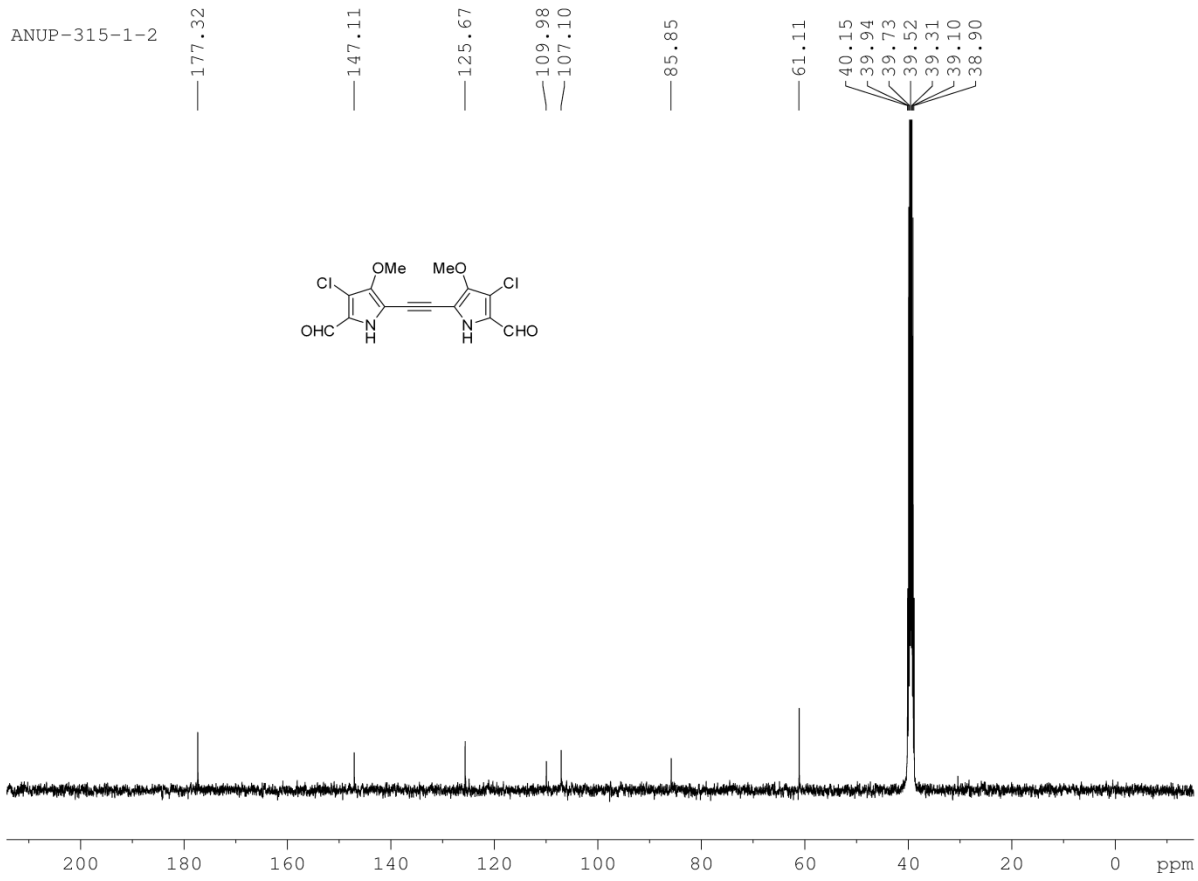

Figure 7.22 ^{13}C NMR spectrum of **7.21c** in DMSO-d_6.

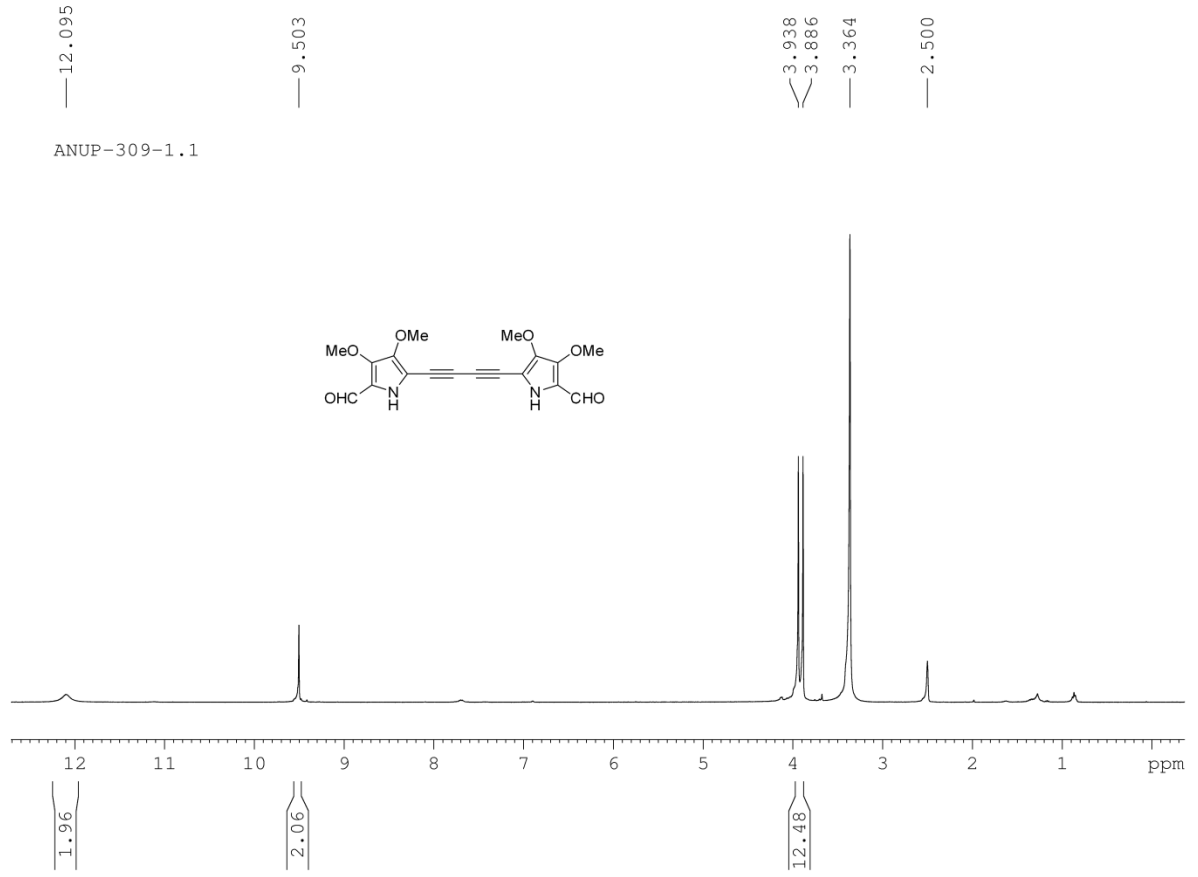

Figure 7.23 ^{1}H NMR spectrum of **7.22b** in DMSO-d_6.

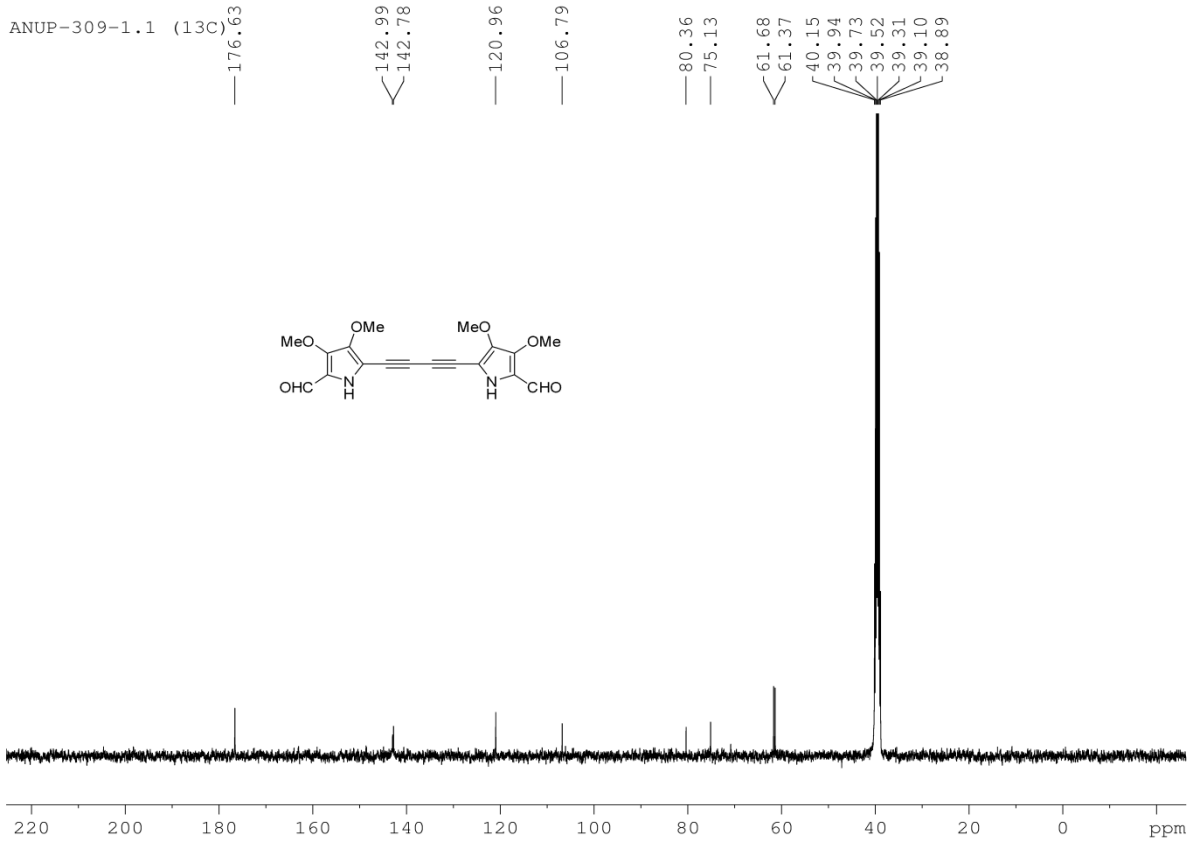

Figure 7.24 ^{13}C NMR spectrum of **7.22b** in DMSO-d_6.

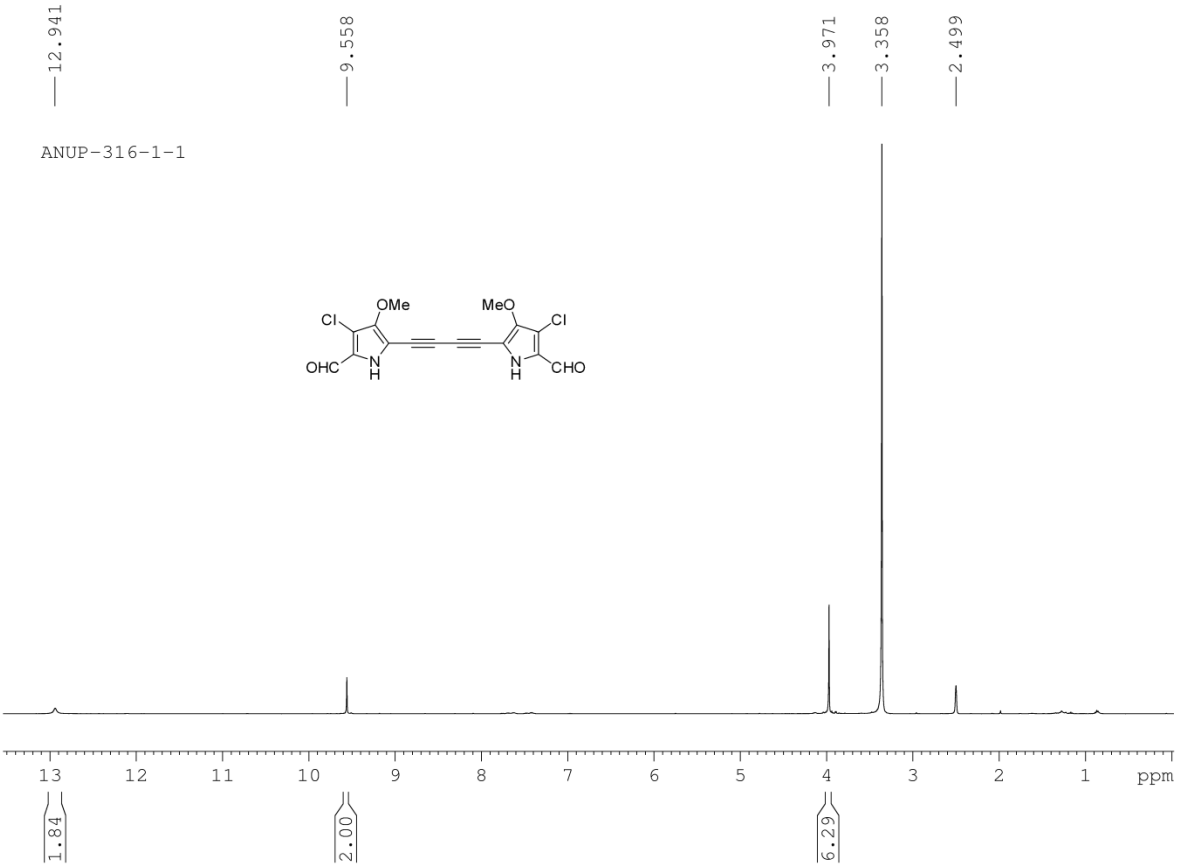

Figure 7.25 ^{1}H NMR spectrum of **7.22c** in DMSO-d_6.

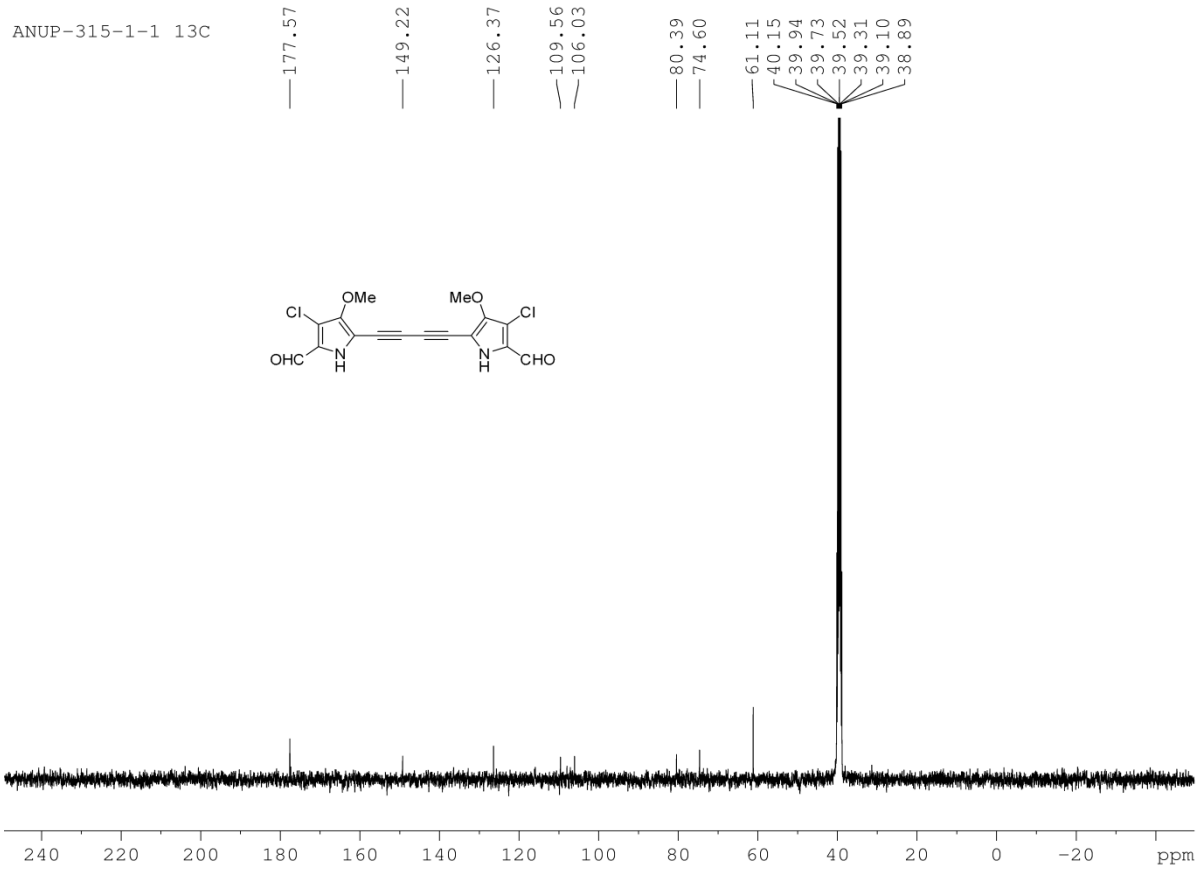

Figure 7.26 ^{13}C NMR spectrum of **7.22c** in DMSO-d_6.

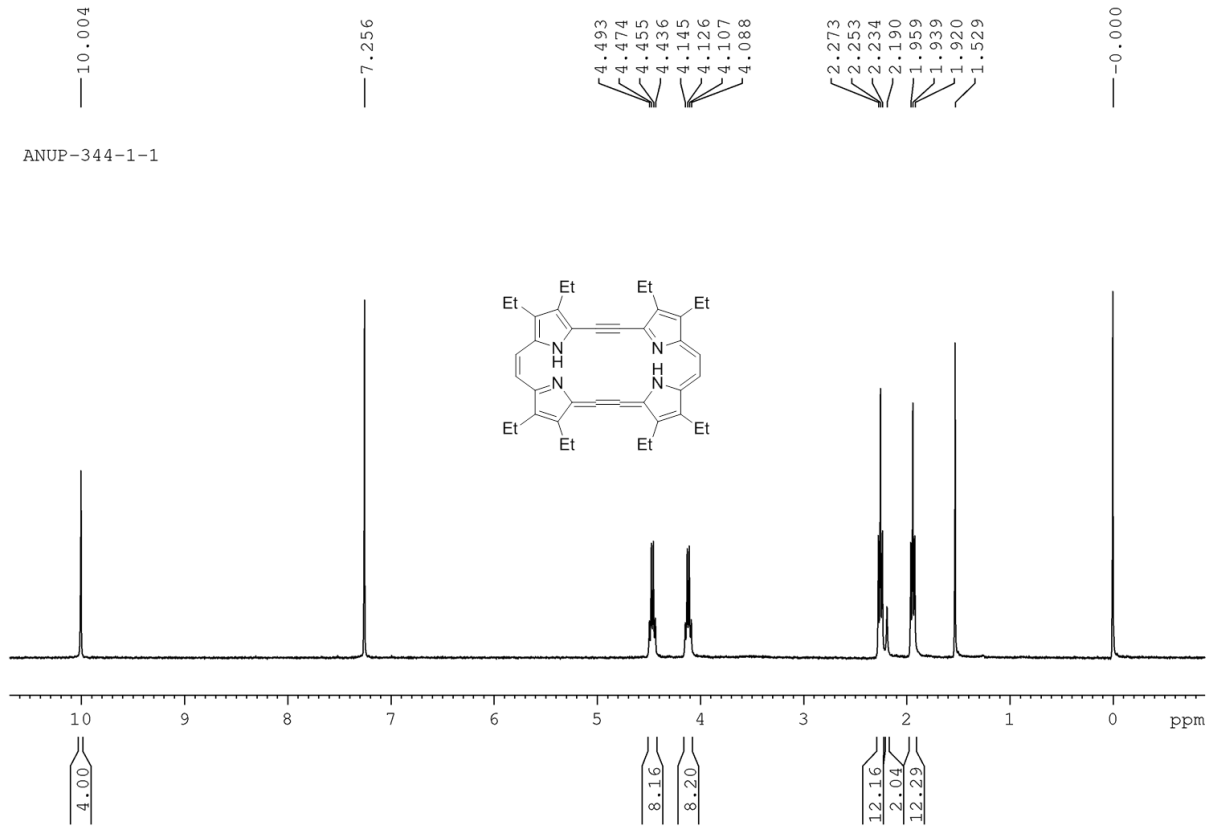

Figure 7.27 ^{1}H NMR spectrum of **7.8** in $CDCl_3$.

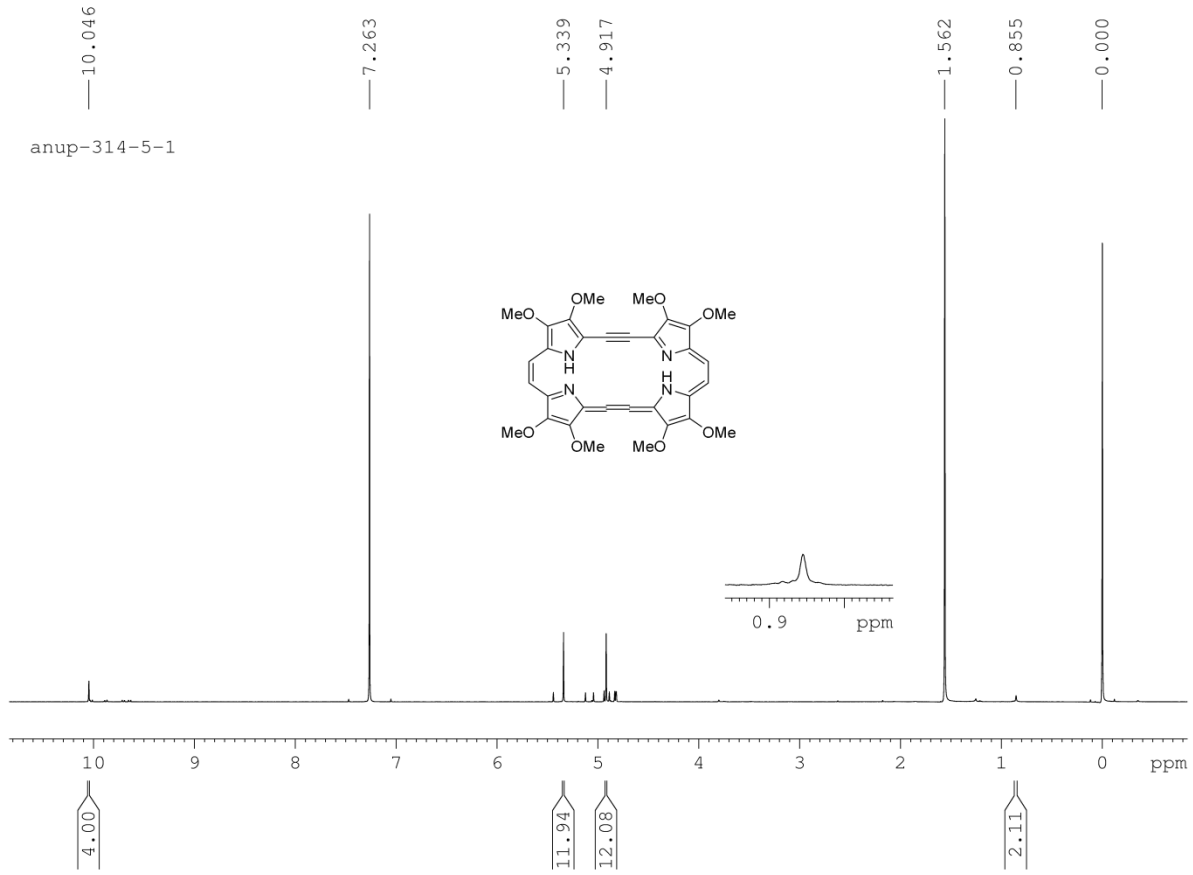

Figure 7.28 ^{1}H NMR spectrum of **7.15** in $CDCl_3$.

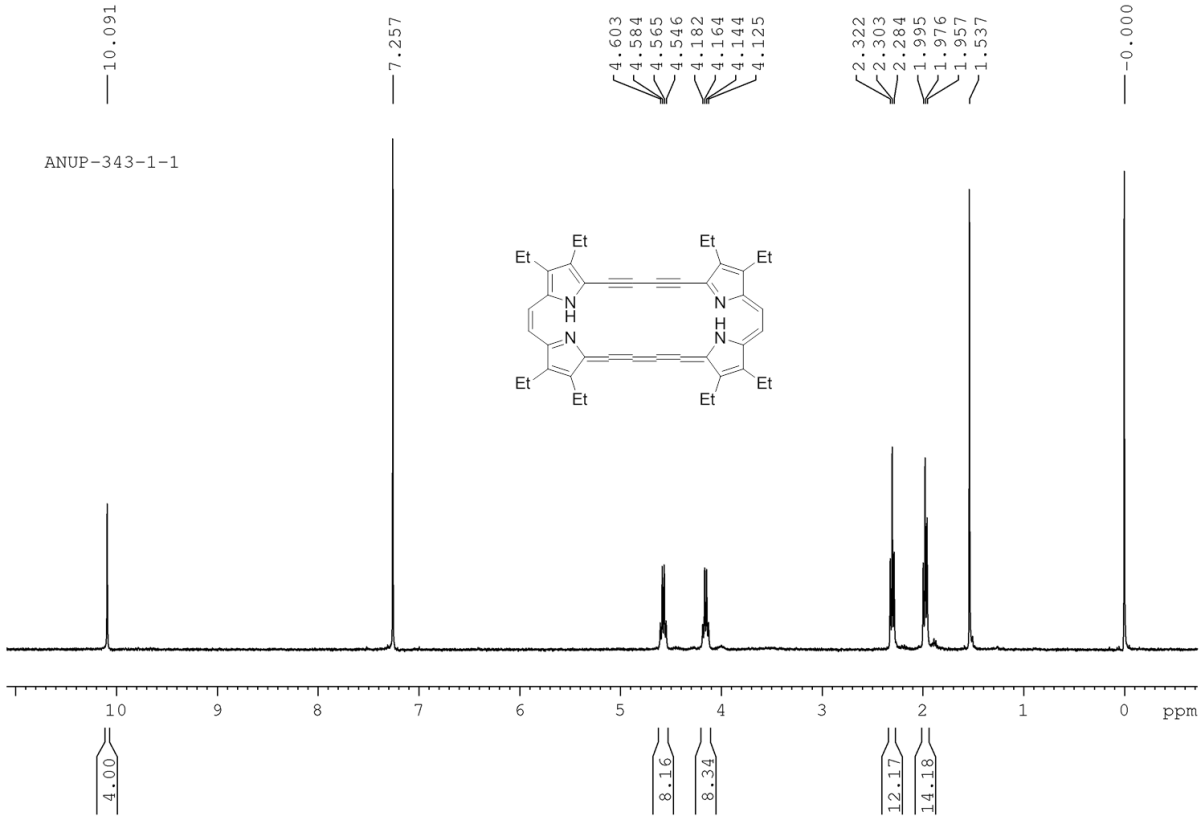

Figure 7.29 ^{1}H NMR spectrum of **7.9** in $CDCl_3$.

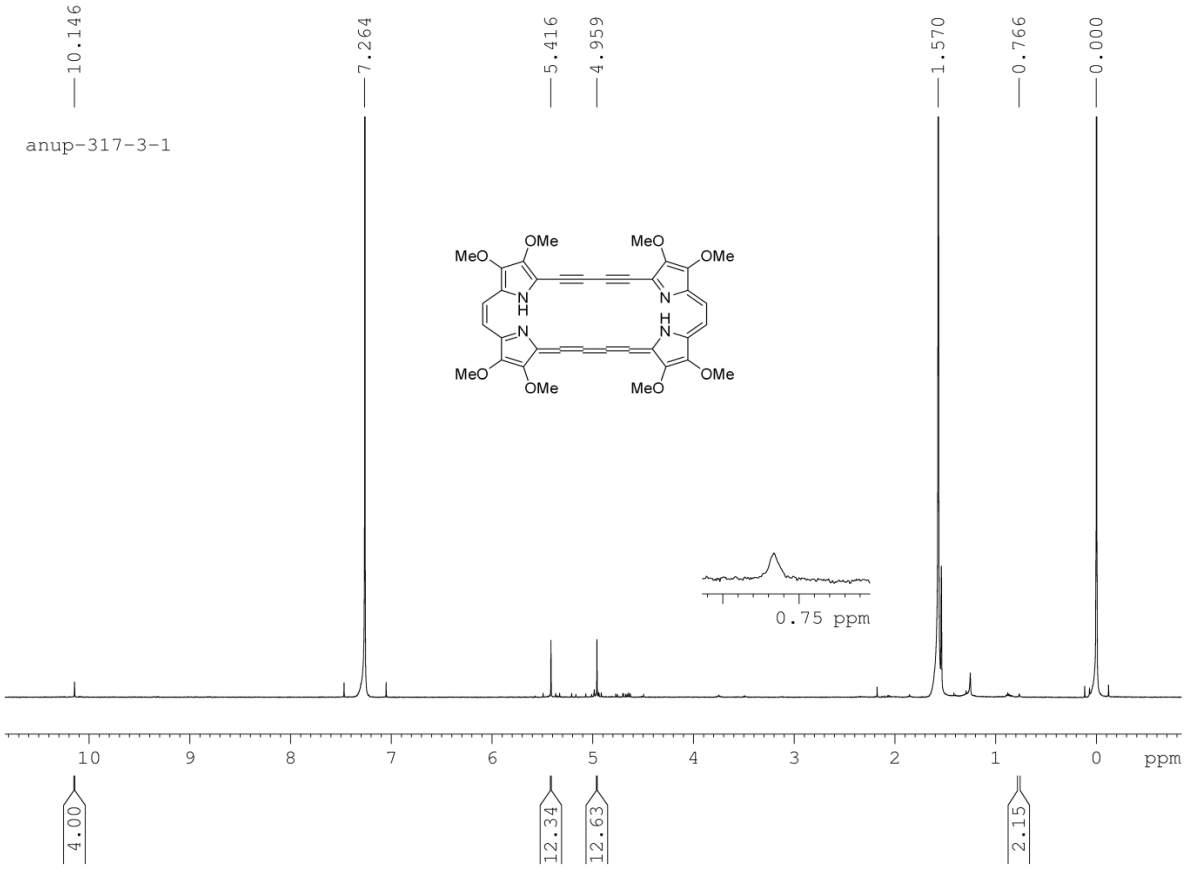

Figure 7.30 ^{1}H NMR spectrum of **7.16** in $CDCl_3$.

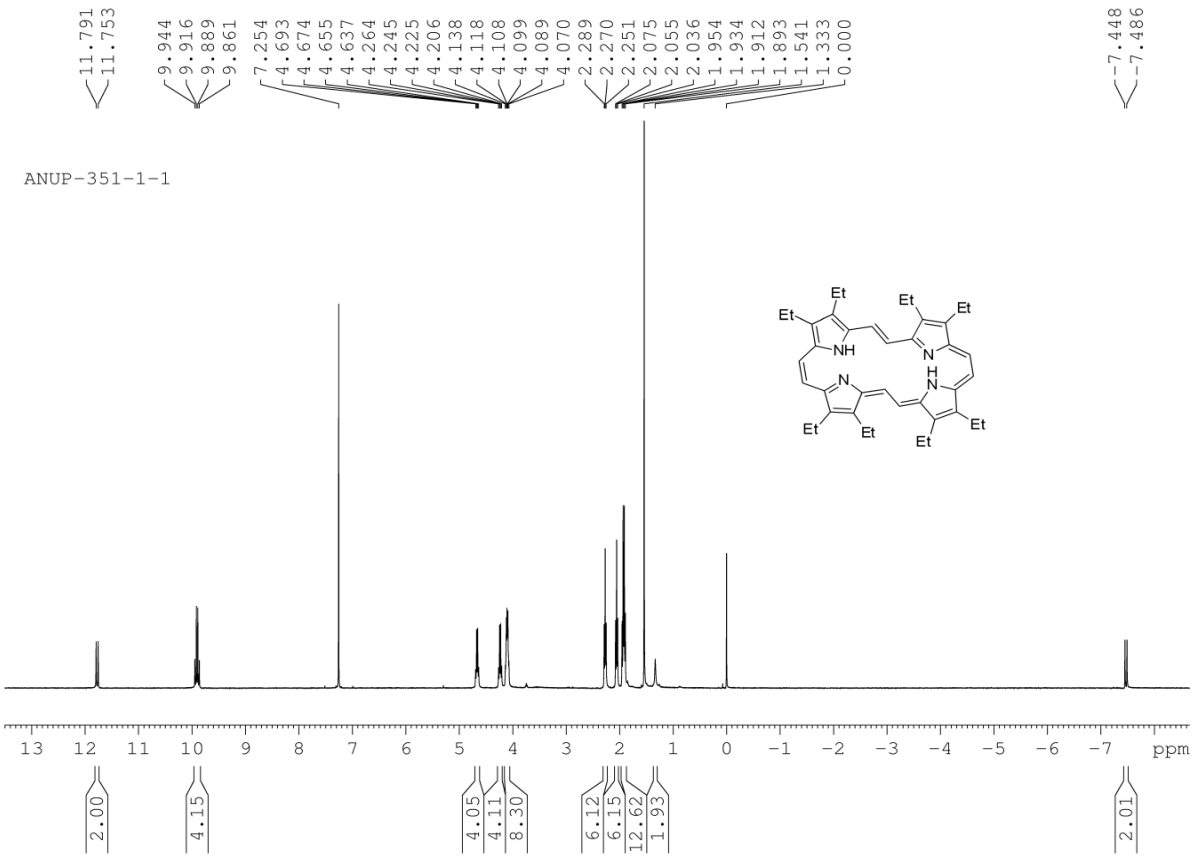

Figure 7.31 ^{1}H NMR spectrum of **7.10** in $CDCl_3$.

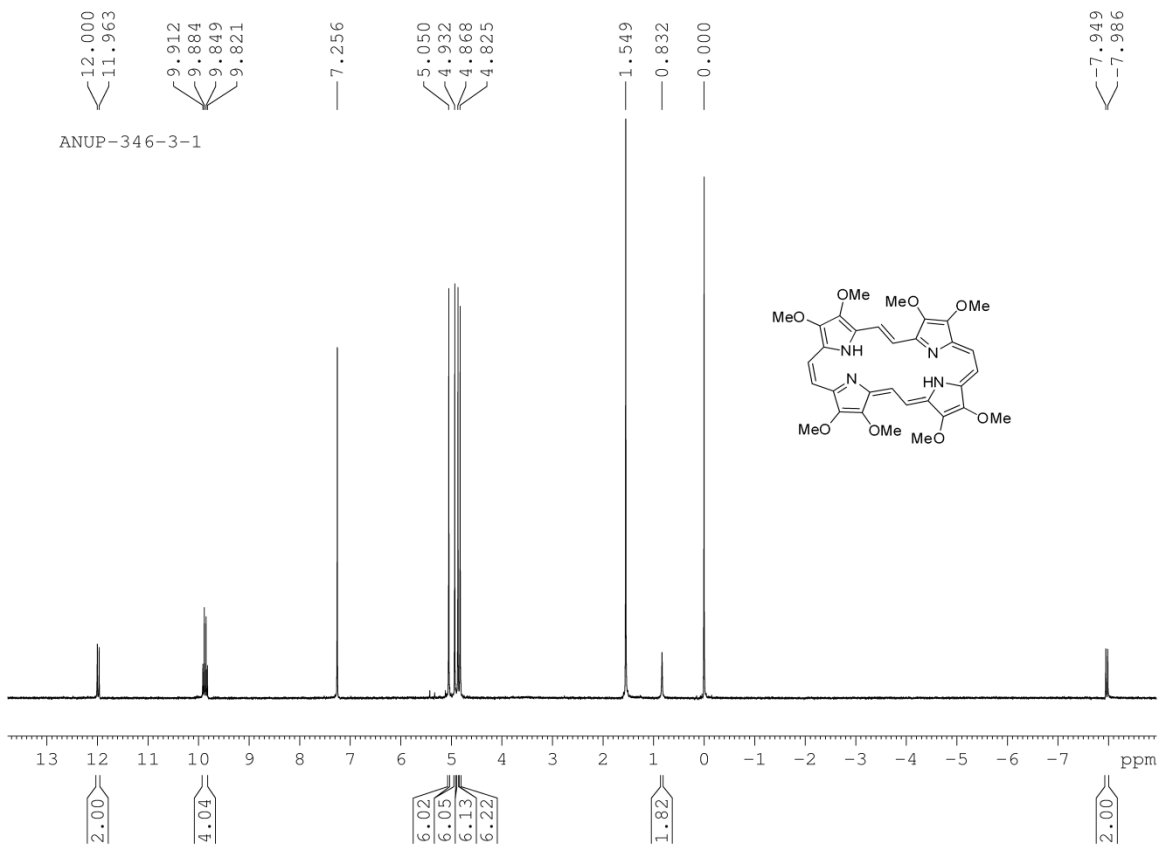

Figure 7.32 ^{1}H NMR spectrum of **7.17** in $CDCl_3$.

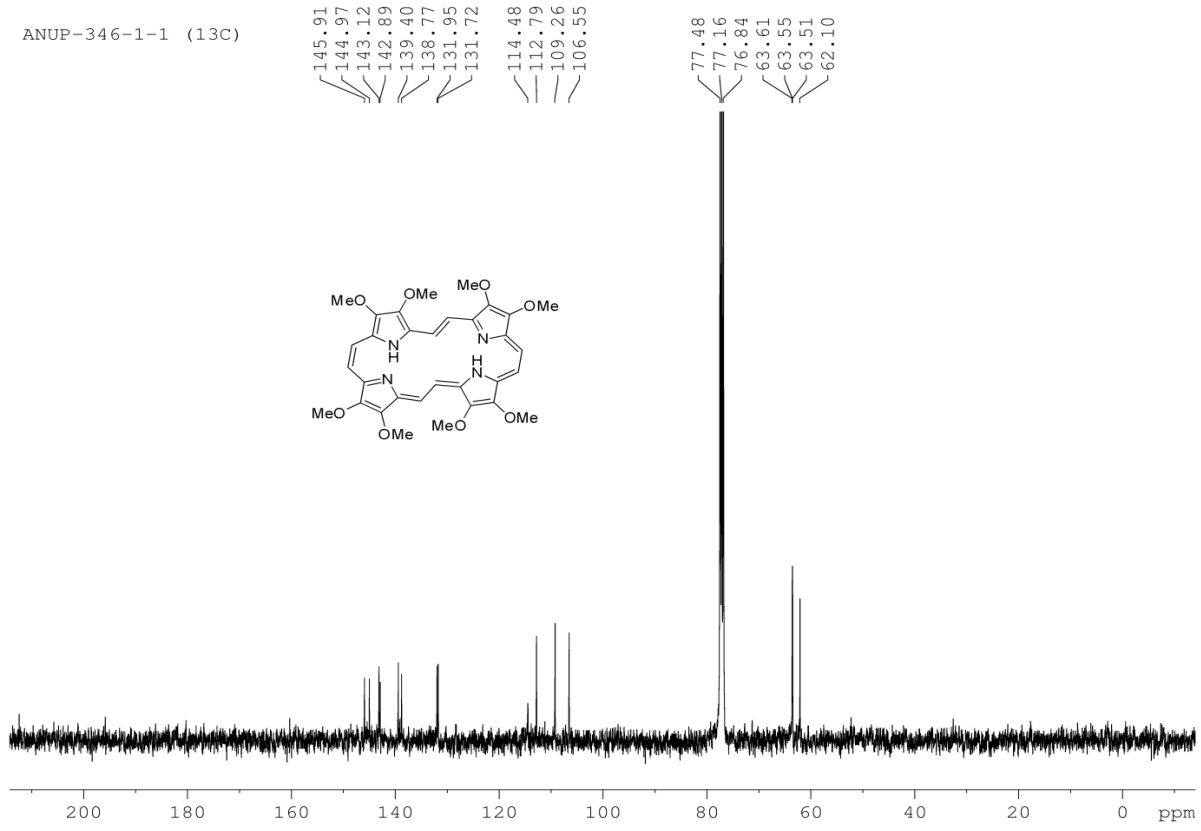

Figure 7.33 ^{13}C NMR spectrum of **7.17** in $CDCl_3$.

CHAPTER 8

β-Decamethoxysapphyrins: Structural Diversity and Anion Binding Study

8.1 Introduction

Expanded porphyrins can be synthesized by introducing extra pyrrole unit(s) or/and meso carbon atom(s) onto porphyrin skeleton.[1] Replacement of one pyrrole moiety of a porphyrin macrocycle with a bipyrrolic entity leads to [22]pentaphyrin-(1.1.1.1.0) or sapphyrin, discovered accidentally by Woodward and coworkers[2] during the synthesis of vitamin B_{12}, but however, the dioxa-analogue was first reported in detail by Johnson and coworkers[3] as a

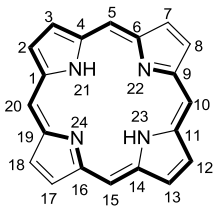

8.1 (Porphyrin)

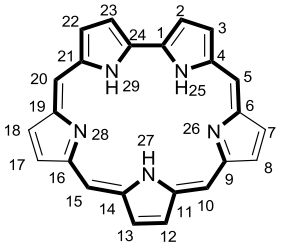

8.2 (Sapphyrin)

side product of dioxacorroles. Initially it was thought that sapphyrin may coordinate with comparatively larger metal ion. In 1990, Sessler and coworkers demonstrated that sapphyrin in diprotonated state can bind with anion both in solution as well as in solid states, making it one of the widely studied expanded porphyrin system.[4] It not only act as anion binding agent but receptor for drug delivery, studied as photodynamic therapeutic agent and very recently as third order nonlinear optical (NLO) material.[5]

8.1.1 Synthetic protocols

Most commonly used method for synthesis of sapphyrin is [3+2] McDonald type condensation of bipyrrole dialdehyde and tripyrrane (Scheme 8.1). This protocol, which was originally introduced by Woodward group[2b] and Johnson group[6] independently, works exceptionally well. Later, this method was popularized by Sessler and coworkers with improved synthesis of tripyrrane and bipyrrole dialdehyde.[4a,7] Another route, to sapphyrin also developed by Woodward and coworkers, involves [4+1] condensation (Scheme 8.1) of bipyrrolyldipyrromethane and pyrrole dialdehyde and subsequent oxidation to form desired sapphyrin.[2b] Later, Lash and coworkers improved the yield of sapphyrin by employing $FeCl_3$ as oxidant for aromatization (**8.8a-e** and **8.9-11**).[8] However, this method didn't get wide applicability over [3+2] condensation method due to the difficulty associated with the synthesis of precursors. Smith and coworkers introduced alternative [4+1] condensation approach, (Scheme 8.1) involving the reaction of biladiene and 2-formylpyrrole to produce sapphyrin **8.17** in 20% yield.[9] An alternative [3+2] condensation approach, (Scheme 8.1) also

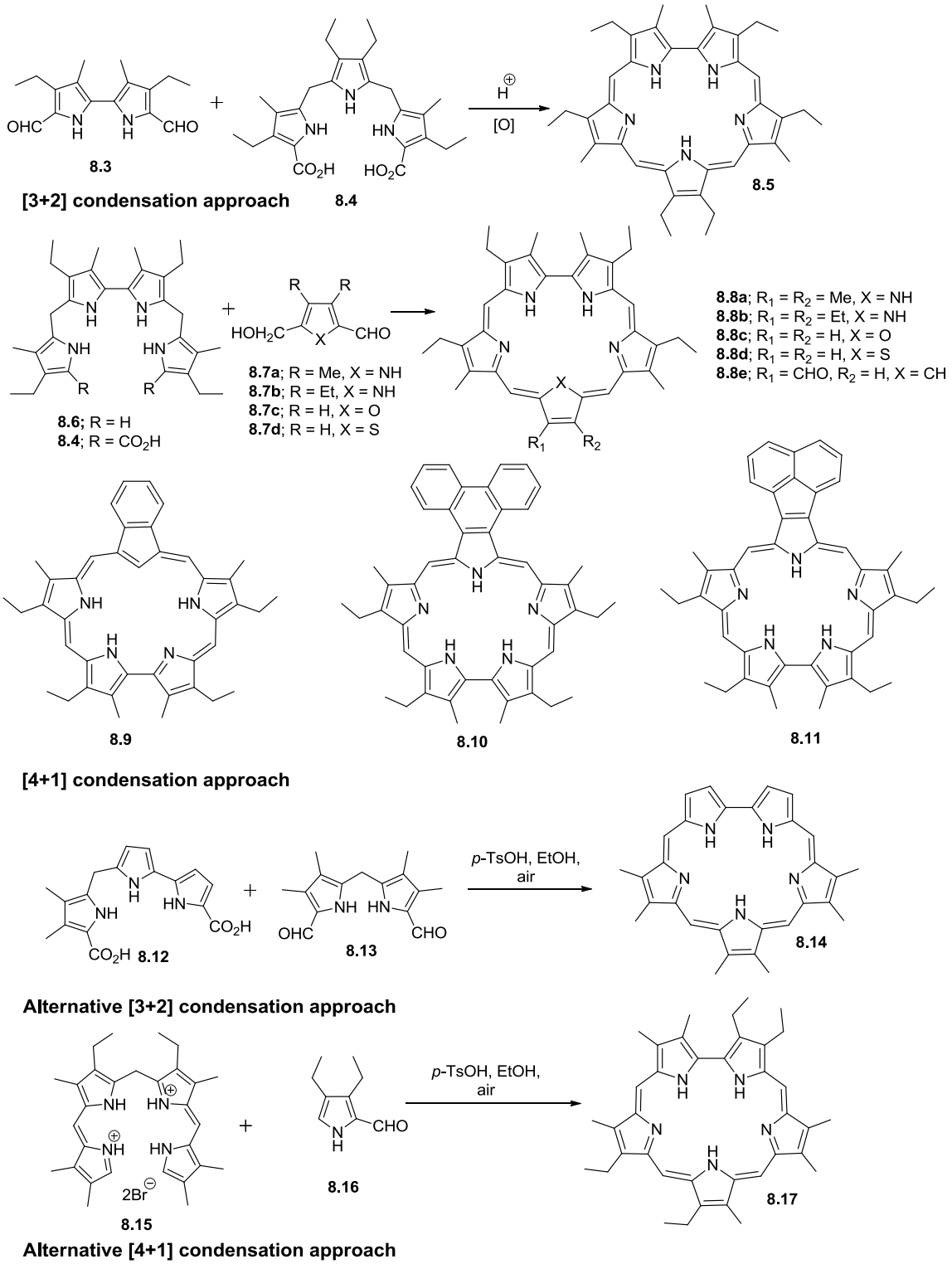

Scheme 8.1 [3+2] and [4+1] approach for synthesis of sapphyrins.

reported by Woodward and coworkers, involves the condensation of pyrrolyl bipyrrole **8.12** and diformyldipyrromethane **8.13** to synthesize desired sapphyrin **8.14**.[10] Although this approach produced desired sapphyrin in 35% yield, difficulties associated with the synthesis of precursors limited further utility of this method. Several "one pot" synthetic approaches

were reported by quite a few groups. This approach was first introduced by Woodward and coworkers, (Scheme 8.2) involving the condensation of 3,4-dimethylpyrrole **8.18** and pyrrole

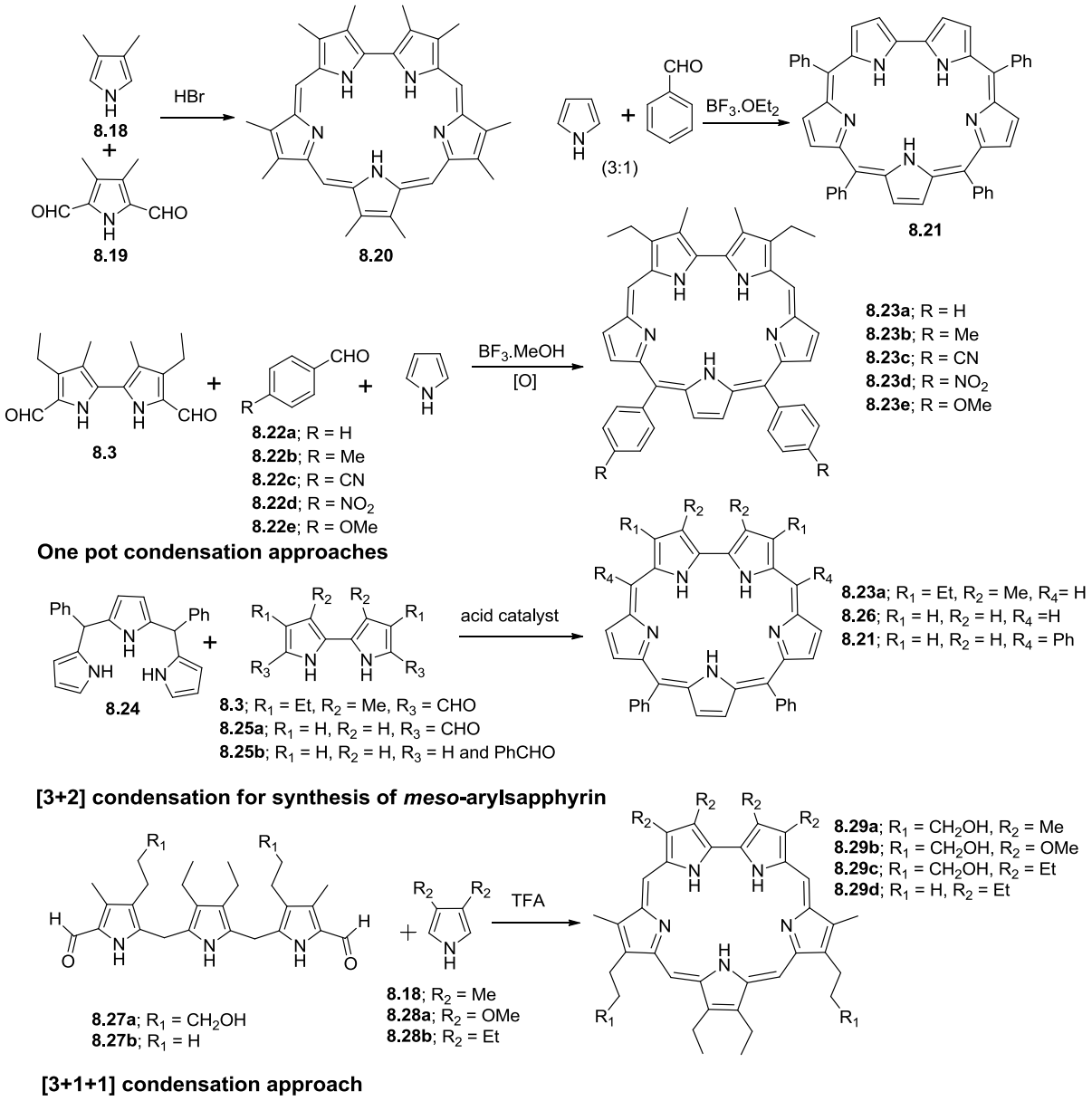

Scheme 8.2 Methods for synthesis of sapphyrins.

dialdehyde **8.19** to obtained sapphyrin **8.20** directly.[2b] Similarly, Sessler and coworkers reported the condensation (Scheme 8.2) of pyrrole and bipyrrole dialdehyde in presence of arylaldehyde to synthesize the desired sapphyrin (**8.23a-e**).[11] Later, Latos-Grażyński and coworkers found that simple condensation of pyrrole and benzaldehyde in 3:1 ratio in presence of acid catalyst, results in the formation of *meso*-tetraphenylsapphyrin **8.21** (Scheme 8.2).[12] However, these simple approaches suffer with poor yield to limit their wider utility. Further, Dolphin and coworkers introduced [3+2] approach (Scheme 8.2) involving the

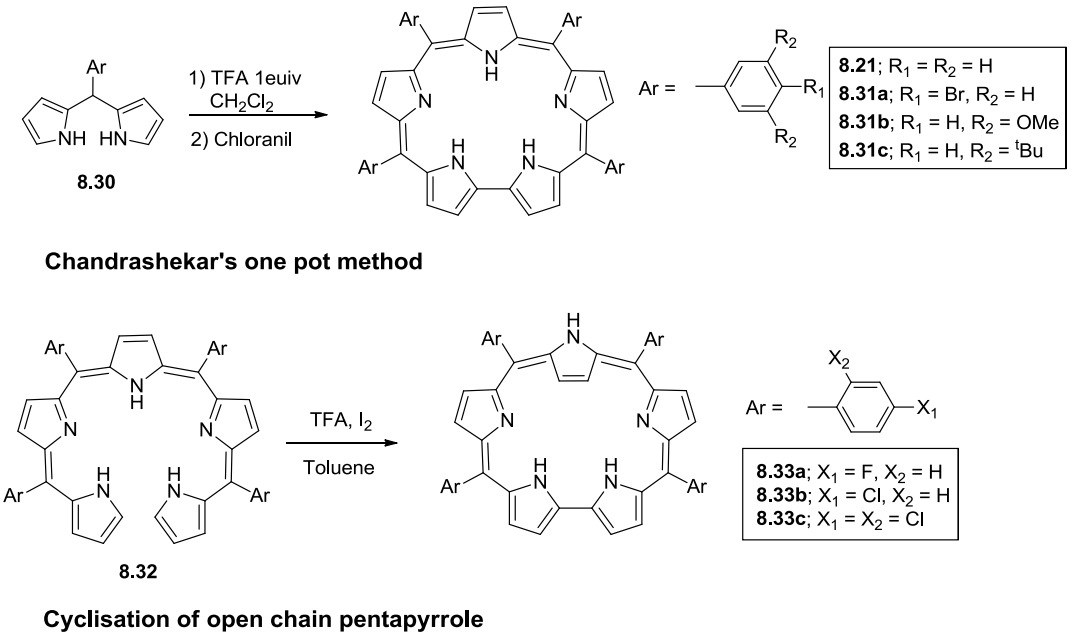

Scheme 8.3 Synthesis of *meso*-tetraarylsapphyrin.

condensation of 5,10-diphenyltripyrrane **8.24** with bipyrrole dialdehydes for the synthesis of *meso*-diphenyl- and *meso*-tetraphenyl- sapphyrins (**8.23a**, **8.26** and **8.21**).[13] Recently, Sessler and coworkers reported [3+1+1] condensation using tripyrrane dialdehyde (**8.27a-b**) and pyrrole, in presence of acid to yield sapphyrins **8.29a-d** in good yield.[14] Major advantage of this method is we can avoid bipyrrolic precursors and can be employed for pyrrolic precursors, whose bipyrrolic precursors are difficult to synthesize. Further, Chandrasekhar and coworkers reported *meso*-tetraarylsapphyrins (**8.21** and **8.31a-c**) (Scheme 8.3) by the reaction of 5-aryldipyrromethane in presence of 1 equiv. TFA and subsequent oxidation with DDQ yields desired sapphyrin upto 11% yield.[15] Also they found that formation of sapphyrins is largely dependent on acid catalyst, for example use of *p*-TsOH instead of TFA, resulted in formation of porphyrin along with N-confused porphyrin, instead of sapphyrin. However, the easy access of dipyrromethane precursors may find this one pot protocol attractive towards the synthesis of *meso*-tetraarylsapphyrin. Very recently, *meso*-tetraarylsapphyrin **8.33a-c** have been synthesized form open chain pentapyrrole in presence of TFA and iodine (Scheme 8.3).[16]

8.1.2 Spectroscopic properties of sapphyrins

The ^{1}H NMR spectrum of sapphyrin e.g. **8.5** exhibits the external *meso* protons at 10.8 ppm and internal NH protons at -2 ppm, a characteristic for aromatic system. Similarly, UV-Vis spectrum of **8.5**.2HCl reveals very intense Soret type band at 456 nm and several weak Q-

type bands at 616-711 nm range. The absorption spectrum of sapphyrin strongly dependent on protonation and aggregation and accordingly Soret band may appear anywhere in between 410-460 nm.[2,4] Grażyński and coworkers found that in the ^{1}H NMR spectrum of **8.21**, one of the NH proton resonating at -2.74 ppm in diprotonated state leaps to 11.75 ppm in freebase sapphyrin and similarly, some external β-protons resonating at 14.49 ppm in diprotonated state moved to -1.21 in freebase form, indicating one of the pyrrole ring undergoing inversion in freebase form.[12,17] Since then structural diversity of sapphyrin became one of the widely studied aspects in sapphyrin chemistry.

8.1.3 π-extended sapphyrins

Richter and Lash first introduced π-extended sapphyrins during the improved synthesis of sapphyrin by using $FeCl_3$ for aromatization.[8] The absorption spectra of reported phenanthrosapphyrin **8.10** and acenapthosapphyrin **8.11**, exhibits a red shifted Soret band at 473 and 500 nm respectively, compare to β-substituted analogues, originated from extended conjugation. Further, Ono and coworkers introduced benzopyrrole fused sapphyrins **8.34-35**,

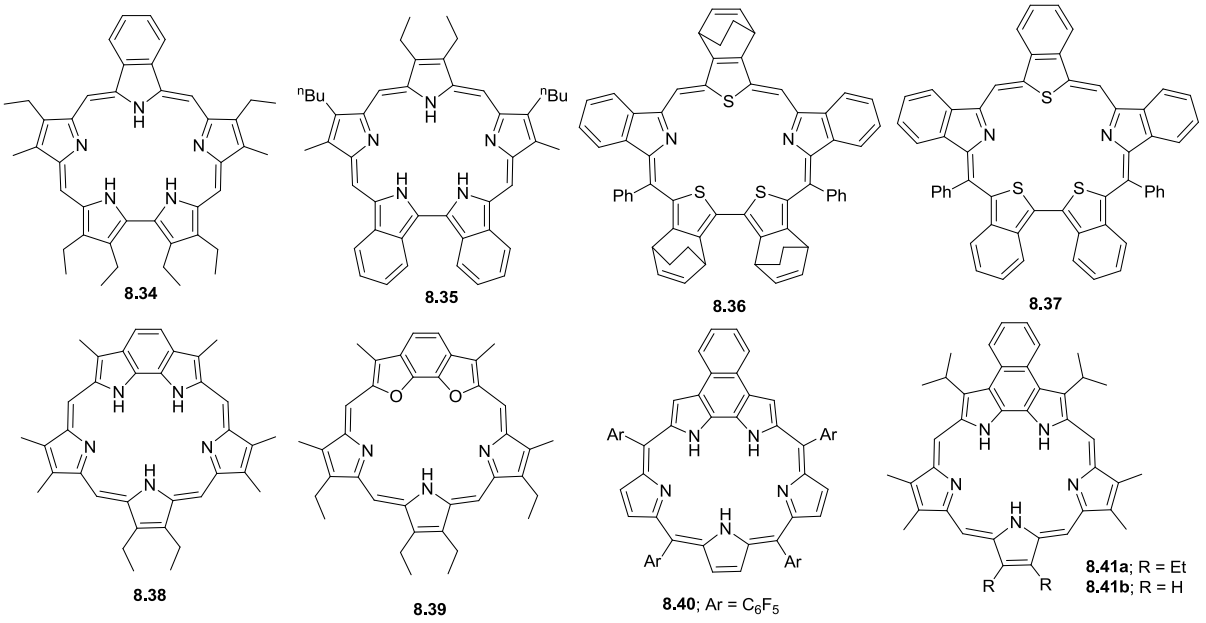

Figure 8.1 π-extended sapphyrins.

by employing retro Diels-Alder reaction of BCOD fused pyrrole analogues; display 12-22 nm red shifted absorption maxima compare to their BCOD analogues.[18] In extension of their work, they have reported trithiadibenzosapphyrin **8.36** and trithiapentabenzosapphyrin **8.37** by using earlier developed protocol. Introduction of sulfur-atom along with benzo fusion clearly reflected in their absorption spectra with an intense Soret band at 551 nm and lowest

energy Q- band appeared at 915 nm.[19] Lee and coworkers introduced benzobipyrrole fused sapphyrin **8.38**, where Soret band appears at 466 and 469 nm in freebase and diprotonated form respectively in absorption spectra, arising from extension of π-conjugation.[20] Further, Lee and Sessler introduced dioxabenzosapphyrin **8.39** originated from benzofused-difuran precursor.[21] The absorption spectrum of freebase sapphyrin **8.39** displays weak absorption maxima at 400 nm along with broad Q-type band at 650 and 750 nm. However, diprotonated form displays strong Soret band at 455 nm along with relatively sharp Q-bands. Introduction of two furan ring leads to weaker affinity towards fluoride and chloride ion in diprotonated state compare to diaza analogue. However, due to the presence of H-bond acceptors, it displays weaker interaction with Ar-OH (phenols) in diprotonated form. Recently, Lee and coworkers introduced *meso*-tetraarylnaphthosapphyrin **8.40** by one pot condensations of naphthobipyrrole, pyrrole and pentafluorobenzaldehyde in presence of TFA and subsequent oxidation with DDQ in 2% yield.[22] Napthobipyrrole fusion leads to appearance of Soret band at 508 nm and lowest energy Q-band at 781 nm in the absorption spectrum. Very recently, our group introduced naphthobipyrrole-fused β-substituted sapphyrins **8.41a-b** by following rational [3+2] condensation of naphthobipyrrole dialdehyde and tripyrrane diacid in presence of *p*-TsOH. Importantly, these naphthosapphyrins exhibit significant two photon absorption (TPA).[5g]

8.1.4 Anion binding studies of sapphyrins

Anion binding studies of sapphyrin could be probed by absorption, emission and ^{1}H NMR spectroscopic techniques in solution. In general, it has been found that decaalkylsapphyrin **8.5** in monoprotonated and diprotonated state bind fluoride ion stronger than phosphate ion, which in turn is stronger than chloride ion.[4] However, the diprotonated salt exhibits stronger binding affinity towards anion compared to monoprotonated form. Further, it was found that water-soluble monoprotonated sapphyrins (e.g., **8.42**) would strongly bind DNA at near neutral pH.[23] Covalently incorporated sapphyrin **8.43** on silica gel was used as HPLC column phase for separation of short oligonucleotides.[24] Further, this column was found effective for anion binding studies.[24c] It was more effective for phosphate and arsenate ions than carboxylate or halide, when used to enhance the rate of elution of AMP from solid support.[24c] Sessler and coworkers employed nucleotide incorporated sapphyrins e.g. **8.44** capable of transporting complementary nucleotide monophosphates at neutral pH through DCM layer.[25] Similarly, sapphyrin-oligonucleotide conjugate **8.45** was employed for sequence specific photo-modification of complementary DNA targets upon irradiation with 620 nm light.[5d] An

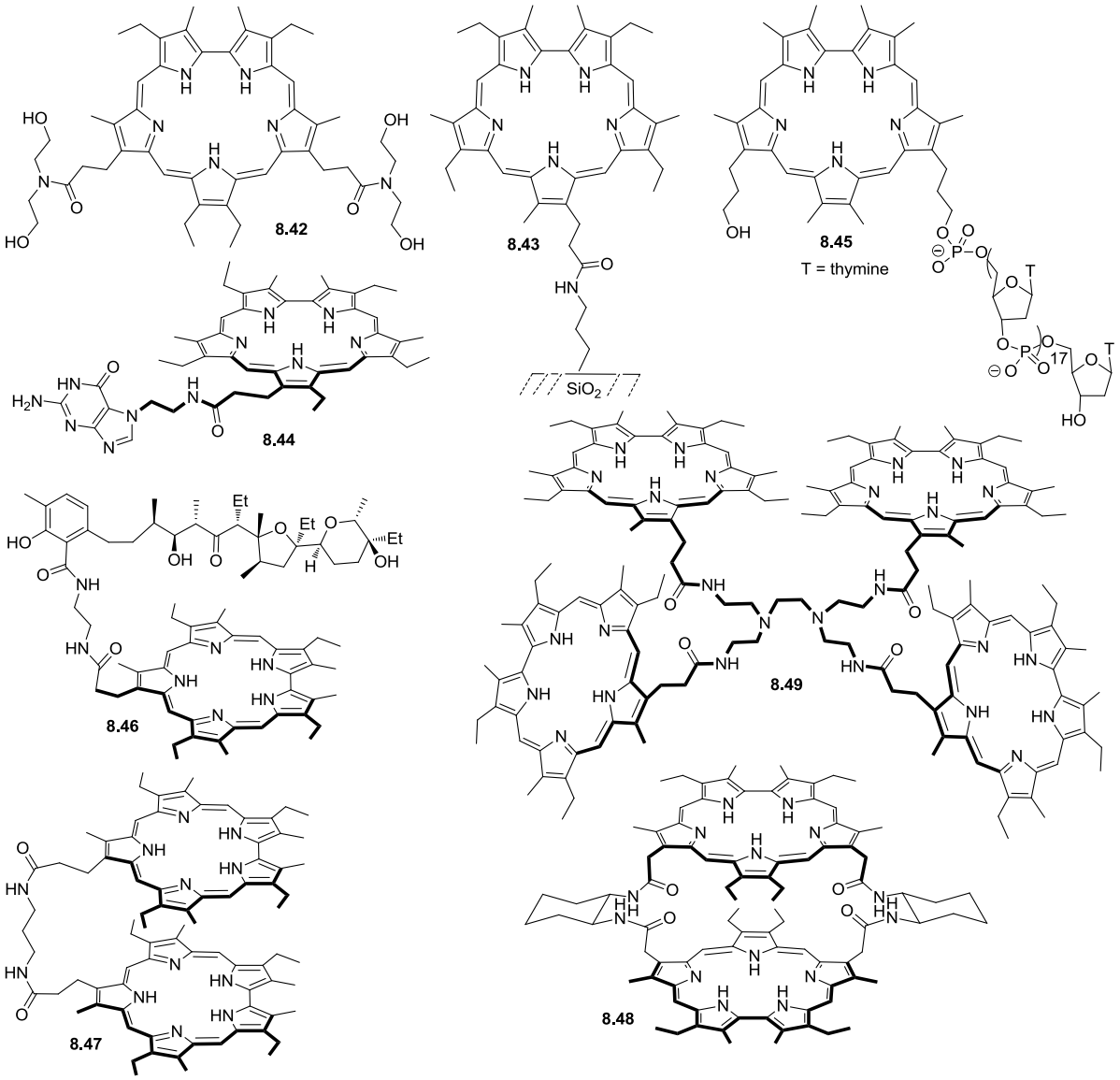

Figure 8.2 Sapphyrin designed for anion binding and transportation.

interesting sapphyrin-lasalocid conjugate **8.46** was designed towards recognition and transportation of amino acids.[26] Covalently linked sapphyrin dimer **8.47** was reported for dicarboxylate anion binding and transportation.[27] The absorption spectra of these sapphyrin dimers, found to exhibit two Soret like maxima, both in methanol (422 and 441 nm) and DCM (426 and 450 nm), originated from *endo*-like self-stacked and *exo*-like extended π-stacked forms, respectively. Sapphyrin dimers show enhanced transportation rate for dicarboxylate ion through Pressman type U-tube, compared to monomers.[27a] Further, chiral-spacer linked sapphyrin dimer **8.48** exhibits enantioselective recognition of N-protected amino acids.[27b] Oligosapphyrin **8.49** was found to acts as good solution phase receptors for multiply charged anionic species such as diphosphate, triphosphate, dicarboxylate and amino acids.[28]

8.1.5 Structural diversity in sapphyrins

Initial sapphyrin research was directed towards anion binding chemistry, until Grażyński and coworkers found something unusual during their studies with *meso*-tetraphenylsapphyrin. As discussed earlier, the pyrrole opposite to bipyrrole unit undergoes inversion in freebase form

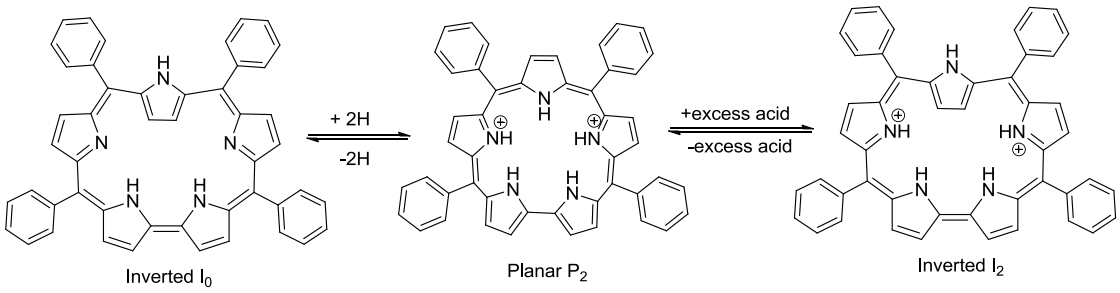

Scheme 8.4 Proton induced interconversion between inverted and planar form in tetraphenylsapphyrin.

I_0 and exists in normal all nitrogen P_2 form in diprotonated state (Scheme 8.4). This unusual behavior of sapphyrin open up a new arena named "structural diversity of sapphyrin".[12] Later, their detailed studies showed that inversion of pyrrole ring of sapphyrin dependent on the concentration of acid used for protonation. For instance, when sapphyrin:acid molar ratio is 1:2, it exists in dicationic planar conformation P_2. However, the dicationic planar P_2 conformation again undergoes inversion to I_2 conformation, in presence of excess acid (~50 equiv).[17] In a similar fashion, dicationic form of π-extended *meso*-tetraarylnaphthosapphyrin undergoes inverted conformation in presence of excess acid, determined by the change observed in ^{1}H NMR and absorption spectral pattern.[22]

Other than *meso*-tetraarylpentaazasapphyrin, some specially designed heterosapphyrins also display structural diversity. Chandrashekar and coworkers introduced a series of heterosapphyrins (**8.50** and **8.52**) found to display inverted conformation in solution.[29] They have found that presence of heavier atoms (S or Se) **8.53** at 26- and 28-positions lead to planar structure while, presence of smaller atom like N and O leads to the sapphyrin adopting an inverted conformation.[30] The structural analysis of inverted heterosapphyrins revealed that the relatively larger core may allow it to attain inverted conformation. Again, Grażyński and coworkers introduced dithia-*meso*-tetratolylsapphyrin **8.55**, in which by ^{1}H NMR studies they found the planar and inverted conformers exist in equilibrium in solution.[31] Further, Lee and coworkers assumed that the inversion of thiophene unit in **8.50** (X = S) is caused by strain arising from the larger Cα-Cα′ distance, rather than the presence of meso aryl substituents. To prove this hypothesis they synthesized oxa-dithiasapphyrin **8.51**, which undergoes inversion

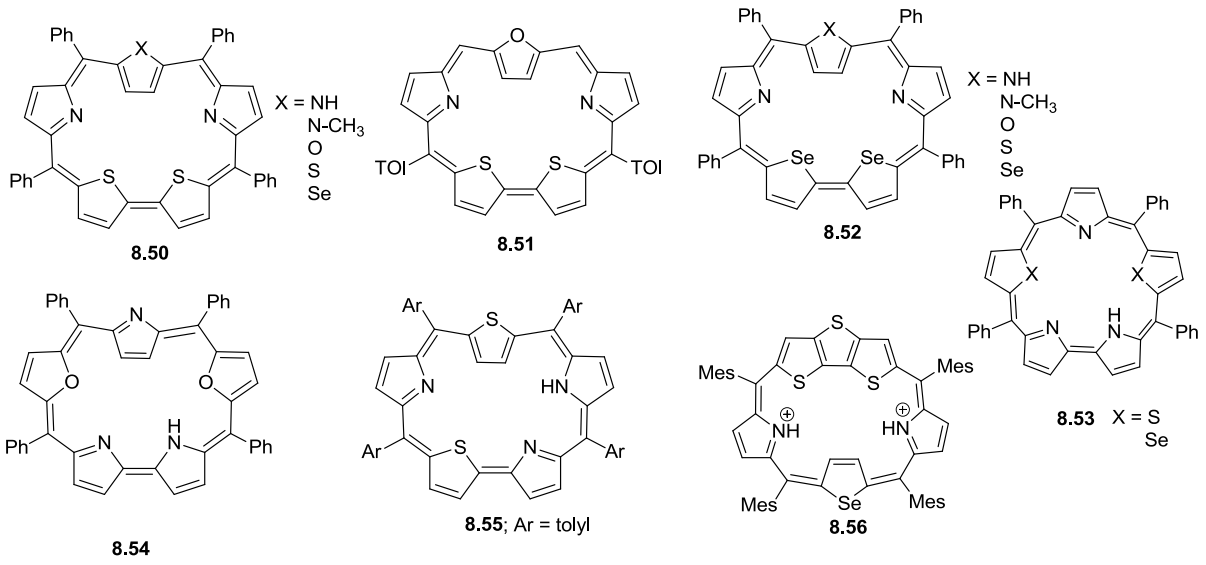

Figure 8.3 Structural diversity of heterosapphyrins.

of furan ring, despite the absence of 10,15-aryl substituents, as proved by ^{1}H NMR spectroscopy and solid state structural analysis.[32] Very recently, Chandrashekar and coworkers reported dithienothiophene fused sapphyrin **8.56**, which remains in equilibrium between normal planar and inverted conformation in free base form, and undergoes complete inversion in diprotonated state only.[33]

8.2 Research goal

The above depicted summary revealed that sapphyrin have been widely studied for its unique anion binding properties and structural diversity. Our present interest on methoxy substituted macrocycles motivated us to synthesize 2,3,7,8,12,13,17,18,22,23-decamethoxysapphyrin **8.57** to study the effect of methoxy substituents on macrocyclic structure, photophysical

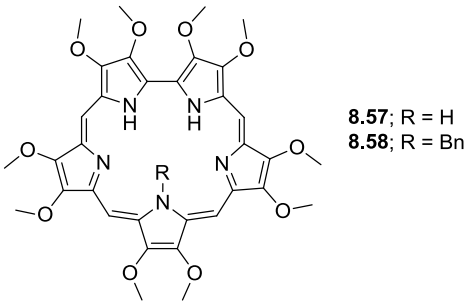

properties and anion binding studies.[34] Further, we have designed its 27-N-benzylated analogue **8.58** not only owing to its relatively easier synthetic access, but also in order to explore the possible structural diversity resulting from the probable disposition of the benzyl group in the freebase, and more importantly, its interaction with the incoming anions in the

diprotonated state. Further, we also evaluated the electrochemical properties of sapphyrins in both its freebase and diprotonated states, which is least explored compared to other expanded porphyrinoids.

8.3 Results and discussion

8.3.1 Synthesis of decamethoxysapphyrins

The synthesis of sapphyrins were achieved by following the conventional [3 + 2] McDonald type acid catalyzed condensation of bipyrrole dialdehyde and tripyrrane diacid. Recently, we have reported the synthesis of 3,3',4,4'-tetramethoxy-[2,2'-bipyrrole]-5,5'-dialdehyde **8.66**,[35] therefore in order to achieve our target, focus could be zeroed on the synthesis of precursor hexamethoxytripyrranediacids **8.65a-b** (Scheme 8.5). The synthesis of **8.65a-b** started with

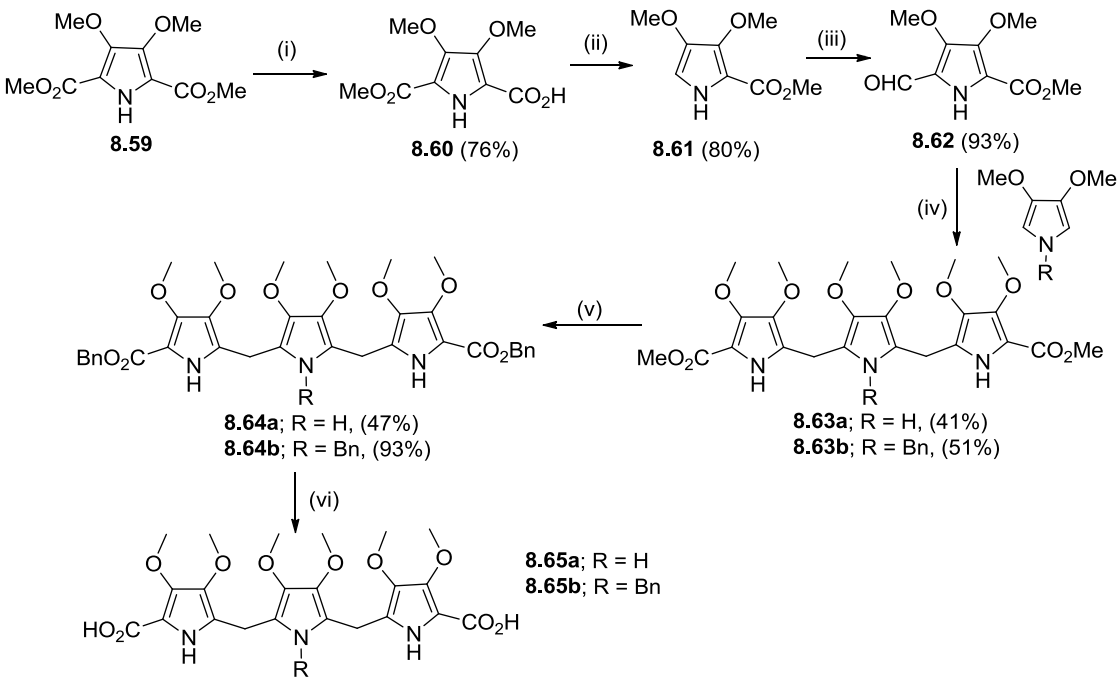

Scheme 8.5 Synthesis of precursor hexamethoxytripyrrane diacids (**8.65a** and **8.65b**). Reagent and conditions: (i) LiOH, THF/MeOH/H_2O (3:1:1), RT, 5 day; (ii) 180 °C, 10 min; (iii) $POCl_3$, DMF, DCE, reflux, 4 h; (iv) (a) $NaBH_4$, THF/MeOH (9:1), RT, 4 h, (b) *p*-TsOH, MeOH, reflux, 5 h; (v) Na, $PhCH_2OH$, 90 °C, 10 mmHg, 2 h; (vi) 5 % Pd/C (10 mol%), THF, H_2 (1 atm), RT, 18 h.

hydrolysis of one methyl ester group of dimethyl 3,4-dimethoxypyrrole-2,5-dicarboxylate **8.59**[36] with 1 eqv of LiOH in THF/MeOH/H_2O (3:1:1) at room temperature to obtain the mono de-esterified product 3,4-dimethoxy-5-(methoxycarbonyl)-pyrrole-2-carboxylic acid **8.60** in 76% yield,[37] followed by heating of **8.60** at 180 °C under nitrogen atmosphere led to the formation of methyl 3,4-dimethoxypyrrole-2-carboxylate **8.61** in 80% yield. Subsequent

Vilsmeier-Haack formylation of **8.61** under reflux condition provided the desired methyl 5-formyl-3,4-dimethoxypyrrole-2-carboxylate **8.62** in 93% yield. The reduction of **8.62** with sodium borohydride at room temperature provided methyl 5-(hydroxymethyl)-3,4-dimethoxypyrrole-2-carboxylate, which was used immediately for acid catalyzed condensation with the α-free pyrrole (3,4-dimethoxypyrrole for **8.63a** and N-benzyl-3,4-dimethoxypyrrole for **8.63b**) under reflux condition, in MeOH to provide the desired

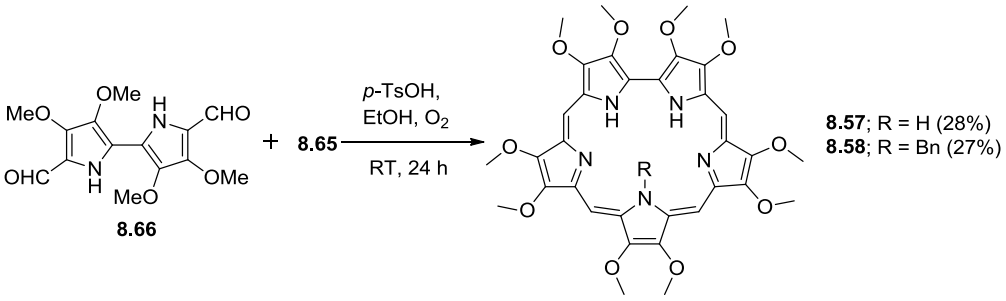

Scheme 8.6 Synthesis of decamethoxysapphyrins (**8.57**-**58**).

tripyrrane diesters **8.63a** and **8.63b** in 41 and 51% yield respectively.[38] The transesterification of tripyrrane dimethyl esters (**8.63a** and **8.63b**) in presence of sodium in benzyl alcohol (under 10 mm Hg pressure at 90 °C) to the corresponding dibenzyl esters **8.64a** and **8.65b** were achieved in 47 and 93% yield, respectively.[39] Debenzylation of benzyl esters (**8.64a** and **8.64b**) were carried out with 5% Pd/C (10 mol%) in THF under 1 atm hydrogen pressure, led to the corresponding tripyrrane diacid **8.65a** and **8.65b**, which were used immediately for next step because color of this product changed from white to brown under ambient condition. With both the starting material **8.65a-b** and **8.66** in hand, [3+2] type McDonald condensation of tetramethoxybipyrrole dialdehyde **8.66** and hexamethoxytripyrrane diacids (**8.65a** and **8.65b**) in presence of *p*-toluenesulphonic acid in EtOH with continuous bubbling of oxygen provided the desired decamethoxysapphyrins **8.57** and **8.58** in 28 and 27% yield, respectively (Scheme 8.6). The diprotonated salts were prepared by washing the freebase sapphyrins in dichloromethane with corresponding acids. All the precursors and final products were characterized by standard spectroscopic techniques.

8.3.2 ^{1}H NMR analysis of sapphyrins

The ^{1}H NMR spectrum of **8.57** consists of meso protons at 10.98, 10.71 ppm and a relatively sharp (for freebase sapphyrins) NH signal at -5.88 ppm, which is more deshielded and shielded respectively, compared to the decaalkylsapphyrin **8.5**.[40] Further, the position of NH signal varies with the amount of water present in $CDCl_3$. The large shielding of NH signals in

8.57 compared to **8.5**, along with concomitant absence of any weak NH signals, indicates fast water assisted NH tautomerisation in NMR time scale.[5g,40] Sessler et al. assumed the weak

Table 8.1 Chemical shifts (ppm) in ^{1}H NMR spectra of **8.57** and **8.58** along with their diprotonated salts in $CDCl_3$.

Compounds	*meso*-CH	pyrrole NH	*p*-CH[a]	*m*-CH[a]	*o*-CH[a]	CH_2[a]
8.57	10.98, 10.71	-5.88				
8.57.2HCl	11.86, 11.84	-5.42, -5.52, -5.76				
8.57.2HBr	11.85, 11.82	-5.69, -5.90, -6.05				
8.57.2TFA	11.87, 11.83	-6.64, -6.89, -7.14				
8.57.2$HClO_4$	11.87, 11.86	-7.13, -7.55, -7.67				
8.57.2PTSA	11.67, 11.64	-6.42, -6.51, -6.69				
8.58	10.97, 10.96	-2.43	5.93	5.57	2.29	-6.60
8.58.2HCl	11.80, 11.42	-4.60, -5.32	6.08	5.73	2.64	-7.15
8.58.2HBr	11.80, 11.38	-5.184, -5.49	6.04	5.69	2.59	-7.19
8.58.2TFA	11.94, 11.61	-6.31, -6.52	6.16	5.77	2.42	-7.65
8.58.2PA	11.75, 11.30	---	5.87	5.45	1.99	-7.39
8.58.2$HClO_4$	11.68, 11.25	-6.35, -6.91	6.25	6.00	3.48	-6.72
8.58.2PTSA	11.51, 11.19	-4.82, -6.09	6.21	5.93	3.36	-6.71

[a] indicates chemical shift for benzyl protons.

signals might be emerging from decomposition products, however the presence of weak NH signals in benzosapphyrin is noticed,[20] where probably interaction with water is much less (owing to its relatively electron defficient character). This indicates water plays a big role in the tautomerization process and when the basicity of sapphyrin increases, probably it enhances it affinity and hence interaction with water. Therefore, in our case i.e. **8.57**, owing to the presence of ten electron donating methoxy substituents, the basic sapphyrin moiety interact strongly with water (even in K_2CO_3 dried $CDCl_3$), hence we did not see any peaks corresponding to the pure freebases and peaks appearing at very much shielding region (**8.57**: -5.88 ppm *vs* **8.5**: ~ -3.5 ppm). The protonation of freebase sapphyrin **8.57** led to formation of diprotonated salts, where the *meso* protons were downfield shifted (~1 ppm) and three set of NH signals appeared with 1:2:2 ratios ranging from -5.42 to -7.67 ppm. Though minimal change was observed in the *meso*-proton signals among various diprotonated salts, but NH signal positions vary widely, depending on counter anions, probably arise from interaction of

counter anion with diprotonated sapphyrins (Table 8.1). Similar trend was observed in the ^{1}H NMR spectrum of N-benzylsapphyrin **8.58**, consisting of meso protons at 10.97, 10.96 and NH at -2.43 ppm, which clearly indicates that N-benzyl substitution at 27-position didn't affect the aromaticity, symmetry, and planarity of the macrocycle. Most importantly benzyl

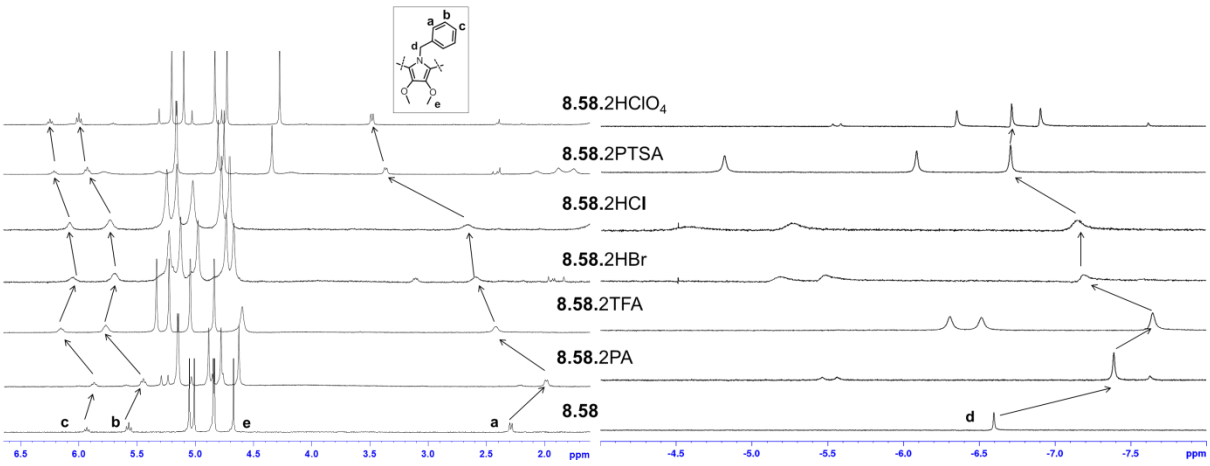

Figure 8.4 Selected regions of ^{1}H NMR spectra of **8.58** and its diprotonated salts.

group situated inside the core of macrocycle, confirmed by large upfield shift of benzyl –CH_2 proton signal (at -6.6 ppm) along with phenyl protons. Upon protonation, *meso* protons were shifted downfield (~1 ppm) and NH protons appeared in the range of -4.60 to -6.91 ppm, depending on the counter anions, with 2:2 ratio for the diprotonated salts of **8.58** (Table 8.1). Again, benzylic CH_2 protons reside in upfield region, indicating that the diprotonated salts also achieved the all-N-in conformer, in spite of the presence of bulky 27-N-benzyl substituent. However, the position of protons from benzyl moiety varies with counter anions, indicative of some unusual behavior (Figure 8.4 and Table 8.1). If N-benzylpyrrole moiety is flipping out of plane of the macrocycle then there will be downfield shift of benzyl protons and upfield shift of methoxy group signals of pyrrole at 12- and 13-positions in ^{1}H NMR. Similar type of behavior with diprotonated salts indicative of unusual displacement of benzyl group, probably arising from the steric or/and electronic repulsion (anion-π interaction) with incoming counter anion towards macrocyclic core. Among the studied diprotonated salts, maximum downfield shift was observed for *o*-CH, followed by *m*-CH > -CH_2 (determined by D_2O exchange) > *p*-CH in the benzyl group. If we compare displacement of N-benzylpyrrole signals of dipicrate **8.58**.2PA, dichloride **8.58**.2HCl and dibromide **8.58**.2HBr salts by ^{1}H NMR, the order is **8.58**.2PA < **8.58**.2HBr < **8.58**.2HCl**,** which clearly indicates the bulky counter anions remain away from macrocyclic core, leading to minimal distortion of the structure. The ditrifluoroacetate salt **8.58**.2TFA shows higher degree of displacement

compare to **8.58**.2PA due to less bulky nature. The maximum displacement of N-benzylpyrrole moiety is observed for diperchlorate salt **8.58**.2$HClO_4$, which preceded by di-*p*-toluenesulphonate salt **8.58**.2PTSA probably owing to relatively more bulky nature of *p*-toluenesulphonate ion. Notably, we could observe an equilibrium between planar and nonplanar macrocyclic cores, which is more evident in case of **8.58**.2$HClO_4$ and **8.58**.2PA (small peaks were observed, where *meso* protons were more downfield shifted and benzylic CH_2 more upfield shifted compare to major contributor) (Figure 8.39 and 8.41). So, from the above results, we can conclude that the counter anion induced displacement of N-benzylpyrrole moiety opposite to the bipyrrole unit, depend on the size of the counter anions. However, the complete inversion of N-benzylpyrrole moiety didn't occur probably due to the presence of β-methoxy substituents.

8.3.3 Photophysical properties of sapphyrins

The UV-Vis spectrum of sapphyrin **8.57** consists of soret band at 449 nm and four Q-type bands at 586, 632, 647 and 720 nm in $CHCl_3$, which is quite similar to other decaalkylated sapphyrins (Figure 8.5 and Table 8.2).[4b] The protonation of **8.57** with perchloric acid leads to large intensification of Soret band (almost doubled) and Q-bands due to eradication of tautomerism in the protonated state. Minimal shift in the Soret band could be observed

Table 8.2 Photophysical data for **8.57**, **8.58** and their diprotonated salts

Comp Name	Solvent	Absorption (λ_{max}) nm (log ε)	Emission (λ_{max}) nm	ϕ_f [a]
8.57	$CHCl_3$	449 (5.43), 586 (4.06), 632 (4.12), 647 (4.10), 720 (3.72)	724	0.017
8.57.2HF	MeOH	443 (5.43), 614 (3.98), 661 (3.83)	679	0.065
8.57.2HCl	MeOH	443 (5.46), 613(4.04), 661(3.95)	683	0.043
8.57.2HBr	MeOH	443(5.53), 614(4.08), 661(3.93)	680	0.029
8.57.2$HClO_4$	$CHCl_3$	451(5.75), 619(4.33), 674(4.13)	688	0.067
8.58	$CHCl_3$	456 (5.51), 582 (4.26), 626 (4.09), 662 (4.07), 732 (3.80)	739	0.030
8.58.2HCl	$CHCl_3$	458 (5.37), 626 (3.96), 676 (3.85)	697	0.017
8.58.2HBr	$CHCl_3$	462 (5.43), 632 (4.07), 685 (3.94)	698	0.005
8.58.2$HClO_4$	$CHCl_3$	462 (5.70), 632 (4.31), 693 (4.17)	697	0.016

[a] for fluorescent quantum yield measurements in $CHCl_3$, **H_2TPP** (ϕ_f 0.11) in toluene was taken as standard.[41]

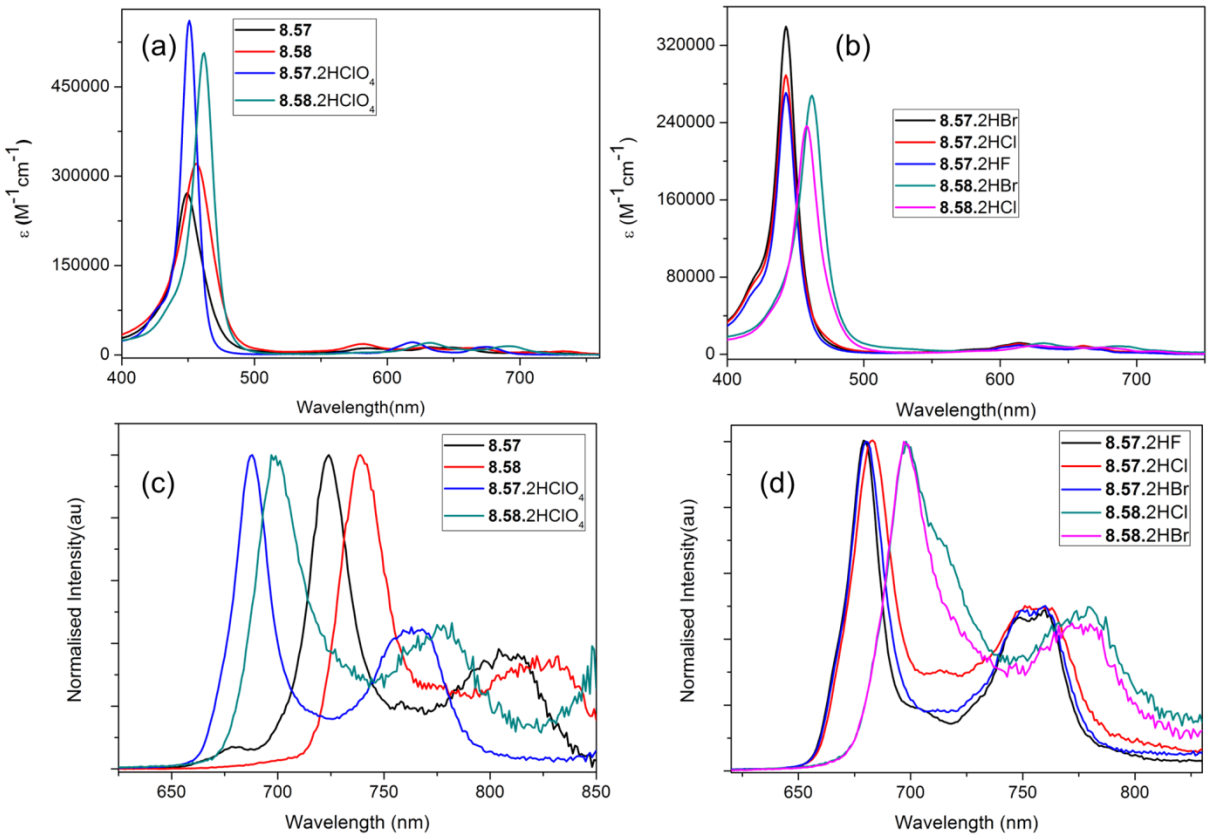

Figure 8.5 (a-b) UV-Vis and (c-d) fluorescence spectra of **8.57**, **8.58** and their diprotonated salts at 25 °C.

(only 2 nm red shift), however the increased symmetry led to two characteristic blue shifted Q-bands at 619 and 674 nm compared to freebase **8.57** (Figure 8.5). The freebase sapphyrin **8.57** and its diprotonated salts display emission with maxima at 724 and 679-688 nm, respectively (Figure 8.5 and Table 8.2). The enhancement of fluorescence quantum yield for diprotonated salts (ϕ_f, 0.029-0.067) compared to freebase **8.57** (ϕ_f, 0.017) may be attributed to the more rigid structure of the latter, along with absence of tautomerism (Table 8.2).

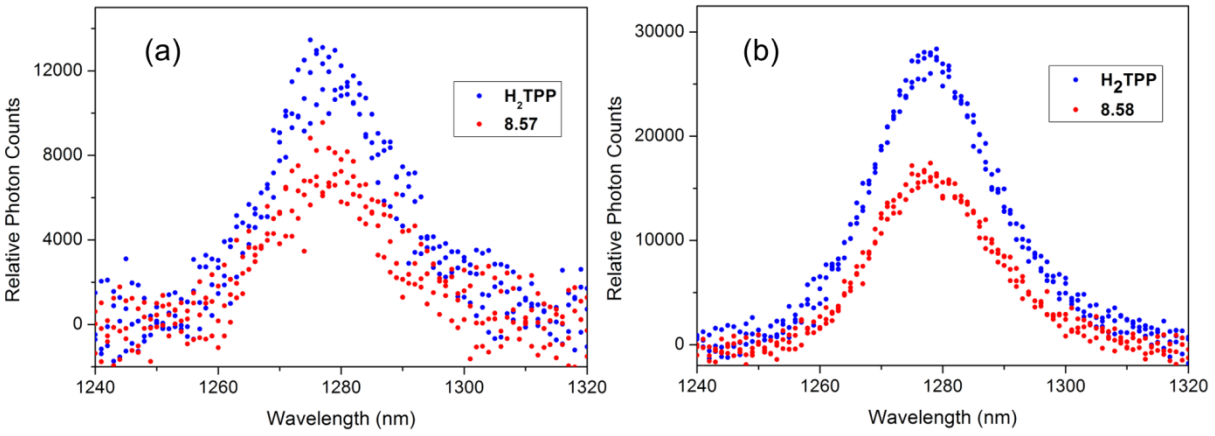

Figure 8.6 Singlet oxygen luminescence of optically matched (a) **H_2TPP** and **8.57** and (b) **H_2TPP** and **8.58** in air saturated toluene at 25 °C.

Similarly, UV-Vis spectrum of **8.58** consists of Soret band at 456 nm and four Q-bands at 582, 626, 662, and 732 nm (in $CHCl_3$), where Soret and lowest energy Q-bands are 7 and 12 nm red shifted respectively, compared to **8.57** due to the distortion of the core, induced by N-benzyl substituent (Figure 8.5 and Table 8.2). More interestingly, Q-bands of **8.58** shows a four-banded pattern, more generally noticed in freebase porphyrins, which however is quite unexpected in sapphyrin chemistry. This may be attributed to the lesser no. of tautomer's (four only) upon N-benzylation at the 27-position (in **8.58**) compared to the free base sapphyrins (six). The protonation of **8.58** leads to red shifted Soret band (2-6 nm) and blue shifted two Q-type bands in the range of 626-693 nm (Figure 8.5). Again, the freebase **8.58** and its diprotonated salts weakly emit with emission maxima at 739 and ~ 697 nm respectively (Figure 8.5). The reduced fluorescence quantum yield of diprotonated salts (0.005-0.017) compared to freebase **8.58** probably arise due to the distortion of core of the macrocycle caused by steric interaction between the benzyl moiety and the counter anion, as evident by ^{1}H NMR studies (Table 8.2). Both freebases **8.57** and **8.58** have absorption above 700 nm and hence may find application as photosensitizer for PDT. We have observed both freebases **8.57** and **8.58** generate singlet oxygen in aerated toluene with moderate efficiencies (ϕ_Δ , 0.44 for **8.57** and 0.42 for **8.58**), making them useful as possible photosensitizers for deep-site PDT (Figure 8.6).

8.3.4 Protonation of sapphyrins

The protonation of freebase sapphyrins **8.57** and **8.58** were studied by successive addition of TFA in dichloromethane solution (Figure 8.7). Gradual addition of TFA leads to increase in the intensity of the Soret band with minimal red shift (449 to 450 nm for **8.57** and 455 nm to 460 nm for **8.58**), whereas the four Q-bands reduce to two blue shifted bands. Also, in both cases intensity of Soret band undergoes saturation after addition of ~ 6 eqv of TFA and no further change was observed, even after addition of excess TFA. In addition, owing to the strong basicity of these sapphyrins, we could observe diprotonation even with a weak acid like acetic acid, *albeit* upon addition of much higher equivalents (Figure 8.7). However, as the changes are quite gradual in nature, therefore we could not clearly identify stepwise protonation events in both TFA and acetic acid.

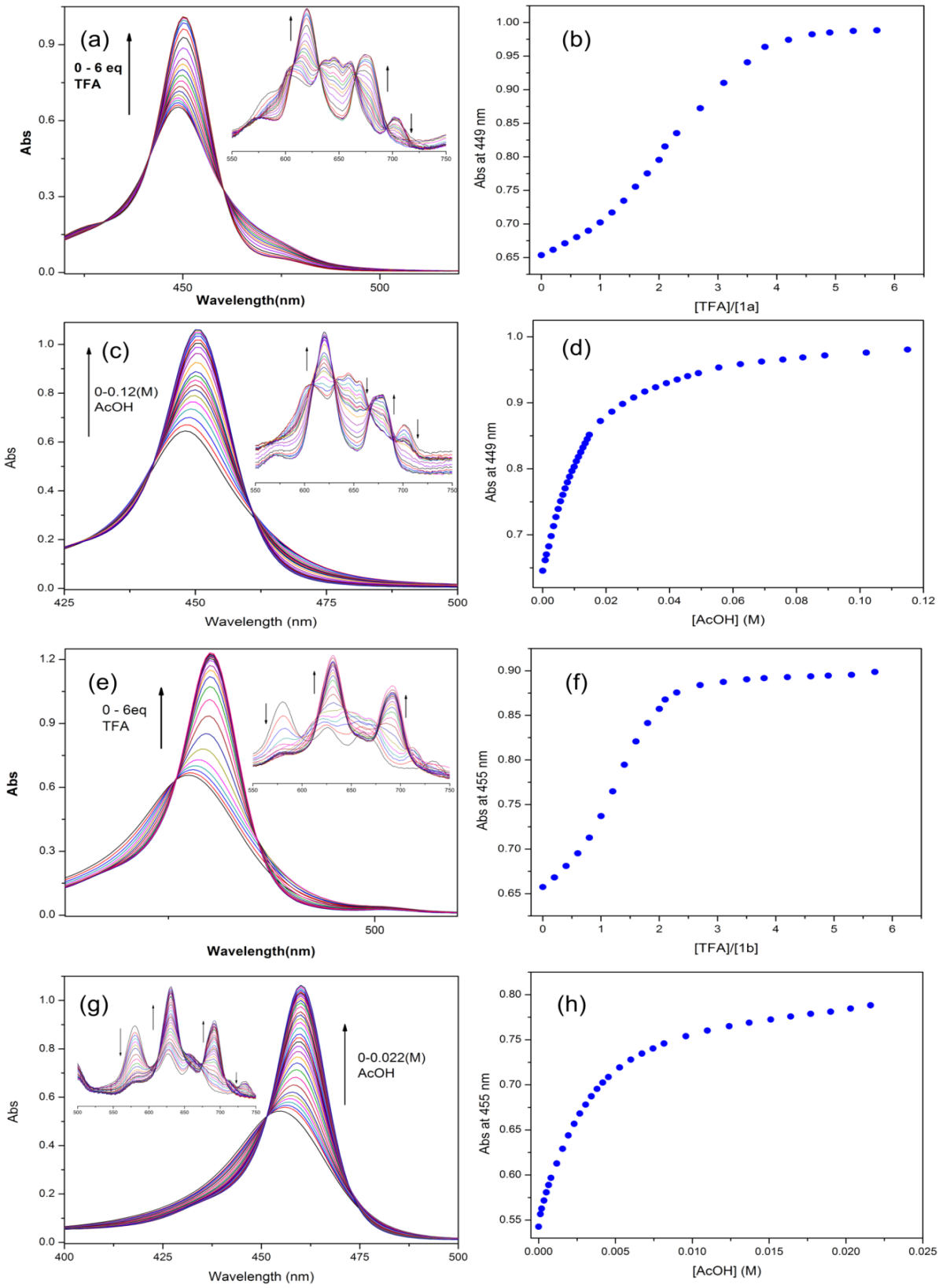

Figure 8.7 Change in UV-Vis spectra on protonation of (a) **8.57** *vs* TFA, (c) **8.57** *vs* AcOH, (e) **8.58** *vs* TFA and (g) **8.58** *vs* AcOH in dichloromethane at 25 °C (Insets represents the Q-bands of sapphyrin). (b), (d), (f) and (g) represent the change in absorption maxima with successive addition of acid. Concentration of sapphyrin used for titration (a), (e) 2.47×10^{-6} (M) and (c), (g) 2×10^{-6} (M).

8.3.5 Anion binding studies of sapphyrins

The anion binding studies of sapphyrin **8.57** was carried out in methanol with diprotonated salts by UV-Vis spectroscopic method (Figure 8.8). The UV-Vis absorption spectra of **8.57**.2HF, **8.57**.2HCl, and **8.57**.2HBr in methanol consist of Soret band at 443 nm and two Q-bands at 614 and 661 nm revealing that sapphyrin **8.57** exist as planar diprotonated salt, whereas anions are solvated in methanol (Figure 8.5b). Successive addition of tetrabutyl-

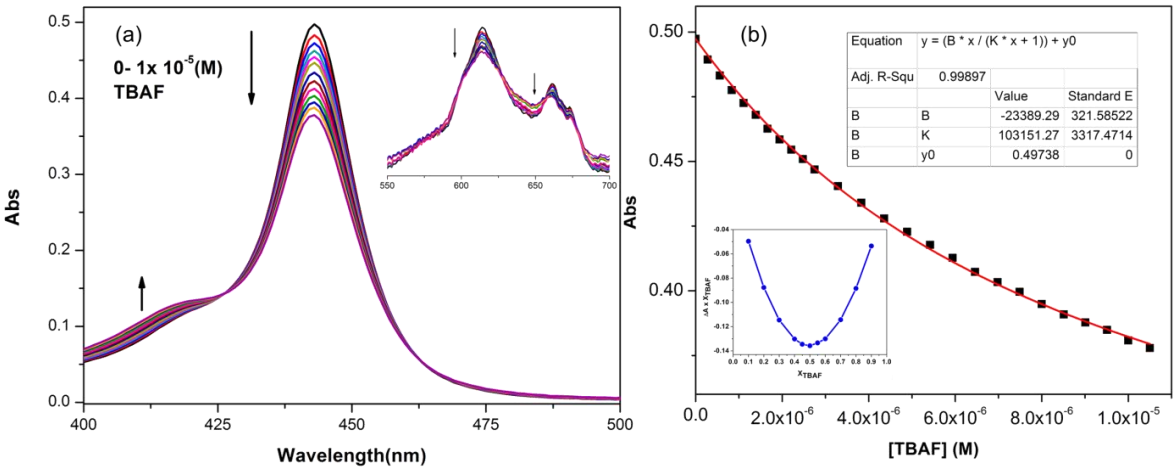

Figure 8.8 (a) Change in absorbance after successive addition of TBAF to a methanol solution of **8.57.**2HF and inset represents change in Q-type bands. (b) Plot of the absorption change of **8.57.**2HF at 443 nm vs. the concentration of TBAF, overlaid by calculated 1:1 binding profile using Connor equation. The concentration of **8.57.**2HF was 2.91 × 10^{-6} (M) used for measurement. Inset of Figure b represent Job's plot revealing 1:1 binding profile.

ammonium fluoride (TBAF) to **8.57**.2HF salt in methanol leads to decrease in intensity of Soret band, with a new peak evolving around ~ 416 nm (Figure 8.8a). The binding constant was measured by Connor equation, which could nicely fit with 1:1 binding stoichiometry (Figure 8.8b). Also, Job's plot analysis for TBAF and **8.57**.2HF in methanol by UV-Vis titration confirms with 1:1 equilibrium process (Figure 8.8b inset). The binding constant obtained for fluoride interaction was (1.03 ± 0.03) × 10^5 M^{-1}, (Figure 8.8b) which is weaker compared to decaalkylated sapphyrin (**8.5**.2HF) ((2.8 ± 0.5) × 10^5 M^{-1}) reported by Sessler and coworkers, and may be attributed to the electron rich nature of the macrocycle owing to the introduction of methoxy groups.[4b] Further, titration of **8.57**.2HCl and **8.57**.2HBr with TBACl and TBABr, respectively didn't show any detectable binding. We anticipate interesting anion binding behavior for diprotonated **8.58** owing to the presence of 27-N-benzyl substituent, which further reduces the total number of binding sites. But unfortunately, we could not able to prepare **8.58**.2HF salt, whereas we could obtain only monoprotonated

salt, probably 10% HF solution is not strong enough to diprotonate **8.58**. Though we are able to synthesized **8.58**.2HCl and **8.58**.2HBr salts but they (including **8.58**.HF) undergo deprotonation in methanol, denying us to study their anion binding behavior.

8.3.6 Structural analysis of decamethoxysapphyrins

The structure of *p*-toluenesulphonate salt of sapphyrin **8.57** i.e. **8.57**.2PTSA was further characterized by single crystal XRD technique, which acquires near planar macrocyclic core where two tosylate units resided symmetrically (distance of O^- unit of tosylate from mean plane 1.35 Å) from mean plane drawn through core of the macrocycle excluding methoxy groups (Figure 8.9). Further, each tosyl group is hydrogen bonded to three pyrrolic units with N-O distances ranging from 2.83-3.07 Å. The distance between N2-N4 units is 5.43 Å, which is quite similar to dihydrogenchloride complex of decaalkylatedsapphyrin (5.50 Å) reported by Sessler and coworkers.[4a] All nitrogen atoms remain closer to the mean plane (deviation from mean plane in the range 0.059-0.182 Å) with maximum deviation occurs for N1 unit.

Similarly, diprotonated perchlorate salt of **8.58** i.e. **8.58**.2$HClO_4$ and mono protonated *p*-toluenesulphonate salt, **8.58**.PTSA were structurally characterized. The asymmetric unit of **8.58**.2$HClO_4$ consists of three diprotonated sapphyrin units. The presence of N-benzyl substituent at 27-position leads to distortion of macrocyclic core (Figure 8.9). More strikingly, structural parameters of three sapphyrin asymmetric units are different from each other. First of all, the distance between N2-N4 is in the range from 5.31-5.41 Å, which is little bit narrower compare to **8.57**.2PTSA. Unlike **8.57**.2PTSA, two perchlorate units are asymmetrically disposed in **8.58**.2$HClO_4$, where comparatively nearer perchlorate ion (distance from mean plane 0.92 Å) hydrogen bonded with four pyrrole NHs, whereas the other one (distance from mean plane 2.48 Å) H-bonded with only one pyrrole NH. Interestingly, the closer perchlorate moiety resided in the center of core with N-O distance ~2.93 Å, revealing stronger H-bonded interaction. Also, further ruffling of structure occurs due to the nonbonding interaction between perchlorate ion with the benzyl unit. The maximum displacement of β-C's of N3 pyrrole unit from the mean plane drawn through N1,N2, N4, N5 pyrrole units is 1.29 Å and the maximum angle between mean planes drawn through N1, N2, N4, N5 and N3 pyrrole units excluding benzyl group is 36.22°. The above result proves our previous presumption of ^{1}H NMR studies that approach of perchlorate ion towards the macrocyclic core leads to flipping out of benzyl substituted N3 pyrrole unit. On the other hand, the N2-N4 distance (5.46 Å) for mono protonated *p*-toluenesulphonate salt

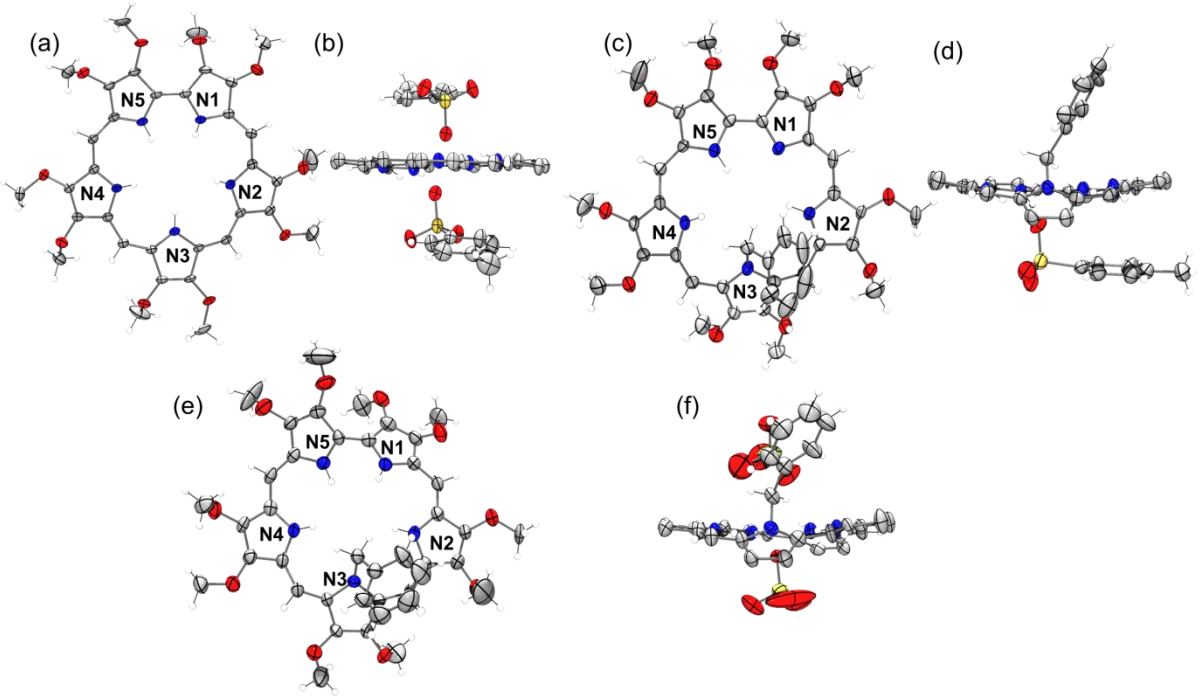

Figure 8.9 Molecular structure of **8.57.**2PTSA where (a) represents front view and (b) side view, **8.58.**PTSA where (c) represents front view and (d) side view, **8.58.**2$HClO_4$ where (e) represents front view and (f) side view drawn in 35% probability level. In front view corresponding counter anion and in side view methoxy groups are removed for clarity. Color code: C, grey; N, blue; O, red; S, yellow; Cl, yellow green; H, white.

8.58.PTSA is similar to that of **8.57**.2PTSA and little bit wider compared to **8.58**.2$HClO_4$ (Figure 8.9). Further, *p*-toluenesulphonate unit hydrogen bonded with N4 and N5 pyrrolic units with O-N distance ~2.77 Å and the distance from mean plane drawn through macrocycle excluding benzyl and methoxy group is 1.40 Å. Again, displacement of nitrogens from the mean plane is in the range of 0.013-0.231 Å. Similar to perchlorate salt of **8.58**, the N-benzyl pyrrole unit flipping out of macrocyclic plane and the maximum displacement of β-C's of N3 pyrrole unit from the mean plane drawn through N1, N2, N4, N5 is 1.18 Å, which is 0.11 Å lesser compared to **8.58**.2$HClO_4$. Further, the angle between mean plane drawn through N1, N2, N4, N5 and N-benzyl pyrrole unit is 31.87°, which can also be correlated with ^{1}H NMR studies and confirms the relatively lesser degree of displacement of N-benzylpyrrole unit in **8.58**.PTSA compared to **8.58**.2$HClO_4$. Therefore, from the above structural data we can conclude that one of the counter anion play major role in out of plane displacement of N-benzylpyrrole unit. The anion dependent displacement of N-benzylpyrrole unit matched quite well with ^{1}H NMR data and structural data from XRD analysis.

8.3.7 Electrochemical studies of decamethoxysapphyrins

Electrochemical measurements of freebase sapphyrins **8.57**, **8.58** and their perchlorate salts were carried out by cyclic voltammetry (CV) and differential pulse voltammetry (DPV) in dichloromethane by using tetrabutylammonium hexafluorophosphate as supporting electrolyte at 25 °C (Figure 8.10 and Table 8.3). Though, sapphyrin got wide attention as

Table 8.3 Comparative oxidation and reduction potentials (V vs Ag/AgCl) for sapphyrins and their perchlorate salts

Sapphyrins	Reduction	Oxidation
8.57	-1.16[a]	+0.56[a], +1.04, +1.23
8.58	-1.30[a]	+0.48[a], +0.86[a], +1.22
8.57.2$HClO_4$	-1.09, -0.86, -0.74[a]	+1.23
8.58.2$HClO_4$	-1.20, -0.76, -0.61	+1.24

[a] measured by DPV.

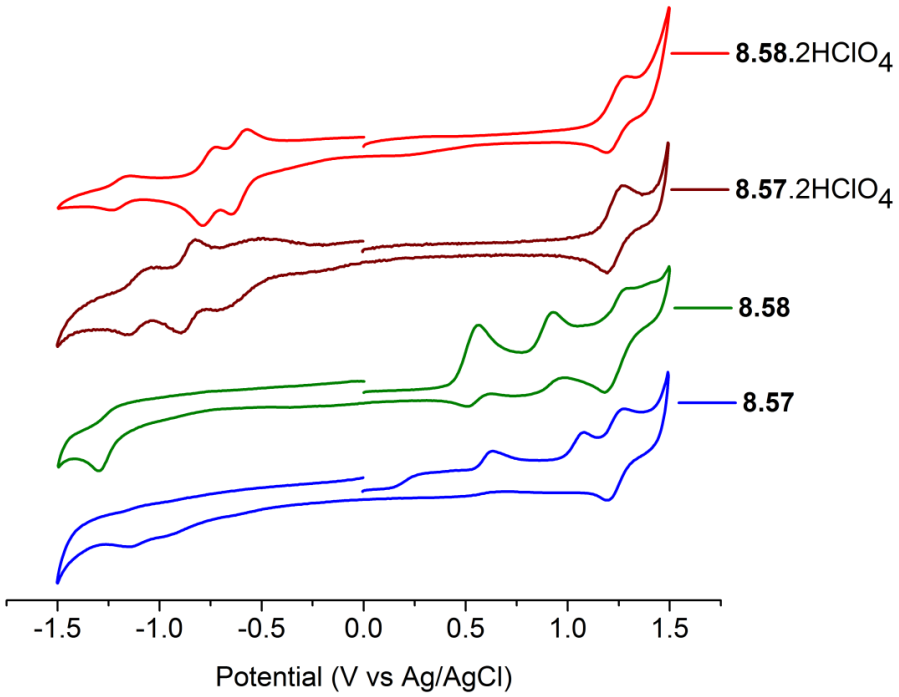

Figure 8.10 Cyclic voltammograms of **8.57**, **8.58**, **8.57**.2$HClO_4$ and **8.58**.2$HClO_4$ in dichloromethane at 25 °C (scan rate 50 mV/sec).

anion receptors, however there are few reports on their electrochemical properties,[4b,42] and only recently, Kadish and coworker studied electrochemistry in details for open chain pentapyrroles as well as meso-tetraarylsapphyrins.[16,43] We observed three reversible and/or

quasi reversible oxidation potentials and one detectable irreversible reduction potential for freebase sapphyrins **8.57** and **8.58**. Kadish and coworkers observed three irreversible reduction potential and upto three oxidation potential for freebase meso-tetraaryl sapphyrins. However, in the present case, as the decamethoxysapphyrins are already highly electron rich in nature, hence we could notice only one reduction potential at -1.16 and -1.30 V for sapphyrins **8.57** and **8.58**, respectively. Whereas, the oxidation potentials of freebase sapphyrins may be attributed to the formation of π-cation radical, dicationic species and tricationic species. The first oxidations were observed at +0.56 and +0.48 V respectively, for **8.57** and **8.58**. It is difficult to determine the HOMO-LUMO energy gap for free base sapphyrins due to the difficulties in detection of their reduction potentials. On the other hand, the diprotonated sapphyrins i.e. **8.57**.2$HClO_4$ and **8.58**.2$HClO_4$ display one reversible oxidation and three reversible reduction potentials. Most interestingly, protonation leads to disappearance of first two oxidation potentials of the freebase sapphyrins and appearance of two more reversible reduction potentials. Also, third oxidation potential of freebase and the oxidation potential of the diprotonated salts are very similar, indicating that probably they originate from the same electrochemical oxidation states. The chemically generated diprotonated state of sapphyrins leads to disappearance of first two oxidation potentials and appearance of two more reductions at more positive potentials, which may arise from electrochemically induced successive deprotonations of diprotonated sapphyrins. Similar type of trend was observed by Kadish and coworkers during electrochemical reduction and oxidation of chemically generated mono-anionic tetraarylsapphyrins, which cause disappearance of first electrochemically reduced state followed by appearance of reversible one electron oxidation state.[18b] Further, the third reduction potential of diprotonated sapphyrins probably evolve from the generation of sapphyrin anion radical species. However, further detailed studies are needed to understand these interesting electrochemical properties of sapphyrins and their diprotonated salts. Again, similar to freebase sapphyrins, determination of HOMO-LUMO energy gap could not be accomplished in these protonated sapphyrins owing to the absence of their first oxidation potentials.

8.4 Conclusions

In conclusion, we have synthesized and characterized β-decamethoxysapphyrin and its 27-N-benzyl analogue along with their various diprotonated salts. Among them **8.57**.2HF binds selectively with fluoride ion in methanol. Both **8.57** and **8.58** generates singlet oxygen with moderate yield and hence may find application as good photosensitizers. Electrochemical

studies of **8.57** and **8.58** and their perchlorate salts provide important information about electronic properties of both freebase and protonated sapphyrins. Most interestingly, both ^{1}H NMR studies and solid state characterization of diprotonated **8.58** reveal anion induced out of plane deformation of N-benzylpyrrole unit opposite to bipyrrole moiety for the first time. We believe the presence of methoxy substituents at the 12 & 13-positions probably hinder complete flipping out of the N-benzylpyrrolic moiety from the macrocyclic core. Therefore, at present efforts are underway to synthesize sapphyrin analogue with 12,13-unsubstituted N-benzylpyrrole moiety, which may show the path to interesting anion induced inversion of pyrrole unit in diprotonated sapphyrins.

8.5 Experimental details

Synthesis of 3,4-dimethoxy-5-(methoxycarbonyl)-pyrrole-2-carboxylic acid (8.60): Lithium hydroxide monohydrate (1.38 g, 32.89 mmol) was added to a solution of dimethyl 3,4-dimethoxypyrrole-2,5-dicarboxylate **8.59** (8 g, 32.89 mmol) in THF/CH_3OH/H_2O (3:1:1, 120 mL) under nitrogen atmosphere and the resulting reaction mixture was stirred at room temperature for 5 days. Water (~30 mL) was added to the reaction mixture and MeOH/THF was evaporated under reduce pressure. Aqueous layer was extracted with diethyl ether to remove unreacted starting materials **8.59** and acidified with 10% aqueous HCl, to precipitate **8.60** as white solid. Solution was kept in freeze (4 °C) for 1 h to complete precipitation and precipitate was filtered and washed with ice cooled water twice, which leaves **8.60** as white fibrous solid. Filtrate was extracted with diethylether for three times. Combined organic layer was passed through anhydrous Na_2SO_4 and evaporated under reduce pressure provides additional amount of **8.60** as white solid. Yield: 5.7 g (76%); m.p.: 158.4 °C (dec); IR (neat): ν (cm^{-1}) 3248, 1717, 1664; ^{1}H NMR (400 MHz, DMSO-d_6), δ (ppm): 12.87 (br s, 1H), 11.39 (br s, 1H), 3.80 (s, 3H), 3.79 (s, 3H), 3.75 (s, 3H); ^{13}C NMR (100 MHz, DMSO-d_6), δ (ppm): 160.50, 159.57, 141.93, 141.46, 114.23, 112.21, 61.74, 61.59, 51.39; HRMS (ESI+): m/z: calculated for $C_9H_{12}NO_6$ ($M+H^+$): 230.0659; found: 230.0666.

Synthesis of methyl 3,4-dimethoxypyrrole-2-carboxylate (8.61): 3,4-Dimethoxy-5-(methoxycarbonyl)-pyrrole-2-carboxylic acid **8.60** (2 g, 8.73 mmol) was heated at 180 °C for 10 min under nitrogen atmosphere in Kugelrohr with rotation. Residue was purified by silica gel column chromatography by using EtOAc/Hexane (3:7) as eluent to provide **8.61** (1.3 g) as white crystalline solid. Yield: 1.3 g (80%); m.p.: 84.7 °C; IR (neat): ν (cm^{-1}) 3317, 1673; ^{1}H NMR (400 MHz, $CDCl_3$), δ (ppm): 8.61 (br s, 1H), 6.48 (d, 1H, J = 3.6 Hz), 3.96 (s, 3H),

3.87 (s, 3H), 3.76 (s, 3H); ^{13}C NMR (100 MHz, $CDCl_3$), δ (ppm): 161.40, 140.33, 139.98, 109.31, 105.84, 61.70, 58.88, 51.56; HRMS (ESI+): m/z: calculated for $C_8H_{12}NO_4$ ($M+H^+$): 186.0761; found: 186.0761.

Synthesis of methyl 5-formyl-3,4-dimethoxypyrrole-2-carboxylate (8.62): Methyl 3,4-dimethoxypyrrole-2-carboxylate **8.61** (1.5 g, 8.10 mmol) dissolved in dry DCE (20 mL) was added slowly to ice cooled stirred Vilsmeier-Haack formylating mixture prepared from $POCl_3$ (1.5 mL, 16.20 mmol) and DMF (1.3 mL, 17.01 mmol) in dry DCE (20 mL) under nitrogen atmosphere. After addition was over, ice-bath was replaced with oil bath and the reaction mixture was refluxed for 4 h. Then it was cooled on ice bath and NaOAc (6.64 g, 81 mmol) in water (30 mL) added carefully and refluxed the reaction mixture for additional 2 h. After cooling to room temperature, the organic layer was separated and aqueous layer was extracted with DCM for three times. Combined organic layer was washed with aqueous sodium bicarbonate solution, passed through anhydrous Na_2SO_4 and evaporated to dryness. Crude reaction mixture was purified by silica gel column chromatography using EtOAc/Hexane (3:7) as eluent to obtain compound **8.62** (1.6 g) as white crystalline solid. Yield: 1.6 g (93%); m.p.: 59.3 °C; IR (neat): ν (cm^{-1}) 3286, 1701, 1654; ^{1}H NMR (400 MHz, $CDCl_3$), δ (ppm): 9.73 (s, 1H), 8.98 (br s, 1H), 4.07 (s, 3H), 3.94 (s, 3H), 3.92 (s, 3H); ^{13}C NMR (100 MHz, $CDCl_3$), δ (ppm): 178.08, 160.16, 145.37, 140.66, 120.73, 116.61, 62.59, 61.63, 52.23; HRMS (ESI+): m/z: calculated for $C_9H_{12}NO_5$ ($M+H^+$): 214.0710; found: 214.0715.

General procedure for synthesis of dimethyl 5,5'-((1-substituted-3,4-dimethoxypyrrole-2,5-diyl)bis(methylene))bis(3,4-dimethoxypyrrole-2-carboxylate) (8.63a-b): Methyl 5-formyl-3,4-dimethoxypyrrole-2-carboxylate **8.62** (400 mg, 1.88 mmol) was taken in dry THF/MeOH (9:1) (10 mL) under nitrogen atmosphere. Sodium borohydride (142 mg, 3.75 mmol) was added to the reaction mixture in small amount and stirred at room temperature for 4 h. Then, water was added to the reaction mixture and extracted with DCM. Combined organic layer was passed through anhydrous Na_2SO_4 and evaporated to dryness under reduced pressure, to result methyl 5-(hydroxymethyl)-3,4-dimethoxypyrrole-2-carboxylate as colourless viscous liquid. Compound was used in the next step immediately without further purification. ^{1}H NMR (400 MHz, $CDCl_3$), δ (ppm): 9.22 (br s, 1H), 4.61 (s, 2H), 3.95 (s, 3H), 3.87 (s, 3H), 3.82 (s, 3H); ^{13}C NMR (100 MHz, $CDCl_3$), δ (ppm): 161.68, 143.13, 135.75, 124.54, 107.78, 62.51, 61.81, 54.98, 51.72.

Compound obtained in previous step and 3,4-dimethoxypyrrole were taken in dry MeOH (20 mL) under nitrogen atmosphere. *Para*-toluenesulphonic acid monohydrate (34 mg, 0.18 mmol) was added to the reaction mixture and refluxed for 5 h. Then methanol was evaporated under reduce pressure and residue was dissolve in DCM. The DCM layer was washed with aqueous $NaHCO_3$ solution, passed through anhydrous Na_2SO_4 and evaporated to dryness under reduced pressure. Crude product was purified by silica gel column chromatography with EtOAc/Hexane (1:1) as eluent to obtain pure **8.63a** (191 mg) as white solid.

Dimethyl 5,5'-((3,4-dimethoxypyrrole-2,5-diyl)bis(methylene))bis(3,4-dimethoxypyrrole-2-carboxylate) (8.63a): Yield: 191 mg (41%); m.p.: 159.2 °C; IR (neat): ν (cm^{-1}) 3282, 1646; ^{1}H NMR (400 MHz, $CDCl_3$), δ (ppm): 9.99 (br s, 2H), 8.32 (br s, 1H), 3.94 (s, 6H), 3.82 (s, 6H), 3.80 (s, 6H), 3.78 (s, 4H), 3.41 (s, 6H); ^{13}C NMR (125 MHz, $CDCl_3$), δ (ppm): 162.40, 143.33, 135.27, 134.62, 124.06, 111.89, 106.64, 62.34, 61.92, 61.39, 51.62, 20.10; HRMS (ESI+): m/z: calculated for $C_{24}H_{32}N_3O_{10}$ ($M+H^+$): 522.2082; found: 522.2087.

Dimethyl 5,5'-((N-benzyl-3,4-dimethoxypyrrole-2,5-diyl)bis(methylene))bis(3,4-dimethoxypyrrole-2-carboxylate) (8.63b): Methyl 5-formyl-3,4-dimethoxypyrrole-2-carboxylate (**8.62**) (600 mg, 2.81 mmol) and N-benzyl-3,4-dimethoxypyrrole (290 mg, 1.33 mmol) were used. Reaction was run for 15 h under reflux condition. Crude product was purified by silica gel column chromatography with EtOAc/Hexane (1:1) as eluent to yield pure **8.63b** (437 mg) as white crystalline solid. Yield: 437 mg (51%); m.p.: 149.7 °C; IR (neat): ν (cm^{-1}) 3297, 3247, 1652; ^{1}H NMR (400 MHz, $CDCl_3$), δ (ppm): 8.08 (br s, 2H), 7.21-7.09 (m, 3H), 6.64 (d, 2H, *J* = 6.8 Hz), 4.86 (s, 2H), 3.89 (s, 6H), 3.83 (s, 6H), 3.82 (s, 6H), 3.67 (s, 4H), 3.62 (s, 6H); ^{13}C NMR (100 MHz, $CDCl_3$), δ (ppm): 160.67, 143.19, 138.15, 136.10, 135.04, 128.65, 127.07, 125.17, 122.76, 114.01, 106.99, 61.98, 61.85, 61.70, 51.35, 46.68, 18.69; HRMS (ESI+): m/z: calculated for $C_{31}H_{38}N_3O_{10}$ ($M+H^+$): 612.2552; found: 612.2558.

General procedure for synthesis of dibenzyl 5,5'-((1-substituted-3,4-dimethoxypyrrole-2,5-diyl)bis(methylene))bis(3,4-dimethoxypyrrole-2-carboxylate) (8.64): Sodium metal (11 mg) was dissolved in dry benzyl alcohol (2 mL) under nitrogen. Dimethyl 5,5'-((3,4-dimethoxypyrrole-2,5-diyl)bis(methylene))bis(3,4-dimethoxypyrrole-2-carboxylate) (**8.63a**) (258 mg, 0.49 mmol) in dry benzyl alcohol (3 mL) was added. Reaction mixture was stirred at 90 °C for 2 h under ~10 mmHg pressure. Benzyl alcohol was evaporated under reduce

pressure and residue was dissolved in DCM. The DCM layer was washed with water, passed through anhydrous Na_2SO_4 and evaporated to dryness under reduce pressure. Crude product was purified by silica gel column chromatography with EtOAc/Hexane (3:7) as eluent to provide the pure **8.64a** (155 mg) as white solid.

Dibenzyl 5,5'-((3,4-dimethoxypyrrole-2,5-diyl)bis(methylene))bis(3,4-dimethoxypyrrole-2-carboxylate) (8.64a): Yield: 155 mg (47%); m.p.: 129.4 °C (dec); IR (neat): ν (cm^{-1}) 3257, 1653; ^{1}H NMR (400 MHz, $CDCl_3$), δ (ppm): 10.35 (br s, 2H), 8.52 (s, 1H), 7.30-7.24 (m, 3H), 7.19 (d, 2H, *J* = 7.2 Hz), 4.70 (s, 4H), 3.81 (s, 6H), 3.80 (s, 6H), 3.70 (s, 6H), 3.60 (s, 4H); ^{13}C NMR (100 MHz, $CDCl_3$), δ (ppm): 161.57, 143.76, 136.29, 135.25, 134.72, 128.43, 127.79, 127.14, 124.39, 112.03, 106.76, 65.86, 62.20, 61.96, 61.69, 19.99; HRMS (ESI+): m/z: calculated for $C_{36}H_{40}N_3O_{10}$ ($M+H^+$): 674.2708; found: 674.2626.

Dibenzyl 5,5'-((N-benzyl-3,4-dimethoxypyrrole-2,5-diyl)bis(methylene))bis(3,4-dimethoxypyrrole-2-carboxylate) (8.64b): Sodium metal (8 mg) and **8.63b** (200 mg, 0.33 mmol) were used for reaction. Crude product was purified by silica gel column chromatography with EtOAc/Hexane (3:7) as eluent to obtain the pure **8.64b** (233 mg) as colorless viscous liquid which solidifies slowly at low temperature.Yield: 233 mg (93%); m.p.: 72.1 °C; ^{1}H NMR (400 MHz, $CDCl_3$), δ (ppm): 8.27 (br s, 2H), 7.42 (d, 4H, *J* = 6.8 Hz), 7.37-7.31 (m, 6H), 7.11-7.04 (m, 3H), 6.62 (d, 2H, *J* = 7.2 Hz), 5.27 (s, 4H), 4.85 (s, 2H), 3.83 (s, 6H), 3.79 (s, 6H), 3.64 (s, 4H), 3.61 (s, 6H); ^{13}C NMR (100 MHz, $CDCl_3$), δ (ppm): 159.96, 143.57, 138.13, 136.62, 136.00, 135.13, 128.61, 127.09, 125.17, 122.92, 114.08, 107.12, 65.67, 61.89, 61.83, 60.54, 46.68, 18.68; HRMS (ESI+): m/z: calculated for $C_{43}H_{46}N_3O_{10}$ ($M+H^+$): 764.3178; found: 764.3184.

General Procedure for synthesis of 5,5'-((N-substituted-3,4-dimethoxypyrrole-2,5-diyl)bis(methylene))bis(3,4-dimethoxypyrrole-2-carboxylic acid) (8.65a-b): Dibenzyl 5,5'-((3,4-dimethoxypyrrole-2,5-diyl)bis(methylene))bis(3,4-dimethoxypyrrole-2-carboxylate) (**8.64a**) (155 mg, 0.23 mmol) and 5% Pd/C (49 mg, 0.023 mmol) were taken in dry THF (20 mL) under hydrogen atmosphere (1 atm, hydrogen balloon). Reaction mixture was stirred in dark at room temperature for 18 h and passed through celite and washed with THF repeatedly. THF was evaporated under reduced pressure to provide entitled compound **8.65a** as white solid, which turns brown with time. Product was used directly in the next step immediately.

5,5'-((N-benzyl-3,4-dimethoxypyrrole-2,5-diyl)bis(methylene))bis(3,4-dimethoxypyrrole-2-carboxylic acid) (8.65b): Dibenzyl 5,5'-((N-benzyl-3,4-dimethoxypyrrole-2,5-diyl)bis(methylene))bis(3,4-dimethoxypyrrole-2-carboxylate) (**8.64b**) (233 mg, 0.30 mmol) and 5% Pd/C (65 mg, 0.030 mmol) were taken in dry THF (20 mL).

General procedure for synthesis of 2,3,7,8,12,13,17,18,22,23-decamethoxy-27-N-substituted sapphyrins (8.57-58): Tripyrrane diacid obtained in previous reaction (**8.65a**) (0.23 mmol, assuming 100% conversion) and 3,3',4,4'-tetramethoxy-[2,2'-bipyrrole]-5,5'-dialdehyde **8.66** (71 mg, 0.23 mmol) were taken in dry EtOH (240 mL). *Para*-toluenesulphonic acid monohydrate (175 mg, 0.92 mmol) was added to the reaction mixture and stirring was continued in dark for 24 h with continuous O_2 bubbling. Solvent was evaporated under reduced pressure and residue was dissolved in DCM. The organic layer was washed with aqueous $NaHCO_3$ and passed through anhydrous Na_2SO_4 and evaporated to dryness under reduced pressure. Crude product was purified by silica gel column chromatography by using $CHCl_3$/ MeOH (ratio gradually changed from 100:0 to 90:10). Green fraction was collected, evaporated and purified again by neutral alumina column chromatography by using $CHCl_3$/ MeOH (99:1) as eluent to obtain pure **8.57** (44 mg) as blue purple solid. Corresponding diprotonated salts were prepared by washing chloroform solution of freebase sapphyrin with the relevant acids.

2,3,7,8,12,13,17,18,22,23-decamethoxysapphyrins (8.57): Yield: 44 mg (28%); m.p.: 182.8 °C; ^{1}H NMR (400 MHz, $CDCl_3$), δ (ppm): 10.98 (s, 2H), 10.71 (s, 2H), 5.22 (s, 6H), 5.18 (s, 6H), 5.17 (s, 6H), 5.08 (s, 6H), 4.90 (s, 6H), -5.88 (br s, 6H); ^{13}C NMR (100 MHz, $CDCl_3$), δ (ppm): 147.78, 143.83, 143.80, 142.82, 142.24, 129.84, 127.96, 127.20, 126.32, 126.16, 92.87, 87.92, 64.77, 64.10, 63.69, 63.58, 62.75; UV-Vis data in $CHCl_3$, λ_{max} nm (log ε): 449 (5.43), 586 (4.06), 632 (4.12), 647 (4.10), 720 (3.72); Fluorescence in $CHCl_3$, λ_{max} nm (λ_{exc} 445 nm): 724; Fluorescence quantum yield in $CHCl_3$ (ϕ_f): 0.017; HRMS (ESI+): m/z: calculated for $C_{34}H_{38}N_5O_{10}$ ($M+H^+$): 676.2613; found: 676.2617.

8.57.2TFA**:** ^{1}H NMR (400 MHz, $CDCl_3$), δ (ppm): 11.87 (s, 2H), 11.83 (s, 2H), 5.28 (s, 6H), 5.21 (s, 12H), 5.16 (s, 6H), 4.97 (s, 6H), -6.64 (br, s, 1H), -6.89 (br s, 2H), -7.14 (br s, 2H).

8.57.2HBr**:** ^{1}H NMR (400 MHz, $CDCl_3$), δ (ppm): 11.84 (s, 2H), 11.82 (s, 2H), 5.19 (s, 18H), 5.15 (s, 6H), 5.03 (s, 6H), -5.69 (br s, 1H), -5.90 (br s, 2H), -6.05 (br s, 2H); UV-Vis data in

MeOH, λ_{max} nm (log ε): 443 (5.53), 614 (4.08), 661 (3.93); Fluorescence in $CHCl_3$, λ_{max} nm (λ_{exc} 443 nm): 680; Fluorescence quantum yield in $CHCl_3$ (ϕ_f): 0.029.

8.57.2HCl**:** ^{1}H NMR (400 MHz, $CDCl_3$), δ (ppm): 11.86 (s, 2H), 11.84 (s, 2H), 5.19 (s, 18H), 5.15 (s, 6H), 5.04 (s, 6H), -5.42 (br s, 1H), -5.52 (br s, 2H), -5.76 (br s, 2H); UV-Vis data in MeOH, λ_{max} nm (log ε): 443 (5.46), 614 (4.04), 661 (3.95); Fluorescence in $CHCl_3$, λ_{max} nm (λ_{exc} 443 nm): 683; Fluorescence quantum yield in $CHCl_3$ (ϕ_f): 0.043.

8.57.2HF**:** Due to poor solubility we are not able to record ^{1}H NMR spectrum. UV-Vis data in MeOH, λ_{max} nm (log ε): 443 (5.43), 614 (3.98), 661 (3.83); Fluorescence in $CHCl_3$, λ_{max} nm (λ_{exc} 443 nm): 679; Fluorescence quantum yield in $CHCl_3$ (ϕ_f): 0.065.

8.57.2$HClO_4$**:** ^{1}H NMR (400 MHz, $CDCl_3$), δ (ppm): 11.87 (s, 2H), 11.86 (s, 2H), 5.24 (s, 6H), 5.21 (s, 6H), 5.20 (s, 6H), 5.15 (s, 6H), 4.98 (s, 6H), -7.13 (s, 1H), -7.55 (s, 2H), -7.67 (s, 2H); UV-Vis data in $CHCl_3$, λ_{max} nm (log ε): 451 (5.75), 619 (4.33), 674 (4.13); Fluorescence in $CHCl_3$, λ_{max} nm (λ_{exc} 450 nm): 688; Fluorescence quantum yield in $CHCl_3$ (ϕ_f): 0.067.

8.57.2PTSA**:** ^{1}H NMR (400 MHz, $CDCl_3$), δ (ppm): 11.67 (s, 2H), 11.64 (s, 2H), 5.42 (d, 4H, *J* = 5.6 Hz), 5.27 (s, 6H), 5.23 (s, 6H), 5.22 (s, 6H), 5.19 (s, 6H), 5.02 (s, 6H), 2.23 (s, 4H), 1.96 (s, 6H), -6.42 (br s, 1H), -6.51 (br s, 2H), -6.69 (br s, 2H).

2,3,7,8,12,13,17,18,22,23-decamethoxy-27-N-benzylsapphyrins (8.58): Tripyrrane diacid obtained in previous reaction (**8.65b**) (0.305 mmol, assuming 100% conversion) and 3,3',4,4'-tetramethoxy-[2,2'-bipyrrole]-5,5'-dialdehyde (**8.66**) (94 mg, 0.305 mmol) were taken in dry EtOH (300 mL). Yield: 63 mg (27%); m.p.: 95.5 °C; ^{1}H NMR (400 MHz, $CDCl_3$), δ (ppm): 10.97 (s, 2H), 10.96 (s, 2H), 5.93 (t, 1H, *J* = 7.4 Hz), 5.57 (t, 2H, *J* = 7.6 Hz), 5.05 (s, 6H), 5.01 (s, 6H), 4.84 (s, 6H), 4.83 (s, 6H), 4.66 (s, 6H), 2.29 (d, 2H, *J* = 7.6 Hz), -2.43 (br s, 4H), -6.60 (s, 2H); ^{13}C NMR (100 MHz, $CDCl_3$), δ (ppm): 147.68, 144.64, 143.94, 143.04, 140.71, 134.04, 133.88, 131.45, 131.26, 128.19, 125.73, 125.30, 125.26, 123.43, 96.41, 90.18, 64.66, 64.14, 63.19, 63.08, 62.95, 39.52; UV-Vis data in $CHCl_3$, λ_{max} nm (log ε): 456 (5.51), 582 (4.26), 626 (4.09), 662 (4.07), 732 (3.80); Fluorescence in $CHCl_3$, λ_{max} nm (λ_{exc} 455 nm): 739; Fluorescence quantum yield in $CHCl_3$ (ϕ_f): 0.030; HRMS (ESI+): m/z: calculated for $C_{41}H_{44}N_5O_{10}$ ($M+H^+$): 766.3083; found: 766.3087.

8.58.2HCl **:** ^{1}H NMR (400 MHz, $CDCl_3$), δ (ppm): 11.80 (s, 2H), 11.42 (s, 2H), 6.08 (s, 1H), 5.73 (s, 2H), 5.24 (s, 6H), 5.16 (s, 6H), 5.02 (s, 6H), 4.77 (s, 6H), 4.70 (s, 6H), 2.64 (s, 2H), -4.60 (br s, 2H), -5.31 (br s, 2H), -7.15 (s, 2H); UV-Vis data in $CHCl_3$, λ_{max} nm (log ε): 458 (5.37), 626 (3.96), 676 (3.85); Fluorescence in $CHCl_3$, λ_{max} nm (λ_{exc} 458 nm): 697; Fluorescence quantum yield in $CHCl_3$ (ϕ_f): 0.017.

8.58.2HBr **:** ^{1}H NMR (400 MHz, $CDCl_3$), δ (ppm): 11.80 (s, 2H), 11.38 (s, 2H), 6.04 (s, 1H), 5.69 (s, 2H), 5.23 (s, 6H), 5.13 (s, 6H), 4.98 (s, 6H), 4.73 (s, 6H), 4.67 (s, 6H), 2.59 (s, 2H), -5.18 (br s, 2H), -5.49 (br s, 2H), -7.19 (s, 2H); UV-Vis data in $CHCl_3$, λ_{max} nm (log ε): 462 (5.43), 632 (4.07), 685 (3.94); Fluorescence in $CHCl_3$, λ_{max} nm (λ_{exc} 462 nm): 698; Fluorescence quantum yield in $CHCl_3$ (ϕ_f): 0.005.

8.58.2$HClO_4$ **:** ^{1}H NMR (400 MHz, $CDCl_3$), δ (ppm): 11.67 (s, 2H), 11.25 (s, 2H), 6.23 (t, 1H, *J* = 7.4 Hz), 6.00 (t, 2H, *J* = 7.6 Hz), 5.20 (s, 6H), 5.10 (s, 6H), 4.83 (s, 6H), 4.73 (s, 6H), 4.27 (s, 6H), 3.48 (d, 2H, *J* = 8 Hz), -6.35 (s, 2H), -6.72 (s, 2H), -6.91 (s, 2H); UV-Vis data in $CHCl_3$, λ_{max} nm (log ε): 462 (5.70), 632 (4.31), 693 (4.17); Fluorescence in $CHCl_3$, λ_{max} nm (λ_{exc} 462 nm): 697; Fluorescence quantum yield in $CHCl_3$ (ϕ_f): 0.016.

8.58.2PA **:** ^{1}H NMR (400 MHz, $CDCl_3$), δ (ppm): 11.75 (s, 2H), 11.30 (s, 2H), 5.87 (t, 1H, *J* = 7.4 Hz), 5.45 (t, 2H, *J* = 7.2 Hz), 5.16 (s, 6H), 5.15 (s, 6H), 4.89 (s, 6H), 4.78 (s, 6H), 4.63 (s, 6H), 1.98 (d, 2H, *J* = 8 Hz), -7.39 (s, 2H).

8.58.2PTSA **:** ^{1}H NMR (400 MHz, $CDCl_3$), δ (ppm): 11.52 (s, 2H), 11.19 (s, 2H), 6.21 (t, 1H, *J* = 7 Hz), 5.93 (t, 2H, *J* = 7.2 Hz), 5.78 (s, 2H), 5.32 (s, 2H), 5.17 (s, 6H), 5.16 (s, 6H), 4.80 (s, 6H), 4.75 (s, 6H), 4.34 (s, 6H), 4.18 (s, 2H), 3.36 (d, 2H, *J* = 7.2 Hz), 2.06 (s, 2H), 1.88 (s, 3H), 1.74 (s, 3H), -4.82 (br s, 2H), -6.09 (br s, 2H), -6.71 (s, 2H).

8.58.2TFA **:** ^{1}H NMR (400 MHz, $CDCl_3$), δ (ppm): 11.94 (s, 2H), 11.61 (s, 2H), 6.15 (s, 1H), 5.77 (s, 2H), 5.33 (s, 6H), 5.22 (s, 6H), 5.04 (s, 6H), 4.84 (s, 6H), 4.60 (s, 6H), 2.42 (s, 2H), -6.31 (br s, 2H), -6.52 (br s, 2H), -7.65 (s, 2H).

8.6 Crystallographic details

Crystallographic data for **8.57.**2PTSA, **8.58.**2$HClO_4$ and **8.58.**PTSA were collected on Oxford Gemini A Ultra diffractometer with dual source. Mo-Kα (λ = 0.71073 Å) radiation

was used for **8.58.**2$HClO_4$ and **8.58.**PTSA to collect the X-ray reflections of the crystal. Cu-Kα (λ = 1.54184 Å) radiations was used for **8.57.**2PTSA to collect the X-ray reflections of the crystals. Relevant crystallographic data collection and refinement parameters are shown in the following table:

Crystal Data	**8.57.**2PTSA	**8.58.**2$HClO_4$	**8.58.**PTSA
CCDC No.	1047320	1057321	105.7322
Formula unit	$C_{48}H_{53}N_5O_{16}S_2$	$C_{41}H_{45}N_5O_{18}Cl_2$	$C_{48}H_{51}N_5O_{13}S$
Formula Weight	1020.70	966.72	938.00
Crystal system	Monoclinic	Triclinic	Monoclinic
T [K]	293(2)	293(2)	293(2)
a [Å]	9.5948(3)	18.7180(14)	10.656(3)
b [Å]	11.7166(3)	20.1801(14)	38.925(9)
c [Å]	43.6295(16)	21.555(2)	11.435(3)
α [°]	90.00	63.466(8)	90.00
β [°]	91.392(4)	65.800(8)	111.21(3)
γ [°]	90.00	82.646(9)	90.00
volume [$Å^3$]	4903.3(3)	6629.1(9)	4422(2)
Space group	P 21/n	P -1	P 21/c
Z´	1	3	1
Z	4	6	4
D_{calc} [$g.cm^{-3}$]	1.382	1.453	1.409
μ/mm^{-1}	1.633	0.230	0.148
Reflns collected	13819	52197	16969
Unique reflns	7416	23322	7349
Obs. reflns	5550	6937	2497
R(int)	0.0414	0.1173	0.1316
R_1 [$I > 2\sigma(I)$],	0.0921(5550)	0.1032(6937)	0.0854(2497)
wR_2	0.2745(7416)	0.3480(23322)	0.2325(7349)
GOF	1.115	0.965	0.980

8.7 References

1. (a) Sessler, J. L.; Weghorn, S. J. *Expanded, Contracted and Isomeric Porphyrins*, **1997**, 253. (b) Sessler, J. L.; Gebauer, A.; Weghorn, S. J. *Porphyrin Handbook*, **2000**, *2*, 55.
2. (a) Woodward, R. B. *Presented at the Aromaticity Conference, Sheffield, U.K.* **1966**. (b) Bauer, V. J.; Clive, D. L. J.; Dolphin, D.; Paine III, J. B. P.; Harris, F. L.; King, M. M.; Loder, J.; Wang, S.-W. C.; Woodward, R. B. *J. Am. Chem. Soc.* **1983,** *105*, 6429.
3. Broadhurst, M. J.; Grigg, R.; Johnson, A. W. *J. Chem. Soc. D, Chem. Commun.* **1969**, 1480.
4. (a) Sessler, J. L.; Cry, M.; Lynch, V.; McGhee, E.; Ibers, J. A. *J. Am. Chem. Soc.* **1990**, *112*, 2810. (b) Shionoya, M.; Furuta, H.; Lynch, V.; Harriman, A.; Sessler, J. L. *J. Am. Chem. Soc.* **1992**, *114*, 5714. (c) Sessler, J. L.; Devis, J. M. *Acc. Chem. Res.* **2001**, *34*, 989. (d) Sessler, J. L.; Camiolo, S.; Gale, P. A. *Coord. Chem. Rev.* **2003**, *240*, 17.
5. (a) Maiya, B. G.; Cyr, M.; Harriman, A.; Sessler, J. L. *J. Phys. Chem.* **1990**, *94*, 3597. (b) Král, V.; Davis, J.; Andrievsky, A.; Kralova, J.; Synytsya, A.; Pouckova, P.; Sessler, J. L. *J. Med. Chem.* **2002**, *45*, 1073. (c) Wang, Z.; Lecane, P.; Thiemann, P.; Fan, A.; Cortez, C.; Ma, X.; Tonev, D.; Miles, D.; Lin, A.; Hemmi, G.; Naumovski, L.; Miller, R. A.; Magda, D.; Cho, D.-G.; Sessler, J. L.; Pike, B. L.; Yeligar, S. M.; Karaman, M. W.; Hacia, J. G. *Mol. Cancer* **2007**, *6*, 9. (d) Sessler, J. L.; Sansom, P. I.; Král, V.; O'Connor, D.; Iverson, B. L. *J. Am. Chem. Soc.* **1996**, *118*, 12322. (e) Hooker, J. D.; Nguyen, V. H.; Taylor, V. M.; Cedeño, D. L.; Lash, T. D.; Jones, M. A.; Robledo, S. M.; Vélez, I. D. *Photochem. Photobiol.* **2012**, *88*, 194. (f) Naumovski, L.; Sirisawad, M.; Lecane, P.; Chen, J.; Ramos, J.; Wang, Z.; Cortez, C.; Magda, D.; Thiemann, P.; Boswell, G.; Miles, D.; Cho, D. G.; Sessler, J. L.; Miller, R. *Mol Cancer Ther.* **2006**, *5*, 2798. (g) Sarma, T.; Anusha, P. T.; Pabbathi, A.; Rao, S. V.; Panda, P. K. *Chem. -Eur. J.* **2014**, *20*, 15561.
6. Broadhurst, M. J.; Grigg, R.; Johnson, A. W. *J. Chem. Soc. Perkin Trans. 1* **1972**, 2111.
7. Sessler, J. L.; Johnson, M. R.; Lynch, V. *J. Org. Chem.* **1987**, *52*, 4394.
8. (a) Richter, D. T.; Lash, T. D. *Tetrahedron Lett.* **1999**, *40*, 6735. (b) Richter, D. T.; Lash, T. D. *J. Org. Chem.* **2004**, *69*, 8842.

9. Paolesse, R.; Licoccia, S.; Spagnoli, M.; Boschi, T.; Khoury, R. G.; Smith, K. M. *J. Org. Chem*. **1997**, *62*, 5133.
10. King, M. M. Ph. D. Dissertation, Harvard University, Cambridge, MA, USA, **1970**.
11. Sessler, J. L.; Lisowski, J.; Boudreaux, K. A.; Lynch, V.; Barry, J.; Kodadek, T. J. *J. Org. Chem*. **1995**, *60*, 5975.
12. Chmielewski, P. J.; Latos-Grażyński, L.; Rachlewicz, K. *Chem. Eur. J*. **1995**, *1*, 68.
13. Brückner, C.; Sternberg, E. D.; Boyle, R. W.; Dolphin, D. *Chem. Commun*. **1997**, 1689.
14. Sessler, J. L.; Shevchuk, S.; Davis, J. M. *Tetrahedron Lett.* **2001**, *42*, 2447.
15. Narayanan, S. J.; Sridevi, B.; Srinivasan, A.; Chandrashekar, T. K.; Roy, R. *Tetrahedron Lett.* **1998**, *39*, 7389.
16. Yuan, M.; Ou, Z.; Fang, Y.; Huang, S.; Xue, Z.; Lu, G.; Kadish, K. M. *Inorg. Chem*. **2013**, *52*, 6664.
17. Rachlewicz, K.; Sprutta, N.; Latos-Grażyński, L.; Chmielewski, P. J.; Szterenberg, L. *J. Chem. Soc. Perkin Trans. 2* **1998**, 959.
18. Ono, N.; Kuroki, K.; Watanabe, E.; Ochi, N.; Uno, H. *Heterocycles* **2004**, *62*, 365.
19. Okujima, T.; Kikkawa, T.; Kawakami, S.; Shimizu, Y.; Yamada, H.; Ono, N.; Uno. H. *Tetrahedron*, **2010**, *66*, 7213.
20. Panda, P. K.; Kang, Y.-J.; Lee, C.-H. *Angew. Chem., Int. Ed.* **2005**, *44*, 4053.
21. Cho, D.-G; Plitt, P.; Kim, S. K.; Lynch, V.; Hong, S.-J.; Lee, C.-H.; Sessler, J. L. *J. Am. Chem. Soc.* **2008**, *130*, 10502.
22. Kee, S.-Y.; Lim, J. M.; Kim, S.-J.; Yoo, J.; Park, J.-S.; Sarma, T.; Lynch, V. M.; Panda, P. K.; Sessler, J. L.; Kim, D.; Lee, C.-H. *Chem. Commun.* **2011**, *47*, 6813.
23. Král, V.; Furuta, H.; Shreder, K.; Lynch, V.; Sessler, J. L. *J. Am. Chem. Soc*. **1996**, *118*, 1595.
24. (a) Iverson, B. L.; Thomas, R. E.; Král, V.; Genge, J. W.; Sessler, J. L. *J. Am. Chem. Soc*. **1994**, *116*, 2663. (b) Sessler, J. L.; Genge, J. W.; Král, V.; Iverson, B. L. *Supramol. Chem*. **1996**, *8*, 45. (c) Sessler, J. L.; Král, V.; Genge, J. W.; Thomas, R. E.; Iverson, B. L. *Anal. Chem*. **1998**, *70*, 2516.
25. (a) Král, V.; Sessler, J. L.; Furuta, H. *J. Am. Chem. Soc*. **1992**,*114*, 8704. (b) Sessler, J. L.; Furuta, H.; Král,V. *Supramol.Chem*. **1993**, *1*, 209. (c) Král, V.; Sessler, J. L. *Tetrahedron* **1995**, *51*, 539.
26. (a) Sessler, J. L.; Andrievsky, A. *Chem. Commun*. **1996**, 1119. (b) Sessler, J. L.; Andrievsky, A. *Chem. Eur. J*. **1998**, *4*, 159.

27. (a) Král, V.; Andrievsky, A.; Sessler, J. L. *J. Am. Chem. Soc*. **1995**, *117*, 2953. (b) Sessler, J. L.; Andrievsky, A.; Král, V.; Lynch, V. *J. Am. Chem. Soc*. **1997**, *119*, 9385.
28. Král, V.; Andrievsky, A.; Sessler, J. L. *J. Chem. Soc. Chem. Commun*. **1995**, 2349.
29. (a) Srinivasan, A.; Anand, V. G.; Narayanan, S. J.; Pushpan, S. K.; Kumar, M. R.; Chandrashekar, T. K.; Sugiura, K.-I.; Sakata, Y. *J. Org. Chem.* **1999**, *64*, 8693. (b) Rachlewicz, K.; Sprutta, N.; Chmielewski, P. J.; Latos-Grazynski, L. *J. Chem. Soc., Perkin Trans. 2* **1998**, 969.
30. Narayanan, S. J.; Sridevi, B.; Chandrashekar, T. K.; Vij, A.; Roy, R. *J. Am. Chem. Soc*. **1999**, *121*, 9053.
31. Sprutta, N.; Latos-Grażyński, L. *Org. Lett*. **2001**, *3*, 1933.
32. Shin, K.; Lim, C.; Choi, C.; Kim, Y.; Lee, C.-H. *Chem. Lett*. **1999**, *28*, 1331.
33. Karthik, G.; Srinivasan, A.; Chandrashekar, T. K. *Org. Lett*. **2014**, *16*, 3472.
34. Rana, A.; Panda, P. K. *Communicated*.
35. Rana, A.; Panda, P. K. *Org. Lett.* **2014**, *16*, 78.
36. Merz, A.; Schropp, R.; Dötterl, E. *Synthesis* **1995**, 795.
37. Boger, D. L.; Patel, M. *J. Org. Chem.* **1988**, *53*, 1405.
38. Uno, H.; Nakamoto, K.-i.; Kuroki, K.; Fujimoto, A.; Ono, N. *Chem. -Eur. J.* **2007**, *13*, 5773.
39. Boudif, A.; Momenteau, M. *J. Chem. Soc., Perkin Trans. 1* **1996**, 1235.
40. Rachlewicz, K.; Latos-Grażyński, L.; Gebauer, A.; Vivian, A.; Sessler, J. L. *J. Chem. Soc., Perkin Trans. 2* **1999**, 2189.
41. Ohno, O.; Kaizu, Y.; Kobayashi, H. *J. Chem. Phys*. **1985**, *82*, 1779.
42. Kang, S.; Hayashi, H.; Umeyama, T.; Matano, Y.; Tkachenko, N. V.; Lemmetyinen, H.; Imahori, H. *Chem. -Asian J.* **2008**, *3*, 2065.
43. Ou, Z.; Meng, D.; Yuan, M.; Huang, W.; Fang, Y.; Kadish, K. M. *J. Phys. Chem. B* **2013**, *117*, 13646.

8.8 Representative NMR spectra

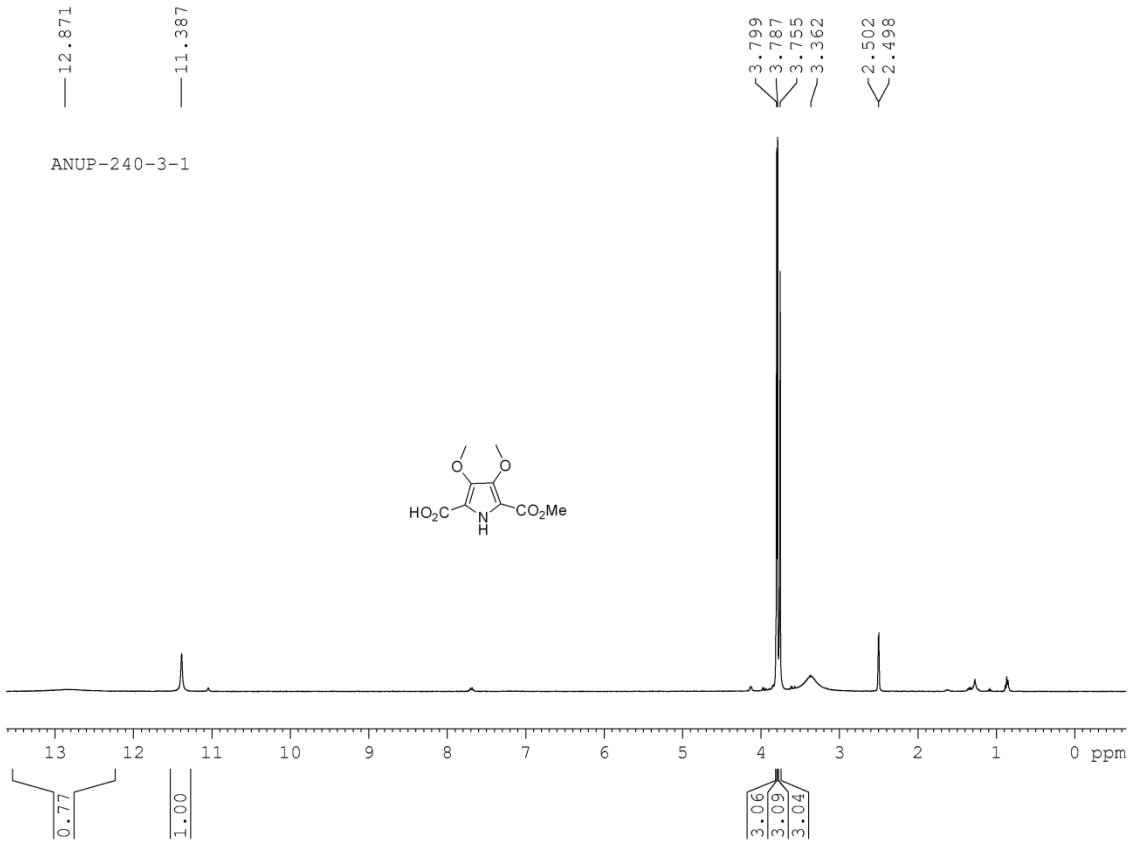

Figure 8.11 ^{1}H NMR spectrum of **8.60** in DMSO-d_6.

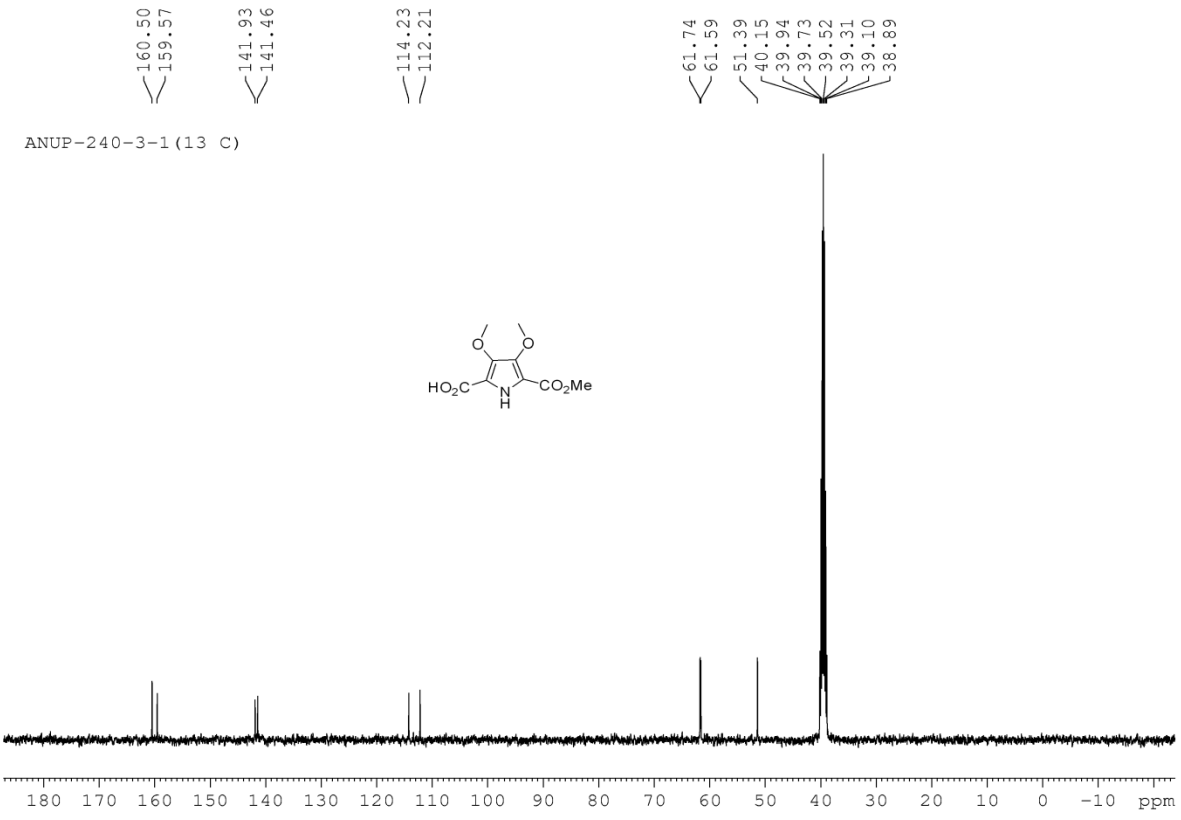

Figure 8.12 ^{13}C NMR spectrum of **8.60** in DMSO-d_6.

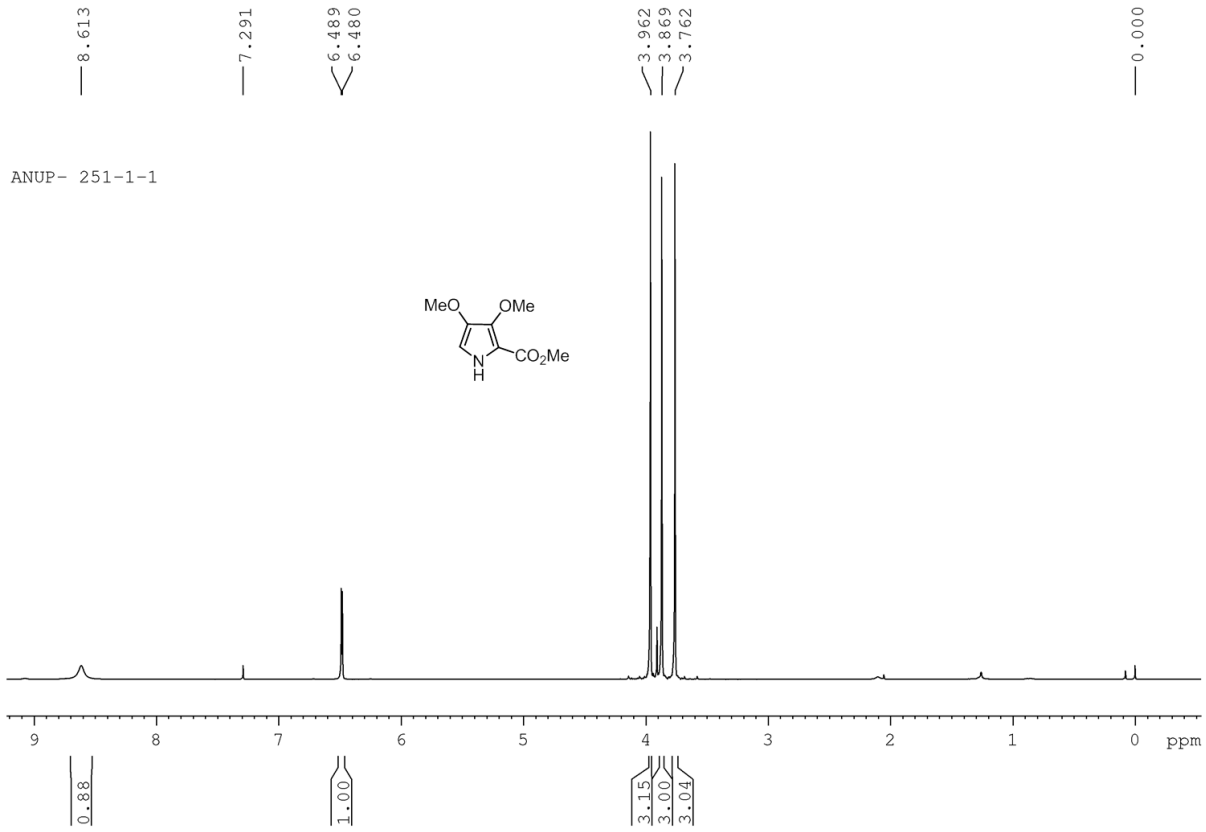

Figure 8.13 ^{1}H NMR spectrum of **8.61** in $CDCl_3$.

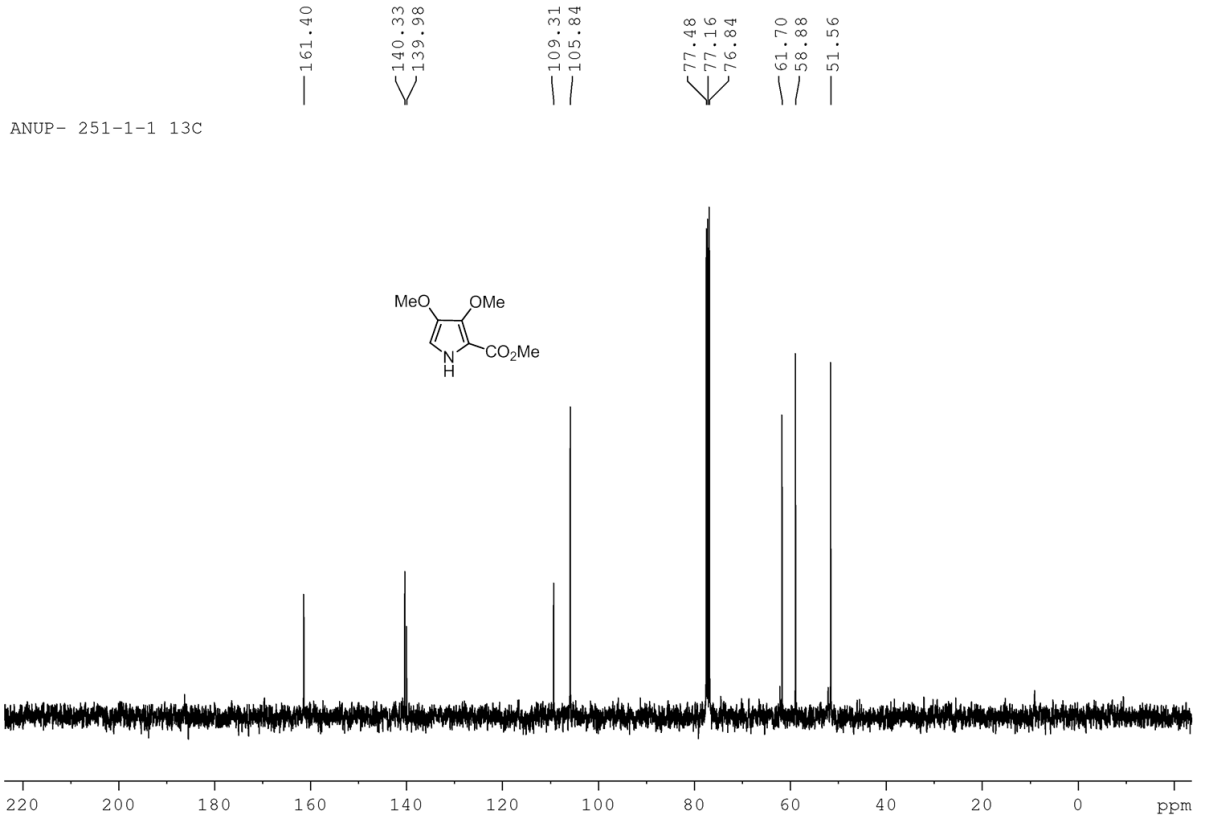

Figure 8.14 ^{13}C NMR spectrum of **8.61** in $CDCl_3$.

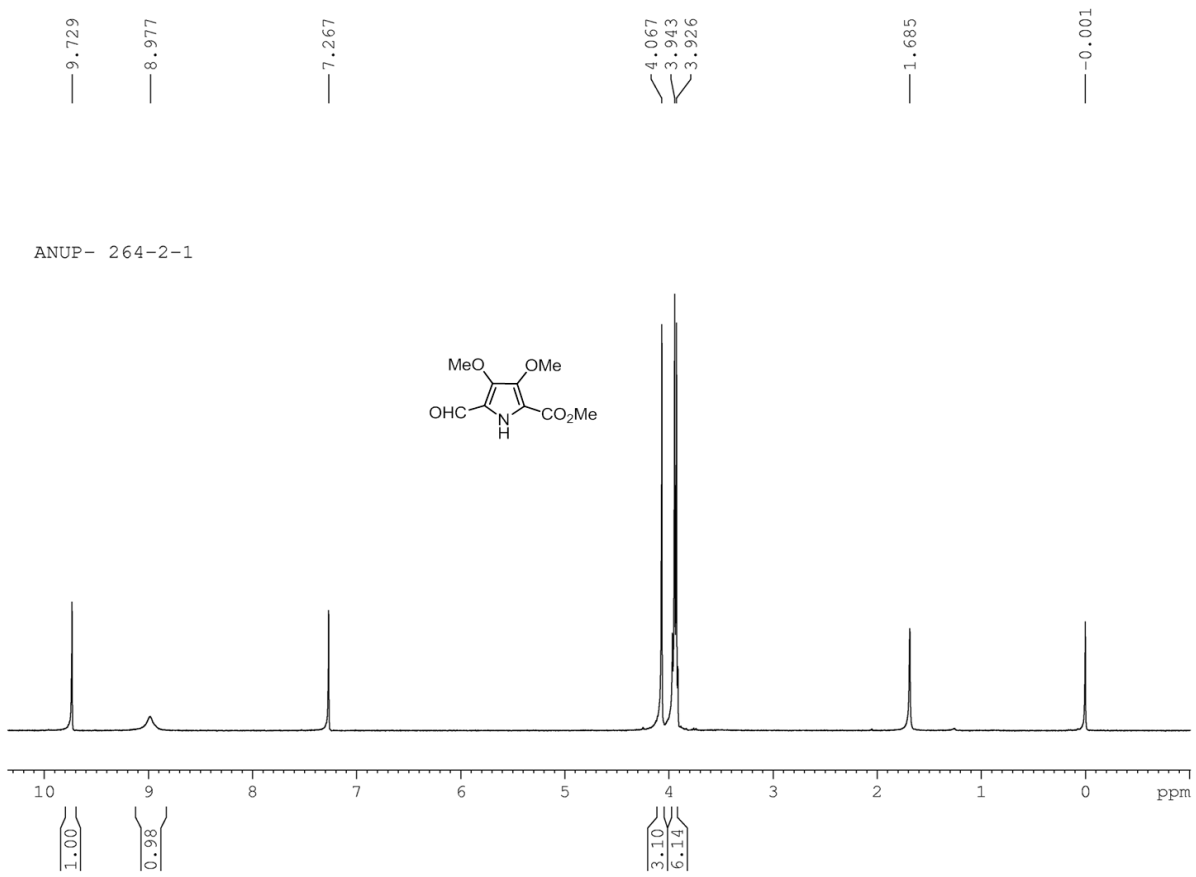

Figure 8.15 ^{1}H NMR spectrum of **8.62** in $CDCl_3$.

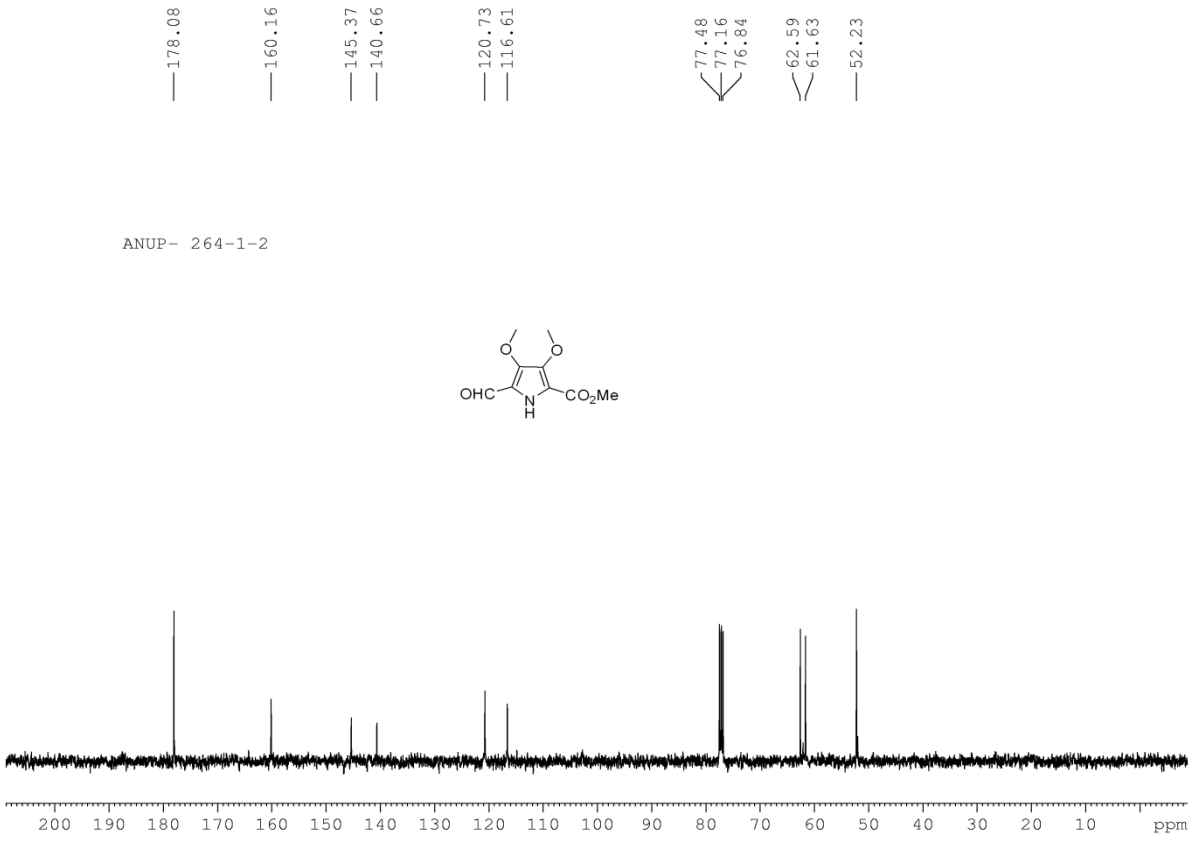

Figure 8.16 ^{13}C NMR spectrum of **8.62** in $CDCl_3$.

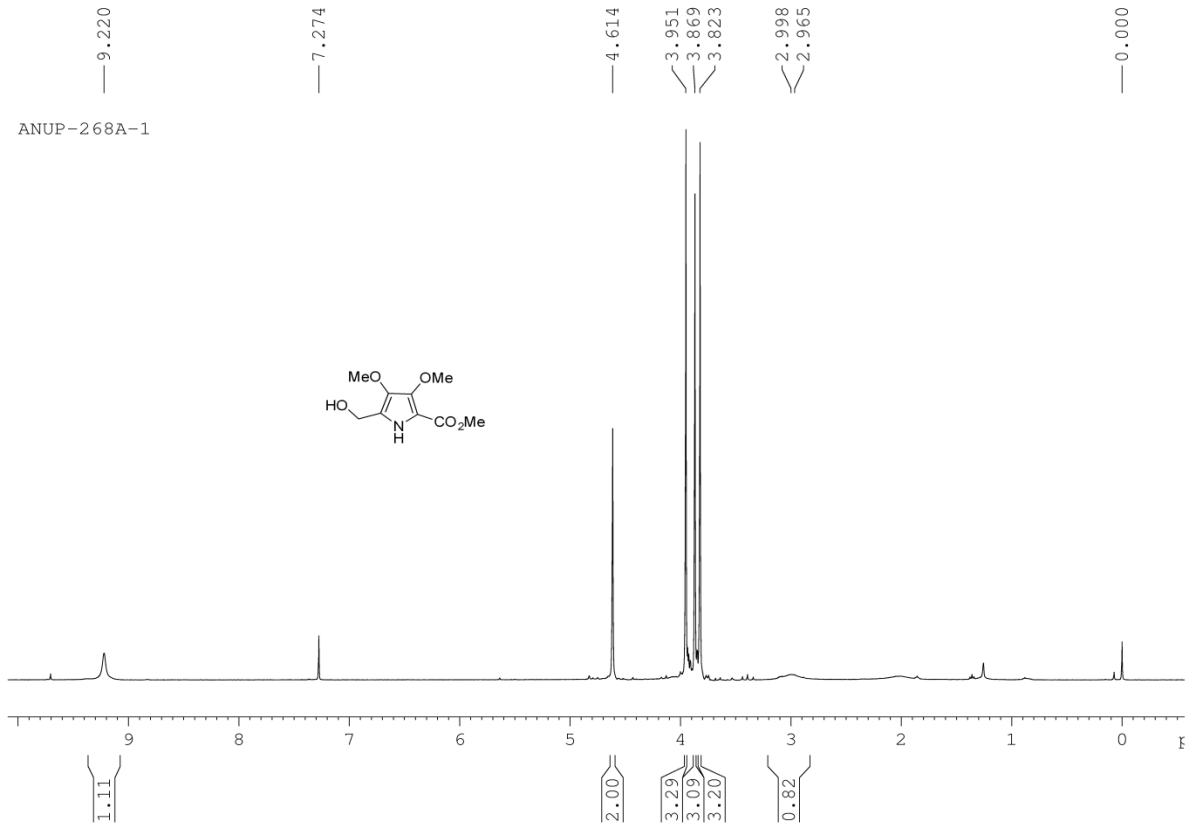

Figure 8.17 ^{1}H NMR spectrum of methyl 5-(hydroxymethyl)-3,4-dimethoxy-1H-pyrrole-2-carboxylate in $CDCl_3$.

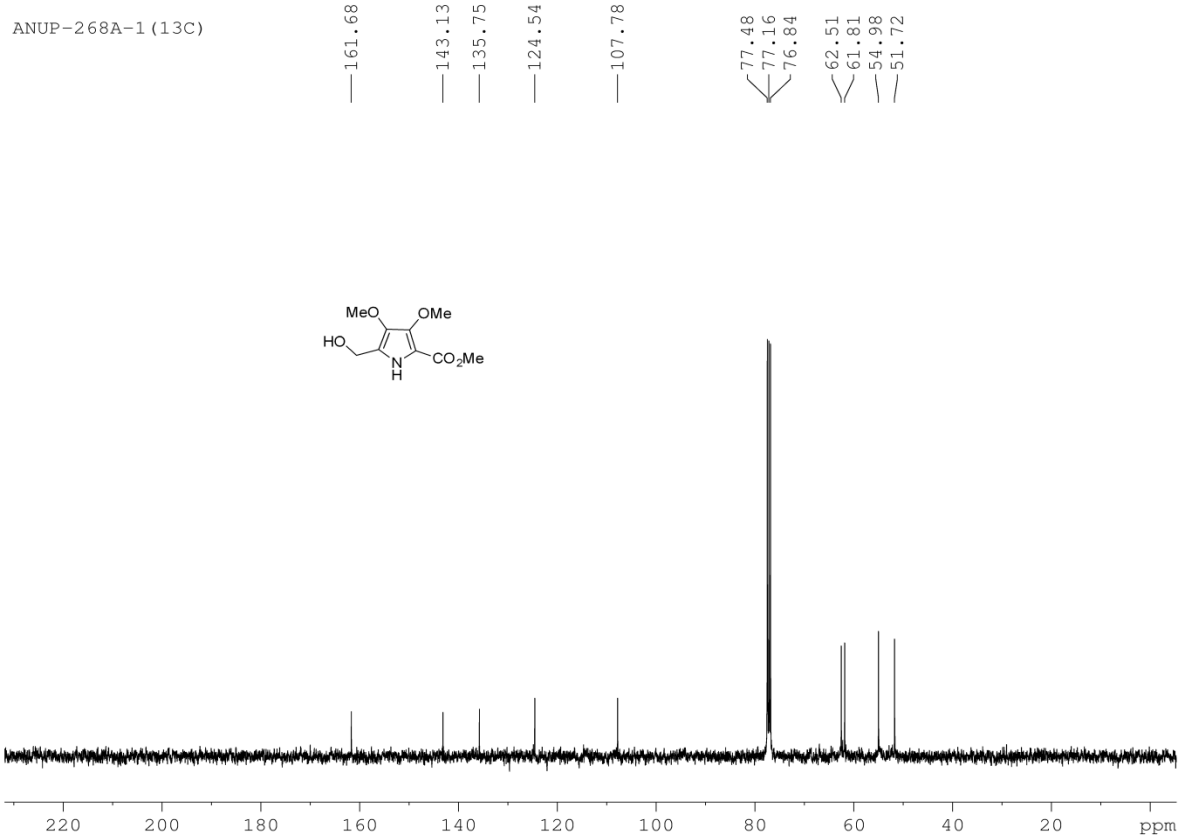

Figure 8.18 ^{13}C NMR spectrum of methyl 5-(hydroxymethyl)-3,4-dimethoxy-1H-pyrrole-2-carboxylate in $CDCl_3$.

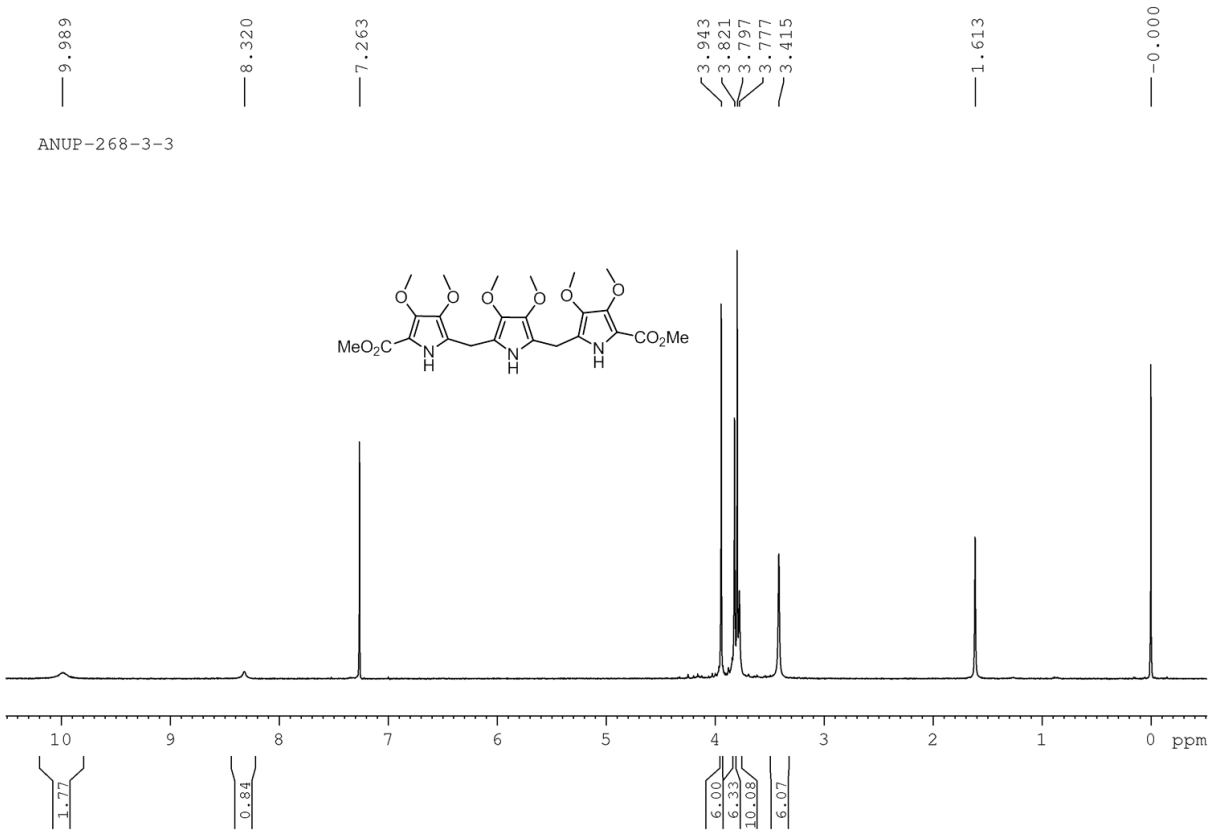

Figure 8.19 ^{1}H NMR spectrum of **8.63a** in $CDCl_3$.

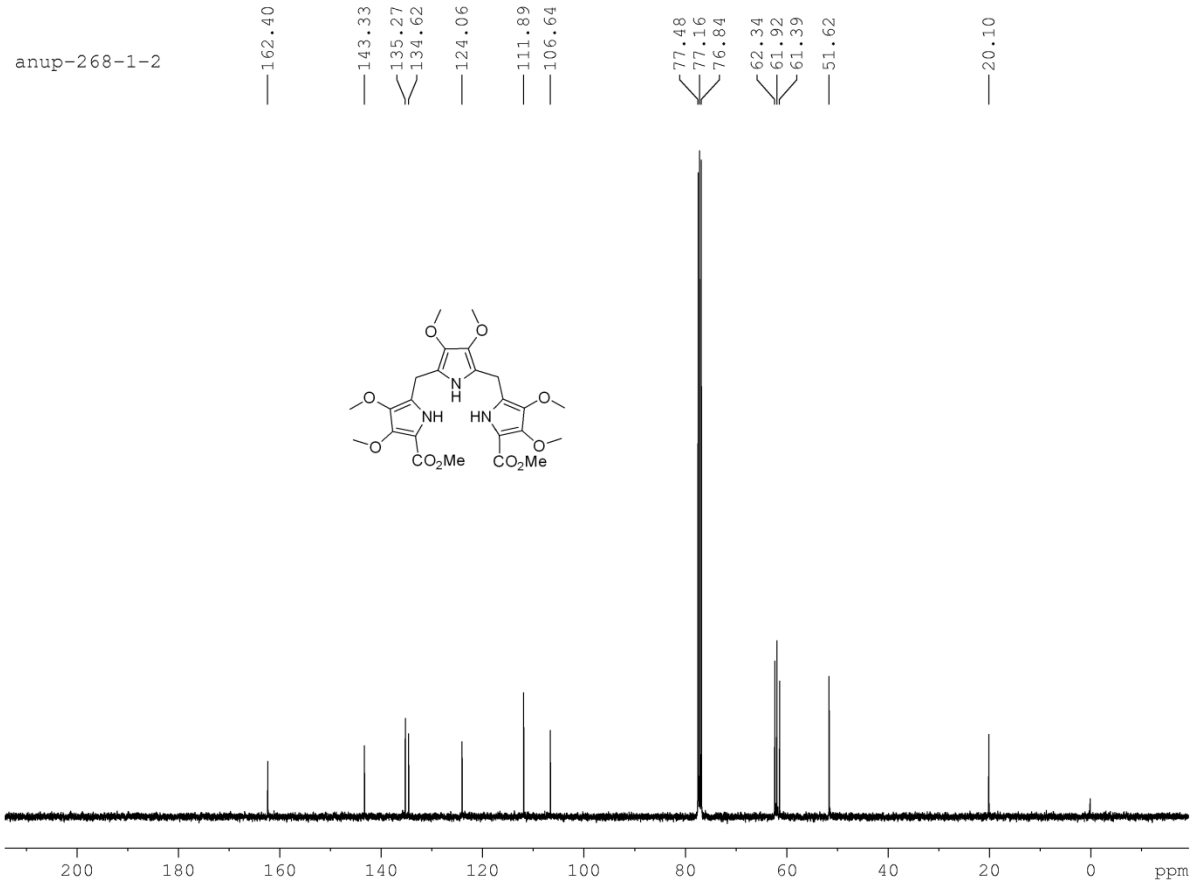

Figure 8.20 ^{13}C NMR spectrum of **8.63a** in $CDCl_3$.

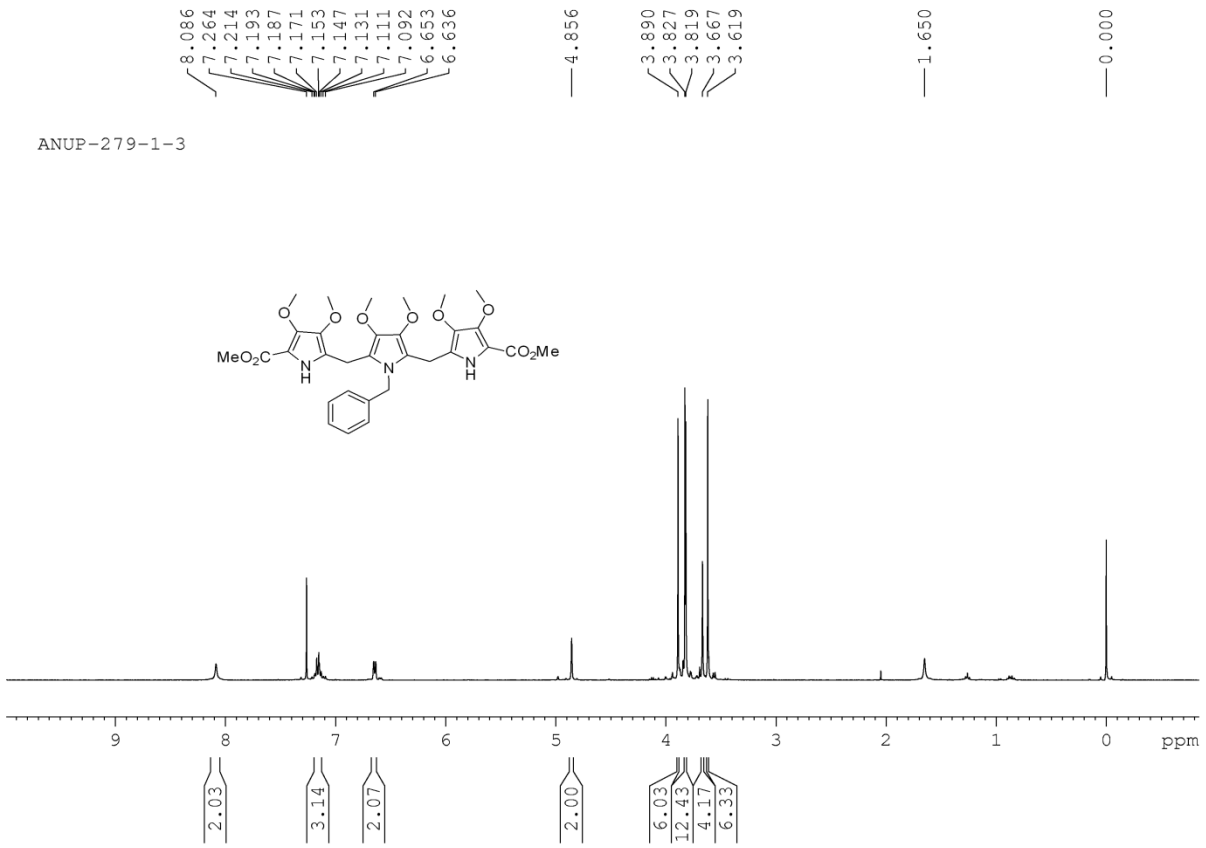

Figure 8.21 ^{1}H NMR spectrum of **8.63b** in $CDCl_3$.

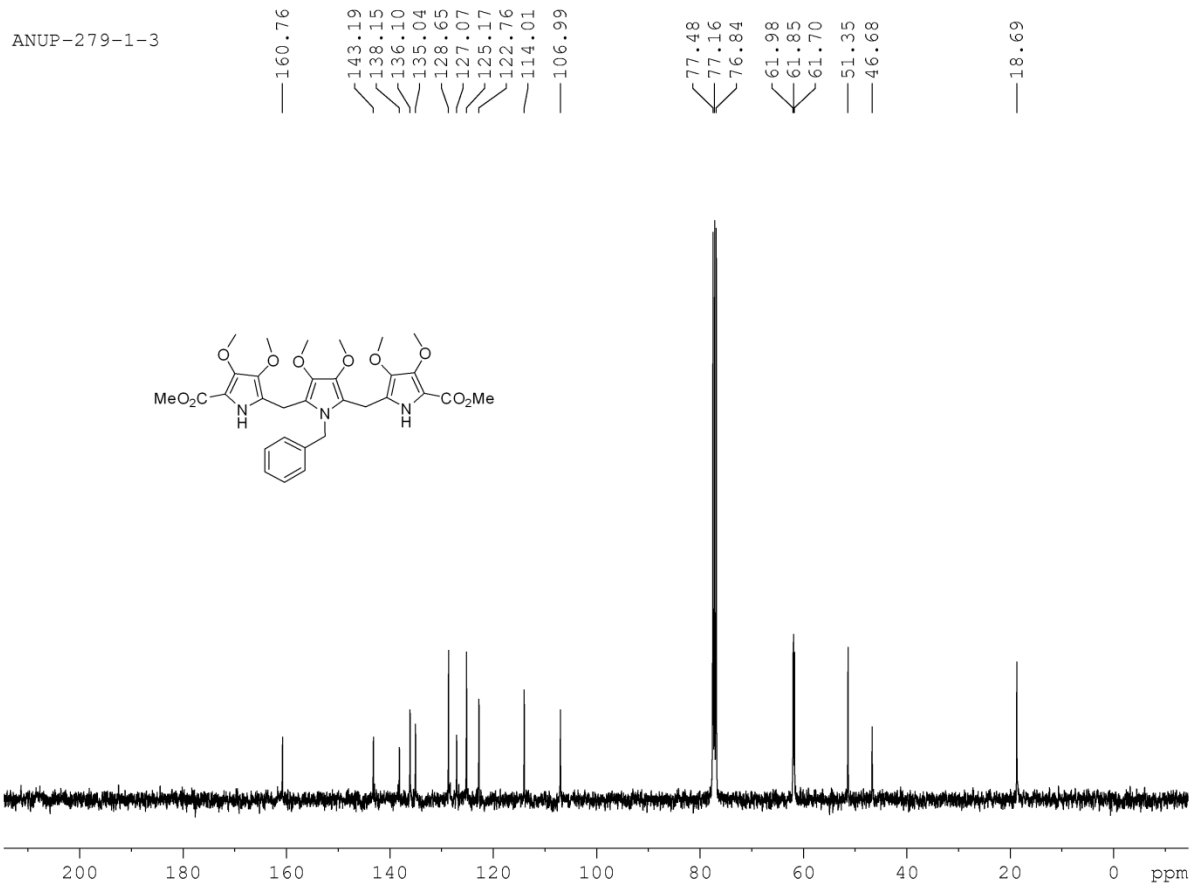

Figure 8.22 ^{13}C NMR spectrum of **8.63b** in $CDCl_3$.

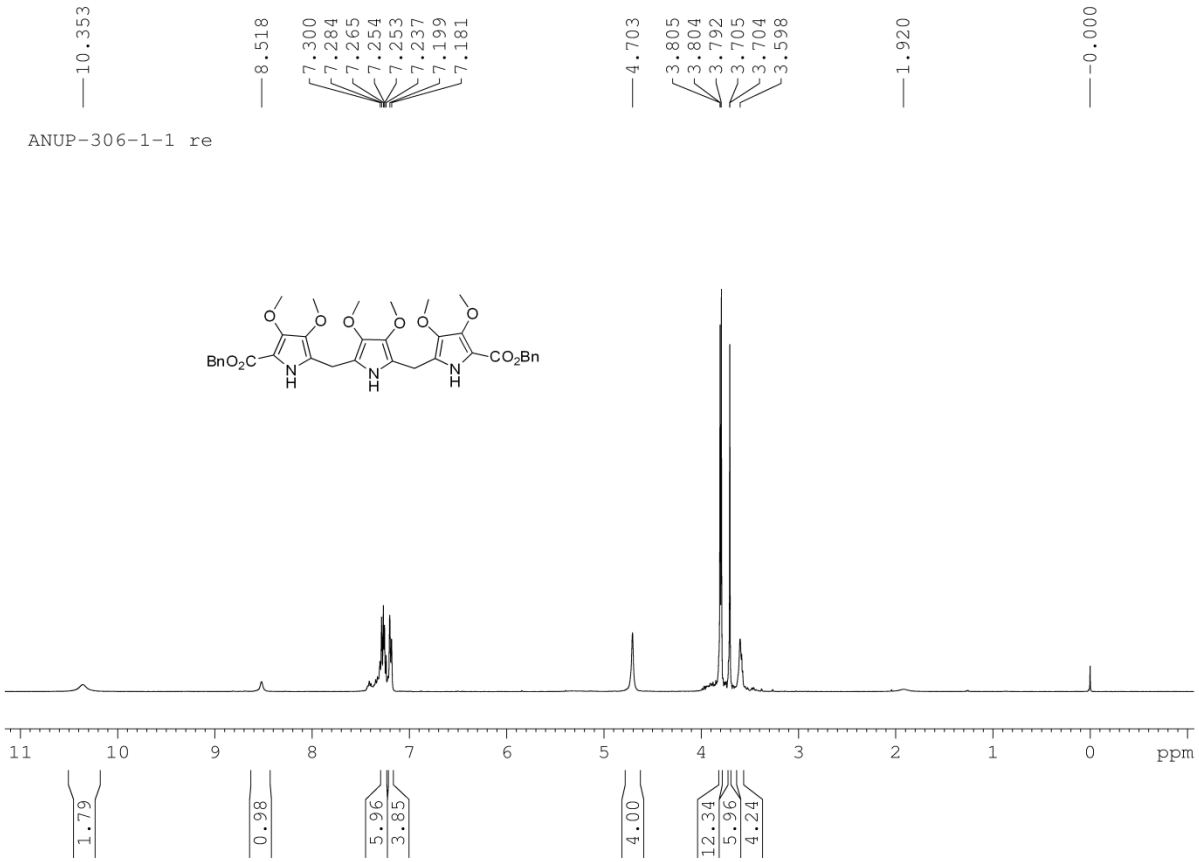

Figure 8.23 ^{1}H NMR spectrum of **8.64a** in $CDCl_3$.

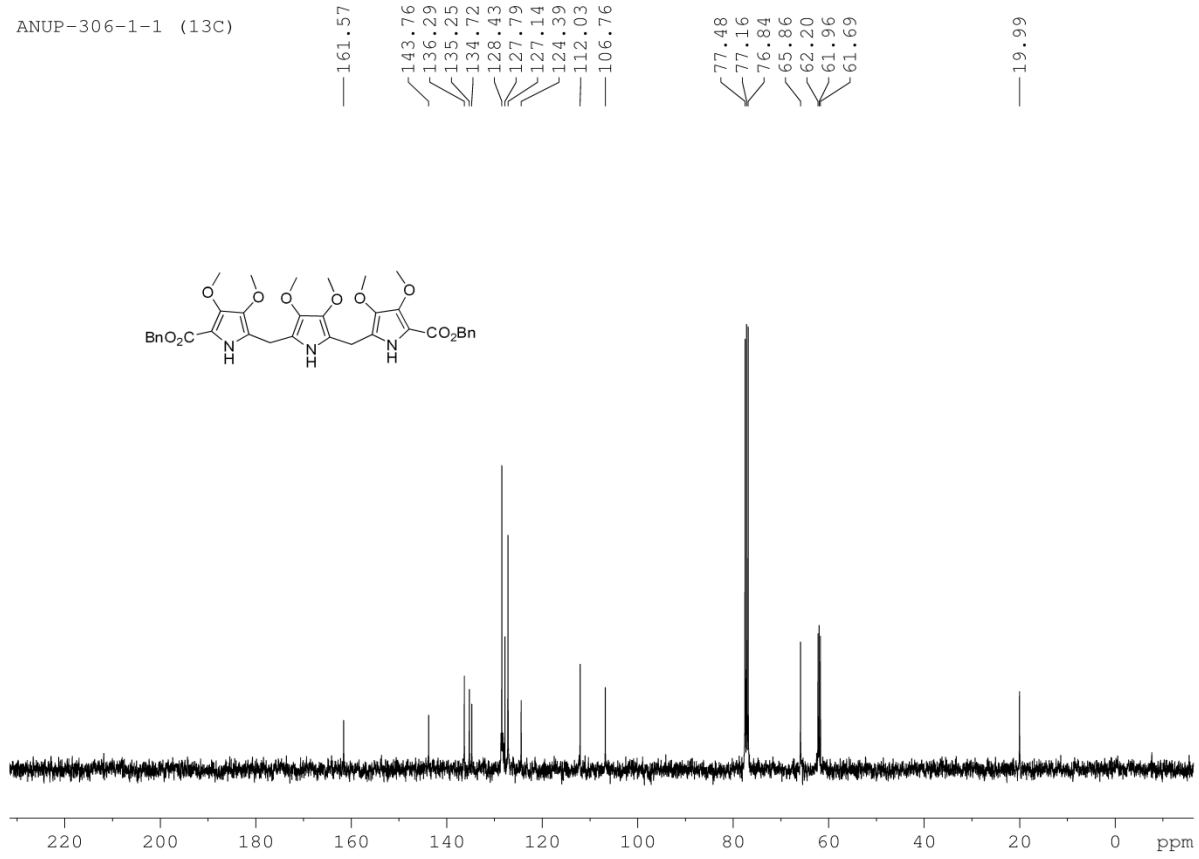

Figure 8.24 ^{13}C NMR spectrum of **8.64a** in $CDCl_3$.

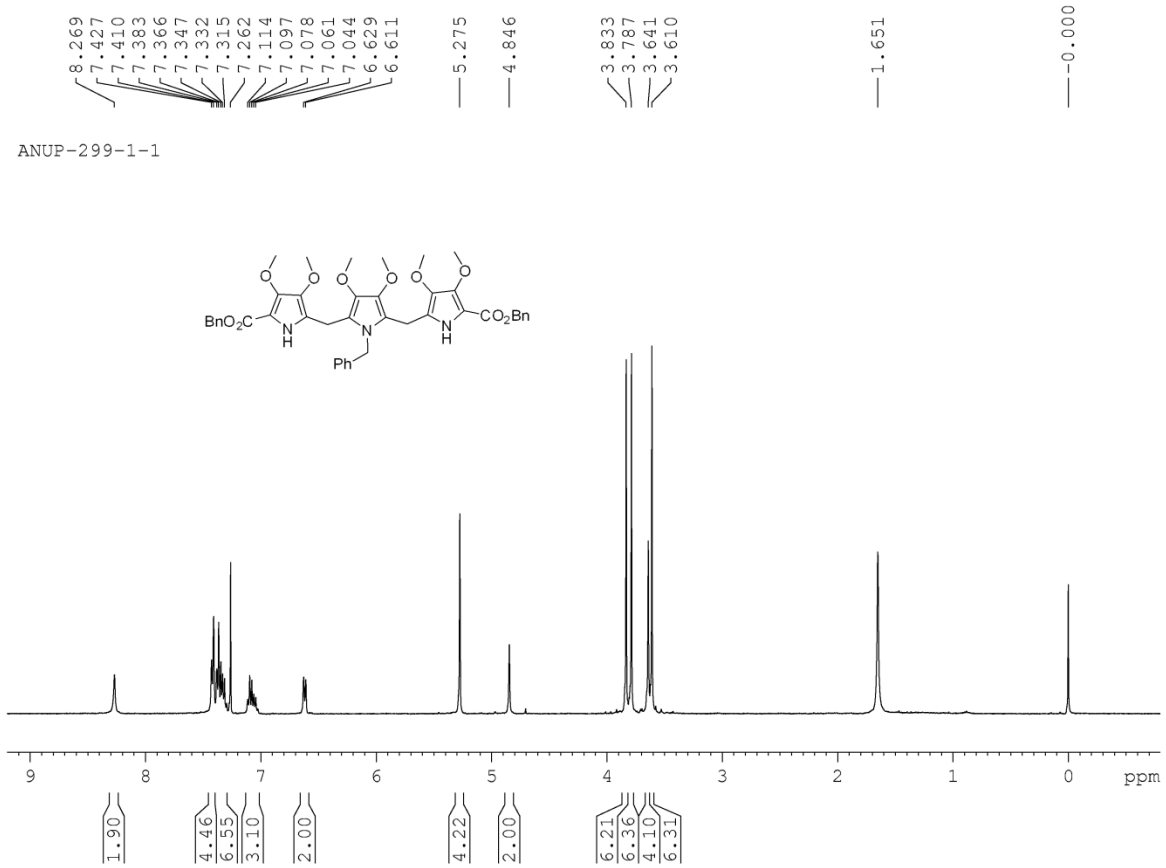

Figure 8.25 ^{1}H NMR spectrum of **8.64b** in $CDCl_3$.

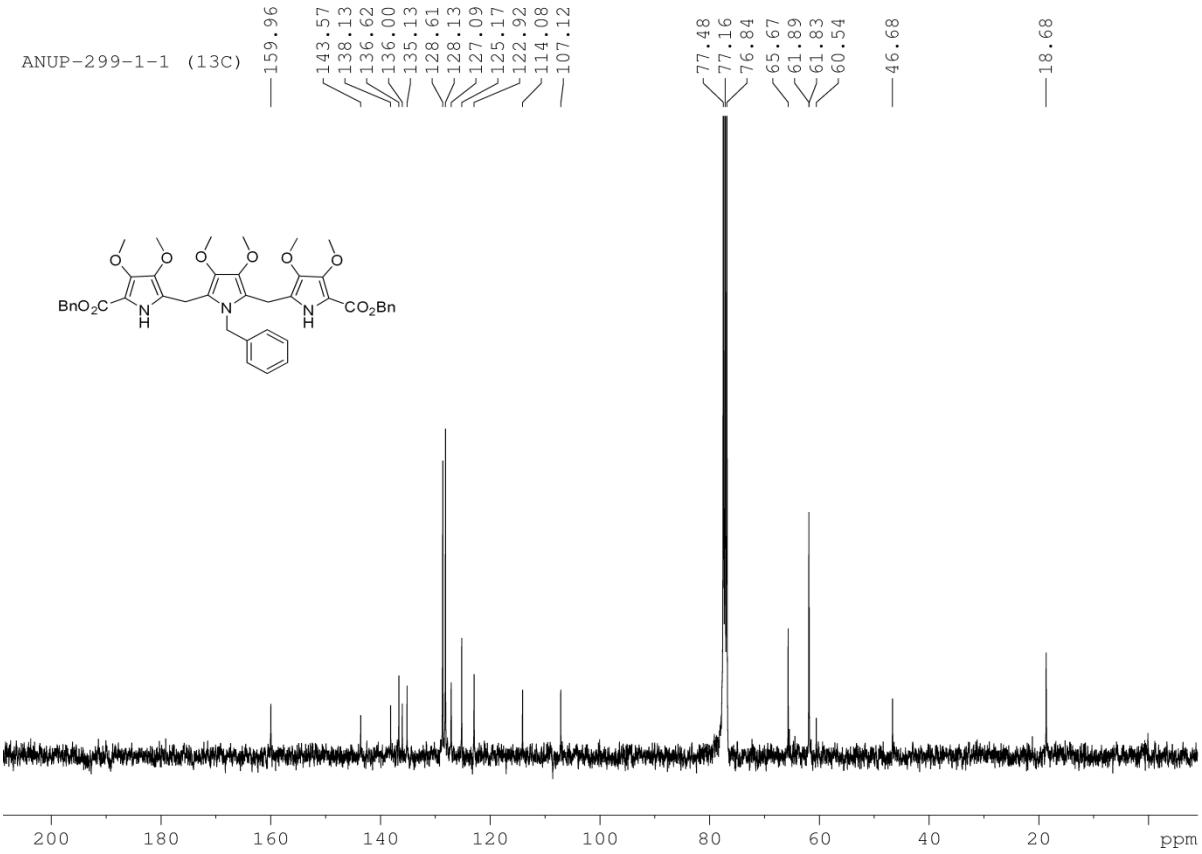

Figure 8.26 ^{13}C NMR spectrum of **8.64b** in $CDCl_3$.

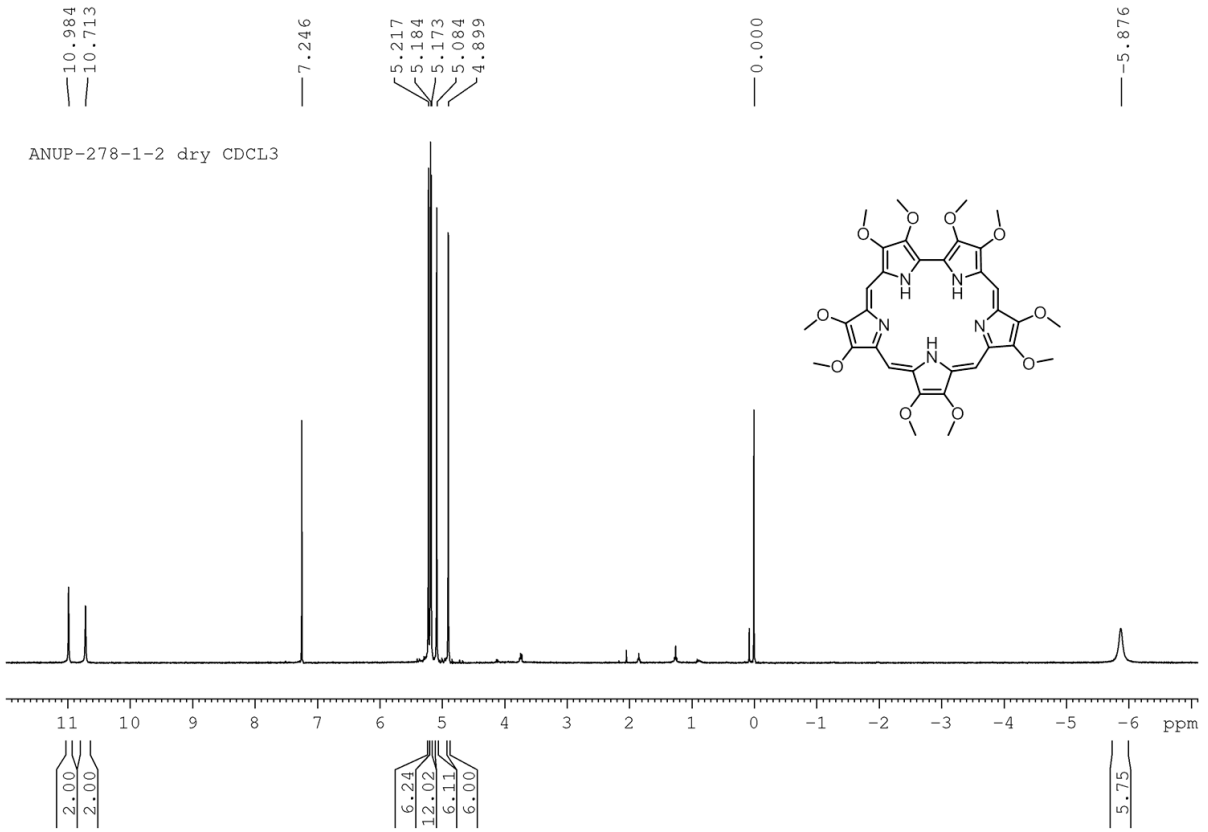

Figure 8.27 ^{1}H NMR spectrum of **8.57** in $CDCl_3$.

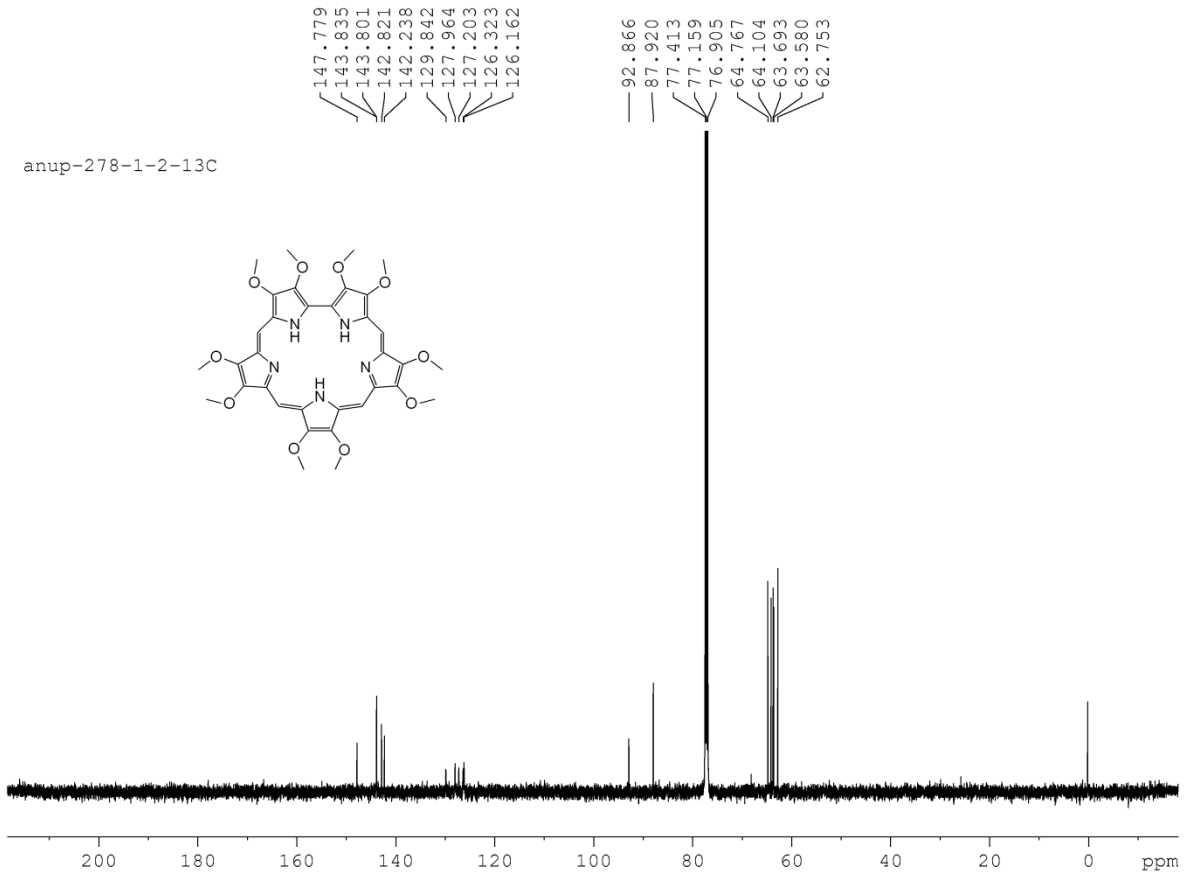

Figure 8.28 ^{13}C NMR spectrum of **8.57** in $CDCl_3$.

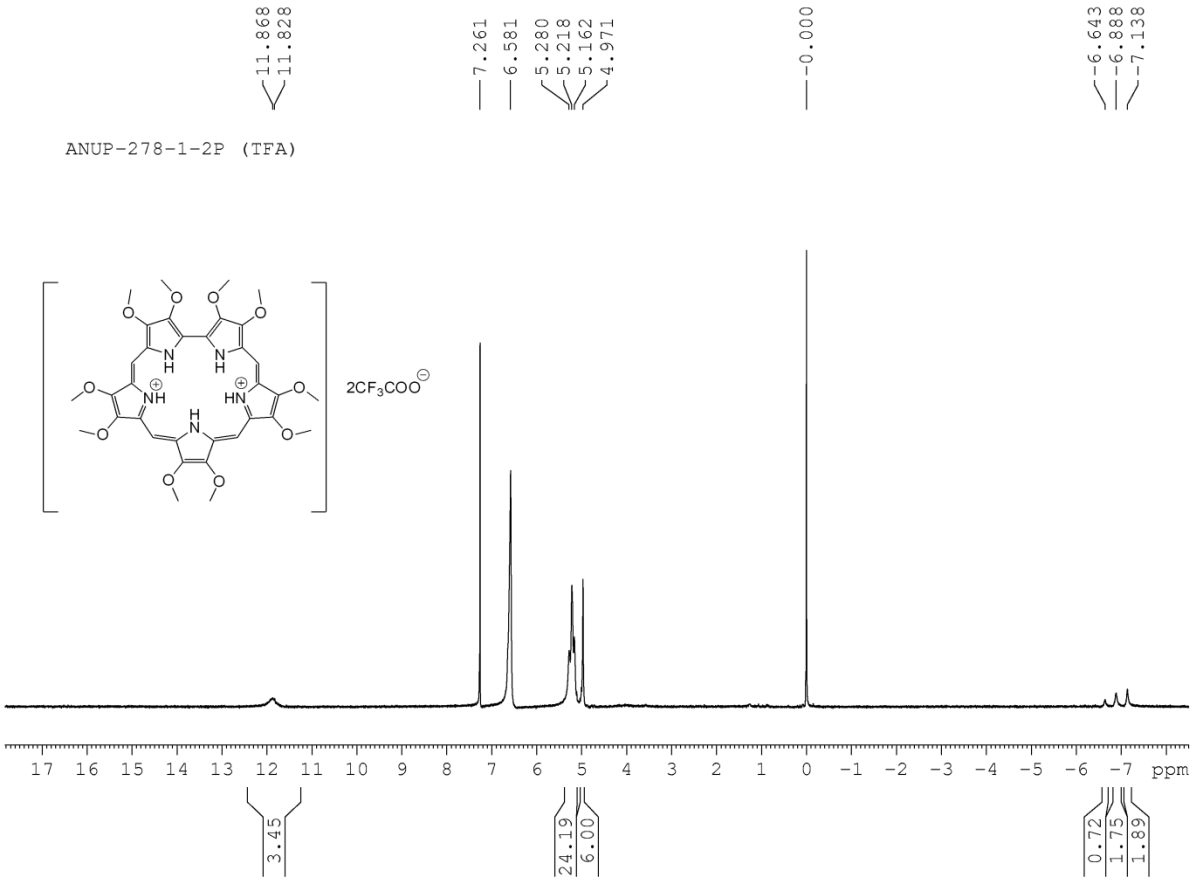

Figure 8.29 ^{1}H NMR spectrum of **8.57.**2TFA in $CDCl_3$.

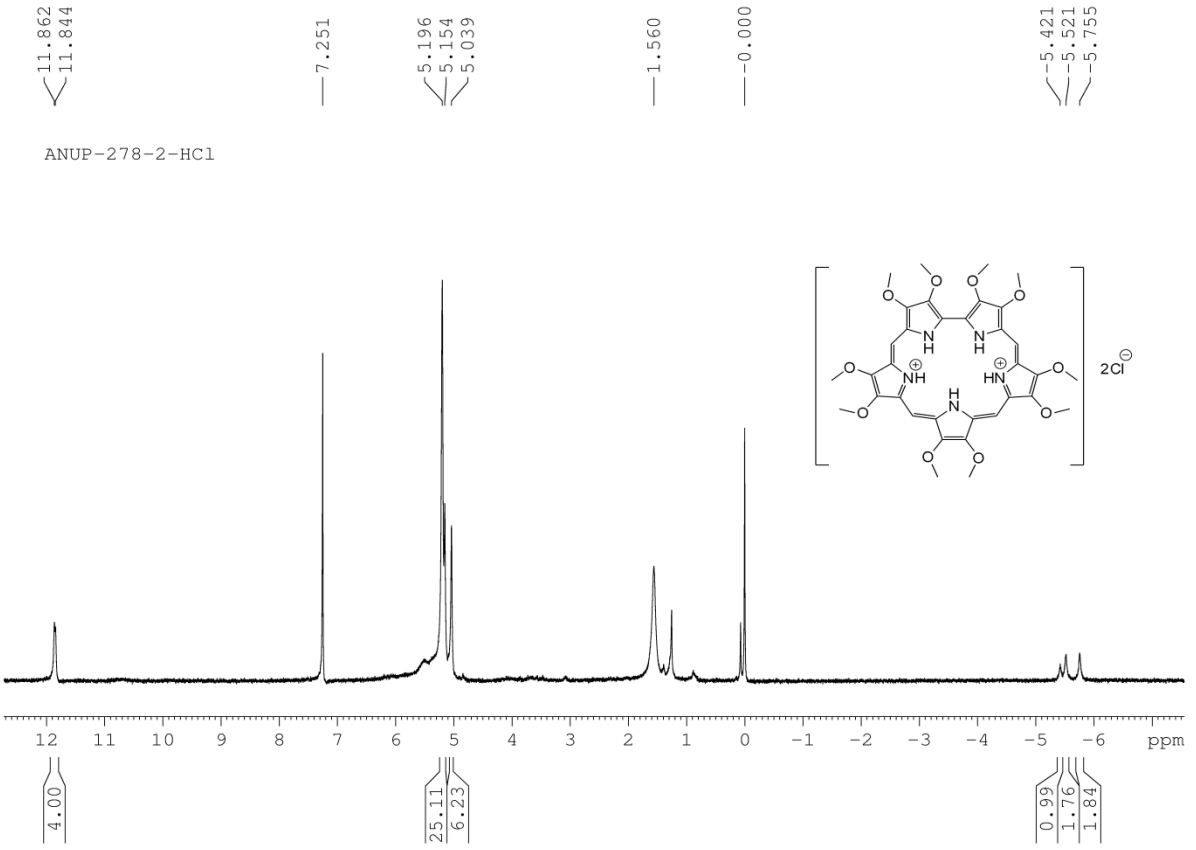

Figure 8.30 ^{1}H NMR spectrum of **8.57.**2HCl in $CDCl_3$.

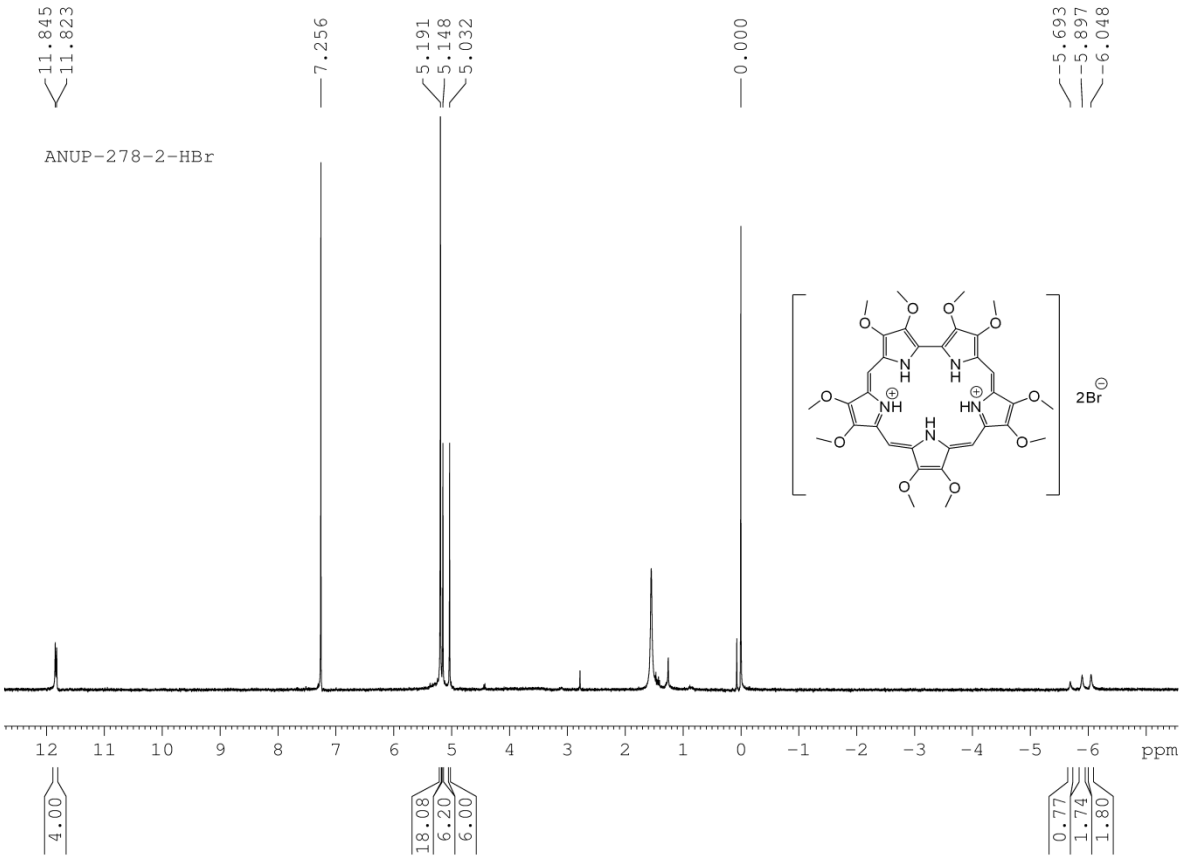

Figure 8.31 ^{1}H NMR spectrum of **8.57**.2HBr in $CDCl_3$.

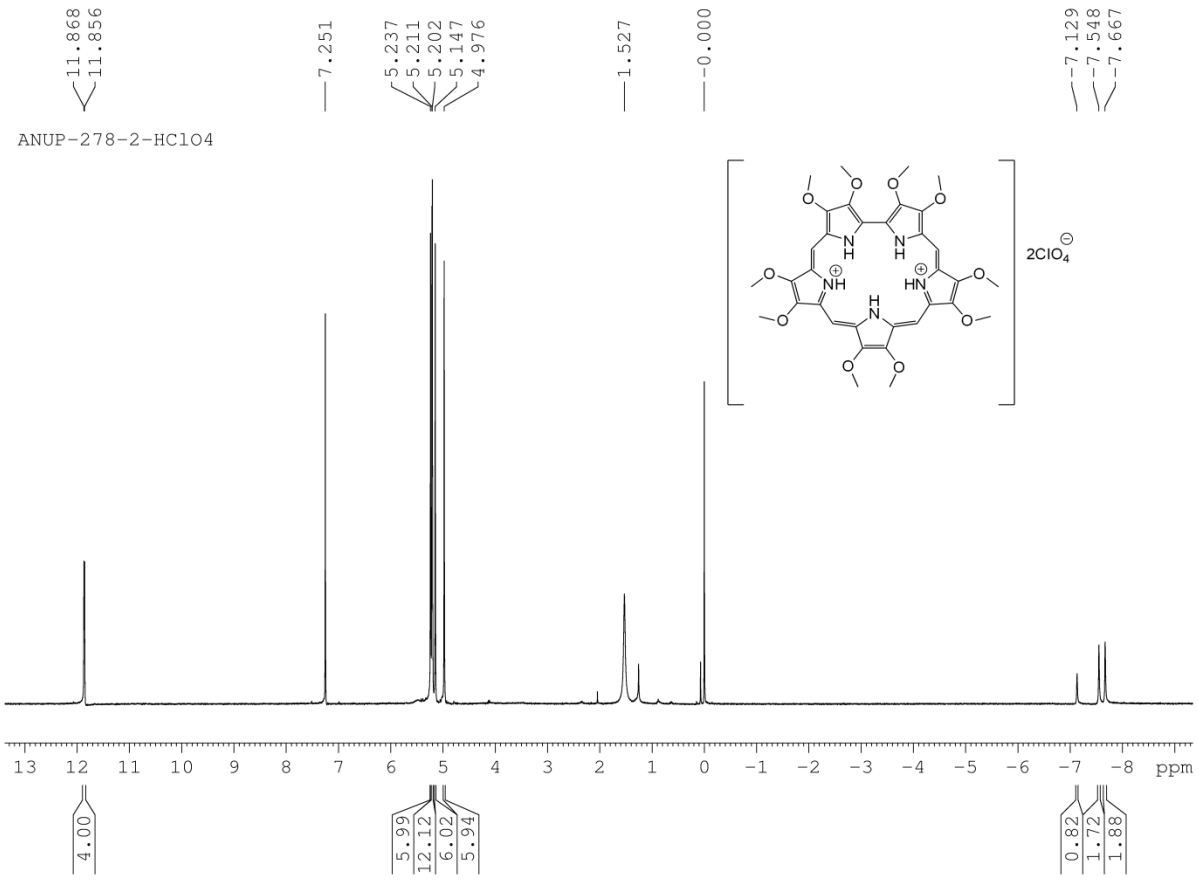

Figure 8.32 ^{1}H NMR spectrum of **8.57**.2$HClO_4$ in $CDCl_3$.

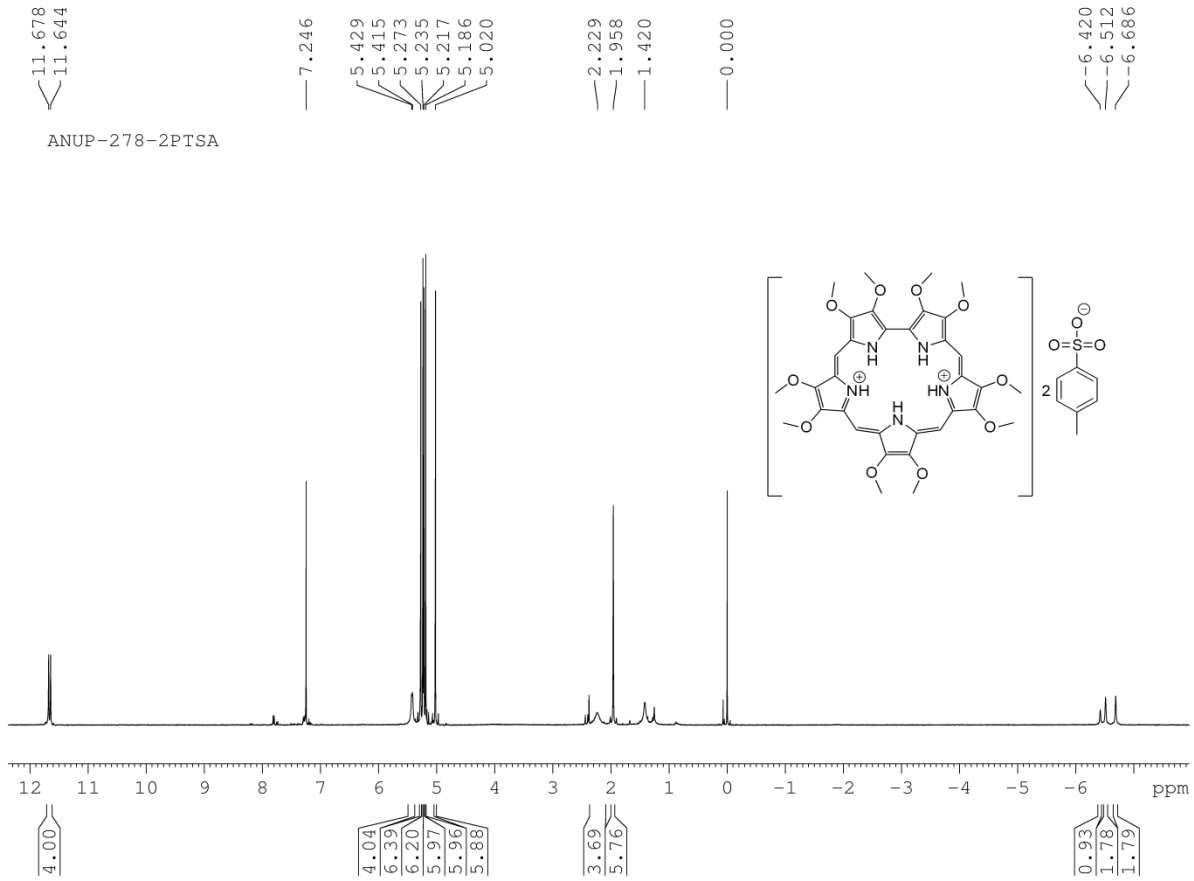

Figure 8.33 ^{1}H NMR spectrum of **8.57.**2PTSA in $CDCl_3$.

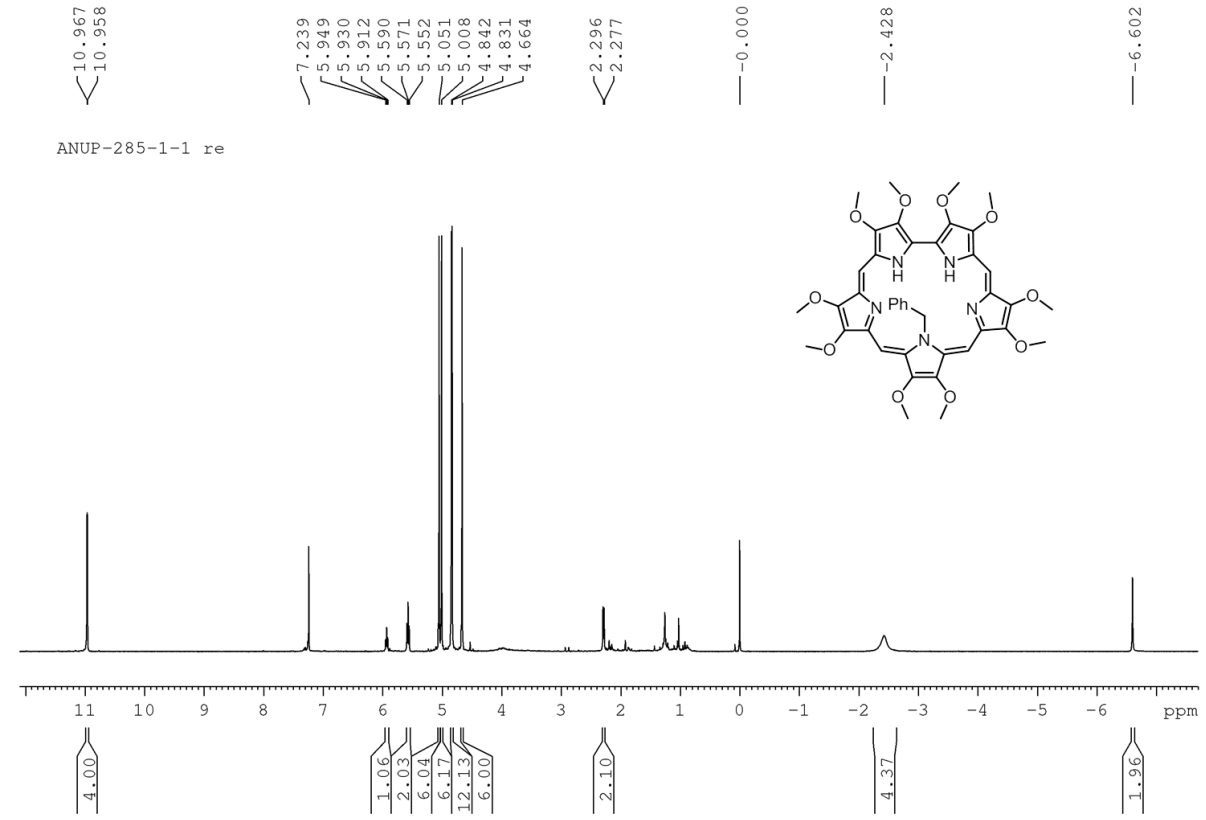

Figure 8.34 ^{1}H NMR spectrum of **8.58** in $CDCl_3$.

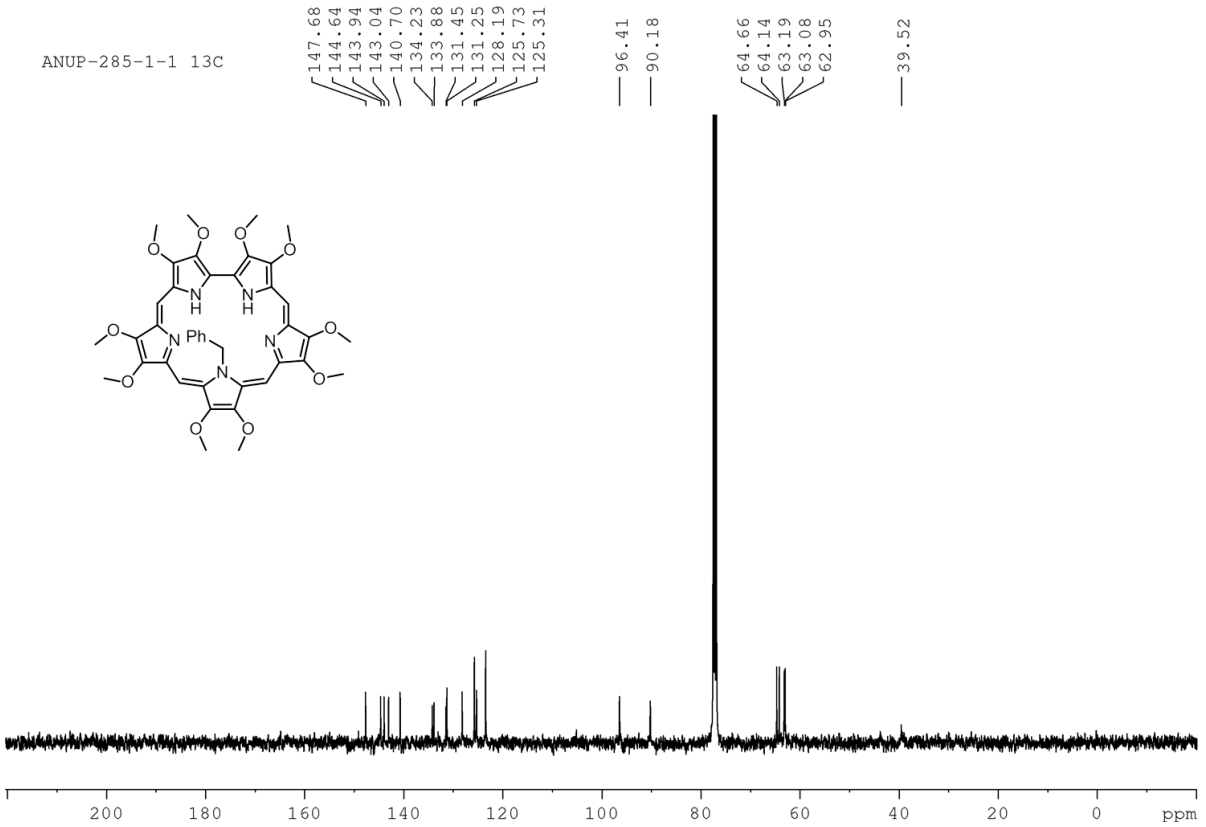

Figure 8.35 ^{13}C NMR spectrum of **8.58** in $CDCl_3$.

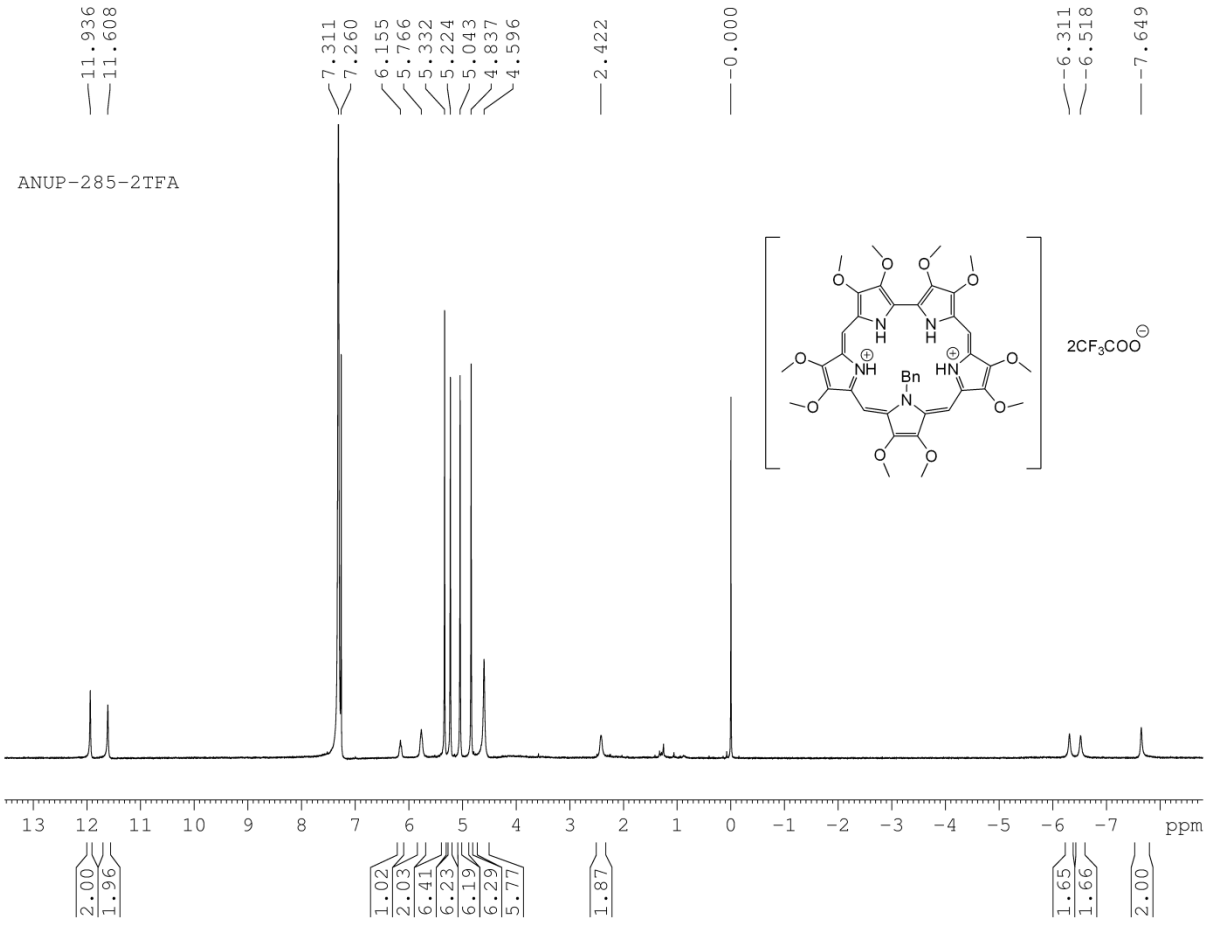

Figure 8.36 ^{1}H NMR spectrum of **8.58**.2TFA in $CDCl_3$.

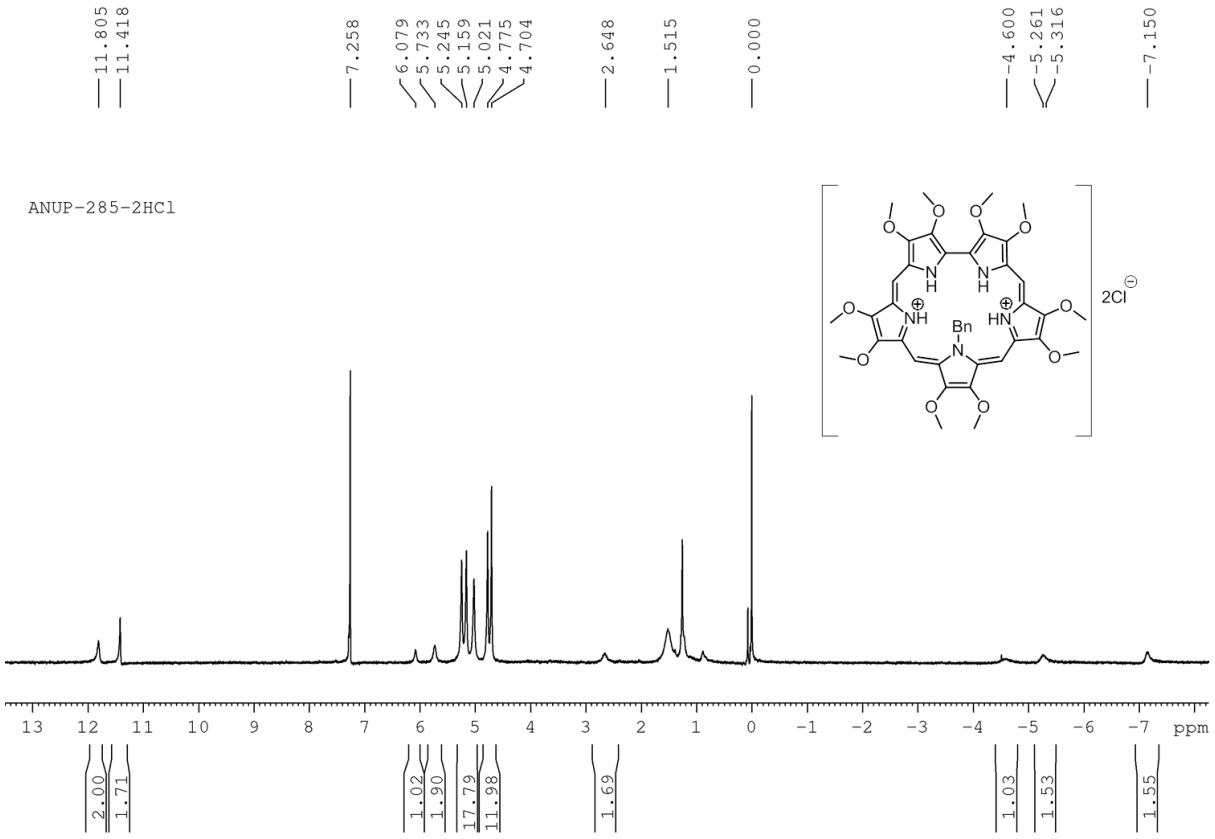

Figure 8.37 ^{1}H NMR spectrum of **8.58.**2HCl in $CDCl_3$.

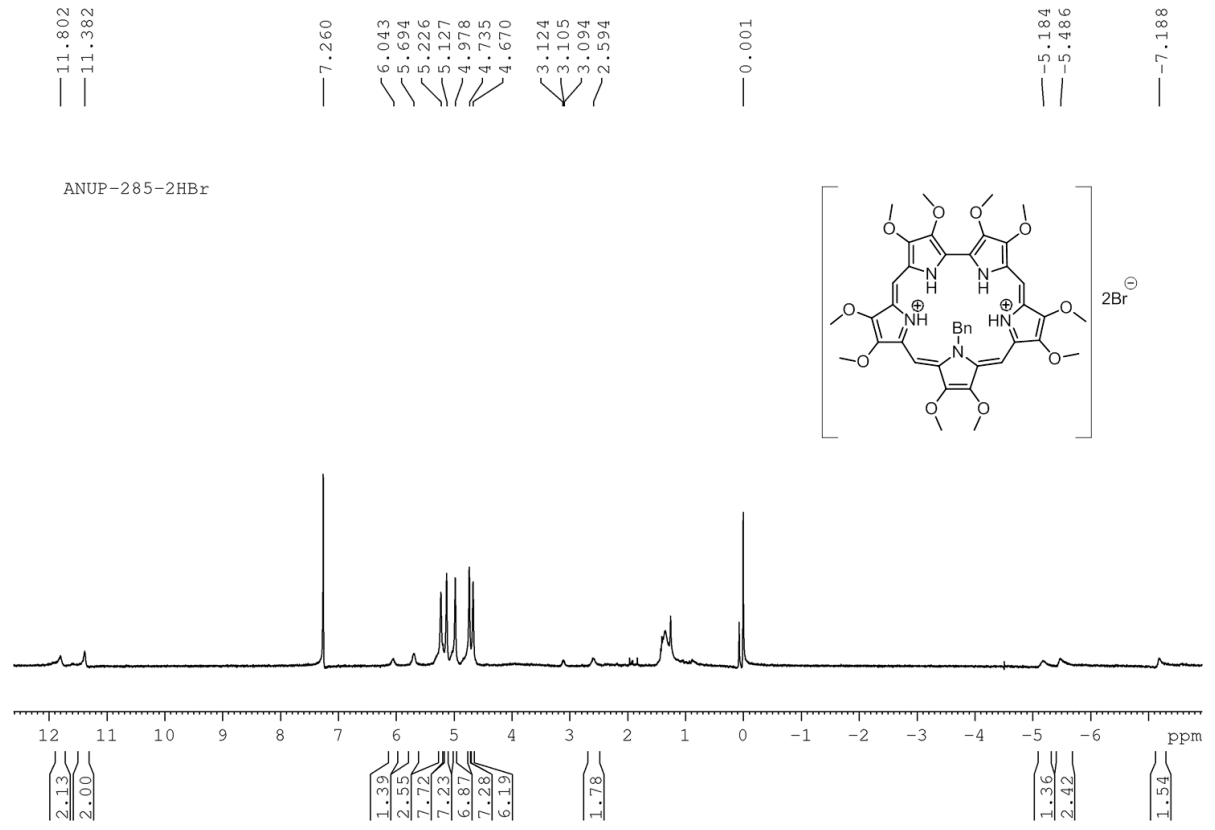

Figure 8.38 ^{1}H NMR spectrum of **8.58.**2HBr in $CDCl_3$.

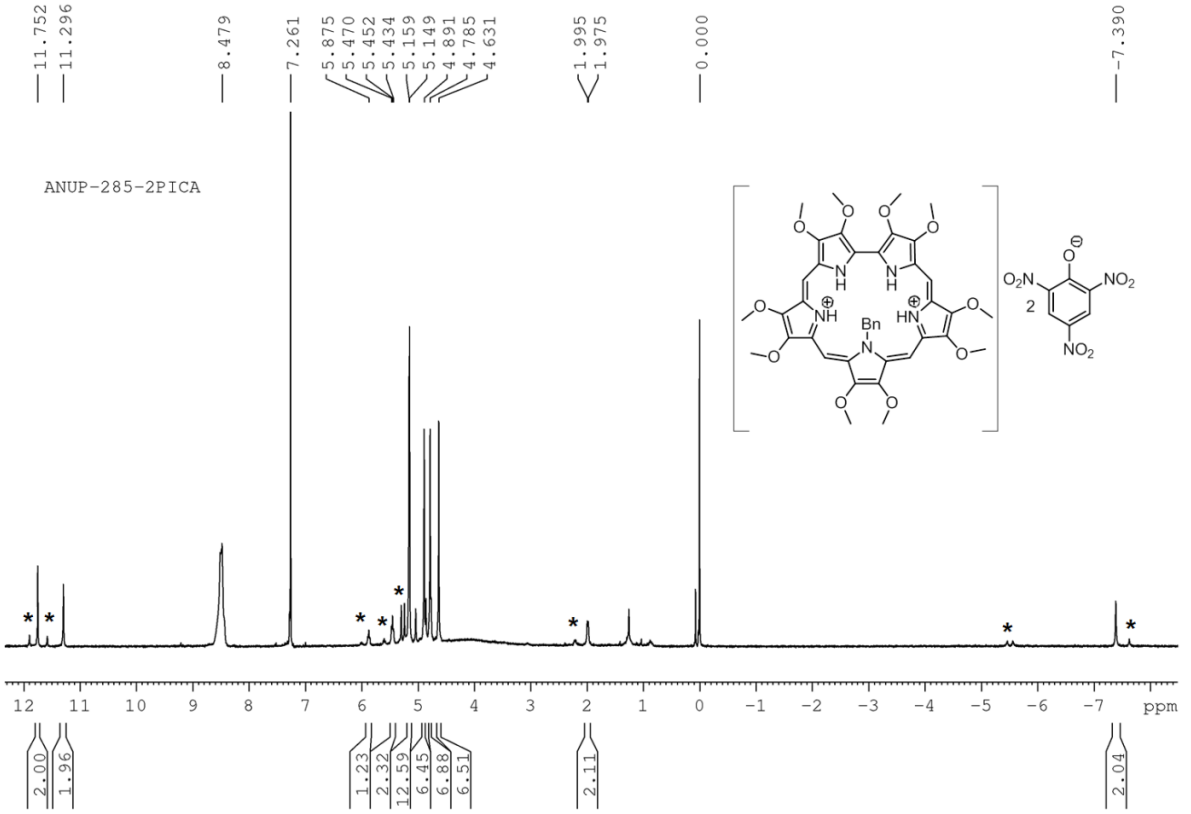

Figure 8.39 ^{1}H NMR spectrum of **8.58.**2PA in $CDCl_3$ and * indicates proton resonance arise from minor component.

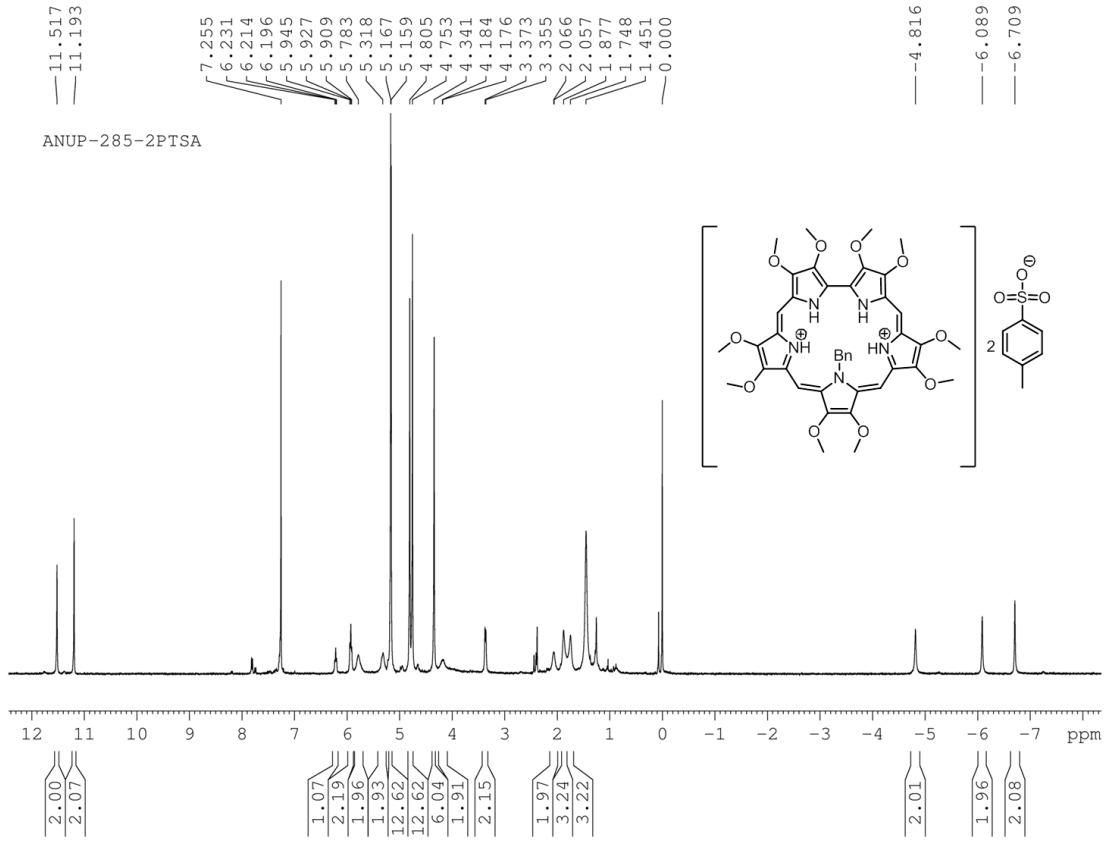

Figure 8.40 ^{1}H NMR spectrum of **8.58.**2PTSA in $CDCl_3$.

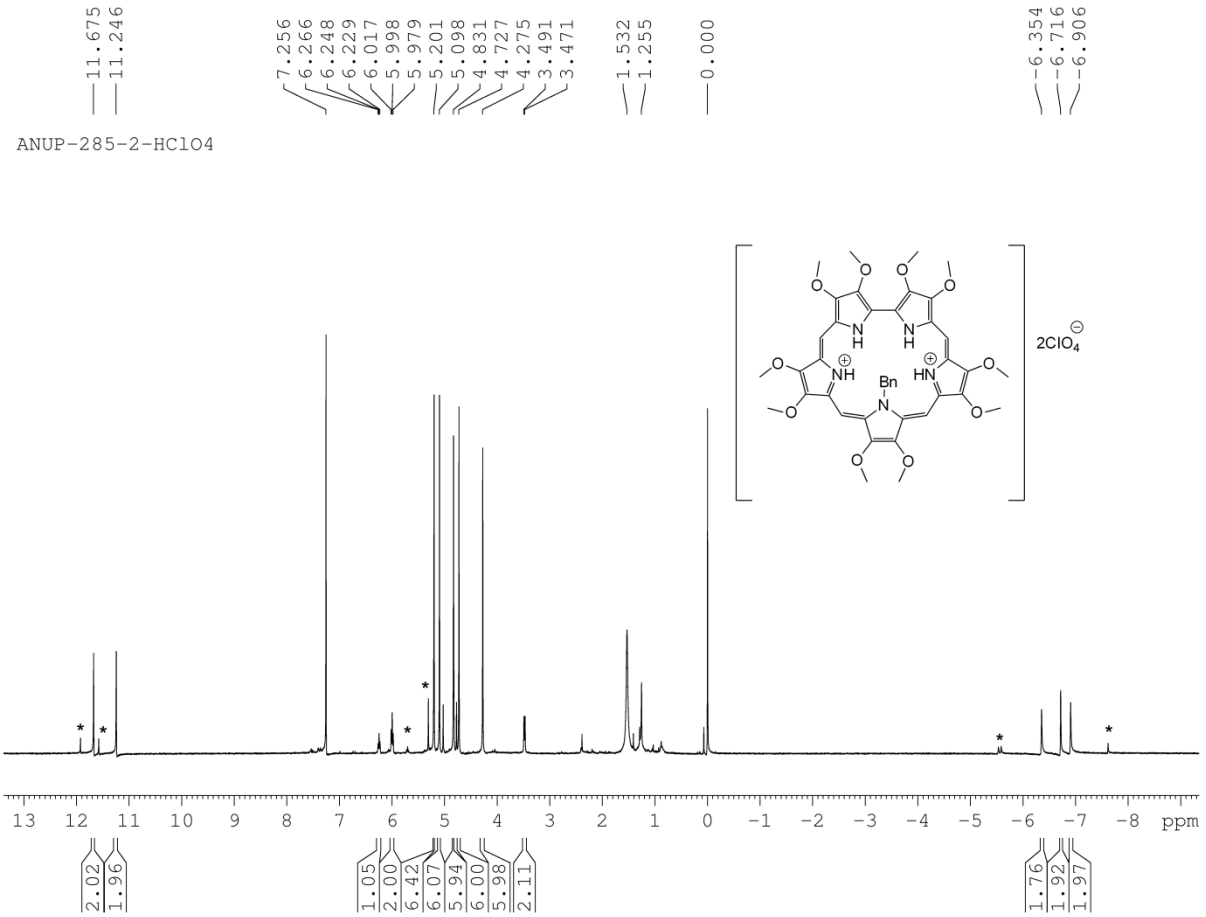

Figure 8.41 ^{1}H NMR spectrum of **8.58.**2$HClO_4$ in $CDCl_3$ and * indicates proton resonance arise from minor component.

CHAPTER 9

Conclusion

9.1 Summary

The thesis entitled "Novel β-substituted (alkoxy and methylthio) porphyrinoids: synthesis, characterization and optical properties" consists of nine chapters, which includes six working chapter along with introduction, conclusion and a chapter devoted to the material and methods employed during course of studies. It deals with the syntheses and characterizations of novel β-substituted porphyrinoids derived from 3,4-dialkoxy and 3,4-di(methylthio)pyrroles. These include porphyrins and its isomer, porphycenes and expanded porphyrins viz. stretched porphycenes and sapphyrins. The effect of β-substituents on these porphyrinoids has been thoroughly investigated in terms on their structure, photophysical and third order nonlinear optical properties, sensing application, coordination and electrochemical behaviors.

It is believed that without porphyrin life in earth is not viable. Porphyrin containing proteins play major roles from energy harvesting to reduce it to energy, hence most prominently known as "pigment of life". Further, the close resemblance of β-substituted porphyrinoids with naturally occurring porphyrinoids make them comparatively better promising material towards application like light harvesting antenna, photosensitizers for photodynamic treatment of cancer. Again, β-substituted porphyrinoids are excellent test bed to check reactivity of *meso* positions and some substituents can act as excellent leaving group, allowing further transformation at their periphery. These interesting properties of β-substituted porphyrins motivate us to explore β-substituted porphyrinoids. We have selected methoxy group, in β-position of pyrrole moiety, where it acts as electron donor, making porphyrinoids electron rich in nature. Also, methoxy group can enhance the hydrophilicity and help further derivatize upon deprotection, thereby enhancing its importance in biomedical application.

Sensing and environmental cleaning of explosives are among few major global challenges. Keeping this in view, we have demonstrated (Chapter-3) a series of porphyrins along with their Zn(II) complexes, endowed with electron deficient and electron rich substituents in their periphery to study the effect of substitution in solution and vapor phase sensing of potentially hazardous nitro explosive materials by fluorescence quenching method. In solution phase sensing study, we found that porphyrins endowed with electron rich substituents showed greater sensitivity compare to electron deficient analogues. Also, we found that among electron rich porphyrins, alkoxy analogues showed greater sensitivity towards nitroaromatic

explosives and moderate sensitivity towards alkyl nitro (NM, DMNB) and N-nitramine (RDX and HMX) explosives.[1] Therefore, on the basis of these results, we further extended our investigation to vapor phase explosive detection by fluorescence quenching method with electron rich porphyrins and their Zn(II) complexes. Preliminary vapor phase study revealed good sensitivity towards not only the nitroaromatics, but also towards plastic explosive taggant (alkyl nitro compound). Further, alkoxyporphyrins showed better sensitivity towards explosive molecules compare to non-alkoxy analogues and sensitivity is comparable and sometimes better than previously reported porphyrins. To the best of our knowledge, there are very few reports where good sensitivity was observed for both nitroaromatics and alkyl nitro compounds, indicating importance of the alkoxyporphyrins. Easy synthetic access along with simple fabrication techniques and good sensitivity towards a series of explosive molecules indicates alkoxporphyrins can act as versatile sensor for explosives detection.

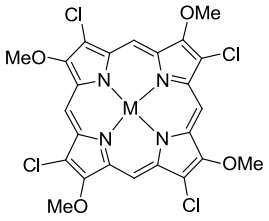

M = H_2, Ni(II), Zn(II)

Presence of donor-acceptor moieties or substituents that impart that type of attribute, make the systems act as excellent candidate for NLO and biomedical application. Towards this we have investigated (Chapter-4) the synthesis and characterization of 3,8,13,18-tetrachloro-2,7,12,17-tetramethoxyporphyrin along with their M(II) (Zn and Ni) complexes, which could be achieved owing to the unexpected synthesis of 3-chloro-4-methoxypyrrole-2-aldehyde during exhaustive formylation of 3,4-dimethoxypyrrole.[2] We extended this protocol towards selective bromination at 3-postion and 3-chlorination for higher alkoxypyrroles. Selective halogenation of pyrrole required expensive catalytic condition to achieve, further enhancing the importance of the halogenation of alkoxypyrrole. Further, careful control of reaction condition led to formation of unique type-I porphyrin, endowed with electron donating and withdrawing substituents at each pyrrole unit on its β-positions. We have observed strong two photon absorption (TPA) cross-section in chloromethoxyporphyrins (6440-53690 GM at 800 nm) compared to corresponding octamethoxyporphyrin analogues, endowed with all eight electron donating methoxy groups (1960-4000 GM).[3] Ultrafast excited state dynamics of porphyrins were also investigated using femtosecond degenerate pump-probe techniques.

In chapter 5 we have synthesized methoxysubstituted porphycenes which may find promising application towards photodynamic therapy (PDT). As literature indicates presence of methoxy group in porphycene led to faster cell localization, therefore, it motivated us to design and synthesize β-octamethoxyporphycene along with its M(II) complexes.[4] The

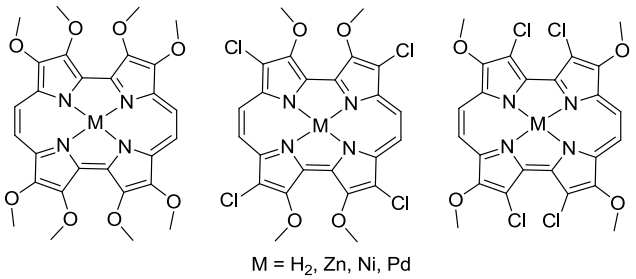

oxidative coupling of 3,4-dimethoxypyrrole enable us to synthesize octamethoxyporphycene efficiently, in three steps. Further, as presence of halogen groups in periphery leads to improved singlet oxygen generation efficiency of porphycenes, this motivated us to synthesize for the first time regio-specifically two positional isomers of β-tetrachlorotetramethoxyporphycenes along with their M(II) complexes.[5] Further, we have introduced synthetic protocol to avoid unstable bipyrrole intermediates towards the synthesis of porphycene. Solid state structures of all porphycenes revealed planar macrocyclic core arising from reduced van der Waals interaction at 3,6- and 13,16-positions. Also, we noticed significant positional effects of substituents for the two isomers of tetrachlorotetramethoxyporphycene on their structure, ^{1}H NMR spectral data, photophysical and electrochemical properties. The presence of methoxy groups led to an increase in their hydrophilicity, and Zn(II)- and Pd(II)-complexes of these porphycenes can efficiently generate singlet oxygen, enhancing their potential utility towards PDT application.

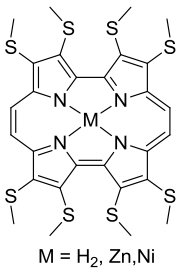

In chapter 6 we have reported the first porphycene endowed with all electron-deficient substituents at their β-positions, namely octa(methylthio)-porphycene, efficiently by employing oxidative coupling of 3,4-di(methylthio)pyrrole.[6] Current modified protocol might enable efficient synthesis of electron deficient bipyrroles directly, from their constituent pyrroles in single step. Introduction of methylthio groups led to ruffling of structure of porphycene and intense NIR absorption (~750 nm) along with unusual Q-band pattern. The third order nonlinear optical studies for freebase porphycene and its Ni(II) complex revealed enhanced two photon absorption compare to corresponding octaethyl and octamethoxy analogues. Femtosecond transient absorption and its decay profiles reveals shorter excited state lifetime observed for octamethoxy and octamethylthio porphycenes compare to octaethyl analogue. Electrochemical studies revealed electron deficient nature of methylthio-substituted porphycene. Further, we could successfully deprotect all methylthio groups of porphycene, leading to formation of unsubstituted porphycene efficiently, under mild condition. Owing to its mild deprotection ability, methylthio groups can be employed towards the synthesis of novel functionalized porphycenes.

Chapter 7 deals with three new β-octamethoxy substituted acetylene-cumuleneporphycene and stretched [22]porphyrin-(2.2.2.2).[7] The UV-Vis spectra of octamethoxy derivatives show minimal substituent effect owing to absence of van der Waals repulsion caused by introduction of acetylenic and vinylinic spacers between the bipyrrolic moieties. The methoxy analogues possess enhanced third order NLO absorption cross-section compared to ethyl analogues, indicating dominant internal charge transfer (ICT) characteristic induced by methoxy groups. Most importantly, the expansion of π-conjugation network either by introduction of meso methine groups or increasing the number of pyrrole moieties, behaves

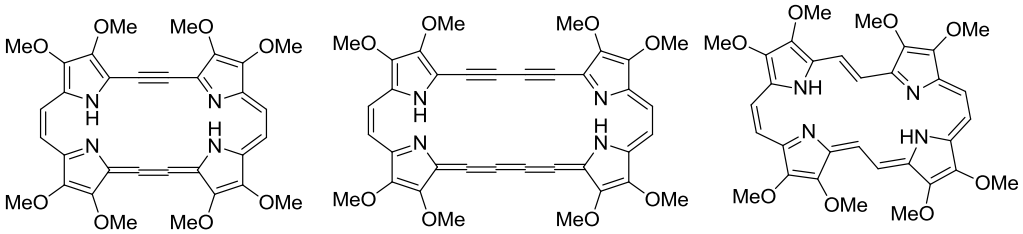

similarly towards NLO response. The NLO properties of studied expanded porphycenes are dominated not only by the π-conjugated network, but also conformational flexibility plays an important role. Femtosecond transient absorption studies revealed shorter excited state lifetime for methoxy substituted stretched porphycenes compare to octaethyl analogues, again arising from dominant ICT characteristic of methoxy groups. Electrochemical studies of stretched porphycenes revealed the characteristic electron rich features of these macrocycles.

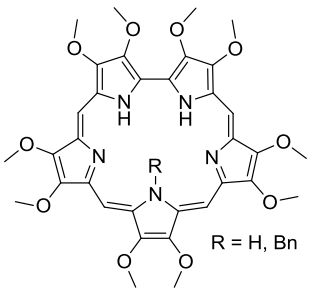

In chapter 8, we have reported the synthesis of decamethoxysapphyrin and its 27-N-benzyl congener. We have thoroughly investigated the effect of methoxy and 27-N-benzyl substituent on their structure, anion binding, photophysical and electrochemical properties.[8] Interestingly decamethoxysapphyrin dihydrogenfluoride salt binds selectively with fluoride ion. Both freebase sapphyrins can generate singlet oxygen with moderate efficiencies and hence may act as good photosensitizer. Electrochemical studies of freebase sapphyrins and their perchlorate salts provide important information about electronic properties of both freebase and protonated sapphyrins. Most interestingly, both ^{1}H NMR studies and solid state structural characterization of diprotonated N-benzyl sapphyrin analogue reveal anion induced out of plane deformation of N-benzylpyrrole unit opposite to bipyrrole unit for the first time.

In conclusion, β-substituted porphyrins are more closely related to naturally occurring porphyrins, however studies directed towards their potential application in light harvesting antenna, as photosensitizers for photodynamic treatment of cancer and materials for NLO applications are limited due to difficulties associated in term of synthesis and diverse reactivity of β-substituted pyrroles. For example, 3,4-dialkoxypyrrole finds wide applicability as electro-polymerized conductive polymer, however find very limited applicability in porphyrinoid chemistry, owing to instability at ambient condition and higher reactivity. The important features of methoxy group include greater hydrophilicity, electron donating character and further substitution scope, motivated us to explore these β-methoxy substituted novel porphyrinoids. Also, we found that by simple modulation of substitution at β-positions, we can modulate the properties of macrocycles. Moreover, we found some of these macrocycles can generate singlet oxygen efficiently and with increased hydrophilicity induced by methoxy groups, may find application for PDT. Further, ICT character of methoxy groups and methylthio groups enhanced their third order NLO response. We believe that our findings will be considered as important additions in this direction.

9.2 References

1. Rana, A.; Panda, P. K. *RSC Adv*. **2012**, *2*, 12164.
2. Rana, A.; Panda, P. K. *Tetrahedron Lett*. **2011**, *52*, 2697.
3. Swain, D.; Rana, A.; Panda, P. K.; Rao, S. V. *Chem. Phys. Lett*. **2014**, *610-611*, 310.
4. Rana, A.; Panda, P. K. *Org. Lett*. **2014**, *16*, 78.
5. Rana, A.; Panda, P. K. *Manuscript under preparation*.
6. Rana, A.; Lee, S.; Kim, D.; Panda, P. K. *Chem. Commun*. **2015**, DOI: 10.1039/C5CC02279G.
7. Rana, A.; Lee, S.; Kim, D.; Panda, P. K. *Communicated*.
8. Rana, A.; Panda, P. K. *Communicated*.

Publications

1. Synthesis of 3,8,13,18-tetrachloro-2,7,12,17-tetramethoxyporphyrin, **Rana, A.**; Panda, P. K. *Tetrahedron. Lett*. **2011**, *52*, 2697.
2. Fluorescent turn-off based sensing of nitrated explosives using porphyrins and their Zn(II)-derivatives, **Rana, A.**; Panda, P. K. *RSC. Adv*. **2012**, *2*, 12164.
3. β-Octamethoxyporphycenes, **Rana, A.**; Panda, P. K. *Org. Lett*. **2014**, *16*, 78.
4. Strong two-photon absorption properties and ultrafast pump-probe studies of novel porphyrin derivatives, Swain, D.; **Rana, A.**; Panda, P. K.; Rao, S. V. *Chem. Phys. Lett*. **2014**, *610-611*, 310.
5. β-Octakis(methylthio)porphycenes: synthesis, characterisation and third order nonlinear optical studies, **Rana, A.**; Lee, S.; Kim, D.; Panda, P. K. *Chem. Commun*. **2015**, DOI: 10.1039/C5CC02279G.
6. New 22π and 26π stretched porphycenes: synthesis, characterization, photodynamics and nonlinear optical studies, **Rana, A.**; Lee, S.; Kim, D.; Panda, P. K. *Communicated*.
7. β-Decamethoxysapphyrins: structural diversity and anion binding study, **Rana, A.**; Panda, P. K. *Communicated*.
8. Chloro-substituted porphycenes: regio-specific synthesis of positional isomers of β-tetrachloro-tetra-methoxyporphycene, **Rana, A.**; Panda, P. K. *Manuscript under preparation*.

Conference proceedings

1. Ultrafast nonlinear optical studies of 3,8,13,18-tetrachloro-2,7,12,17-tetramethoxyporphyrin and its derivatives, Swain, D.; **Rana, A.**; Panda, P. K. Rao, S. V. *Proc. of SPIE* **2012**, *8258*, 82581B.

Conference presentations

1. Presented poster on "3,8,13,18-Tetrachloro-2,7,12,17-tetramethoxyporphyrin", 13th CRSI National Symposium in Chemistry and 5th CRSI-RSC Symposium, February 4, **2011**, NISER and KIIT, Bhubaneshwar, INDIA.
2. Poster presented on "3,8,13,18-tetrachloro-2,7,12,17-tetramethoxyporphyrin", 8th Annual In-House Symposium of the School of Chemistry, ChemFest, 25-26th February, **2011**, University of Hyderabad.

3. Poster presented on "Synthesis of free base and metallated 2,3,6,7,12,13,16,17-octamethoxyporphycene and their photophysical properties", 10th Annual In-House Symposium of the School of Chemistry, ChemFest, **2013**, University of Hyderabad, Hyderabad, India.
4. **Oral presentation** and poster presented on "β-Methoxysubstitutedporphycenes: Potential Photosensitizers for Photodynamic Therapy (PDT)", 11th Annual In-House Symposium of the School of Chemistry, ChemFest, 21-22nd February, **2014**, University of Hyderabad, Hyderabad, India.
5. Poster presented on "2,3,7,8,12,13,17,18,22,23-Decamethoxysapphyrins", 8th International Conference on Porphyrins and Phthalocyanines (ICPP-8), 22-27th June, **2014**, Istanbul, Turkey.
6. Poster presented on "Vapor phase sensing of nitroaromatics by β-octaalkoxy-porphyrins", 8th International Conference on Porphyrins and Phthalocyanines (ICPP-8), 22-27th June, **2014**, Istanbul, Turkey.
7. Poster presented on "Novel β-substituted porphycenes towards photo dynamic therapy (PDT)", Indo-German Conference on Bio-inspired Chemistry 2014 (IGCBIC-2014), 10-11th September, **2014**, Indian Institute of Science, Bangalore, India.
8. Poster presented on "Novel β-substituted porphycenes towards photo dynamic therapy (PDT)", Indian Roadshow Workshop organized by Royal Society of Chemistry, 7th November, **2014**, University of Hyderabad, Hyderabad, India.
9. Poster presented on "Novel β-substituted porphycenes towards photo dynamic therapy (PDT)", 1st Indo-Taiwan Symposium on "Recent Trends in Chemical Sciences (RTCS)", 17-18th November, **2014**, University of Hyderabad, Hyderabad, India.